



**ENGINEERING SERVICE CENTER**  
Port Hueneme, California 93043-4370

## **CONTRACT REPORT**

### **CR-NAVFAC ESC-EV-1202**

# **Dense Non Aqueous Phase Liquid (DNAPL) Removal from Fractured Rock Using Thermal Conductive Heating (TCH)**

By  
Carmen A. Lebrón; NAVFAC ESC  
Devon Phelan, Dr. Gorm Heron, John LaChance and Steffen G. Nielsen; TerraTherm,  
Inc.  
Dr. Bernard Kueper, David Rodriguez, Ashley Wemp and Daniel Baston; Queen's  
University  
Pierre Lacombe and Dr. Francis H. Chapelle; USGS



# **FINAL REPORT**

---

## **Environmental Restoration Project ER200715**

### **Dense Non Aqueous Phase Liquid (DNAPL) Removal from Fractured Rock Using Thermal Conductive Heating (TCH)**

**August 2012**

**Prepared by:**

**Carmen A. Lebrón NAVFAC ESC  
Devon Phelan, Dr. Gorm Heron, John LaChance and Steffen G.  
Nielsen, TerraTherm, Inc.  
Dr. Bernard Kueper, David Rodriguez, Ashley Wemp and Daniel  
Baston, Queen's University  
Pierre Lacombe and Dr. Francis H. Chapelle, USGS**

**REPORT DOCUMENTATION PAGE***Form Approved  
OMB No. 0704-0188*

The public reporting burden for this collection of information is estimated to average 1 hour per response, including the time for reviewing instructions, searching existing data sources, gathering and maintaining the data needed, and completing and reviewing the collection of information. Send comments regarding this burden estimate or any other aspect of this collection of information, including suggestions for reducing the burden, to the Department of Defense, Executive Services and Communications Directorate (0704-0188). Respondents should be aware that notwithstanding any other provision of law, no person shall be subject to any penalty for failing to comply with a collection of information if it does not display a currently valid OMB control number.

**PLEASE DO NOT RETURN YOUR FORM TO THE ABOVE ORGANIZATION.**

<b>1. REPORT DATE (DD-MM-YYYY)</b>		<b>2. REPORT TYPE</b>		<b>3. DATES COVERED (From - To)</b>	
<b>4. TITLE AND SUBTITLE</b>				<b>5a. CONTRACT NUMBER</b>	
				<b>5b. GRANT NUMBER</b>	
				<b>5c. PROGRAM ELEMENT NUMBER</b>	
<b>6. AUTHOR(S)</b>				<b>5d. PROJECT NUMBER</b>	
				<b>5e. TASK NUMBER</b>	
				<b>5f. WORK UNIT NUMBER</b>	
<b>7. PERFORMING ORGANIZATION NAME(S) AND ADDRESS(ES)</b>				<b>8. PERFORMING ORGANIZATION REPORT NUMBER</b>	
<b>9. SPONSORING/MONITORING AGENCY NAME(S) AND ADDRESS(ES)</b>				<b>10. SPONSOR/MONITOR'S ACRONYM(S)</b>	
				<b>11. SPONSOR/MONITOR'S REPORT NUMBER(S)</b>	
<b>12. DISTRIBUTION/AVAILABILITY STATEMENT</b>					
<b>13. SUPPLEMENTARY NOTES</b>					
<b>14. ABSTRACT</b>					
<b>15. SUBJECT TERMS</b>					
<b>16. SECURITY CLASSIFICATION OF:</b>			<b>17. LIMITATION OF ABSTRACT</b>	<b>18. NUMBER OF PAGES</b>	<b>19a. NAME OF RESPONSIBLE PERSON</b>
<b>a. REPORT</b>	<b>b. ABSTRACT</b>	<b>c. THIS PAGE</b>			<b>19b. TELEPHONE NUMBER (Include area code)</b>

# Table of Contents

1.0 INTRODUCTION .....	1
1.1 BACKGROUND.....	1
1.2 OBJECTIVE OF THE DEMONSTRATION .....	3
1.3 REGULATORY DRIVERS.....	3
2.0 TECHNOLOGY .....	4
2.1 TECHNOLOGY DESCRIPTION.....	4
2.2 TECHNOLOGY DEVELOPMENT .....	7
2.2.1 Harwell TCH Project in Chalk.....	8
2.2.2 NASA Demonstration with Limestone.....	8
2.2.3 Confidential Site with Saprofite and Gneiss .....	8
2.3 ADVANTAGES AND LIMITATIONS OF THE TECHNOLOGY .....	9
2.4 MODELING TCH TECHNOLOGY .....	10
2.4.1 Screening Calculations to Evaluate the Cooling Effect of Groundwater Influx.....	10
2.4.2 Numerical Modeling of TCH Treatment in Bedrock.....	11
3.0 PERFORMANCE OBJECTIVES .....	13
3.1 DISCUSSION OF PERFORMANCE OBJECTIVES .....	15
3.1.1 Performance Objective: Faster Remediation .....	15
3.1.2 Performance Objective: Achieve Acceptable Concentrations .....	17
3.1.3 Performance Objective: Ease of Combining with Existing Operations.....	17
3.1.4 Performance Objective: Ease of Use/Operator Acceptance .....	17
3.1.5 Performance Objective: Achieve and Maintain Target Treatment Temperatures ..	18
3.1.6 Performance Objective: Reduce COC Mass in Rock Matrix .....	19
3.1.7 Performance Objective: Assess Magnitude and Impact of Cooling Due to Groundwater Flux through Treatment Volume .....	20
3.1.8 Performance Objective: Estimate Contaminant Mass in the Contaminated Zone while Quantifying Mass Recovered from Demonstration Area .....	21
3.1.9 Performance Objective: Estimate Hazardous Materials Generated.....	23
3.1.10 Performance Objective: Estimate Waste Generated.....	23
3.1.11 Performance Objective: Factors Affecting Performance .....	23
4.0 SITE DESCRIPTION .....	26
4.1 SITE LOCATION AND HISTORY .....	26
4.2 PRESENT OPERATIONS.....	28
4.3 SITE GEOLOGY .....	29
4.4 SITE HYDROGEOLOGY .....	34
4.5 CONTAMINANT DISTRIBUTION .....	35
5.0 TEST DESIGN AND OPERATIONAL CONDITIONS .....	38
5.1 DESIGN AND LAYOUT OF TECHNOLOGY COMPONENTS.....	38
5.1.1 TCH Well Installations .....	38
5.1.2 Vapor Handling/Treatment Equipment.....	42
5.1.3 System Controls .....	46
5.1.4 Electrical Distribution Equipment .....	46
5.2 BASELINE CHARACTERIZATION .....	46
5.3 TREATABILITY AND LABORATORY STUDY RESULTS .....	57
5.3.1 Treatability and Laboratory Heating Study .....	58

5.3.2	Treatability and Laboratory Study Results for NAWC Site Microbial Characterization.....	69
5.4	DESIGN AND LAYOUT OF TECHNOLOGY COMPONENTS.....	75
5.5	FIELD TESTING.....	75
5.6	SAMPLING METHODS.....	77
5.6.1	Bedrock Samples.....	78
5.6.2	Process Vapor Samples.....	82
5.6.3	Sampling Locations and Equipment.....	83
5.6.4	Field Screening.....	83
5.6.5	Summa Canister Sampling.....	84
5.6.6	Process Flow, Pressure and Temperature Measurements.....	84
5.6.7	Condensate Samples.....	84
5.6.8	Rock Temperature.....	85
5.6.9	Wellfield Vapor Samples.....	87
5.6.10	Ambient Air Samples.....	87
5.6.11	Groundwater Samples.....	87
5.6.12	Borehole Pressure Test.....	89
5.6.13	Microbial Parameters.....	91
5.6.14	Sample Identification and Labeling.....	91
5.6.15	Sample Handling, Packaging, and Shipping.....	92
5.7	SAMPLING RESULTS.....	92
5.7.1	TCE Mass Removal.....	92
5.7.2	Bedrock TCE Concentrations.....	96
5.7.3	Bedrock TCE Mass Estimates.....	105
5.8	WASTE GENERATED.....	106
5.8.1	Drill Cuttings.....	106
5.8.2	Sludge.....	106
5.8.3	Vapor Phase Carbon.....	106
5.8.4	Extracted Water.....	107
5.9	TCH SYSTEM SHUTDOWN.....	107
5.10	DECOMMISSIONING AND DEMOBILIZATION.....	107
6.0	PERFORMANCE ASSESSMENT.....	108
6.1	ASSESSING SITE PARAMETER'S IMPACT ON PERFORMANCE.....	108
6.1.1	Pre-Treatment Groundwater Sampling.....	108
6.1.2	Pre-Treatment Pressure Tests.....	110
6.1.3	Power Usage.....	113
6.1.4	Energy Injected and Extracted.....	115
6.1.5	Water and Air Balances.....	117
6.1.6	Temperatures during Operation and Cool-Down.....	122
6.1.7	Wellfield Vapor Samples.....	128
6.1.8	Numerical Modeling of TCE Pilot Test.....	130
7.0	COST ASSESSMENT.....	131
7.1	COST MODEL.....	131
7.1.1	Interpretation of Costs and Scale.....	134
7.2	COST DRIVERS.....	134
8.0	IMPLEMENTATION ISSUES.....	141

8.1 GUIDELINES TO PRACTITIONERS.....	142
9.0 REFERENCES .....	145

## Appendices

- Appendix A: Points of Contact
- Appendix B: Modeling Results
- Appendix C: Lab Treatability Results
- Appendix D: Temperature Profiles
- Appendix E: Decontamination and Calibration

## List of Figures

- Figure 2.1. Proprietary TerraTherm Heater Element
- Figure 2.2. Sketch of TCH Implementation
- Figure 2.3. TCH system installed at NAWC Site
- Figure 3.1. Average Temperatures at Different Depths during Heating Operations
- Figure 3.2. Temperature at T1 during Heating Operations
- Figure 3.3. Temperature at T1 during Cool-Down
- Figure 3.4. Vapor Stream VOC Concentrations for the Dominant Compounds
- Figure 3.5. Liquid Stream VOC Concentrations for the Dominant Compounds
- Figure 3.6. Cumulative Water Removed during Treatment
- Figure 3.7. Water Removal Rate during Treatment
- Figure 4.1. Map showing TCE Concentration Contours in Groundwater and the Approximate Location of Field Demonstration Area
- Figure 4.2. Aerial View Showing the Approximate Location of Field Demonstration's Process Treatment Equipment, Electrical Equipment, and Heater Wellfield
- Figure 4.3. Geologic Map Showing Locations of Subcrops of Selected Strata around the TCH Demonstration Site and the Location of Sections A-A' and B-B', NAWC, Trenton, NJ
- Figure 4.4. Geologic Column of the TCH Demonstration Site, NAWC, Trenton, NJ
- Figure 4.5. Section A-A' Showing Geologic and Natural Gamma Geophysical Strata for the TCH Demonstration Site (red box) and USGS/SERDP Research Site (orange box), NAWC, Trenton, NJ
- Figure 4.6. Geologic Section B-B' of the TCH Demonstration Site Showing Strata, Weathered and Competent Bedrock, and Natural Gamma Geophysical Logs from 3 of 23 Boreholes, NAWC, Trenton, NJ
- Figure 4.7. TCE Concentrations in Water Samples from Hydraulically Active Fractures (A) near Land Surface and (B) at 100 Feet below Land Surface, NAWC, Trenton, NJ
- Figure 4.8. Section G-G' Showing the Local Geology and Concentrations (micrograms per liter) of Aqueous Phase TCE in Hydraulically Active Fractures, NAWC, Trenton, NJ
- Figure 4.9. Graphs Showing Concentrations of Aqueous Phase TCE, cis-DCE, and Vinyl Chloride in Water Samples from Hydraulically Active Fractures Wells (A) 07BR and (B) 24BR, NAWC, Trenton, NJ
- Figure 5.1. TCH Heater Boring with Co-Located Vacuum Extraction Point
- Figure 5.2. Temperature Monitoring Point
- Figure 5.3. Completed TCH Field Demonstration Well Installation
- Figure 5.4. Conceptual Process Flow Diagram for Treatment System

- Figure 5.5. Aerial View of Completed Process Treatment System
- Figure 5.6. Correlation of Natural Gamma Logs for 15 HO Wells, Relative Gamma Counts Range from 50 to 200 Counts per Second, TCH Demonstration Site, NAWC, Trenton, NJ
- Figure 5.7. Water-Level Hydrographs for Wells MW-07BR and MW-24BR Showing TCH Drilling and Heating Periods, NAWC, Trenton, NJ, October 2008 to September 2009
- Figure 5.8. Water-Level Hydrographs for Wells 15BR and 4BR and TCH Drilling and Heating Periods, NAWC, Trenton, NJ, October 2008 to September 2009
- Figure 5.9. Water-Level Hydrographs for Wells 68BR-A and 68BR-F and TCH Drilling and Heating Periods, NAWC, Trenton, NJ, October 2008 to September 2009
- Figure 5.10. Water-Level Hydrographs for Wells 70BR-10 and 70BR-72, and TCH Drilling and Heating Periods, NAWC, Trenton, NJ, October 2008 to September 2009
- Figure 5.11. Water-Level Hydrographs for Wells 71BR-A, 71BR-B, 71BR-C, and TCH Drilling and Heating Periods, NAWC, Trenton, NJ, October 2008 to September 2009
- Figure 5.12. Water-Level Hydrographs for Wells 71BR-D, and 71BR-E, and TCH Drilling and Heating Periods, NAWC, Trenton, NJ, October 2008 to September 2009
- Figure 5.13. Water-Level Hydrographs for Wells 73BR-A, 73BR-BC, 73BR-E, and TCH Drilling and Heating Periods, NAWC, Trenton, NJ, October 2008 to September 2009
- Figure 5.14. Water-Level Hydrographs for Wells BRP1 and 47BR and TCH Drilling and Heating Periods, NAWC, Trenton, NJ, October 2008 to September 2009
- Figure 5.15. Summary of Disc Samples Used for Each Rock Type in Heating Experiments
- Figure 5.16. Heating Temperature Profile Illustrating the Six Temperature Points at which Rock Discs Were Removed from the Convection Oven during Heating Tests
- Figure 5.17. Heating Duration Profile Illustrating the Six Temperature Points at which Rock Discs Were Removed from the Convection Oven during Heating Tests
- Figure 5.18. Normalized TCE Concentration versus Temperature Point in Heating Temperature Profile Tests
- Figure 5.19. Normalized PCE Concentration versus Temperature Point in Heating Temperature Profile Tests
- Figure 5.20. Normalized TCE Concentration versus Temperature Point in Heating Duration Profile Tests
- Figure 5.21. Normalized PCE Concentration versus Temperature Point in Heating Duration Profile Tests
- Figure 5.22. Principal Component Analysis (PCA) of the Results of the Heating Tests on Different Rock Types, and the Results of the Porosity and Fraction Organic Carbon Analysis
- Figure 5.23. Concentrations of Cells before, during and after Thermal Heating
- Figure 5.24. Results of CO<sub>2</sub> Production Assays pre- and post-Thermal Heating
- Figure 5.25. TCH Field Demonstration Schedule
- Figure 5.26. Drill Rig on Vapor Cap during Post-Treatment Bedrock Sampling
- Figure 5.27. Core Barrels Containing Hot Bedrock Being Cooled Before Rock Sampling
- Figure 5.28. Cutting and Methanol Preservation of the Cores
- Figure 5.29. Pre-Treatment Rock Cores
- Figure 5.30. Location of Temperature Monitoring Points in the Wellfield

- Figure 5.31. Location of Pre-Treatment Groundwater Sampling Locations
- Figure 5.32. Packer, Pressure Tank and Water Meter Used During the Borehole Pressure Test
- Figure 5.33. PID Readings on Vapor Stream Samples and Associated Mass Removal Estimate
- Figure 5.34. Estimated VOC Mass Removal Rate during Operations
- Figure 5.35. Vapor Stream VOC Concentrations for the Dominant Compounds
- Figure 5.36. Liquid Stream VOC Concentrations for the Dominant Compounds
- Figure 5.37. Pre- and Post-Treatment Rock Concentration Sampling Locations
- Figure 5.38. Pre- and Post-Treatment TCE Rock Matrix and Fracture Concentrations at Sampling Location BR1/BRP1
- Figure 5.39. Pre- and Post-Treatment TCE Rock Matrix and Fracture Concentrations at Sampling Location BR2/BRP2
- Figure 5.40. Pre- and Post-Treatment TCE Rock Matrix and Fracture Concentrations at Sampling Location BR3/BRP3
- Figure 5.41. Location and Size of Fractures for BR1 Based on Borehole Generally Representing Inspections in One Foot Increments
- Figure 5.42. Screenshot from the Video Borehole Logging Showing a Category 0 (picture at left) and a Category 4 (picture at right) Fracture
- Figure 5.43. Vertical Pre- and Post-Treatment Concentration Profile from BR1/BRP1 Indicating Samples Close to a Category 3 and 4 Fracture (red circles)
- Figure 5.44. Pre- and Post-Treatment TCE Rock Matrix Concentrations at Sampling Location BR1/BRP1
- Figure 6.1. Pre-Treatment VOC Groundwater Concentration in HO-8
- Figure 6.2. Pre-Treatment VOC Groundwater Concentration in HO-12
- Figure 6.3. Pre-Treatment VOC Groundwater Concentration in HO-13
- Figure 6.4. Calculated Average Hydraulic Conductivity with Depth Based on the Pressure Tests
- Figure 6.5. Cumulative Power Usage during Treatment
- Figure 6.6. Estimated Power Usage Rate during Treatment
- Figure 6.7. Cumulative Energy Balance
- Figure 6.8. Energy Injection and Extraction Rates during Treatment
- Figure 6.9. Cumulative Water Removed during Treatment
- Figure 6.10. Water Removal Rate during Treatment
- Figure 6.11. Cumulative Vapor Removal during Treatment
- Figure 6.12. Thermocouple Temperature Readings ( F) at Temperature over the Duration of Operations
- Figure 6.13. Thermocouple Temperature Readings ( F) at Temperature over the Duration of Operations
- Figure 6.14. Thermocouple Temperature Readings ( F) at Temperature over the Duration of Operations
- Figure 6.15. Thermocouple Temperature Readings ( F) at Temperature over the Duration of Operations ng Wall Temperature Monitoring
- Figure 6.16. Thermocouple Temperature Readings ( F) at Temperature over the Duration of Operations
- Figure 6.17. Thermocouple Temperature Readings ( F) at Temperature over the Duration of Operations
- Figure 6.18. Thermocouple Temperature Readings ( F) at Temperature over the Duration of Operations

- Figure 6.19. Thermocouple Temperature Readings ( □F) at Temperature over the Duration of Operations
- Figure 6.20. Average Temperatures at Different Depths during Heating Operations
- Figure 6.21. Temperature at T1 during Heating Operations
- Figure 6.22. Temperature at T1 during Cool-Down
- Figure 6.23. PID Readings at Vapor Extraction Points HO1 through HO8
- Figure 6.24. PID Readings at Vapor Extraction Points HO9 through HO15
- Figure 7.1. Project Duration by Task for Small Project Implementation
- Figure 7.2. Project Duration by Task for Medium Project Implementation
- Figure 7.3. Project Duration by Task for Large Project Implementation

## List of Tables

- Table 3.1. Performance Objectives
- Table 5.1. Average Rock Property Values Obtained from the Rock Properties Analysis in Triplicate of the Seven Types of Rock Utilized during Heating Experiments
- Table 5.2. Summary of Initial Concentration ( $C_0$ ) in Each Rock Type
- Table 5.3. Average Contaminant Mass Removal Attained at the Last Three Temperature Points of the Heating Tests for All Rock Types
- Table 5.4. Average Contaminant Mass Removal Attained at the Last Three Temperature Points of the Heating Tests for All Rock Types Excluding Black Mudstone
- Table 5.5. Non-Parametric Analysis (P-values) on the Results of the Heating Temperature Profile and Heating Duration Profile Tests at the Last Three Stages of Heating
- Table 5.6. Background Characterization of Bacteria at the NAWC Site
- Table 5.7. Cell Counts in Groundwater Samples Collected Prior to Thermal Treatment (2-11-2009)
- Table 5.8. Cell Counts in Groundwater Samples Collected during Thermal Treatment (5-29-2009)
- Table 5.9. Cell Counts in Groundwater Samples Collected after Thermal Treatment (8-21-2009)
- Table 5.10. Cell Counts in Groundwater Samples Collected after Thermal Treatment (11-4-5-2009)
- Table 5.11. Bedrock Samples Collected Pre- and Post-Treatment
- Table 5.12. Process Vapor Samples Collected during Treatment
- Table 5.13. Process Flow, Pressure and Temperature Measurements Collected during Treatment
- Table 5.14. Condensate Samples Collected during Treatment
- Table 5.15. Temperatures Collected during Treatment
- Table 5.16. Depth, Number of Sensors and Location of the Temperature Monitoring Wells
- Table 5.17. Wellfield Vapor Samples Collected during Treatment
- Table 5.18. Approximate Sample Depth for Pre-Treatment Groundwater Samples
- Table 5.19. Groundwater Samples Collected Pre-Treatment
- Table 5.20. Pre-Treatment Pressure Tests
- Table 5.21. Number of Pre- and Post-Treatment Sampling Locations
- Table 5.22. Pre- and Post-Treatment TCE Rock Concentrations
- Table 5.23. Pre- and Post-Treatment TCE Rock Matrix Concentrations
- Table 5.24. Pre- and Post-Treatment TCE Mass
- Table 6.1. Pre- and Post-Treatment TCE Mass
- Table 6.2. Pressure Test Results for BR2

Table 6.3. Pressure Test Results for BR1

Table 6.4. Comparison of Starting Volume of Water in TTZ with Volume Removed During Treatment

Table 7.1. Comparison of Starting Volume of Water in TTZ with Volume Removed During Treatment

Table 7.2. Volume and Heat Capacity Design Input Parameters

Table 7.3. Energy Balance Design Input Parameters

Table 7.4. Total Operational Duration

Table 7.5. Total Number of Wells

Table 7.6. Implementation Costs for Small, Medium and Large Volume TCH Projects

## List of Acronyms

A	Ampere
AFCEE	Air Force Center for Engineering and the Environment
ATS	Automatic Transfer Switch
AWG	American Wire Gauge
bgs	Below ground surface
BTU/hr	British Thermal Units per hour
C	Celsius
cis-DCE	cis-Dichloroethene
cm/s	centimeters per second
CO <sub>2</sub>	Carbon Dioxide
COC	Contaminant of concern
cu ft	cubic feet
cu yd	cubic yard
CVOCs	Chlorinated Volatile Organic Compound
DEM/VAL	Demonstration and Validation
DNAPL	Dense Non Aqueous Phase Liquid
DoD	Department of Defense
EPA	Environmental Protection Agency
ERH	Electrical Resistance Heating
ESTCP	Environmental Security Technology Certification Program
eV	Electron Volt
F	Fahrenheit
F.L.A.	Full Load Amperes
ft	Feet
FY	Fiscal Year
GAC	Granular Activated Carbon
Gal	Gallons
GJ	Gigajoules
gpm	Gallons per minute
GWP	Global Warming Potential
HASP	Health and Safety Plan
Hg	Mercury
Hz	Hertz
ISTD	In Situ Thermal Desorption
kW	Kilowatt
kWh	kilowatt-hour
kWh/cy	kilowatt-hour per cubic yard
lbs	Pounds
LCA	Life Cycle Assessment

LED	Light Emitting Diode
M	Million
m	meters
MCL	Maximum Contaminant Level
mg/kg	milligrams per kilogram
MNA	Monitored Natural Attenuation
MS/MSD	Matrix spike and Matrix Spike Duplicate
MSFC	Marshall Space Flight Center
N.J.A.C.	New Jersey Administration Code
NAPL	Non Aqueous Phase Liquid
NASA	National Aeronautics and Space Agency
NAVFAC ESC	Naval Facilities Engineering Service Center
NAWC	Naval Air Warfare Center
NEC	National Electrical Code
NEMA	National Electrical Manufacturers Association
NFESC	Naval Facilities Engineering Service Center
Nox	Nitrogen Oxides
NRC	National Research Council
OSHA	Occupational Safety and Health Administration
P&T	Pump and Treat
PAH	Polycyclic Aromatic Hydrocarbon
PCA	Principal component analysis
PCB	Polychlorinated Biphenyl
PCE	Perchloroethene
PE	Person Equivalent
PEL	Permissible Exposure Limit
PFD	Process Flow Diagram
PID	Photoionization Detector
PLC	Programmable Logic Controller
POC	Points of Contact
ppb	Parts per billion
ppmv	parts per million by volume
psig	Pounds per square inch gauge
QA	Quality Assurance
QC	Quality Control
R&D	Research and Development
RemS	Remediation Strategy for Soil and Groundwater Pollution Tool
RPM	Remedial Project Manager
SCFM	Standard cubic feet per minute
SCR	Silicon Controlled Rectifier

SERDP	Strategic Environmental Research and Development Program
Shell E&P	Shell Exploration and Production
Sox	Sulfur Oxides
SRT	Sustainable Remediation Tool
SVE	Soil Vapor Extraction
SVOC	Semi-Volatile Organic Compounds
TCA	Trichloroethane
TCE	Trichloroethene
TCH	Thermal Conductive Heating
TCs	Thermocouples
TDH	Total Dynamic Head
TESI	TerraTherm Environmental Services
TI	Technical Impracticability
TMP	Temperature Monitoring Points
TTZ	Target Treatment Zone
UCL	Upper Concentration Limit
UK	United Kingdom
UKAEA	United Kingdom Atomic Energy Authority
um	micrometer
U.S.	United States of America
USEPA	United States Environmental Protection Agency
USGS	United States Geological Survey
UT	University of Texas at Austin
VAC	Voltage in Alternating Current
VC	Vinyl Chloride
VOA	Volatile Organic Analysis
VOC	Volatile Organic Compounds
W	Width
wt	Water Temperature

## **Acknowledgements**

The project team consisted of the following organizations (details regarding these points of contact are provided in Appendix A):

- NAVFAC Engineering Service Center (NAVFAC ESC): Carmen A. Lebrón
- TerraTherm, Inc.: Gorm Heron, John LaChance, David Brogan, Steffen Griepke Nielsen, and Devon Phelan
- Queen's University: Dr. Bernie Kueper, David Rodriguez, Ashley Wemp, and Daniel Baston
- U.S. Geological Survey: Pierre Lacombe, Dr. Frank Chapelle, Daniel Goode and Claire Tiedeman.

The team greatly appreciates the support of the organizations and individuals that assisted in this endeavor, and through which the successful on-site execution and generation of the Final Report was possible. We would like to thank NAVFAC BRAC PMO North East, ECOR Solutions and the U.S. Geological Survey who contributed to the implementation of the field demonstration. Specifically:

- Robert Lewandowski (now retired), Brian Helland and Jeffrey Dale (BRAC PMO NE);
- Patrick Schauble, Matt Lapp, William Torres and Ed King (ECOR Solutions);
- Donna Gaffigan and Bill Hanrahan (NJDEP);
- Kathy Davies (EPA); and
- Claire Tiedeman, Daniel J. Goode and Pierre Lacombe without whom executing the on-site demonstration would have been impossible.

We would also like to thank the U.S. Navy and the parcel owners and their representatives for their support.

## Executive Summary

The removal of Dense, Non-Aqueous Phase Liquids (DNAPLs) and associated dissolved phase compounds is challenging in fractured rock given permeability, matrix diffusion, and fracture connectivity issues. In fact, in 2005, the National Research Council concluded, that: *“Most of the technologies [used to treat DNAPLs] are not applicable in fractured materials”* (NRC, 2005). Yet, despite the fact that there have been no reported cases of DNAPL sites where remediation has achieved drinking water standards, there is still regulatory pressure to achieve strict remedial goals and absolute objectives at DNAPL sites (NRC, 2005).

Furthermore, the same NRC panel concluded that *“There is no experience with conductive heating in saturated fractured media or karst. As control of water inflow may be problematic in fractured media and karst, and capture of contaminants may be difficult, effectiveness is expected to be limited in these settings”* (NRC, 2005). Hence, ESTCP project ER0715 was carried out in such context and results from the project have improved our understanding both in terms of what is achievable, and in terms of the technical challenges presented regarding the application of thermal heating in fractured bedrock.

TCH was selected for the demonstration as it is the only existing thermal approach that can reach temperatures in excess of 100°C (boiling) between heater borings installed into intact bedrock, and it is the only thermal technology that can effectively heat all types of rock matrix including, igneous, metamorphic and sedimentary bedrocks. TCH has the potential to reduce the challenges presented by fractured bedrock because it can directly heat the bedrock matrix. It is expected that potential limitations include the fact that it may be difficult to convey fluids through a low permeability matrix, which in turn results in higher boiling points. The site selected for the demonstration was the NAWC in Trenton, NJ.

The former NAWC is within the Newark Basin geologic province and is underlain by mudstone of the Skunk Hollow, Byram, and Ewing Creek Members of the Lockatong Formation (Lacombe, 2010). The conceptual model for the site is that TCE mass is held tightly in the rock matrix, and potentially in some of the fractures at the site. The TCE has dissolved, diffused, and adsorbed to the rock matrix (silt and mudstones). The CVOC plume in the field demonstration area consists of TCE and its degradation products cDCE and VC. Water samples from wells 07BR and 24BR, located less than 50 ft from the TCH field demonstration site, have exhibited TCE concentrations that ranged from 5,000 to 60,000 ug/L during the past 3 years. cDCE concentrations have ranged from 10,000 to 25,000 ug/L, and VC concentrations have ranged from 500 to 2,000 ug/L. At present, the major CVOC contamination plume is 75 to 125 ft bgs.

The DEM/VAL objectives for the on-site TCH demonstration were to:

- a) Demonstrate the feasibility of TCH to heat the target volume of rock and water to steam distillation temperatures and the boiling point of water via energy applied to vertical TCH borings. This included evaluating the cooling influence of inflowing groundwater.
- b) Validate the degree of heating to temperatures above boiling (100°C) at different distances from the heater borings. This included validating whether the temperatures recommended for effective treatment in this particular geology (derived from the laboratory work) were achieved.

- c) Demonstrate capture of steam and other fluids from the heated boreholes such that vaporized and mobilized contaminants are extracted from the available fractures.
- d) Show that the surface equipment meets regulatory demands for contaminant reduction efficiency and emissions.
- e) Collect detailed temperature data to support numerical simulations of the heating and effect on remediation progress.
- f) Collect rock chip samples to demonstrate temporal changes in contaminant concentrations within the pilot test volume as a function of the TCH application.
- g) Collect microbial characterization data to evaluate the effect of the heating process on the potential for natural attenuation or enhanced bioremediation at the site.

The overall project management approach that was adopted included:

- 1) Treatability studies to ascertain a treatment strategy (duration and temperature) for several rock types,
- 2) Modeling to perform screening calculations and carry out mass estimates; and,
- 3) Application of TCH at a fractured bedrock site.

The focus of the treatability study was to assess removal rates and establish necessary treatment temperatures and duration in the field. The focus of the field demonstration was to validate the heating strategy, achievable heating rates and fluid control, as well as matrix heating and desaturation. In addition, a microbial characterization was conducted before and after TCH field application, with the purpose of investigating changes in the microbial population as a result of the elevated temperatures.

Accordingly, results are summarized below:

***Modeling Results:***

Numerical modeling was carried out as part of this project to evaluate the influence of inflowing cold groundwater on the ability to heat fractured rock, and to evaluate the influence of various rock properties on the ability to achieve boiling in the rock matrix using TCH.

The results of this modeling indicate that careful attention should be given to groundwater influx into a target treatment zone in order to determine whether the boiling of water can be achieved, and the length of heating time required to reach boiling. Calculating the groundwater influx at a fractured rock site is typically carried out using measurements of bulk rock hydraulic conductivity and hydraulic gradient. Given the likely variability of flow rate amongst individual fractures in a treatment zone (flow proportional to fracture aperture cubed), however, more accurate assessment of the influence of inflowing cold groundwater can be determined on the basis of knowledge of individual fracture apertures and fracture spacing. Groundwater influx may prevent or delay the heating of fractured rock during application of TCH. When bulk groundwater influx is high, temperatures in the fractures are influenced by the aperture and spacing of fractures. For medium and low values of influx, fracture properties do not appear to be as important in determining the temperature in fractures. In these cases, it appears not to be important to characterize discrete fracture features in the treatment zone; only a quantification of the total groundwater influx through the treatment zone is necessary.

The performance of TCH in fractured rock environments is expected to be strongly dependent on the hydraulic properties of the rock matrix (permeability, porosity) and the aperture and spacing of fractures. If complete removal of all liquid water is the goal of thermal treatment, treatment time will be strongly governed by the magnitude of the pressure spike that occurs in the rock matrix during heating. When the rock matrix has a low permeability, high porosity, or sparse fracturing, this pressure rise may be enough to significantly raise the boiling point of water in the matrix, thus delaying treatment. Because a clear temperature plateau may not be observed in the matrix during boiling, it may be difficult to determine if boiling has occurred throughout a treatment area from temperature measurements alone.

Modeling results also showed that variations in material properties (rock density, rock thermal conductivity, and rock heat capacity) amongst rock types do have a small effect on the early-time temperature distribution in the rock, but on the whole are less significant than variations in hydrogeological parameters (hydraulic gradient, fracture aperture, and fracture spacing). It is noted that the range of variation in material properties is much smaller than the range of hydrogeological properties, which may vary by several orders of magnitude. This stresses the need for proper site characterization.

Low matrix permeability, high matrix porosity, and wide fracture spacing can contribute to boiling point elevation in the rock matrix. Consequently, knowledge of these properties is important for the estimation of treatment times. Because of the variability in boiling point throughout a fractured rock treatment zone and the absence of a well-defined constant temperature boiling plateau in the rock matrix, it may be difficult to monitor the progress of thermal treatment using temperature measurements alone. This is particularly relevant in low matrix permeability rock where thermal expansion of groundwater leads to pressure increases which in turn result in elevated boiling points for water. Due to the importance of fracture spacing in determining the pressure rise in the matrix, a discrete fracture model is more appropriate than an equivalent porous medium model for simulating boiling in this context.

Furthermore, semi-analytical transient solutions were developed as part of the project to evaluate what level of fractured porous media (e.g., bedrock or clay) matrix clean-up must be achieved in order to achieve compliance of fracture pore water concentrations within a specified time at specified locations of interest. The developed mathematical solutions accounted for forward and back diffusion in a fractured porous medium where the initial condition comprises a spatially uniform, non-zero matrix concentration throughout the domain. Illustrative simulations incorporating the properties of mudstone fractured bedrock demonstrate that the time required to reach a desired fracture pore water concentration is a function of the distance between the point of compliance and the upgradient face of the domain where clean groundwater is inflowing. Shorter distances correspond to reduced times required to reach compliance, implying that shorter treatment zones will respond more favorably to remediation than longer treatment zones in which back-diffusion dominates the fracture pore water response. For a specified matrix clean-up goal, compliance of fracture pore water concentrations will be reached sooner for decreased fracture spacing, increased fracture aperture, higher matrix fraction organic carbon, lower matrix porosity, shorter aqueous phase decay half-life, and a higher hydraulic gradient. The parameters dominating the response of the system can be measured using standard field and laboratory techniques.

### ***Laboratory Treatability Studies Results:***

Laboratory studies conducted in support of this project included:

- a) Bench scale evaluations to identify optimum temperatures (*temperature profile* testing) and duration (*duration profile* testing) on different types of rock: three (3) types of mudstone (found at the NAWC site), siltstone, limestone, sandstone and dolostone.
- b) Microbial enumeration both before and after heating to determine the effect of the heating on on-site microflora and if that effect was temporary.

The seven (7) rock types were employed to assess the relationships between temperature, heating duration and degree of contaminant mass removal. Core samples of each rock type were cut to provide 40 discs (total of 280 discs) measuring 1 cm in thickness and 5 cm in diameter. A total of 28 discs were retained for heating experiments involving trichloroethylene (TCE) and tetrachloroethylene (PCE) for each of the 7 rock types, while 12 discs were retained for physical characterization measurements (Figure 5.15) for each of the 7 rock types.

Results indicate that heating duration had a greater effect on the degree of TCE and PCE mass removal compared to heating temperature. In heating *duration profile* tests the majority of contaminant mass removal was achieved in the early stages of heating. In samples of sandstone, dolostone, limestone and siltstone further heating did not lead to a significant decrease in contaminant concentration. Heating *temperature profile* tests required final target temperatures of 200°C to remove the majority of the contaminant mass. In thermal field applications, extending treatment duration under standard operational temperatures beyond the boiling point of water would, therefore, be more effective than elevating temperatures above the boiling point of water. The removal of TCE and PCE from the rock matrix by heating was not found to be sensitive to the chemical properties of the compounds.

Rock properties had a significant effect on contaminant mass removal during heating experiments. It was determined that the rock properties observed in samples of sandstone and dolostone, such as high porosity and low fraction organic carbon, contributed to the increase in contaminant mass removal during the heating tests. In field applications, fractured bedrock with higher porosities and lower fraction organic carbon would favor the performance and effectiveness of thermal treatment in the removal of TCE and PCE.

PCA analysis revealed that porosity favored the degree of contaminant mass removal from the rock matrix. In contrast, fraction organic carbon had a negative effect on the contaminant mass removal. Samples of sandstone and dolostone with a combination of higher porosity and lower fraction organic carbon exhibited higher degrees of contaminant mass removal. Samples of gray mudstone, limestone, red mudstone and siltstone had similar porosities and fraction organic carbon. The latter indicates that in a field application, such types of rock could present a similar contaminant mass removal under heat treatment at similar conditions. Finally, with a combination of lower porosity and higher fraction organic carbon, black mudstone (found at the NAWC site) exhibited the lowest degree of contaminant mass removal.

### ***Field Demonstration Results:***

TCH operations ran continuously for 106 days, 24 hours per day, 7 days per week without any major shutdowns other than shutdowns for scheduled maintenance and minor equipment replacement and GAC change-outs. The heating period lasted a total of 97 days, while the

extraction system operated for 106 days. This included 6 days of startup, 97 days of operation and 3 days of cool down.

During the course of the TCH demonstration, data was collected and compiled to monitor the performance of the TCH system. These data include energy expenditures for the target treatment zone (TTZ) and volumes for water and air removed from the subsurface. Furthermore, an energy balance was set up and maintained during operation to keep track of energy injected and extracted from the TTZ on a daily basis. The energy balance was used to optimize the thermal treatment.

A sampling and analysis program was implemented to provide the data required for evaluation of the TCH system effectiveness on the impacted bedrock and groundwater at the site, and to provide sufficient data for applying the technology to other sites in the future. To achieve these project objectives, the sampling and analysis program implemented the following activities:

- Collection of samples of the bedrock within the TTZ for quality analysis before and after treatment;
- Collection of samples of process vapor generated during operation of the TCH system to evaluate mass removal of COCs;
- Collection of process flow, pressures and process temperature data to ensure that the process treatment system was running properly and to gain data needed to evaluate the mass removal of COCs;
- Collection of samples of condensate generated during operation of the TCH system to evaluate mass removal of COCs;
- Collection of detailed temperature data during the project to support numerical simulations of the heating and its effect on remediation progress;
- Collection of rock samples for analysis of physical attributes before and after treatment;
- Collection of groundwater samples from bedrock borings within the TTZ before treatment; and,
- Monitoring of the ambient air quality to confirm that project-specific HASP criteria were not exceeded during construction or operation of the TCH system.

Bedrock samples were collected from borings within the TTZ in order to evaluate TCH performance both before and after treatment. Three boreholes were cored prior to treatment in order to collect the rock samples and establish baseline conditions. Three boreholes were also cored after treatment in order to collect a similar set of rock samples. The pre- and post-treatment core locations were located approximately 2-3 feet apart to ensure that the post-treatment cores would not intersect fractures that had been filled with grout from the pre-treatment coring activities.

Results from the bedrock samples indicate that the average reduction in TCE concentrations was 41-69%. However, careful examination of selected points in the rock matrix revealed that the rock matrix did not achieve targeted temperature in all locations (due mostly to contaminated groundwater influx thru existing fractures). Since discrete sampling was done at 5 feet intervals, it was possible to identify at which depth there was incomplete heating and correlate that with observed fractures from a video log of the boreholes. If we eliminate from the performance data the points where boiling water temperature was not achieved due to cool water influx, the average reduction was higher at 94.5%. The 94.5% COC mass removal rate is consistent with

others findings. For example, in a literature survey conducted by NAVFAC ESC and Geosyntec Consultants under ESTCP project ER0424, thermal technologies typically achieved levels of DNAPL mass removal ranging between 94% to 96% (Lebron, et al. 2011). McGuire and others also reported in 2005 that thermal treatment exhibited a median parent reduction of 95% or greater.

The data also shows that most rock concentrations were lowered to around 0-5 mg/kg, but that higher concentrations were maintained at distinct depth intervals. These depths correlated reasonably well with the depth showing the highest TCE concentrations prior to heating. A total (vapor and liquid) of approximately 530 lbs based on daily PID readings and approximately 680 lbs based on analytical data of TCE was extracted from the site.

The more or less consistent level of VOCs in the vapor stream during the last two months of heating indicates that VOCs are entering from outside the TTZ and supplying additional mass to the treatment area. As cold, contaminated water flows towards the heaters, the groundwater is heated by thermal conduction from the matrix, and while some of the VOCs are vaporized, the fracture zones remain cooler than the larger matrix blocks.

It is noteworthy that the VC concentration remained significant in the entire operations period. Since VC is the most volatile VOC at most sites, it is normally removed within the first month of heating. The persistent level of VC in the vapor stream indicates that groundwater flowing into the TTZ was providing a constant source of contaminant mass entering the TTZ.

System performance was likely impacted by groundwater flow (both regional and induced by the vapor extraction system) which is likely responsible for the cooling that led to ineffective TCE remediation. In addition, the flow of contaminated water into the TTZ continuously supplied TCE and other VOCs to the field demonstration area. This finding is consistent with NRC findings in 2005, i.e., *“There is limited field experience applying conductive heating below the water table... As control of water inflow may be problematic in fractured media and karst, and capture of contaminants may be difficult, effectiveness is expected to be limited in these settings. If water inflow can be limited, then conductive heating would be expected to be effective in all granular media.”* Furthermore, Kingston, et al. reported in 2009 that *“Better performance might be achieved if system footprints are over-designed to extend beyond the source zone boundaries.”*

The relatively smooth temperature profiles during cool-down indicate that regional groundwater flow may not have dominated the cooling. The high groundwater extraction rates observed during the thermal treatment are hypothesized to have been caused by liquid entrainment within the extracted steam. These rates were quickly reduced during cooling, as no more steam was flowing out of the vapor extraction points. In fact, it is believed that the induced flow of cool groundwater into the demonstration volume through the dominant fractures was the result of the design of the vacuum extraction system.

The results of a microbial presence treatability tests demonstrated that, as expected, heating groundwater to approximately 200°F resulted in sterilization. However, the results also indicated that the aquifer was rapidly reseeded with microorganisms, and that both numbers of microorganisms and microbial activity in groundwater just four months after thermal treatment were actually greater than prior to treatment. These results show that, while thermal treatment does decrease both numbers and activity of microorganisms in the short term, the aquifer quickly regained its ability to support microbial populations as well as microbial activity.

Based on the laboratory studies, modeling and on-site field demonstration several guidelines are offered to practitioners. The guidelines can be found in Section 8 of the report and include:

- Careful attention should be given to groundwater influx into a target treatment zone in order to determine whether the boiling of water can be achieved, and the length of heating time required to achieve boiling.
- System design must take into account the induced flow of cool groundwater into the treatment volume through the dominant fractures as a result of the vacuum extraction system.
- Because of the variability in boiling point throughout a fractured rock treatment zone and the absence of a well-defined constant temperature boiling plateau in the rock matrix, it may be difficult to monitor the progress of thermal treatment using temperature measurements alone.
- A site manager must consider impacts of drilling techniques on the potential for water influx and a system design should include contingencies to limit or mitigate groundwater influx if cooling is detected. The high vibrations created during sonic drilling in this case may have induced fractures in the field demonstration area and increased the hydraulic conductivity of the bedrock.
- Use of larger-diameter vapor extraction points (so that the steam can bubble through the standing water without pushing it out) should be considered.
- Regional groundwater flow cooling can possibly be reduced using a hydraulic barrier such as a freeze-wall or a grout curtain.
- Practitioners should consider longer treatment and/or higher temperatures to remove contaminants from difficult regions.
- Hydraulic conductivity measurements should be taken at relatively small scales to assess individual strata or rock types. Further, as much as possible, fractures should be characterized as well as possible.
- The impacts of different rock types present in the contaminated zone should be understood.

## 1.0 INTRODUCTION

### 1.1 BACKGROUND

The removal of Dense, Non-Aqueous Phase Liquids (DNAPLs) and associated dissolved phase compounds is challenging in fractured rock given permeability, matrix diffusion, and fracture connectivity issues. In fact, in 2005, the National Research Council concluded, that: *“Most of the technologies [used to treat DNAPLs] are not applicable in fractured materials”* (NRC, 2005). Yet, despite the fact that there have been no reported cases of DNAPL sites where remediation has achieved drinking water standards, there’s still regulatory pressure to achieve strict remedial goals and absolute objectives at DNAPL sites (NRC, 2005).

The common perception is that bedrock sites are few in number, therefore research and development (R&D) efforts addressing their remediation will yield a low return. Furthermore, in years past, regulatory agencies recognized the remedial challenges that fractured bedrock sites represented and as a result, fractured bedrock site owners were at times able to obtain Technical Impracticability (TI) waivers without much difficulty. However, as new aggressive remedial technologies emerge, regulatory agencies have adopted a more conservative approach to minimizing health risks and TI waivers have become more difficult to obtain. In many cases, site owners find themselves spending millions of dollars while developing a site conceptual model that would support their strategy for a TI waiver whereas the same financial investment directed to remediation could have lowered health risks considerably.

Fractured bedrock sites, although perhaps not the norm, are still quite abundant. In a survey conducted by the Navy and Geosyntec Consultants, 29% of the 118 cases evaluated were fractured media sites (NFESC, Geosyntec, 2004). Fractured rock settings offer rather unique challenges, however, resulting in consumption of a much larger ratio of U.S. Department of Defense (DoD) financial resources. In fractured rock settings, unique challenges arise from the difficulty of characterizing the fracture and flow patterns, and the diffusion of contaminants into the rock matrix, where fluid flow is negligible.

Unless treatment removes mass from the matrix, back-diffusion of contaminants can continue for hundreds of years following removal of DNAPL from the open fractures. Therefore, a successful fractured rock remediation technology must target contaminants in both the open fractures and the porous rock matrix.

In August 2001, U.S. Department of Defense Strategic Environmental Research and Development Program (SERDP), and the Environmental Security Technology Certification Program (ESTCP) sponsored a workshop in which research and development needs for cleanup of chlorinated solvent sites were identified. The panel reached consensus that in situ thermal treatment: 1) is the emerging technology most in need of research (assessment based on the promise of the technology and the uncertainties regarding implementation); and 2) has the potential to remove a very large fraction of the DNAPL mass and may be able to treat even the less permeable areas within the source zone as opposed to technologies relying on hydraulic delivery of reagents (SERDP/ESTCP, 2001).

In 2005, a panel put together by the National Academy of Sciences concluded that *“There’s limited field experience applying conductive heating below the water table. If water inflow can*

*be limited, then conductive heating would be expected to be effective in all granular media. However, achieving adequate capture of vapors and liquids and limiting water inflow may be more difficult as heterogeneity increases. There is no experience with conductive heating in saturated fractured media or karst. As control of water inflow may be problematic in fractured media and karst, and capture of contaminants may be difficult, effectiveness is expected to be limited in these settings” (NRC, 2005).*

Thus, ESTCP project ER0715 was conducted in part to improve our understanding both in terms of what’s achievable in situ in addition to a better understanding of the physical properties affecting thermal remediation of fractured bedrock. The project was funded with the objective of evaluating the efficiency of Thermal Conductive Heating (TCH) to treat DNAPL in fractured bedrock.

The overall project approach adopted included:

- 4) Treatability studies to ascertain a treatment strategy (duration and temperature) for several rock types
- 5) Modeling to perform screening calculations and carry out mass estimates; and
- 6) Application of TCH at a fractured bedrock site.

The focus of the treatability study was to calculate removal rates and establish necessary treatment temperatures and duration in the field. The focus of the field demonstration was to validate: the heating strategy, achievable heating rates and fluid control, as well as matrix heating and de-saturation. In addition, a microbial characterization was conducted before and after TCH field application, with the purpose of investigating changes in the microbial population as a result of the elevated temperatures. The on-site application took place at the former NAWC in Trenton, NJ. The conceptual model for the site is that TCE mass is held tightly in the rock matrix, and potentially in some of the fractures at the site. The TCE has dissolved, diffused, and adsorbed to the solid rock matrix (silt and mudstones).

Although TCH had been proven effective for DNAPL removal from fractured clay settings (LaChance et al., 2004), its effectiveness had not yet been demonstrated in bedrock, the most challenging geological setting, at the start of this project. Therefore, TCH was selected for the demonstration as it is the only thermal technology that can reach temperatures in excess of 100°C (boiling) between heater borings installed into intact bedrock. There was/is a need to DEM/VAL successful DNAPL remedial technologies from bedrock sites and determine what type of performance should be expect from the technology.

TCH involves the placement of heater wells that have the capacity of operating at temperatures as high as 800°C, and thereby raise the temperature of the surrounding rock to a target temperature through conductive heating. TCH uses simple electrical heaters suspended inside a cased borehole to deliver energy to the surrounding formation. The heat migrates away from the heater borings by a combination of thermal conduction (driven by a temperature gradient) and convection (migration of steam produced by boiling ground water). Heater borings are typically located in a triangular pattern, using a spacing of between 10 to 20 feet. In porous media, DNAPL is treated by heating the target volume to a minimum of the boiling point of water combined with vapor extraction.

## **1.2 OBJECTIVE OF THE DEMONSTRATION**

The goal of the ER200715 project was to demonstrate and validate TCH performance in fractured bedrock and develop guidelines to practitioners on how to apply TCH.

The DEM/VAL objectives for the TCH demonstration were to:

1. Demonstrate the feasibility of TCH to heat the target volume of rock and water to steam distillation temperatures via energy applied to vertical TCH borings. This included evaluating the cooling influence of inflowing groundwater.
2. Validate the degree of heating to temperatures above boiling (100°C) at different distances from the heater borings. This included validating whether the temperatures recommended for effective treatment in this particular geology (derived from the laboratory work) were achieved.
3. Demonstrate capture of steam and other fluids from the heated boreholes such that vaporized and mobilized contaminants are extracted from the available fractures.
4. Show that the surface equipment meets regulatory demands for contaminant reduction efficiency and emissions.
5. Collect detailed temperature data to support numerical simulations of the heating and effect on remediation progress.
6. Collect rock chip samples to demonstrate temporal changes in contaminant concentrations within the pilot test volume as a function of the TCH application.
7. Collect microbial characterization data to evaluate the effect of the heating process on the potential for natural attenuation or enhanced bioremediation at the site.

## **1.3 REGULATORY DRIVERS**

In 1976, trichloroethene (TCE) was designated by the United States Environmental Protection Agency (USEPA) a priority pollutant. The Safe Drinking Water Act Amendments of 1986 strictly regulate this chlorinated ethene at a Maximum Contaminant Level (MCL) in drinking water of 5 parts per billion (ppb) (USEPA, 1996). When concentrations at a contaminated site exceed this criterion, remedial action is required to lower these concentrations and reduce the risk to human health and the environment.

## 2.0 TECHNOLOGY

### 2.1 TECHNOLOGY DESCRIPTION

In Situ Thermal Desorption (ISTD) is the simultaneous application of TCH and vacuum to the subsurface. TCH's primary application uses thermal heating wells, along with extraction wells, which can be placed to almost any depth in virtually any media. TerraTherm's proprietary In Situ Thermal Desorption technology is an off-the-shelf remediation technology that has been demonstrated to be capable of remediating the full range of Volatile Organic Compounds (VOCs) and Semi-Volatile Organic Compounds (SVOCs) to levels at or below typical regulatory agency clean-up standards (Stegemeier and Vinegar, 2001).

During the TCH process, the subsurface is heated and treated in the following manner:

Heat is applied to the subsurface using simple electrical heaters (as shown in Figure 2.1), installed inside a casing in contact with the soil, so that radiation and thermal conduction heat transfer are effective near the heater. As a result, thermal conduction and convection occur in the bulk of the soil volume. As the heating progresses by thermal conduction, the heater wells are heated to temperatures around 500 to 800°C, creating significant temperature gradients in the formation around each heater. Since the thermal conductivity of soil materials only varies by a factor of 2 (Stegemeier and Vinegar 2001), TCH can be considered to be very precise and predictable regardless of the permeability of the soil or its degree of heterogeneity.



**Figure 2.1. Proprietary TerraTherm Heater Element**

The metal rod has a diameter of approximately 0.5 inches. The white beads are ceramic isolators. Electric power flows through the steel rod, causing it to heat resistively. Covered by one or more of the following: U.S. Patent Nos. 5,190,405, 5,318,116, 6,485,232 and 6,632,047.

As the heat front moves away from the heaters through the soil by thermal conduction and convection, the superposition of heat from the many heaters results in a temperature rise throughout the Target Treatment Zone (TTZ). As soil temperatures increase, contaminants and water contained in the soil matrix are vaporized. While locations close to heaters may achieve temperatures well above the boiling point of water, locations in between heaters need only achieve temperatures to the boiling point of water to accomplish steam distillation for effective removal of CVOCs. Very high (>99%) removal rates have been repeatedly measured for TCH

treatment of CVOCs (Heron et al. 2005; 2009 and Nielsen et al. 2010) both in unconsolidated and consolidated media. Groundwater concentrations within the treatment zone were reduced between 74.5% and 99.7% at a confidential fractured rock site using TCH (Heron et al. 2008).

Heating the subsurface to temperatures around the boiling point of water can lead to significant changes in the thermodynamic conditions in the subsurface and can make CVOCs and NAPL more mobile and removable. The major effects of heating are:

- The vapor pressure of the NAPL increases markedly with temperature. As the subsurface is heated from ambient temperature to temperatures in the range of 100°C, the vapor pressure of the NAPL constituents will typically increase by between 10 and 30-fold (Udell, 1996).
- Adsorption coefficients are reduced moderately during heating, leading to an increased rate of desorption of CVOCs from the soil (Heron et al., 1998).
- Viscosity of NAPL is reduced by heating. The higher the initial viscosity, the greater the reduction. For TCE and other chlorinated solvents, the viscosity typically is reduced by about a factor of two.
- NAPL-water interfacial tensions are reduced (Heron et al. 2006), which can lead to improved recovery as a liquid, but can also present a mobilization risk if appropriate measures are not implemented. However, this change is very modest compared to the vaporization mechanism.
- Boiling of NAPL at temperatures below the boiling point of water (DeVoe and Udell, 1998). Heating the subsurface to above the boiling point of site contaminants will make the DNAPL thermodynamically unstable, causing it to boil and convert to a vapor. Thus, once the temperature throughout the saturated portion of the TTZ has reached the contaminant boiling point, NAPL will no longer be able to exist as a separate phase. Other mechanisms, as discussed below, will then work to remove the remaining contamination.

For chlorinated solvents such as TCE and perchloroethene (PCE), vaporization is the most important physical removal / remediation mechanism. In addition to the physical removal described above, biological and chemical degradation mechanisms may occur during and after thermal remediation. These mechanisms may include thermal destruction by oxidation and pyrolysis near heating elements (for thermal conductive heating) at temperatures around 400°C, microbial mineralization of NAPL components, and hydrolysis at elevated temperature (Baker and Kuhlman, 2002).

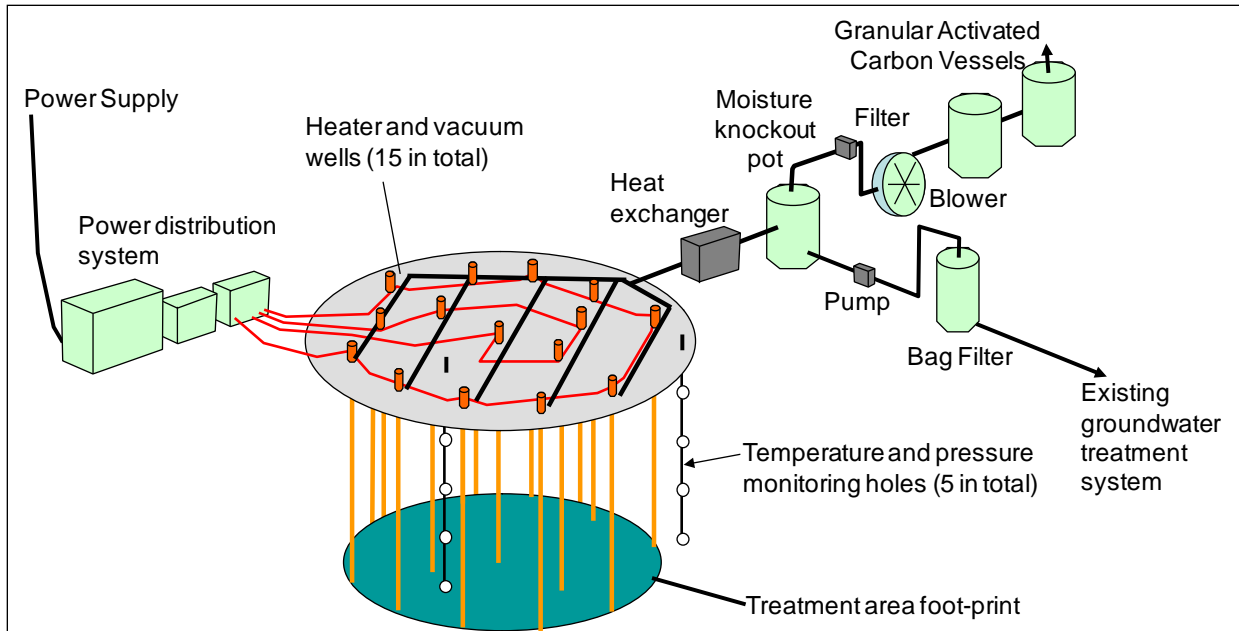


**Figure 2.2. Sketch of TCH Implementation**

Figure 2.2 contains a simple sketch of a TCH system. The major equipment used in a TCH installation includes:

- A transformer delivering power for the electrical circuits;
- A power distribution system with switches, meters, and controllers;
- Cables and wiring for the TCH heaters, which are located in vertical borings (heater borings);
- The wells and borings:
  - Heater borings;
  - Vapor and fluid recovery borings/wells;
  - Monitoring points;
- Manifold and conveyance piping for extracted fluids; and,
- Treatment system for extracted fluids (vapor and liquids, as required).

Typically, an office trailer is used for housing data management computers and other monitoring equipment. The entire process is usually automated, with operators overseeing the system and collecting data and samples during the daytime. As the site is heated, fluids are extracted, cooled, separated, and treated. The subsurface process is monitored using temperature and pressure sensors and detailed sampling and analysis of subsurface fluids. Figure 2.3 shows the TCH system installed at the NAWC site.

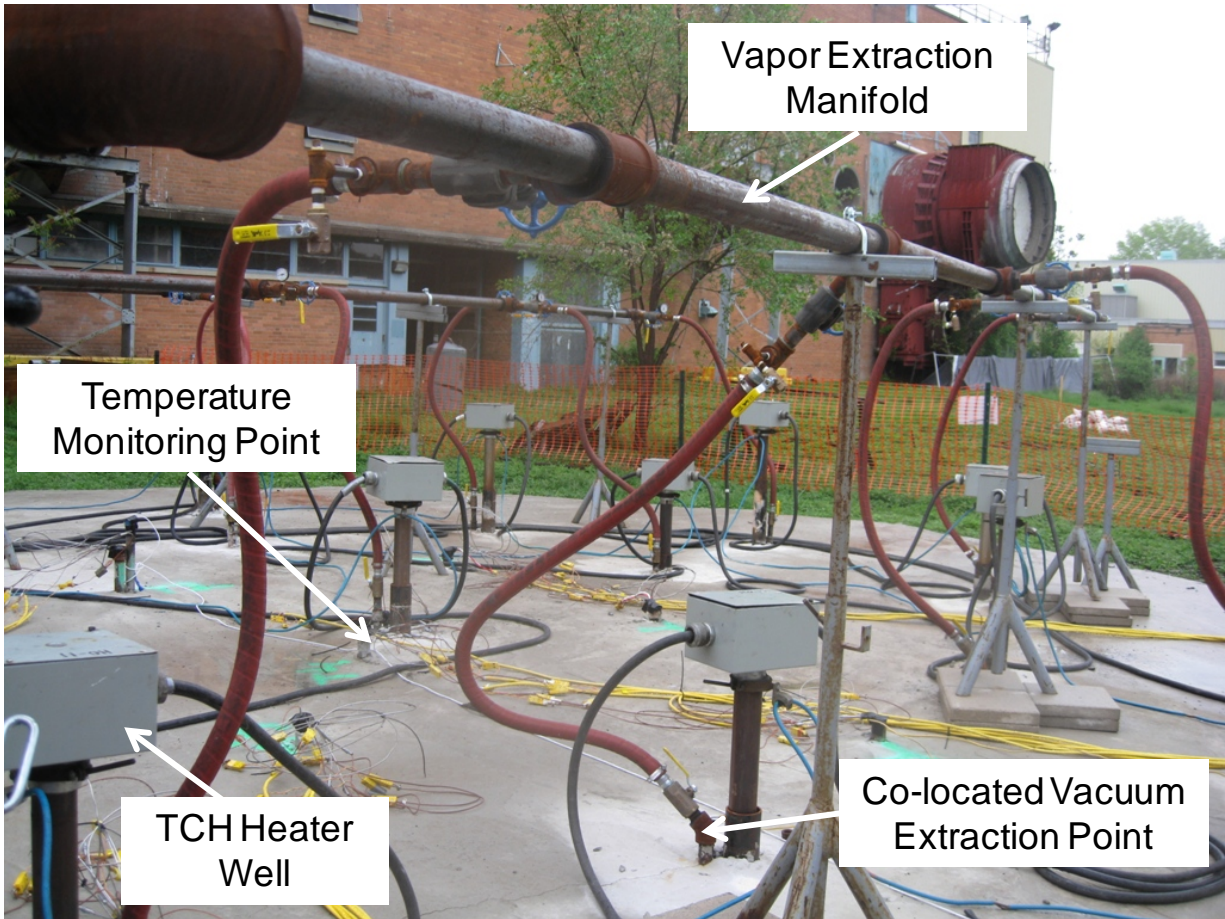


**Figure 2.3. TCH system installed at NAWC Site**

## **2.2 TECHNOLOGY DEVELOPMENT**

The ISTD/TCH technology was originally developed by Shell Exploration and Production (Shell E&P), a division of Royal Dutch Shell (Shell) over 15 years ago to accomplish enhanced oil recovery. Shell E&P soon recognized the technology's application to the cleanup of contaminated sites. From 1994 to 1996, Shell Technology Ventures, Inc., a wholly owned subsidiary of Shell E&P that held the TCH patents, conducted several TCH demonstrations, and established TerraTherm Environmental Services Inc. (TESI) to be a stand-alone remediation company based in Houston, Texas, offering TCH services to both the public and private sectors. From August 1996 through September 1998, TESI implemented TCH at six sites located within the U.S. and its territories. Shell subsequently elected to exit the environmental cleanup business. In January of 2000, Shell donated the TCH rights within the U.S. to the University of Texas at Austin (UT), and a new company, TerraTherm, Inc. (TerraTherm) secured the exclusive license from UT to commercialize TCH within the U.S. In 2002, Shell granted TerraTherm exclusive rights to commercialize the TCH technology outside the U.S. Since then, TerraTherm has successfully completed approximately 30 TCH projects, including the successful treatment of fractured clay in the Midwest and three field projects with fractured rock. In total, there are over 30 completed field projects documenting the technological maturity of TCH.

Shell E&P and TerraTherm have invested over \$40M since the early 1990s on basic research and development of TCH for soil and groundwater remediation. Through these efforts, TCH has been demonstrated to be effective in removing a variety of contaminants from porous media including polychlorinated biphenyls (PCBs), pesticides, CVOCs, polycyclic aromatic hydrocarbons (PAHs), dioxins, and heavy and light petroleum hydrocarbons (Stegemeier and Vinegar, 2001). Three of these early efforts were performed at DoD sites: Former Mare Island Naval Shipyard, Vallejo, CA; Tanapag Village, Saipan, NMI; and Naval Facility Centerville Beach, Ferndale, CA. Treatment goals were achieved at all completed sites. TerraTherm has since used the TCH technology successfully to remediate approximately 20 sites across the US. The following sections describe sites with a component in fractured rock.

### **2.2.1 Harwell TCH Project in Chalk**

In 2005, a pilot-scale demonstration of TCH in fractured chalk (at the UK Atomic Energy Authority [UKAEA] site in Harwell, UK) was completed. This pilot test demonstrated how TCH can significantly enhance soil vapor extraction in chalk. The removal rate for TCE increased fourfold when the unsaturated zone was heated to ~100°C (CL:AIRE, 2010). Currently, full-scale TCH operation is on-going. Six waste pits were treated between 2005 and 2011, one each year, and operations continue at the site. Though on-site work continues, as of May 2012, 7 pits have been treated thus far. Though performance monitoring at the site does not include taking rock samples routinely for determination of percent removal, limited data suggests much better than 90% reductions, and simultaneous peaking of the mass removal rates.

### **2.2.2 NASA Demonstration with Limestone**

In the summer of 2007, TerraTherm completed a pilot-scale test at the NASA Marshall Space Flight Center (MSFC) Source Area 13 in Huntsville, AL (Cole et al., 2008). The study area volume included a clayey residuum from land surface to a depth of approximately 32 ft below ground surface (bgs); the groundwater-bearing rubble zone at the base of the residuum; and the top 5 ft of limestone bedrock beneath the rubble zone demonstrating the ability of TCH to treat saturated bedrock zones. Post-treatment soil samples taken at the site had a mean concentration of 0.06 mg/kg with a maximum post-treatment concentration of 0.56 mg/kg TCE, demonstrating an average reduction of TCE in the subsurface of 99.87%.

### **2.2.3 Confidential Site with Saprolite and Gneiss**

A third TCH project located in the southeastern U.S. with a treatment zone encompassing bedrock was also completed in the summer of 2007 (Heron et al., 2008). At the southeastern U.S. site, the TTZ extended to approximately 87 feet bgs. Saprolite was present from 30 to 70 ft bgs, underlain by weathered and unweathered gneiss. The water table was encountered at approximately 55 bgs. This resulted in a total saturated thickness of approximately 25 feet of soil and partially weathered bedrock overlying fractured bedrock. TCH heaters extended approximately 10 feet into the fractured gneiss bedrock. The site was heated and treated for a period of 100 days. Post-treatment concentrations at this site indicated that the 95% UCL of the mean concentration of TCE in soil within the treated area (including bedrock) was 0.017 mg/kg. Although the southeastern U.S. site was a saturated DNAPL site, the effectiveness of TCH on removal of DNAPL/contaminant mass from the fractured rock was not demonstrated as there were no pre- or post-treatment samples within the rock to quantify the effectiveness of TCH at

removal of the contaminants. However, an effective and efficient heating strategy for gneiss rock was demonstrated.

Additionally, TCH has been effectively demonstrated for DNAPL removal from dense fractured clays both above and below the water table at a site located on San Francisco Bay in Richmond, CA (LaChance et al., 2004). At this site, pre-treatment maximum and average concentrations of PCE in soil were reduced by greater than 99.9% (the post treatment average concentration of PCE based on 64 samples was 0.012 mg/kg. These experiences with TCH at rock and fractured clay supported the technology maturity needed for demonstration and use at fractured rock sites with DNAPL below the water table.

This project augmented the scope of SERDP project ER-1423: Large-Scale Physical Models of Thermal Remediation of DNAPL Source Zones in Aquifers, (PIs Drs. Ralph Baker and Uwe Hiester) whose goal was to (1) determine the significance of the various contaminant removal mechanisms during TCH; (2) assess the percentage of DNAPL source removal at various treatment temperatures/durations through boiling; and (3) evaluate the potential for DNAPL mobilization during heating. ER-1423 focused on PCE and TCE DNAPL placed below the water table in heterogeneous, but unconsolidated materials (sand, silt, clay). It elucidated the mechanisms of thermal removal of DNAPL from zones without a rock matrix, and focused on heating to the boiling point of water. Therefore, the TCH field demonstration in fractured rock complements ER-1423 well, and did not overlap with it.

### **2.3 ADVANTAGES AND LIMITATIONS OF THE TECHNOLOGY**

The major advantage of TCH is that it has a very high probability of success when applied to a well defined target volume. In brief, the advantages include:

- Readily predictable heating due to simplicity of the conductive heating approach.
- Uniform heat distribution and treatment.
- No practical limitation on treatment depth or area (the TCH technology is used for enhanced oil recovery applications to depths > 1,000 ft and for volumes exceeding 100,000 cubic yards).
- Shorter treatment duration. Average treatment duration is 228 days (McGuire, et al 2005).

Potential disadvantages include:

- Energy demand. Typical sites require on the order of 120 to 300 kWh per cubic yard treated. This equals an energy cost of \$10-30 per cubic yard. Also, the energy consumption, depending on the source of electricity, may contribute to emissions of carbon dioxide, which contributes to global warming.
- The technology requires invasive drilling and on-site construction activities, which may disrupt site activities temporarily.
- Sensitivity to groundwater flow and cooling. Excessive flow through the heated volume can slow heating, or in some cases prevent certain fracture areas from getting to the target temperature.

For fractured rock sites, any in situ treatment technology will be faced with the upfront challenge of defining the three-dimensional treatment volume. This is particularly important for highly effective technologies such as TCH. Thus, the application of a technology that is suited for removal of all the DNAPL at a site poses difficult questions such as (1) what is the foot-print within which the source has spread, and (2) how deep is the DNAPL? These questions are just as important for full-scale implementation as the question of effectiveness of the TCH technology. For instance, if one can remove 99.9% of the mass inside a selected treatment volume using TCH, it becomes important to select the right target volume. In certain situations the characterization effort required to define the treatment volume may be more costly than the remedy itself.

Conductive heating offers distinct advantages over fluid flushing technologies and other thermal technologies. In comparison to fluid flushing technologies (e.g., oxidant flushing, surfactant flushing), heat migration is not as adversely affected by geological heterogeneity as is fluid migration. In comparison to other thermal technologies, TCH has the advantages of (1) not relying on fluid injection (e.g., steam flooding) for heat delivery to the subsurface; (2) being able to achieve temperatures above boiling (which cannot be achieved by steam flooding or electrical resistance heating [ERH]); and (3) the ability to destroy contaminants in situ as a result of the high temperatures that can be achieved, thereby reducing the need for ex situ produced fluids treatment.

## **2.4 MODELING TCH TECHNOLOGY**

Numerical modeling was carried out as part of this project to evaluate the influence of inflowing cold groundwater on the ability to heat fractured rock, and to evaluate the influence of various rock properties on the ability to achieve boiling in the rock matrix using TCH. Results are summarized below and details are included in Appendix B.

### **2.4.1 Screening Calculations to Evaluate the Cooling Effect of Groundwater Influx**

A two-dimensional semi-analytical heat transfer solution was developed and a parameter sensitivity analysis performed to determine the relative importance of rock material properties (density, thermal conductivity and heat capacity) and hydrogeological properties (hydraulic gradient, fracture aperture, fracture spacing) on the ability to heat fractured rock using TCH. The solution was developed using a Green's function approach in which an integral equation is constructed for the temperature in the fracture.

Results indicate that groundwater influx may prevent or delay the heating of fractured rock during application of thermal conductive heating (TCH). When bulk groundwater influx is high, temperatures in the fractures are influenced by the aperture and spacing of fractures. For medium and low values of influx, fracture properties do not appear to be important in determining the temperature in fractures. In these cases, it appears not to be important to characterize discrete fracture features in the treatment zone; only a quantification of the total groundwater influx through the treatment zone is necessary.

Variations in material properties (rock density, rock thermal conductivity, and rock heat capacity) amongst rock types do have a small effect on the early-time temperature distribution in the rock, but on the whole are less significant than variations in hydrogeological parameters (hydraulic gradient, fracture aperture, and fracture spacing). It is noted that the range of variation in material properties is much smaller than the range of hydrogeological properties, which may vary by several orders of magnitude.

Transient analysis shows that influx cooling affects treatment zone temperatures only once a certain temperature threshold has been passed during heating. It is possible that, if target treatment temperatures are low, influx cooling may not pose a problem.

One solution to the problem of groundwater influx cooling is to simply increase the power delivered to the thermal wells. In the case where this may not be done due to equipment limitations or other concerns, preheating wells installed outside of the treatment zone may be used to partially mitigate the cooling effects.

Further, results indicate that subsurface temperature distributions are far more sensitive to hydrogeological properties than rock material properties. The bulk groundwater influx can provide a good estimate of the extent of influx cooling when influx is low to moderate, allowing the prediction of temperatures during heating without specific knowledge of the aperture and spacing of fractures. However, target temperatures may not be reached, or may be significantly delayed, when the groundwater influx is large.

The results of this modeling indicate that careful attention should be given to groundwater influx into a target treatment zone in order to determine whether the boiling of water can be achieved, and the length of heating time required to achieve boiling. Calculating the groundwater influx at a fractured rock site is typically carried out using measurements of bulk rock hydraulic conductivity and hydraulic gradient. Given the likely variability of flow rate amongst individual fractures in a treatment zone (flow proportional to fracture aperture cubed), more accurate assessment of the influence of inflowing cold groundwater can be determined on the basis of bulk rock hydraulic conductivity measurements carried out at smaller scales, rather than at larger scales. Further details of this modeling effort are presented in Appendix B.

#### **2.4.2 Numerical Modeling of TCH Treatment in Bedrock**

Numerical modeling was employed to study the performance of TCH in fractured shale under a variety of hydrogeological conditions. Model results show that groundwater flow in fractures does not significantly affect the minimum treatment zone temperature, except near the beginning of heating or when groundwater influx is high. However, fracture and rock matrix properties can significantly influence the time necessary to remove all liquid water (i.e., reach superheated steam conditions) in the treatment area. Low matrix permeability, high matrix porosity, and wide fracture spacing can contribute to boiling point elevation in the rock matrix. Consequently, knowledge of these properties is important for the estimation of treatment times. Because of the variability in boiling point throughout a fractured rock treatment zone and the absence of a well-defined constant temperature boiling plateau in the rock matrix, it may be difficult to monitor the progress of thermal treatment using temperature measurements alone. This is particularly relevant in low matrix permeability rock where thermal expansion of groundwater leads to

pressure increases which in turn result in elevated boiling points for water. Further details are provided in Appendix C.

The performance of thermal conductive heating in fractured rock environments is expected to be strongly dependent on the hydraulic properties of the rock matrix (permeability, porosity) and the aperture and spacing of fractures. If complete removal of all liquid water is the goal of thermal treatment, treatment time will be strongly governed by the magnitude of the pressure spike that occurs in the rock matrix during heating. When the rock matrix has a low permeability, high porosity, or sparse fracturing, this pressure rise may be enough to significantly raise the boiling point of water in the matrix, thus delaying treatment. Because a clear temperature plateau may not be observed in the matrix during boiling, it may be difficult to determine if boiling has occurred throughout a treatment area from temperature measurements alone.

Due to the importance of fracture spacing in determining the pressure rise in the matrix, a discrete fracture model is more appropriate than an equivalent porous medium model for simulating boiling in this context. However, treatment zone temperatures are only moderately affected by the location of fractures, for a given value of bulk permeability.

### 3.0 PERFORMANCE OBJECTIVES

This section contains a summary of the performance objectives and whether they were met and, if not met, the principal reason for failure. The performance objectives are summarized in Table 3.1.

**Table 3.1. Performance Objectives**

Performance Objective	Data Requirements	Success Criteria	Results
<b>Qualitative Performance Objectives</b>			
Faster remediation	Collection of rock-chip TCE concentrations data before thermal treatment. Quantification of the mass of TCE removed during thermal treatment. Collection of rock-chip TCE concentrations data after thermal treatment. Calculations of changes in average TCE concentrations, and changes in TCE concentration in the larger matrix blocks within the demonstration volume.	Document that COC mass in the rock can be substantially reduced in months or few years of operation.	Objective met. Approximately 530-680 lbs of TCE were removed in 3.5 months of operation. Rock chip concentrations were reduced by 41-69% on average in the rock samples close to fractures where cooling influence hindered complete heating; 94.5% removal accomplished in the samples where target temperatures were achieved. For details please refer to tables 5.22 and 5.23.
Achieve acceptable concentrations	Source area TCE concentrations before and after thermal treatment. Modeling of groundwater impacts of the treatment.	Reach endpoints faster by reducing mass discharge from source area.	Objective not met. Due to small test volume surrounded by contaminants, and influx of fluids to the treatment zone, end-points could not be validated. Results are consistent with Kingston, et al 2010, i.e., " <i>worse performance occurs when the treatment footprint is smaller than the extent of the source zone.</i> " Further, results are also consistent with Kingston, et al in that 1-2 orders of magnitude (10X to 100X) reductions in dissolved groundwater concentrations are achieved with in-situ thermal systems.
Ease of combining with existing operations	Observation of operations at the thermal test site and the existing pump and treat (P&T) system.	No upset of existing P&T systems including acceptable treatment of vapors and liquids.	Objective met. TCH system successfully operated with existing P&T system.
Ease of Use Operator acceptance	Recording of operation up-time. Observation of any operational challenges or difficulties.	Successful operation of TCH system with >95% uptime.	Objective met. TCH system successfully operated with 95% uptime.

<b>Quantitative Performance Objectives</b>			
Achieve and maintain target treatment temperatures	Thermocouple data from eight locations, each with approximately 10 sensors (76 sensors total), recorded at least daily.	Achieve and maintain > 95°C above the water table and 100°C below the water table in target treatment volume.	Objective met in the upper 35 ft of the volume, but not in the bottom 15 ft. Higher than expected groundwater flow at these depths prevented target temperatures from being achieved at the bottom 14 ft.
Reduce COC mass in rock matrix	Collection of rock-chip TCE concentrations data before thermal treatment. Collection of rock-chip TCE concentrations data after thermal treatment. Calculations of changes in average TCE concentrations, and changes in TCE concentration in the larger matrix blocks within the demonstration volume.	Reduce contaminant concentration and mass inside the inner treatment volume in matrix > 99% or below 0.1 mg/kg in rock matrix	Objective not met. Rock chip concentrations were reduced by 41-69% on average in the rock samples close to fractures where cooling influence hindered complete heating; 94.5% removal accomplished in the samples where target temperatures were achieved. For details please refer to tables 5.22 and 5.23.
Assess magnitude and impact of cooling due to groundwater flux through treatment volume	Thermocouple data collected weekly during cool-down inside treatment area and in downgradient wells.	Support observations and interpretation of heating progress, and the impact of groundwater flow on the overall performance	Objective met. Groundwater flux documented to be 5-10 times higher than expected during treatment. Liquid entrainment caused heating at the bottom 10-15 ft and in major fractures to be slower than expected. Cooling data was obtained during 8.5 months after thermal treatment. Regional groundwater flow, vapor extraction and fractures possibly created during sonic drilling are believed to have exacerbated cooling.
Estimate contaminant mass in the contaminated zone while quantifying mass recovered from demonstration area	Mass flux and totals calculated using flow rate and concentration data for vapor and water streams conveyed to treatment system; based on data collected from the cooled streams.	Maintain water and vapor balances, obtain TCE concentration data, and estimate mass removed	Objective met. Approximately 500-650 lbs of TCE removed in the vapor phase, and 33 lbs in the liquid phase.
Estimate hazardous materials generated	NAPL recovered from condensing effluent vapors	Quantify any NAPL collected.	Objective met. No NAPL was collected.
Estimate waste generated	Drilling, construction and demobilization wastes.	Quantify or estimate all major waste streams.	Objective met. Drilling waste (soil and rock cores) disposed of or archived, demobilization waste quantified (Section 5.8).

Factors affecting performance	Groundwater flow through treatment zone (interpreted). Rock type, porosity, organic carbon content. Contaminant boiling point and hydrophobicity.	Data to be collected throughout implementation.	Objective met. Estimated effect of groundwater flow through treatment zone, rock type impact, porosity, Organic carbon content and contaminant boiling point and hydrophobicity
-------------------------------	---	---	---

### 3.1 DISCUSSION OF PERFORMANCE OBJECTIVES

This section presents each performance objective, the data collected, and the result of the evaluation. Table 3.1 contains a summary of the performance objectives and the field demonstration results.

#### 3.1.1 Performance Objective: Faster Remediation

Success Criteria: Document that COC mass in the rock can be substantially reduced in months or few years of operation.

The data collected to evaluate this criterion were:

- Collection of rock-chip TCE concentration data before thermal treatment.
- Quantification of the mass of TCE removed during thermal treatment.
- Collection of rock-chip TCE concentration data after thermal treatment.
- Calculations of changes in average TCE concentrations and changes in TCE concentration in the larger matrix blocks within the demonstration volume.

Interpretation and results: Heating lasted for 97 days. The vapor extraction system operated for 106 days. Therefore, documented reductions in rock TCE concentrations were accomplished over a period of 3.5 months. Based on the rock-chip TCE data, the average reduction in TCE concentrations was 41-69%. However, careful examination of selected points in the rock matrix revealed that the rock matrix did not achieve targeted temperature in all locations (due mostly to contaminated groundwater influx thru existing fractures). Since discrete sampling was done at 5 feet intervals, it was possible to identify at which depth there was incomplete heating and correlate that with observed fractures from a video log of the boreholes. If we eliminate from the performance data the points where boiling water temperature was not achieved due to cool water influx, the average reduction was higher at 94.5 %. For details, please see Tables 5.22 and 5.23.

The 94.5% COC mass removal rate is consistent with findings from other studies. For example, in a literature survey conducted by NAVFAC ESC and Geosyntec Consultants under ESTCP project ER0424, thermal technologies typically achieved levels of DNAPL mass removal ranging between 94% to 96%. As a reference, median removals for anaerobic EISB, ISCO, SEAR and co-solvent flushing ranged from 64% to 81% (Lebron, et al. 2011). McGuire and others also reported in 2005 that thermal treatment exhibited a median parent reduction of 95% or greater. Further, in a field-scale TCH project conducted by TerraTherm at a confidential fractured rock site, 99% or higher reductions were observed in saprolite/gneiss (Heron et al. 2008). The 95% reduction observed here is therefore much lower than what would be expected

at full scale, where the treatment would be more complete than could be accomplished in the small pilot test.

Data from the ER0715 on-site demonstration show that most rock concentrations were lowered to around 0-5 mg/kg, but that higher concentrations were maintained at distinct depth intervals. These depths correlated reasonably well with the depth showing the highest TCE concentrations prior to heating. Relatively good heating and remediation occurred in the larger matrix blocks. Concentrations in the thick zones without evident fractures were reduced substantially to levels below 5 mg/kg. The most probable explanation for the observed post-treatment concentrations is:

- Substantial flow of contaminated groundwater occurred in distinct fracture zones during the thermal operations. This influx of water has two negative effects: it introduces new contamination in addition to cooling the treatment zone which can prevent reaching boiling point. This being the case during the ER0715 field demonstration is supported by the following observations: (1) slower heating at certain depth intervals, (2) the high groundwater extraction rates observed, and (3) consistently elevated VOC concentrations in extracted vapor and water.
- The steam created in the matrix led to partial desaturation and to a push of steam and water towards the permeable fractures. As the steam migrated towards the fractures, it encountered lower temperatures and condensed near the fractures. Where the cool water flow continued (and was sufficient to keep the fractures below the boiling point of groundwater), TCE accumulated in the matrix near the fractures.

In summary, groundwater flow was likely responsible for the local cooling that led to ineffective TCE remediation. In addition, the flow of contaminated water into the TTZ continuously supplied TCE and other VOCs to the field demonstration area. This finding is consistent with NRC findings in 2005, i.e., *“control of water inflow may be problematic in fractured media and karst, and capture of contaminants may be difficult, effectiveness is expected to be limited in these settings. If water inflow can be limited, then conductive heating would be expected to be effective in all granular media.”* Furthermore, Kingston, et. al reported in 2009 that *“Better performance might be achieved if system footprints are over-designed to extend beyond the source zone boundaries.”*

Nonetheless, the following observations indicate that a carefully designed TCH application can be effective in removing TCE and other VOCs from the bedrock at the site:

- The site was brought to temperatures near or at the boiling point of water from a depth of 5 to 35 ft bgs. This shows that the electrical energy was effectively delivered, and that the rock matrix was heated as desired.
- Between 500 and 650 lbs of VOCs were removed in the vapor phase during the pilot scale operation.
- Rock concentrations were lowered, and mass removal continued up until the end of the operations period, indicating that the TCH treatment was still occurring.

### **3.1.2 Performance Objective: Achieve Acceptable Concentrations**

Success Criteria: Reach endpoints faster by reducing mass discharge from source area.

The data collected to evaluate this criterion were:

- Source area TCE concentrations before and after thermal treatment.
- Modeling of groundwater impacts of the treatment.

Interpretation and results: The CVOC concentration in the major fractures was not reduced substantially during this demonstration, therefore the performance objective was not met. Flow of cool groundwater into the demonstration volume through the dominant fractures, and the associated TCE mass, impacted target temperature in the vicinity of the fractures. As such, during this demonstration, the mass discharge from the small target volume was not reduced substantially. For full-scale applications, the cooling water flow should be reduced or eliminated, and in such cases a positive effect on the mass discharge would be expected. This was documented for the Knullen site in Denmark, where thermal treatment (based on TCH and steam injection) eliminated a source area and essentially removed the mass discharge of PCE feeding a long groundwater plume (Heron, 2010). However, though possible, limiting water inflow at a fractured bedrock site may be challenging. Therefore an effective TCH application should include site-specific testing to discover these issues and make modifications prior to full-scale treatment. In fact, practitioners should pay particular attention to the potential for groundwater influx when designing and implementing a TCH application in fractured bedrock.

### **3.1.3 Performance Objective: Ease of Combining with Existing Operations**

Success Criteria: No upset of existing P&T systems including acceptable treatment of vapors and liquids.

The data collected to evaluate this criterion were:

- Observation of operations at the thermal test site and the existing P&T system.

Interpretation and results: This performance objective was met. The existing P&T system operation continued, and the P&T system functioned without upsets caused by the thermal treatment system. In order to smooth out the water treatment rate, a large surge/buffer tank was installed between the two systems, removing any issues related to variable flow rates into the existing system. This was an easy and routine activity.

### **3.1.4 Performance Objective: Ease of Use/Operator Acceptance**

Success Criteria: Successful operation of TCH system with >95% uptime.

The data collected to evaluate this criterion were:

- Recording of operation up-time.
- Observation of any operational challenges or difficulties.

Interpretation and results: The thermal system operated with minimal down-time. Very minor changes were necessary throughout operation, even when much higher than anticipated liquid recovery rates were observed. The process equipment was designed and built to handle fluctuations in the incoming water and vapor rates, which ensured very limited periods with less than optimal operation. Therefore, this performance objective was met.

### 3.1.5 Performance Objective: Achieve and Maintain Target Treatment Temperatures

Success Criteria: Achieve and maintain  $> 95^{\circ}\text{C}$  above the water table and  $100^{\circ}\text{C}$  below the water table in target treatment volume.

The data collected to evaluate this criterion were:

- Thermocouple data from eight locations, each with approximately 10 sensors (76 sensors total), recorded daily.

Interpretation and results: Thermocouple data was collected and is included in Figure 3.1 which shows the average temperatures at depths between 5 and 50 ft bgs. It can be seen that generally, all zones from 35 ft bgs and above reached temperatures in the range of  $210\text{-}230^{\circ}\text{F}$ , consistent with in situ boiling temperatures of groundwater. It can also be seen that at depths of 40, 45, and 50 ft bgs the temperatures reached were somewhat lower and below the boiling point of water thereby impacting treatment performance.

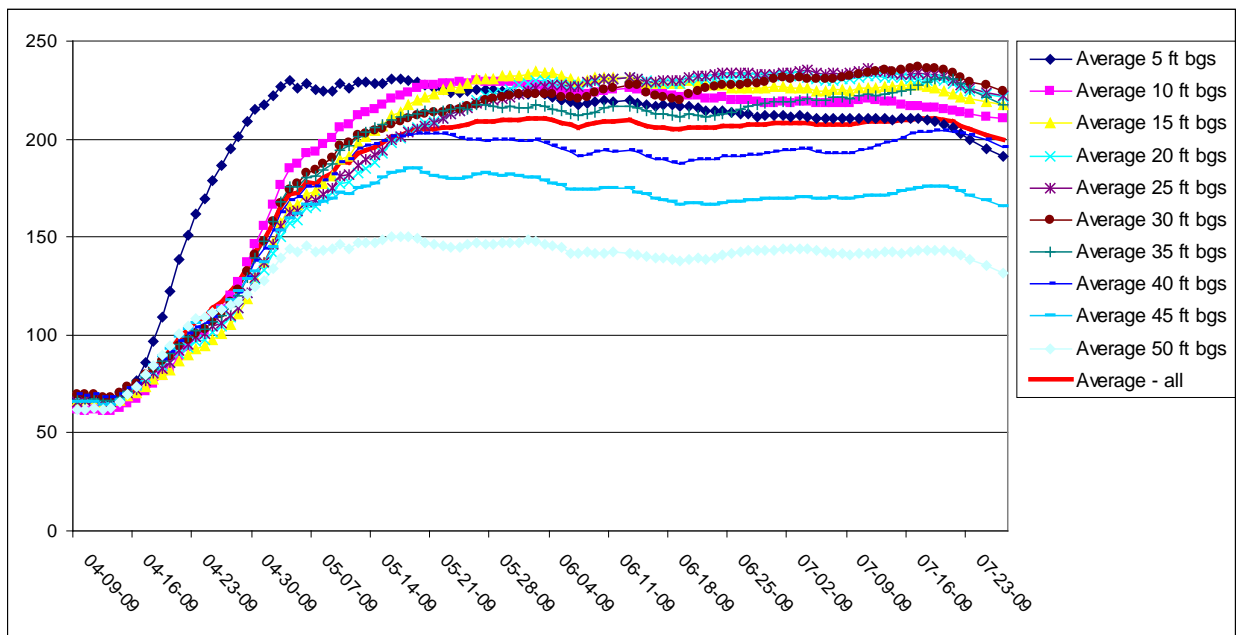


**Figure 3.1. Average Temperatures at Different Depths during Heating Operations**

Figure 3.2 shows, as an example, the temperature profile in T1 as it developed over time. A noticeable lag in heating is observed at a depth around 10 to 25 ft bgs, and at depth of 40 ft bgs and deeper. Such lagging is consistent with more groundwater flow at these depths, as discussed previously. In summary, the performance objective was met in the upper 35 ft of the volume, but not in the bottom 15 ft, which was explained by the higher than expected groundwater flow at these depths. As a consequence of this, the TCE mass removal was also lower than anticipated.

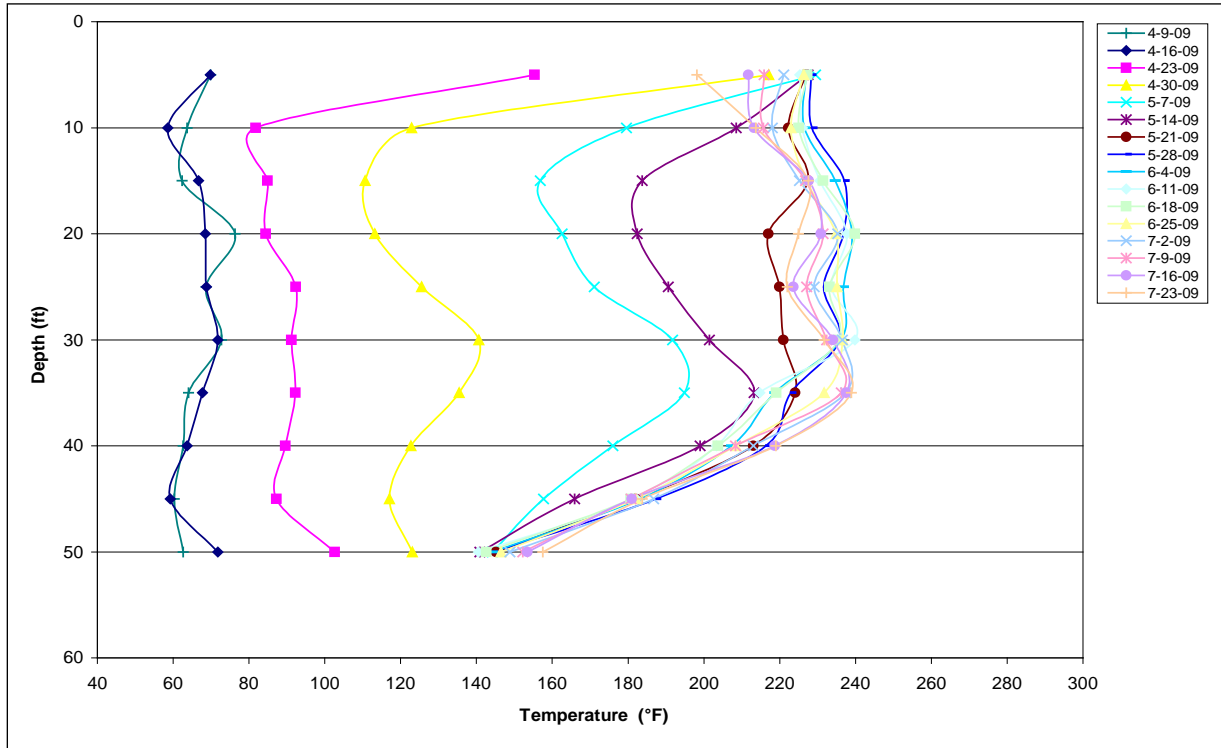


**Figure 3.2. Temperature at T1 during Heating Operations**

### 3.1.6 Performance Objective: Reduce COC Mass in Rock Matrix

Success Criteria: Reduce contaminant concentration and mass inside the inner treatment volume in matrix > 99% or below 0.1 mg/kg in rock matrix.

The data collected to evaluate this criterion were:

- Collection of rock-chip TCE concentrations data before thermal treatment.
- Collection of rock-chip TCE concentrations data after thermal treatment.
- Calculations of changes in average TCE concentrations and changes in TCE concentration in the larger matrix blocks within the demonstration volume.

Interpretation and results: This objective was not met in this demonstration. An average TCE concentration reduction of 58% was achieved (64% in boring BR1/BRP1, 69% in boring BR2/BRP2 and 41% in BR3/BRP3 – see Table 5.22 for details). Proposed improvements for full-scale application of the TCH technology are provided in Section 8 of this report. However, the 0.1 mg/kg remedial goal in the matrix may be difficult to reach in some rock formations,

especially those with high content of organic matter, and/or substantial groundwater flux in the fractures, both of which are the case at the NAWC site. In the portions of the matrix where fractures were minimal (therefore the matrix not affected by the cooling effect), 94.5% removal was achieved (see Table 5.23 for details). The data also shows that most rock concentrations were lowered to around 0-5 mg/kg, but that higher concentrations were maintained at distinct depth intervals. These depths correlated reasonably well with the depth showing the highest TCE concentrations prior to heating.

### **3.1.7 Performance Objective: Assess Magnitude and Impact of Cooling Due to Groundwater Flux through Treatment Volume**

Success Criteria: Thermocouple data collected weekly during cool-down inside treatment area and in downgradient wells.

The data collected to evaluate this criterion were:

- Thermocouple data from eight locations, each with approximately 10 sensors (76 sensors total), recorded weekly.

Interpretation and results: Thermocouple data were collected. Figure 3.3 shows T1 as an example. The period of monitoring was extended, and the frequency of reading reduced, such that the cooling effect data was obtained over a period of approximately 8.5 months. The temperatures did show that cooling was faster at the top and bottom of the treatment interval. However, no significant anomalies were observed locally, indicating that regional groundwater flow was not dominant in controlling the cooling of the matrix and fracture systems. This corresponds well with the interpretation of the elevated groundwater flows during thermal treatment being caused by the vapor extraction, not by regional groundwater flow. In other words, groundwater moved much faster during the thermal operations, as a result of liquid entrainment occurring in the vapor extraction points as steam was extracted, and pulled large quantities of groundwater with it. Further, after completion of the field demonstration, the team hypothesized that the primary cause of this cooling effect was the induced flow of cool groundwater into the demonstration volume through the dominant fractures as a result of the design of the vacuum extraction system. The induced flow of groundwater impacted the ability of the demonstration to reach the target temperature in the vicinity of the water bearing fractures at specific depths and introduced additional TCE mass into the demonstration volume, and the associated TCE mass, likely reduced the positive impacted target temperature effects of the thermal treatment in the vicinity of the fractures. As such, during this demonstration, the mass discharge from the small target volume was not reduced substantially. For full-scale applications of thermal technologies, the influx of cool groundwater into the treatment zone, whether potentially induced by the design or due to regional gradients cooling water flow would should be reduced or eliminated, and in such cases a very positive effect on the mass discharge would be expected.

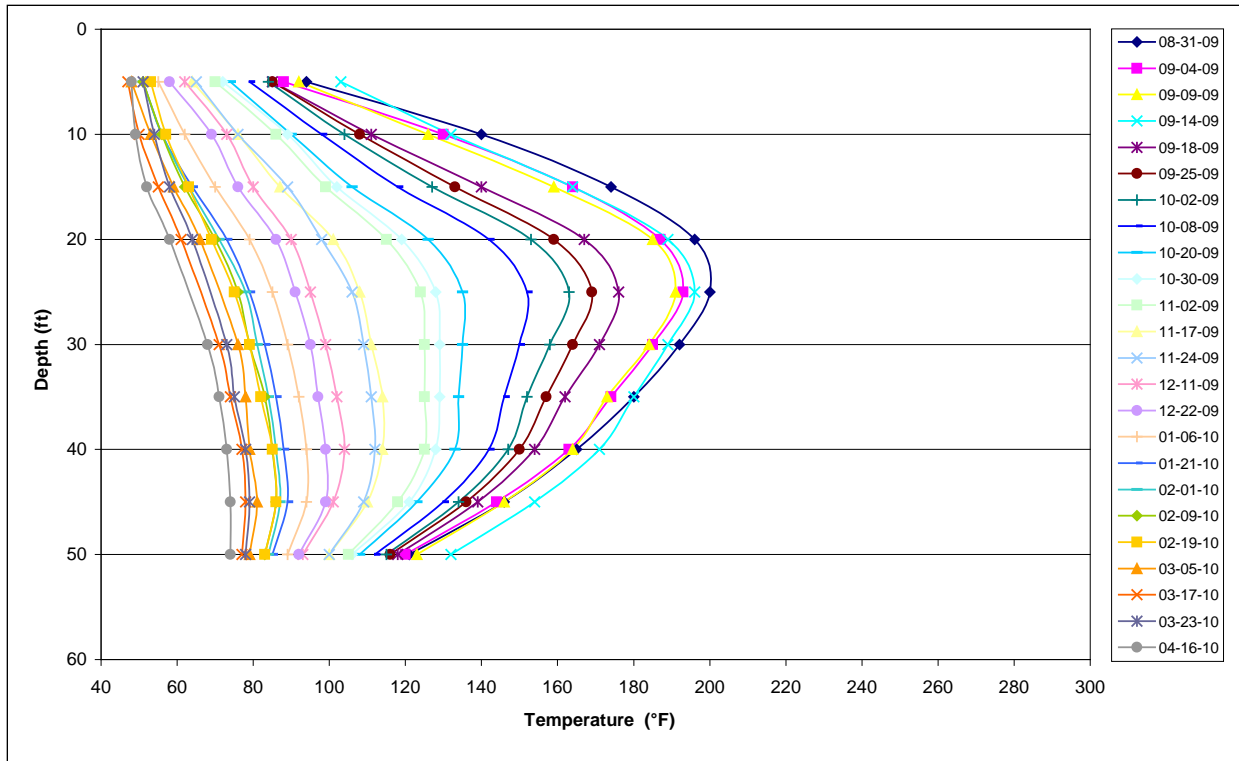


**Figure 3.3. Temperature at T1 during Cool-Down**

### **3.1.8 Performance Objective: Estimate Contaminant Mass in the Contaminated Zone while Quantifying Mass Recovered from Demonstration Area**

Success Criteria: Mass flux and totals will be calculated using flow rate and concentration data for vapor and water streams conveyed to treatment system; based on data collected from the cooled streams.

The data collected to evaluate this criterion were:

- Water and vapor balances.
- TCE concentration data in vapor and liquids.
- Estimate mass removed.
- Compare to mass estimates in the treatment volume based on rock chip data.

This objective was met, and the data presented in Figures 3.4 and 3.5. Approximately 500 to 650 lbs of TCE removed in the vapor phase, and 33 lbs in the liquid phase. Note that the mass removed was significantly higher than the estimated difference between TCE mass estimates in the rock before and after the treatment (Section 5.7).

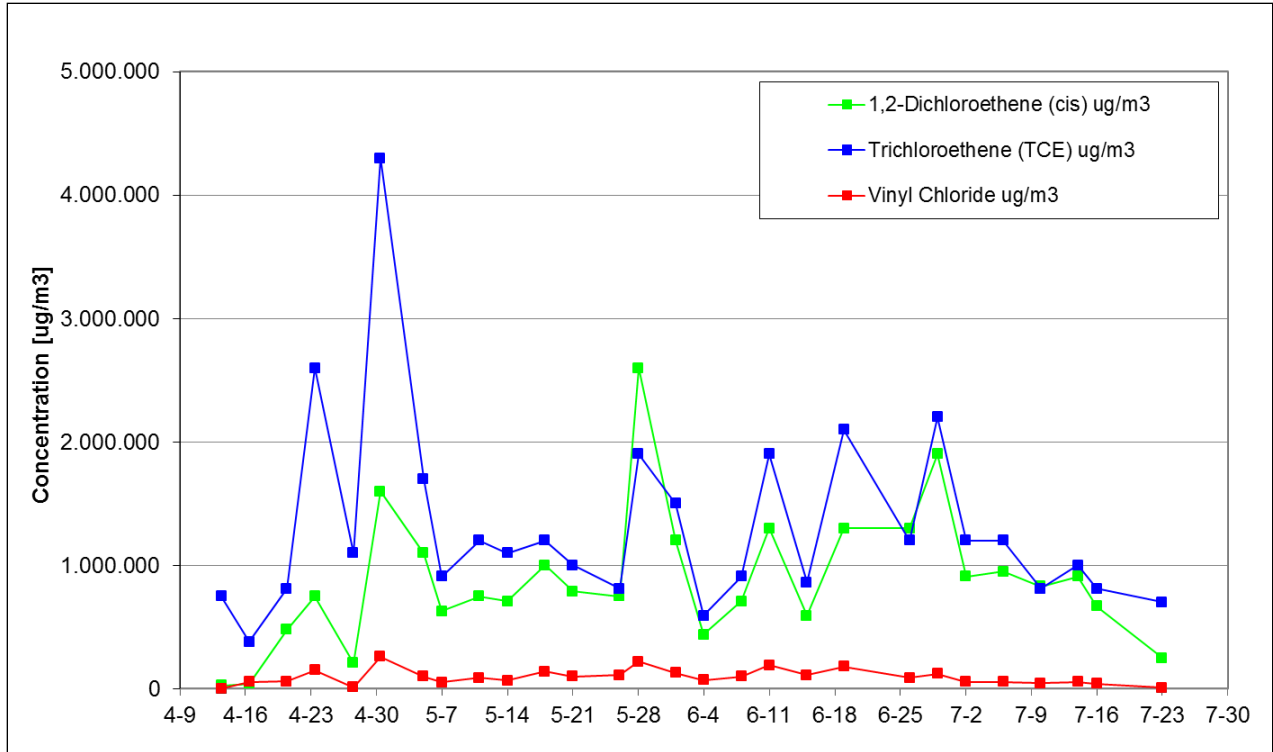


**Figure 3.4. Vapor Stream VOC Concentrations for the Dominant Compounds**

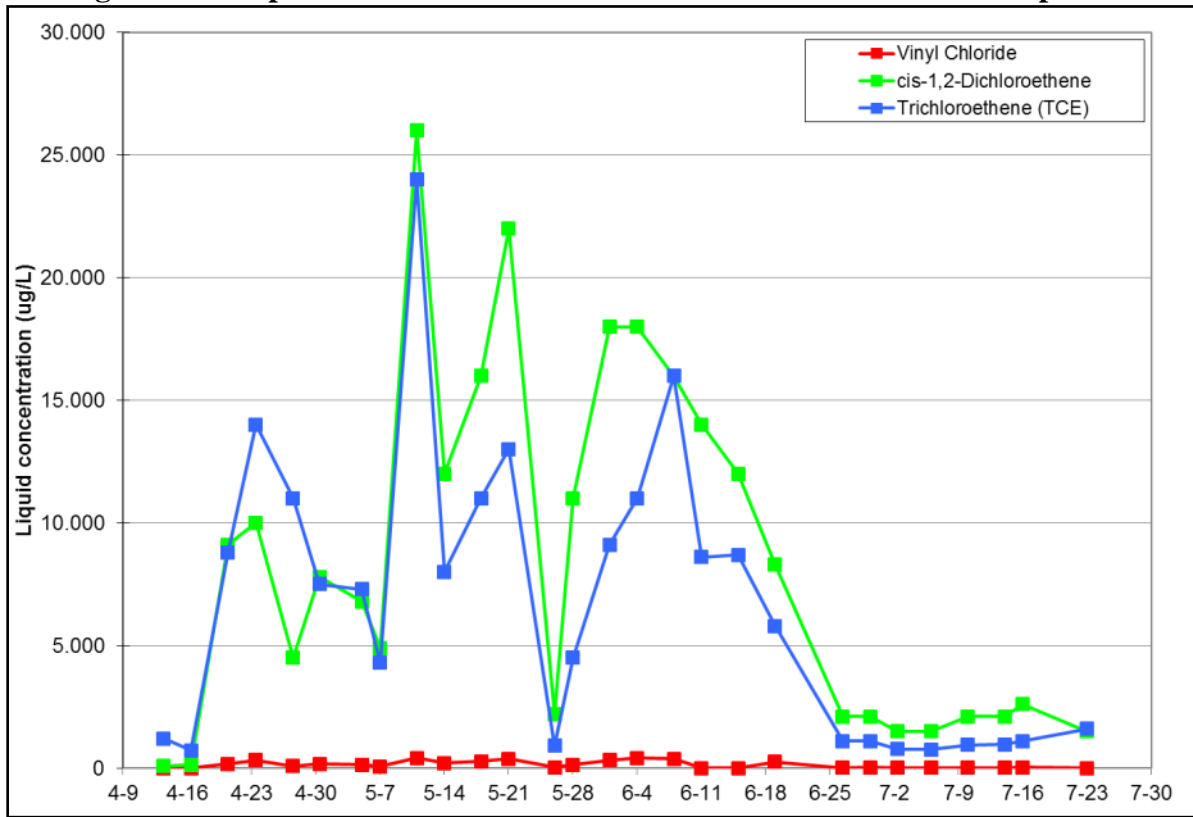


**Figure 3.5. Liquid Stream VOC Concentrations for the Dominant Compounds**

### **3.1.9 Performance Objective: Estimate Hazardous Materials Generated**

Success Criteria: NAPL recovered from condensing effluent vapors.

The data collected to evaluate this criterion was:

- Observation of any NAPL accumulating in the treatment system.

Interpretation and results: The objective was met. No NAPL was observed.

### **3.1.10 Performance Objective: Estimate Waste Generated**

Success Criteria: Quantify or estimate all major waste streams.

The data collected to evaluate this criterion was:

- Archiving/quantification of drill cuttings and recovered cores.
- Listing of all major wastes leaving the site.

Interpretation and results: The objective was met. Refer to Section 5.8.

### **3.1.11 Performance Objective: Factors Affecting Performance**

Success Criteria: Determine effect of groundwater flow through treatment zone, rock type impact, porosity, Organic carbon content and contaminant boiling point and hydrophobicity in treatability studies prior to the field demonstration. Validate effect during the field demonstration.

The data collected to evaluate these factors were:

- Estimate effect of groundwater flow through treatment zone.
- Rock type.
- Porosity.
- Organic carbon content.
- Contaminant boiling point and hydrophobicity.

Interpretation and results: The objective was met. The groundwater flow during thermal treatment was quantified (Figures 3.6 and 3.7), and shown to be five to ten times higher than expected. This was explained by the large quantities of groundwater entrained on the way through the vapor extraction points. This in turn affected the subsurface temperatures and reduced the heating efficiency in zones with large fractures, such as the depth interval between 40 and 50 ft bgs. Data on rock type, porosity, organic carbon content and contaminant properties were collected at Queen's University and are attached in Appendix C.

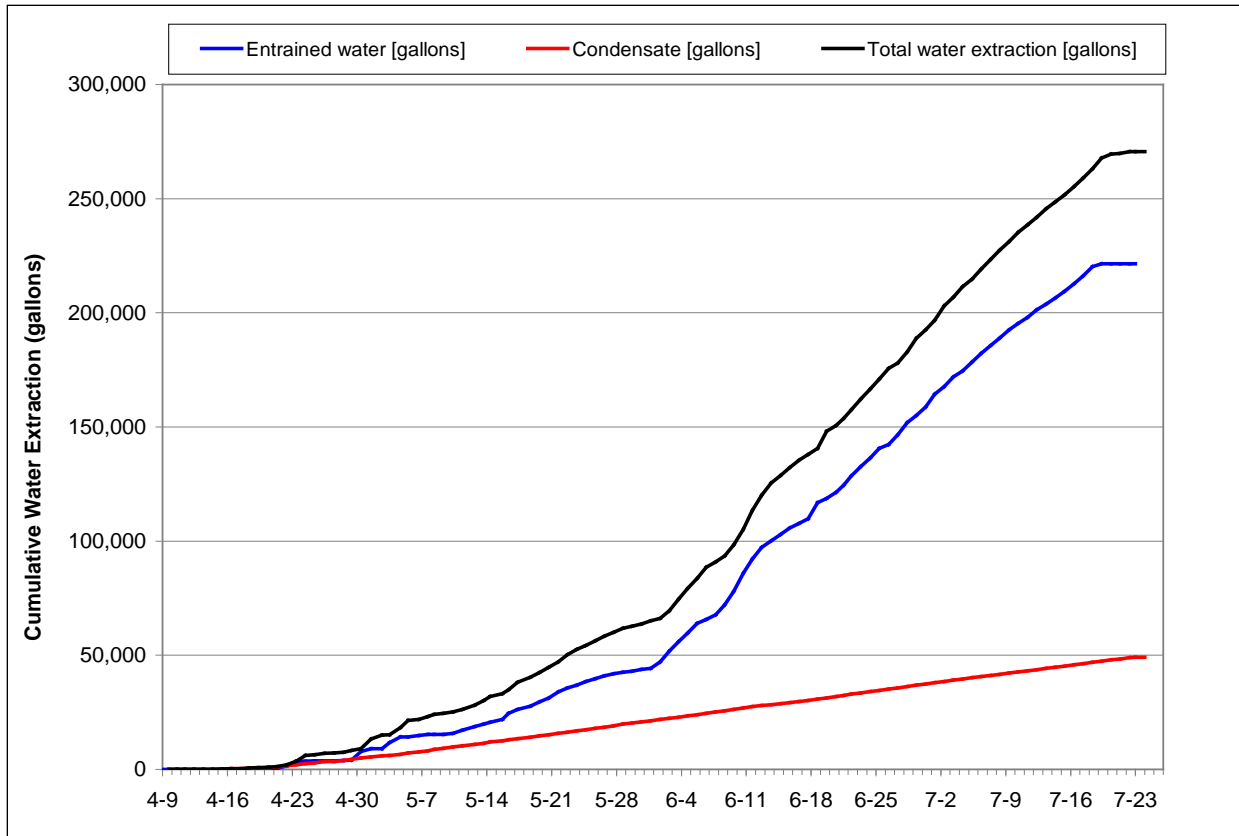


**Figure 3.6. Cumulative Water Removed during Treatment**

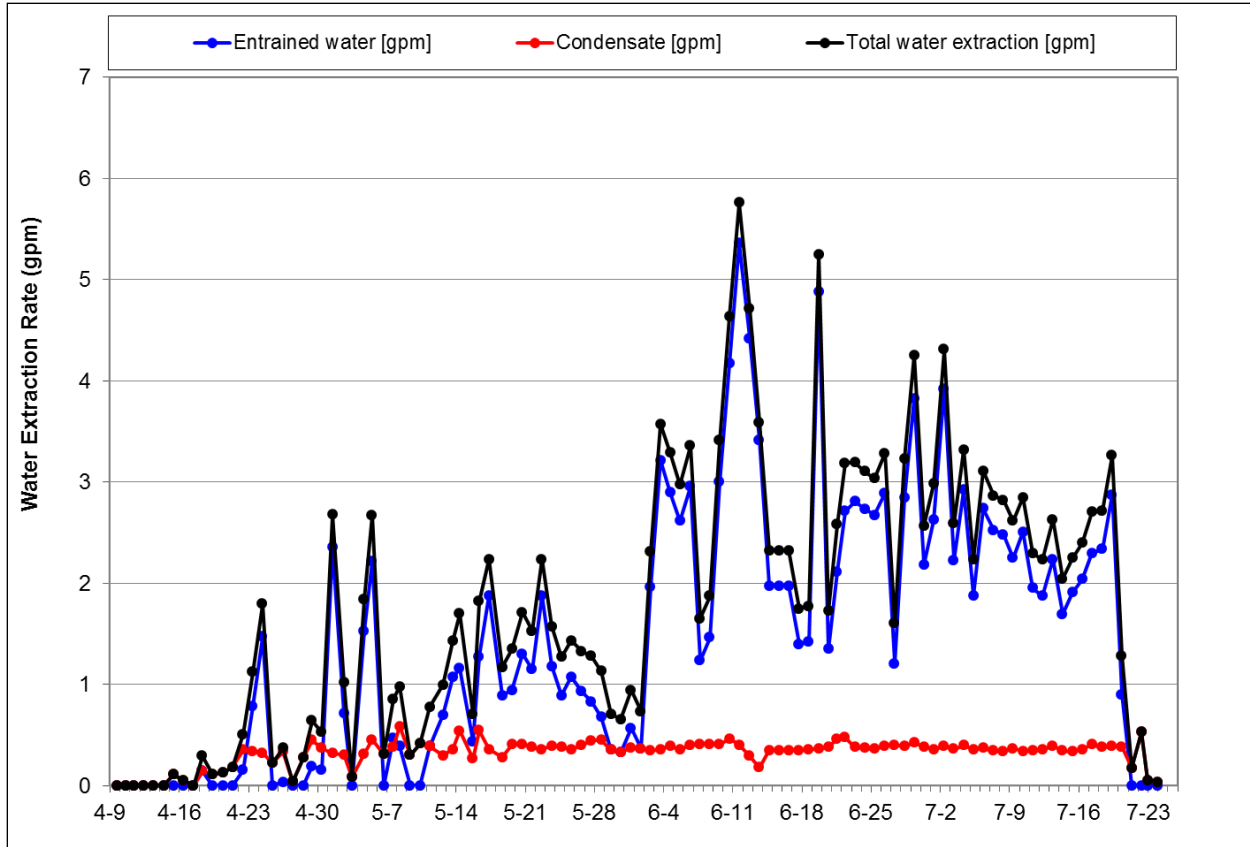


**Figure 3.7. Water Removal Rate during Treatment**

## **4.0 SITE DESCRIPTION**

The TCH field demonstration was conducted at a TCE impacted fractured rock site (USGS Chlorinated Solvents in Fractured Sedimentary Rock Research Site at the Naval Air Warfare Center (NAWC)) in West Trenton, New Jersey (resources available at: [http://toxics.usgs.gov/sites/nawc\\_page.html](http://toxics.usgs.gov/sites/nawc_page.html)). The NAWC site was ideal for this demonstration as it is well characterized, having in excess of 100 wells (at least 70 bedrock wells and 30 shallow wells). Several other technology demonstrations have been hosted at the site as well. These other demonstrations include: 1) single-well hydraulic testing to measure transmissivity, 2) assessment of contaminant distribution, 3) gauging evidence of intrinsic biodegradation and natural processes, 4) assessing efficacy of biostimulation and bioaugmentation, and 5) long term monitoring tools. Future and on-going work at the NAWC site includes: 1) estimating matrix diffusion, porosity and transport pathways, 2) understanding relationships between microbial degradation and rock geochemistry, 3) carbon isotope analysis, 4) geophysical time lapse monitoring, and 5) modeling. All demonstrations at the NAWC site (present and future) complement and did not duplicate the efforts of this project.

### **4.1 SITE LOCATION AND HISTORY**

The NAWC site was a U.S. Navy jet engine testing facility for military aircraft from the mid-1950's until the late 1990's. As a result of the activities at the facility, TCE, jet fuel, and other chemicals leaked into the subsurface. The NAWC covers 67-acres and has large jet-engine test buildings, associated service buildings, hangars, and scores of smaller support structures all interconnected with a vast network of aboveground and underground service lines.

NAWC was decommissioned on October 15, 1998 and since then it has been sub-parceled and sold. It is bordered by the Mercer County Airport on the east, north, and west and by Parkway Avenue on the south. Commercial and industrial firms occupy the south side of Parkway Avenue. Freight train tracks separate the eastern from the western part of the base.

Investigations of the ground water contamination at the site began in the late 1980's. By the mid-1990's, the pump and treat (P&T) facility was in operation. The Navy demonstrated to the EPA that the pump and treat facility remedy was operating properly and successfully.

The site subsurface is dominated by sedimentary rocks, with silt- and mudstone making up the majority of the sequence. The rocks are heavily weathered from land surface to a depth of about 5 ft and as a result, this portion of the bedrock behaves like an unconsolidated aquifer. Bedrock from 5 to 50 ft ranges from very weathered to unweathered. Water is transmitted in heavily weathered zones and in succinct fractures and partings. At depths greater than 50 ft below land surface, the bedrock is generally unweathered and water is transmitted via succinct fractures or partings. The unstressed regional hydraulic gradient in the bedrock aquifer is southward toward the west branch of Gold Run, but the ground-water flow direction is westward toward the spring. The cone of depression caused by pumping of contaminant and recovery wells at the site is asymmetric with a ratio of at least 4:1. The preferential flow directions in the bedrock aquifer are along bedding, strike, and dip.

TCE and jet fuel in the Site 1 area leaked onto land surface between buildings 40 and 41. Some of the TCE and the jet fuel were intercepted by storm sewer lines and discharged to a local creek, a tributary to the Delaware River. The remaining TCE evaporated, sorbed onto the sediments, and flowed downward into the fractured bedrock aquifer. The remaining jet fuel infiltrated to the water table. TCE that intercepted spilled jet fuel began to biodegrade rather rapidly. TCE that flowed deeply into the fractured bedrock did not biodegrade rapidly, if at all.

The conceptual model for the site is that TCE mass was held tightly in the rock matrix, and potentially in some of the fractures at the site. The TCE had dissolved, diffused, and adsorbed to the solid rock matrix (silt and mudstones). The demonstration location at the site is shown on Figure 4.1 and an aerial view of the demonstration location at the site is shown on Figure 4.2.

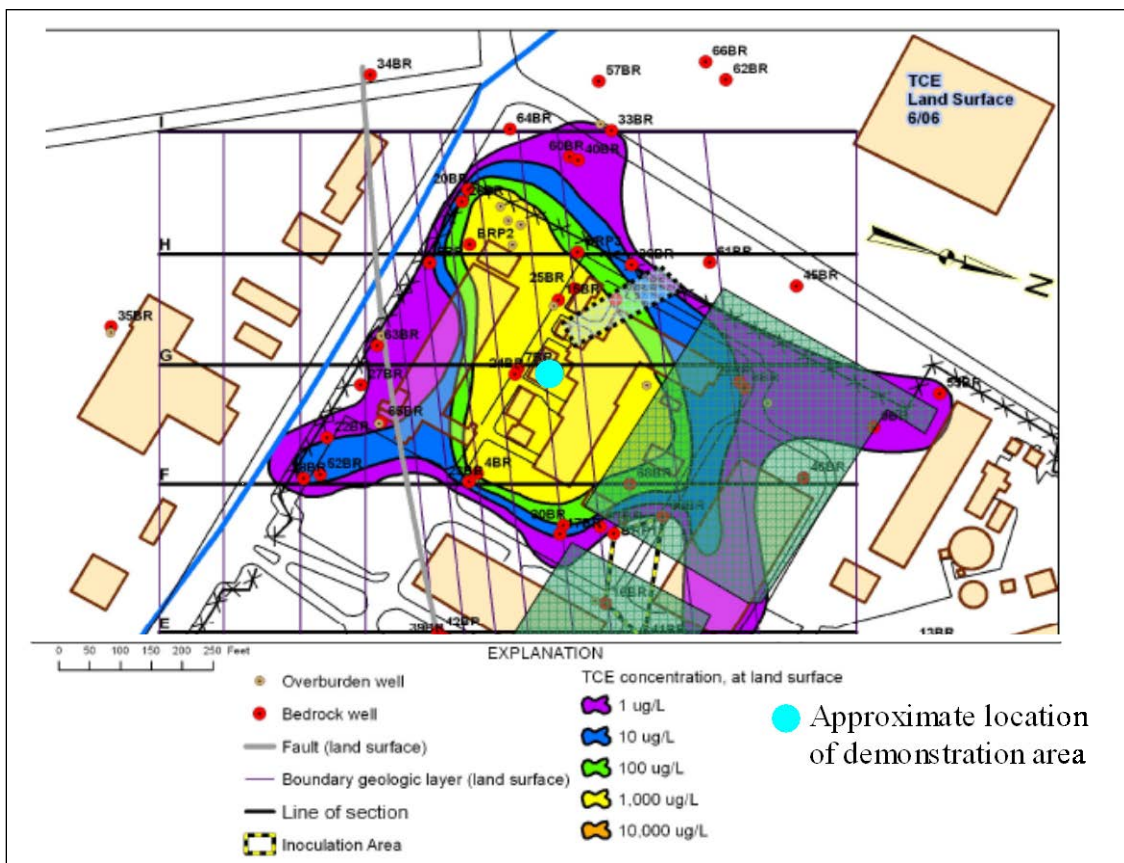


**Figure 4.1. Map showing TCE Concentration Contours in Groundwater and the Approximate Location of Field Demonstration Area**  
*Courtesy of USGS*

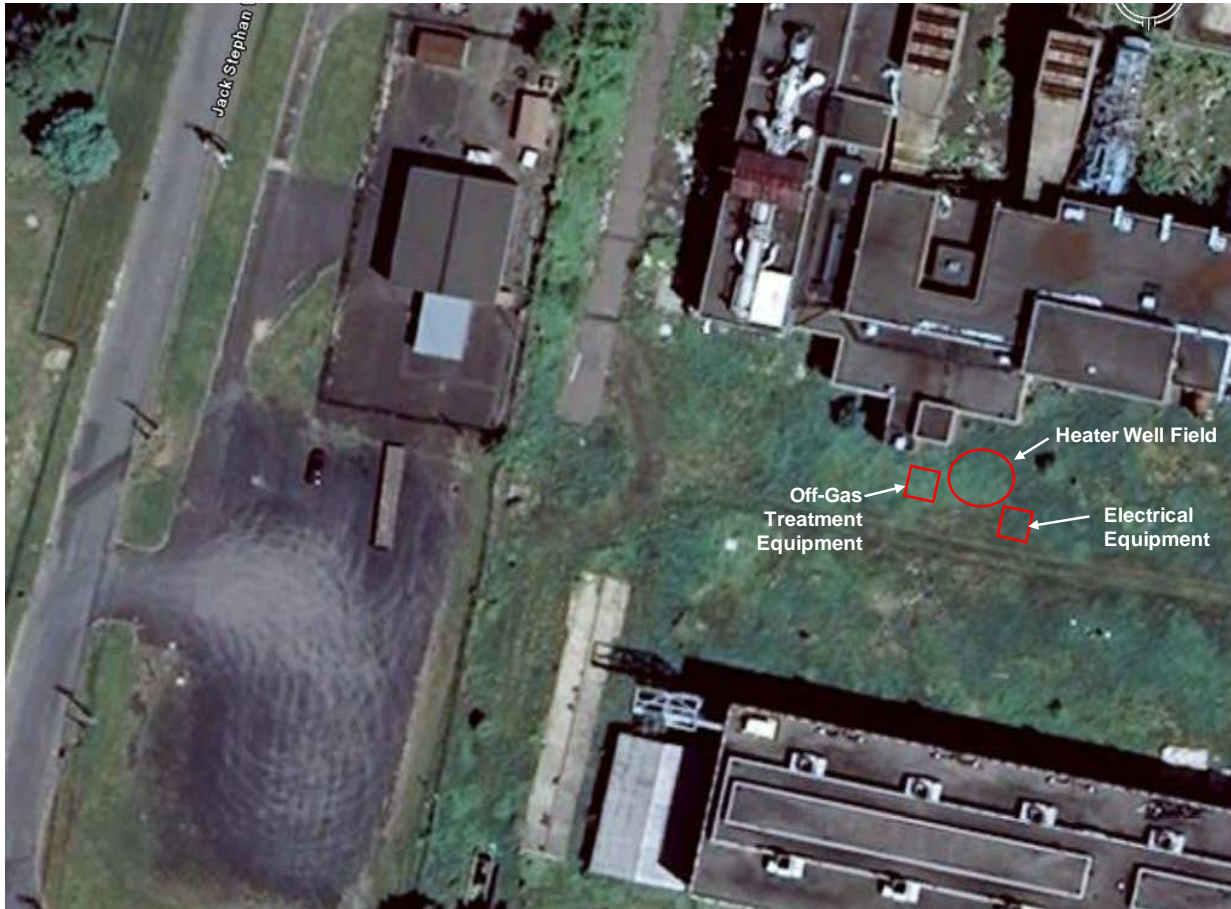


**Figure 4.2. Aerial View Showing the Approximate Location of Field Demonstration's Process Treatment Equipment, Electrical Equipment, and Heater Wellfield**

## **4.2 PRESENT OPERATIONS**

In 1993, the USGS began studies at the NAWC site in cooperation with the U.S. Navy. In 2001 the NAWC site became a fractured rock research site under USGS Toxics Substances Hydrology Program. The NAWC site was selected as a Test Site because the site's hydrogeologic conditions are well characterized. Research being conducted at the NAWC will help improve the understanding of the transport and fate of chlorinated solvents in fractured-rock aquifers and will compare the effectiveness of different remedial approaches. The cooperative effort that began in 2001 includes scientists from the Navy, New Jersey Department of Environmental Protection, New Jersey Geological Survey, and universities and other research institutions. In 2005 a biostimulation and bioaugmentation study was conducted by Geosyntec Consultants and ECOR Solutions on behalf of the Navy. Research support is mostly sponsored by the USGS, the Navy, the U.S. Environmental Protection Agency (EPA), and the U.S. Department of Defense SERDP and ESTCP.

Current operations at the site include an active P&T system. As mentioned earlier, the site was sold as parcels to several parties. The portion where the TCH demonstration took place is currently owned by Nassimi Realty. Nassimi Realty has plans to develop the parcel into a retail sale shopping area which will include a Lowes Home Improvement Warehouse.

### 4.3 SITE GEOLOGY

The Thermal Conductive Heating (TCH) research site at the former Naval Air Warfare Center (NAWC) (Figure 4.3) is within the Newark Basin geologic province and is underlain by mudstone of the Skunk Hollow, Byram, and Ewing Creek Members of the Lockatong Formation (Lacombe and Burton, 2010). Lacombe divided the bedrock at the NAWC into strata using two techniques. The first and simplest technique divides the strata using the natural gamma signature. This method divided the bedrock into 11 layers (L-11 to L-22) on the basis of high and low counts per second of natural gamma logs. This geophysical method is rapid but provides low resolution of individual strata. The second method divides the strata on the basis of rock-core descriptions following a modified Van Houten deposition scheme (Olsen and others, 1996). The rock-core method divided the bedrock at NAWC into 43 strata on the basis of the following four broad rock types (a generic identifier is included for each rock type; fig. 4.2):

- |   |  |
|---|--|
| (1) black, carbon-rich mudstone [Carb.190], | (2) dark gray, layered mudstone [Lay.201], |
| (3) light gray, massive mudstone [Mas.191], | (4) red, massive mudstone [Red.279].       |

A geologic column for the TCH research site (Figure 4.4) was created by correlating three natural gamma and rock-core logs for the TCH site with similar logs from wells that are along strike and within the USGS/SERDP research site and logs for the full NAWC site. The three natural gamma logs for the most updip, central, and most downdip boreholes are shown in Figure 4.2. The composite natural gamma logs are coupled with the lithologic descriptions of the rock core from the TCH site, the USGS/SERDP 2008-12 research site, and other NAWC borehole sites to create a geologic column showing and describing the geologic and natural gamma stratigraphy.

The pilot study area geologic map, geologic column, and section A-A (Figures 4.3-4.5) show the TCH research site is predominately in layer L-19, a low gamma-count-per-second strata, and partly in the base of layer L-20, a high gamma-count-per-second strata. The map and section show that the TCH research site crosses the 14 rock-core stratigraphic layers from Lay.251 to Lay.178. The rock cores show that the bedrock includes four thin carbon-rich mudstones; six layered mudstones; and five massive, light gray mudstones. Section B-B' (Figure 4.6) provides high definition of the strata from borehole HO-01 to HO-15 through the center of the TCH array of heating wells.

Folds, faults, and joints within the bedrock were developed at great depths by tectonic compression during the Jurassic (Herman 2005). All strata in the TCH area are gently folded with a similar strike and dip. Three-point computation of the strike and dip confirm that the bedrock at the TCH research site is N66°E and 28°NW, which is similar to the strike and dip determined from other boreholes in areas along strike at the NAWC. The carbon-rich strata generally developed the greatest number of bedding slip faults and the highest density of strata bound joints. As a result, these strata are much more fissile than most of the other strata. The massive strata developed the least bedding faults and the lowest density of strata bound joints and, therefore, are more indurated. The layered mudstone has fewer joints and fault features than the carbon-rich strata and more than the massive strata.

Weathered mudstone from land surface to about 25 to 30 feet (ft) below land surface (BLS) is visually, chemically, geophysically, and hydraulically different from the same stratum that is unweathered and from about 25 or 30 ft BLS to 55 ft BLS. The weathered mudstone stratum ranges from unconsolidated muds to highly fissile and highly fractured bedrock as a result of differential degradation of the various types of mudstone strata. Weathered mudstone contains a great deal of iron oxide staining and rarely contains secondary minerals, such as calcite and analcime, in fracture and vug fillings. Pyrite and other sulfide crystals generally are fully weathered. Strata that are at depth and that have a high natural gamma count signature owing to uranium concentrations generally have a greatly diminished gamma count signature in the weathered zone as a result of mobilization of uranium during weathering. Weathered mudstone has a higher hydraulic conductivity than the same strata located at a greater depth.

Mudstone strata from about 30 ft BLS to about 250 ft BLS is physically and hydraulically different from the same strata that are at a depth greater than 250 ft BLS. The physical and hydraulic differences are predominantly due to lithostatic pressures. The reduced lithostatic pressure at 30 to 250 ft BLS permits bedding plain faults and orthorhombic joints to open and transmit small but important amounts of water. The most transmissive zones at this depth may show minor iron staining features.

Mudstone strata at depths greater than 250 ft BLS are physically and hydraulically different than the same strata at a shallower depth. A deeply buried stratum generally shows no chemical or physical changes. All deep strata are indurated. Bedding faults, bedding partings, and joints are rarely open and groundwater flow is virtually nonexistent.

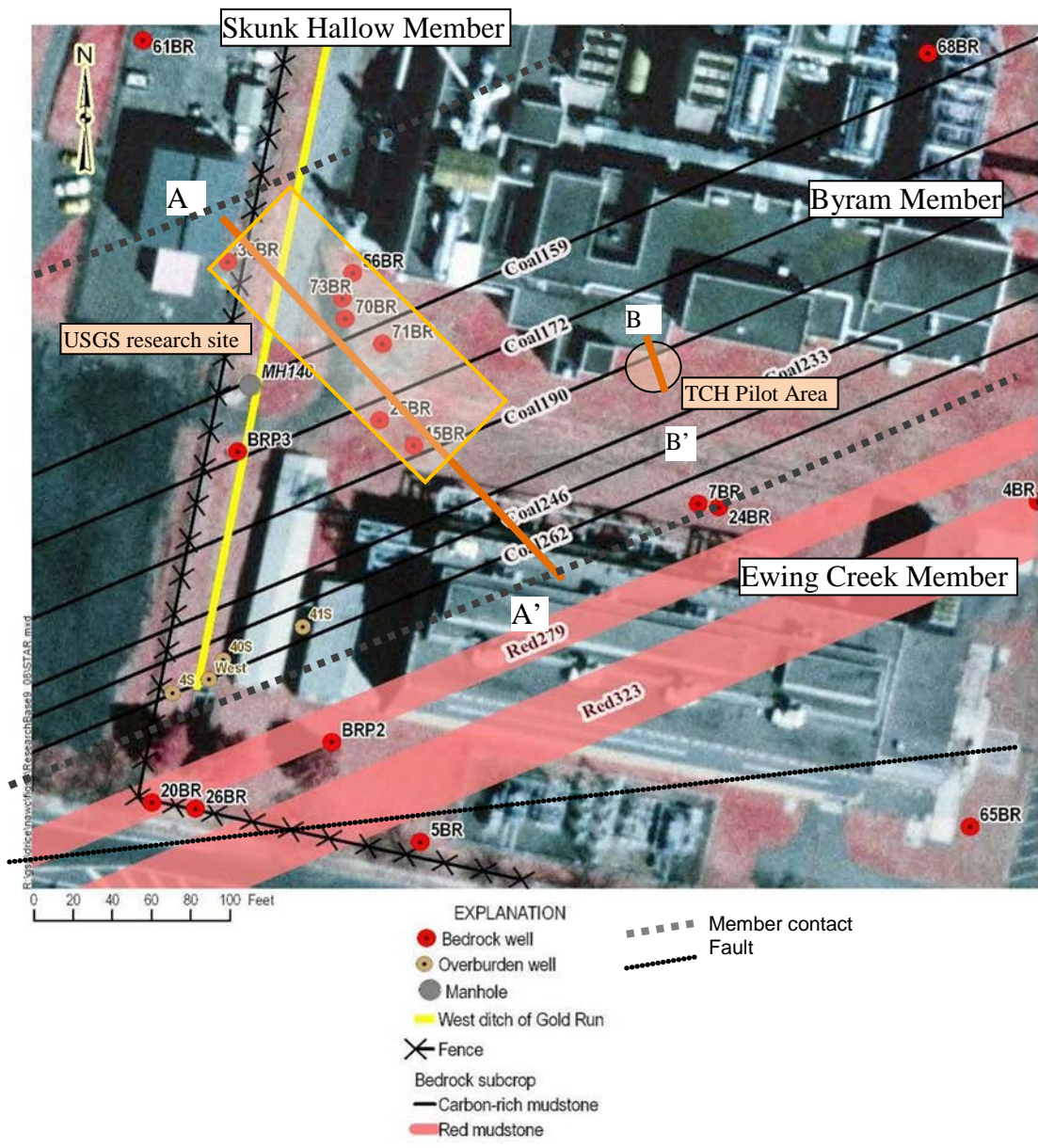


**Figure 4.3. Geologic Map Showing Locations of Subcrops of Selected Strata around the TCH Demonstration Site and the Location of Sections A-A' and B-B', NAWC, Trenton, NJ**  
*Courtesy of USGS*

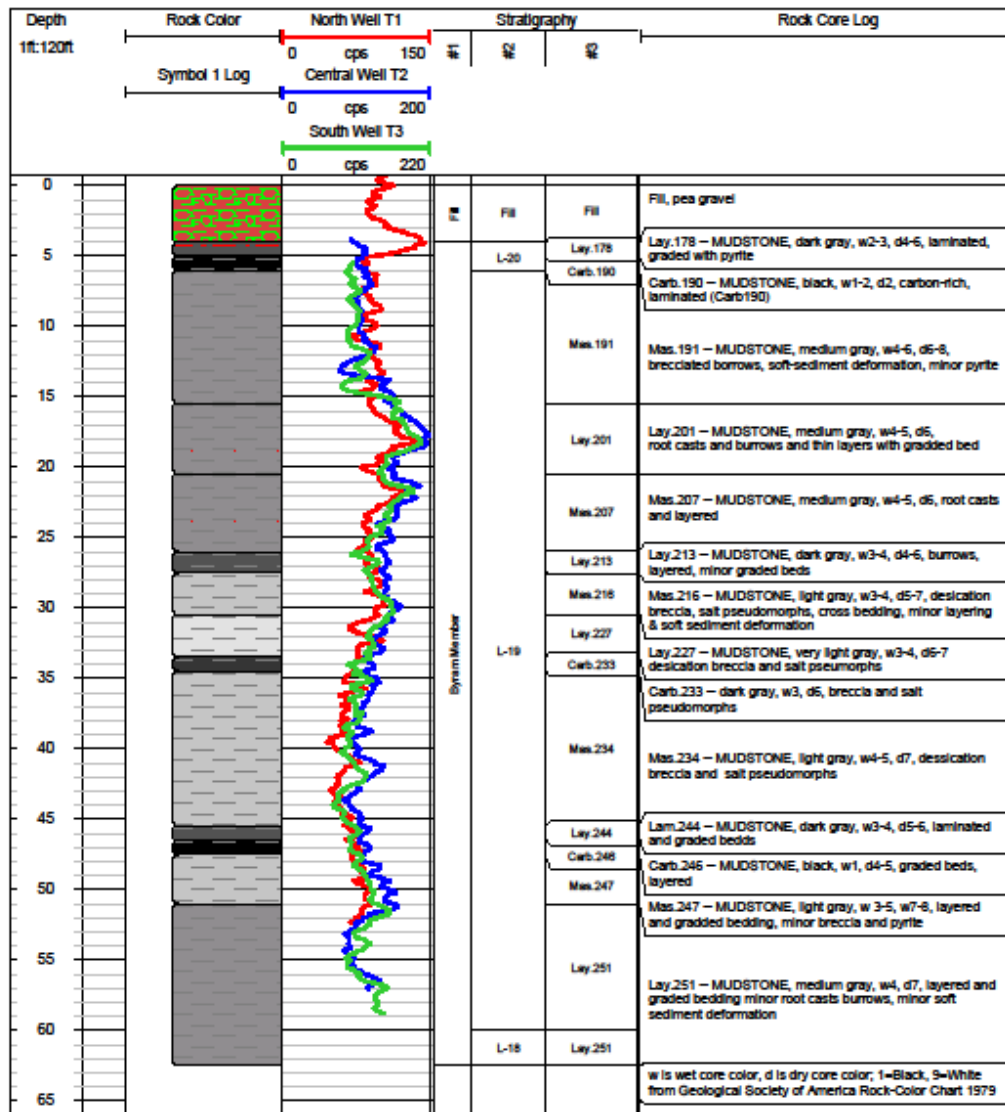
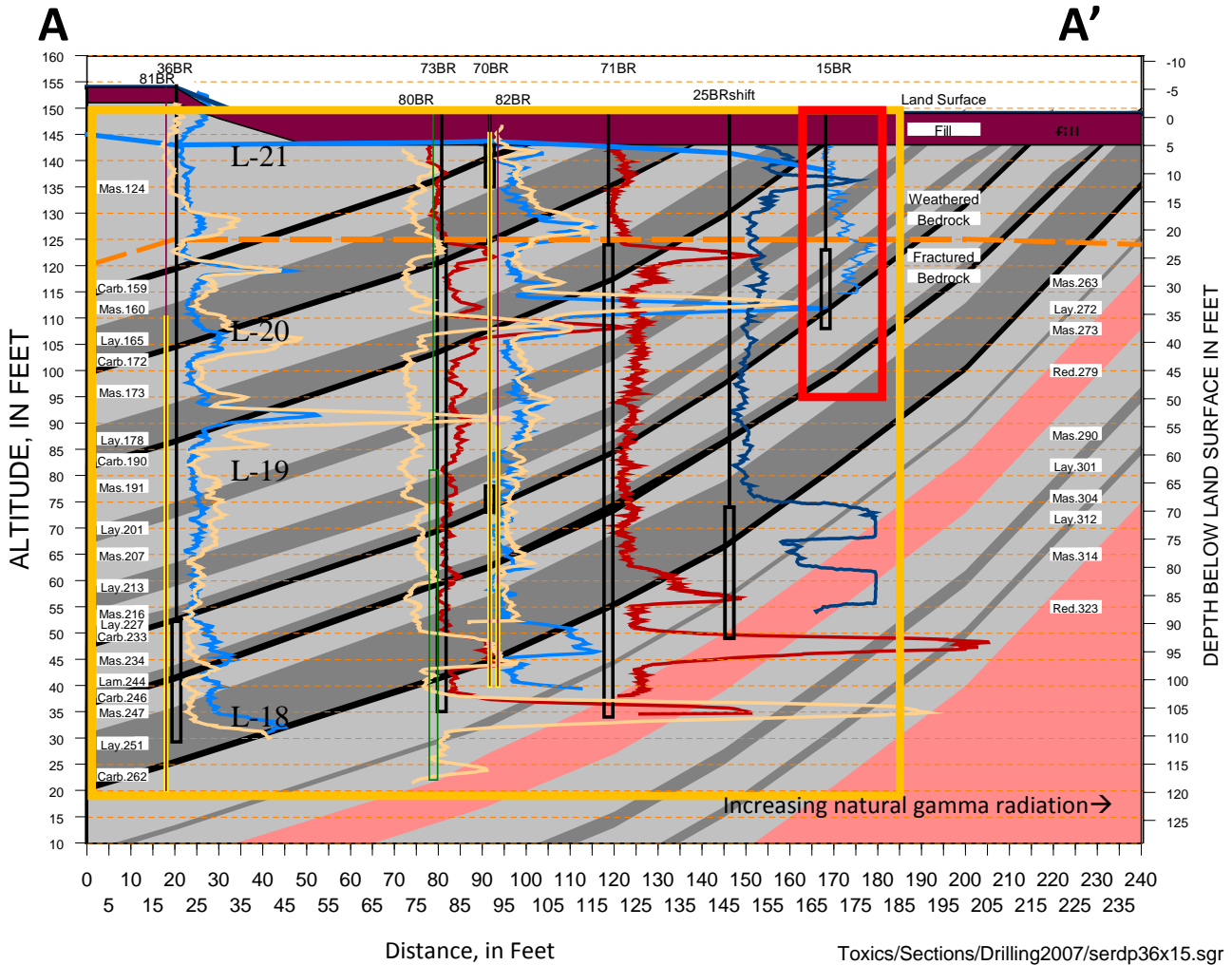
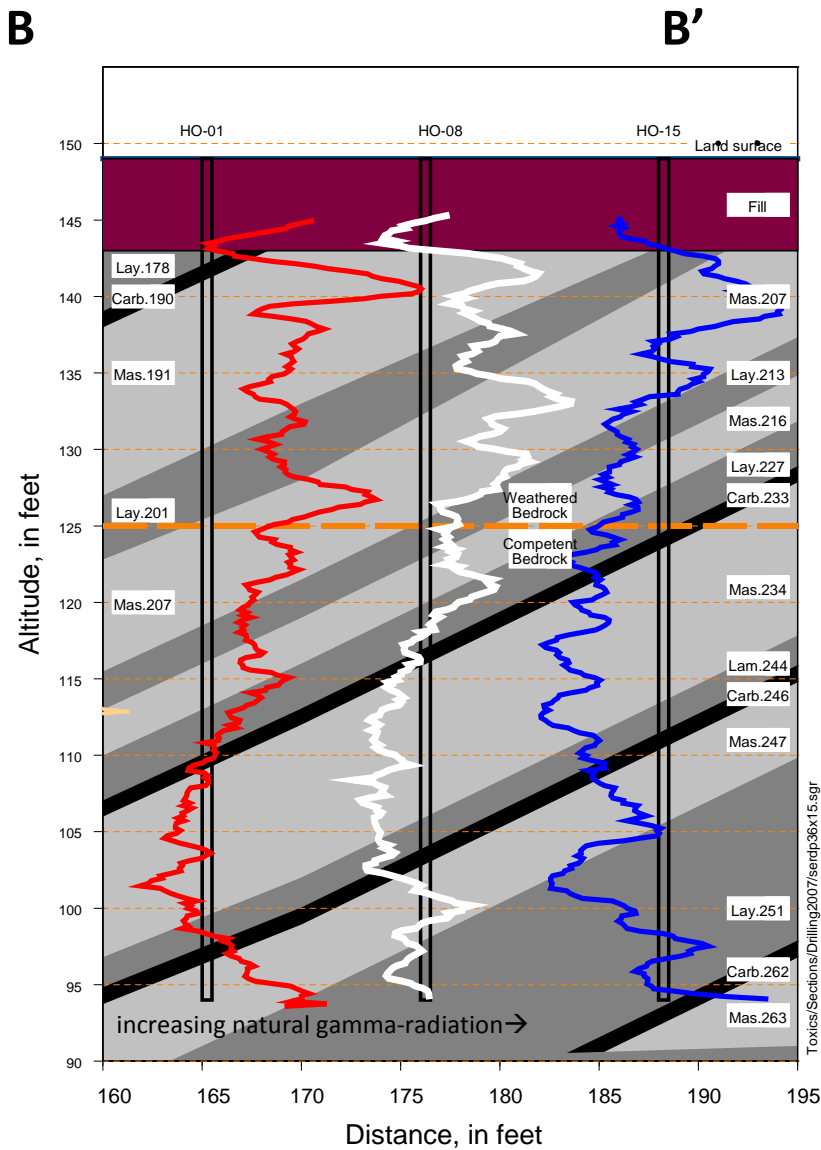


Figure 4.4. Geologic Column of the TCH Demonstration Site, NAWC, Trenton, NJ (Color of Core Range from 1 Black to 9 White and Shades of Gray from 2 through 8, w, wet; d, dry)  
 Courtesy of USGS



**Figure 4.5. Section A-A' Showing Geologic and Natural Gamma Geophysical Strata for the TCH Demonstration Site (red box) and USGS/SERDP Research Site (orange box), NAWC, Trenton, NJ**  
*Courtesy of USGS*



**Figure 4.6. Geologic Section B-B' of the TCH Demonstration Site Showing Strata, Weathered and Competent Bedrock, and Natural Gamma Geophysical Logs from 3 of 23 Boreholes, NAWC, Trenton, NJ**  
*Courtesy of USGS*

#### 4.4 SITE HYDROGEOLOGY

Two major hydrostratigraphic zones are present within the bedrock at the NAWC and the TCH research site. The shallow zone (0 to 25 ft BLS) contains highly weathered mudstone that is

gently dipping and has a low lithostatic pressure. This zone is hydraulically conductive, and groundwater flows as it would in porous media. The deeper zone (25 to 60 ft BLS) contains unweathered mudstone that is gently dipping and under medium lithostatic pressure. This zone has a greatly diminished hydraulic conductivity when compared to shallower strata. Groundwater flow in this zone is within discreet fractures, such as bedding faults and joints, and is truly fractured bedrock flow.

Lewis-Brown and others (2006) report hydraulic characteristics that are based on an aquifer test during pumping of well 15BR (Figure 4.3). The well used for the aquifer test intersects strata identical to that at the TCH research site and is less than 100 ft southwest and along strike of the TCH research site. The transmissivity for the test was 1,300 square feet per day ( $\text{ft}^2/\text{d}$ ), and the storage coefficient was  $5 \times 10^{-3}$ . Lewis-Brown and others also report that the vertical hydraulic conductivity for 15BR is 140 feet per day ( $\text{ft}/\text{d}$ ), which is based on a slug test, and 9.4  $\text{ft}/\text{d}$ , based on the groundwater flow model. Tiedeman and others (2010) report the transmissivity for the following strata in the USGS/SERDP research site: upper weathered zone (184  $\text{ft}^2/\text{d}$ ), lower weathered zone (0.68  $\text{ft}^2/\text{d}$ ), unweathered dipping mudstone with high hydraulic conductivity (0.99 to 990  $\text{ft}/\text{d}$ ), and unweathered dipping mudstone with low hydraulic conductivity ( $2.6 \times 10^{-3}$   $\text{ft}/\text{d}$ ). Primary porosity of the shallow, highly weathered but indurated bedrock is up to 15 percent. Fissile rocks likely have a much higher porosity. At depth, the indurated rock has a porosity of 3 to 5 percent.

The ambient hydraulic characteristics at the TCH research site were likely altered after installation of 23 boreholes in a cylindrical area that is 22 ft in diameter and 55 ft deep. Each borehole was drilled using a sonic drilling rig with a 6-inch drill bit. Holes are generally 1.5 to 6 ft from a nearby borehole. The closely spaced boreholes and the high vibrations created during sonic drilling produced a massive network of fractures in the TCH research site and radically increased the hydraulic conductivity of the bedrock. The New Jersey licensed driller reported that the first completed borehole in the TCH research site pumped at a maximum rate of less than 1 gallon per minute (gpm); a pumping rate that is typical for many of the 105 monitoring wells located at the NAWC. The driller also reported that the last three or four boreholes were pumped at a rate of about 40 gpm. The average pumping rate of higher producing wells at the NAWC typically is 4 to 10 gpm. Only one well (15BR) is known to produce water at greater than 10 gpm (15 gpm).

The geologic strata of the TCH field demonstration area from land surface to 6 ft BLS, shown in section B-B' (Figure 4.6), consists of highly weathered native material that was excavated in 1998 because of high chlorinated volatile organic compounds (CVOC) concentrations and replaced with clean fill. From 6 ft BLS to about 24 ft BLS, bedrock contains fractures, faults, and joints that are open, and chemical weathering has increased the transmissivity. From 24 to 55 ft BLS, the major fractures are bedding plane faults with some strata bound by vertical joints.

#### **4.5 CONTAMINANT DISTRIBUTION**

The TCH pilot study area (Figure 4.3) is near the center of the main CVOC plume (Figures 4.7 and 4.8). The plume is defined using concentrations of trichloroethylene TCE in groundwater samples from transmissive fractures. TCE at the NAWC also is present as pure phase, aqueous

phase in the primary porosity and adsorbed phase attached to carbon-rich, clay, and zeolite minerals. CVOCs in the groundwater have been contained by a pump and treat (P&T) system since 1996. Concentrations in water samples from most monitoring wells have decreased as a result of P&T and monitored natural attenuation (MNA).

In the TCH research area, the CVOC plume consists of TCE and the degradation products cis-1,2-dichloroethene (cDCE) and vinyl chloride (VC). Water samples collected during 2009–11 from wells 07BR and 24BR, located less than 50 ft from the TCH field demonstration site, contained TCE concentrations ranging from 5,000 to 60,000 micrograms per liter ( $\mu\text{g/L}$ ) (Figure 4.9). cDCE concentrations ranged from 10,000 to 25,000  $\mu\text{g/L}$ , and VC concentrations ranged from 500 to 2,000  $\mu\text{g/L}$ . As of 2012, the major CVOC contamination plume is 75 to 125 ft BLS. Excavation, P&T, and MNA have reduced the aqueous phase TCE in the fractures. The extent of TCE in the aqueous phase or as DNAPL in the primary porosity is unclear.

Drill cutting samples collected in 2008 from well 70BR located 120 ft west of the TCH study area contained DNAPL TCE (Figure 4.8). Rock-chip samples from 70 BR (Figure 4.3) contained TCE in the rock pores and adsorbed to the rock in concentrations exceeding 100,000,000  $\mu\text{g/L}$ . CVOC concentrations that are adsorbed and in the primary porosity of rock core for the TCH site are found in Section 5.7.2.

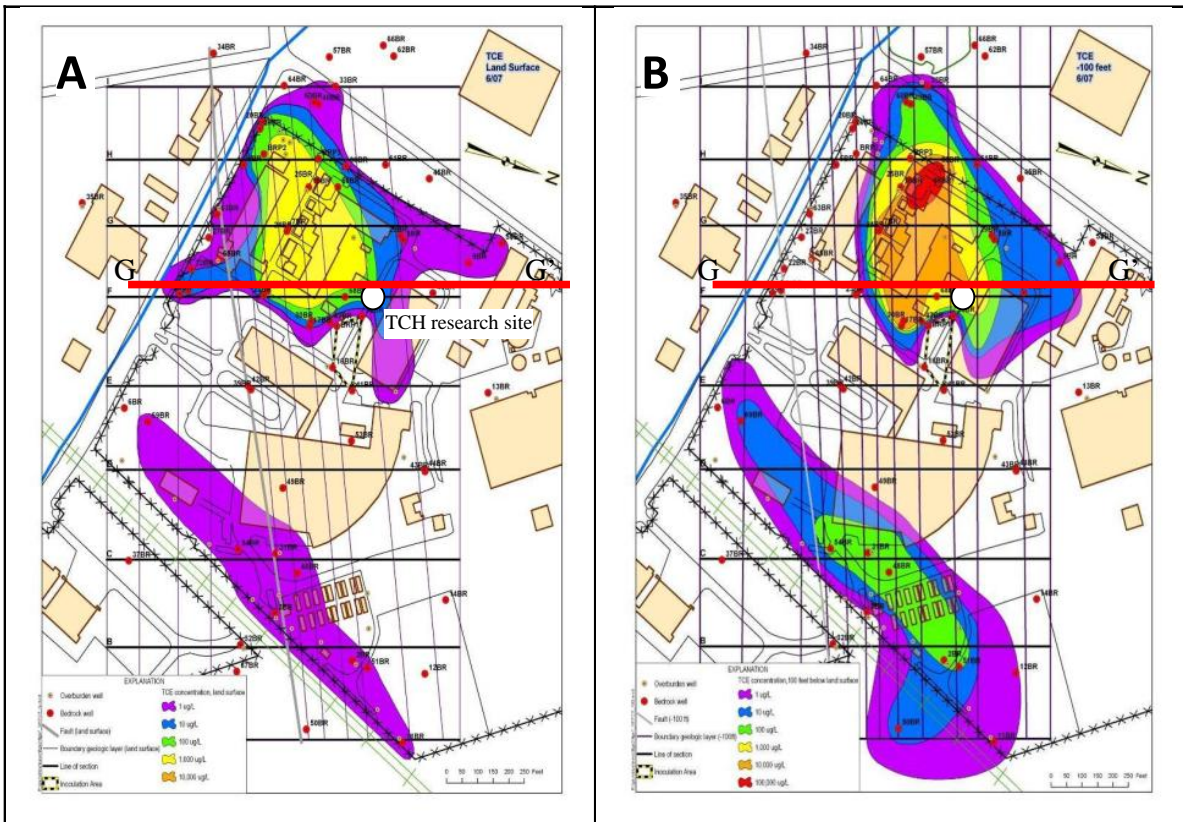


**Figure 4.7. TCE Concentrations in Water Samples from Hydraulically Active Fractures (A) near Land Surface and (B) at 100 Feet below Land Surface, NAWC, Trenton, NJ**  
*Courtesy of USGS*

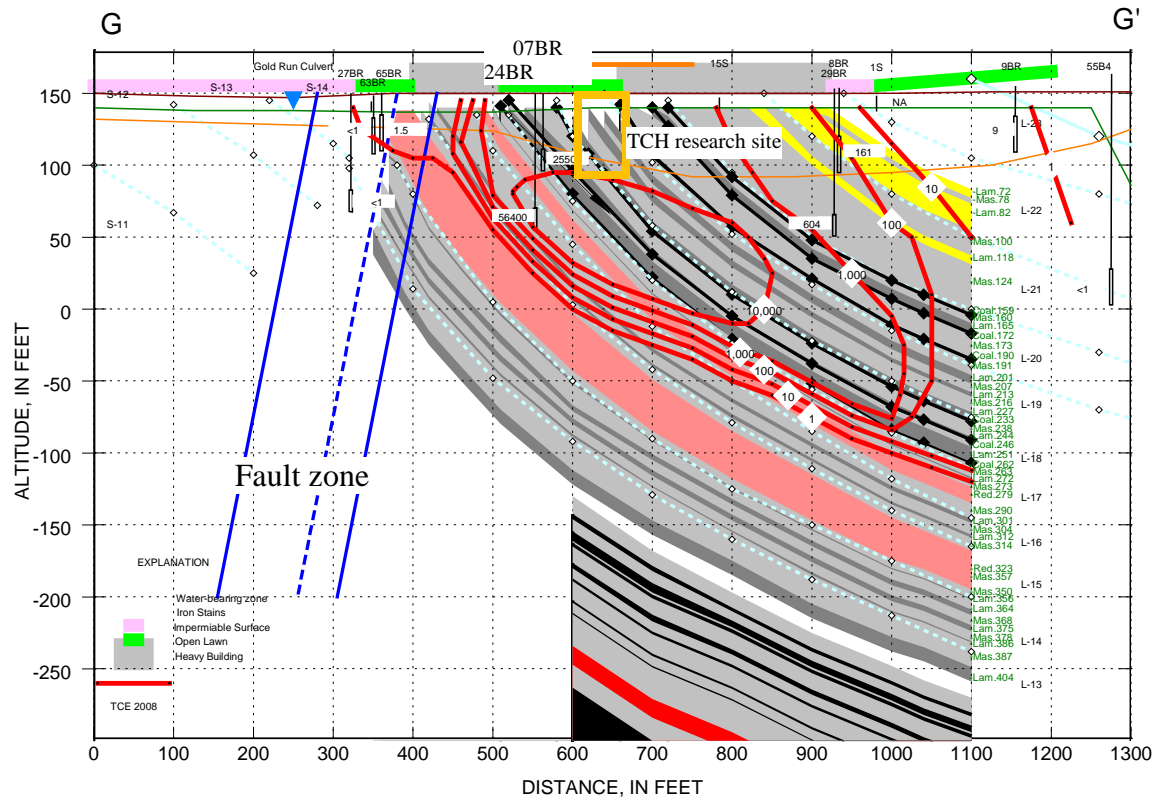
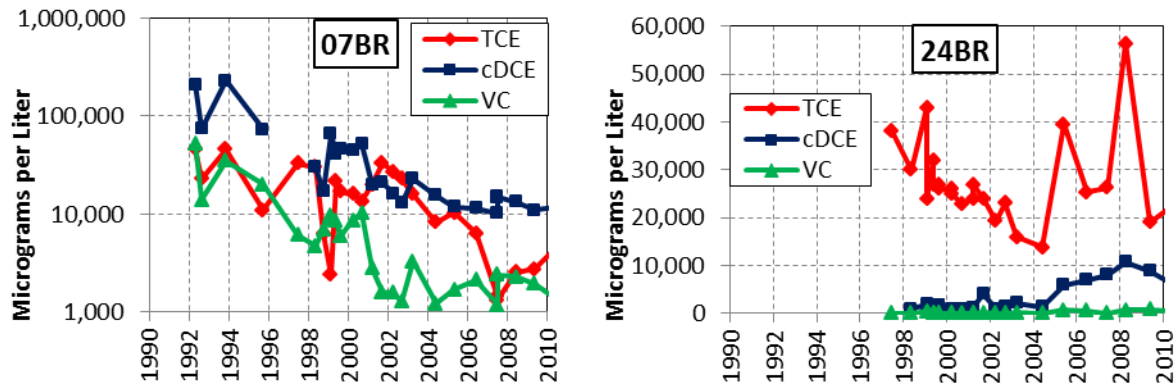


Figure 7g. Section G-G' showing TCE concentrations and contour lines, Summer 2008, Naval Air Warfare Center, West Trenton, N.J.

SPlus//Toxics/Sections/June07/FrameGG.TCE07.sgr Apr. 24, 2009 3:43:31 PM

**Figure 4.8. Section G-G' Showing the Local Geology and Concentrations (micrograms per liter) of Aqueous Phase TCE in Hydraulically Active Fractures, NAWC, Trenton, NJ**  
*Courtesy of USGS*



**Figure 4.9. Graphs Showing Concentrations of Aqueous Phase TCE, cis-DCE, and Vinyl Chloride in Water Samples from Hydraulically Active Fractures Wells (A) 07BR and (B) 24BR, NAWC, Trenton, NJ**  
*Courtesy of USGS*

## **5.0 TEST DESIGN AND OPERATIONAL CONDITIONS**

The following sections present the conceptual experimental design and the baseline characterization completed prior to mobilization to the TCH field demonstration site. A description of the most significant phases of the demonstration and the sample methods used are described in this section as well. As TCH is an off the shelf commercial technology, the conceptual experimental design typically described in Section 5.1 was not required. Instead, Section 5.1 of this document describes the design and layout of technology components and has been expanded so as to provide additional details on the operating components of the technology.

### **5.1 DESIGN AND LAYOUT OF TECHNOLOGY COMPONENTS**

The TCH remediation process entails the use of equipment installed above and below ground for the treatment of subsurface contaminants. The major underground and aboveground operating components of the TCH system are described in general terms in the sections below.

#### **5.1.1 TCH Well Installations**

A summary of well installations is provided below. The well system consists of heater borings, vapor extraction points, and temperature monitoring points.

Design of TerraTherm's thermal wells is proprietary and protected by one or more U.S. and international patents. The total number of borings installed for the field demonstration was as follows:

- 15 TCH heater borings (designated HO-1 through HO-15);
- 15 vapor extraction points installed next to the heater wells (co-located borehole); and,
- 8 temperature monitoring points

The wells are further described below.

##### **5.1.1.1 Drilling Method**

Sonic drilling was used to install the wells at the Site. The sonic drilling rig uses a combination of mechanically generated vibrations and limited rotary power to penetrate the rock. The drill head attached to the drill pipe has two counter-rotating out-of-balance rollers that cause the drill pipe to vibrate. The frequency of the vibrations can be adjusted and optimized by the drillers. Resonance occurs when the frequency of the vibrations induced by the drill head equals to the natural frequency of the drill pipe. This resonance and the weight of the drill pipe along with the downward thrust of the drill head permits easier penetration of the formation. The inner-core barrel was attached to a small steel inner rod that was removed for core retrieval and sample collection.

The boreholes at the Site were installed as close as 1.2 ft apart. The heater well spacing was as close as 5 ft for the demonstration. On a full scale TCH project the heater spacing is typically 12 to 15 ft. The combination of the close well spacing and the vibrations induced to the rock formation during drilling may have created additional fractures and have caused the hydraulic conductivity of the fractured bedrock in the demonstration area to increase.

### 5.1.1.2 Heater Borings with Co-Located Vacuum Extraction Points

The heaters were used to apply energy to the TTZ. A total of 15 heater borings were installed at NAWC in a cylindrical area approximately 20ft in diameter. Each heater boring consisted of a 3-inch diameter, non-perforated carbon steel casing with a bottom seal, installed to a depth of ~ 56 ft bgs. Each vacuum extraction point consisted of 1-inch diameter, stainless steel screen with bottom seal, installed in the same borehole as a heater well, to a depth of ~45 ft and screened from 5 to 45 ft. The heater borings with co-located vacuum extraction points are conceptually shown in Figure 5.1 below.

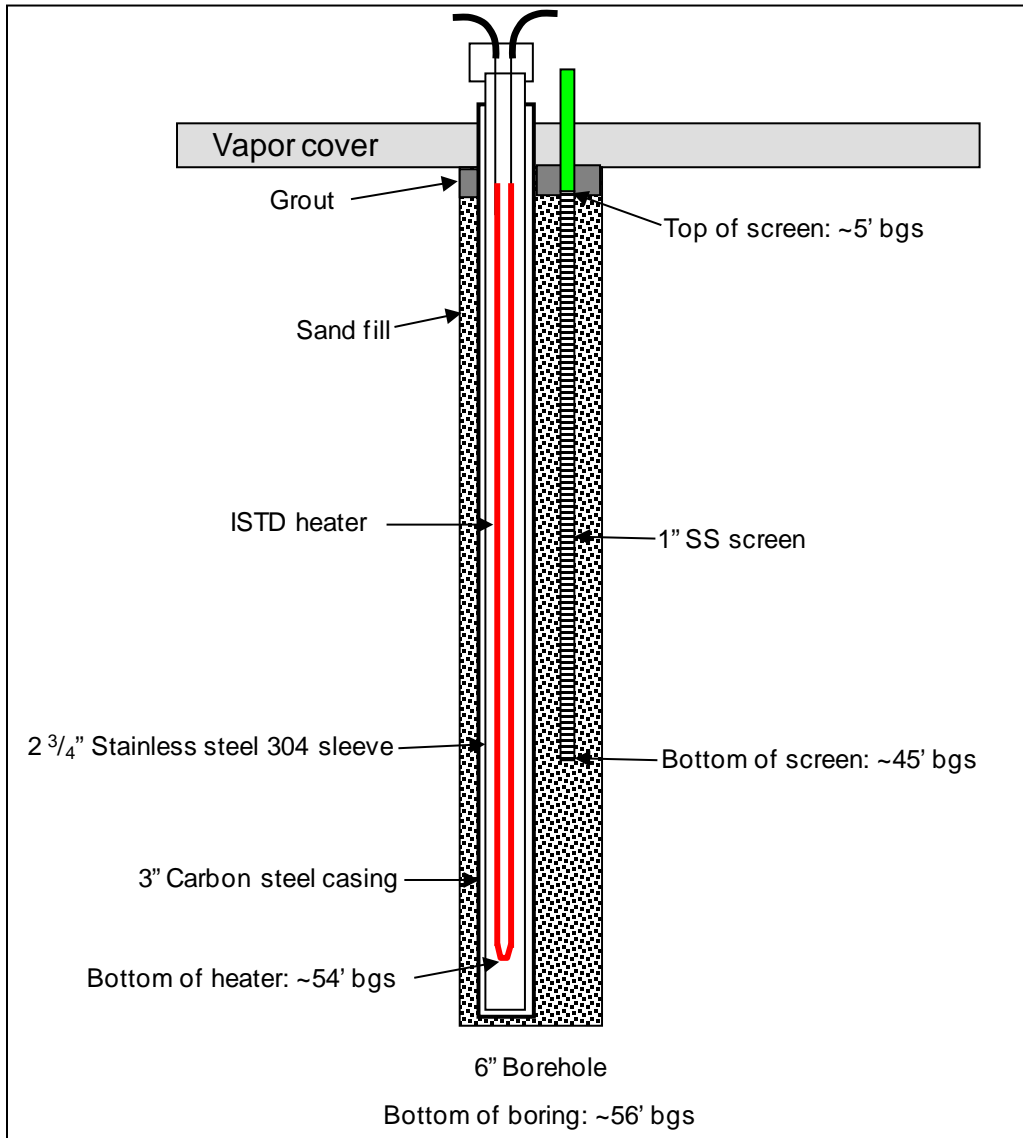


**Figure 5.1. TCH Heater Boring with Co-Located Vacuum Extraction Point**

The co-located heater and vacuum extraction point installation was performed in accordance with the following general procedure. The carbon steel heater casings were bundled together with the threaded extraction screen and riser segments to allow for ease of handling and

installation. The bundled heater can and vacuum extraction screen was then hoisted and placed into the borehole using an all-terrain forklift with extendable boom.

Following the installation of the heaters and vacuum extraction points into the borehole, a sand pack was installed in the annular space from the bottom of the borehole to a depth of 1 ft bgs. The sand pack used for the first 6-7 well completions had a significant fines percentage. Therefore, the sand pack material was substituted with a coarser grained sand pack for the remainder of the heater and vacuum extraction point installations. The annular space above the sand pack was then filled with a Class H high-temperature grout to the ground surface to create a surface seal.

A single ISTD heater element was placed inside each stainless steel liner and set inside the heater can. Groups of heater wells were wired in series, to deliver up to approximately 350 watts per foot of heated length to the subsurface at full power.

A silicon controlled rectifier (SCR) power controller and remote temperature controllers were used to regulate the power application to the ISTD heaters based on temperature input from thermocouples (TCs). The TCs were placed on the outside of the stainless steel sleeve adjacent to selected heaters to allow monitoring and control of the temperature of the heaters. Data from the TCs were used to control the amount of power delivered to each heater electrical circuit to maintain an optimum heater temperature. The amount of power delivered to each circuit was controlled manually by the operator during the initial start-up and ramping period, after which the heaters were set to constant power outputs based on the observed operating temperature of the heater.

#### **5.1.1.3 Temperature Monitoring System**

The temperature monitoring system was used to monitor heating progress during and after treatment. A total of 8 monitoring points were installed for the field demonstration. The temperature monitoring points were constructed of 1.5-inch diameter non-perforated carbon steel pipe with bottom cap, installed to a depth of ~50 feet bgs in a 4-inch cased hole. Each temperature monitoring well had approximately 10 thermocouples located 5, 10, 15, 20, 25, 30, 35, 40, 45, and 50 ft bgs. The annular space between the pipe and the borehole wall was filled with a cement-bentonite grout using a tremie pipe to the ground surface. The points were further sealed at the ground surface as the surface cover was installed. The temperature monitoring points are conceptually shown in Figure 5.2 below.

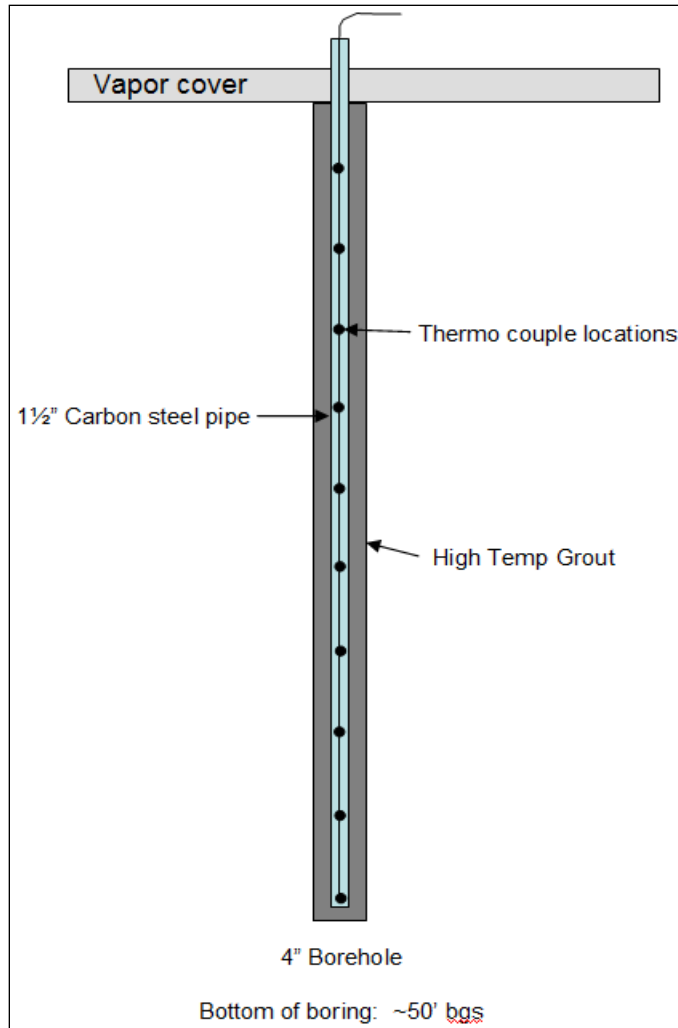


**Figure 5.2. Temperature Monitoring Point**

Figure 5.3 below provides an aerial view of the completed well installations for the TCH field demonstration.

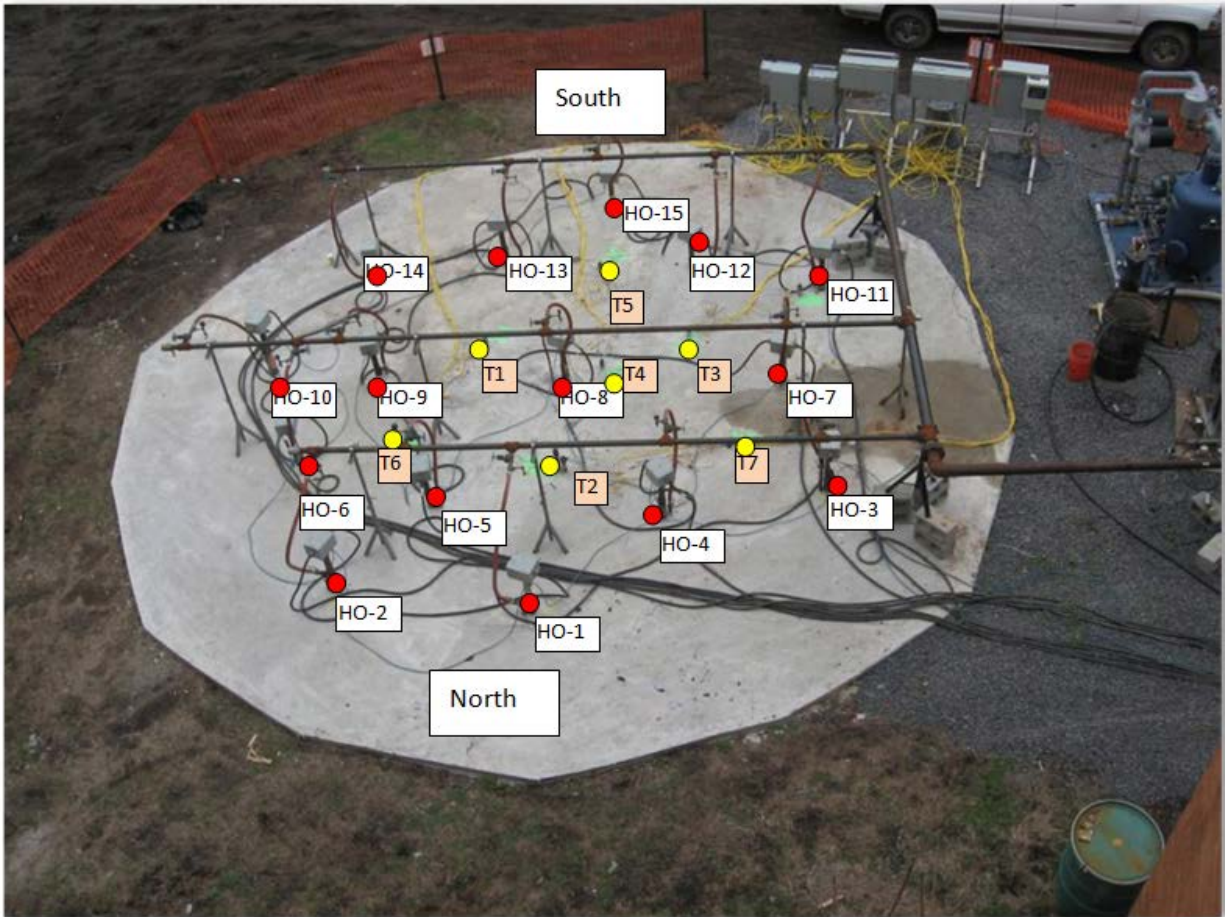


**Figure 5.3. Completed TCH Field Demonstration Well Installation**  
*Courtesy of USGS*

### 5.1.2 Vapor Handling/Treatment Equipment

The following paragraphs describe the components of the aboveground vapor collection and treatment system. A conceptual treatment system process flow diagram is shown in Figure 5.4.

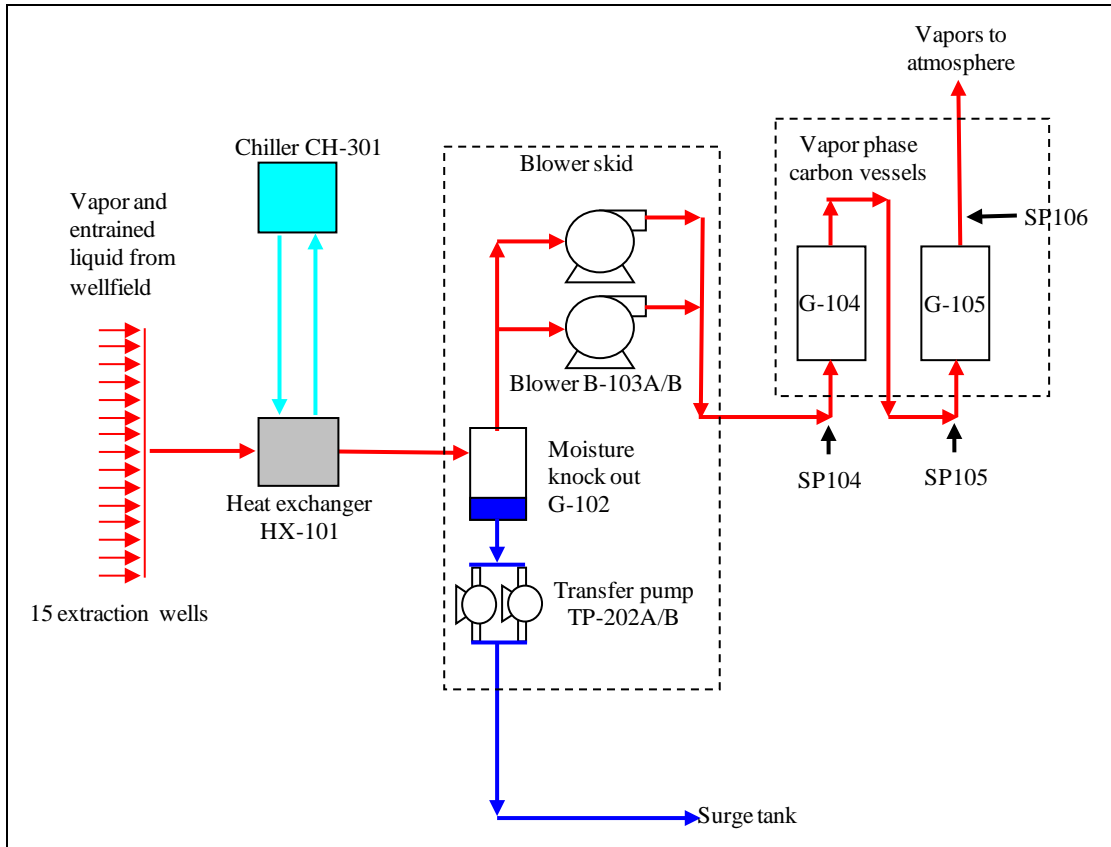


**Figure 5.4. Conceptual Process Flow Diagram for Treatment System**

Figure 5.5 below shows an aerial view of the completed process treatment equipment for the TCH field demonstration.

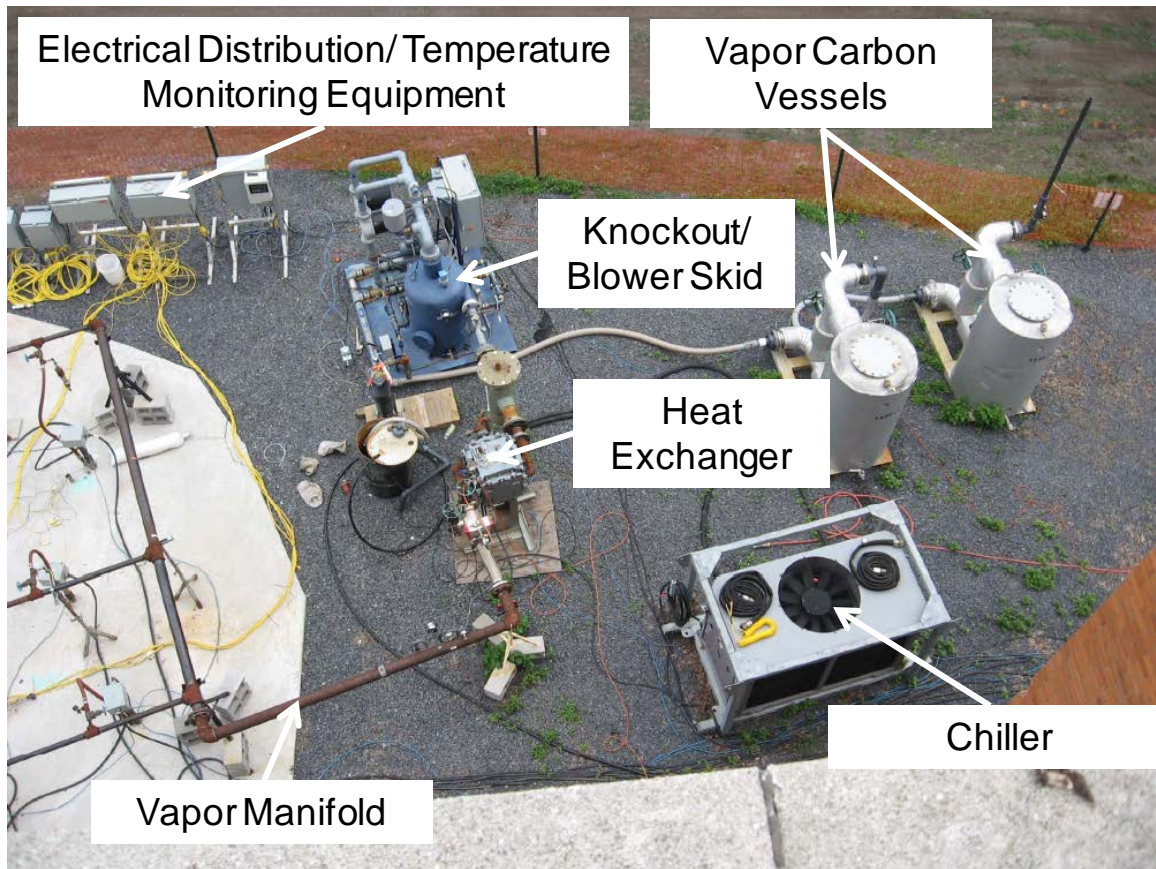


**Figure 5.5. Aerial View of Completed Process Treatment System**  
*Courtesy of USGS*

### 5.1.2.1 Soil Vapor Extraction System

The soil vapor extraction (SVE) system was a skid mounted unit consisting of two regenerative vacuum blowers, two transfer pumps, a moisture knock out, valves, transmitters and controls.

The packaged skid mounted SVE system included the following components:

Steam, vapors, and liquid droplets were extracted from the 15 vapor extraction points, passed through a heat exchanger and separated in the knockout pot. The extracted vapors passed through the knockout pot for subsequent treatment, while the separated liquids were pumped to the existing groundwater treatment plant operated by ECOR Solutions, who operates the site's P&T system.

### 5.1.2.2 Graphite Block Heat Exchanger

Vapors were extracted from the wellfield under vacuum (provided by vacuum blowers). Vapors extracted from the wellfield were cooled to condense extracted steam. A graphite heat exchanger was provided to cool the extracted wellfield vapors. Chilled water for the heat exchanger was supplied by a non-contact packaged rental chiller.

Cooled wellfield vapors were condensed in, or immediately following the heat exchanger and the condensate was collected in the knockout pot.

### **5.1.2.3 Chiller**

A packaged chiller (rental unit) was used to provide non-contact cooling for the graphite heat exchanger. The chiller was a self-contained air cooled, refrigerated chiller unit, with nominal 18 tons (108,000-228,000 BTU/hr) of cooling capacity. The chiller was capable of maintaining a water temperature of approximately 45-50°F for the heat exchanger cooling water supply.

The packaged chiller unit included all necessary circulating pumps, refrigeration equipment and controls. Since it was a closed loop system, minimal make-up water was required for the chiller.

### **5.1.2.4 Knockout Pot**

After exiting the graphite heat exchanger, the cooled vapor stream was drawn through a liquid knockout pot to remove condensate and entrained liquid droplets. Although the primary function of the knockout pot was to remove condensate and liquid droplets, it also served to remove entrained particulate matter. Water collected in the knockout pot was pumped to the surge tank and then pumped to the existing groundwater treatment plant on site operated by the on-site CLEAN contractor, ECOR.

### **5.1.2.5 Transfer Pumps**

Level sensors installed through ports in the side of the knockout tank provided discrete input signals to the local control panel to control operation of the two knockout pot condensate transfer pumps and provided a high-high level interlock alarm. In addition, a flow switch on the discharge side of the transfer pumps provided an interlock in the event of a pump flow failure. Both pumps were powered through a local disconnect on the SVE skid and were automatically operated by a local control panel. The discharge from the pumps was routed to the groundwater treatment plant.

### **5.1.2.6 Vapor Phase Carbon Vessels**

Two vapor phase activated carbon vessels, each containing 750 pounds of vapor phase granular activated carbon (GAC), were installed downstream of the vacuum blowers. The carbon vessels were equipped with local differential pressure indicators that displayed the pressure drop across each vessel. The operators noted the normal pressure drop across the vessel in the log and reported any sudden or substantial change to the project engineer and/or project manager.

In line sample ports were installed upstream and downstream of the carbon vessel. The operator collected vapor samples from the inlet and outlet using a polymer bag resistant to weather, chemicals, and oils. The operator monitored and recorded influent (inlet) and effluent (discharge) vapor concentrations to evaluate VOC loading and/or potential breakthrough of the GAC beds.

The two vapor phase carbon beds were plumbed together in series and contaminant levels were monitored after the first and second carbon beds. While the first carbon vessel was absorbing the majority of the contaminant load, the second vessel provided backup protection from excessive contaminant discharge. Upon breakthrough of the first vessel (i.e., concentrations in excess of the permitted discharge level), the carbon was changed out. Three GAC changeouts were performed during operation (106 days of extraction system operation).

### **5.1.3 System Controls**

A Programmable Logic Controller (PLC) operated and monitored the heating and vapor collection system functions. The PLC was connected to a telephone line for remote monitoring and for automated alarm notifications in the event of system faults. This PLC also had the capability to remotely shut down the vapor and liquid extraction and treatment systems if necessary.

The PLC was accessed locally either through a light emitting diode (LED) interface located at the control panel, with a laptop computer using the serial port connection on the controller, or remotely through a phone line. The operator's computer was configured to dial in to the PLC controller through the remote access feature.

The central PLC panel contained the data recording, remote access, and reporting for the process equipment.

### **5.1.4 Electrical Distribution Equipment**

The main electrical service disconnect was a 600A, 3-phase circuit, 480VAC breaker fed from new service installed along Jack Stephans Way. Two 400 Amp frame/400 Amp trip circuit breakers provided power to the heater circuits. An additional 400 Amp frame/400 Amp trip circuit breaker fed power through an automatic transfer switch (ATS), then out to the sub-panel that distributed power to the vapor treatment system components and the control and monitoring systems.

There were no exposed, live electrical parts. Heater element electrical connections were made inside National Electrical Manufacturers Association (NEMA) 3R or NEMA 4 rated electrical junction boxes mounted to the top of each boring. Connections to the primary and secondary sides of transformers and the various power distribution panels were made inside approved electrical enclosures. The SCRs required flow-through ventilation and therefore the tops and bottoms of the SCRs were open. As such, all SCRs were located in a locked structure accessible only to authorized TerraTherm personnel.

Exposed well risers and conductive metal equipment were bonded and grounded with a #2 AWG copper conductor to an earth ground (i.e., grounding rods). Eight foot ground rods were installed adjacent to the electrical equipment and transformer as required by the National Electrical Code (NEC) 70.

## **5.2 BASELINE CHARACTERIZATION**

Baseline characterization of the NAWC has been ongoing since 1995. The U.S. Navy, in cooperation with the U.S. Geological Survey (USGS) and environmental consulting firms, has been investigating contamination fate and transport since 1988. The USGS developed the first detailed hydrogeologic framework, which is based on bedrock geologic mapping, an understanding of the geology of the Newark Basin, implementation of borehole and surface geophysics, aquifer and slug testing, water-quality sampling and analysis, and groundwater/surface-water flow modeling. In 2002, the NAWC was selected to be a national

research site for the USGS Toxics Substances Hydrology Program. The USGS has supported the TCH research, as well as other research, as part of its mission.

Baseline characterization specific to the TCH site involved the following steps:

- Collection of three sonic drilling cores. Rock chips from the sonic cores were immersed in methane and processed to determine the CVOC concentration in the primary porosity and adsorbed to the matrix. CVOC concentrations are included in Appendix C.
- Collection of rock samples to determine rock characteristics. Samples were collected to determine the following rock characteristics: matrix porosity, organic carbon, pore throat distribution, and bulk density. Results are included in Appendix C.
- Geophysical logging. The 15 HO boreholes (Figure 5.3) were natural-gamma logged to compare with the locally developed geologic framework. The uphole natural gamma logs are correlated to show similar signature features from borehole to borehole (Figure 5.6). Digital copies of the files are available at the USGS New Jersey Water Science Center, West Trenton, NJ. Plans to collect optical and acoustic borehole image logs and heat-pulse flow meter geophysical logs at the TCH site were abandoned because the competency of the boreholes was questionable, and it was feared that the geophysical tool would get stuck in the holes.

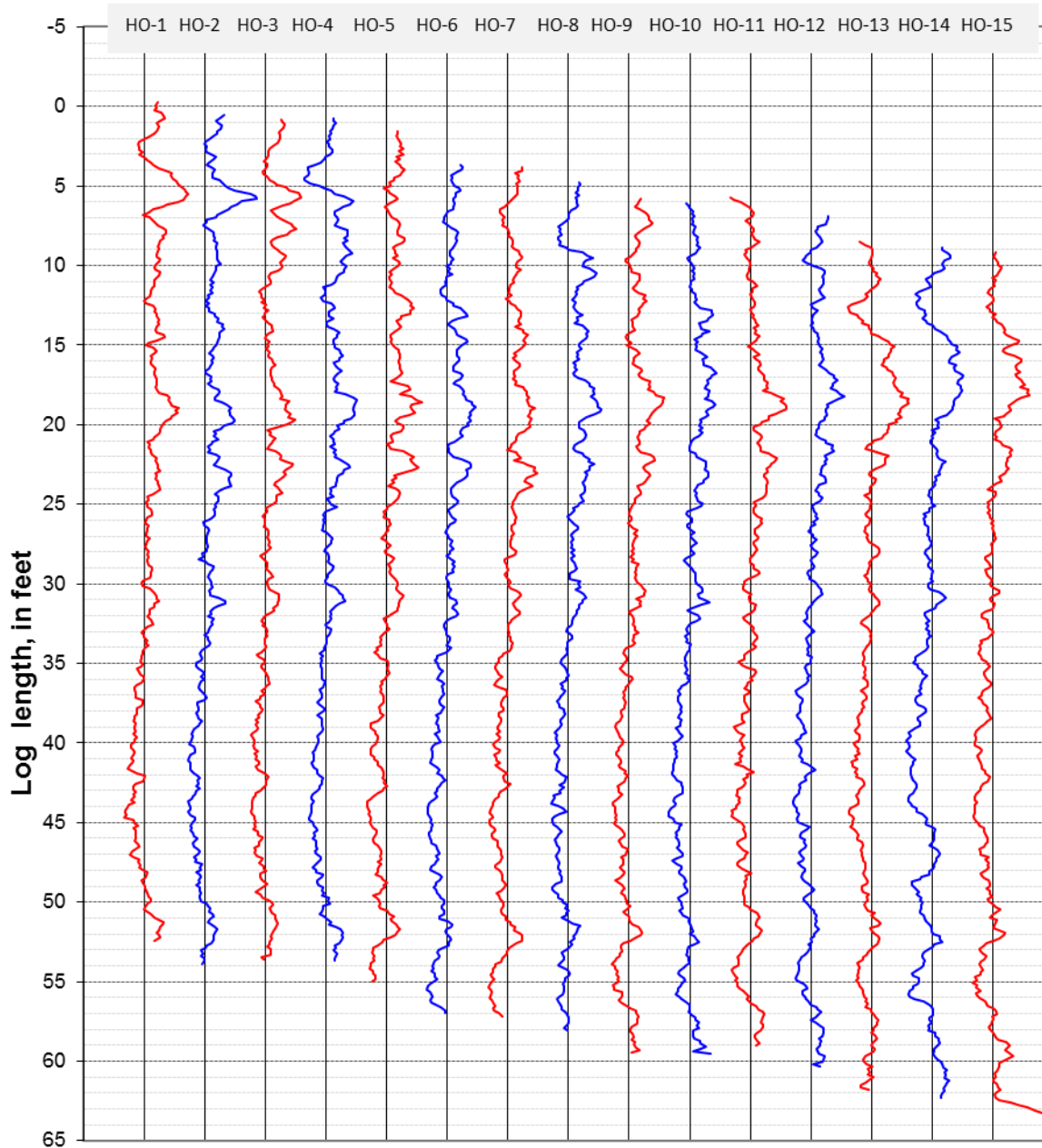


**Figure 5.6. Correlation of Natural Gamma Logs for 15 HO Wells, Relative Gamma Counts Range from 50 to 200 Counts per Second, TCH Demonstration Site, NAWC, Trenton, NJ**

- Water-level monitoring of nearby wells. Water levels were monitored in 18 intervals in a network of 9 bedrock wells within 200 ft of the TCH research site. Monitoring began October 1, 2008, and continued to October 30, 2009. The monitoring was designed to collect water levels prior to and during drilling of the TCH boreholes, November 20 through December 31, 2008, and prior to, during, and after the TCH heating period, April 9 through July 23, 2009. The purpose of the water-level monitoring was to determine whether drilling or heating and steam/water withdrawal caused water-level fluctuations in areas near the TCH site.

The water-level hydrographs in Figures 5.7 through 5.14 show depth to water below land surface at 15-minute intervals for the period of record. The hydrographs also show the period when drilling occurred (brown line) and the period when thermal conductive heating occurred and groundwater and steam were recovered (red line).

Wells 07BR and 24BR are about 50 ft south of the TCH research site (Figure 5.7). Well 07BR is open to stratum Lay.251, the basal strata of the TCH research site. Well 24BR is open to strata that is about 40 ft below the strata of the TCH research site. Water levels in well 07BR apparently were not affected during drilling November 20, 2008, through December 31, 2009. In addition, water levels apparently were not affected during heating and recovery of the contaminated water during April 9–July 23, 2009.

Well 15BR is about 80 to 100 ft along strike and west of the TCH research site Figure 5.8. The well was an active P&T recovery well pumping at a rate of 10 to 12 gpm during drilling and heating. Water levels in well 15BR fluctuated as a result of seasonal changes in evapotranspiration, precipitation, and pump shut downs for maintenance or power outages. Water-level fluctuations cannot be directly attributed to TCH drilling or heating operations.

Wells 4BR, 68BR-A, 68BR-F, 70BR-10, 70BR-72, 71BR-A, 71BR-B, 71BR-C, 71BR-D, 71BR-E, 73BR-A, 73BR-BC, 73BR-E, BRP1, and 47BR are 100 to 200 ft from the TCH site (Figures 5.8-5.14). Water levels in these wells fluctuate as a result of seasonal changes in evapotranspiration, precipitation, and P&T operations. Water-level fluctuations cannot be directly attributed to TCH drilling or heating operations.

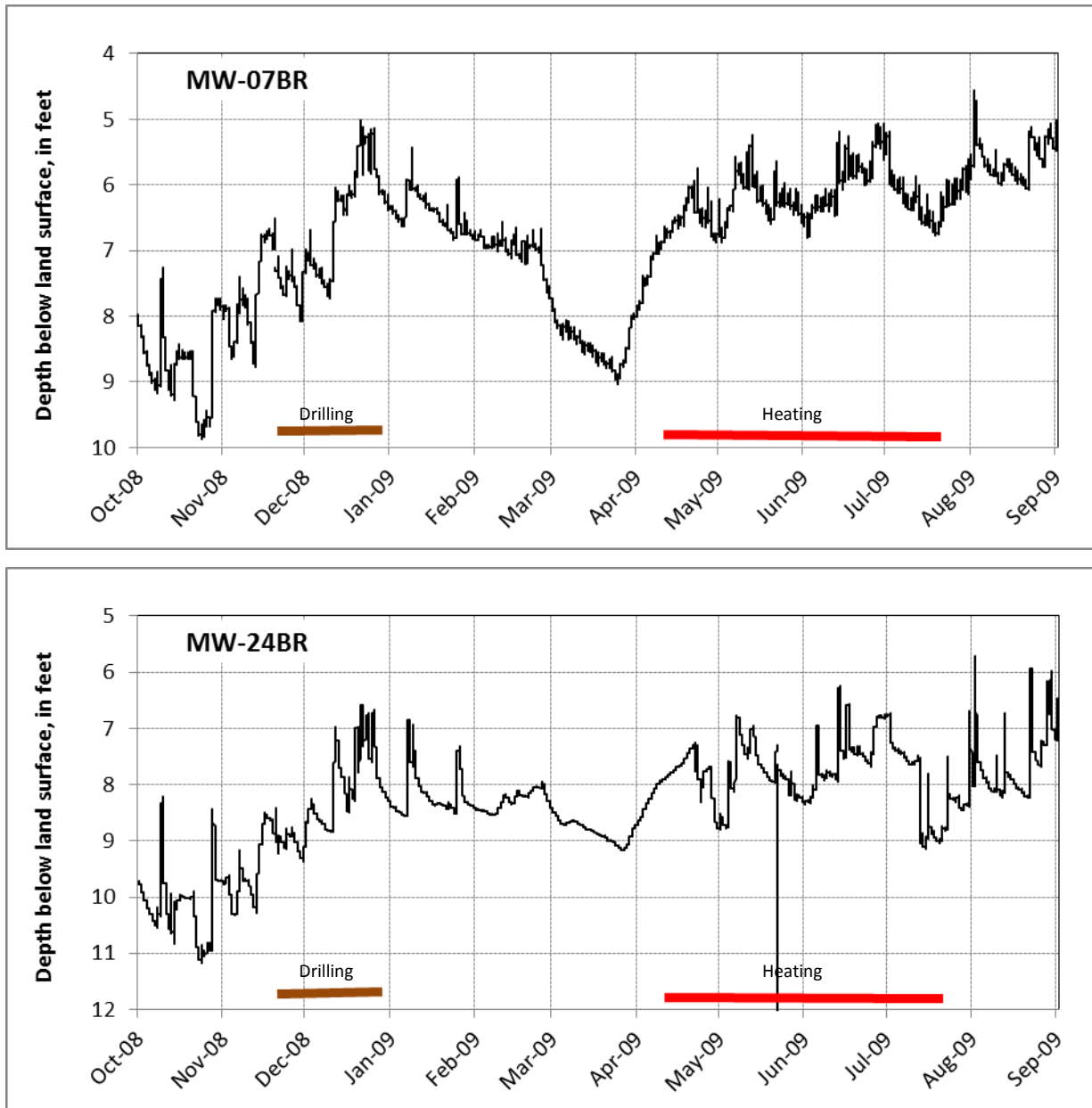


**Figure 5.7. Water-Level Hydrographs for Wells MW-07BR and MW-24BR Showing TCH Drilling and Heating Periods, NAWC, Trenton, NJ, October 2008 to September 2009**

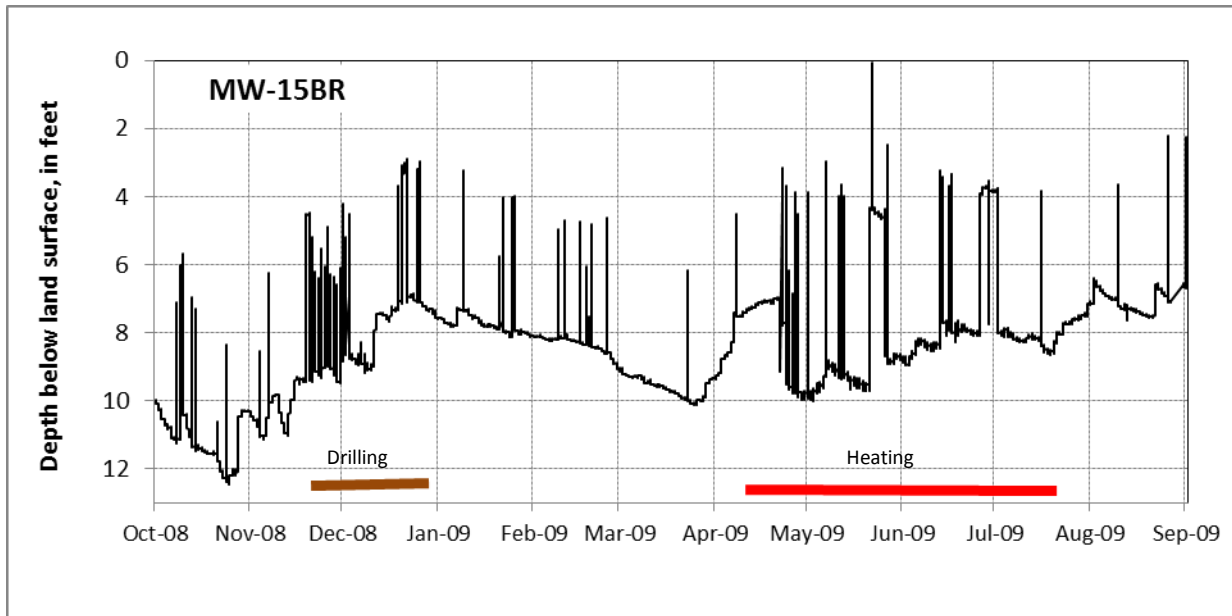


**Figure 5.8. Water-Level Hydrographs for Wells 15BR and 4BR and TCH Drilling and Heating Periods, NAWC, Trenton, NJ, October 2008 to September 2009**

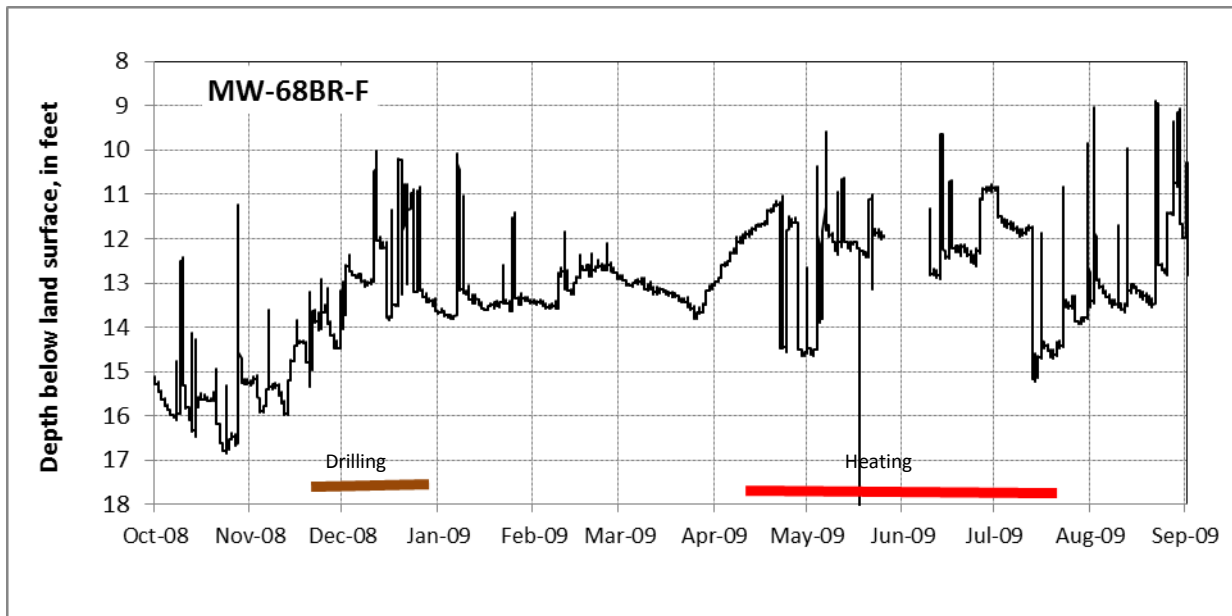
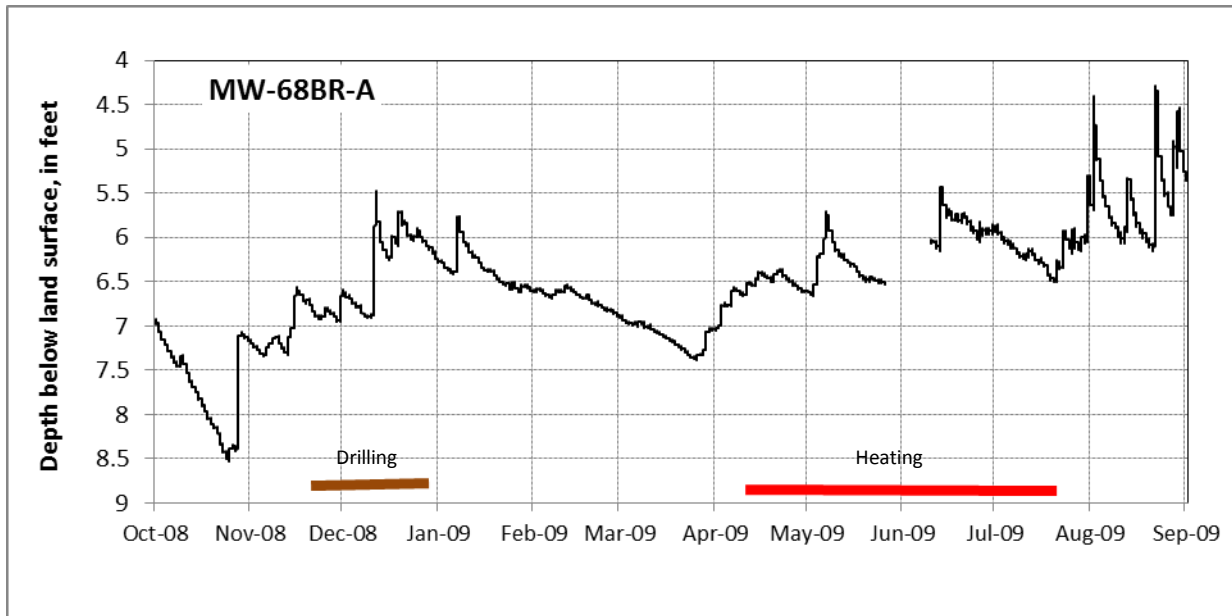


**Figure 5.9. Water-Level Hydrographs for Wells 68BR-A and 68BR-F and TCH Drilling and Heating Periods, NAWC, Trenton, NJ, October 2008 to September 2009**

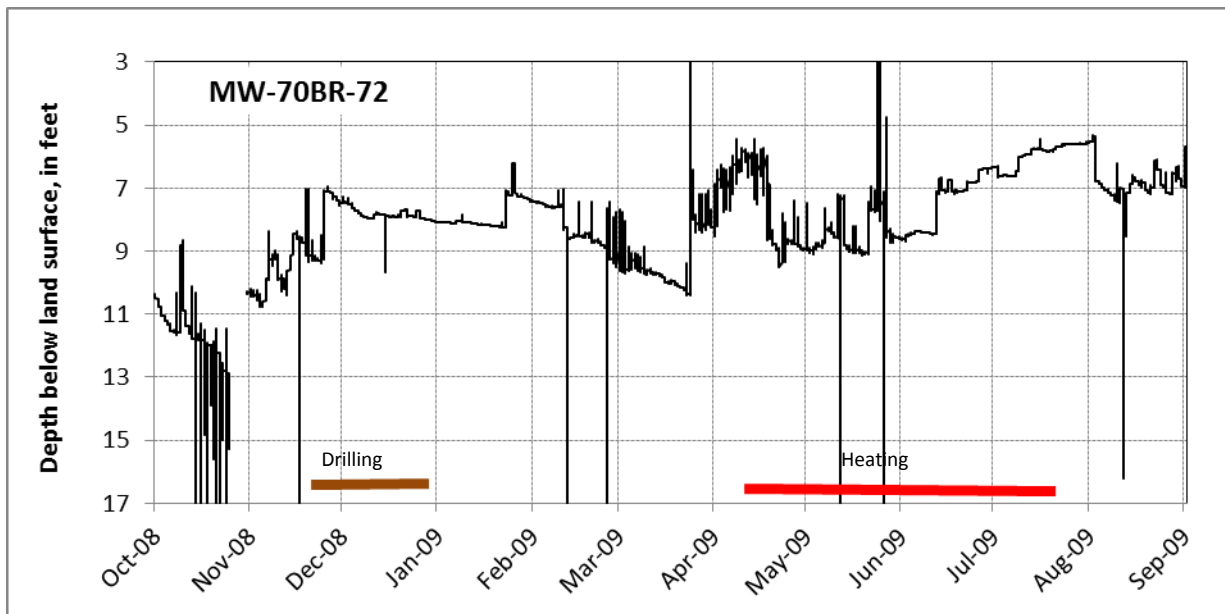
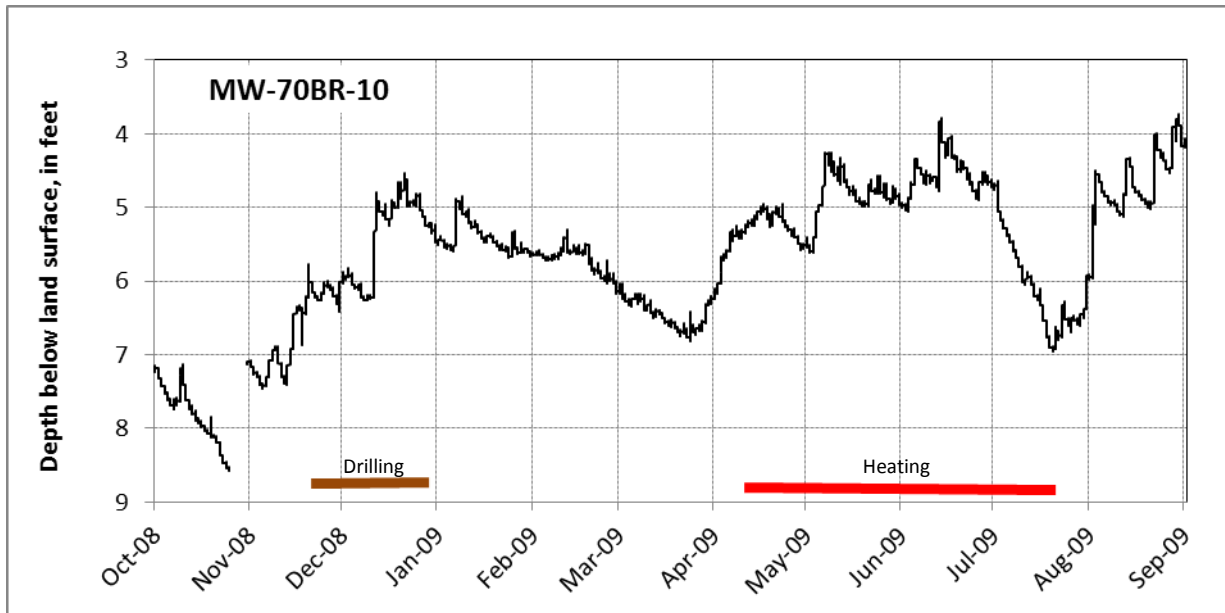


**Figure 5.10. Water-Level Hydrographs for Wells 70BR-10 and 70BR-72, and TCH Drilling and Heating Periods, NAWC, Trenton, NJ, October 2008 to September 2009**

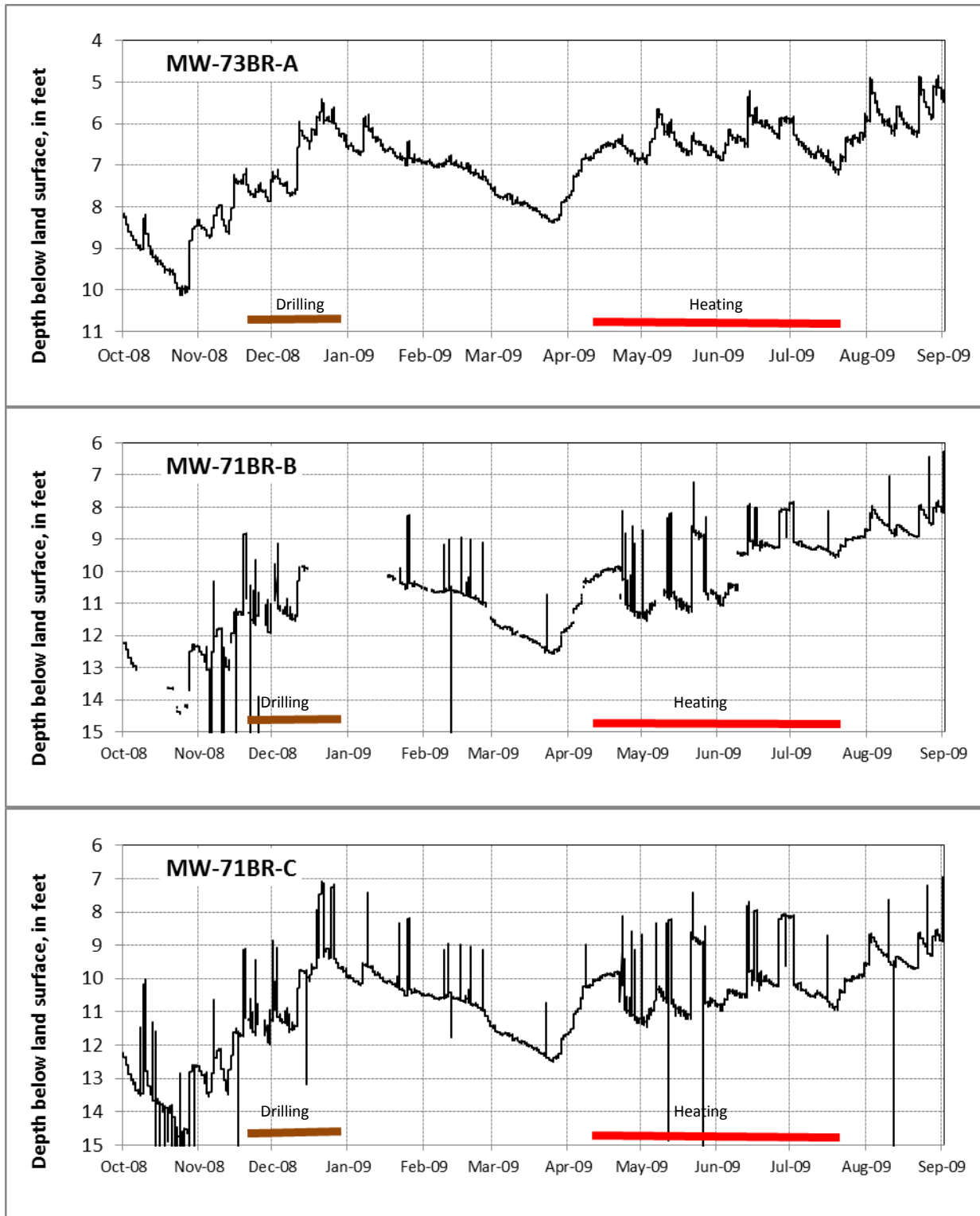


**Figure 5.11. Water-Level Hydrographs for Wells 71BR-A, 71BR-B, 71BR-C, and TCH Drilling and Heating Periods, NAWC, Trenton, NJ, October 2008 to September 2009**

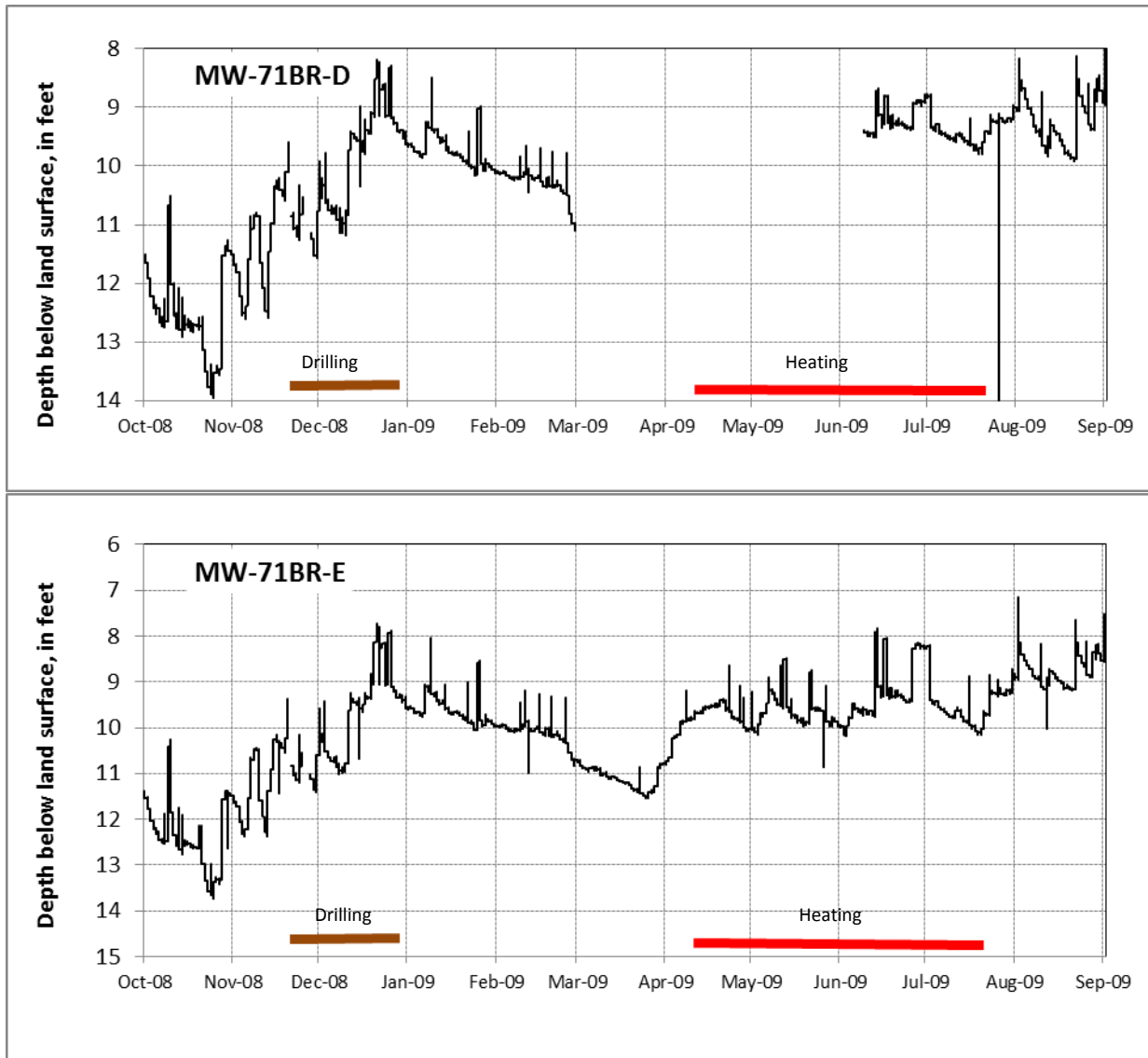


**Figure 5.12. Water-Level Hydrographs for Wells 71BR-D, and 71BR-E, and TCH Drilling and Heating Periods, NAWC, Trenton, NJ, October 2008 to September 2009**

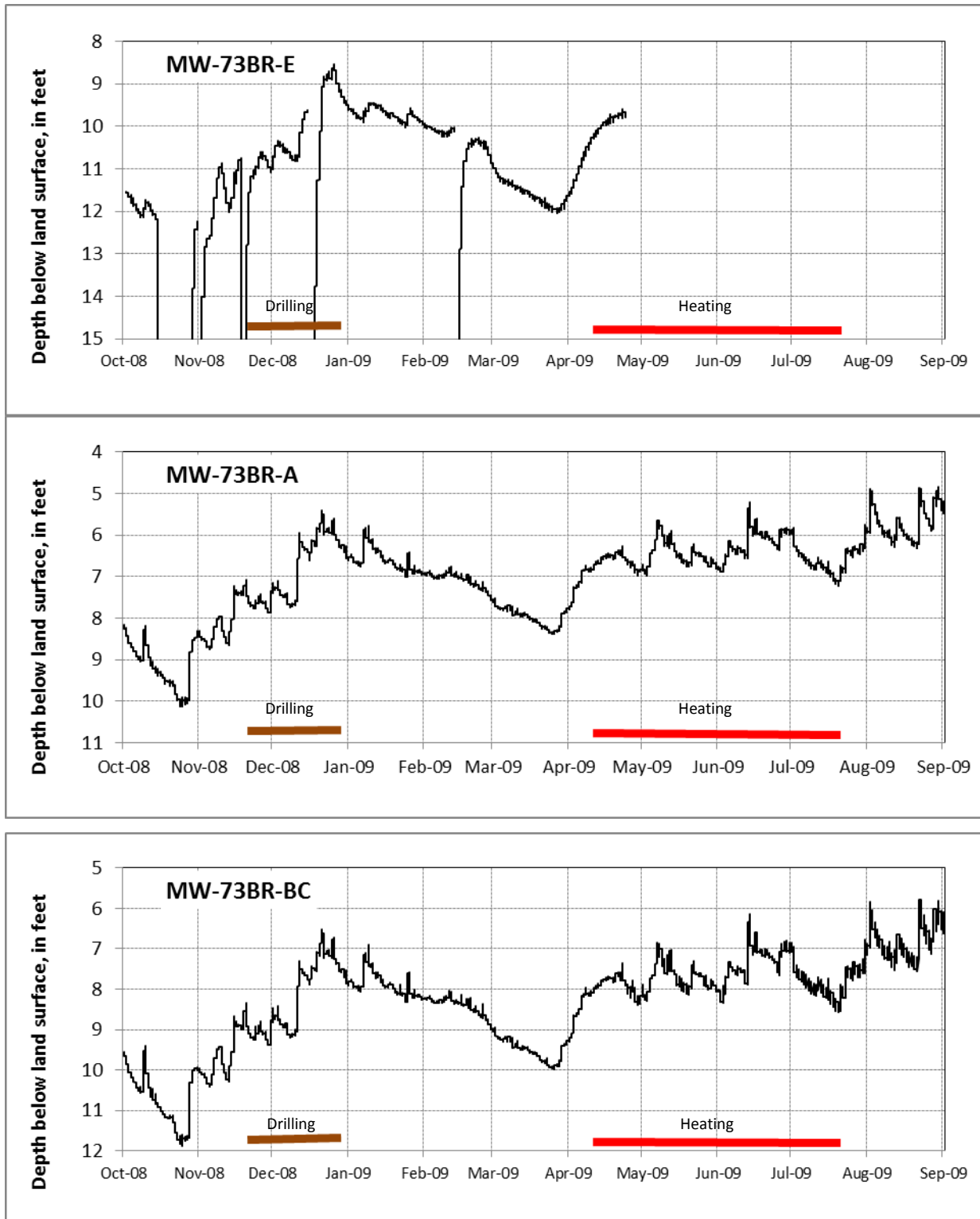


**Figure 5.13. Water-Level Hydrographs for Wells 73BR-A, 73BR-BC, 73BR-E, and TCH Drilling and Heating Periods, NAWC, Trenton, NJ, October 2008 to September 2009**

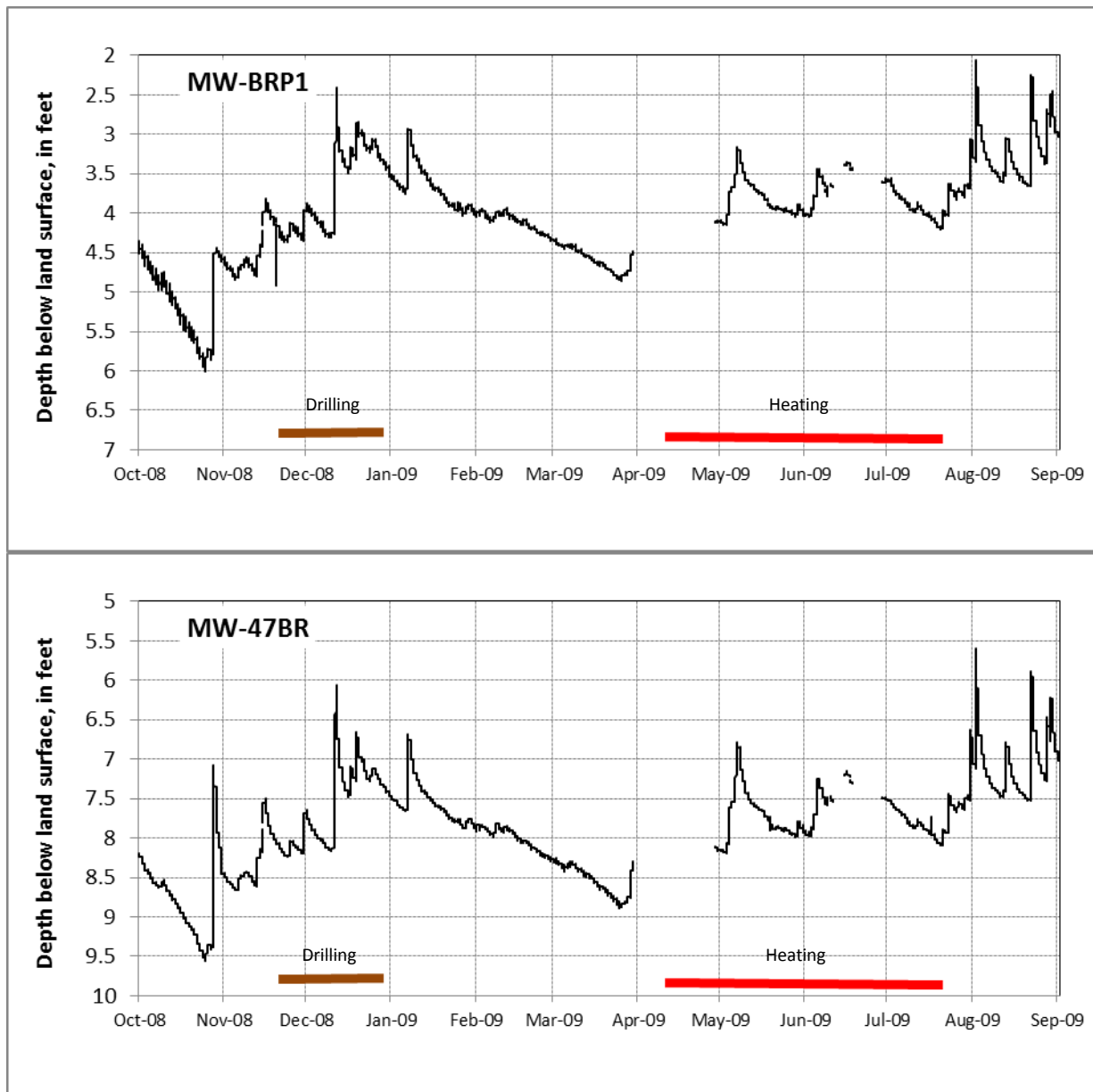


**Figure 5.14. Water-Level Hydrographs for Wells BRP1 and 47BR and TCH Drilling and Heating Periods, NAWC, Trenton, NJ, October 2008 to September 2009**

### 5.3 TREATABILITY AND LABORATORY STUDY RESULTS

Laboratory studies conducted in support of this project included:

- a) Bench scale evaluations to identify optimum temperatures (*temperature profile testing*) and duration (*duration profile testing*) on different types of rock; mudstone (found at the NAWC site), siltstone, limestone, sandstone and dolostone.

b) Microbial enumeration both before and after heating to determine the effect of the heating on on-site microflora and if that effect was temporary.

A summary of the results of the laboratory treatability heating studies can be found in Section 5.3.1 below. Details from the evaluations are included in Appendix D. A description and results of the laboratory studies dealing with the microbial characterization before and after heating are described below in Section 5.3.2.

### 5.3.1 Treatability and Laboratory Heating Study

#### 5.3.1.1 Methodology

Seven rock types were employed to assess the relationships between temperature, heating duration and degree of contaminant mass removal. Cores of siltstone, limestone, sandstone, dolostone and three types of mudstone were obtained from a variety of locations in the US and Canada, including three types of mudstone from the NAWC Site. Core samples of each rock type were cut to provide 40 discs measuring 1 cm in thickness and 5 cm in diameter. A total of 28 discs were retained for heating experiments involving trichloroethylene (TCE) and tetrachloroethylene (PCE), while 12 discs were retained for physical characterization measurements (Figure 5.15).

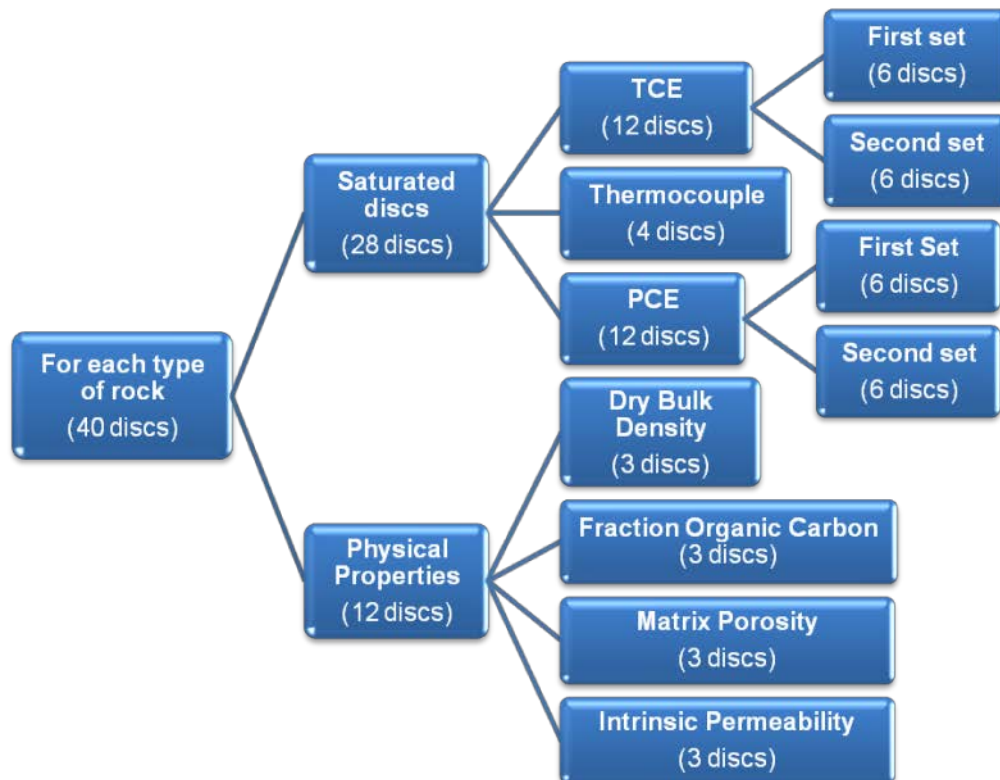
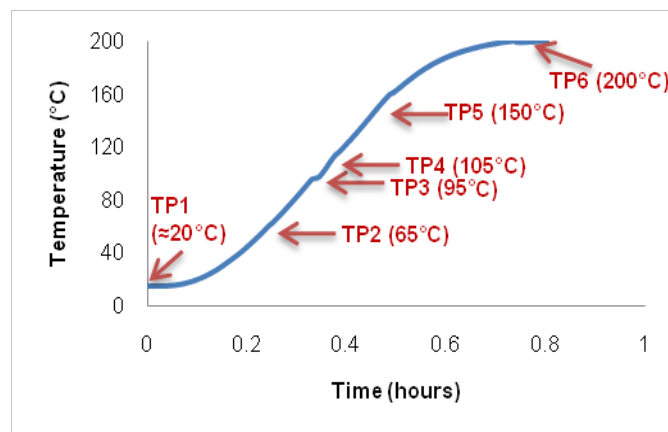


Figure 5.15. Summary of Disc Samples Used for Each Rock Type in Heating Experiments

The set of 28 discs was dried for a period of 24 hrs at 30°C, following which the discs were pre-saturated with carbon dioxide (CO<sub>2</sub>) in a pressure chamber (413.7 kPa) and subsequently saturated with distilled de-aired water under atmospheric pressure for one week. Twenty-four of the water-saturated discs were spiked with either Fisher Scientific reagent grade (>99%) TCE (12 discs), or PCE (12 discs). The discs were placed in 4L sealed vessels filled with the respective DNAPL, allowing diffusion to load the rock matrix. A four month period was required to reach TCE and PCE saturation above an estimated 80 % of capacity. Saturation time was calculated using an analytical solution for three-dimensional mass transfer into water-saturated matrix blocks (Parker et al., 1996). Four discs were kept under water saturation until the end of the TCE and PCE spiking period. These four discs were employed to monitor temperature during the heating experiments.

The set of 12 discs was sent to an independent laboratory for rock property characterization. The analyses included measurements of dry bulk density, fraction organic carbon, matrix porosity, pore throat distribution, and intrinsic permeability. Three discs were analyzed for dry bulk density using gravimetric method ASTM D2937-04 (ASTM, 2004a); three discs were analyzed for fraction organic carbon using the Walkley-Black method EPA 9060 (USEPA, 1999); three discs provided the pore throat distribution and total porosity using mercury porosimetry method ASTM D4404-84 (ASTM, 2004b); and three discs were used to measure intrinsic permeability using method EPA 9100 (USEPA, 1986).

Following TCE and PCE spiking, the 12 TCE and 12 PCE rock discs were divided into two sets of six discs, respectively. Heating experiments were conducted during which each set of six discs was heated with a specified heating profile in a convection oven vented to a fumehood. During the heating *temperature profile* testing, each set of six TCE and six PCE spiked discs was heated to six different temperature points (Figure 5.16): TP1 to approximately 20°C [room temperature], TP2 to 60°C, TP3 to 95°C, TP4 to 105°C, TP5 to 150°C and TP6 to 200°C. Six discs were placed into the oven following which it was set to 200°C. Discs were removed from the oven immediately after reaching their respective target temperature. The more elevated temperatures [150°C and 200°C] in this procedure were used to determine whether temperatures above the boiling point of water could yield lower TCE and PCE matrix concentrations than simply heating the discs to 100°C, thereby providing a more efficient treatment.



**Figure 5.16. Heating Temperature Profile Illustrating the Six Temperature Points at which Rock Discs Were Removed from the Convection Oven during Heating Tests**

During the heating *duration profile* testing, the effect of heating duration on matrix concentrations was evaluated. The second set of six TCE and six PCE spiked discs were heated to 105°C (Figure 5.17). The first three discs in this set were removed from the oven at approximately 20°C (TP1), 65°C (TP2), and 95°C (TP3). Once the oven reached 105°C, the remaining three discs were maintained at this temperature and were removed after 24 hrs (TP4), 48 hrs (TP5), and 72 hrs (TP6) of heating.

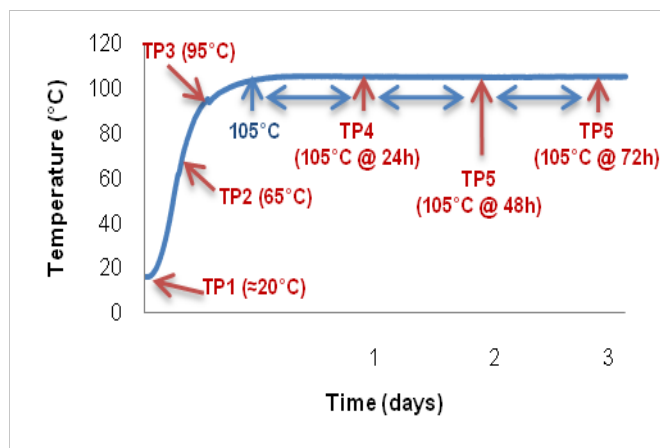


**Figure 5.17. Heating Duration Profile Illustrating the Six Temperature Points at which Rock Discs Were Removed from the Convection Oven during Heating Tests**

In each set of tests, one of the four water-saturated discs was used to monitor the internal temperature of the rock discs within the oven. This was facilitated by drilling a hole into the side of the disk and cementing in place a type T thermocouple. The thermocouple equipped disc was placed in the oven for each heating test and linked to a data logger located outside of the convection oven.

Upon removal from the oven, rock discs were immediately crushed in a sealed stainless steel rock crusher containing methanol (reagent grade, >99 % pure) to extract the TCE or PCE according to preservation methods outlined by USEPA (2002). The resultant methanol extract was analyzed for TCE or PCE content at Queen’s University using USEPA methods 5035A (USEPA, 2002) and 8260B (USEPA, 1996), closed-system purge-and-trap and extraction for volatile organics in soil and waste samples and volatile organic compounds by gas chromatography/mass spectrometry (GC/MS), respectively. The analyses were performed in a gas chromatograph/mass selective detector system with purge-and-trap concentrator. The method detection limits for TCE and PCE were both on the order of 2 ppb. Further details of the disc crushing process and chlorinated compound extraction are presented in Appendix D.

### 5.3.1.2 Rock Core Sample Collection

Siltstone core samples were collected from a depth of 19.2 m to 22.4 m at a confidential facility in northern Pennsylvania. The cores were collected from a bedrock system of the Lock Haven formation which comprises low-permeability material of very-fine grained sandstone, siltstone and silty shale. The Lock Haven formation is moderately resistant to weathering and forms hills and ridges of moderate relief slopes. It is known for its brackish or saline water and the presence of hydrogen sulfide (Low and Galeone, 2006; Geyer and Wilshusen, 1982).

Limestone cores were collected in the south-eastern side of Frontenac County in Ontario, Canada. The bedrock is part of the Gull River formation and consists largely of inter-bedded limestone and silty dolostone with occasional inter-beds of shale and fine-grained quartz sandstone (Marich, 2009). Sandford (1993) reported that the Gull River formation is largely composed of underlying limestone beds that consist of gray, lithographic to finely crystalline limestone exhibiting a laminated appearance on weathered surfaces. Limestone core samples were collected at a depth of 20.6 m to 21.8 m.

Core samples of sandstone were collected in a geologic zone that comprises Precambrian igneous and metamorphic rocks of the Canadian Shield overlain by Palaeozoic sedimentary rocks in and to the north of the Village of Lansdowne in Ontario, Canada (Sterling et al., 2010). The geology of Precambrian bedrock within the Lansdowne area is a mixture of rock types including felsic plutonic rocks and clastic meta-sedimentary rocks (Sterling et al., 2010). Sandstone core samples were collected from a depth of 9.1 m to 13.8 m. At this depth, the bedrock system is part of the Palaeozoic sedimentary rock of the Nepean formation, which consists primarily of medium-grained, well-sorted quartz sandstone (Williams and Wolf, 1984).

Dolostone core samples were collected in southern Ontario, Canada at a depth of 13.7 m to 17.2 m. The bedrock system in this area is part of the Lockport formation that extends from Western New York to southern Ontario. The Lockport formation is primarily composed of buff-colored, aphanitic- to medium-crystalline, soft, porous dolostone (Reichart, 1992).

Mudstone core samples were collected from the Lockatong formation at the former Naval Air Warfare Center (NAWC) in West Trenton, NJ. The four lithotypes identified by Lacombe and Burton (2010) in the Lockatong formation are divided into massive red mudstone, massive light gray mudstone, dark-gray laminated mudstone and laminated black carbon-rich mudstone. For this study, three types of rock were utilized in the heating experiments: massive red mudstone, laminated black mudstone and light-dark gray mudstone. Samples of light-dark gray mudstone consisted of a combination of massive and laminated grey mudstone. Red mudstone core samples were composed of a high percentage of analcime. Core samples of grey and black mudstone had distinct laminated bands. Gray mudstone had the least distinct shaley bands, while black mudstone had the most distinct shaley bands. Red mudstone core samples were collected from a depth of 85.8 m to 87.7 m, gray mudstone core samples from a depth of 7.4 m to 7.8 m and 15.7 m to 16.7 m, and black mudstone core samples from a depth of 77.9 m to 80.3 m.

### **5.3.1.3 Statistical Analysis**

A two-way analysis of variance (ANOVA) without replication (95 % significance level) was utilized to determine the variability within each rock property analysis, and between the results

of rock property analyses for each type of rock. A two-way ANOVA with replication (95 % significance level) was utilized to evaluate the variability of the heating tests between the different heating profiles, rock types, and contaminants. The two-way ANOVA with replication was utilized independently for each of the six temperature points in the heating tests. In addition, parametric and non-parametric tests (95 % significance level) were performed to corroborate the results of the ANOVA with replication. The k-sample comparison of variances [parametric] and the Friedman's test [non-parametric] were utilized to evaluate any statistically significant difference between the results of the heating temperature profile test and the heating duration profile test, as well as between the contaminant mass removal in each type of rock. The Student *t*-test [parametric] and Wilcoxon test [non-parametric] were utilized to evaluate any statistically significant difference between TCE and PCE mass removal in each heating profile test.

Principal component analysis (PCA) was utilized to evaluate the influence of the rock properties on the removal of TCE and PCE from the rock matrix for the heating temperature profile and the heating duration profile tests. The statistical analyses were performed utilizing an Analysis Toolpak. Non-parametric and PCA analyses were performed using a statistical software program.

#### 5.3.1.4 Results and discussion.

#### Rock Property Analysis

Table 5.1 summarizes the average values and corresponding standard deviations obtained for the rock property analyses for each rock type (detailed summary of rock property testing result is presented in Appendix D). The two-way ANOVA without replication revealed no statistically significant difference within the results of the replicates of dry bulk density, fraction organic carbon, matrix porosity and intrinsic permeability ( $P = 0.25, 0.19, 0.85$  and  $0.41$ , respectively). In addition, the values of dry bulk density and intrinsic permeability showed no statistically significant difference between each type of rock investigated in this study ( $P = 0.14$  and  $0.46$ , respectively). Therefore, values of dry bulk density and intrinsic permeability were considered similar for all the types of rock employed in this study. However, the fraction organic carbon and matrix porosity showed a statistically significant difference ( $P$ -value =  $9.44E-10$  and  $2.63E-04$ , respectively) between rock types.

**Table 5.1. Average Rock Property Values Obtained from the Rock Properties Analysis in Triplicate of the Seven Types of Rock Utilized during Heating Experiments**

Type of rock	$\rho_b$ (g/cm <sup>3</sup> )	foc (g/g)	porosity (%)	permeability (cm <sup>2</sup> )
Red Mudstone	$2.59 \pm 0.0$	$1.88E-03 \pm 0.1E-03$	$1.00 \pm 0.3$	$9.90E-15 \pm 0.0E-15$
Gray Mudstone	$2.69 \pm 0.1$	$4.08E-03 \pm 0.1E-03$	$6.30 \pm 0.3$	$3.69E-13 \pm 1.0E-13$
Black Mudstone	$2.80 \pm 0.3$	$8.65E-03 \pm 1.0E-03$	$0.17 \pm 0.1$	$6.77E-13 \pm 1.3E-13$
Siltstone	$2.67 \pm 0.0$	$2.80E-03 \pm 0.4E-03$	$0.47 \pm 0.2$	$2.78E-12 \pm 0.1E-12$
Limestone	$2.71 \pm 0.0$	$2.52E-03 \pm 0.2E-03$	$2.13 \pm 1.5$	$1.05E-12 \pm 0.9E-12$
Sandstone	$2.54 \pm 0.0$	$5.90E-04 \pm 3.5E-04$	$5.87 \pm 2.8$	$1.06E-12 \pm 1.1E-12$
Dolostone	$2.64 \pm 0.1$	$1.80E-03 \pm 0.5E-03$	$4.93 \pm 1.2$	$5.32E-11 \pm 9.9E-11$

## Heating Tests

Variations in fraction organic carbon and matrix porosity resulted in differing initial contaminant concentrations in each rock type (Table 5.2). TCE and PCE concentrations in the rock discs retrieved at ambient temperature (TP1) were considered as the initial concentration ( $C_0$ ). Results (normalized  $C/C_0$ ) of the heating *temperature profile* tests for the removal of TCE and PCE are presented in Figures 5.18 and 5.19, respectively. Figure 5.20 presents the results of the heating *duration profile* tests for the removal of TCE, while Figure 5.21 presents the results for the removal of PCE. The amount of obtained red mudstone material was not sufficient to complete all heating tests due to sample loss during the cutting process and unusable sections of the core. The heating *duration profile* test was, consequently, not carried out on red mudstone spiked with TCE. The internal temperature of the rock discs increased steadily requiring approximately 45 minutes to reach target temperatures during the heating *temperature profile* tests, and 40 minutes during the heating *duration profile* tests.

**Table 5.2. Summary of Initial Concentration ( $C_0$ ) in Each Rock Type**

Type of rock	Heating temperature profile		Heating duration profile	
	TCE (mg/kg)	PCE (mg/kg)	TCE (mg/kg)	PCE (mg/kg)
Red mudstone	6.2	12.35	8.6	10.8
Gray mudstone	43,722.8	22,163	604.9	14,376.2
Black mudstone	1,334.3	1,310.5	509	350.3
Siltstone	12,040.4	21,248.7	11,344.5	12,762.6
Limestone	16,432.4	30,654.2	31,577.8	30,192.6
Sandstone	47,976.3	13,687.9	15,315	19,537.6
Dolostone	15,778.8	21,248.7	27,296.1	22,272.3

Heating profiles for the removal of TCE and PCE from the black mudstone were noted to be more erratic than for the other rock types. A possible explanation is that the black mudstone exhibited the highest fraction organic carbon and the lowest matrix porosity. The low matrix porosity would have resulted in limited water content within the matrix following the water saturation. In a dry environment, the amount that a chlorinated solvent such as TCE or PCE is sorbed to solid surfaces can increase four orders of magnitude (e.g., Peterson et al. 1988). This could have been dominant in the black mudstone given the high matrix organic carbon content. Also relevant (to explaining the erratic results of the black mudstone) is that it was found to contain frequent bands of shaley material, and was hence considered to be highly heterogeneous, which likely affected the initial contaminant concentrations in each individual rock sample. For example, in Figures 5.18 and 5.19 final concentrations were observed to be higher than  $C_0$  in black mudstone. Based on the aforementioned, the results of the heating tests were statistically analyzed, firstly by including all of the different types of rock, and secondly with the exclusion of black mudstone.

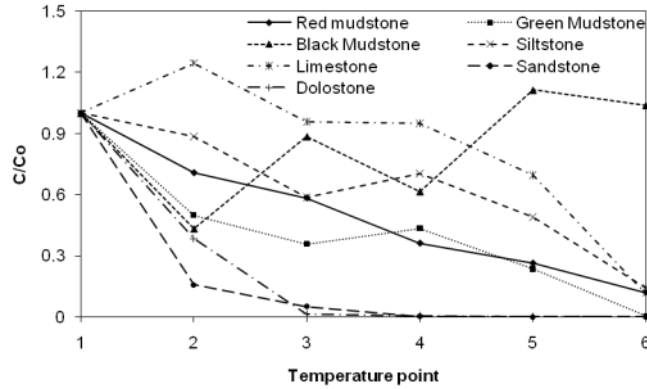


**Figure 5.18. Normalized TCE Concentration versus Temperature Point in Heating Temperature Profile Tests**

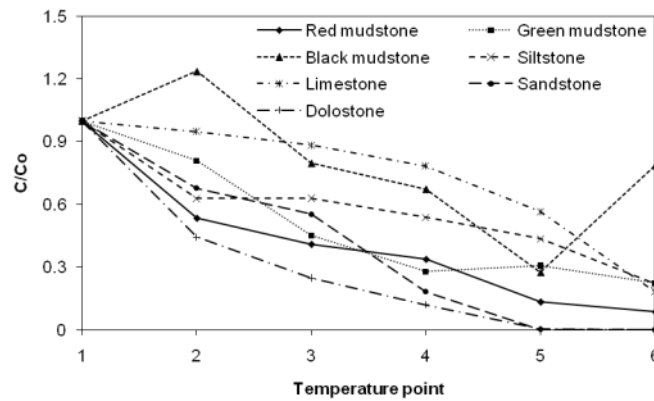


**Figure 5.19. Normalized PCE Concentration versus Temperature Point in Heating Temperature Profile Tests**

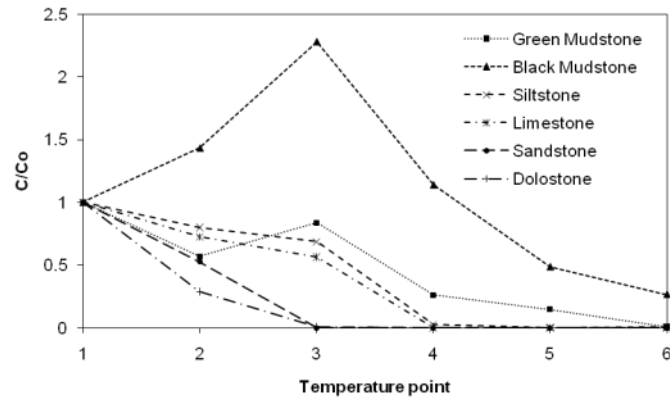


**Figure 5.20. Normalized TCE Concentration versus Temperature Point in Heating Duration Profile Tests**

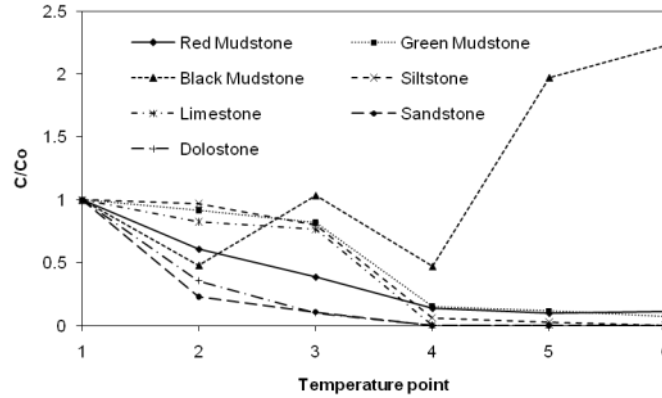


**Figure 5.21. Normalized PCE Concentration versus Temperature Point in Heating Duration Profile Tests**

### Effect of Heating Profile on Contaminant Removal

The two-way ANOVA with replication performed on the seven different types of rock showed that when the sixth temperature point (TP6) was reached, the contaminant mass removal achieved in the heating *temperature profile* tests showed no statistically significant difference to that of the heating *duration profile* tests ( $P = 0.96$ ). Similar results were observed at the fifth temperature point (TP5) ( $P = 0.41$ ). However, the two-way ANOVA revealed that there was a statistically significant difference ( $P = 3.89E-04$ ) at the fourth temperature point (TP4) between the heating *temperature profile* and the heating *duration profile* tests. Heating *temperature profile* tests removed on average  $56.1 \pm 35.3$  % of TCE and  $58.4 \pm 25.3$  % of PCE after reaching the fourth temperature point. In contrast, heating *duration profile* tests removed on average  $76.2 \pm 45.3$  % of TCE and  $88.2 \pm 16.9$  % of PCE.

Overall, TCE and PCE matrix concentrations were reduced further during the heating *duration profile* tests. In addition, during heating *duration profile* tests more than 98 % of the contaminant mass removal was achieved within the first 24 to 25 hours, in samples of sandstone, dolostone, limestone and siltstone. Heating for an additional 24 to 48 hours resulted in a less significant decrease in concentration. The latter is an important consideration in field applications, where attaining water boiling temperatures within the subsurface requires several weeks, whereas attaining temperatures above 200°C would require longer periods of time. The average TCE and PCE mass removal obtained by the two different heating profiles at TP6, TP5 and TP4 of the seven different types of rock is summarized in Table 5.3.

**Table 5.3. Average Contaminant Mass Removal Attained at the Last Three Temperature Points of the Heating Tests for All Rock Types**

Temperature point	Average contaminant mass removal (%)			
	Heating temperature profile		Heating duration profile	
	TCE	PCE	TCE	PCE
TP6	$79.7 \pm 37.4$	$78.5 \pm 27.0$	$95.3 \pm 10.7$	$65.5 \pm 83.2$
TP5	$60.0 \pm 40.2$	$75.4 \pm 21.4$	$89.3 \pm 6.6$	$68.3 \pm 73.2$
TP4	$56.1 \pm 35.3$	$58.4 \pm 25.3$	$76.2 \pm 45.3$	$88.2 \pm 16.9$

When black mudstone was excluded from the statistical analysis, there was a statistically significant difference throughout the heating process between the degree of contaminant mass removal achieved during the heating *temperature profile* tests and the heating *duration profile* tests. The heating *duration profile* tests removed significantly more TCE and PCE mass from the rock matrix than the heating *temperature profile* tests at TP6, TP5 and TP4 ( $P = 0.01, 1.12E-07$  and  $8.11E-07$ , respectively). The average TCE and PCE mass removal achieved by the two different heating profiles at TP6, TP5 and TP4 in the different types of rock, with the exclusion of black mudstone, is shown in Table 5.4.

**Table 5.4. Average Contaminant Mass Removal Attained at the Last Three Temperature Points of the Heating Tests for All Rock Types Excluding Black Mudstone**

Temperature point	Average contaminant mass removal (%)			
	Heating temperature profile		Heating duration profile	
	TCE	PCE	TCE	PCE
TP6	93.6 ± 6.9	88.1 ± 10.4	99.6 ± 5.2	96.8 ± 4.8
TP5	71.9 ± 27.3	75.9 ± 23.4	96.9 ± 6.6	95.9 ± 5.3
TP4	59.1 ± 37.7	62.7 ± 24.7	94.2 ± 11.5	94.1 ± 7.1

Higher concentrations of PCE were noted in samples of black mudstone in the last stages of the heating duration profile tests (TP6 and TP5), likely as a consequence of the drying out of the rock matrix (Figure 5.21). Such concentrations decreased the overall degree of contaminant mass removal achieved during the heating *duration profile* tests (Table 5.3) making it similar to that of the heating *temperature profile* tests.

The Friedman's test confirmed the that when all the rock types were included in the analysis, the only statistically significant difference between the degree of contaminant mass removal observed in the heating *temperature profile* and heating *duration profile* tests was found at TP4 ( $P = 0.01$ ). There was no significant difference between the degree of contaminant mass removal achieved in the heating *temperature profile* tests and that of the heating *duration profile* tests at TP6 and TP5 ( $P = 0.22$  and  $0.12$ , respectively). However, when black mudstone was excluded from the statistical analysis, the Friedman's tests revealed a statistically significant difference at TP6 and TP5, but not at TP4 ( $P = 0.17, 0.04$  and  $2.0E-03$ , respectively). In general, heating at the boiling point of water for an extended period of 72 hours was more effective than elevating the operational temperatures to 200°C.

### Effect of Chemical Compound

The two-way ANOVA with replication did not reveal a statistically significant difference between the results of TCE and PCE mass removal (when black mudstone was included in the analysis), for neither the heating *temperature profile* nor the heating *duration profile* tests, at any of the temperature points of the heating process, except at TP4 ( $P = 0.97, 0.32$  and  $3.31E-03$  for TP6, TP5 and TP4, respectively). At this heating temperature point, the degree of TCE removal was significantly different to that of PCE during the heating experiments, indicating that heating was affected by the chemical properties of the chlorinated compound. During heating, with either

the heating *temperature profile* or the heating *duration profile*, the main bulk of the contaminant concentration in the rock matrix, which is present as aqueous phase, is removed by boiling. This bulk concentration represents the higher percentage of the contaminant mass that is frequently removed during the first stages of heating. However, at the end of the heating process a recalcitrant fraction frequently remains, often as a sorbed phase (Uzgiris et al., 1995). In general, rock samples spiked with PCE presented higher rock matrix concentrations than samples spiked with TCE. The latter due to the higher organic carbon-water partitioning coefficient for PCE (= 364 mL/g; Pankow and Cherry, 1996) compared to that for TCE (= 126 mL/g; Pankow and Cherry, 1996).

This difference between the removal of TCE and PCE were slightly more noticeable when black mudstone was excluded from the statistical analysis. It was confirmed that at the end of the heating process (TP6) there was no significant difference between the degree of TCE mass removal and that of PCE ( $P = 0.09$ ); however, a significant difference was noticed in TP5 and TP4 ( $P = 1.64E-06$  and  $1.39E-05$ , respectively). More PCE was removed than PCE during the heating tests at TP4 and TP5, but this was only noted during the heating *temperature profile* tests. Hence, a field application operated with a similar profile to that of the heating *temperature profile* tests could be more sensitive to the chemical properties of the contaminant.

However, the Wilcoxon test revealed that no statistically significant difference could be noted at TP6, TP5 or TP4, neither when the black mudstone was included nor when it was excluded from the analysis ( $P < 0.05$ ). The difference between the results of the two-way ANOVA and the non-parametric analysis indicated that the results of both the heating temperature profile and the heating duration profile tests were not normally distributed. Hence, the removal of the contaminants from the rock matrix by heating does not appear to be sensitive to the chemical properties of the chemical compound. The  $P$  values produced by the Wilcoxon test for both heating profiles are showed in Table 5.5.

**Table 5.5. Non-Parametric Analysis (P-values) on the Results of the Heating Temperature Profile and Heating Duration Profile Tests at the Last Three Stages of Heating**

	Wilcoxon test ( $P$ -values)			
	Heating temperature profile		Heating duration profile	
TP6	0.55	0.16*	0.45	0.84*
TP5	0.27	0.56*	0.67	1.0*
TP4	0.8	0.69*	0.35	0.69*
* Statistical analysis did not include samples of black mudstone				

### Effect of Rock Type on Contaminant Removal

The two-way ANOVA with replication showed that the contaminant mass removal was significantly different for each type of rock throughout the heating process, regardless of the heating profile utilized during the heating tests (95 % significance level). The latter was observed independently of the inclusion or exclusion of black mudstone. When black mudstone was included in the analysis, the  $P$ -values were 0.01, 0.02 and  $1.48E-04$  for the TP6, TP5 and TP4 temperature points, respectively. When black mudstone was excluded from the analysis the  $P$

*values* for TP6, TP5 and TP4 were 0.04, 2.17E-06 and 2.43E-05, respectively. In addition, the Friedman's test confirmed the statistically significant difference between the degrees of contaminant mass removal for each type of rock. The *P values* produced by the Friedman's test when black mudstone was included in the analysis were 2.0E-03, 0.01 and 0.03 for TP6, TP5 and TP4, respectively. When black mudstone was excluded from the analysis the resulting *P values* were 0.01, 0.02 and 0.04 for TP6, TP5 and TP4, respectively. Therefore, the rock properties influenced the effectiveness of heating, which is further discussed in the following paragraphs with the aid of PCA.

### **Effect of Rock Properties**

Figure 5.22 illustrates a representative example of the PCA performed on the results of the two different heating profile tests at TP6 and the results of the rock property analyses for the seven different rock types. The two-way ANOVA analysis revealed that the results of the dry bulk density and permeability analyses showed no statistically significant difference among the seven rock types utilized during the heating experiments. Hence, such results were excluded from the PCA analysis to reduce the number of variables and facilitate the examination of the relationships between variables. In addition, to reduce the number of factors (relationships between variables), the Kaiser criterion was utilized to select only factors with eigen values greater than 1 (greater than their original variable value) (Kaiser, 1960). Hence, Factor 1 was the only factor that was retained (eigen value = 5.1), which explained 85.4% of the relationships between variables and represented the effect of rock properties on the degree of contaminant mass removal during heating (Figure 5.22).

The PCA analysis revealed that porosity favored the degree of contaminant mass removal from the rock matrix. In contrast, fraction organic carbon had a negative effect on the contaminant mass removal. In Figure 5.22, rock samples in which higher degrees of contaminant mass removal were achieved are located on the right side. Samples of sandstone and dolostone with a combination of higher porosity and lower fraction organic carbon exhibited higher degrees of contaminant mass removal. Samples of gray mudstone, limestone, red mudstone and siltstone are clustered together at the proximity of the centerline of the plot with similar porosities and fraction organic carbon. The latter indicates that in a field application, such types of rock could present a similar contaminant mass removal under heat treatment at similar conditions. Finally, with a combination of lower porosity and higher fraction organic carbon, black mudstone exhibited the lowest degree of contaminant mass removal. In addition, a lower fraction organic carbon would result in a lowered sorbed mass in the rock matrix, which would facilitate the removal of the contaminant from the rock matrix.

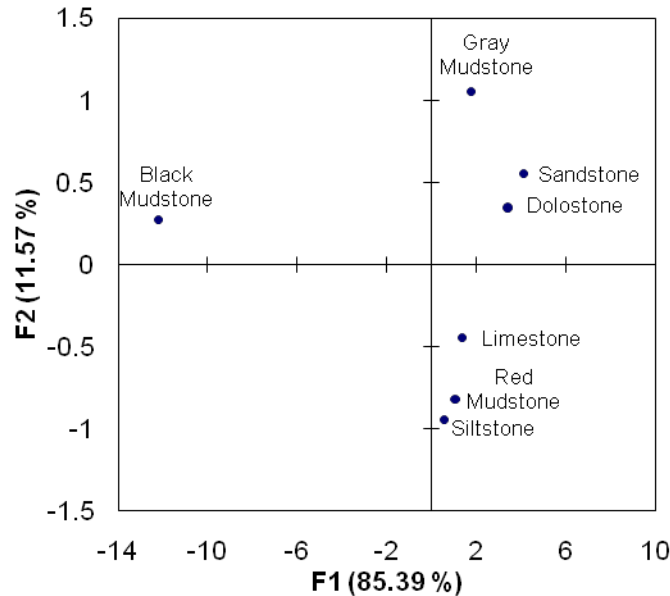


**Figure 5.22. Principal Component Analysis (PCA) of the Results of the Heating Tests on Different Rock Types, and the Results of the Porosity and Fraction Organic Carbon Analysis**

### 5.3.1.5 Conclusions

Heating duration had a greater effect on the degree of TCE and PCE mass removal compared to heating temperature. In heating *duration profile* tests the majority of contaminant mass removal was achieved in the early stages of heating. In samples of sandstone, dolostone, limestone and siltstone further heating did not lead to a significant decrease in contaminant concentration. Heating *temperature profile* tests required final target temperatures of 200°C to remove the majority of the contaminant mass. In thermal field applications, extending treatment duration under standard operational temperatures beyond the boiling point of water would, therefore, be more effective than elevating temperatures above the boiling point of water. The removal of TCE and PCE from the rock matrix by heating was not sensitive to the chemical properties of the compounds.

Rock properties had a significant effect on contaminant mass removal during heating experiments. It was determined that the rock properties observed in samples of sandstone and dolostone, such as high porosity and low fraction organic carbon, contributed to the increase in contaminant mass removal during the heating tests. In field applications, fractured bedrock with higher porosities and lower fraction organic carbon would favor the performance and effectiveness of thermal treatment in the removal of TCE and PCE.

### 5.3.2 Treatability and Laboratory Study Results for NAWC Site Microbial Characterization

This evaluation was conducted in order to determine the effects of thermal heating on the aquifer microorganisms. The hypothesis was that because of the high temperatures used, the possibility existed that the aquifer may be thermally sterilized. That, in turn, could deactivate microbial processes that naturally biodegrade the aquifer. If the aquifer can be thermally sterilized, it is not

known if it will remain sterile or whether it can be repopulated with microorganisms after temperatures cool. The purpose of this investigation was to assess these possibilities by (1) counting microorganisms in groundwater before, during, and after thermal heating using microscopic techniques, and (2) using carbon dioxide production assays to compare microbial activity in groundwater before and after thermal heating.

The conceptual design of this study was to (1) establish baseline numbers of microorganisms in groundwater from selected wells at the NAWC site, (2) measure baseline numbers of microorganisms in groundwater produced from the thermal heating wells prior to the initiation of thermal heating, and measure baseline microbial activity using CO<sub>2</sub> production assays with groundwater, (3) measure numbers of microorganisms and CO<sub>2</sub> production microbial activity in groundwater from the thermal heating wells during thermal heating, and (4) measure numbers of microorganisms and CO<sub>2</sub> production microbial activity in groundwater from the thermal heating wells after thermal heating has ceased. The working hypothesis was that heating the bedrock to ~200°F would effectively sterilize the groundwater. After the heating ceased, there was the possibility that (1) numbers of microorganisms and microbial activity would return to pre-heating levels or (2) that numbers of microorganisms and microbial activity would remain lower than pre-heating levels.

#### **5.3.2.1 Methods and Materials**

Water samples from the NAWC site were collected from selected wells in the vicinity of TCH demonstration area. Samples were collected in sterile 1 L glass bottles, chilled to 4°C and shipped to the laboratory for processing. The epifluorescent microscopic method of Hobbie et al. (1977) was used to enumerate numbers of bacterial cells. Depending on cell concentrations, between one and ten mls of water was filtered onto a black filter (0.2 micron, 10 mls diameter) and stained with acridine orange. The damp filter was placed between a microscope slide and a coverslip using immersion oil. An epifluorescent microscope with a mercury lamp was used to observe the stained cells at x 1000 magnification. The number of bacteria per milliliter was estimated from a count of 10 random fields. Sterile blanks typically exhibited 5 cells per ten fields yielding a lower detection limit of approximately 2.5 x10<sup>3</sup> cells/ml. Cell counts were made in duplicate and reported ± 1 standard deviation.

Microcosms for bioassays of CO<sub>2</sub> production were constructed in duplicate by adding 5 mls of unfiltered water to 20 ml septated serum vials. Initial treatments were immediately frozen. Killed controls were prepared in duplicate by autoclaving the microcosms three times for 1hr on three successive days. Final treatments and killed controls were incubated in the dark at 25°C for varying lengths of time. For the pre-heating assays, the incubations began on February 14, 2009 and ended on August 21, 2009 giving an incubation period of 188 days. For the first post-heating assays, the incubations began on August 21, 2009 and ended on November 9, 2009 for an incubation period of 80 days. For the second post-heating assays, the incubations began on November 10, 2009 and ended on January 18, 2010 for an incubation period of 70 days. After the incubation periods, the frozen initials were thawed. Duplicate initial, final, and killed treatments were acidified below pH 2.0, a 0.5 ml aliquot of headspace gas removed and CO<sub>2</sub> quantified using gas chromatography with thermal conductivity detection. The concentrations of CO<sub>2</sub> present in the headspace gas were reported in unites of µmol/L CO<sub>2</sub> ± 1 standard deviation.

### 5.3.2.2 Baseline Characterization

Three kinds of baseline characterization were performed for this study. First, numbers of microorganisms present in eleven different wells at the NAWC site were counted. The results of this baseline characterization are shown in Table 5.6. Groundwater from these wells consistently showed numbers of microorganisms in the  $10^4$  to  $10^5$  cells per milliliter. These microbial cell numbers are typical of many groundwater systems (Wilson et al, 1983 and Balkwill, 1989)). In addition, this baseline characterization suggested that different wells produced microbial cells with different rates of growth. Acridine Orange is a fluorescent dye that binds to nucleic acids. The DNA-acridine orange complex fluoresces green, whereas the RNA-acridine orange complex fluoresces orange. Because actively growing cells have a preponderance of RNA, they fluoresce an orange color. On the other hand, cells that are largely dormant have a preponderance of DNA and fluoresce green. Thus, the color of fluorescence is a qualitative indicator of microbial growth rates. The data shown in Table 5.6 indicates that apparent microbial growth rates vary across the site, with some samples containing mostly green cells (lower growth rates) and others containing orange cells (higher growth rate).

The second kind of baseline characterization was numbers and apparent growth rates of cells in groundwater produced from the thermal heating wells HO-1, HO-3, HO-8, HO-1-, and HO-15. The numbers of cells present in these wells (Table 5.7) were similar to those found throughout the site (Table 5.6). The apparent growth rates of the cells, as indicated by the color of fluorescence, was more uniform. Most of the wells produced microorganisms that fluoresced green indicating low growth rates. Only two wells, HO-8 and HO-1 produced cells with noticeably orange fluorescing cells.

The third kind of baseline characterization was assays of CO<sub>2</sub> production from unfiltered groundwater collected at the site prior to thermal heating.

### 5.3.2.3 Results and Discussion

The results of microbial counts performed before, during and after thermal heating are shown in Tables 5.6-5.10 and Figure 5.23. The pre-heating counts were on the order of  $10^4$  cells/ml. In contrast, the counts in the hot composite sample (Table 5.8) were on the order of  $10^3$  cells/ml and were not significantly different from the sterile blanks prepared in the lab. Counts of microorganisms in the warm composite sample, taken from the cooling chamber, were on the order of  $10^6$  cells/ml and were notable because they exhibited evidence of active growth (Table 5.8). The first post-heating samples (t=1) showed microbial counts not significantly different than the pre-heating counts (Figure 5.23, Table 5.9). However, the second post heating samples (t=2) were significantly higher than the pre-heating samples (Figure 5.23).

The results of the CO<sub>2</sub> production bioassays are summarized on Figure 5.24. There was no measurable activity either prior to heating (February, 2009) or immediately after thermal heating (August, 2009). However, by November of 2009, there was CO<sub>2</sub> production during the incubation period (70 days) that was statistically significant.

The results of the microbial cell counts and the results of the CO<sub>2</sub> production bioassays are consistent with each other. Both methods indicate a largely inactive microbial population in the wells prior to thermal heating. The cell counts also indicate that, as expected, thermal heating

resulted in groundwater being sterilized (Table 5.8). By just a month after heating ended, the microbial cell counts had rebounded to pre-heating levels (Table 5.9, Figure 5.23), but microbial activity was still below measurable levels (Figure 5.24). By four months after heating ended, both cell counts (Figure 5.23) and CO<sub>2</sub> production were greater than they had been prior to thermal heating.

The results of this study demonstrate that, as expected, heating groundwater to approximately 200°F resulted in sterilization. However, the results also indicate that the aquifer was rapidly reseeded with microorganisms, and that both numbers of microorganisms and microbial activity in groundwater just four months after thermal treatment were actually greater than prior to treatment. These results show that, while thermal treatment does decrease both numbers and activity of microorganisms in the short term, the aquifer quickly regained its ability to support microbial populations as well as microbial activity.

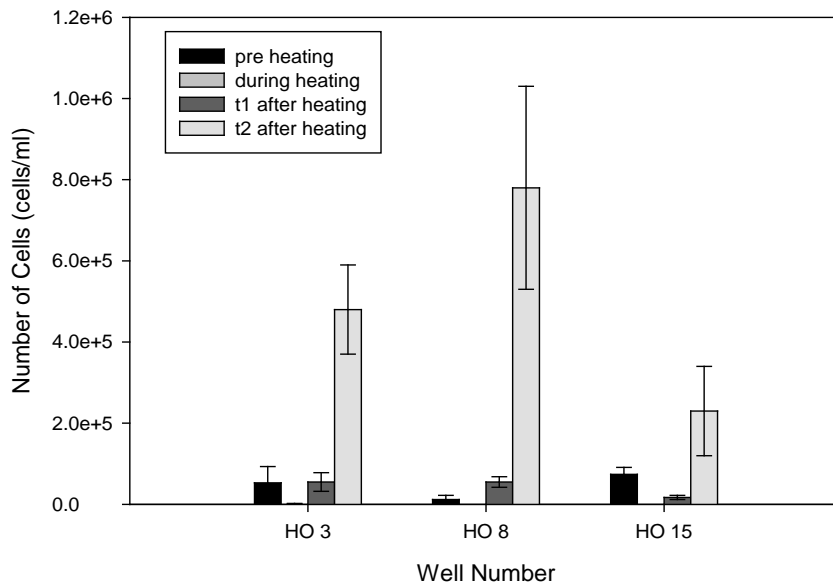


**Figure 5.23. Concentrations of Cells before, during and after Thermal Heating**

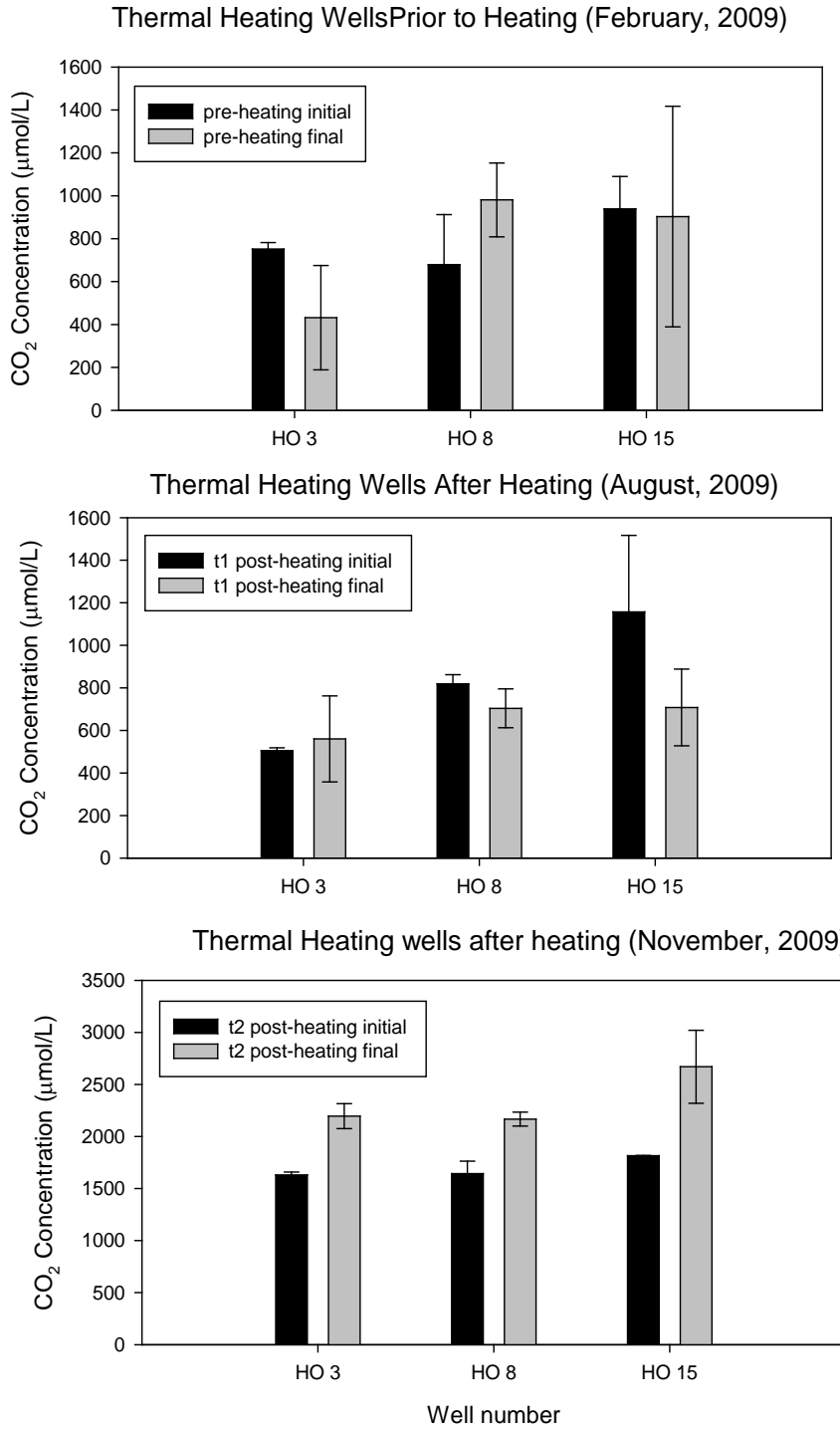


**Figure 5.24. Results of CO<sub>2</sub> Production Assays pre- and post-Thermal Heating**

**Table 5.6. Background Characterization of Bacteria at the NAWC Site**

<i>Well Number</i>	<i>Cells/ml</i>	<i>Description</i>
68BR A	$6.8 \times 10^4$	v/ small, green cells & rods
68BR B	$9.3 \times 10^4$	v/ small, green cells & rods, dividing cell observed
68BR C	$6.7 \times 10^4$	Green w/ orange cells
68BR D	$7.6 \times 10^4$	Green and orange cells noticeably larger than zone A
68BR E	$6.8 \times 10^4$	Green and orange cells noticeably smaller than zone D
68BR F	$6.9 \times 10^4$	Green and orange cells noticeably larger than zone E
<sup>1</sup> 4BR	$6.7 \times 10^5$	Cells mostly orange and large
<sup>1</sup> 30BR	$6.0 \times 10^4$	v/ small, green cells & rods
<sup>2</sup> 2BR	$2.3 \times 10^5$	Cells mostly orange and large
<sup>2</sup> 51BR	$2.1 \times 10^5$	Cells mostly orange and large
<sup>3</sup> 16BR	$8.0 \times 10^5$	Large orange, dividing cells
DIW Blank	$<2.8 \times 10^3$	v/ small, green cells

<sup>1</sup>background well within fence

<sup>2</sup>background well outside fence

<sup>3</sup>well impacted by vegetable oil

Green cells denote predominance of DNA with relatively little RNA, implying a lack of active growth.

Orange cells denote higher amounts of RNA, implying active growth

**Table 5.7. Cell Counts in Groundwater Samples Collected Prior to Thermal Treatment (2-11-2009)**

<i>Well Number</i>	<i>Cells/ml</i>	<i>Description</i>
HO-15	$7.4 \pm 1.7 \times 10^4$	very small, greenish-white cocci
HO-10	$3.7 \pm 0.3 \times 10^4$	very small, greenish-white cocci
HO-8	$1.2 \pm 0.0 \times 10^4$	small green w/ orange cells
HO-3	$5.3 \pm 0.4 \times 10^4$	very small, greenish-white cocci
HO-1	$5.2 \pm 0.2 \times 10^4$	small green w/ orange cells
Filtered DIW Blank	$2.2 \pm 0.9 \times 10^3 \pm$	very small, green cells

Green cells denote predominance of DNA with relatively little RNA, implying a lack of active growth.

Orange cells denote higher amounts of RNA, implying active growth

**Table 5.8. Cell Counts in Groundwater Samples Collected during Thermal Treatment (5-29-2009)**

<i>Well Number</i>	<i>Cells/ml</i>	<i>Description</i>
Hot composite <sup>1</sup>	$1.4 \pm 0.1 \times 10^3$	very small orange cocci
Warm composite <sup>2</sup>	$1.17 \pm 0.05 \times 10^6$	large orange rods and cocci
Filtered DIW Blank	$7.5 \times 10^2 \pm 0.05$	very small, green cells

<sup>1</sup>Water temperature ~140°F

<sup>2</sup>Water temperature ~ 60°F

Green cells denote predominance of DNA with relatively little RNA, implying a lack of active growth.

Orange cells denote higher amounts of RNA, implying active growth

**Table 5.9. Cell Counts in Groundwater Samples Collected after Thermal Treatment (8-21-2009)**

<i>Well Number</i>	<i>Cells/ml</i>	<i>Description</i>
HO-15	$1.7 \pm 0.5 \times 10^4$	very small, greenish-white cocci
HO-10	$9.9 \pm 3.2 \times 10^4$	very small, greenish-white cocci w/ few reddish cells
HO-8	$5.5 \pm 1.3 \times 10^4$	very small, greenish-white cocci
HO-3	$5.5 \pm 2.3 \times 10^4$	very small, greenish-white cocci
HO-1	$1.0 \pm 2.5 \times 10^5$	very small, greenish-white cocci w/ some orange cells
Filtered DIW Blank	$3.3 \pm 1.0 \times 10^3$	very small, green cells

Green cells denote predominance of DNA with relatively little RNA, implying a lack of active growth.

Orange cells denote higher amounts of RNA, implying active growth

**Table 5.10. Cell Counts in Groundwater Samples Collected after Thermal Treatment (11-4-5-2009)**

<i>Well Number</i>	<i>Cells/ml</i>	<i>Description</i>
HO-15	$2.3 \pm 1.1 \times 10^5$	small, greenish-white cocci
HO-14	$4.4 \pm 2.2 \times 10^5$	very small, greenish-white cocci
HO-11	$3.8 \pm 0.5 \times 10^5$	long green and orange rods
HO-8	$7.8 \pm 2.5 \times 10^5$	small, greenish-white cocci
HO-3	$4.8 \pm 1.1 \times 10^5$	very small, greenish-white cocci w/ some orange cells
Filtered DIW Blank	$2.4 \pm 1.0 \times 10^3$	very small, green cells

Green cells denote predominance of DNA with relatively little RNA, implying a lack of active growth.

Orange cells denote higher amounts of RNA, implying active growth

## 5.4 DESIGN AND LAYOUT OF TECHNOLOGY COMPONENTS

The design and layout of TCH components is provided in Section 5.1.

## 5.5 FIELD TESTING

TCH operations ran continuously for 106 days, 24 hours per day, 7 days per week without any major shutdowns other than shutdowns for scheduled maintenance and minor equipment replacement and GAC change-outs.

The heating period lasted a total of 97 days, while the extraction system operated for 106 days. This included 6 days of startup, 97 days of operation and 3 days of cool down. The operational phases are as follows:

- Extraction phase (day 1 to day 6, 6 days from 4/10/09 to 4/15/09): The vacuum system was turned on and vapors extracted from the wellfield. During this phase, the vacuum was adjusted, and the individual flows regulated in order to achieve a relatively uniform vapor extraction rate between the different vapor extraction screens. When the screens were all operational, the performance of the treatment equipment was verified, and the achieved wellhead vacuum distribution was monitored. The TCH heating was initiated on day 1 (4/10/09) by slowly ramping up the power to the heater circuits, such that the heater borings heated first to 100°C, then to higher temperatures as the water in the boreholes vaporized and was removed as steam.
- Heat-up and boiling phase (day 7 to day 103, 97 days from 4/16/09 to 07/21/09): Starting on 4/16/09 the heaters were slowly ramped up to full operation mode and the power input reached its design input of approximately 300 KW around 4/20/09. The demonstration volume slowly heated up during days 7 to 52 (45 days) and approached the maximum temperatures reached. The shallow zone reached the boiling point on day 22 (05/01/09), but the majority of the site heated up more slowly. The average site temperature on day 54 (06/02/09) was 211°F and all depth intervals from the surface and down to 35 ft bgs had average temperatures of 216°F or more. After achieving the boiling point at the different treatment depths, heating continued until day 103 (07/21/09). The bottom of the site did not heat up as expected. In the final heating period different attempts were made to limit the inflow of cooling groundwater into the TTZ, which was believed to be the major reason for the low temperatures at the bottom of the TTZ. This is further described in Section 6.1.6.
- Cool-down phase (3 days from day 104 to 106, 07/22/09 to 07/24/09): The TCH heating was stopped, and vacuum extraction continued for a short period, during which time the steam was removed from the subsurface to begin cooling of the site. Due to an excessive inflow of cooling groundwater, the heating period was ~ 5.5 weeks longer than expected, and the initial cool-down phase was approximately one week shorter than anticipated.

Figure 5.25 below provides a schedule of the field activities during the TCH on-site demonstration.

Task Name	2007			2008									2009												
	Oct	Nov	Dec	Jan	Feb	Mar	Apr	May	Jun	Jul	Aug	Sep	Oct	Nov	Dec	Jan	Feb	Mar	Apr	May	Jun	Jul	Aug	Sep	
Site Inspection	■																								
Review of NAWC Site Data			■	■	■																				
Draft Demonstration Plan		■	■	■	■	■	■																		
Demonstration Plan Review (by others)							■	■	■																
Final Demonstration Plan									■	■	■	■	■	■	■										
Permitting and Regulatory Interface													■	■	■	■	■	■							
Engineer Site Inspection									■																
TCH System Materials Procurement													■	■	■	■	■	■							
Site Preparation - Survey/Grading/Brush Removal													■	■											
Mobilization													■	■											
Drilling - Well Installation/Pre-Treatment Sample Collection and Analysis													■	■											
TCH System Construction																									
TCH System Shakedown/Startup																									
TCH System Operations																									
Post-Treatment Data Collection and Analysis																									
Demobilization																									
Well Abandonment/Cover Removal - To be Completed																									

**Figure 5.25. TCH Field Demonstration Schedule**

## 5.6 SAMPLING METHODS

The overall goal of the sampling and analysis program for the TCH demonstration at the NAWC site was to provide the data required for evaluation of the TCH system effectiveness on the impacted bedrock and groundwater at the site, and provide sufficient data for applying the technology to other sites in the future.

Specific objectives of the sampling were:

- Evaluate the effectiveness of the TCH technology in removing COCs from bedrock;
- Evaluate the effectiveness of the process treatment system;
- Evaluate the impact of treatment on the groundwater quality within the TTZ;
- Calculate COC mass removed from the subsurface;
- Provide data for site-specific validation of a heat conduction/steam migration model; and,
- Demonstrate that the Health and Safety Plan (HASP) criteria were maintained during operation of the TCH system.

To achieve these project objectives, the sampling and analysis program implemented the following activities:

- Collection of samples of the bedrock within the TTZ for quality analysis before and after treatment;
- Collection of samples of process vapor generated during operation of the TCH system to evaluate mass removal of COCs;

- Collection of process flow, pressures and process temperature data to ensure that the process treatment system was running properly and to gain data needed to evaluate the mass removal of COCs;
- Collection of samples of condensate generated during operation of the TCH system to evaluate mass removal of COCs;
- Collection of detailed temperature data during the project to support numerical simulations of the heating and its effect on remediation progress;
- Collection of rock samples for analysis of physical attributes before and after treatment;
- Collection of groundwater samples from bedrock borings within the TTZ before treatment; and,
- Monitoring of the ambient air quality to confirm that project-specific HASP criteria were not exceeded during construction or operation of the TCH system.

### 5.6.1 Bedrock Samples

Bedrock samples were collected from borings within the TTZ in order to evaluate TCH performance after treatment. Three boreholes were cored prior to treatment in order to collect the rock samples and enable collection of the groundwater samples required to establish baseline conditions. Three boreholes were also cored after treatment in order to collect a similar set of rock samples. The pre- and post-treatment core locations were located approximately 2-3 feet apart to ensure that the post-treatment cores would not intersect fractures that had been filled with grout from the pre-treatment coring activities. Figure 5.26 shows the drill rig on the vapor cover during the post-treatment bedrock sampling.



**Figure 5.26. Drill Rig on Vapor Cap during Post-Treatment Bedrock Sampling**

Comparison of the pre- vs. post-demonstration data provided the basis to evaluate remediation performance. The sampling results are further described in Section 5.7. Locations for the rock samples are shown on Figure 5.37. Table 5.11 shows an overview of the bedrock sampling conducted.

**Table 5.11. Bedrock Samples Collected Pre- and Post-Treatment**

<i>Data</i>	<i>Media</i>	<i>Number of locations</i>	<i>Frequency</i>	<i>Total Samples</i>	<i>QA/QC Samples</i>	<i>Method</i>
Rock-chip VOC concentrations	Rock	3 borings: BR1/BR P1 BR2/BR P/2 BR3/BP R3	1 sample round before treatment (BR1-BR3)  1 sample round after treatment (BRP1-BRP3)	BR1: 50 samples BRP1: 48 samples  BR2: 10 samples BRP2: 46 samples  BR3: 10 samples BRP3: 45 samples	5 duplicate rock samples  5 trip blanks	Methanol extracts analyzed by EPA Method 8260B/503 5A/5030B

Bedrock cores from pre-remedy and post-remedy borings were screened using a Photoionization detector (PID) to identify zones of high concentration. A total of 70 pre-remedy samples and 139 post-remedy samples were collected from the borehole cores. Five duplicate rock samples were collected and analyzed pre-treatment from BR-1 at 10, 20, 30, 40 and 59 ft bgs respectively. Furthermore, five trip blanks were analyzed during the pre-treatment rock sample analysis.

Because the post-demonstration cores were collected immediately after the heating ceased, the cores were generally at or near 100°C. To minimize vapor loss and ensure accurate characterization of post-treatment concentrations in the rock, the core barrels were retrieved from the subsurface and the ends were immediately capped. The sealed core barrels were then placed in an ice bath to quickly cool them to approximately 12°C, see Figure 5.27. This methodology conforms to the guidelines presented by Gaberell et al. (2002). This methodology was validated during the Cape Canaveral Inter-Agency demonstration project, and has been used successfully by TerraTherm in several states throughout the U.S., to verify attainment of soil cleanup goals. It has been shown to yield representative samples without significant loss of volatile COCs due to the elevated sample temperatures.



**Figure 5.27. Core Barrels Containing Hot Bedrock Being Cooled Before Rock Sampling**

Once the cores were cooled, they were removed from the core barrel for logging, screening, and sampling. The depth of each sample was marked on the plastic liner protecting the core to minimize evaporative contaminant loss. The larger rock sections were washed by hand, removing dust generated during the drilling process. One centimeter thick discs were then cut from the core from the appropriate depth using a portable wet-saw and immediately placed into methanol for crushing and extraction. The cutting process was necessary to isolate samples from the intact core sections, but was not expected to result in significant VOC losses given that the majority of contaminant mass was expected to be diffused into the matrix and sorbed to grain surfaces. The rock samples collected were then crushed in a rock crusher, placed in jar of methanol on a shaker for contaminant extraction and preservation for at least 12 hours whereupon the methanol extract was collected in vials and shipped to the laboratory.

Some core intervals came to the surface in relatively small pieces. From such cores the samples were collected without cutting the core in the field with the wet-saw. After extraction, the samples were shipped to an independent laboratory for EPA Method 8260B analysis. Figure 5.28 shows cutting of the discs with the wet-saw and subsequent preparation for laboratory analysis.



**Figure 5.28. Cutting and Methanol Preservation of the Cores**

After all samples were collected from the cores, the cores were rinsed in water, allowed to air dry and then labeled and organized in cardboard boxes as shown in Figure 5.29. Furthermore, as the picture indicates, only a few of the core pieces brought to the surface were longer than 12-15 inches. The results of the pre- and post-treatment rock analyses are presented in Section 5.7. Section 6.1.1 presents the results of the pre-treatment groundwater analyses.



**Figure 5.29. Pre-Treatment Rock Cores**

### 5.6.2 Process Vapor Samples

TerraTherm obtained process vapor samples (i.e., influent from the vapor extraction wellfield manifold and effluent from the vapor phase GAC vessels) in order to document the amount of COC mass removed from the subsurface, in order to allow the system operator to track the progress of remediation, monitor influent contaminant concentrations during operation, and to provide a record of VOC concentrations for demonstrating regulatory compliance.

Daily grab samples for field screening with a PID field instrument were collected on the discharge side of the vacuum blowers; samples were obtained at the vapor inlet to the first GAC vessel (SP104), in between GAC vessels (SP105), and at the discharge stack (SP106). In addition, periodic Summa canister sampling for VOC analysis using EPA method TO-15 was conducted. The Summa samples were collected in duplicate with the daily grab samples for PID screening, and were shipped to a qualified laboratory for analysis. Results from these samples allowed a correlation to be developed between the PID reading and total VOC and analyte specific (e.g., TCE) concentration in the vapor stream. The resulting correction factors were applied to the daily PID readings to estimate the daily VOC concentrations. The daily VOC concentrations were combined with the measurements of the daily flow rate to estimate the daily VOC mass flux during system operations (i.e., mass removed).

During the first week of operation, one duplicate sample was collected during a Summa canister sampling event from the lead GAC vessel influent (SP104), and one duplicate sample was collected during a Summa canister sampling event from lag GAC vessel influent (SP105). Additional duplicate samples were collected during Summa canister sampling events from the GAC vessel influent (SP104) on days 40 and 71 of operation. Duplicate samples were collected using a Y-tubing assembly to collect samples from the sampling port. The purpose of the duplicate sampling was to evaluate potential variability in the field sampling technique.

The vapor sample data provided the basis to evaluate the COC mass extraction rate and the overall remediation performance. Results are further described in Section 5.7.1. Table 5.12 provides an overview of the process vapor sampling conducted.

**Table 5.12. Process Vapor Samples Collected during Treatment**

<i>Data</i>	<i>Media</i>	<i>Number of locations</i>	<i>Frequency</i>	<i>Total Samples</i>	<i>QA/QC Samples</i>	<i>Method</i>
Extracted vapor VOC concentration	Process Vapor	Inlet to Vapor-phase GAC system (SP104) Between Vapor-phase GAC vessels (SP105) Discharge from Vapor-phase GAC system	Grab samples daily	318		PID calibrated to isobutylene, sample collected in tedlar bags

<i>Data</i>	<i>Media</i>	<i>Number of locations</i>	<i>Frequency</i>	<i>Total Samples</i>	<i>QA/QC Samples</i>	<i>Method</i>
		(SP106)				
Extracted vapor VOC concentration	Process Vapor	Inlet to vapor-phase GAC system (SP104)	1-Hour samples approximately twice a week during treatment	28	3 dup.	EPA Method TO-15, sample collected in Summa canister
Efficiency of primary GAC vessel	Process Vapor	Between vapor-phase GAC vessels (SP105)	1-Hour samples four times during treatment	4		EPA Method TO-15, sample collected in Summa canister
Efficiency of GAC treatment system	Process Vapor	Discharge from vapor-phase GAC system (SP106)	1-Hour samples two times during treatment	2		EPA Method TO-15, sample collected in Summa canister

### 5.6.3 Sampling Locations and Equipment

Both daily field screening and periodic Summa canister sampling were conducted at two sampling locations. The first sample port, SP104, was located at the influent to the lead GAC vessel. The second sample port, SP105, was located between the two GAC vessels at the influent to the lag vessel. Additional daily field screening was also performed at sample port SP106 located at the discharge from the second GAC vessel. The readings from SP106 represented the treated vapor extracted from the site.

Daily field screening was performed with a portable PID system, equipped with a 10.6 eV lamp.

Verification samples collected for laboratory analysis were collected using evacuated 6.0-Liter Summa sampling canisters equipped with 1-hour flow regulator valves. Summa canisters were certified clean and provided by Test America's analytical laboratory in Burlington, Vermont.

### 5.6.4 Field Screening

Samples were collected from sample ports SP104, SP105 and SP106 by connecting 1.0-Liter Tedlar sample bags to the port using Teflon tubing. Since each of these sample ports was on the pressure discharge side of the system blowers, no additional sampling pump was required to collect the sample. Once the sample was collected, the tubing was disconnected from the sample port and attached to the inlet of the PID.

Prior to sampling, the PID was calibrated daily using isobutylene span gas and following the manufacturer's recommended calibration procedure. The PID was programmed with the manufacturer's published correction factor of 0.54 for TCE as a rough approximation of the actual volumetric concentration observed in the field.

### 5.6.5 Summa Canister Sampling

Samples were collected using the evacuated Summa canisters by attaching the canister's flow regulator valve to the sample port with Teflon tubing. The flow regulator was calibrated to provide a one-hour sampling time once the valve was opened. Once the sample was obtained, the sample container was shipped to an independent analytical laboratory in Burlington, Vermont for analysis by EPA Method TO-15.

### 5.6.6 Process Flow, Pressure and Temperature Measurements

Temperature, pressure and flow rate of fluid streams were measured using in-line meters and gauges. These data were used to calculate the standard flow rate and mass emissions for the TCH process system. Data were collected on a daily basis and used to maintain the mass and energy balance presented in Section 6.1.4. Table 5.13 provides an overview of the process data collected during treatment.

**Table 5.13. Process Flow, Pressure and Temperature Measurements Collected during Treatment**

<i>Data</i>	<i>Media</i>	<i>Number of locations</i>	<i>Frequency</i>	<i>Total Samples</i>	<i>Method</i>
Flow rates, pressure, and temperature of vapor streams	Process Vapor	Multiple process lines in treatment system, daily manual readings	Daily	106	Meters and gauges

### 5.6.7 Condensate Samples

Liquid generated from steam condensation during the project was sampled from the liquid discharge line to the on-site surge tank. Samples were collected from sample port SP207. Grab samples were shipped to an independent analytical laboratory for analysis by EPA Method 8260B.

A total of 28 condensate samples were collected during treatment. The liquid sample data provided the basis to evaluate the COC mass extraction rate and the overall remediation performance.

Condensate duplicate samples were collected on days 11, 42 and 71 of operation. The purpose of the duplicate sampling was to evaluate potential variability in the field sampling technique.

Results are further described in Section 5.7. Table 5.14 provides an overview of the process vapor sampling conducted.

**Table 5.14. Condensate Samples Collected during Treatment**

<i>Data</i>	<i>Media</i>	<i>Number of locations</i>	<i>Frequency</i>	<i>Total Samples</i>	<i>Method</i>
Extracted water VOC concentration	Condensate	Liquid line to surge tank	Grab samples every ~ 4 days	28	EPA Method 8260B

### 5.6.8 Rock Temperature

Thermocouples (TCs) were installed at 8 locations between the thermal wells throughout the ISTD wellfield to monitor soil heating progress. These TCs were used to determine when the target treatment temperature was attained within and at the top and bottom of the TTZ. Attainment of the target treatment temperature was used to gauge when the TCH treatment could be stopped.

After termination of the thermal treatment on 7/24/2009 the cool-down of the site was monitored by collecting the subsurface temperatures on a regular basis. The first data collection in the cool-down phase was conducted 8/31/2009 and the last round of data was collected 4/16/2010.

Table 5.15 shows an overview of temperature readings collected.

**Table 5.15. Temperatures Collected during Treatment**

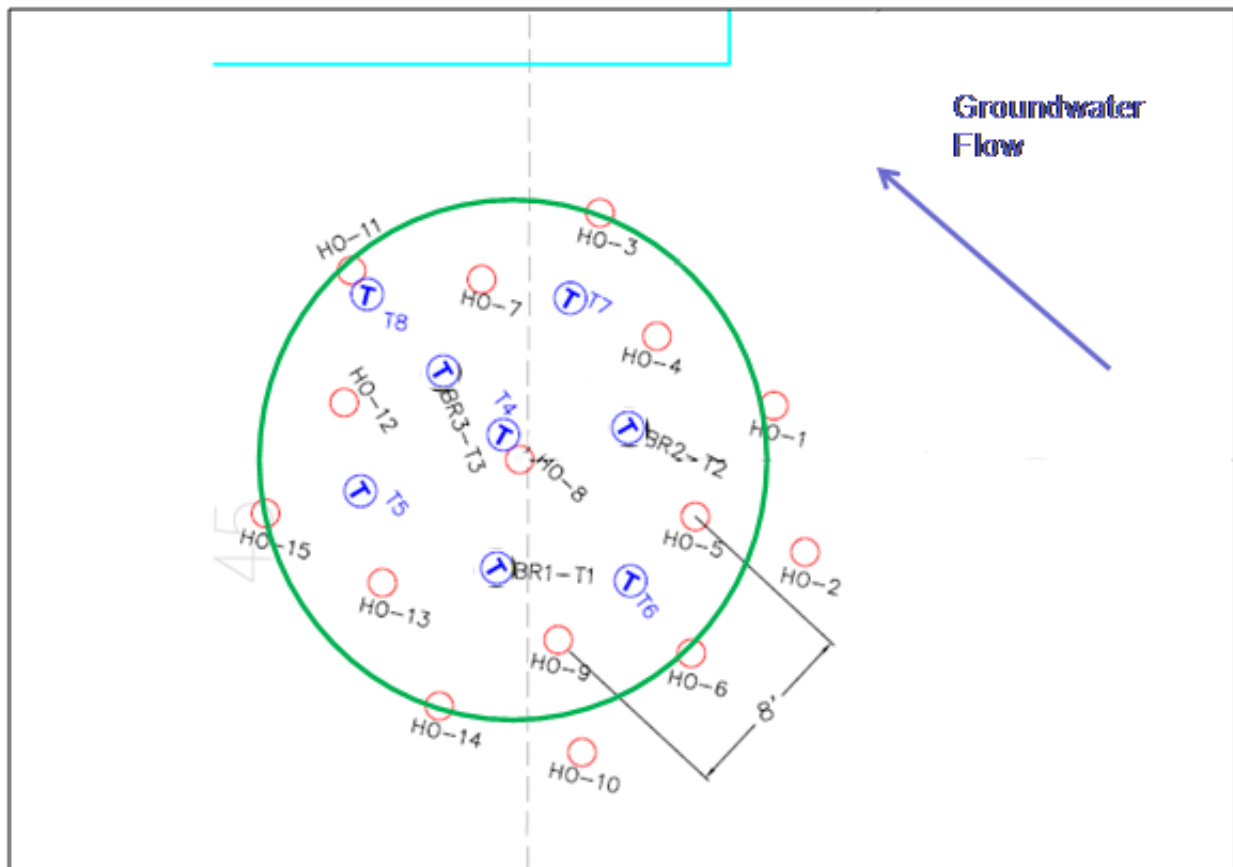
<i>Data</i>	<i>Media</i>	<i>Number of locations</i>	<i>Frequency</i>	<i>Total Readings</i>	<i>Method</i>
Subsurface temperature during operation	Rock	8 borings (TMP 1-8) each with 10 temperature sensors (from 5 to 50 ft bgs)	Daily for 106 days	~ 8,100 readings	Type K thermocouples
Subsurface temperature in cool-down phase	Rock	8 borings (TMP 1-8) each with 10 temperature sensors (from 5 to 50 ft bgs)	24 rounds between 8/31-09 and 4/16-10	~ 1,800 readings	Type K thermocouples

Table 5.16 shows the depth, number of TCs and the location of each of the 8 temperature monitoring locations at the site.

**Table 5.16. Depth, Number of Sensors and Location of the Temperature Monitoring Wells**

Monitoring Point	Total Depth (ft)	Number of Sensors	Distance to Closest Heater Well (ft)	Location
T1	50	10	4.1 (HO9)	Centroid
T2	40	7	4.1 (HO4)	Centroid
T3	50	10	4.4 (HO7)	Centroid
T4	50	9	1.3 (HO8)	Close to heater
T5	50	10	3.9 (HO12)	Between
T6	50	10	3.9 (HO5)	Between
T7	50	10	3.9 (HO3 and HO7)	Between
T8	50	10	1.2 (HO11)	Close to heater
Total		76		

The location of each of the 8 temperature monitoring points in the wellfield is shown in Figure 5.30. Each monitoring string consisted of an array of thermocouples located at a 5 ft vertical interval (e.g., 5, 10, 15, 20, 25, 30, 35, 40, 45 and 50 ft bgs for the deepest monitoring point).



**Figure 5.30. Location of Temperature Monitoring Points in the Wellfield**

In general, the temperature monitoring points were placed in three different locations in relation to the heaters. Three monitoring points were placed between two heaters (herein referred to as “between”), three monitoring points were placed in the centroid (herein referred to as “centroid”), while the remaining two were placed 2 feet from a heater (herein referred to as “close to heater”).

Wellfield temperature results are further described in Section 6.1.6.

### 5.6.9 Wellfield Vapor Samples

Vapor samples from individual vacuum extraction points were collected through a sample pump into 1-liter tedlar bags. Each extraction point had a sampling port from where the sample was collected. Since the sampled stream was under vacuum and contained steam, some condensation on the walls of the tedlar bag occurred. The bags were allowed to cool for approximately 30 minutes such that they reached ambient temperature before being sampled with the PID. This also allowed the CVOCs in the vapor and condensate to come into equilibrium which provided comparative results between sampling events. Vapor samples were analyzed in the field using a handheld PID calibrated to isobutylene.

Results are further described in Section 6.1.7. Table 5.17 shows an overview of the wellfield vapor sampling conducted.

**Table 5.17. Wellfield Vapor Samples Collected during Treatment**

<i>Data</i>	<i>Media</i>	<i>Number of locations</i>	<i>Frequency</i>	<i>Total Samples</i>	<i>Method</i>
PID screening on vapor streams from individual extraction screens	Wellfield Vapor	15 heater borings Collection in 1-liter tedlar bags with sampling pump, cooled to ambient	Grab samples approximately once per week. A total of 12 sample rounds were conducted.	180	PID calibrated to isobutylene, sample collected in tedlar bags

### 5.6.10 Ambient Air Samples

A PID equipped with a 10.6 eV lamp, was used to screen the breathing zone of employees during TCH wellfield installation and system influent and effluent monitoring. A project-specific action limit was calculated based on the OSHA permissible exposure limit (PEL) of 1 ppm for VC using the manufacturer’s reported response factor to the selected compound divided by an applied safety factor of 2. Given the mix of compounds that were likely to be present, a reading of 1.0 unit above background was selected as the action level for the TCH field demonstration.

### 5.6.11 Groundwater Samples

Pre-treatment groundwater samples were obtained from three wellfield locations HO-8, HO-12 and HO-13. The groundwater sample was collected from the co-located vapor extraction screen located adjacent to the heater boring. The location of the three wells is shown in Figure 5.31 below (red circles).

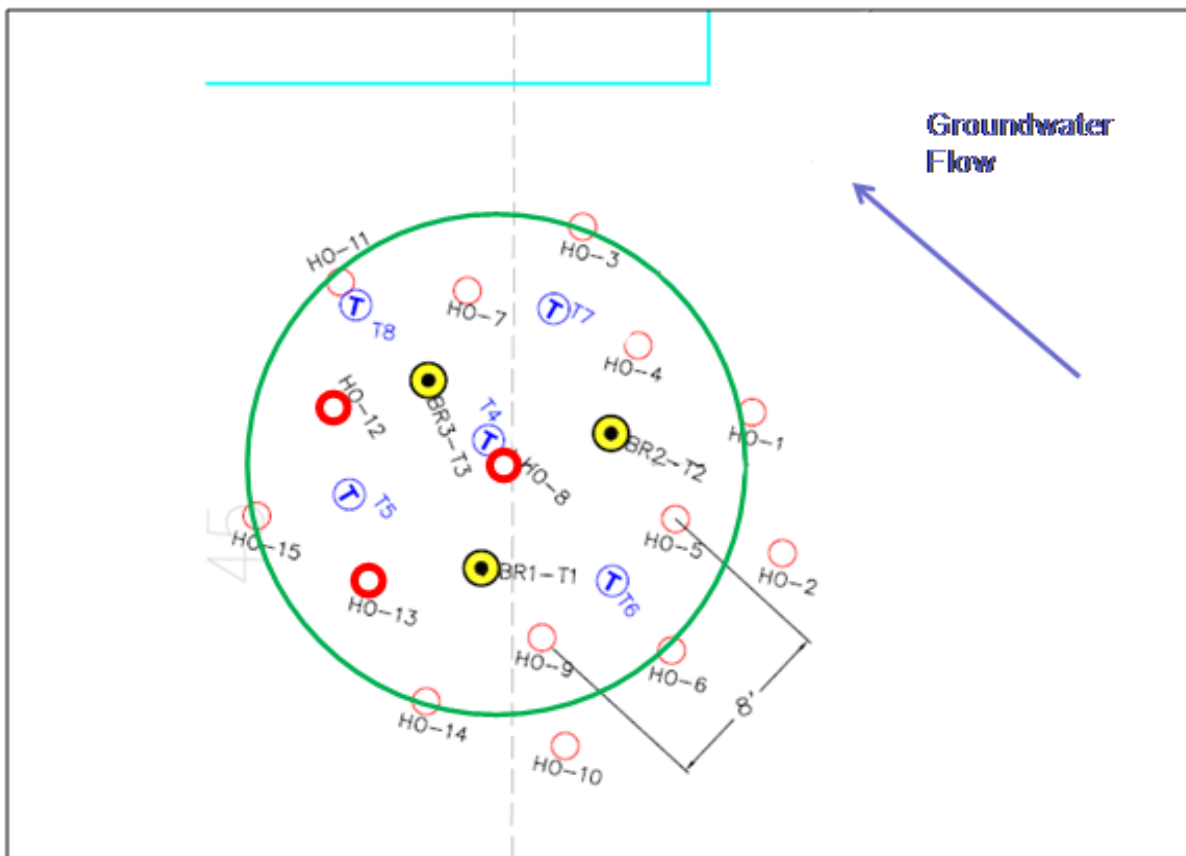


**Figure 5.31. Location of Pre-Treatment Groundwater Sampling Locations**

Three groundwater samples were obtained from each sampling location (i.e., the vapor extraction point co-located to the heaters) in order to characterize the vertical distribution of COCs pre-treatment. The approximate sample depth at each of the three locations is shown in Table 5.18.

**Table 5.18. Approximate Sample Depth for Pre-Treatment Groundwater Samples**

<i>Sample location</i>	<i>Depth of well screen [ft bgs]</i>	<i>Depth to water table [ft bgs]</i>	<i>Saturated thickness [ft]</i>	<i>Depth of top sample tube [ft bgs]</i>	<i>Depth of middle sample tube [ft bgs]</i>	<i>Depth of bottom sample tube [ft bgs]</i>
HO-8	42	5	32	18.00	26.00	34.00
HO-12	45	5	35	18.75	27.50	36.25
HO-13	44	5	34	18.50	27.00	35.50

The groundwater samples were collected using a peristaltic pump and new tubing for each borehole and sample interval. The tubing was cut to length and one end of the tubing was placed into the vacuum side of the peristaltic pump head and attached to the flexible tubing mounted in the pump head. Another short section of tubing was then run from the discharge side of the pump head to a flow through cell equipped with temperature, dissolved oxygen (DO), pH, ORP, and conductivity sensors and then to a bucket to collect purged water. The free end of the tubing was placed into the borehole until the end of the tubing was at the sampling depth indicated in Table 5.18. The peristaltic pump was turned on to produce a vacuum on the well side of the pump head and to remove water from the borehole in order to purge and sample the well. Low flow sampling methods were followed for purging and sampling each interval in the boreholes. In order to ensure a representative sample from the interval and minimize mixing of water from other portions of the borehole, the discharge rate of the pump was set at a low rate (50-100 ml/min). Once the measured values of temperature and conductivity stabilized, a groundwater sample was collected in appropriately labeled sample containers with sampling details and custody information. The sample was collected holding the sample container in a tilted position under the peristaltic pump discharge tube and filled to the desired amount. After sampling was complete, the peristaltic pump was disconnected and the tubing was removed from the well and discarded.

Results are further described in Section 6.1.1. Table 5.19 shows an overview of the pre-treatment groundwater samples collected.

**Table 5.19. Groundwater Samples Collected Pre-Treatment**

<i>Data</i>	<i>Media</i>	<i>Number of locations</i>	<i>Frequency</i>	<i>Total Samples</i>	<i>QA/QC Samples</i>	<i>Method</i>
Groundwater VOC concentrations	Groundwater	3 borings 3 samples per boring	1 sample round before treatment	9	3 duplicates	EPA Method 8260B

Post-treatment samples were planned to be collected, however; since there was evidence of significant inflow of groundwater during treatment, these samples were not collected. Because of the significant groundwater inflow during treatment, the post-treatment groundwater samples would have represented ambient surrounding groundwater conditions, not the conditions inside a TTZ following normal thermal treatment.

#### **5.6.12 Borehole Pressure Test**

The three boreholes BR1, BR2 and BR3 were pressure tested during drilling. The purpose was to gain data to determine a depth specific bedrock hydraulic conductivity for each of the three boreholes.

The pressure test was conducted during drilling at 10 ft intervals by placing a packer approximately 10 ft from the bottom of the borehole. The packer was mounted on a hose that

allowed water injection below the packer. After placement of the packer it was inflated inside of the borehole to serve as a watertight plug between the bottom and top of the borehole. By using this procedure the bottom of the borehole was cut off and it was ensured that injected water in the bottom of the borehole only could migrate away from the borehole through fractures. Water was then injected at different injection pressures for each test and the corresponding water injection flow was read. After the end of the pressure test the packer was removed from the borehole and drilling continued.



**Figure 5.32. Packer, Pressure Tank and Water Meter Used During the Borehole Pressure Test**

A total of 12 depth intervals were pressure tested corresponding to four tests in each of the three boreholes. Each of the 12 depth tests were conducted by injecting water at different injection pressures and reading the corresponding water flow between two and five times per depth interval.

Results from the pressure test are further described in Section 6.1.2. Table 5.20 shows an overview of the pressure tests conducted.

**Table 5.20. Pre-Treatment Pressure Tests**

<i>Data</i>	<i>Media</i>	<i>Number of locations</i>	<i>Frequency</i>	<i>Total Tests</i>	<i>Method</i>
Borehole pressure test	-	3 (BR1, BR2 and BR3)	4 depths per borehole 2-5 pressure test per depth	A total of 39 pressure tests	-

**5.6.13 Microbial Parameters**

Sampling descriptions and data resulting from the microbial characterization is described in detail in Section 5.3.2.

**5.6.14 Sample Identification and Labeling**

Each sample submitted for laboratory analysis was assigned a unique identification number and a unique field sample number. Field sample identification numbers were assigned in the field by the sampling crew. A label was affixed to each individual sample container with the following information written legibly in waterproof ink:

- Field sample identification number.
- Date and time of sample collection.
- Sample matrix.
- Preservative.
- Analysis to be performed.
- Name and initials of the sampler.

Field and laboratory sample custodians or their designated representatives were responsible for maintaining proper custody of samples to ensure the integrity of the samples from collection until analysis.

Chain-of-custody forms were provided by the laboratory contractor. Chain-of-custody records were maintained in accordance with the analyzing laboratory’s standard operating procedure to document sample custody from the time of collection until analysis.

A chain-of-custody record was initiated in the field for each cooler of samples transmitted to the laboratory. This form contained the following information:

- Unique sample identification code.
- Sampling date and time.
- Sample matrix.
- Number and type of containers per sample.
- Analysis required.

- Sampler's name.
- Custody release information including date, location, and technician's signature.
- Assigned shipping cooler number.

The original chain-of-custody record accompanied the cooler, and a copy was retained by the field sampler. If samples were hand delivered, a signed chain-of-custody record was obtained from the laboratory custodian after the samples were received and their condition checked.

Upon receipt in the laboratory, all samples were carefully checked to ensure that there were no broken or leaking sample containers, proper preservation methods were followed, and all labels and custody seals were intact.

Each chain-of-custody record was verified for accuracy and completeness, and any discrepancies were brought to the immediate attention of the person who relinquished custody to the laboratory. If there were discrepancies identified, the sample chain-of-custody record was corrected, signed, and a copy was returned to the field personnel within 24 hours.

From the time of receipt, the laboratory used its standard internal chain-of-custody procedures to ensure that the samples were appropriately tracked through completion of the analytical process or transmittal to the contract laboratory.

#### **5.6.15 Sample Handling, Packaging, and Shipping**

All bedrock, water and vapor samples were packaged and labeled after collection. Bedrock and water samples were placed in coolers with ice as soon as practicable to keep them cold during shipment. The samples were packaged and shipped according to the following procedure:

1. Verified that all sample containers had completed labels;
2. Placed sample containers (rock and water) in plastic resealable bags and place in coolers;
3. Placed blue or sealed bagged ice on top of and between samples in coolers (rock and water);
4. Secured and taped cooler drain plugs (rock and water);
5. Placed a completed Chain-of-Custody form in a plastic resealable bag inside each cooler (rock and water) or box (vapor);
6. Taped coolers/boxes with custody tape at opposite ends; and
7. Delivered to laboratory for analysis.

Calibration procedures for sampling equipment and decontamination procedures are included as Appendix E.

## **5.7 SAMPLING RESULTS**

### **5.7.1 TCE Mass Removal**

Figures 5.33 and 5.34 show the data at the inlet to the vapor phase carbon units. It was estimated that approximately 500 lbs of VOCs calculated as TCE were removed in the vapor stream alone based on observed PID readings and flow rates and by using the PID correction factor for TCE.

The estimate of 650 lbs is based on total VOCs detected by the laboratory in the Summa canister samples.

The VOC mass removal rate based on PID was 4.7 lbs/day on average while the removal rate based on Summa canister samples was 6.2 lbs/average. The vapor mass removal rates were typically 2-10 lbs/day during operation. The mass removal of VOCs in the liquid phase was 0.3 lbs/day on average.

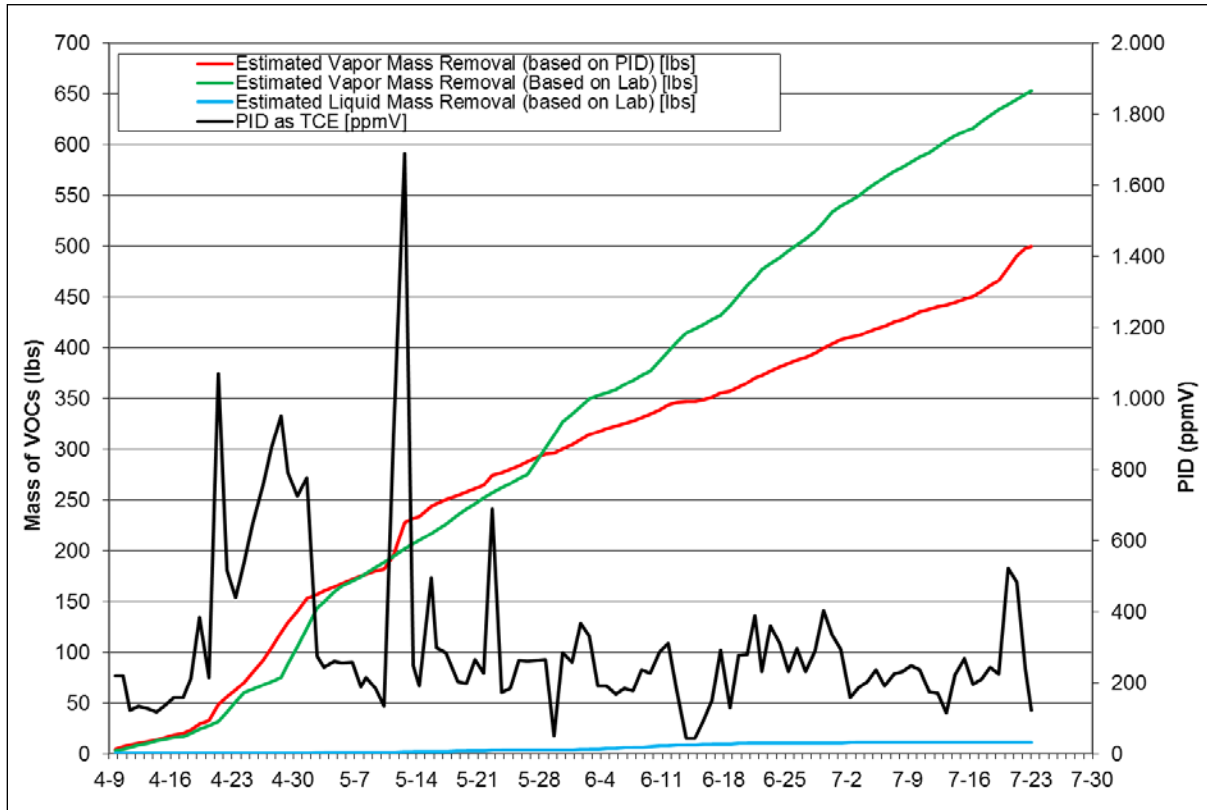


**Figure 5.33. PID Readings on Vapor Stream Samples and Associated Mass Removal Estimate**

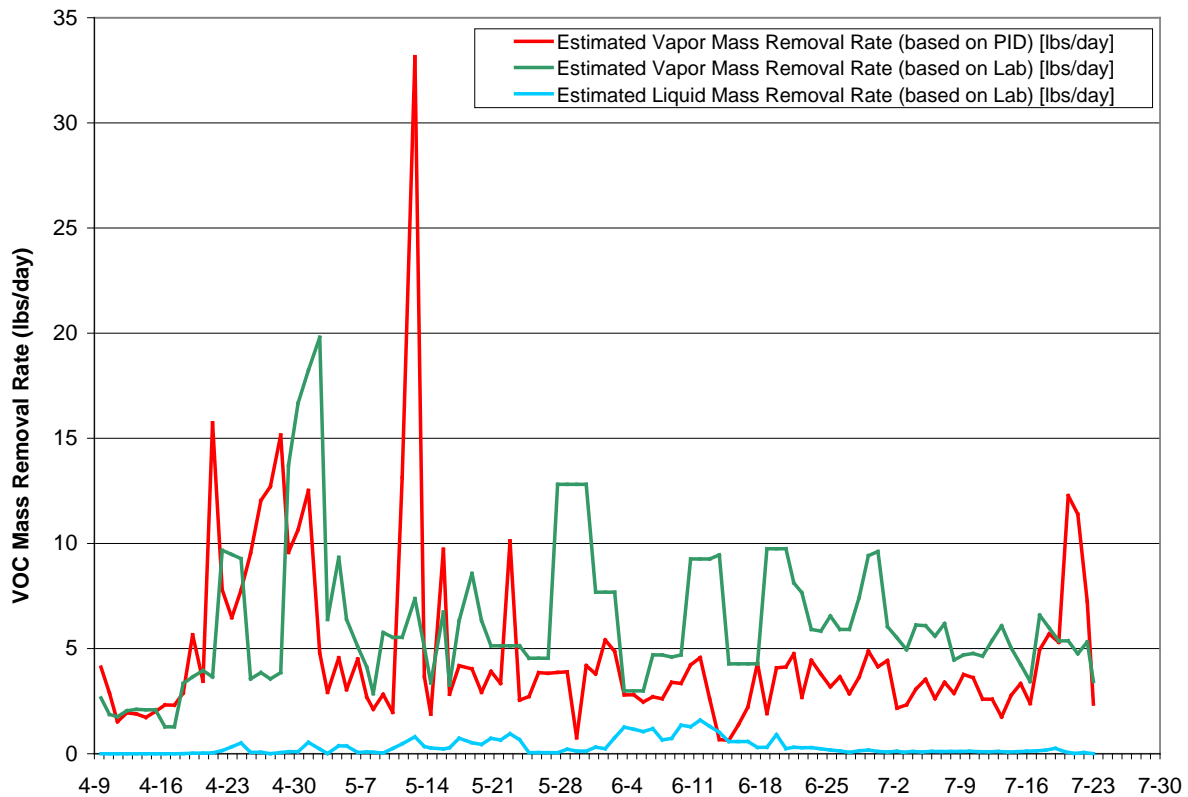


**Figure 5.34. Estimated VOC Mass Removal Rate during Operations**

The PID readings (and thus the mass removal rate) spiked between 4/20/09 and 5/24/09, during the time when the site heated to an average temperature around 200°F. This mass removal increase in the vapor stream is consistent with other TCH field projects. However, it would also be typical that the PID readings decreased to very low levels (less than 10-30 ppmv) toward the end of the heating period, indicating that the mass in the heated volume was exhausted. As shown in Figure 5.34, that did not occur.

The laboratory data collected from the vapor stream show a similar trend (Figure 5.35).

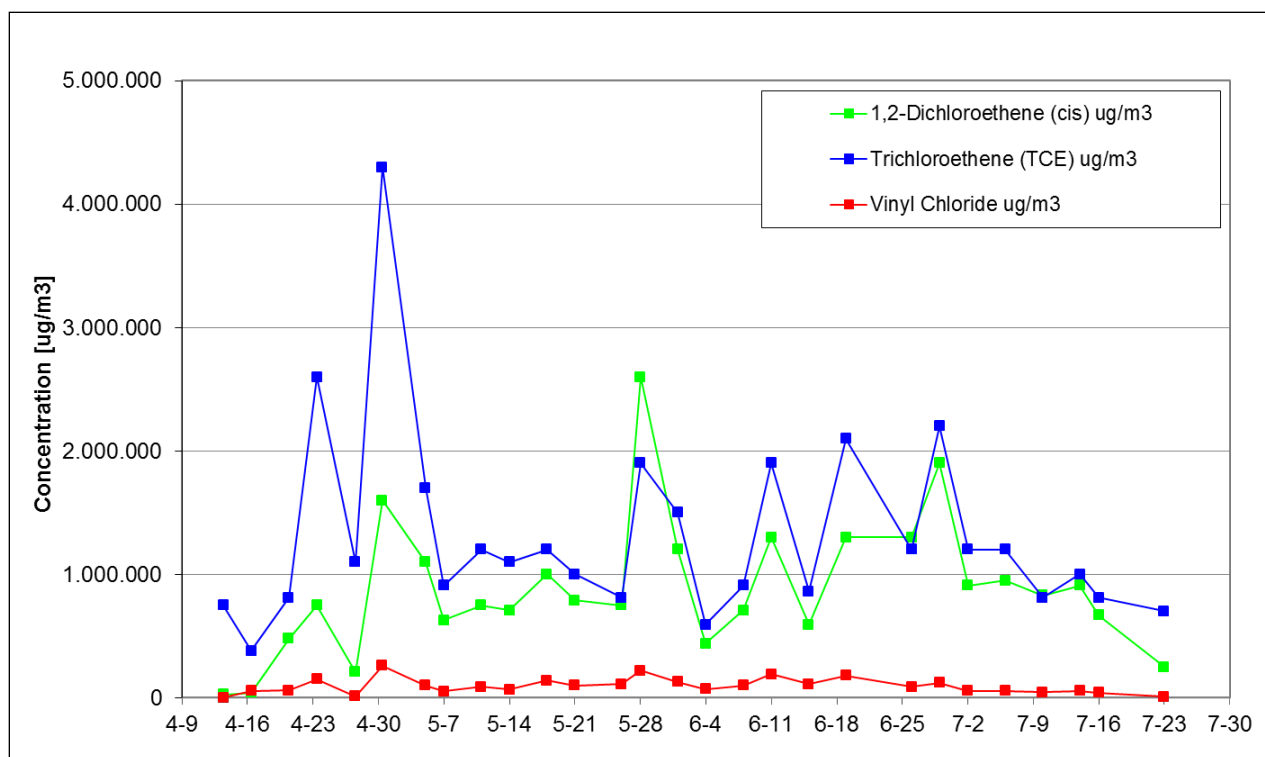


**Figure 5.35. Vapor Stream VOC Concentrations for the Dominant Compounds**

The more or less consistent level of VOCs in the vapor stream during the last two months of heating indicates that VOCs are entering from outside the TTZ and supplying additional mass to the treatment area. As cold, contaminated water flows towards the heaters, the groundwater is heated by thermal conduction from the matrix, and while some of the VOCs are vaporized, the fracture zones remain cooler than the larger matrix blocks.

It is noteworthy that the VC concentration remains significant in the entire operations period. Since VC is the most volatile VOC at most sites, it is normally removed within the first month of heating. The persistent level of VC in the vapor stream indicates that groundwater flowing into the TTZ was providing a constant source of contaminant mass entering the TTZ.

Figure 5.36 shows the VOC concentrations in the entrained water from the TTZ. The trends are similar to those seen for the extracted vapor. Based on these concentrations and measured liquid extraction rates, an estimated 33 lbs of TCE was removed in the liquid phase during TCH operations.

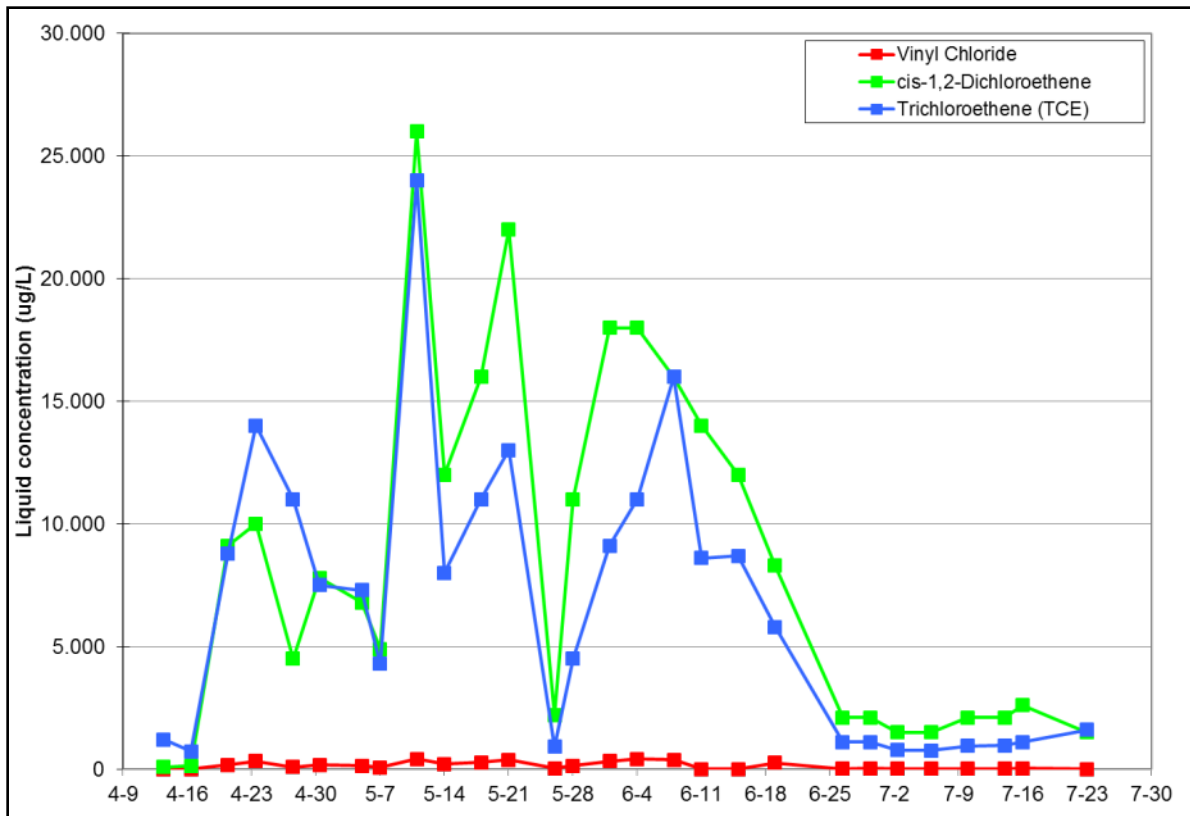


**Figure 5.36. Liquid Stream VOC Concentrations for the Dominant Compounds**

The trend in the extracted water VOC content supports the theory that VOCs entered the treatment area via influent groundwater.

Based on these data, a total (vapor and liquid) of approximately 530 lbs based on daily PID readings and approximately 680 lbs based on analytical data of TCE was extracted from the site.

### 5.7.2 Bedrock TCE Concentrations

The rock concentration of TCE was measured at three locations inside the TTZ pre- and post-thermal treatment. Pre-treatment rock concentrations were collected from BR1, BR2, and BR3, all located in centroid points. After collecting the pre-treatment rock samples temperature monitoring point T1 through T3 were installed at the three sampling locations, respectively. Approximately one week after heating ceased post-treatment rock samples were collected from neighboring holes located less than 1-2 ft from the pre-treatment borehole. The three pre- and post-treatment rock sampling locations are shown in Figure 5.37 below.

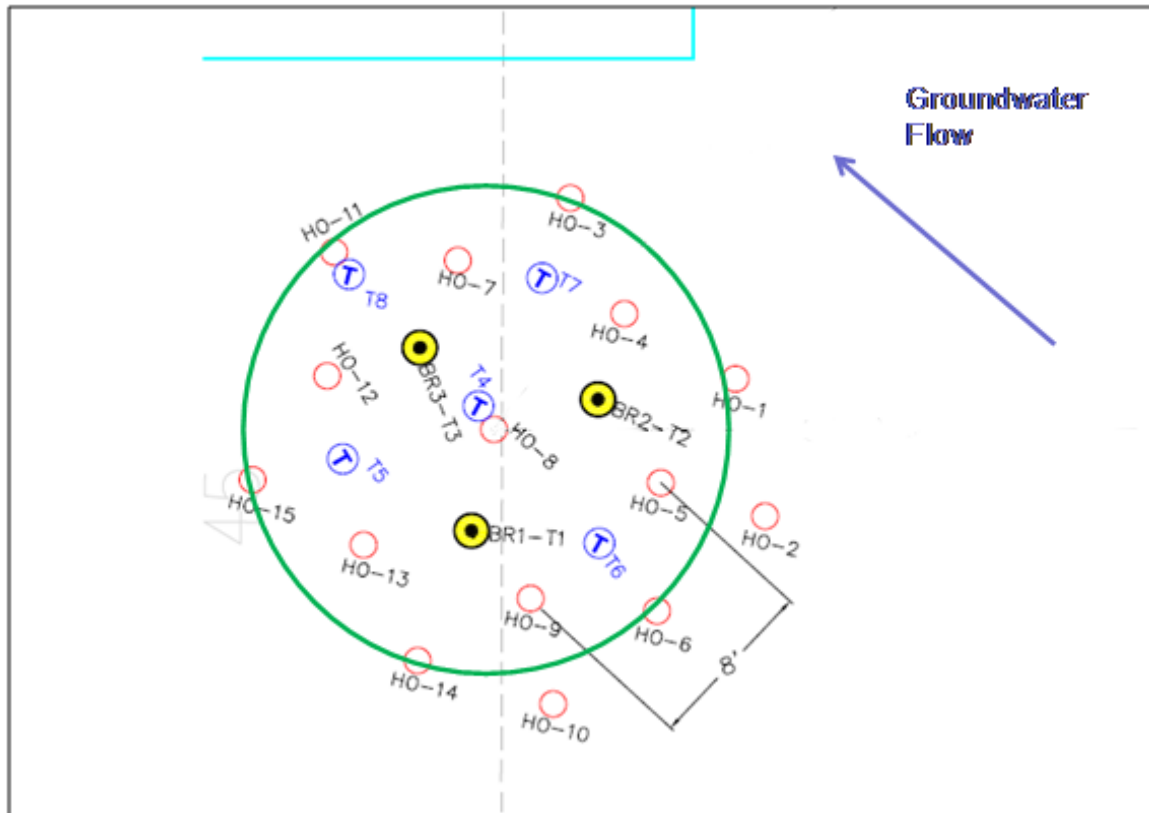


**Figure 5.37. Pre- and Post-Treatment Rock Concentration Sampling Locations**

The performance of the thermal treatment has been evaluated using two different measures:

- Comparison of all pre- and post-treatment rock matrix and fracture concentrations at each of the three sampling locations, not taking into account that not all sampling locations have been sampled both post- and pre-treatment and not taking into account that some of the sample depths may represent rock fractures.
- Comparison of all pre- and post-treatment rock matrix sampling locations by excluding what is believed to be all sample locations close to the major rock fractures (locations directly affected by the influx of cool ambient groundwater with significant CVOC concentrations).

#### **5.7.2.1 Pre- and Post-Treatment Rock Matrix and Fracture Concentrations**

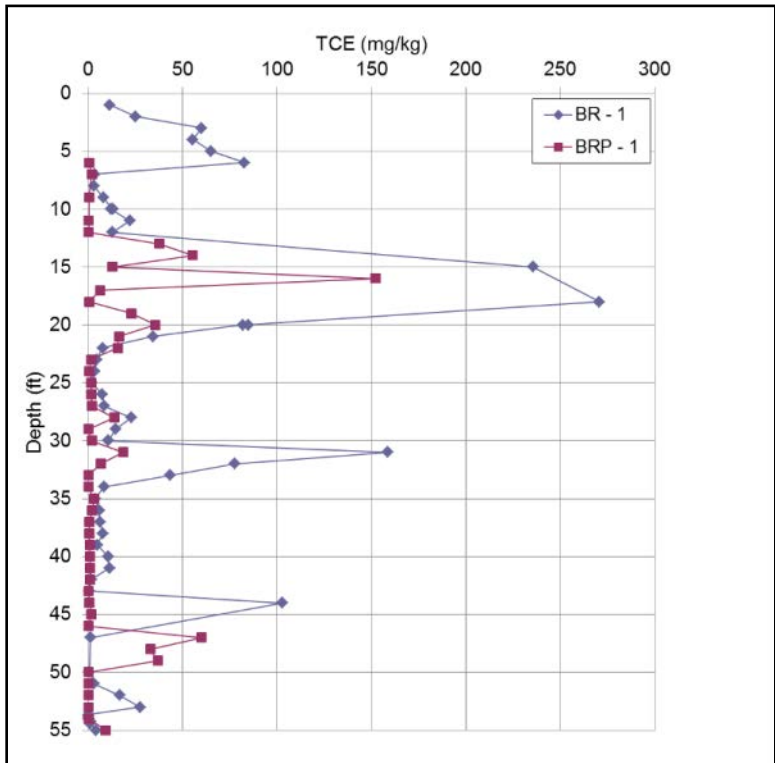
The following sections present the pre- and post-treatment rock concentration based on all samples collected at the site.

Table 5.21 below shows the rock samples collected from each of the three sampling locations pre- and post-thermal treatment. Please note that additional samples were collected from BRP2 and BRP3 at the post-treatment sampling event, which explains the higher post-treatment sampling density.

**Table 5.21. Number of Pre- and Post-Treatment Sampling Locations**

<i>Sampling location</i>	<i>Pre-treatment samples</i>	<i>Post-treatment samples</i>
BR1/BRP1	55	48
BR2/BRP2	10	46
BR3/BRP3	10	45

Figures 5.38-5.40 show pre- and post-treatment concentrations with depth for each of the sampling locations. While BR-1 was sampled at a 0-ft increment for both pre- and post-treatment sampling, BR-2 and BR-3 were sampled at a 5-ft increment during pre-treatment sampling and a 1-ft increment during post-treatment sampling. This accounts for the greater resolution of the post-treatment data for these locations.



**Figure 5.38. Pre- and Post-Treatment TCE Rock Matrix and Fracture Concentrations at Sampling Location BR1/BRP1**

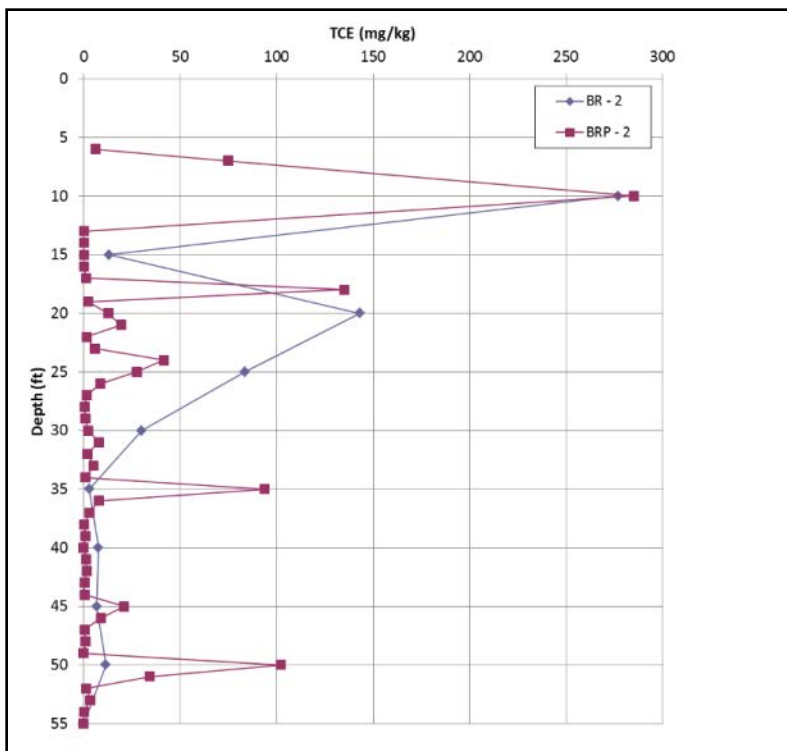


**Figure 5.39. Pre- and Post-Treatment TCE Rock Matrix and Fracture Concentrations at Sampling Location BR2/BRP2**

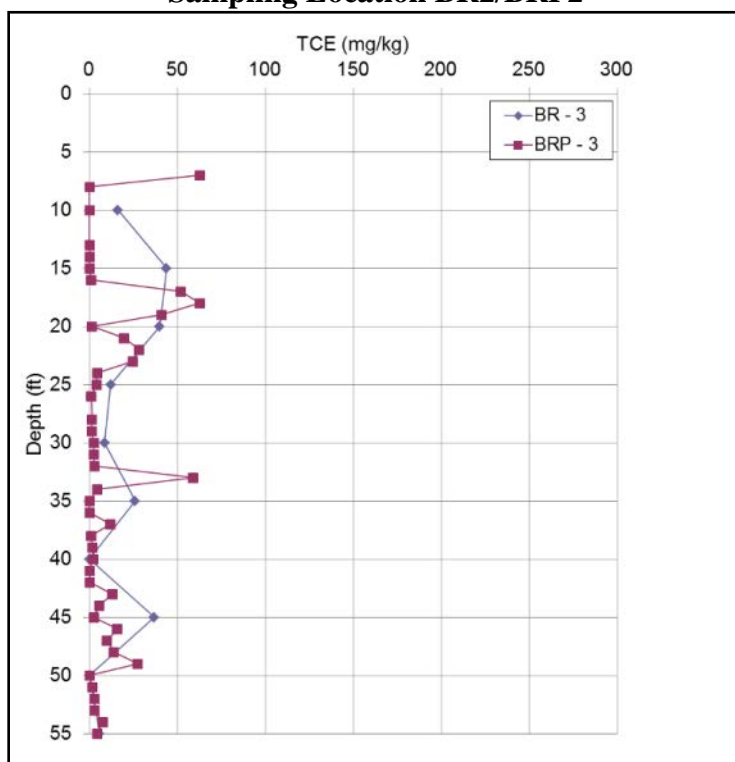


**Figure 5.40. Pre- and Post-Treatment TCE Rock Matrix and Fracture Concentrations at Sampling Location BR3/BRP3**

While a general decrease is observed in the TCE concentrations, some apparent increases are also seen. However, these typically do not represent depths where pre-operational samples were collected. Therefore, rather than indicating an accumulation of TCE, the data show that post-treatment concentrations are high in some rock sections that were not sampled before the thermal treatment (i.e., the pre-treatment concentrations are unknown).

Table 5.22 below shows the average, maximum and minimum pre- and post-treatment TCE rock concentration based on all data collected at the site. Please note that only samples collected inside the treated volume, e.g. from the surface and to 50 ft bgs, have been included in the comparison.

**Table 5.22. Pre- and Post-Treatment TCE Rock Concentrations**

<i>All samples</i>		<i>BR1</i>	<i>BRP1</i>	<i>BR2</i>	<i>BRP2</i>	<i>BR3</i>	<i>BRP3</i>
	<i>Unit</i>	<i>Pre-treatment</i>	<i>Post-treatment</i>	<i>Pre-treatment</i>	<i>Post-treatment</i>	<i>Pre-treatment</i>	<i>Post-treatment</i>
Average	[mg/kg]	35.38	12.73	63.94	19.60	20.43	12.10
Max	[mg/kg]	270.77	152.00	276.93	285.00	43.85	63.00
Min	[mg/kg]	0.48	ND	2.86	ND	0.07	ND
No of samples	[-]	46	43	9	40	9	40
Average remedial efficiency	[%]	64%		69%		41%	

ND: Not detected at the laboratory reporting limit

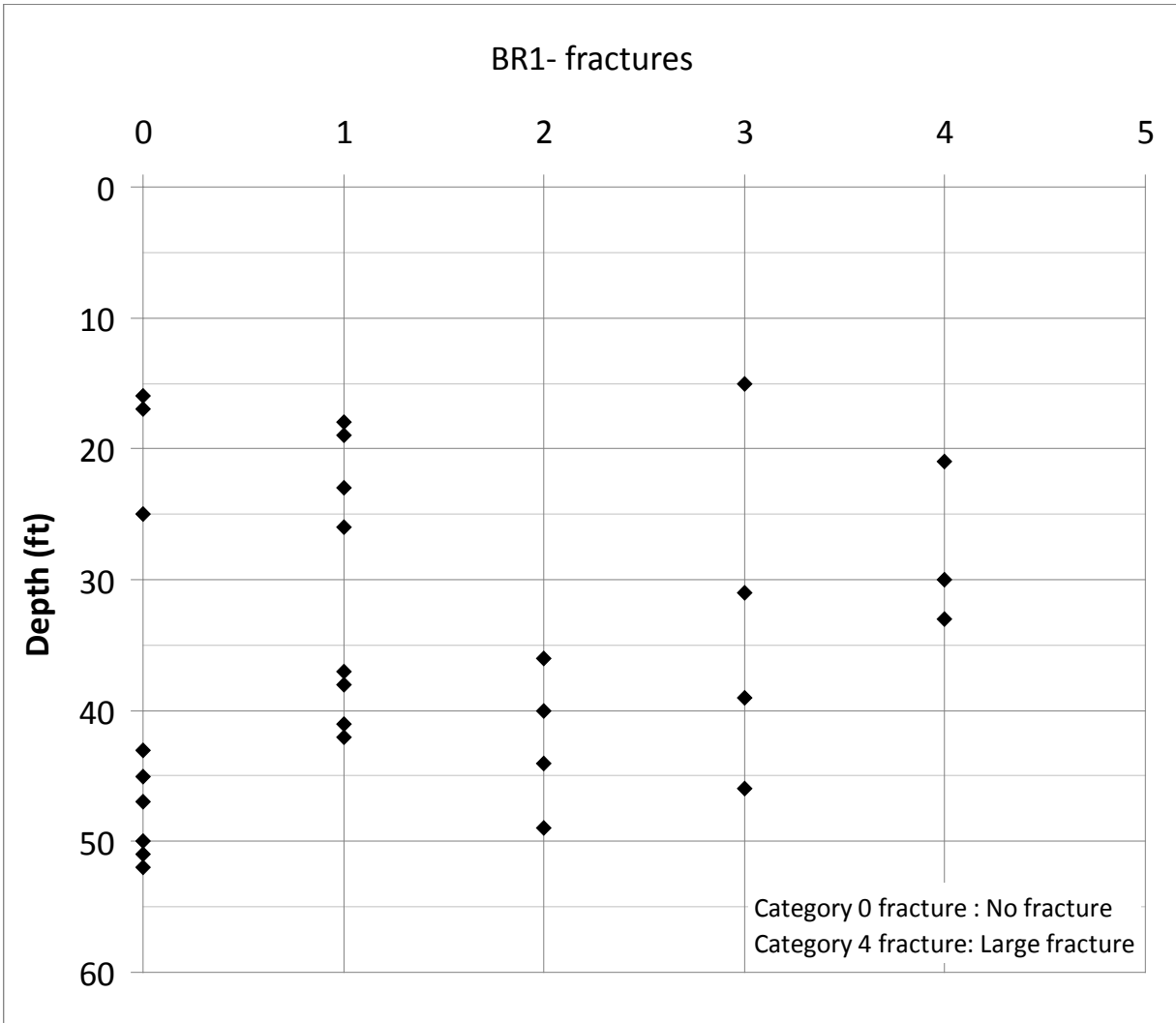
The mass reduction indicated by the data in Table 5.22 is lower, reflecting a concentration reduction in the range of 41-69% when all rock data are considered. This will be discussed further below.

### 5.7.2.2 Pre- and Post-Treatment Rock Matrix Concentrations

This section presents the pre- and post-treatment rock matrix concentrations for BR1/BRP1. Data that are believed to represent fracture concentrations are not included. The same analysis has not been conducted for BR2/BRP2 and BR3/BRP3, since the number of pre-treatment rock concentrations samples are limited.

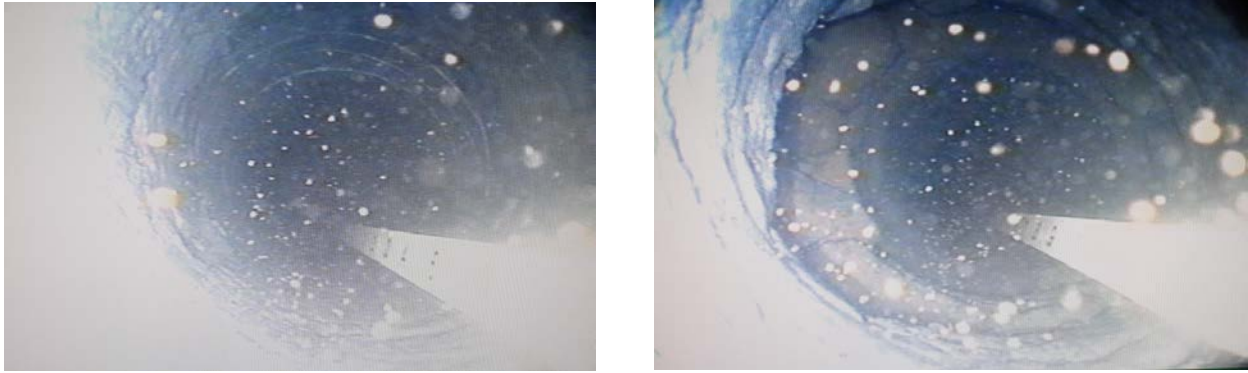
During pre-treatment rock sampling the three open rock boreholes were inspected using a down hole video camera. The videos recorded were subsequently analyzed, and all fractures observed in the borehole were categorized from category 0 being none or a very small fracture not visible on the borehole video to category 4 being a large fracture.

Figure 5.41 shows an example of this analysis for borehole BR1. As shown in the figure, some depths were found to have a higher fracture density, while the size of the fractures varied with depth.



**Figure 5.41. Location and Size of Fractures for BR1 Based on Borehole Generally Representing Inspections in One Foot Increments**

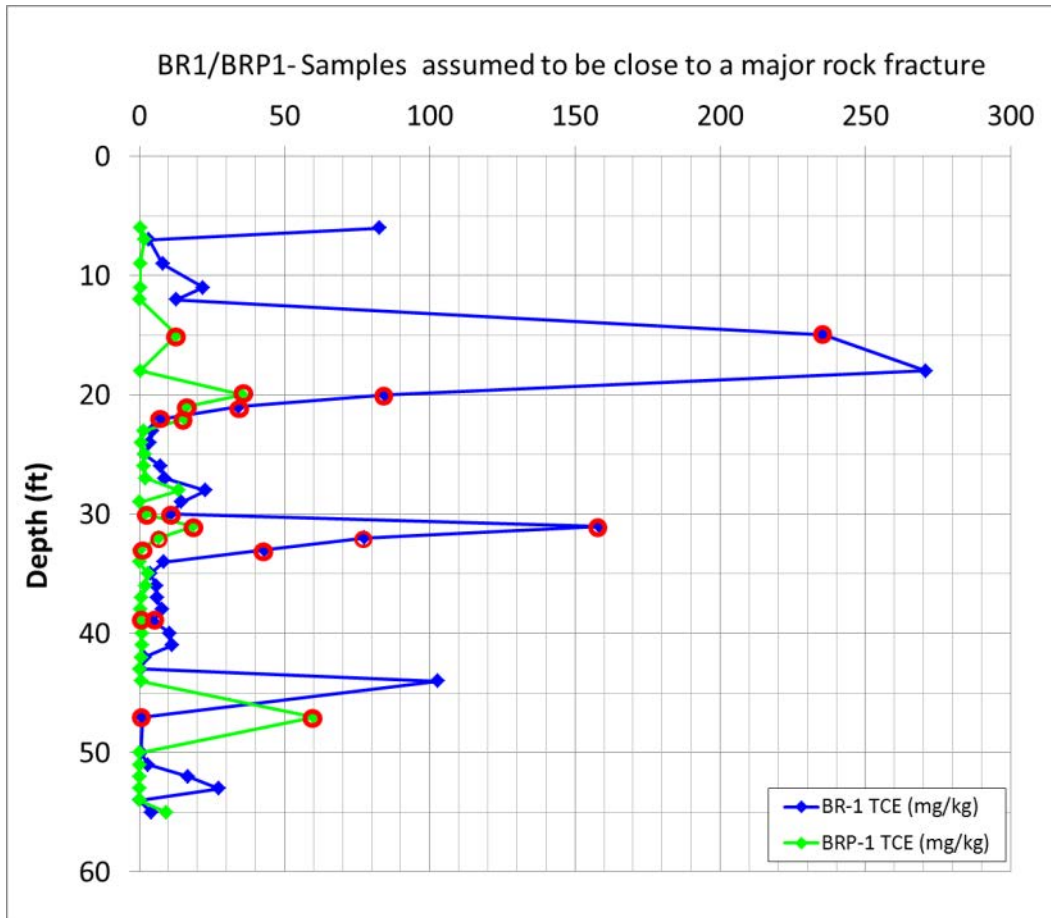
Figure 5.42 shows two screenshots from the borehole video for BR1 showing an example of a category 0 fracture and a category 4 fracture.



**Figure 5.42. Screenshot from the Video Borehole Logging Showing a Category 0 (picture at left) and a Category 4 (picture at right) Fracture**

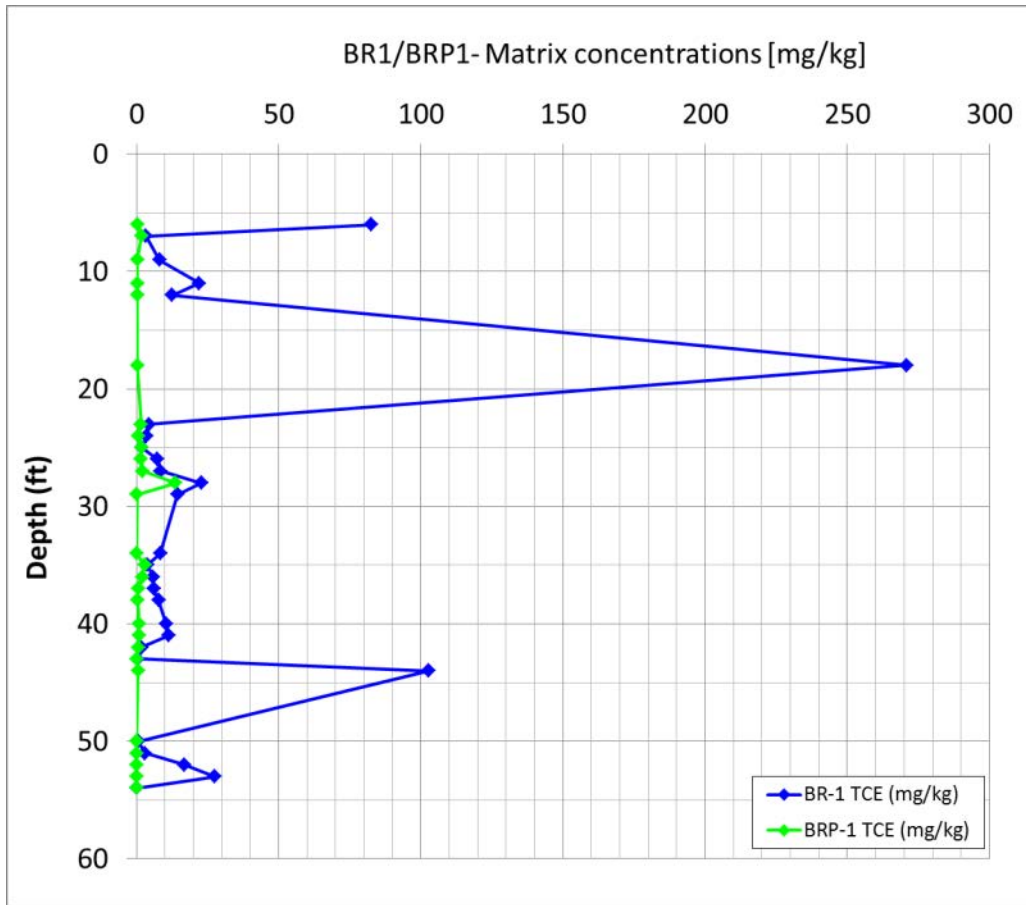
Based on the borehole inspection it was determined that all areas containing category 3 and 4 fractures did not represent rock matrix and had the potential to transport substantial amounts of water and contaminants from outside of the treatment area into the central parts of the treatment area. Therefore, all samples located at these depths were omitted to allow a comparison of pre- and post-treatment rock matrix concentrations.

Figure 5.43 shows what sample depths were estimated to represent fracture concentrations (red circles). The sample depths suggested to represent fractures were 15, 20, 21, 22, 30, 31, 32, 33, 39, and 47 ft bgs.



**Figure 5.43. Vertical Pre- and Post-Treatment Concentration Profile from BR1/BRP1 Indicating Samples Close to a Category 3 and 4 Fracture (red circles)**

Figure 5.44 shows pre- and post-treatment concentrations with depth for BR1/BRP1 after removal of expected rock samples representing fracture locations.



**Figure 5.44. Pre- and Post-Treatment TCE Rock Matrix Concentrations at Sampling Location BR1/BRP1**

A decrease in TCE concentration is observed in all samples. The decrease is as low as 6% at 25 ft bgs and as much as 99.4% at 44 ft bgs.

Table 5.23 below shows the average, maximum and minimum pre- and post-treatment TCE rock matrix concentration. Please note that only samples collected inside the treated volume, e.g. from the surface and to 50 ft bgs, have been included in the comparison.

**Table 5.23. Pre- and Post-Treatment TCE Rock Matrix Concentrations**

<i>Rock matrix</i>		<i>BR1</i>	<i>BRP1</i>
	<i>Unit</i>	<i>Pre-treatment</i>	<i>Post-treatment</i>
Average	[mg/kg]	25.90	1.43
Max	[mg/kg]	270.77	13.70
Min	[mg/kg]	0.48	ND
No of samples	[-]	24	24
Average remedial efficiency	[%]	94.5%	

ND: Not detected at the laboratory reporting limit

An average mass reduction in the 95% range is closer to the usual performance expected during a thermal remediation (NRC, 2005, NAVFAC and Geosyntec 2004, and Lebron, et al. 2012).

### 5.7.3 Bedrock TCE Mass Estimates

Table 5.24 shows the estimated pre- and post-treatment TCE mass inside the treatment area and the estimated mass dissolved in the groundwater flowing into the treatment area during operations.

Based on pre-treatment soil concentrations and assuming that the samples collected from BR1, BR2 and BR3 were representative for the entire TTZ, the TCE mass present inside the TTZ was estimated to be 210 lbs. When only matrix concentrations are considered, the total pre-treatment mass estimate was 146 lbs.

The same calculation conducted based on post-treatment fracture and matrix TCE concentrations indicate that approximately 83 lbs of TCE were left inside the treatment area when thermal operations were terminated.

If expected matrix concentrations are used in the post-treatment mass estimate, only approximately 8 lbs of TCE were left at the end of the demonstration.

The mass flowing into the treatment area in the 271,000 gallons of water extracted during operations was estimated to be 51 lbs. The mass estimates are shown in Table 5.24.

**Table 5.24. Pre- and Post-Treatment TCE Mass**

<b>Mass location</b>	<b>Mass in fractures and matrix <i>pre-treatment</i> [lbs]</b>	<b>Mass in matrix <i>pre-treatment</i> [lbs]</b>	<b>Mass in fractures <i>pre-treatment</i> [lbs]</b>	<b>Mass flowing into the treatment area during operations [lbs]</b>	<b>Mass in fractures and matrix <i>Post-treatment</i> [lbs]</b>	<b>Mass in matrix <i>post-treatment</i> [lbs]</b>	<b>Mass in fractures <i>post-treatment</i> [lbs]</b>
TCE in bedrock	209.8	64.1	145.7	-	83.0	75.0	8.0
TCE in fractures based on groundwater concentrations	0.0		0.0	-	0.0		0.0
TCE flowing into the treatment area during operations	-			51.4	-		-
<b>Total</b>	<b>209.8</b>	<b>64.1</b>	<b>145.7</b>	<b>51.4</b>	<b>83.0</b>	<b>75.0</b>	<b>8.0</b>

It was estimated that 500 lbs of VOCs were removed in the vapor stream only during the remedy based on observed PID readings and flow rates and 650 lbs based on analytical vapor samples. The mass removed in the liquid stream was estimated to be 33 lbs based on collected analytical samples (see Section 5.7.1).

As seen in Table 5.24 above, the mass of TCE calculated in the fractures and matrix pre-treatment was 209.8 lbs. When this is combined with the 51.4 lbs of mass estimated to have flowed into the treatment area during operations the total mass in the treatment zone during operations was 261.2 lbs. Post-treatment, there was an estimated 83.0 lbs of mass remaining in the matrix and fracture for a total mass removed of 178 lbs.

The mass difference between the numbers shown in Table 5.24 and the TCE mass detected in the treatment system is substantial. The data indicate that up to 300-500 lbs of TCE was present in the treatment area as a NAPL phase, and/or that more CVOC mass than anticipated in the calculations above was flowing into the treatment area with the groundwater during the thermal remedy.

## **5.8 WASTE GENERATED**

During the TCH field demonstration a variety of waste streams were generated which required proper management, classification, transportation and disposal. Presented below is a discussion of the wastes generated throughout the duration of TCH operations.

### **5.8.1 Drill Cuttings**

Drill cuttings in the form of soil and rock cores were generated during the installation of the TCH wells and sampling. The drill cuttings were containerized onsite for characterization and disposal. Approximately twenty cubic yards (16.5 tons) plus nineteen 55-gallon drums of soil/rock cores were generated during installation, sampling and decommissioning of the TCH field demonstration. The drill cuttings were classified by the New Jersey Department of Environmental Protection (NJDEP) with a U228 waste code requiring hazardous waste disposal. Additionally, two roll-off containers of concrete were generated during decommissioning requiring hazardous waste disposal.

### **5.8.2 Sludge**

During well installation activities for the TCH field demonstration, a water and soil mixture was produced. This water/soil mixture was containerized in a 21,000 gallon frac tank for settlement before transferring the water to ECOR's groundwater treatment plant for final treatment and discharge. After settlement, sludge was left in both the 21,000 gallon frac tank and in ECOR's equalization tank that received the transferred water. Approximately 1,800 gallons of this sludge were removed and transported for treatment and disposal.

### **5.8.3 Vapor Phase Carbon**

During the TCH field demonstration, approximately 6,000 pounds of waste vapor phase GAC were generated. Three GAC changeouts were required during operations. The waste vapor GAC was removed from the treatment equipment carbon vessels and vacuumed directly into 55-gallon drums or containers called "supersaks". A supersak is a woven polypropylene fabric

treated for ultraviolet resistance used for limited outdoor storage and is commonly used for the storage of GAC. The drums and supersaks were staged onsite to await characterization and removal. The spent carbon was shipped for reactivation/disposal.

#### **5.8.4 Extracted Water**

Approximately 271,000 gallons of water were extracted from the TTZ (in the form of entrained groundwater or condensed steam) over the course of operations. The extracted water was fed in the knockout pot and pumped through a surge tank and then was pumped to the existing groundwater treatment plant on site operated by ECOR.

### **5.9 TCH SYSTEM SHUTDOWN**

The TCH field demonstration was shut down on July 21, 2009 after 97 days of heating operations. The vacuum extraction system was operated from July 22 through July 24, 2009, during which time period the steam was removed from the subsurface. Due to an excessive inflow of cooling groundwater the heating period was ~5.5 weeks longer than expected, and the cool-down phase was approximately one week shorter than anticipated.

### **5.10 DECOMMISSIONING AND DEMOBILIZATION**

Decommissioning and demobilization work began once the extraction and process treatment equipment was shutdown and included the following:

- Removal of the system instrumentation;
- Removal and spooling of all electrical cable connecting heaters and equipment on site;
- Removal and decontamination of heaters (and liners where possible) from the heater borings;
- Decontamination and disassembly of all extraction well head fittings, lines and conveyance manifold;
- Decontamination and disassembly of all process equipment interconnecting piping/hoses;
- Media removal and decontamination of all process equipment;
- Loading and shipping of all TCH demonstration material and equipment; and,
- Removal of office trailer, storage container, and dumpster.

The TCH field demonstration system borings were decommissioned according to N.J.A.C. 7:9D standards and the vapor cover will be removed.

## **6.0 PERFORMANCE ASSESSMENT**

A summary of all data analysis in support of the assessment of performance objectives is provided in detail in Section 6.1. A description of the Performance Objectives and subsections for each performance objective supporting the conclusions are summarized in Section 3.0 and Table 3.1 in particular.

In addition to the performance assessment on specific qualitative and quantitative parameters discussed in Section 3.1, energy balance calculations and parameters affecting heating were monitored through the demonstration. Section 6.1 discusses data collected in support of those parameters. The sustainability of thermal remediation is outlined Section 6.2.

In short, results from the bedrock samples indicate that the average reduction in TCE concentrations was 41-69%. However, careful examination of selected points in the rock matrix revealed that the rock matrix did not achieve targeted temperature in all locations (due mostly to contaminated groundwater influx thru existing fractures). Since discrete sampling was done at 5 feet intervals, it was possible to identify at which depth there was incomplete heating and correlate that with observed fractures from a video log of the boreholes. If we eliminate from the performance data the points where boiling water temperature was not achieved due to cool water influx, the average reduction was higher at 94.5 %. A detailed performance assessment follows.

### **6.1 ASSESSING SITE PARAMETER'S IMPACT ON PERFORMANCE**

During the course of the TCH demonstration, data was collected and compiled to monitor the performance of the TCH system. These data include energy expenditures for the TTZ and volumes for water and air removed from the subsurface. Furthermore, an energy balance was set up and maintained during operation to keep track of energy injected and extracted from the TTZ on a daily basis. The energy balance was used to optimize the thermal treatment. The following sections present the data collected before, during, and after the thermal operation.

#### **6.1.1 Pre-Treatment Groundwater Sampling**

Cis-1,2-DCE, TCE and VC were found to be the dominant VOCs in the pre-treatment groundwater samples. Figures 6.1 through 6.3 depict the concentration of these three VOCs in the groundwater collected at three separate depths in each of the three pre-treatment characterization boreholes. Please note that the VC concentrations were less than the laboratory detection limit of 1000 ug/L in all samples collected from HO-8.

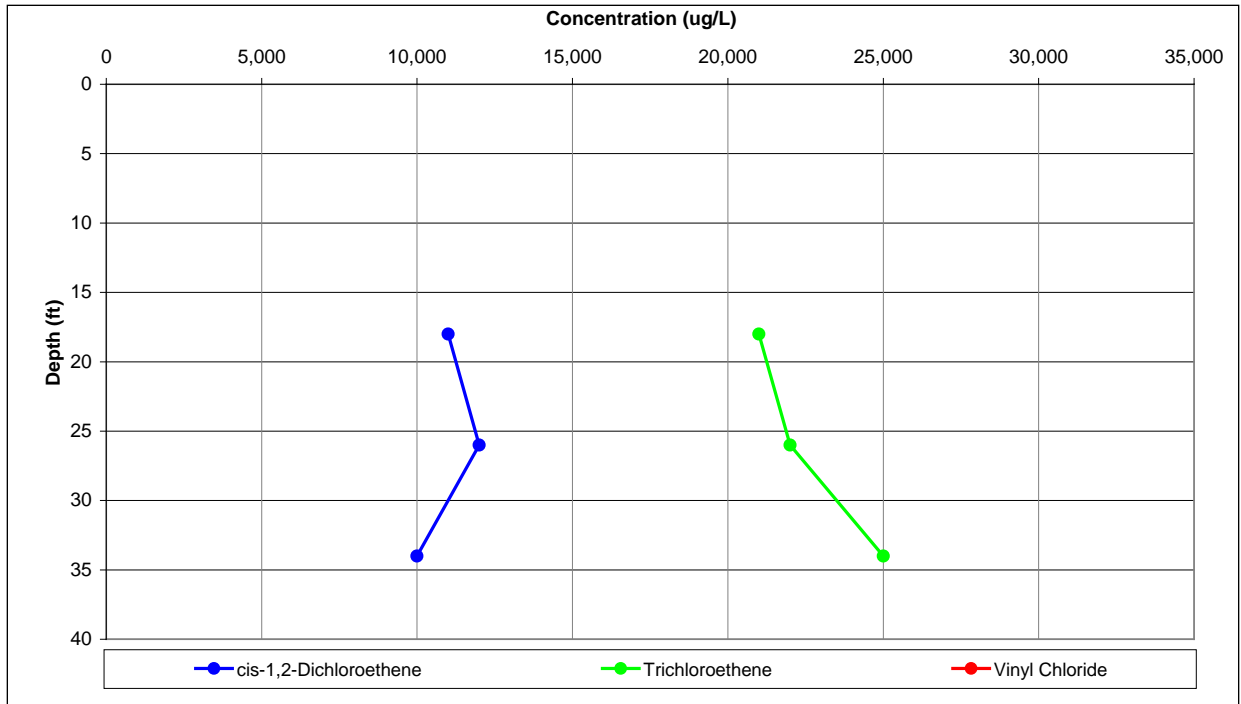


**Figure 6.1. Pre-Treatment VOC Groundwater Concentration in HO-8**

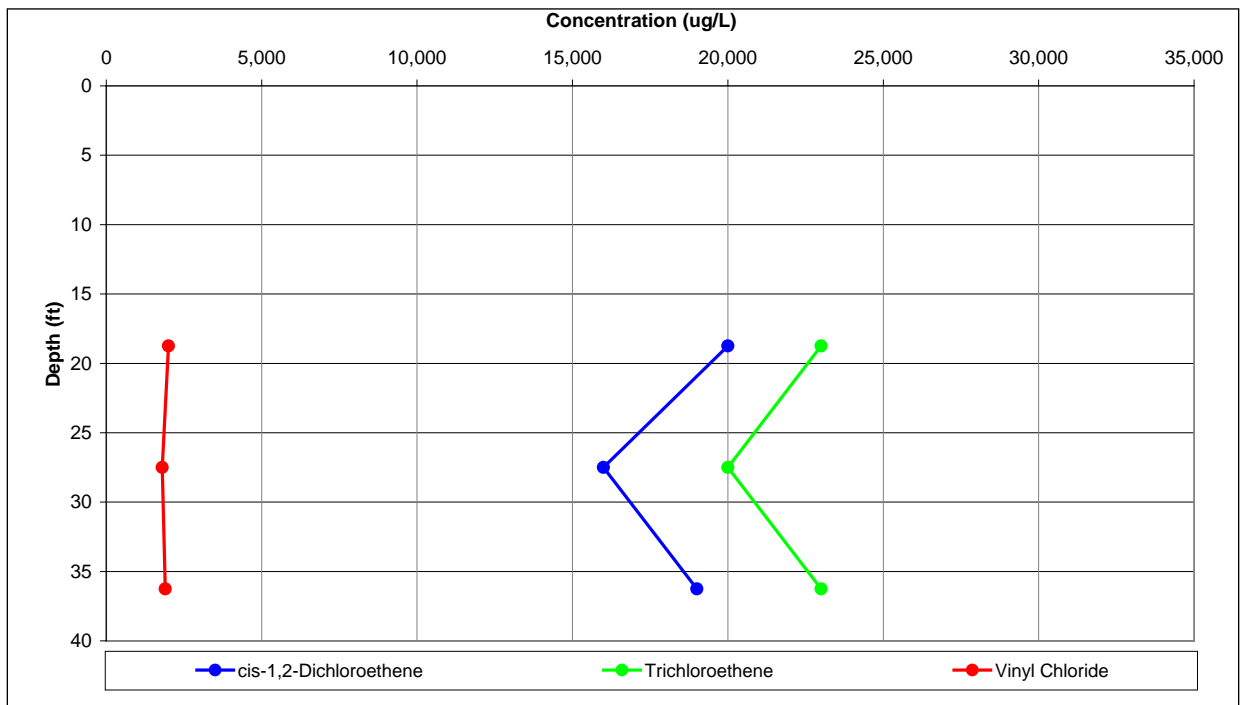


**Figure 6.2. Pre-Treatment VOC Groundwater Concentration in HO-12**

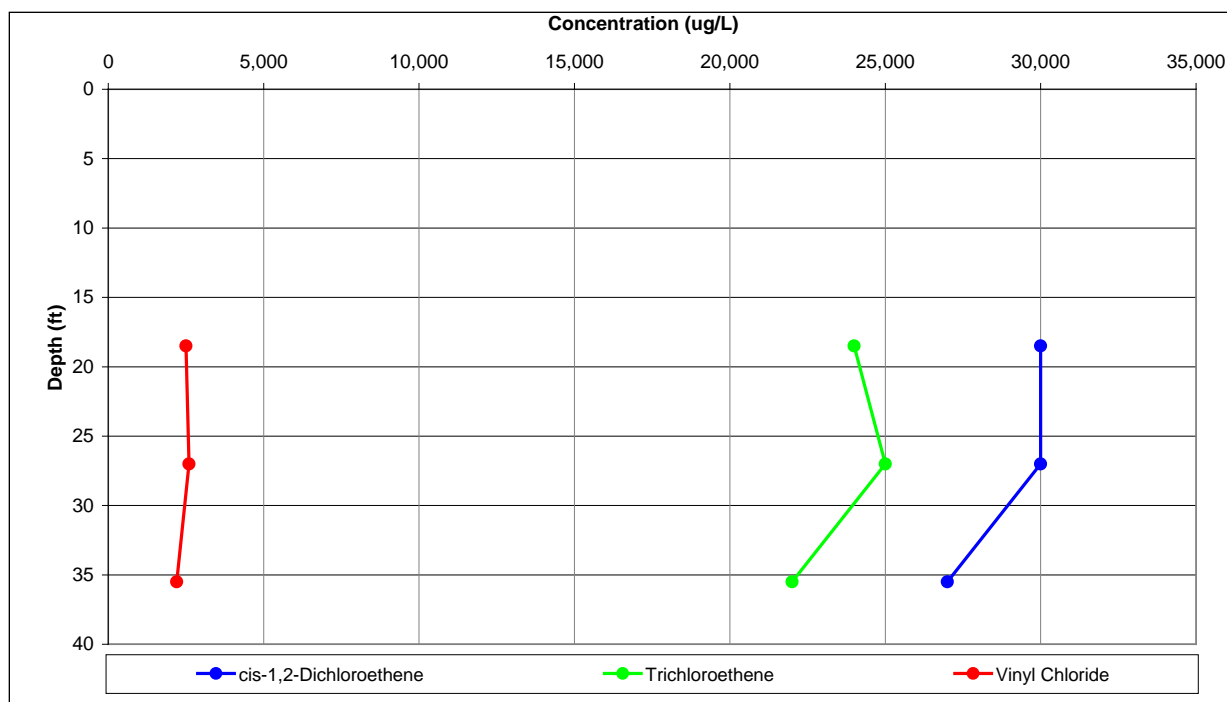


**Figure 6.3. Pre-Treatment VOC Groundwater Concentration in HO-13**

Generally, the concentrations of cis-1,2-DCE, TCE and VC do not vary much with depth at the three sample locations, which may indicate a very uniform contaminant distribution with depth, or that the groundwater at the three sample locations comes from the same major fracture near the sampling well screens.

The concentration of cis-1,2-DCE is in the order of 11,000, 18,300, and 29,000  $\mu\text{g/L}$  across all depths at sample locations HO-8, HO-12, and HO-13, respectively. The corresponding concentration of TCE is 22,700, 22,000, and 23,700  $\mu\text{g/L}$  averaged across all depths at the three sample locations. The average concentration of VC is 1900  $\mu\text{g/L}$  in the three samples collected from HO-12, while the average concentration at sample location HO-13 is 2,430  $\mu\text{g/L}$ .

As described previously, no post-treatment groundwater samples were collected because of the evidence of significant groundwater flux into the TTZ during heating (i.e., the samples would have been representative of ambient surrounding conditions, not conditions inside a treatment zone following thermal treatment). However, 28 samples were collected during operations to represent the VOC concentrations in the liquid stream extracted from the TTZ during treatment. The liquid stream VOC concentrations for the dominant compounds are further described in Section 5.7.1.

### 6.1.2 Pre-Treatment Pressure Tests

Pressure tests are performed to measure the hydraulic properties (e.g., hydraulic conductivity) of boreholes. Pre-treatment pressure tests were conducted at three locations (BR1, BR2 and BR3) in the thermal treatment area. Tables 6.1 through 6.3 show the tested intervals, the location of the packer, the depth of the borehole, injection pressures, water injection flow rate and the calculated

hydraulic conductivity based on the test results. Furthermore the average calculated hydraulic conductivities for each depth interval are shown in Figure 6.4.

**Table 6.1. Pre- and Post-Treatment TCE Mass**

<i>BR1</i> <i>Depth interval tested</i> <i>[ft bgs]</i>	<i>Depth of</i> <i>Packer</i> <i>[ft]</i>	<i>Depth of</i> <i>borehole</i> <i>[ft]</i>	<i>Pressure</i> <i>[psi]</i>	<i>Water</i> <i>injection</i> <i>rate</i> <i>[gpm]</i>	<i>Calculated</i> <i>K</i> <i>[cm/s]</i>	<i>Avg K</i> <i>[cm/s]</i>
11 to 21	11	21	5	1	3.49E-05	2.90E-05
			10	1.5	2.54E-05	
			15	2.4	2.68E-05	
21 to 31	21	31	5	8.0	3.03E-04	1.83E-04
			10	12.4	2.18E-04	
			15	16.2	1.85E-04	
21 to 41	31	41	5	3.0	1.24E-04	1.40E-04
			10	6.0	1.10E-04	
			15	11.0	1.29E-04	
41 to 51	41	51	5	2.3	1.05E-04	1.07E-04
			10	4.6	8.79E-05	
			15	5.2	6.28E-05	

**Table 6.2. Pressure Test Results for BR2**

<i>BR2</i> <i>Depth interval tested</i> <i>[ft bgs]</i>	<i>Depth of</i> <i>Packer</i> <i>[ft]</i>	<i>Depth of</i> <i>borehole</i> <i>[ft]</i>	<i>Pressure</i> <i>[psi]</i>	<i>Water</i> <i>injection</i> <i>rate</i> <i>[gpm]</i>	<i>Calculated</i> <i>K</i> <i>[cm/s]</i>	<i>Avg K</i> <i>[cm/s]</i>
16 to 26	16	26	5	6.0	2.18E-04	2.18E-04
26 to 36	26	36	5	0.0	0.00E+00	9.45E-05
			10	0.0	0.00E+00	
			27	10.0	6.27E-05	
			32	24.0	1.26E-04	
36 to 46	36	46	15	0.0	0.00E+00	5.99E-05
			25	2.5	1.72E-05	
			30	18.0	1.03E-04	
46 to 56	46	56	15	0.8	9.79E-06	1.89E-05
			20	2.5	2.23E-05	
			25	3.5	2.45E-05	

**Table 6.3. Pressure Test Results for BR1**

<i>BR2 Depth interval tested [ft bgs]</i>	<i>Depth of Packer [ft]</i>	<i>Depth of borehole [ft]</i>	<i>Pressure [psi]</i>	<i>Water injection rate [gpm]</i>	<i>Calculated K [cm/s]</i>	<i>Avg K [cm/s]</i>
11 to 21	11	21	5	1.50	5.24E-05	4.73E-05
			10	2.00	3.38E-05	
			15	5.00	5.58E-05	
21 to 31	21	31	5	0.00	0.00E+00	2.94E-05
			10	0.00	0.00E+00	
			15	0.50	5.72E-06	
			20	0.50	4.16E-06	
			30	14.00	7.83E-05	
31 to 41	31	41	5	8.00	3.32E-04	2.17E-04
			10	10.00	1.83E-04	
			15	11.50	1.35E-04	
41 to 51	41	51	5	1.50	6.87E-05	3.44E-05
			10	1.50	2.87E-05	
			15	1.50	1.81E-05	
			20	2.50	2.21E-05	

All of the calculated average hydraulic conductivities are within the  $1.0 \times 10^{-5}$  to  $2.0 \times 10^{-4}$  cm/s interval. BR1 seems to have a relatively consistent hydraulic conductivity with depth, except from the upper interval tested. The hydraulic conductivity varies from  $1.07 \times 10^{-4}$  to  $1.83 \times 10^{-4}$  cm/s from 21 to 51 ft bgs in BR1 (factor of 2). The hydraulic conductivity in BR2 also decreases with depth and varies from  $1.89 \times 10^{-5}$  to  $9.45 \times 10^{-5}$  cm/s (factor of 5) in the depth interval from 26 to 56 ft bgs.

The 21 to 31 ft bgs and the 41 to 51 ft bgs interval in BR3 are both in the range of  $2.94 \times 10^{-5}$  cm/s to  $3.44 \times 10^{-5}$  cm/s interval which is a factor 6-7 lower than the hydraulic conductivity in the 31 to 41 ft bgs interval. This relatively substantial difference may be due to a major fracture located in the 31 to 41 ft depth interval in BR3 and therefore governing the hydraulic conductivity in this depth.

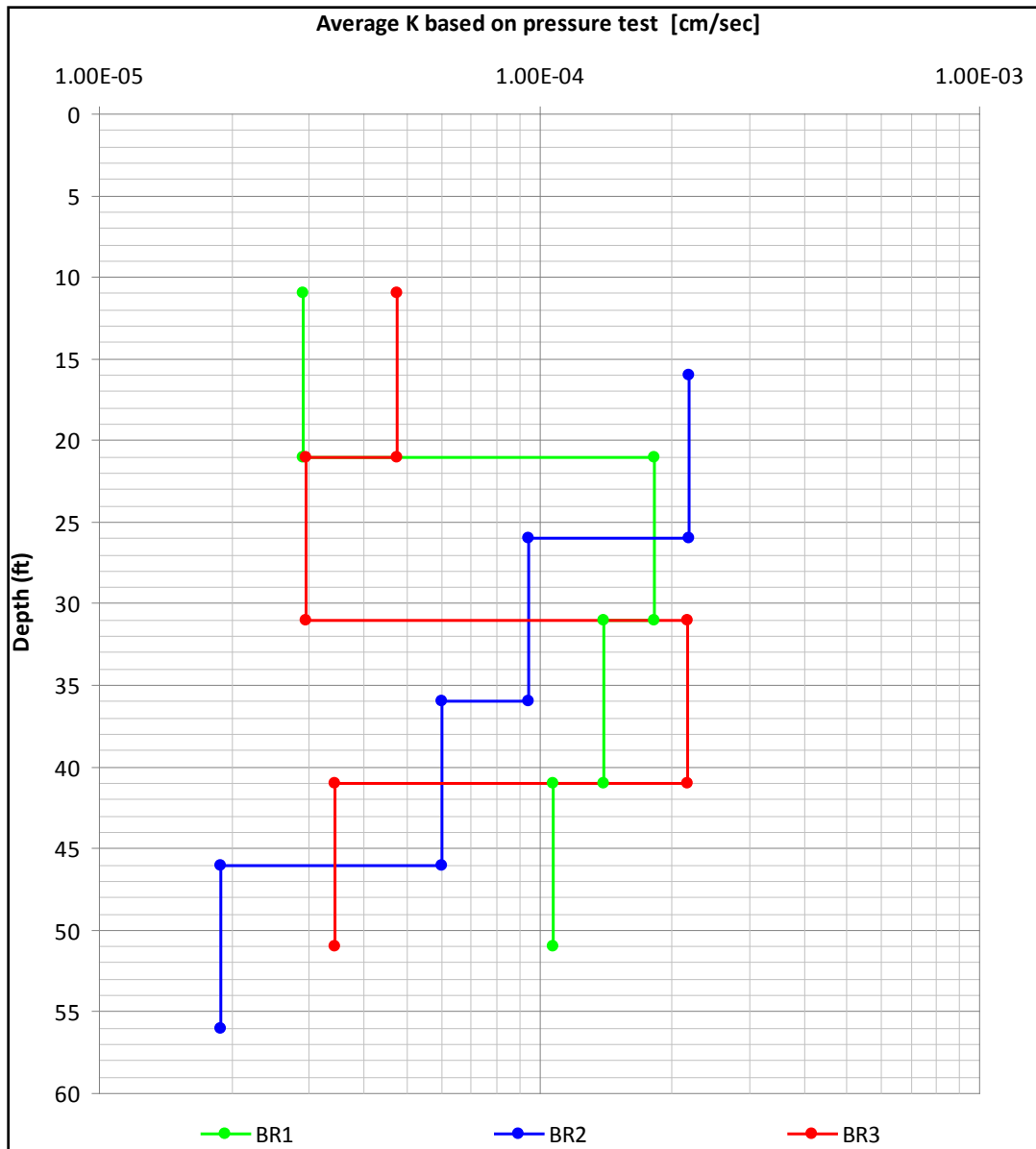


**Figure 6.4. Calculated Average Hydraulic Conductivity with Depth Based on the Pressure Tests**

### 6.1.3 Power Usage

The total amount of energy used during the thermal treatment was 529,000 kiloWatt hours (kWh). Figure 6.5 shows the cumulative power usage during the thermal treatment.

The power usage for the process system was not measured separately, but its energy usage was estimated to be approximately 68,000 kWh over a period of 106 days corresponding to an average power usage for the above ground treatment system of approximately 642 kWh/day or 27 kW.

The energy added to the subsurface was estimated to be approximately 461,000 kWh corresponding to about 87% of the total energy usage. The average amount of energy added each day was approximately 4,550 kWh or 190 kW.

Since the total treatment volume was estimated to be 550 cu yd, the average injected power usage per cu yd was 838 kiloWatt hour per cu yd (kWh/cy). This is much higher than unit power usage for larger sites due to the significant inflow of groundwater and the much higher relative surface area to volume of the small field demonstration TTZ.

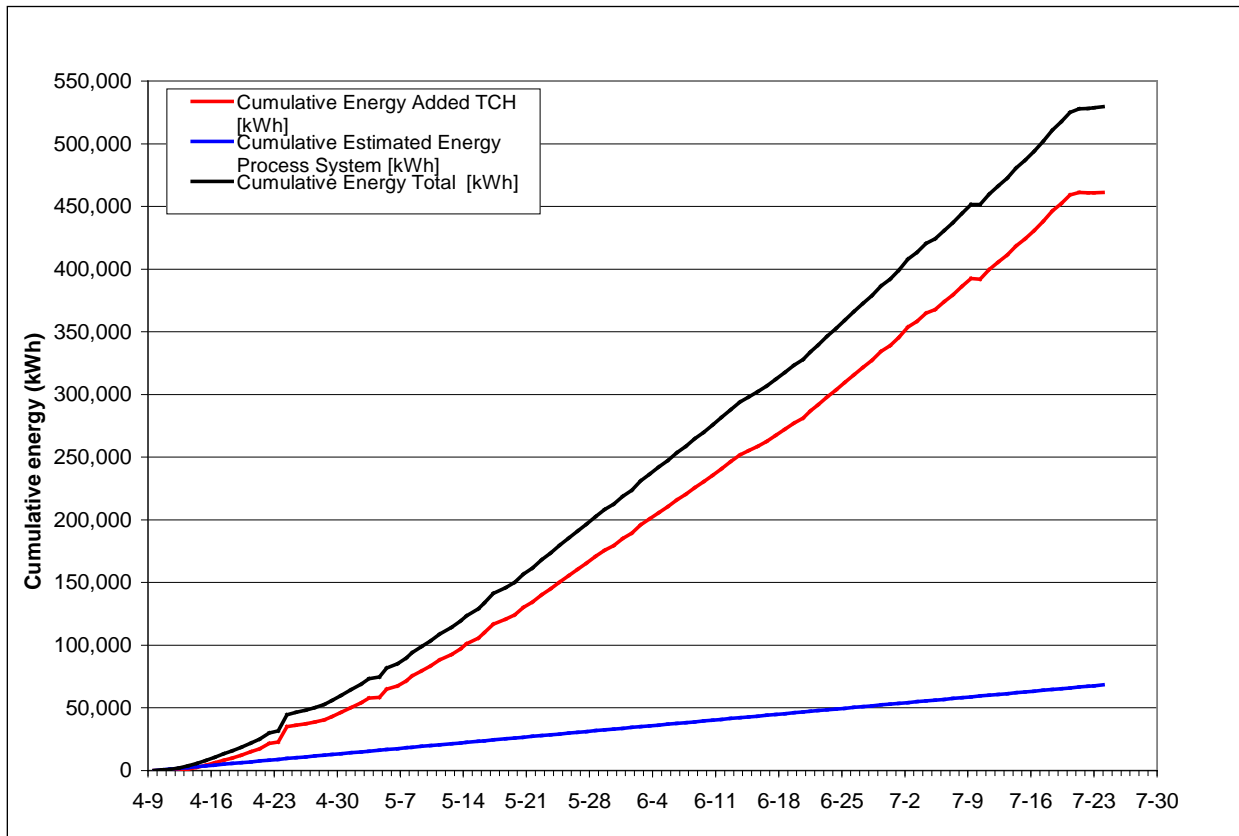


**Figure 6.5. Cumulative Power Usage during Treatment**

Energy was added at varying rates during the thermal treatment to control the temperature of the heaters. Figure 6.6 is the estimated daily power usage shown throughout the operations.

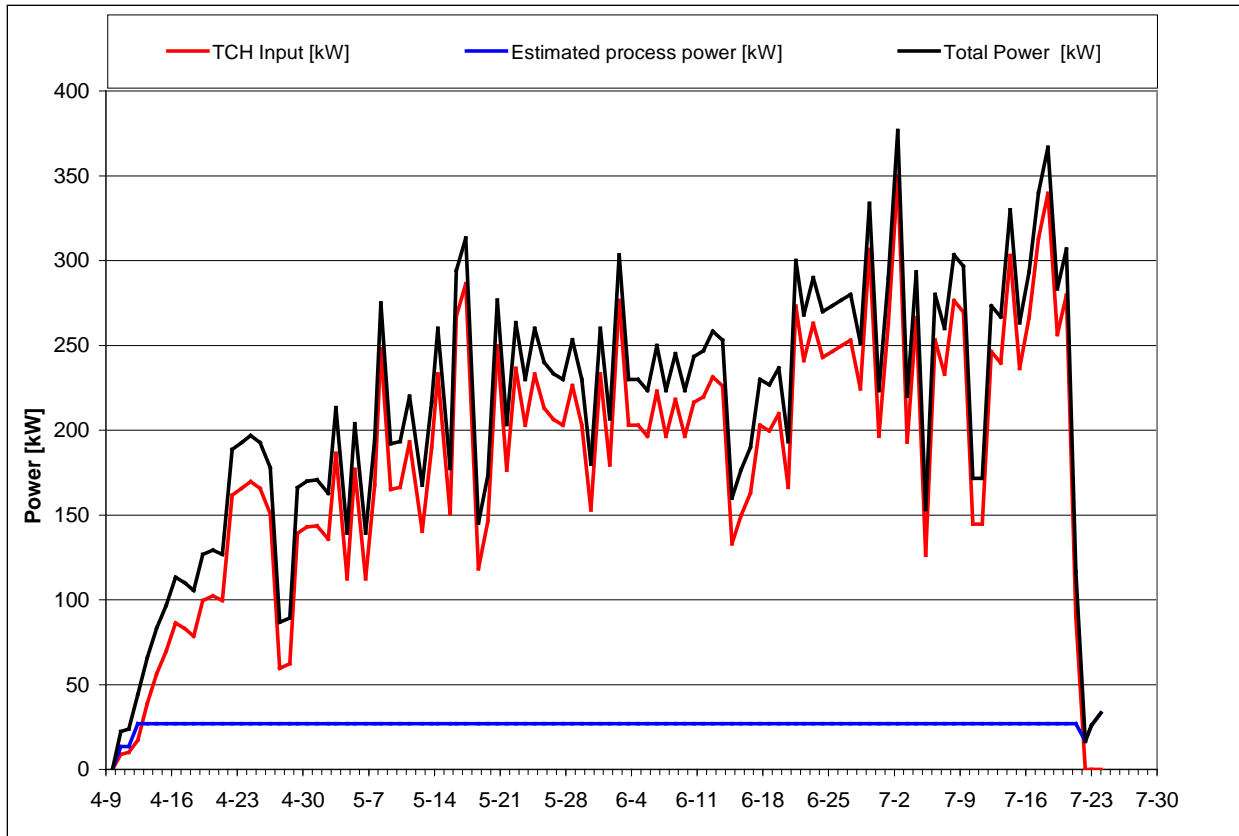


**Figure 6.6. Estimated Power Usage Rate during Treatment**

#### 6.1.4 Energy Injected and Extracted

Figure 6.7 shows the calculated cumulative energy injected and extracted during treatment. A total of 462,000 kWh of energy was added by the ISTD heaters while approximately 134,000 kWh were extracted as steam and condensed out in the process treatment system and 90,000 kWh were extracted as hot water. The net energy injection to the TTZ was approximately 238,000 kWh; approximately 51% of the injected energy remained in the ground.

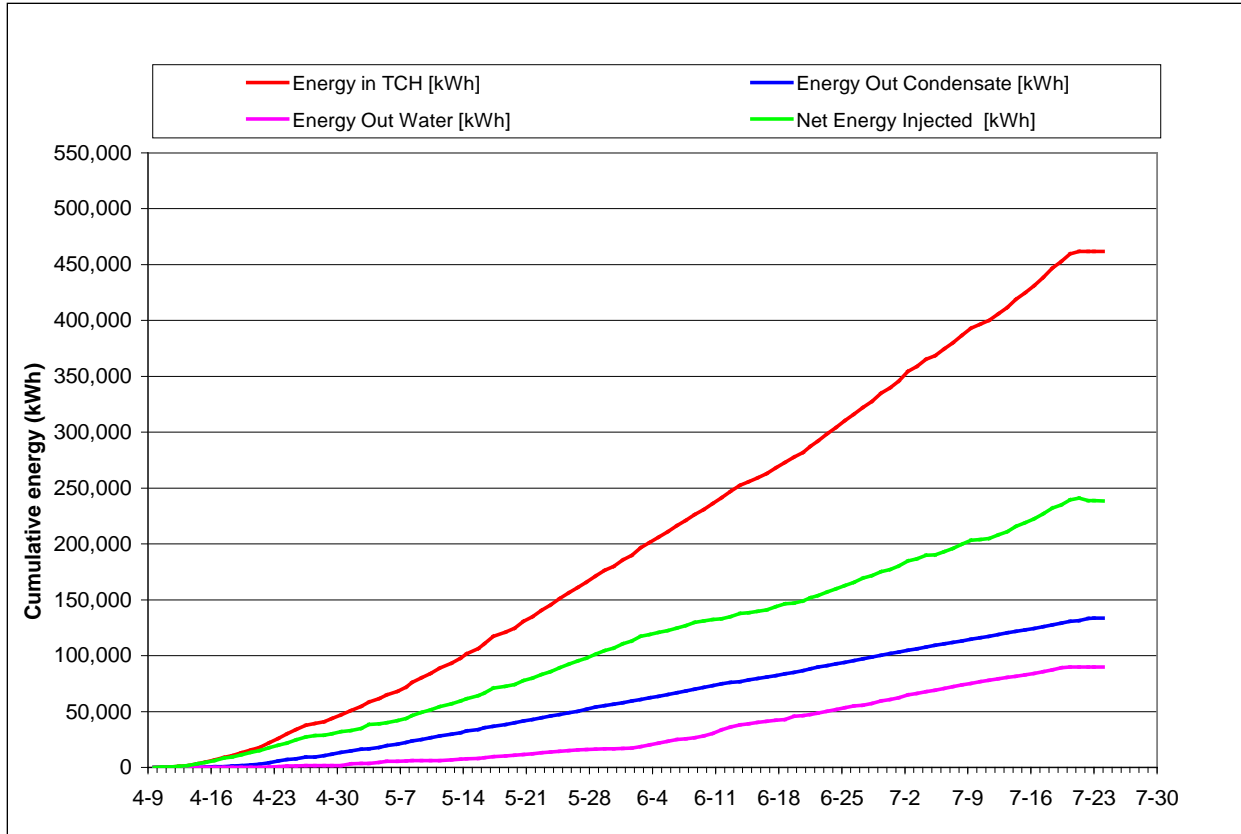


**Figure 6.7. Cumulative Energy Balance**

It is noteworthy that the removal of energy was relatively high in relation to the added energy. During this project, approximately 49% of the added energy was extracted. For TCH projects at other sites, the energy removal has varied between 10 and 35% of the injected energy. The reason for this (i.e., unexpectedly high groundwater removal rates) is discussed below.

Figure 6.8 shows the energy injection and extraction rate during treatment. On average, 187 kW of energy was added by the ISTD heaters while 53 kW was removed as steam and 35 kW was removed as hot water. On average 28% of the total energy injected was extracted as steam, which was within the range predicted in the design. The energy removed as hot water, in contrast, was five to ten times higher than expected.

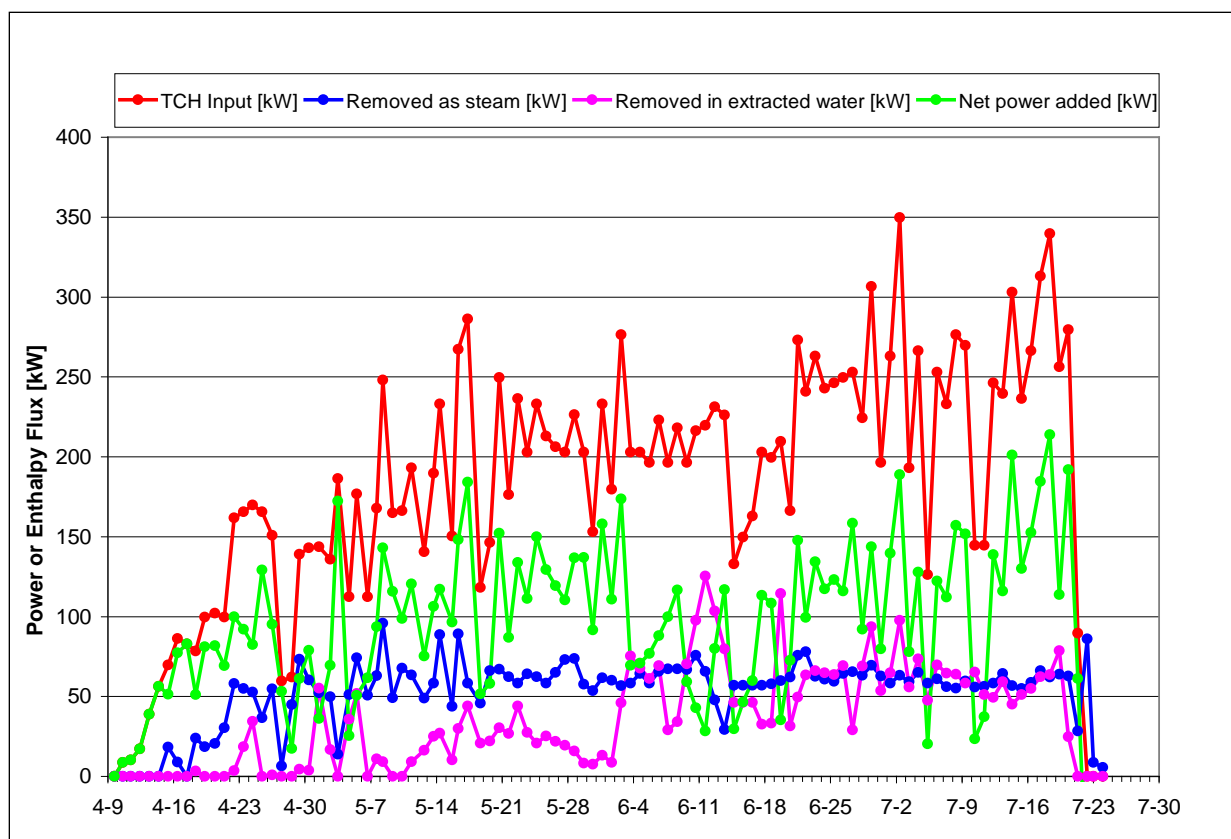


**Figure 6.8. Energy Injection and Extraction Rates during Treatment**

### 6.1.5 Water and Air Balances

During the thermal treatment, the total volume of both the liquid and the vapor phases of the process stream were collected and measured daily. The following sections present key water and vapor balance data.

#### 6.1.5.1 Water Balance

Figure 6.9 depicts the cumulative water balance during remediation. Water was extracted as steam (temperature greater than 100°C) and (hot water temperature less than 100°C) entrained by the vapor extraction system. The total volume of aqueous phase liquid recovered (includes both water entrained and steam condensed) and treated from the site was 271,000 gallons.

The total amount of water entrained during operation was 222,000 gallons, while the amount of water extracted as steam and condensed in the process treatment system was 49,000 gallons. Measurements were recorded from a flow totalizer installed downstream of the knock out tank on the SVE skid. No separate meter was installed to quantify the exact water extraction as entrained water and as steam; instead the quantities have been estimated based on the operator's daily observations.

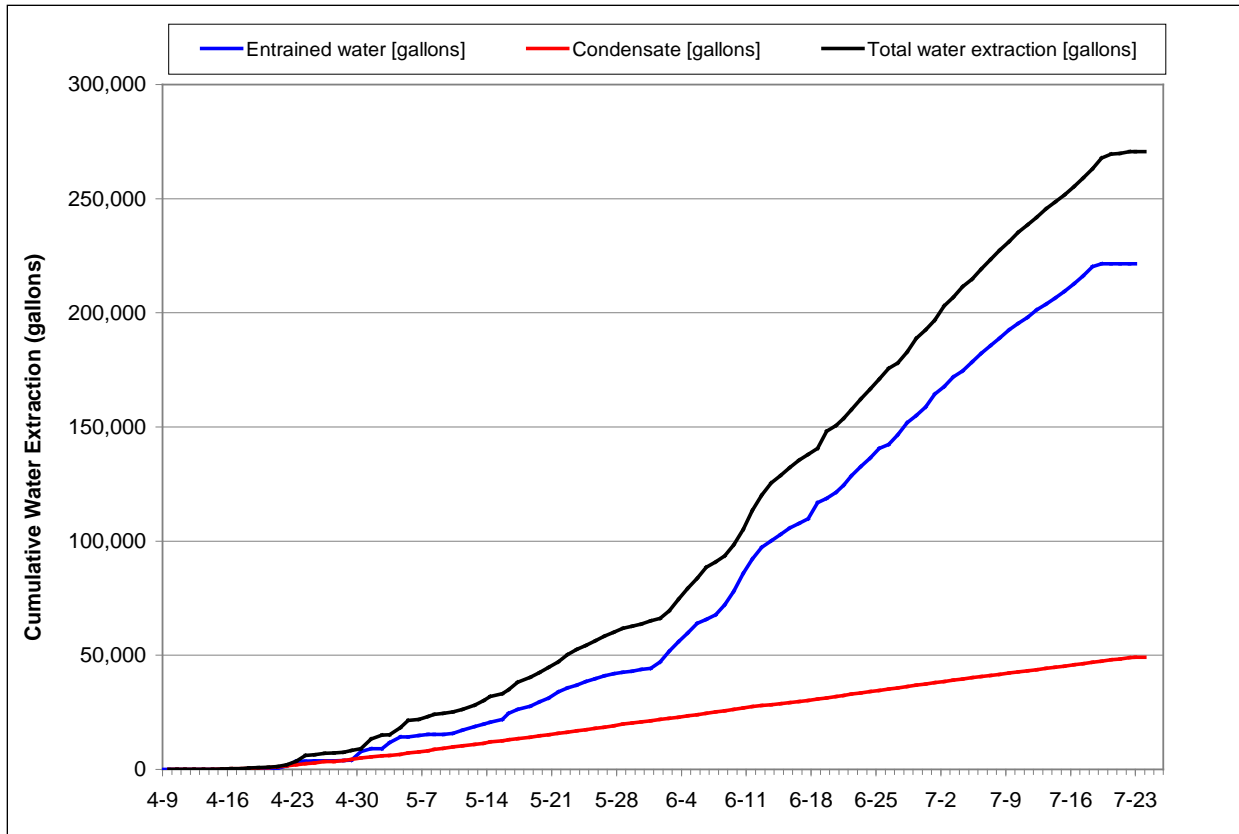


**Figure 6.9. Cumulative Water Removed during Treatment**

Figure 6.10 shows the entrained water rates and the production of steam condensate in the TCH operations period. Furthermore the average site temperature is shown in the figure. The average entrained liquid extraction rate was 1.46 gpm, which is substantially higher than the anticipated design rate of 0.1-0.2 gpm.

The production of steam condensate was estimated to be minimal in the heat-up phase and then stabilized in the range of 0.3-0.4 gpm. The average steam extraction rate was 0.33 gpm.

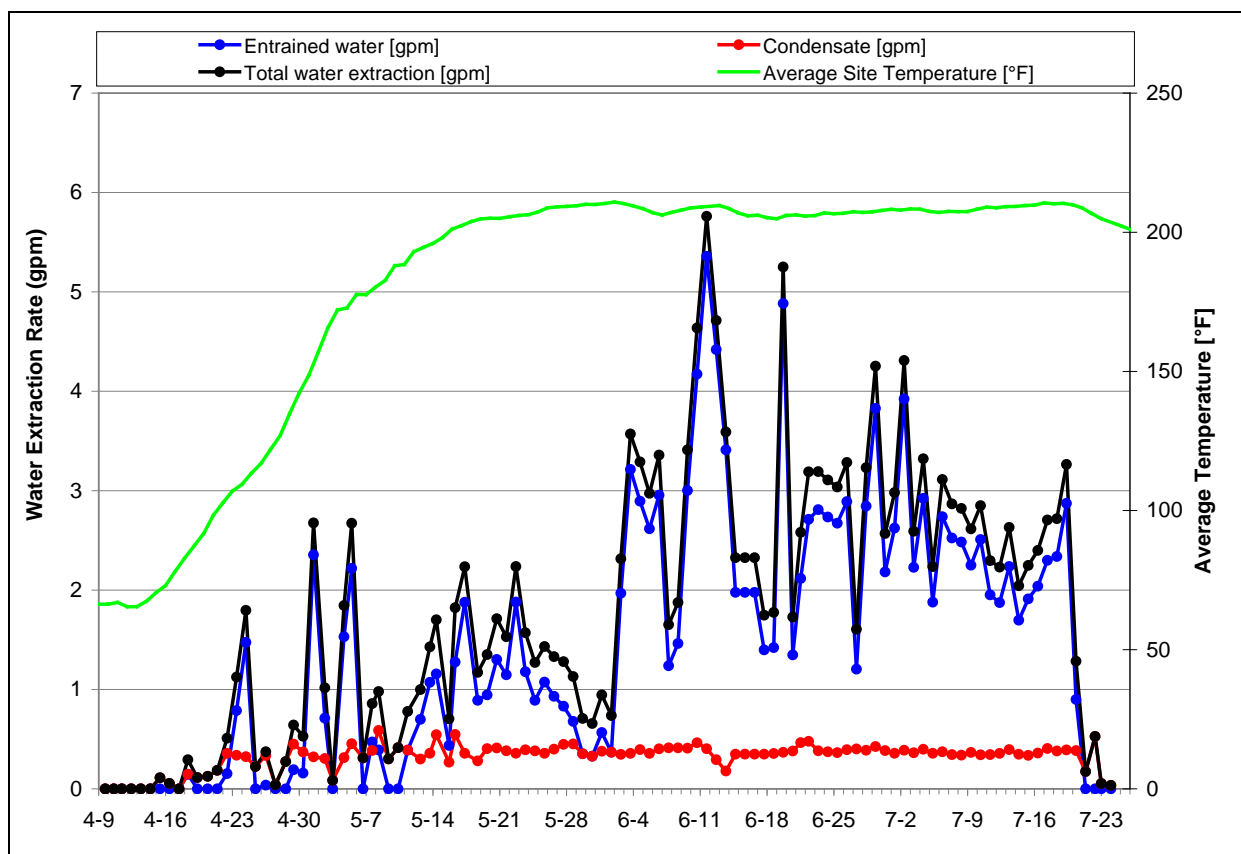


**Figure 6.10. Water Removal Rate during Treatment**

The entrained water flow shows a great deal of variation over time. The trend is upward with increasing rates after the end of May 2009, when the site had reached a temperature near the boiling point of water from 5 to 30 ft bgs. The “jerky” extraction rates are consistent with a removal mechanism where the water is pushed out through the vapor extraction points in a manner similar to steam geysers; steam is formed in the formation, and after some time enough pressure has built to lift the water above it and then the pressure is released as a slug of water that exits the extraction point and is collected in the vapor extraction manifold. This theory is supported by temperature data showing that the average Site temperature peaked at approximately the same time (see Figure 6.10), indicating that most of the energy added to the treatment area from that point was used to generate steam at or near the wells that could support the additional water removal.

We expected a liquid extraction rate in the range of 0.1 to 0.2 gpm or a total extraction volume of between 8,600 and 17,200 gallons over the planned 60 day operational duration. During the second half of operations, the actual water extraction rate fluctuated between 1 and 5 gpm, with an average around 2-3 gpm. In addition, the heating period of the field demonstration was extended by an additional 38 days based on the continued significant mass removal rates. This higher than expected extraction rate and longer heating duration resulted in the removal of a total of approximately 271,000 gallons of liquid from the TTZ.

Table 6.4 presents a summary of the estimated matrix and fracture volumes of the TTZ and a comparison of the volume of water present in the TTZ with the volume of water removed during treatment. Based on this comparison, more than 18 times the volume of water present in the matrix and fractures was removed from the TTZ during treatment. If it is assumed that the water present in the matrix was not directly accessible for extraction (i.e., matrix permeabilities as measured in the lab ranged between  $10^{-9}$  and  $10^{-7}$  cm/s whereas fracture permeabilities measured in the field ranged between  $10^{-5}$  and  $10^{-4}$  cm/s), this water came primarily through the fractures (likely caused by the induced flow) and resulted in more than 10,000 fracture volumes being pulled into, through, and removed from the TTZ.

**Table 6.4. Comparison of Starting Volume of Water in TTZ with Volume Removed During Treatment**

Diameter of TTZ	32	ft	<b>TTZ Dimensions</b>
Area of TTZ	804	ft <sup>2</sup>	
Depth of Unconsolidated Deposits	8	ft	
Depth to Water Table	5	ft	
Bottom of TTZ	50	ft	
Total Volume of TTZ	1,489	cy	
Total Volume of TTZ	1,140	m <sup>3</sup>	
<b>Estimated Matrix and Fracture Volumes</b>			
Volume of Bedrock	1,251	cy	<b>Estimated Matrix and Fracture Volumes</b>
Volume of Bedrock	957	m <sup>3</sup>	
Matrix Porosity	6	%	
Fracture Porosity	0.0100	%	
Fracture Volume	0.0957	m <sup>3</sup>	
Matrix Pore Volume	57	m <sup>3</sup>	
<b>Comparison of Starting and Extracted Water Volumes</b>			
Volume of Water in Matrix	15,172	gals	<b>Comparison of Starting and Extracted Water Volumes</b>
Volume of Water in Fractures	25	gals	
Total Volume of Water in TTZ	15,197	gals	
Total Volume of Water Removed During Treatment	271,000	gals	
Pore Volumes Removed	18		
Fracture Volumes Removed	10,717		

The substantially higher than expected water extraction rate may help to explain the observed post-treatment rock concentrations, as discussed below. The cooling associated with the substantial water flow through the fractures and the continual influx of contaminants from the bedrock surrounding the TTZ, is believed to have limited the remedial efficiency in the bedrock close to such fractures. As discussed below, use of larger diameter vapor extraction points or grouting in the heater borings and use of separate vapor extraction points would have significantly reduced the amount of water produced by eliminating the percolation effect seen at the vapor extraction points during operation. This would have limited the water extraction rate to the rate of in situ steam production from the fractures and the matrix, thereby limiting the rate of contaminant and cold water flux into the TTZ and enabling the efficient heating and treatment

of the TTZ. Another potential remedy for full-scale applications would be the use of steam injection to heat the fractures and minimize groundwater inflow from outside of the TTZ.

### 6.1.5.2 Vapor Balance

In Figure 6.11, the cumulative vapor balance during remediation is shown. The total volume of non-condensable vapors (i.e., the portion of the vapor stream that is not steam) extracted from the site was estimated to be 4.8 million cu ft. An estimated 8.7 million cu ft of steam was extracted during the treatment process.

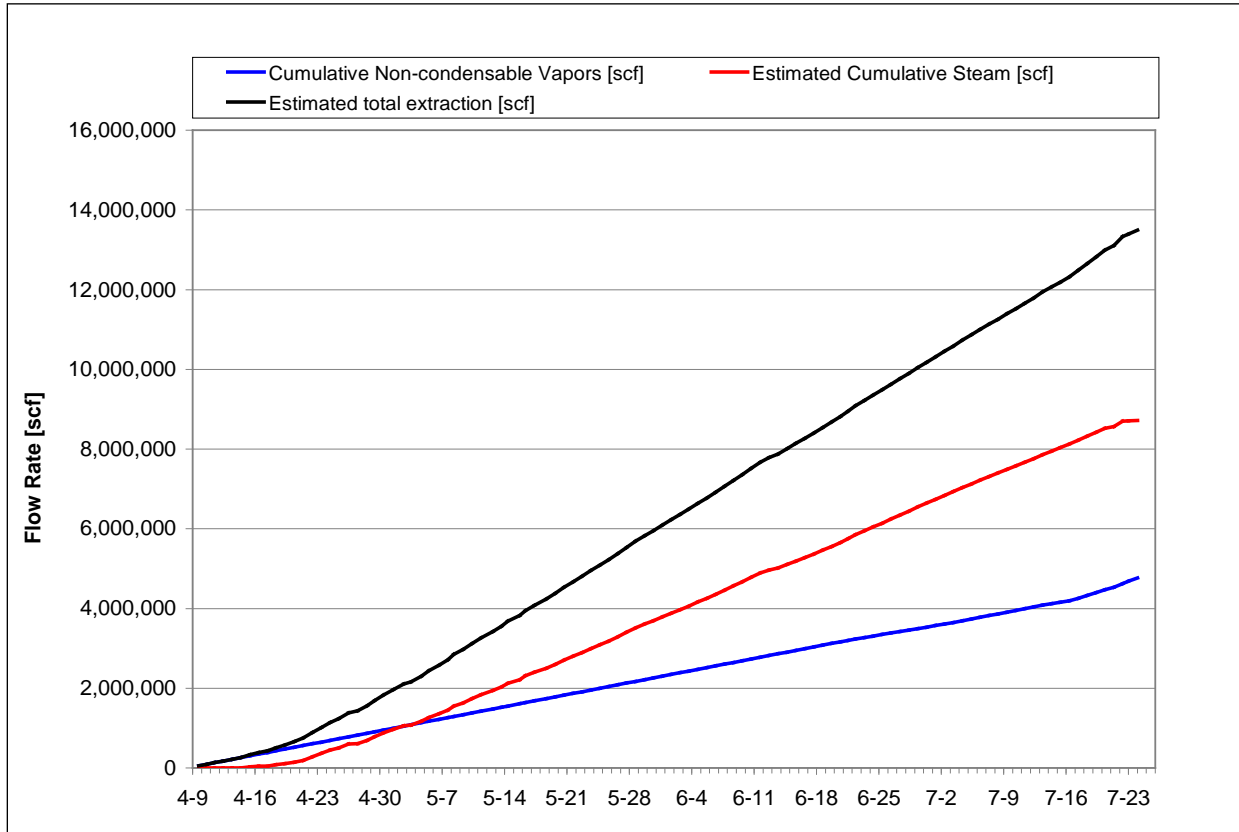


**Figure 6.11. Cumulative Vapor Removal during Treatment**

Non-condensable vapor flows were estimated to be 30 scfm with some fluctuations while the steam extraction rates were in the range of 55 scfm after the initial heat-up. This was sufficient to create pneumatic control and capture of the mobilized, vaporized contaminants.

The vapor points were examined post-treatment with some points showing build up of silt/sand fines. This is believed to be a result of the infiltration of silt/sand fines from initial sand pack used during well installation before switching to a coarser sand pack material. While this may have reduced the vapor extraction rate from some points, a constant vapor extraction rate was maintained across the Site.

### 6.1.6 Temperatures during Operation and Cool-Down

The following sections present temperature data collected during operation and in the cool-down phase.

#### 6.1.6.1 Temperatures during Operation

Figures 6.12–6.19 below show the thermocouple temperature readings at the site over the duration of operations at temperature monitoring points T1 – T8. Refer to Table 5.16 for distances between TCs and nearest wells.

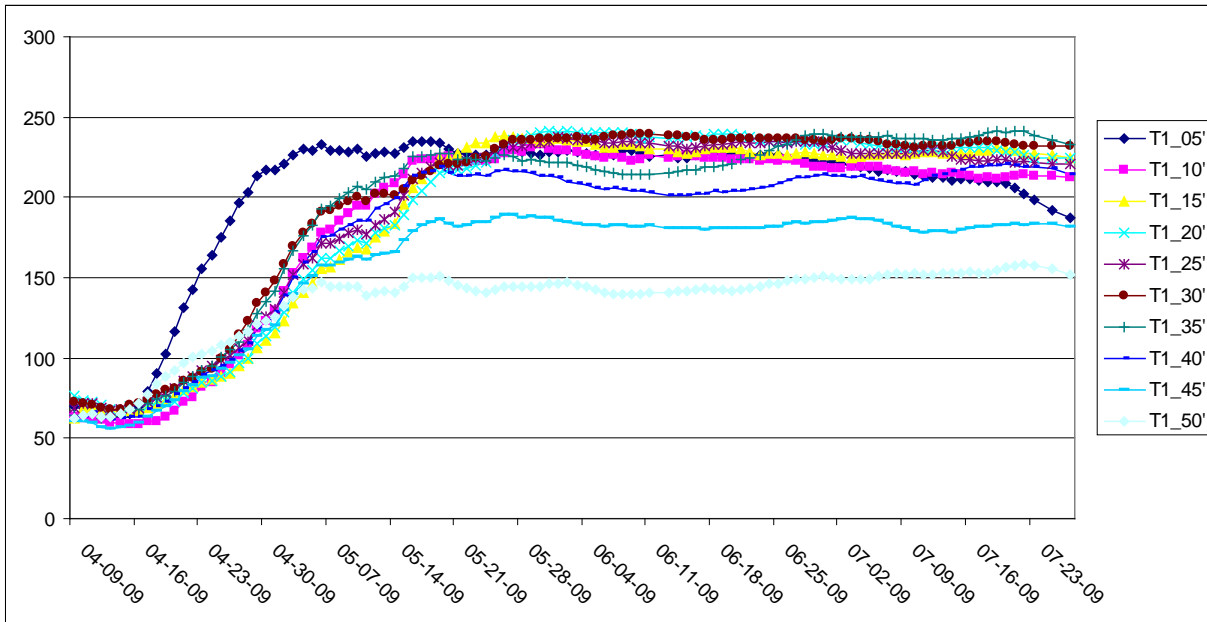
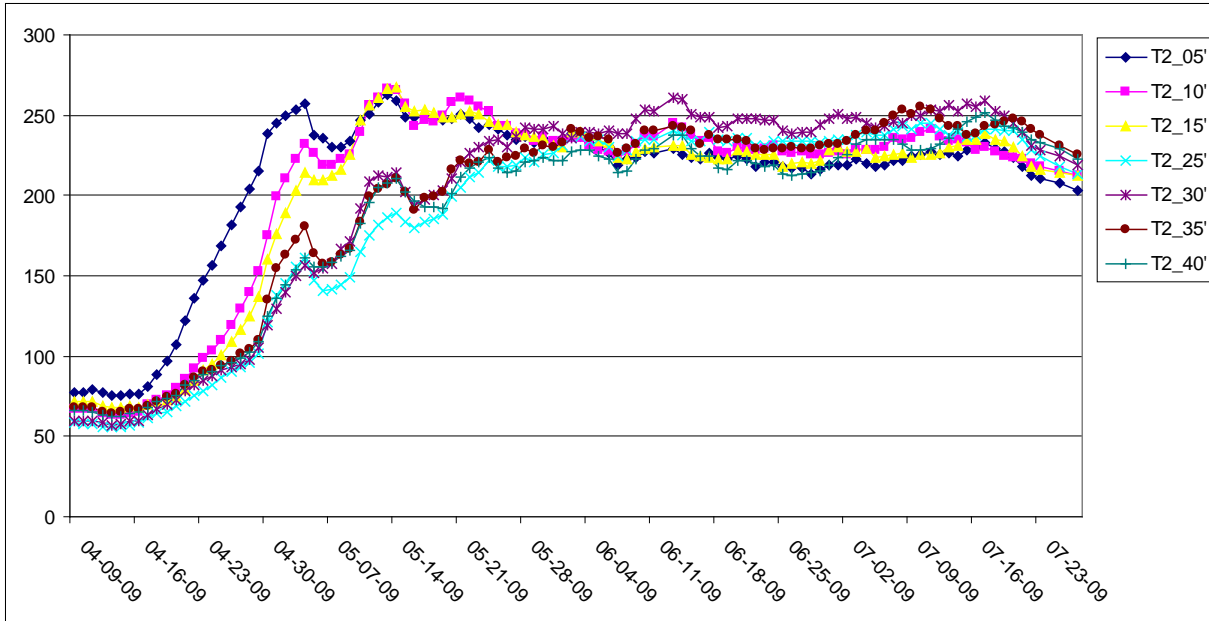


Figure 6.12. Thermocouple Temperature Readings ( °F) at Temperature Monitoring Point T1 over the Duration of Operations

□F) at Tempe



**Figure 6.13. Thermocouple Temperature Readings (T2) over the Duration of Operations**

□F) at Tempe

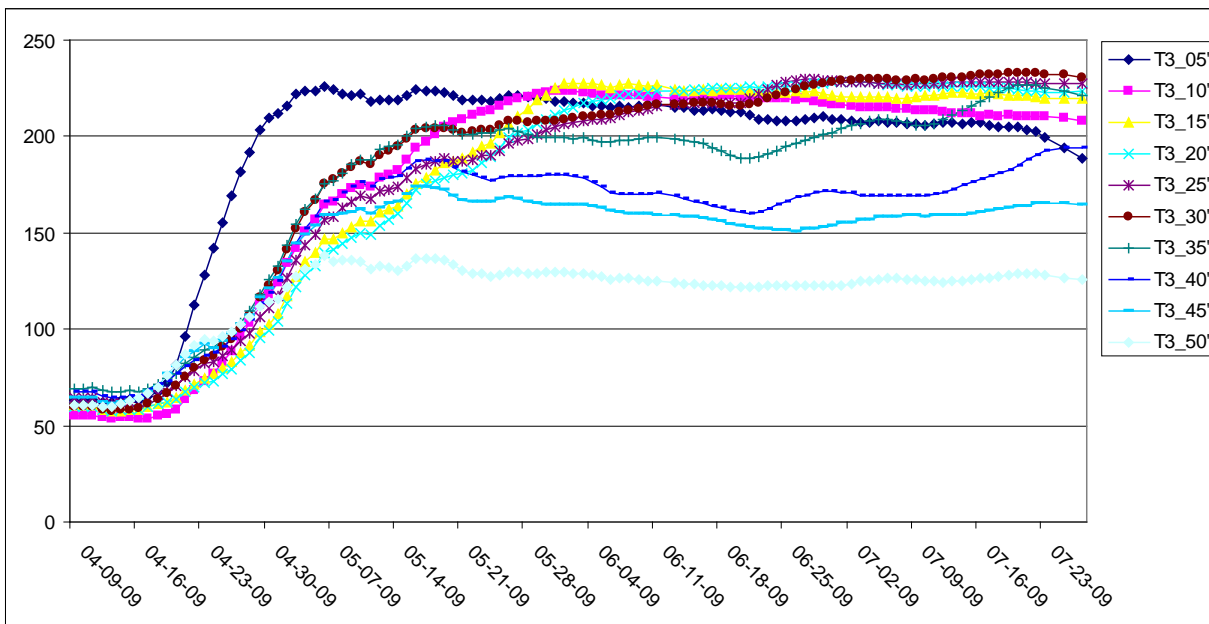


**Figure 6.14. Thermocouple Temperature Readings (T3) over the Duration of Operations**

□F) at Tempe

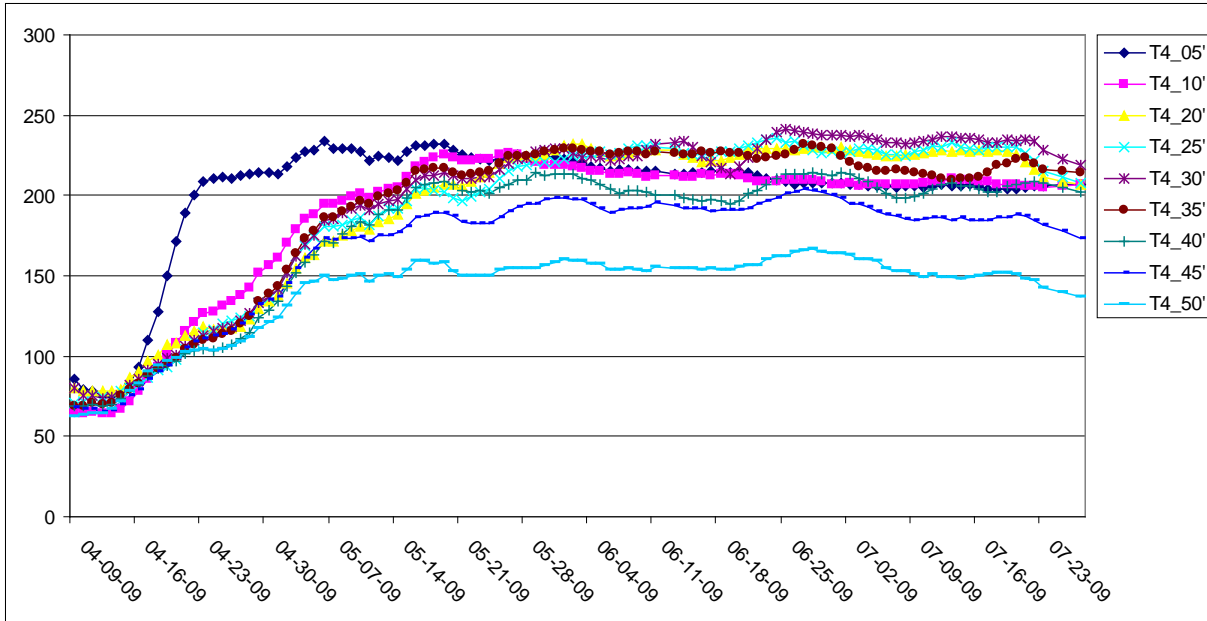


**Figure 6.15. Thermocouple Temperature Readings ( °F) at Temperature T4 over the Duration of Operations**

□F) at Tempe

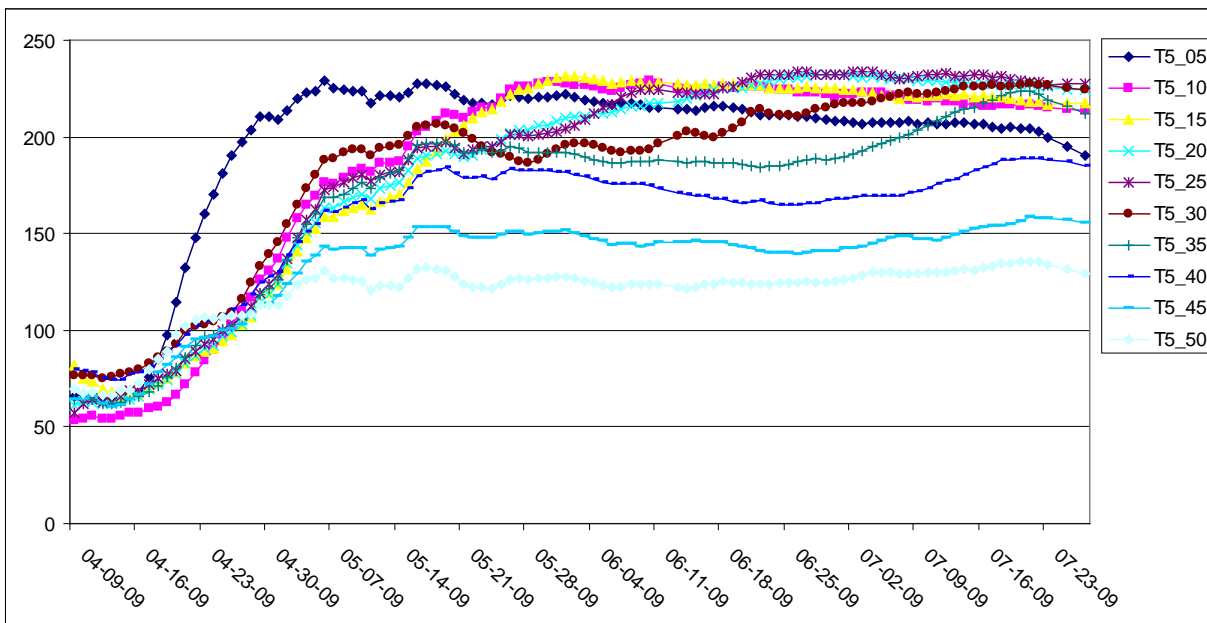


**Figure 6.16. Thermocouple Temperature Readings ( °F) at Temperature T5 over the Duration of Operations**

□F) at Tempe

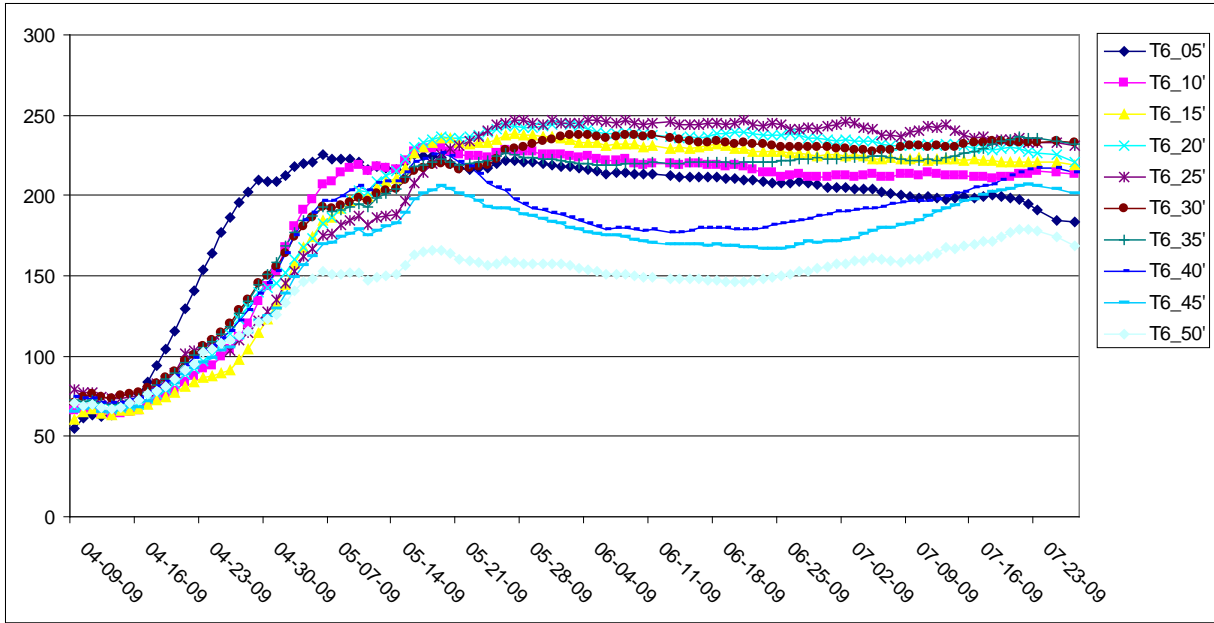


**Figure 6.17. Thermocouple Temperature Readings ( °F) at Temperature T6 over the Duration of Operations**

□F) at Tempe

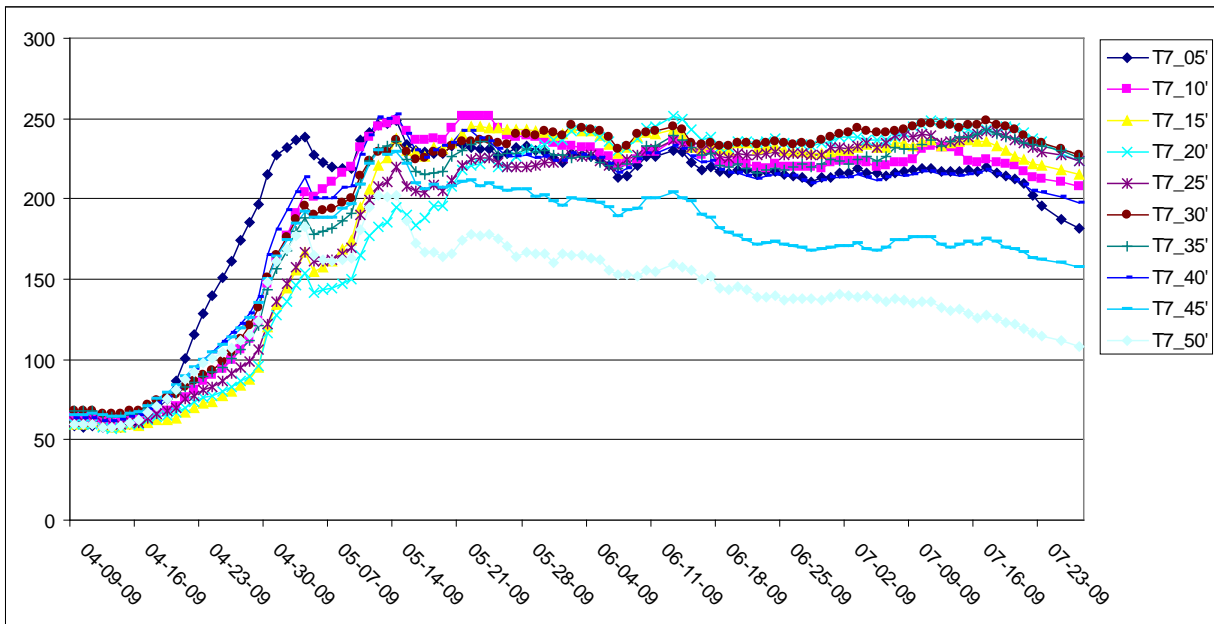


**Figure 6.18. Thermocouple Temperature Readings ( °F) at Temperature T7 over the Duration of Operations**

□F) at Tempe

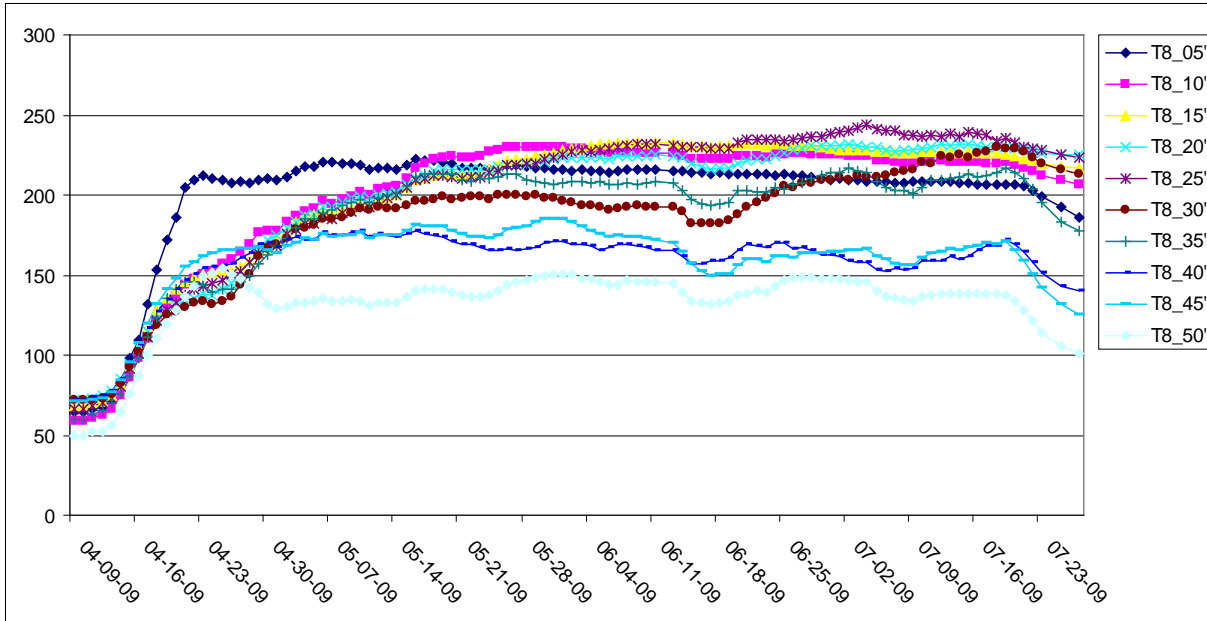
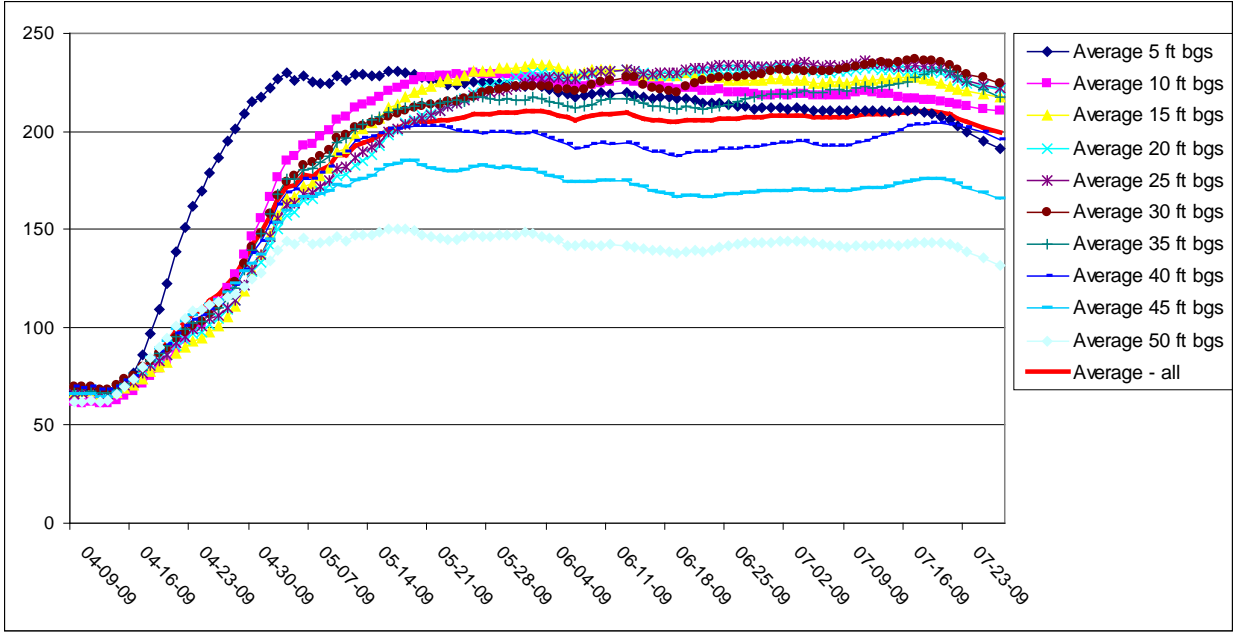


**Figure 6.19. Thermocouple Temperature Readings (T8) over the Duration of Operations**

□F) at Tempe

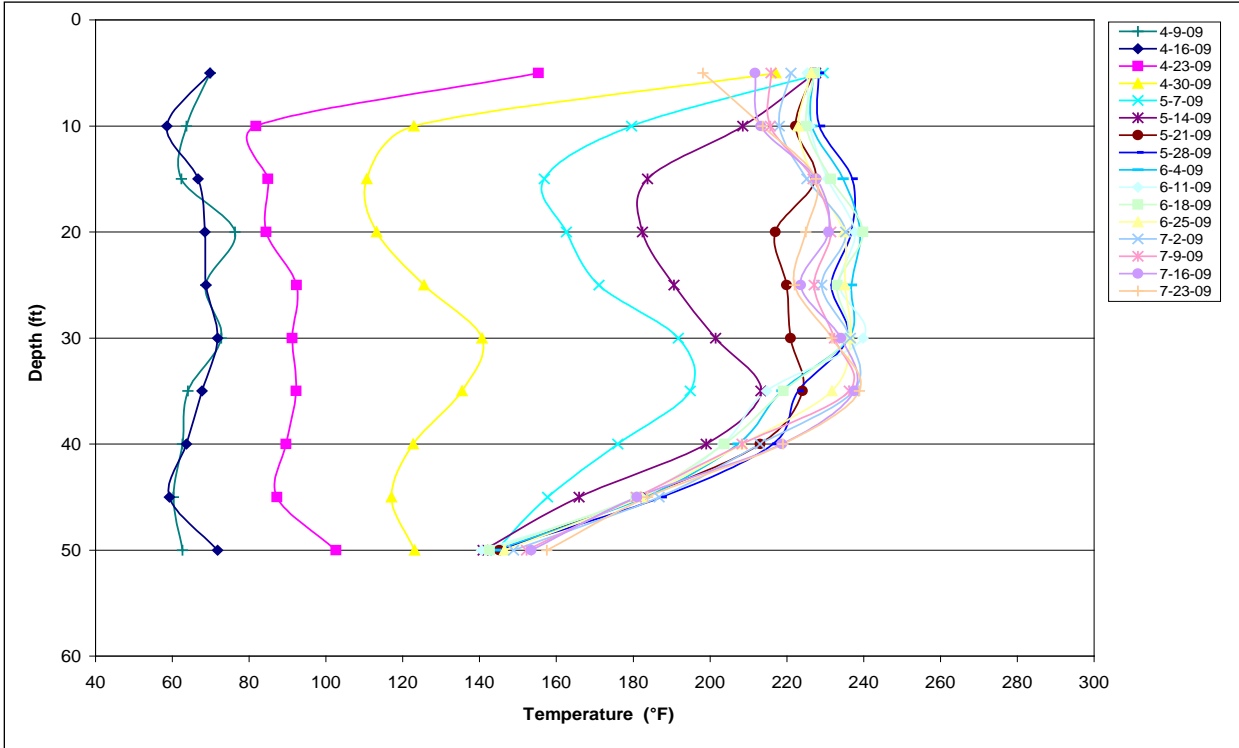
In general all thermocouples from 5 ft bgs to 35 ft bgs reached a maximum temperature at or close to the boiling point of groundwater. The bottom of the TTZ did not reach the boiling point of groundwater. The 40 ft bgs sensors in T3, T5 and T8 and all 45 and 50 ft bgs sensors across the site did not reach the boiling point.

Figure 6.20 shows the average temperatures at depths between 5 and 50 ft bgs. Generally, all zones from 35 ft bgs and above reached temperatures in the range of 210-230°F, consistent with in situ boiling temperatures of groundwater. It can also be seen that at depths of 40, 45, and 50 ft bgs the temperatures reached were somewhat lower, and below the boiling point of groundwater.



**Figure 6.20. Average Temperatures at Different Depths during Heating Operations**

Figure 6.21 shows, as an example, the temperature profile in T1 as it developed over time. In the figure, temperature profiles by depth are shown for every week during operation of the thermal system. Appendix D shows similar figures for the remaining 7 temperature monitoring points.



**Figure 6.21. Temperature at T1 during Heating Operations**

A noticeable lag in heating is observed at a depth around 10 to 25 ft bgs, and at depth of 40 ft bgs and deeper. Such lagging is consistent with more groundwater flow at these depths.

### 6.1.6.2 Temperatures during Cool-Down

Figure 6.22 below shows the thermocouple temperature readings at temperature monitoring point T1 in the cool-down phase. Appendix D shows similar figures for the remaining 7 temperature monitoring points. The data was collected over a cooling period of 8.5 months.

The relatively smooth temperature profiles during cool-down indicated that groundwater flow did not dominate the cooling. The high groundwater extraction rates observed during the thermal treatment, and hypothesized to be caused by liquid entrainment with the extracted steam, are quickly reduced during cooling, as no more steam is flowing out of the vapor extraction points. In fact, the team has hypothesized that the primary cause of this cooling effect was the induced flow as a result of the design of the vacuum extraction system.

The faster cooling at the top (where heat losses through the surface dominate) and at the bottom (where cooling can occur both as a result of heat dissipation downward, and due to groundwater flow in fractures) correspond well to patterns seen at other sites. The site is cooled to near ambient temperatures within approximately 9 months.

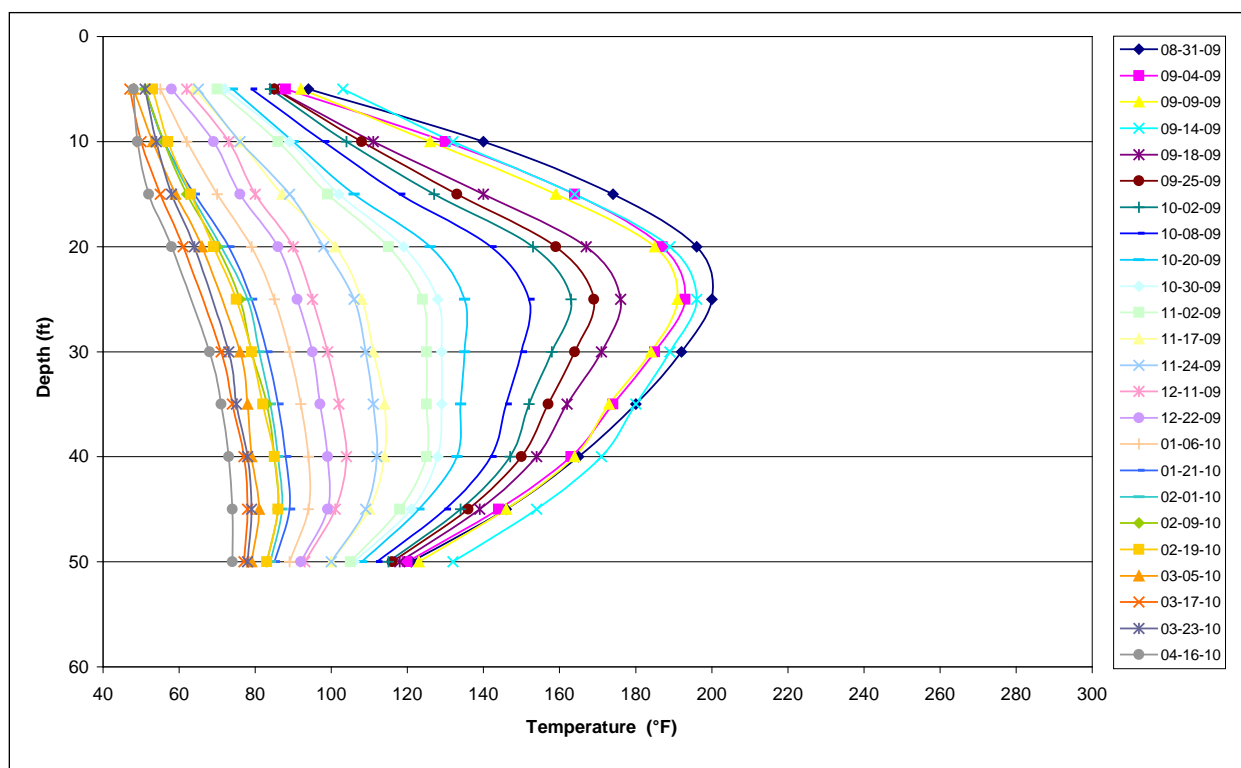
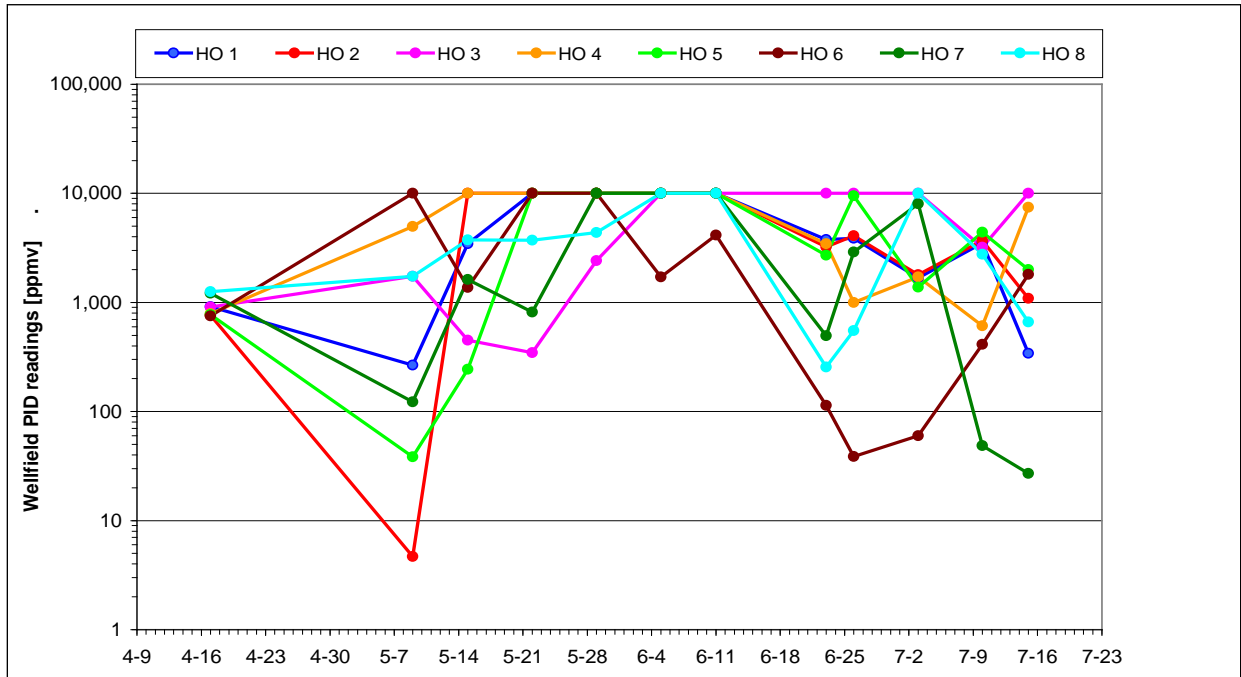


Figure 6.22. Temperature at T1 during Cool-Down

### 6.1.7 Wellfield Vapor Samples

Vapor sampling of the vapor extraction points was performed on a weekly basis with a few exceptions from all 15 vapor extraction locations. Vapor concentrations of total VOCs were

recorded with a calibrated hand-held PID. The concentrations of total VOCs in each of the extraction points (HO1 through HO15) were graphed in Figures 6.23 and 6.24. Note that the values of 10,000 ppmv correspond to the maximum detectable level of VOC for the PID.



**Figure 6.23. PID Readings at Vapor Extraction Points HO1 through HO8**

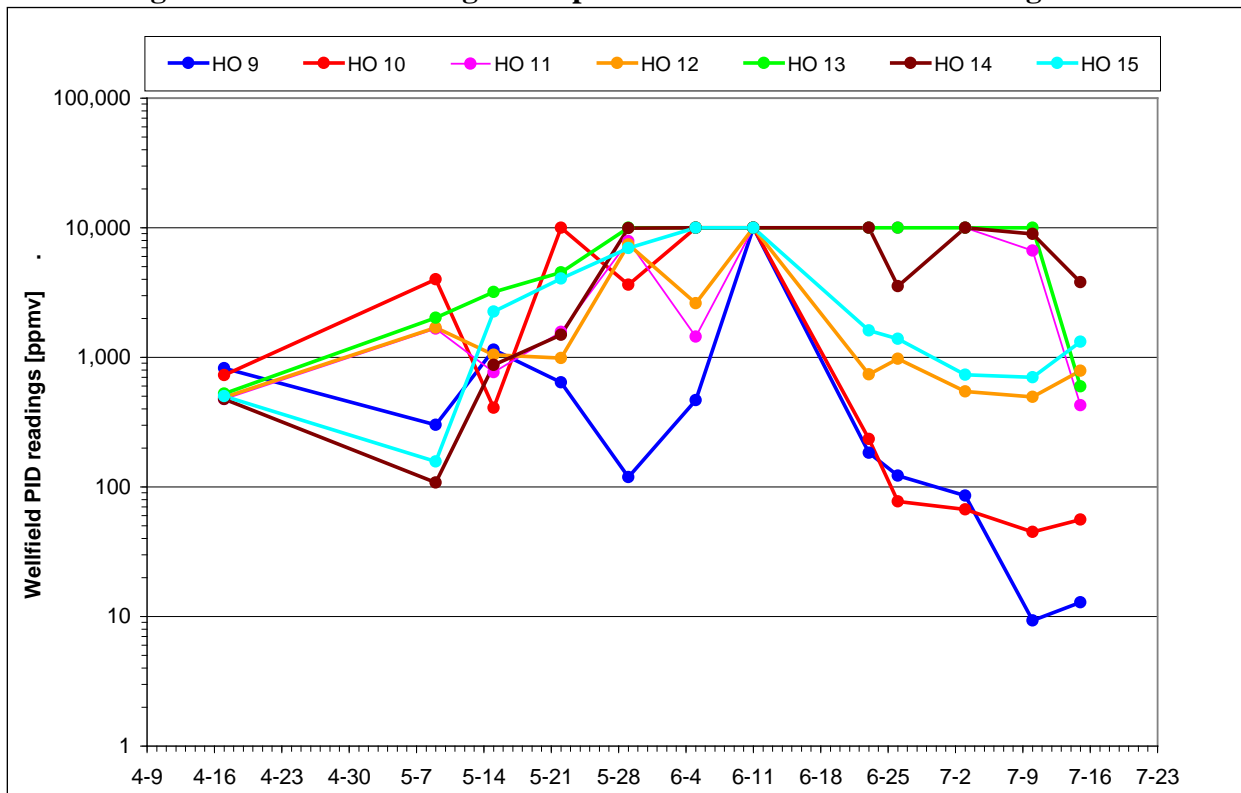


**Figure 6.24. PID Readings at Vapor Extraction Points HO9 through HO15**

In general a small drop in concentration was recorded between the first sample round conducted just after heating system startup and the second round approximately three weeks after. The concentrations peak in the period from mid-May to mid-June with an average concentration in the 15 extraction points of approximately 9,600 ppmv on 06/11/09. At the last sample round collected 07/15/09 the average concentration in the 15 extraction points were just above 2,000 ppmv.

#### **6.1.8 Numerical Modeling of TCE Pilot Test**

Using pilot test data collected at the Site, a 2D numerical model was created using TMVOC in which the primary objective was to examine the TCE mass removal in the rock matrix from the numerical simulations compared to the pilot test. The pilot test was found to have a TCE removal in the rock matrix of 63.5% as compared to the baseline model simulation which had a removal of 31%. The numerical model presented ideal conditions, such as only 3 parallel fractures separated by competent bedrock and no hydraulic gradient, therefore reducing the percentage of TCE being removed. In the field application, it is very likely that vertical fractures existed, thereby providing for smaller matrix blocks than implemented in the numerical model. The smaller matrix blocks in the field explain why the field application removed more mass from the matrix than what was predicted by the model. The fracture zone cells were identified to be the primary area where TCE removal occurred due to the higher permeability in these cells compared to the lower permeability in the rock matrix.

A sensitivity analysis concluded that the greater the maximum temperature sustained in the model, the greater the percentage of TCE removed from the rock matrix. The numerical simulations showed that the greater the duration of remediation at the maximum objective temperature, the greater amount contaminant removed. The field specific parameter of specific heat capacity showed that a lower heat capacity resulted in higher rock matrix temperatures. This parameter is site specific and should be measured prior to designing TCH projects as this may alter the energy input required to heat the subsurface to the desired temperatures. Further details of this modeling are presented in Appendix E.

## 7.0 COST ASSESSMENT

### 7.1 COST MODEL

All costs associated with the TCH Field Demonstration were tracked including: labor hours, materials, supplies, rental equipment, consumables and capital costs. Total costs incurred to date for the field implementation are approximately \$978,000 (including estimated power costs). If normalized to the size of the TTZ, the costs related to the implementation are significantly higher than those that would be expected to be encountered for a full scale project due to the relatively fixed capital costs associated with the aboveground vapor and liquid treatment systems needed to treat extracted fluids from a TCH site. Additionally, the personnel costs to design, procure, manage and operate a TCH remediation project are relatively fixed. While design, procurement, management and operational costs may increase slightly with the size and complexity of a thermal remediation project, there are basic personnel requirements for all sites regardless of the subsurface treatment volume. The total treatment volume for the TCH field demonstration was 740 cubic yards equaling a unit treatment cost of approximately \$1,300/cubic yard (not including electricity). This is in stark contrast to published unit treatment rates by McDade et al (2005) of \$88/cy for thermal treatment, and by Heron et al. (2009) who reported \$79/cy for a large DNAPL site in Tennessee. This illustrates that unit treatment costs are not comparable from site to site, and the substantial dependence on the treatment volume.

Table 7.1 below documents the cost elements that were tracked for the demonstration.

**Table 7.1. Comparison of Starting Volume of Water in TTZ with Volume Removed During Treatment**

<b>Cost Category</b>	<b>Subcategory</b>	<b>Data Tracked During the Demonstration</b>	<b>Costs</b>
Startup Costs and Design	TCH Design including: <ul style="list-style-type: none"> <li>• Review of Existing Site Data</li> <li>• Site Selection</li> <li>• Site Inspection</li> <li>• Prepare Draft/Final Demonstration Plans</li> </ul>	<ul style="list-style-type: none"> <li>• Personnel required</li> </ul>	\$67,000.00
	Permitting and Regulatory Interface	<ul style="list-style-type: none"> <li>• Personnel required</li> <li>• Permit fees</li> </ul>	\$9,800.00
	Engineering Site Inspection	<ul style="list-style-type: none"> <li>• Personnel required and associated support labor</li> </ul>	\$1,200.00
	Site Preparation – Survey/Grading/Brush Removal, Power Drop	<ul style="list-style-type: none"> <li>• Personnel required and associated support labor</li> <li>• Materials</li> <li>• Rental equipment</li> </ul>	\$51,100.00
	Mobilization	<ul style="list-style-type: none"> <li>• Personnel required and associated support labor</li> </ul>	\$6,200.00
	Drilling – Well Installation/Pre-Treatment Sample Collection and Analysis	<ul style="list-style-type: none"> <li>• Personnel required and associated support labor</li> <li>• Materials</li> <li>• Rental equipment</li> <li>• Subcontractor costs</li> <li>• Permit fees</li> </ul>	\$226,000.00
	TCH System Construction and System Shakedown/Startup	<ul style="list-style-type: none"> <li>• Personnel required and associated support labor</li> <li>• Materials</li> <li>• Rental equipment</li> </ul>	\$42,000.00
Capital Costs	TCH System Materials Procurement	<ul style="list-style-type: none"> <li>• Costs included above in TCH System Construction and System Shakedown/Startup</li> </ul>	\$29,900.00
Operating Costs	TCH System Operations	<ul style="list-style-type: none"> <li>• Personnel required and associated support labor</li> <li>• Materials</li> <li>• Rental equipment</li> <li>• Analytical laboratory costs</li> </ul>	\$170,700.00
Direct Environmental Activity Costs	Post-Treatment Data Collection and Analysis	<ul style="list-style-type: none"> <li>• Personnel required and associated support labor</li> <li>• Materials</li> <li>• Rental equipment</li> <li>• Subcontractor costs</li> <li>• Overhead expenses</li> </ul>	\$31,500.00

		<ul style="list-style-type: none"> <li>Analytical laboratory costs</li> </ul>	
	Well Removal	<ul style="list-style-type: none"> <li>Personnel required and associated support labor</li> <li>Materials</li> <li>Rental equipment</li> <li>Subcontractor costs</li> </ul>	\$62,500.00
	Utilities	<ul style="list-style-type: none"> <li>Power drop and electrical usage expense</li> </ul>	<ul style="list-style-type: none"> <li>Power drop costs are site specific. Power drop costs for the TCH Demonstration were \$50,500.00 and are included in the Site Preparation Task above. Power usage costs for the TCH demonstration are estimated to be \$55,000.00.</li> </ul>
Indirect Environmental Activity Costs	Waste Manifesting (if any) and Disposal	Costs included below in Demobilization	\$19,200.00
	Environmental and Safety Training	NA	NA
	OSHA Sampling (if any)	NA	NA
Other	Demobilization	<ul style="list-style-type: none"> <li>Personnel required and associated support labor</li> <li>Materials</li> <li>Rental equipment</li> </ul>	\$33,500.00
	TCH System Installation, Construction, Operation, Post-Treatment Sampling, System Demobilization Overhead Expenses, Project Management, Project Engineering, Project Accounting	<ul style="list-style-type: none"> <li>Overhead expenses such as per diem/living expenses, office trailer rental, shipping charges, etc.</li> </ul>	\$193,800.00
	Project Trips as Necessary	<ul style="list-style-type: none"> <li>Personnel required and associated support labor</li> <li>Overhead expenses such as per diem/living expenses</li> </ul>	\$2,100.00
	Final Reporting	<ul style="list-style-type: none"> <li>Personnel required and associated support labor</li> </ul>	\$31,300.00

### **7.1.1 Interpretation of Costs and Scale**

The costs tracked for the TCH field demonstration should not be used as a linear comparison to cost other TCH remediations at other sites. As discussed above, due to the relatively fixed capital equipment and personnel costs associated with a TCH remediation project, cost estimates must be done using site specific parameters. Due to the relatively incremental cost for heaters and extraction points to be installed into deeper borings, a general rule of thumb is that the deeper a site and the larger the volume, the lower the unit price per cubic yard.

Additionally, as the availability of utilities and the cost for utilities can vary widely for remediation projects in different regions, the cost to install utilities and the cost for utilities is a site-specific cost. Assumptions can be made for estimating purposes, but site-specific costs should be evaluated when preparing a cost estimate.

## **7.2 COST DRIVERS**

The cost of the TCH technology depends primarily on the size and depth of the treated subsurface volume. This defines the volume to be treated, which in turn determines the number and depth of heater borings and extraction points, and the size and type of the process equipment. A secondary parameter is the type of rock or sedimentary deposit, particularly its porosity and heat capacity. These parameters determine the amount of energy necessary to heat the target volume to the treatment temperature.

In fractured rock, several other factors are important. These include:

- The mineralogy of the rock (important for matrix diffusion).
- Organic matter content of the rock and fracture rinds (determining the degree of adsorption and retardation).
- Fracture patterns and permeability (governs the flow of groundwater which could slow heating).

Finally, the type of contaminant is important for the treatment cost. Volatile COCs like TCE and PCE are likely to be effectively removed at the boiling point of water (drying of the site not necessary), whereas less volatile COCs such as PCBs will require heating of the rock to higher temperatures for complete removal and may also require more aggressive aboveground vapor treatment technologies to comply with regulatory requirements.

Costs associated with the implementation of TCH are significantly impacted by the size of the area of concern to be treated. Because of the relatively fixed capital and infrastructure costs associated with the construction of process vapor and liquid treatment systems, the overall size and depth of the area of concern for which TCH will be used impacts the unit cost per volume for the TCH implementation significantly (i.e., the deeper the area of concern, the lower cost per unit volume). While the well head infrastructure cost for each TCH boring and vapor/liquid piping segment is fixed, the cost to extend heater borings and vapor extraction points to deeper depths to treat a larger volume is a relatively minor per foot incremental cost.

Due to the varying boiling points of contaminants of concern (COCs), those COCs with higher boiling points (e.g., chlorobenzenes, PCBs) will typically require more robust heating designs including closer well spacing and longer TCH operational durations to achieve site cleanup. Sites with high groundwater flux or site soils with high organic content (e.g., peat) also require more robust heating designs, typically requiring closer TCH well spacing, longer operational durations or both.

The closer well spacing can be used to heat the subsurface to target treatment temperatures more quickly and in some instances to provide a hydraulic barrier for the site (essentially boiling off groundwater as it enters the area of concern). Longer operational durations may be required to reach higher target treatment temperatures for those COC's with higher boiling points.

### **7.3 COST ANALYSIS**

TerraTherm has utilized its proprietary cost model to produce cost estimates for three treatment scenarios with the same design parameters but with different treatment areas and volumes to demonstrate the range of treatment costs dependent upon the treatment volume at a specific site. TerraTherm's proprietary cost model is based on cost data from approximately 25 completed projects. We have classified the three scenarios as follows:

- Small: treatment zone approximately 12,500 yd<sup>3</sup>;
- Medium: treatment zone approximately 50,000 yd<sup>3</sup>; and,
- Large: treatment zone approximately 250,000 yd<sup>3</sup>.

These cost scenarios are applicable to fractured bedrock as they incorporate assessment of groundwater flow and measures to reduce and manage the rate of flow if necessary (e.g., design of vacuum extraction system, use of steam to prevent groundwater influx and pre heat groundwater, and use of groundwater hydraulic control). Further, Tables 7.2 through 7.3 below outline the design parameters used for the three different costing scenarios. One of the major lessons learned from this TCH field demonstration conducted under ER0715 was the need for not only the utilization of TCH to treat the DNAPL source zone, but also the need for a method to adequately control the incoming flux of groundwater into the TTZ from bedrock fractures. TerraTherm has already incorporated such approach into their TCH applications; thereby transferring technology directly from an ESTCP Project into implementation. To successfully control the groundwater influx, they have included not only multi-phase extraction wells to pump water from the TTZ, but they have also included steam injection well(s) in the design. Steam injection can be used not only to heat and treat permeable matrices, but also can be used to create a pressurized steam zone in the subsurface to effectively block the influx of cool water into the TTZ.

**Table 7.2. Volume and Heat Capacity Design Input Parameters**

<b>Volume and heat capacity</b>	<b>Small</b>	<b>Medium</b>	<b>Large</b>	<b>Unit</b>
Treatment area	2,250	9,000	45,000	ft <sup>2</sup>
Upper depth of treatment	0	0	0	ft bgs
Lower depth of treatment	150	150	150	ft bgs
Thickness of overburden	50	50	50	ft
Thickness of bedrock	100	100	100	ft
Volume, TTZ	12,500	50,000	250,000	yd <sup>3</sup>
Solids volume	10,625	42,500	212,500	yd <sup>3</sup>
Porosity volume	1,875	7,500	37,500	yd <sup>3</sup>
Soil weight	47,443,901	189,775,606	948,878,029	lbs soil
Water weight	2,794,688	11,178,752	55,893,759	lbs water
Soil heat capacity	11,860,975	47,443,901	237,219,507	BTU/F
Water heat capacity	2,794,688	11,178,752	55,893,759	BTU/F
Total heat capacity, whole TTZ	14,655,663	58,622,653	293,113,266	BTU/F

**Table 7.3. Energy Balance Design Input Parameters**

<b>Energy balance</b>	<b>Small</b>	<b>Medium</b>	<b>Large</b>	<b>Unit</b>
Steam injection rate	240	720	2,880	lbs/hr
TCH power input rate	980	2,217	8,056	kW
Water extraction rate during heatup	3	11	52	gpm
Steam extracted, average	1,105	2,552	9,355	lbs/hr
Energy flux into treatment volume	3,577,504	8,260,517	30,279,251	BTU/hr
Energy flux in extracted groundwater	207,916	763,655	3,614,744	BTU/hr
Energy flux in extracted steam	1,073,251	2,478,155	9,083,775	BTU/hr
Net energy flux into treatment volume	2,296,337	5,018,707	17,580,732	BTU/hr
Heating per day	3.7	2	1	F/day
Start temperature	50.0	50	50	F
Target temperature	212.0	212	212	F
Estimated heat loss, worst case	46.3	32	28	%

Tables 7.4 and 7.5 below provide site specific design outputs based on the parameters that were used for modeling the three treatment volume scenarios. Table 7.4 shows the total operational duration for each of the three volume scenarios. This operational time is only for the time spent “heating” the site.

**Table 7.4. Total Operational Duration**

<b>Operating time</b>	<b>Small</b>	<b>Medium</b>	<b>Large</b>	<b>Unit</b>
Shake-down	7	7	7	days
Heating to boiling point	70	103	145	days
Boiling and drying	70	121	167	days
Sampling/analysis phase	10	10	10	days
Post treatment vapor extraction	14	14	14	days
Total operating time	170	255	343	days

**Table 7.5. Total Number of Wells**

<b>Number of wells</b>	<b>Small</b>	<b>Medium</b>	<b>Large</b>
Heater borings	23	52	189
Vertical SVE wells	23	52	189
Steam injection wells	4	8	24
Multi-phase extraction wells	1	2	6
Temperature monitoring wells	7	12	35
Pressure monitoring wells	4	5	10

The total remediation time frame for each of the three volume scenarios is approximately 200 days. In fact, this figure is consistent with published literature; McGuire, et al 2009, which estimated average duration of thermal remediation is 228 days. Project duration, including treatment design, construction and operations and final reporting is less than three years. Figures 7.1 through 7.3 below provide project durations by task for each of the three treatment scenarios. All schedules assume a project start date of January 1, 2012.

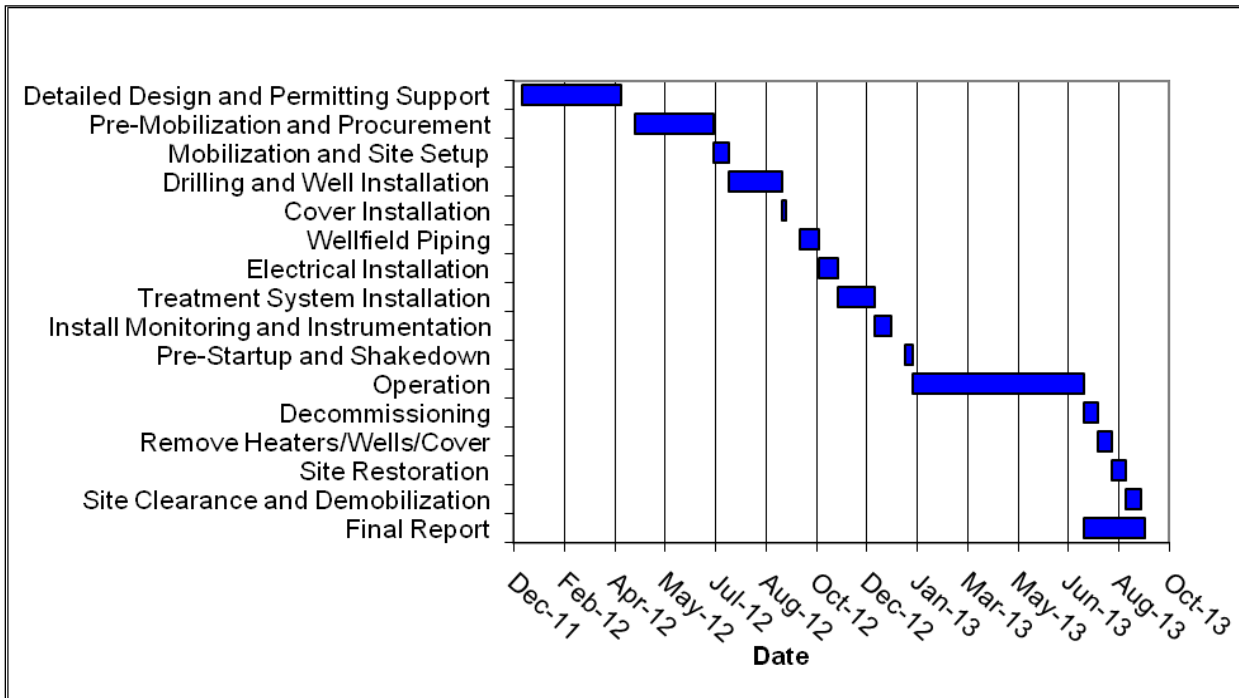


**Figure 7.1. Project Duration by Task for Small Project Implementation**

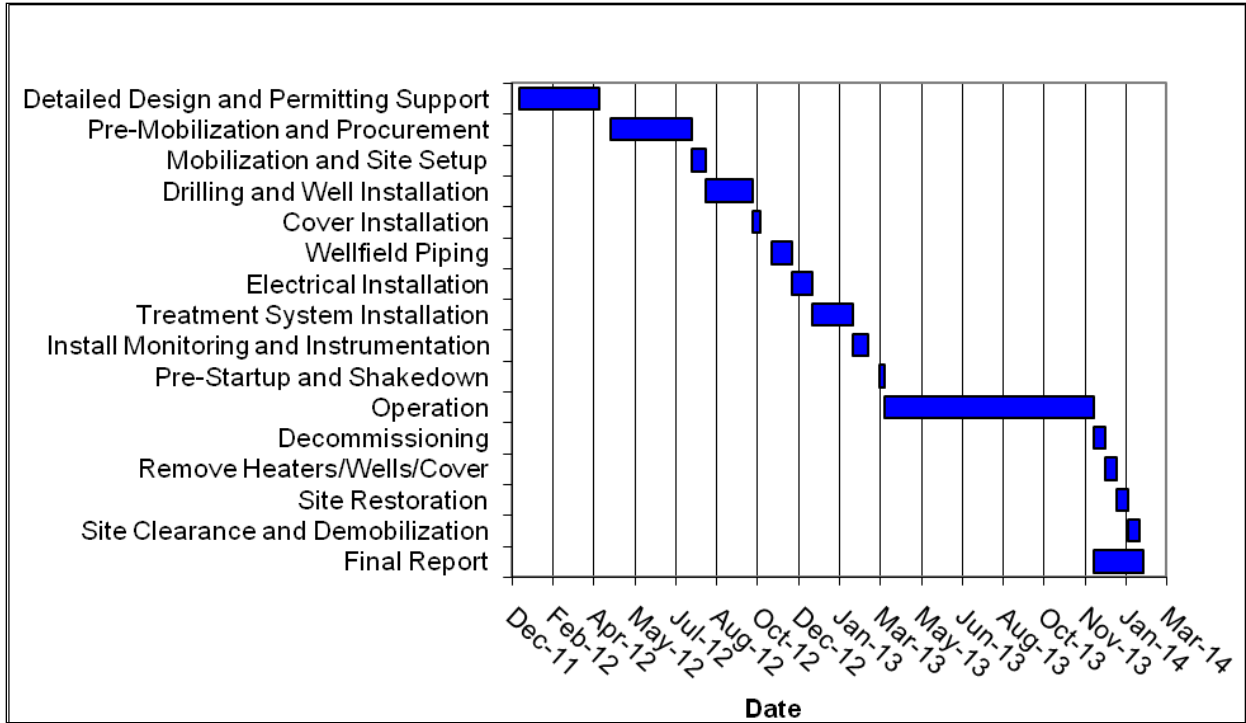


**Figure 7.2. Project Duration by Task for Medium Project Implementation**

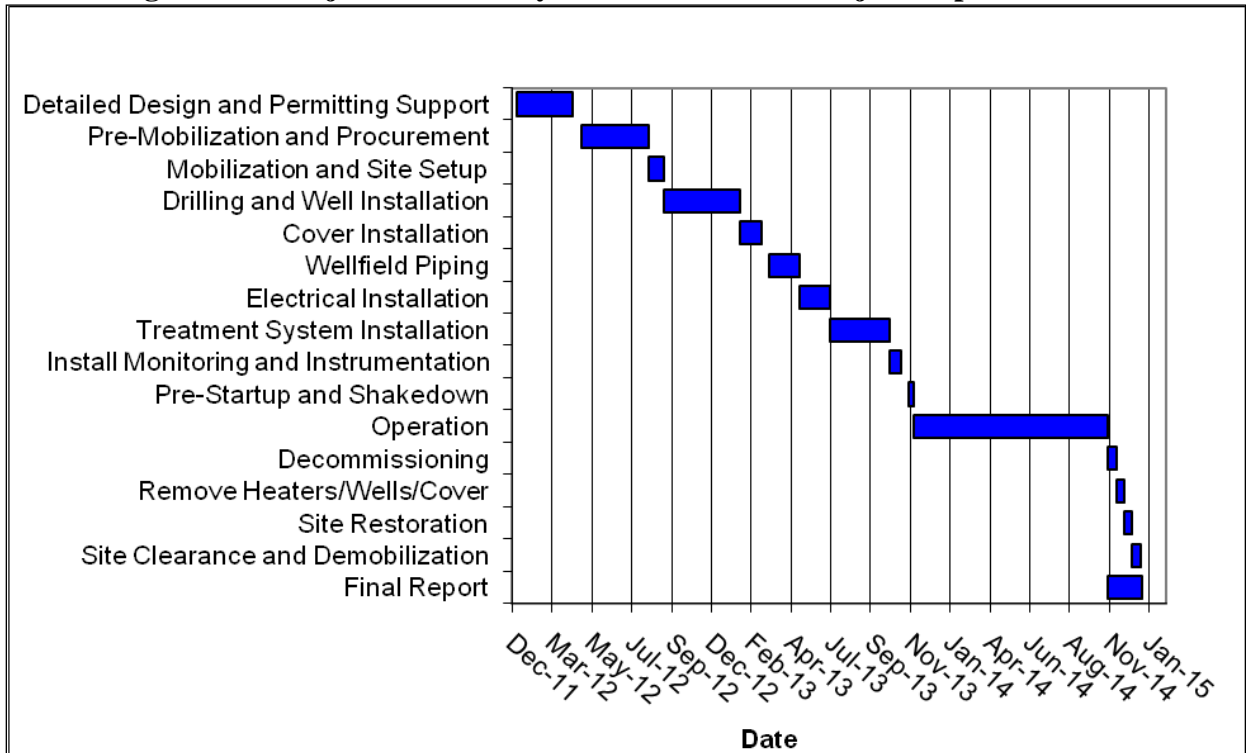


**Figure 7.3. Project Duration by Task for Large Project Implementation**

Costs for three different TCH treatment volumes have been presented in Table 7.6 below. TerraTherm's proprietary design and costing model was used to generate the costs associated with TCH remediation of three sites with the same input parameters with the exception of the surface area of the treatment zone. By keeping all other input parameters constant, it allows us to examine the decrease in unit cost as the overall volume of the area of concern is increased. Because the total remediation time frame is less than three years for each of the scenarios, no discount rate was applied to the costs presented in Table 7.6 (White House OMB, 2010).

The assumptions incorporated in the cost model generated costs are as follows:

- Due to the variability of utility availability, utility hookup charges have not been included in the costs.
- A rate of \$0.12/kWhr has been used for electricity usage charges.
- Permitting fees are excluded; details to support the permitting application process (handled by client) are included in costs.
- Power and other utilities are assumed to be available to the site with service available in a reasonable timeframe. Please note, at most sites it is necessary to bring in power. This typically involves making a new connection (power drop) to an existing nearby power line. In most cases this involves installing one or several poles, running wire, and bringing in and connecting a transformer of the appropriate size for the project.
- Discharge/disposal of treated effluents, drill cuttings and any GAC or NAPL produced during operation is excluded.
- Site will be free of any existing infrastructure not compatible with treatment temperatures or which would interfere with treatment application.
- Sufficient space is provided for unencumbered site construction and thermal operations.
- We have assumed that sacrificial GAC will be used for vapor treatment for both the Small and Medium scenarios. We have assumed that a GAC regeneration system will be used for vapor treatment for the Large scenario.

**Table 7.6. Implementation Costs for Small, Medium and Large Volume TCH Projects**

Task	Subtask	Small Price (\$)	Medium Price (\$)	Large Price (\$)	
<b>Design and preparation</b>	Conceptual design and cost estimate	40,426	40,426	40,426	
	Detailed design, permitting	162,000	162,000	162,000	
	Procurement	100,000	163,000	458,000	
<b>Site activities pre operation</b>	Mobilization and site setup	44,000	76,000	246,000	
	Power drop and transformer	Not included	Not included	Not included	
	Drilling and well installation	725,000	1,483,000	5,012,000	
	Vapor cover installation	46,000	141,000	591,000	
	Wellfield piping	55,000	136,000	986,000	
	ISTD power equipment installation	61,000	97,000	267,000	
	Steam generation system installation	20,000	22,000	30,000	
	Treatment system installation	363,879	578,858	2,216,477	
	Electrical installation, wellfield and process	43,000	58,000	125,000	
	Instrument and monitoring system installation	16,000	22,000	49,000	
	Pre-startup and shakedown	33,000	45,000	100,000	
	<b>Operation</b>	ISTD power equipment rental	90,000	127,000	167,000
		Steam generation system rental	46,000	69,000	113,000
Labor, travel, per diem		282,000	633,000	1,136,000	
Process monitoring, sampling and analysis		16,000	36,000	130,000	
Waste and GAC		27,000	110,000	1,000	
Repair/maintenance		61,000	91,000	123,000	
Tools, rentals and fees		23,000	34,000	46,000	
<b>Demob and other</b>	Decommissioning	42,000	77,000	267,000	
	Remove Heaters/Wells/Cover	237,000	495,000	1,699,000	
	Site Restoration	-	-	-	
	Site Clearance & Demob	17,000	33,000	118,000	
	Reporting	41,000	41,000	41,000	
<b>Indirect costs</b>	Field support	80,000	119,000	160,000	
	Home office support	134,000	200,000	270,000	
	ISTD licensing fees	90,000	157,000	456,000	
	<b>Total (not including electricity)</b>	<b>2,895,000</b>	<b>5,066,000</b>	<b>14,693,000</b>	
<b>Utilities</b>	Electricity	468,000	1,600,000	7,711,000	
	<b>Total (including electricity)</b>	<b>3,363,000</b>	<b>6,846,000</b>	<b>22,721,000</b>	
	<b>Price (\$) per cubic yard</b>	<b>269</b>	<b>137</b>	<b>91</b>	

As seen in Table 7.6 above, the unit costs for TCH implementation vary greatly as a function of the total treatment volume of the site. In the cost model scenarios the cost per cubic yard ranges from \$269/cu yd for the Small 12,500 cu yd scenario to \$91/ cu yd for the Large 250,000 cu yd scenario. These cost ranges agree well with other full-scale implementation costs as observed by TerraTherm at other TCH sites.

## 8.0 IMPLEMENTATION ISSUES

The goal of the field demonstration was to develop useful guidelines so that practitioners could understand how to apply the TCH technology and to help avoid misperceptions regarding what is attainable with TCH, in terms of mass removal, reduction of aqueous phase contaminant flux, reduction of aqueous phase concentrations, and reduction in source zone lifespan. The field demonstration and the data generated help us to understand and evaluate the effectiveness of the thermal treatment of chlorinated ethenes in source zone contamination at bedrock sites.

The following data collected during the field implementation indicate that the TCH application can be effective in removing TCE and other VOCs from the bedrock at the site:

- The site was brought to temperatures near or at the boiling point of water from a depth of 5 to 35 ft bgs. This shows that the electrical energy was effectively delivered, and that the rock matrix at 5 to 35 ft bgs was heated as desired.
- Between 530 and 680 lbs of VOCs were removed during the 106 days of operation.

Rock concentrations were generally lowered substantially, and mass removal continued until the end of the operations period, indicating that the TCH treatment was still occurring.

Field data shows that most rock concentrations were lowered to around 0-5 mg/kg, but that higher concentrations were maintained at distinct depth intervals. These depths correlated reasonably well with the depth showing the highest TCE concentrations prior to heating (as an example, between 15 and 18 ft bgs in BR-1). Relatively good heating and remediation occurred in the larger matrix blocks. Concentrations in thick zones without evident fractures were reduced substantially to levels below 5 mg/kg.

The most probable explanation for the observed concentrations is:

- Substantial flow of contaminated groundwater occurred in distinct fracture zones during the thermal operations. This is supported by (1) slower heating at certain depth intervals, (2) the high groundwater extraction rates observed, and (3) consistently elevated VOC concentrations in extracted vapor and water.
- The steam created in the matrix led to partial desaturation and to a push of steam and water towards the permeable fractures. As the steam migrated towards the fractures, it will encounter lower temperatures and tend to condense near the fractures. Where the cool water flow continues and is sufficient to keep the fractures below the boiling point, TCE will be accumulated in the matrix near the fractures.

Regional groundwater flow is believed to be partially responsible for the local cooling that led to ineffective TCE remediation. In addition, the flow of contaminated water into the TTZ continuously supplied TCE and other VOCs to the field demonstration area. Furthermore, field data corresponds well with the interpretation that elevated groundwater flows during thermal treatment were caused by the vapor extraction, and not solely by regional groundwater flow. In other words, groundwater moved much faster during the thermal operations, as a result of liquid

entrainment occurring in the vapor extraction points as steam was extracted, and pulled large quantities of groundwater with it.

## 8.1 GUIDELINES TO PRACTITIONERS

For the TCH process to be effective in this setting, the flow of cold and contaminated groundwater into the TTZ must be limited and/or controlled. This finding is consistent with NRC findings in 2005, i.e., *“There is limited field experience applying conductive heating below the water table... As control of water inflow may be problematic in fractured media and karst, and capture of contaminants may be difficult, effectiveness is expected to be limited in these settings. If water inflow can be limited, then conductive heating would be expected to be effective in all granular media.”* Furthermore, Kingston, et. al reported in 2009 that *“Better performance might be achieved if system footprints are over-designed to extend beyond the source zone boundaries.”* Though at full scale, this mechanism will be much less pronounced, as the surface area to volume ratio decreases with the scale, it may be necessary to limit the influx of groundwater to limit the cooling effect that prevents target temperatures from being reached. Further, for full-scale applications, the treatment area would typically encompass the entire contaminated zone, so that groundwater entering the treatment area would not re-introduce high VOC concentrations into the treatment zone as was observed at this site.

Other useful guidelines follow:

1. Careful attention should be given to groundwater influx into a target treatment zone in order to determine whether the boiling of water can be achieved, and the length of heating time required to achieve boiling. Calculating the groundwater influx at a fractured rock site is typically carried out using measurements of bulk rock hydraulic conductivity and hydraulic gradient. Given the likely variability of flowrate amongst individual fractures in a treatment zone (flow proportional to fracture aperture cubed), more accurate assessment of the influence of inflowing cold groundwater can be determined on the basis of bulk rock hydraulic conductivity measurements carried out at smaller scales, rather than at larger scales. However, water inflow at a fractured bedrock site may be challenging, therefore an effective TCH application should include site-specific testing to discover these issues and make modifications prior to full-scale treatment. In fact, practitioners should pay particular attention to the potential for groundwater influx when designing and implementing a TCH application in fractured bedrock.
2. System design must take into account the induced flow of cool groundwater into the treatment volume through the dominant fractures as a result of the vacuum extraction system.
3. Because of the variability in boiling point throughout a fractured rock treatment zone and the absence of a well-defined constant temperature boiling plateau in the rock matrix, it may be difficult to monitor the progress of thermal treatment using temperature measurements alone.
4. The combination of the close well spacing and the vibrations induced to the rock formation during the sonic drilling may have created additional fractures and caused the hydraulic conductivity of the fractured bedrock in the demonstration area to increase. Although not likely due to wider well spacing at full scale, drilling methods should be

examined to reduce the possible amount of additional fracturing that may occur during well installation. A site manager must consider impacts of drilling techniques on the potential for water influx and a system design should include contingencies to limit or mitigate groundwater influx if cooling is detected. During this ER0715 TCH demonstration, the ambient hydraulic characteristics of the TCH site were likely altered after installation of 23 boreholes at a site that is 22 ft diameter and 55 ft deep. Each borehole was drilled using a sonic drilling rig and a 6-inch drill bit. The closely spaced boreholes and the high vibrations created during sonic drilling caused a massive network of fracture in the field demonstration area and radically increased the hydraulic conductivity of the bedrock. The NJ licensed driller reported that the first completed borehole pumped at a maximum rate of less than 1 gallon per minute (gpm). A pumping rate that is typical for many of the 105 monitoring wells located at the NAWC. The driller also reported an increased pumping rate for the last 3 or 4 boreholes. The average pumping rate of higher producing wells at the NAWC typically is 4 to 10 gpm.

5. Treatability tests demonstrated that heating duration had a greater effect on the degree of TCE and PCE mass removal compared to heating temperature. In heating *duration profile* tests the majority of contaminant mass removal was achieved in the early stages of heating. In samples of sandstone, dolostone, limestone and siltstone further heating did not lead to a significant decrease in contaminant concentration. Heating *temperature profile* tests required final target temperatures of 200°C to remove the majority of the contaminant mass. In thermal field applications, extending treatment duration under standard operational temperatures beyond the boiling point of water would, therefore, be more effective than elevating temperatures above the boiling point of water. The removal of TCE and PCE from the rock matrix by heating was not sensitive to the chemical properties of the compounds.
6. The results of a microbial presence treatability test demonstrated that, as expected, heating groundwater to approximately 200°F resulted in sterilization. However, the results also indicated that the aquifer was rapidly reseeded with microorganisms, and that both numbers of microorganisms and microbial activity in groundwater just four months after thermal treatment were actually greater than prior to treatment. These results show that, while thermal treatment does decrease both numbers and activity of microorganisms in the short term, the aquifer quickly regained its ability to support microbial populations as well as microbial activity.
7. Use of larger-diameter vapor extraction points (so that the steam can bubble through the standing water without pushing it out) should be considered. In addition, larger extraction points would reduce the steam velocity and the amount of entrained water being extracted from the points.
8. A TCH system should use separate heaters and vacuum extraction points. Grouting of the heater borings into the bedrock is recommended. Grouting the heater borings instead of backfilling the boreholes with sand would prevent the pressurization and steam drive of water out of the boreholes around the heaters.
9. Regional groundwater flow cooling can possibly be reduced using a hydraulic barrier such as a freeze-wall or a grout curtain.
10. TCH can also be combined with steam injection to enhance performance. The injection of steam into the water-bearing fractures, displaces groundwater and heats the fracture system.

11. A site manager should consider smaller-scale testing prior to full-scale deployment to identify potential problems and refine full-scale designs and operations.
12. Practitioners should consider longer treatment and/or higher temperatures to remove contaminants from difficult regions. In fact, a “Critical Evaluation of State-of-the-Art In Situ Thermal Treatment Technologies for DNAPL Source Zone Treatment” conducted under ESTCP Project ER-0314 states: *“The operating duration for most in situ thermal applications seems to arguably have been arbitrary, with cessation of heating after reaching and maintaining a target temperature for some pre-defined period of time. It seems that there is an opportunity here to better define operational endpoints based on metrics more closely related to the conventional cleanup goals (i.e., target soil and groundwater cleanup concentrations).”*
13. Hydraulic conductivity measurements should be taken at relatively small scales to assess individual strata or rock types. Further, as much as possible, fractures should be characterized as well as possible.
14. The impacts of different rock types present in the contaminated zone should be understood. The thorough technical approach employed in the ER0715 validation allowed for laboratory tests that yielded valuable information for the field demonstration. Those treatability tests concluded that rock properties had a significant effect on contaminant mass removal during heating experiments. It was determined that the rock properties observed in samples of sandstone and dolostone, such as high porosity and low fraction organic carbon, contributed to the increase in contaminant mass removal during the heating tests. In field applications, fractured bedrock with higher porosities and lower fraction organic carbon would favor the performance and effectiveness of thermal treatment in the removal of TCE and PCE. Further, a two-way ANOVA with replication showed that the contaminant mass removal was significantly different for each type of rock throughout the heating process, regardless of the heating profile utilized during the heating tests (95 % significance level). The PCA analysis revealed that porosity favored the degree of contaminant mass removal from the rock matrix. In contrast, fraction organic carbon had a negative effect on the contaminant mass removal. Black mudstone (as in the case of NAWC), with a combination of lower porosity and higher fraction organic carbon, exhibited the lowest degree of contaminant mass removal.
15. Last but not least, given the uncertainties intrinsic to site characterization and technology performance, both an adaptive management approach and a performance based contract may fit well in this type of challenge. Clear objectives and goals should be established based on the site’s regulatory, stakeholder and hydrogeological conditions with options to adapt the system design. Performance based contracting is encouraged by DoD whenever possible (DOD 2000).

## 9.0 REFERENCES

- ASTM, 2004a. Standard Test Method for Density of Soil in Place by the Drive-Cylinder Method. ASTM D2937-04. American Society for Testing and Materials (ASTM) International, West Conshohocken, Penn.
- ASTM, 2004b. Standard Test Method for Determination of Pore Volume and Pore Volume Distribution of Soil and Rock by Mercury Intrusion Porosimetry. ASTM D4404-84. American Society for Testing and Materials (ASTM) International, West Conshohocken, Penn.
- Baker R.S., Heron, G., Bierschenk, J.M., LaChance, J.C., 2008. 2-D physical models of thermal conduction heating for remediation of DNAPL source zones in aquitards. ConSoil 2008, Theme E: Remediation concepts and technologies, Lecture session (LeS):E.11 Modeling.
- Baker, R.S. and M. Kuhlman. "A Description of the Mechanisms of In-Situ Thermal Destruction (ISTD) Reactions." In: H. Al-Ekabi (Ed.), *Current Practices in Oxidation and Reduction Technologies for Soil and Groundwater*. Presented at the 2nd International Conf. on Oxidation and Reduction Technologies for Soil and Groundwater, ORTs-2, Toronto, Ontario, Canada, Nov. 17-21, 2002.
- Baker, R.S., Heron, G., 2004. In-situ delivery of heat by thermal conduction and steam injection for improved DNAPL remediation. Proceedings of the fourth international conference on remediation of chlorinated and recalcitrant compounds.
- Baker, R.S., LaChance, J.C., Heron, G., 2006a. Application of thermal remediation techniques for in-situ treatment of contaminated soil and water. NATO Advanced Research Workshop (ARW, Athens, Greece, June 2006.
- Baker, R.S., LaChance, J.C., Heron, G., Hiester, U., Koschitzky, H.-P., Tr ~~ötschler~~, O., F A., Kuhlman, M., 2006b. DNAPL removal from the saturated zone using thermal wells. In Remediation of Chlorinated and Recalcitrant Compounds: Proceedings of the Fifth International Conference.
- Baker, R.S., T. Burdett, S.G. Nielsen, M. Faurbye, N. Ploug, J. Holm, U. Hiester, and V. Schrenk. 2010. "Improving the Sustainability of Source Removal." Paper C-027, in K.A. Fields and G.B. Wickramanayake (Chairs), *Remediation of Chlorinated and Recalcitrant Compounds—2010*. Seventh International Conference on Remediation of Chlorinated and Recalcitrant Compounds (Monterey, CA; May 2010). Battelle Memorial Institute, Columbus, OH.
- Balkwill, D.L. 1989. Numbers, diversity, and morphological characteristics of aerobic, chemoheterotrophic bacteria in deep subsurface sediments from a site in South Carolina. *Geomicrobiology Journal* 7:33-52.

- Baston, D.P., Falta, R.W., Kueper, B.H., 2010. Numerical Modeling of Thermal Conductive Heating in Fractured Bedrock. *Ground Water*, vol. 48, no. 6, pp. 836-843.
- Burghardt, J.M., 2007. Laboratory study evaluating Thermo Remediation of Tetrachloroethylene impacted soil. M.Sc. Thesis, Department of Civil Engineering, Queen's University.
- Burghardt, J.M., Kueper, B.H., 2008. Laboratory Study Evaluating Heating of Tetrachloroethylene Impacted Soil. *Ground Water Monitoring & Remediation* 28, no. 4, pp. 95-106.
- Chen, F., Liu, X., Falta, R.W., Murdoch, L.C., 2010. Experimental Demonstration of Contaminant Removal from Fractured Rock by Boiling. *Environ. Sci. Technol.* 44, 6437-6442.
- CL:AIRE, 2010. TDP24: Application of Thermally Enhanced Soil Vapour Extraction (TESVE) to Remediate the Unsaturated Zone at the Western Storage Area (WSA), Harwell. Technology Demonstration Project Bulletin. CL:AIRE, London, U.K.
- Cole, J., W.J. McElroy, J. Glasgow, G. Heron, J. Galligan, K. Parker and E.F. Davis. 2008. In Situ Thermal Treatment of Trichloroethene at Marshall Space Flight Center. Abstract P-032, in: Bruce M. Sass (Conference Chair), *Remediation of Chlorinated and Recalcitrant Compounds—2008*. Proceedings of the Sixth International Conference on Remediation of Chlorinated and Recalcitrant Compounds (Monterey, CA; May 2008). Battelle Press, Columbus, OH.
- DeVoe, C., and K.S. Udell, 1998. Thermodynamic and Hydrodynamic behavior of water and DNAPLs during heating, In *Proceedings from the First Conference on Remediation of Chlorinated and Recalcitrant Compounds*, May 18-21, Monterey CA, Battelle Press 1 (2): 61-66.
- DoD (Department of Defense), 2000. Guidebook for Performance-Based Services Acquisition (PBSA) in the Department of Defense.  
<http://www.acq.osd.mil/dpap/Docs/pbsaguide010201.pdf>.
- EPA (Environmental Protection Agency), 1997. Cleaning up the Nation's Waste Sites: Markets and Technology Trends. EPA 542-R-96-005. April 1997.
- Friis, A.K., Albrechtsen, H.-J., Heron, G., Bjerg, P.L., 2005. Redox processes and release of organic matter after thermal treatment of a TCE-contaminated aquifer. *Environ. Sci. Technol.* 39, 5787-5795.
- Gaberell, M., A. Gavaskar, E. Drescher, J. Sminchak, L. Cumming, W.-S. Yoon, and S. De Silva. 2002. "Soil Core Characterization Strategy at DNAPL Sites Subjected to Strong Thermal or Chemical Remediation." in: A.R. Gavaskar and A.S.C. Chen (Eds.), *Remediation of Chlorinated and Recalcitrant Compounds—2002*. Proceedings of the Third International Conference on Remediation of Chlorinated and Recalcitrant

- Compounds (Monterey, CA; May 2002). ISBN 1-57477-132-9. Battelle Press, Columbus, OH.
- Geological Society of America Rock-Color Chart Committee, 1948, Rock-Color Chart, the Netherlands, Huyskes-Enschede, reprinted 1979.
- Geyer, A.R., Wilshusen, J.P., 1982. Engineering characteristics of the rocks of Pennsylvania: Environmental geology supplement to the state geologic map. Dept. of Environmental Resources, Office of Resources Management, Bureau of Topographic and Geologic Survey (Harrisburg). 2nd rev. Edition.
- Herman, G. C., 2005, Joints and veins in the Newark basin, New Jersey, in regional tectonic perspective: in Gates, A. E., editor, Newark Basin – View from the 21st Century, 22<sup>nd</sup> Annual Meeting of the Geological Association of New Jersey, College of New Jersey, Ewing, New Jersey, p. 75-116.
- Heron, G., R.S. Baker, J.M. Bierschenk, J.C. LaChance. 2006. Heat it All the Way - Mechanisms and Results Achieved using In-Situ Thermal Remediation. Paper F-13, in: Bruce M. Sass (Conference Chair), Remediation of Chlorinated and Recalcitrant Compounds—2006. Proceedings of the Fifth International Conference on Remediation of Chlorinated and Recalcitrant Compounds (Monterey, CA; May 2006). ISBN 1-57477-157-4, published by Battelle Press, Columbus, OH, [www.battelle.org/bookstore](http://www.battelle.org/bookstore).
- Heron, G., Baker, R.S., Bierschenk, J.M., LaChance, J.C., 2008. Use of Thermal Conduction Heating For the remediation of DNAPL in fractured bedrock. Remediation of Chlorinated and Recalcitrant Compounds: Proceedings of the Sixth International Conference.
- Heron, G., Carroll, S., and Nielsen, S.G.D. 2005. Full-Scale Removal of DNAPL Constituents using steam enhanced extraction and electrical resistance heating. *Ground Water Monitoring and Remediation*, 25(4): 92-107.
- Heron, G., K. Parker, J. Galligan and T.C. Holmes. 2009. “Thermal Treatment of 8 CVOC Source Areas to Near Nondetect Concentrations.” *Ground Water Monitoring and Remediation*. 29 No. 3 / Summer 2009, pp. 56-65.
- Heron, G., M. Van Zutphen, T.H. Christensen, and C.G. Enfield. 1998. Soil heating for enhanced remediation of chlorinated solvents: A laboratory study on resistive heating and vapor extraction in a silty, low-permeable soil contaminated with trichloroethylene. *Environmental Science and Technology*, 32 (10): 1474-1481.
- Heron, G., N. Ploug, S.G. Nielsen, H. Steffensen, T. Heron, H. Skou, N. Just. 2010. Remediation using ISTD and Steam – Source Removal and Plume Effects. Platform presentation at the Consoil 2010 Conference, Salzburg, Austria.

- Heron, G., R.S. Baker, J.M. Bierschenk and J. LaChance. 2008. Use of Thermal Conduction Heating for the Remediation of DNAPL in Fractured Bedrock. Paper P-003, in: Bruce M. Sass (Conference Chair), *Remediation of Chlorinated and Recalcitrant Compounds—2008*. Proceedings of the Sixth International Conference on Remediation of Chlorinated and Recalcitrant Compounds (Monterey, CA; May 2008). Battelle Press, Columbus, OH.
- Hobbie, J.E., R.J. Daley, and S. Jasper. 1977. Use of Nucleopore filters for counting bacteria by fluorescence microscopy. *Applied and Environmental Microbiology* 33:1225-1228.
- Kaiser, H. F., 1960. The application of electronic computers to factor analysis. *Educational and Psychological Measurement*, vol. 20, no. 1, pp. 141-151.
- Kueper, B.H., McWhorter, D.B., 1991. The Behaviour of Dense, Non-Aqueous Phase Liquids in Fractured Clay and rock. *Ground Water*, vol. 29, no. 5, pp. 716-728.
- Kueper, B.H., McWhorter, D.B., 1996. Physics Governing the migration of DNAPLs in Fractured Media. In Pankow, James F. and Cherry, John A., (eds.), *Dense Chlorinated Solvents and other DNAPL's in Groundwater*. Waterloo Press, ch. 11, pp. 337-353.
- LaChance, J.C., Heron, G., Baker, R.S., 2006. Verification of an improved approach for implementing in-situ thermal desorption for the remediation of chlorinated solvents. In *Remediation of Chlorinated and Recalcitrant Compounds: Proceedings of the Fifth International Conference*.
- LaChance, J.C., R.S. Baker, J.P. Galligan, and J.M. Bierschenk. 2004. "Application of 'Thermal Conductive Heating/In-Situ Thermal Desorption (ISTD)' to the Remediation of Chlorinated Volatile Organic Compounds in Saturated and Unsaturated Settings." *Proceedings of Battelle's Conference on Remediation of Chlorinated and Recalcitrant Compounds*, Monterey, CA, May 24, 2004.
- Lacombe, P.J., Burton, W.C., 2010. Hydrogeologic Framework of Fractured Sedimentary Rock, Newark Basin, New Jersey. *Ground Water monitoring & remediation* 30, no. 2, pp. 35-45, doi:10.1111/j.1745-6592.2010.01275.x.
- Lebrón, C.A., D. Major, J. Konzuk, B.H. Keuper, J. Gerhard, 2012. Contract Report CR-NAVFAC ESC-EV-1201, Development of a Protocol and a Screening Tool for the Selection of DNAPL Source Area Remediation.
- Lenczewski, M., Jardine, P., McKay, L., Layton, A., 2003. Natural attenuation of trichloroethylene in fractured shale bedrock. *Journal of Contaminant Hydrology* 64, pp. 151-168.
- Lewis-Brown, J.C., G.B. Carleton, and T.E. Imbrigiotta. 2006. Hydraulic and solute-transport properties and simulated advective transport of contaminated ground water in a fractured rock aquifer at the Naval Air Warfare Center, West Trenton, New Jersey, 2003. U.S.

- Geological Survey Scientific Investigations Report 2005-5049. Reston, Virginia: USGS, 32 p.
- Lipson, D.S., Kueper, B.H., Gefell, M.J., 2005. Matrix Diffusion-Derived Plume Attenuation in Fractured Bedrock. *Ground Water*, vol. 43, no. 1, pp. 30-39.
- Low, D.J., Galeone, D.G., 2006. Reconnaissance of Arsenic Concentrations in Ground Water From Bedrock and Unconsolidated Aquifers in Eight Northern-Tier Counties of Pennsylvania. U.S. Geological Survey (USGS), Open-File Report 2006-1376.
- Marich, A.S., 2009. Project Unit 09-023. Aggregate resources inventory of Frontenac County, Southern Ontario. Ontario Geological Survey, Open File Report 6240, pp. 20-1 to 20-9.
- McDade, J.M., McGuire, T.M., and C.J. Newell. "Analysis of DNAPL Source Depletion Costs at 36 Field Sites." *Remediation*, 2005, 15(2).
- Mundle, K., Reynolds, D.A., West, M.R., Kueper, B.H., 2007. Concentration Rebound Following In Situ Chemical Oxidation in Fractured Clay. *Ground Water*, vol. 45, no. 6 pp 692-702.
- NFESC, GeoSyntec, 2004 Assessing the Feasibility of DNAPL Source Zone Remediation: Review of Case Studies, April, 2004. NFESC Report CR-04-002-ENV.
- Nielsen, S.G., G. Heron, P. Jensen, C. Riis, T. Heron, P. Johansen, N. Ploug, J. Holm, 2010. Thermal Treatment of Thick Peat layers – DNAPL Removal and Shrinkage. E-001, in K.A. Fields and G.B. Wickramanayake (Chairs), Remediation of Chlorinated and Recalcitrant Compounds—2010. Seventh International Conference on Remediation of Chlorinated and Recalcitrant Compounds (Monterey, CA; May 2010). SBN 978-0-9819730-2-9, Battelle Memorial Institute, Columbus, OH, [www.battelle.org/chlorcon](http://www.battelle.org/chlorcon).
- NRC, 2005. Contaminants in the Subsurface: Source Zone Assessment and Remediation. The National Academies Press, Washington, D.C.
- O'Hara, S.K., Parker, B.L., Jørgensen, P.R., Cherry, J.A., 2000. Trichloroethylene DNAPL flow and mass distribution in naturally fractured clay: evidence of aperture variability. *Water Resources Research*, vol. 36, no. 1, pp. 135-147.
- Olsen, P.E., D.V. Kent, B. Cornet, W.K. Witte, and R.W. Schlische. 1996. High resolution stratigraphy of the Newark Rift basin (early Mesozoic, eastern North America). *GSA Bulletin* 108, no. 1: 40–77.
- Pankow, J.F., Cherry, J.A., 1996. Dense Chlorinated Solvents and other DNAPLs in Groundwater. Table A1, p. 508.
- Parker, B.L., Cherry, J.A., Gillham, R.W., 1996. Effects of Molecular diffusion on DNAPL behavior in Fractured Porous Media. In Pankow, James F. and Cherry, John A., (eds.),

- Dense Chlorinated Solvents and other DNAPL's in Groundwater. Waterloo Press, ch. 12, pp. 355-393.
- Parker, B.L., Gillham, R.W., Cherry, J.A., 1994. Diffusive Disappearance of Immiscible-Phase Organic Liquids in Fractured Geologic Media. *Ground Water*, vol. 32, no. 5, pp 805-820.
- Parker, B.L., McWhorter, D.B., Cherry, J.A., 1997. Diffusive loss of Non-Aqueous Phase Organic Solvents from idealized fracture Networks in Geologic Media. *Ground Water*, vol. 35, no. 6, pp. 1077-188.
- Peterson, M.S., Lion, L.W., Shoemaker, C.A., 1988. Influence of Vapor-Phase Sorption and Diffusion on the Fate of Trichloroethylene in an Unsaturated Aquifer System. *Environ. Sci. Technol.* 22, 571-578.
- Pfeilschifter, E., E. Søgaaard, G. Lemming, and M. Møller. 2007. LCA of three soil remediation technologies for PCE contamination at MW Gjøesvej, Reerslev. Unpublished report, Course 42372: Life Cycle Assessment of Products and Systems, Dec. 6, 2007, Technical University of Denmark, Lyngby, Denmark.
- Reichert, T.M., 1992. Influence of vertical fractures in horizontally-stratified rocks. M.Sc. Thesis, University of Waterloo.
- Reynolds, D.A. and Kueper, B.H., 2002. Numerical examination of the factors controlling DNAPL migration through a single fracture. *Journal of Ground Water*, Vol. 40, No. 4, pp. 368-377.
- Sanford, B.V., 1993. Stratigraphic and Structural Framework of Upper Middle Ordovician Rocks in the Head Lake-Burleigh Falls Area of South-Central Ontario. *Géographie physique et Quaternaire*, vol. 47, no. 3, pp. 253-268.
- Stegemeier, G.L., and Vinegar, H.J. 2001. "Thermal Conduction Heating for In-Situ Thermal Desorption of Soils." Ch. 4.6, pp. 1-37. In: Chang H. Oh (ed.), *Hazardous and Radioactive Waste Treatment Technologies Handbook*, CRC Press, Boca Raton, FL.
- Stegemeier, G.L., Vinegar, H.I., 2001. Thermal Conduction Heating for in-situ thermal desorption of soils. In *Hazardous and radioactive Waste Treatment Technologies Handbook*, Chang H. (ed.). CRC Press, Boca Raton, Florida. ch 4.6-1.
- Sterling, S., Murphy, S., West, A., 2010. Lansdowne WHPA and Tier 2 Water Budget Study. Intera Engineering Ltd. Document No. 09-205 Lansdowne Tier 2 WB and WHPA R0.
- SURF, 2009. Sustainable remediation White Paper – Integrating sustainable principles, practices and metrics into remediation projects, *Remediation*. Summer 2009/Vol. 19(3):5-114. The Capital Region of Denmark, Environmental Department, RemS User Guide, Remediation Strategy for Soil and Groundwater Pollution – RemS, Decision Support Tool, Version 2.0, March 2011.

- Tiedeman, C.R., Lacombe, P.J., and Goode, D.J., 2010, Multiple well-shutdown tests and site-scale flow simulation in fractured rocks: *Ground Water*, v. 48, no. 3, p. 401-415, doi:10.1111/j.1745-6584.2009.00651.x.
- U.S. Air Force, May 2010, SRT Sustainable Remediation Tool, User Guide, AFCEE 2010, downloaded 08/19/11 from NAVFAC's Green and Sustainable Remediation webpage at <http://www.ert2.org/t2gsrportal/tools.aspx>
- Udell, K.S. 1996. Heat and mass transfer in clean-up of underground toxic wastes. In *Annual Reviews of Heat Transfer*, Vol. 7, Chang-Lin Tien, Ed.; Begell House, Inc.: New York, Wallingford, UK: 333-405.
- Udell, K.S., 1996. Heat and Mass Transfer in Clean-up of Underground Toxic Wastes. *Annual reviews of heat transfer*, vol. 7, issue 7, pp. 333-405.
- USEPA, 1986. Method 9100: Saturated hydraulic conductivity, saturated leachate conductivity and intrinsic permeability. *Test Methods for Evaluating Solid Waste, Physical/Chemical Methods*. EPA/SW-846, Revision 0.
- USEPA, 1996. Method 8260B: Volatile Organic Compounds by Gas Chromatography/Mass Spectrometry (GC/MS). *Test Methods for Evaluating Solid Waste, Physical/Chemical Methods*. EPA/SW-846, Revision 2.
- USEPA, 1999. Method 9060: Total Organic Carbon (TOC) in soil. *Test Methods for Evaluating Solid Waste, Physical/Chemical Methods*. EPA/SW-846, Revision 1.
- USEPA, 2002. Method 5035A: Closed-system Purge-and-Trap and Extraction for Volatile Organics in soil and waste samples. *Test Methods for Evaluating Solid Waste, Physical/Chemical Methods*. EPA/SW-846, Revision 1.
- USEPA, 2004. *In Situ Thermal Treatment of Chlorinated Solvents: Fundamentals and Field Applications*. USEPA 542-R-04-010. Office of Solid Waste and Emergency Response. Washington, D.C. [online] <http://www.epa.gov/tio/download/remed/epa542r04010.pdf>
- Uzgiris, E.E., Edelstein, W.A., Philipp, H.R., Iben, I.E.T., 1995. Complex thermal desorption of PCBs from soil. *Chemosphere*, Vol. 30, No. 2, pp. 377-387.
- Volkwein, S. 2000. "Decision Support Using Life Cycle Assessment in Soil Remediation Planning." In U.S. Environmental Protection Agency, *NATO/CCMS Pilot Study: Evaluation of Demonstrated and Emerging Technologies for Treatment and Clean-up of Contaminated Land and Groundwater (Phase III)*: Special session - Decision Support Tools, 2000, pp. 92-99. EPA/542/R-01-002.
- West, M. and Kueper, B.H., 2010. Plume detachment and recession times in fractured rock. *Journal of Ground Water*, 48(3), pp. 416-426.

White House Office of Management and Budget. Circular A-94 Appendix C, Revised December 2010, Discount Rates for Cost-Effectiveness, Lease Purchase, and Related Analyses. [http://www.whitehouse.gov/omb/circulars\\_a094/a94\\_appx-c](http://www.whitehouse.gov/omb/circulars_a094/a94_appx-c). Retrieved August 10, 2011.

Williams, D.A., Wolf, R.R., 1984. Paleozoic Geology of the Westport Area, Southern Ontario. Ontario Geological Survey. Map P.2723. Geological Series-Preliminary Map, scale 1:50000.

Wilson, J.T., J.F. McNabb, D.L. Balkwill, and W.C. Ghiorse. 1983. Enumeration and characterization of bacteria indigenous to a shallow water-table aquifer. *Ground Water* 21:134-142.

## APPENDICES

### Appendix A: Points of Contact

POINT OF CONTACT Name	ORGANIZATION Name Address	Phone Fax E-mail	Role in Project
Carmen A. Lebrón	NAVFAC ESC 1100 23 <sup>rd</sup> Avenue Port Hueneme, CA 93043	805-982-1616 / <a href="mailto:Carmen.lebron@navy.mil">Carmen.lebron@navy.mil</a>	Project Manager
Dr. Gorm Heron	TerraTherm, Inc. 28900 Indian Point Keene, CA 93531	661-823-1620 / 978-343-2727 / gheron@terraetherm.com	Field Manager
Dr. Bernard Kueper	Queen's University Ellis Hall Kingston, ON. Canada K7L 3N6	613-533-6834 / 613 533-2128 / <a href="mailto:kueper@civil.queensu.ca">kueper@civil.queensu.ca</a>	Treatability Study Director
Jim Galligan	TerraTherm, Inc. 10 Stevens Road Fitchburg, MA 01420	978-343-0300 / 978-343-2727 / jgalligan@terraetherm.com	Health and Safety Officer
John LaChance	TerraTherm, Inc. 10 Stevens Road Fitchburg, MA 01420	978-343-0300 / 978-343-2727 / jlachance@terraetherm.com	QA Manager

## **Appendix B**

### **Screening Calculations to Evaluate the Cooling Effect of Groundwater Influx**

Baston, D.P. and Kueper, B.H., 2009. Thermal conductive heating in fractured bedrock: screening calculations to assess the effect of groundwater influx. *Advances in Water Resources*, 32, pp. 231-238.

## B1. Introduction

Many of the chemical and physical properties of organic chemicals frequently encountered at hazardous waste sites exhibit a functional dependence on temperature. Elevated temperatures often bring about a decrease in non-aqueous phase liquid (NAPL) viscosity resulting in an increase in NAPL mobility, a decrease in the organic carbon partition coefficient resulting in decreased sorption, an increase in vapor pressure resulting in increased NAPL-air mass transfer (vaporization), and an increase in the Henry's constant leading to increased water-air mass transfer (volatilization) [e.g. 1; 2; 3]. At high temperatures ( $> 100\text{ }^{\circ}\text{C}$ ), heat may also stimulate processes such as aqueous oxidation and pyrolysis that destroy contaminants in-situ and reduce the need for above-ground treatment [4]. Although these in-situ destruction mechanisms are typically significant only at the high temperatures used to treat non-volatile compounds such as polychlorinated biphenyls (PCBs), they may alone provide 95-99% of the removal in these cases [4].

Heat can be delivered to the subsurface using several different approaches. Steam-enhanced extraction (SEE), originally developed by the petroleum industry, has been applied at both pilot and full scales in unconsolidated deposits [e.g. 5]. However, field pilot testing of steam injection in fractured rock has demonstrated the difficulty of achieving large temperature increases throughout a treatment area [6]. Electrical resistive heating (ERH) achieves heating by passing an electrical current between electrodes inserted in-situ throughout the treatment area [e.g. 7]. The amount of resistive heat produced is relatively uniform throughout the treatment area, providing heat to low-permeability areas that may be by-passed by injected steam. Because ERH relies on pore water to conduct electrical current, it only generates temperatures below and at the boiling point of water. Thermal conductive heating (TCH) systems employ arrays of wells containing resistive heating elements to provide heat to the treatment area [e.g. 8]. The resistive heating elements radiate heat to the well casing, from where it is transferred away by conduction. One principal difference between TCH and both SEE and ERH is the ability to heat to temperatures of up to approximately  $800\text{ }^{\circ}\text{C}$ , which allows the technology to target higher boiling point compounds such as PCBs.

Several mechanisms may cause a loss of heat from the treatment area during thermal applications. Strong vertical temperature gradients may cause heat to be lost through conduction; in the case of TCH, wells are typically extended a minimum of two feet (0.6 m) beyond the limit of the treatment zone to mitigate this effect [8]. In addition, insulating blankets may be placed on the ground surface above the treatment area. The influx of cool groundwater may present another source of heat loss. When the temperature of the treatment area is below  $100\text{ }^{\circ}\text{C}$ , groundwater flow may cause heated water to be carried out of the treatment area, representing a loss of energy. At higher temperatures, cool incoming water must be boiled, causing a delay in the attainment of target temperatures. In the presence of a large groundwater influx, the cooling influence may be reduced by steam injection or the installation of an impermeable barrier at the periphery of the treatment zone [9]. Alternatively, an extra row of heater wells could be used to preheat incoming groundwater before it enters the treatment area.

Although the cooling effect of incoming groundwater may be a critical parameter in the design of TCH systems, few published studies have quantitatively examined its importance in porous

media, and none has done so in fractured rock. Elliott et al. [10] used a commercial reservoir simulator to study the cooling influence of groundwater in saturated porous media. They found that the remediation time was largely governed by soil permeability and hydraulic gradient; when these parameters were increased above certain threshold values, treatment temperatures were not reached. A second modeling study [11] examined the effectiveness of several impermeable barrier designs in managing groundwater influx.

The objective of this study is to present a screening-level model that can be used to assess the effect of inflowing groundwater on the ability to heat a treatment zone in fractured rock using TCH. The newly developed semi-analytical solution does not model phase change effects and is therefore best utilized to assess the ability to heat bedrock to the boiling point of water. A base case was established from which six properties were varied to assess their relative importance to treatment time: hydraulic gradient, fracture aperture, fracture spacing, rock density, rock thermal conductivity, and rock heat capacity. Hydrogeological parameters were varied independently; rock properties were varied as a group using measured values from the literature. The potential for the mitigation of groundwater influx cooling by both installation of an upgradient preheating well and increases in thermal well power was also assessed.

## **B2. Model Development**

The fractured rock environment is conceptually modeled using a discrete fracture approach whereby the location and aperture of fractures are specified directly. Fractures, which have an aperture of  $e$ , are assumed to be parallel and evenly spaced by a distance of  $2H$ . A schematic of the conceptual model is shown in Figure B1. The screening model simulates heat transfer within a two-dimensional vertical cross section ( $x - y$  plane) oriented perpendicular to the fractures and in line with the direction of groundwater flow ( $x$ ) which occurs at a specified velocity ( $v$ ) in the fractures only. Thermal wells (line sources of heat) are placed within the cross section at a specified spacing. Although actual wells would intersect the fracture, heating of the water within the fracture itself is not accounted for in the mathematical solution. This is considered acceptable because the actual amount of energy added to the system by inclusion of a heating term in the fracture equation would be insignificant. The screening model does not simulate heat losses from the top or bottom of the overall target zone, implying that lines of symmetry exist at a distance  $H$  above and below each fracture, as well as in the centerline of each fracture. Consequently, the vertical extent of the model domain includes one half of a fracture and one half of a matrix block.

As a result of the two-dimensional treatment of a three-dimensional problem, predicted temperatures at a coordinate  $(x, y)$  can be considered an average of the temperatures at that point along the  $z$  dimension. In other words, temperatures close to a thermal well will be higher than predicted by the model, while temperatures in between two thermal wells will be colder than predicted by the model. If it is desired to predict the temperature at the coldest point in a treatment area (i.e. at a point halfway between two thermal wells), it is important to note that the model will overpredict the temperature at these locations. Consequently, if the model predicts that boiling temperatures cannot be reached, then it can be concluded that the treatment system design must be modified in order to reach boiling temperatures.

Two-dimensional heat transfer within the model plane may be described by two coupled differential equations. In the rock matrix, the heat conduction equation is written as [e.g., 12]:

$$\frac{\partial^2 T}{\partial x^2} + \frac{\partial^2 T}{\partial y^2} + \frac{g(x, y)}{K_r} = \frac{1}{\alpha_r} \frac{\partial T}{\partial t} \quad (1)$$

where  $K_r$  is the thermal conductivity of the rock [W/m·K],  $\alpha_r$  is the thermal diffusivity of the rock [m<sup>2</sup>/s] and  $g$  is the strength of energy generation [W/m<sup>3</sup>] at the point  $(x, y)$ . Performing a heat balance on a control volume of water in a fracture in the  $x$ -direction gives the following equation for the temperature in the fracture [13]:

$$\rho_w c_w \frac{\partial T}{\partial t} = -v \rho_w c_w \frac{\partial T}{\partial x} + \frac{2K_r}{e} \frac{\partial T}{\partial y} \Big|_{y=e/2} \quad (2)$$

where  $\rho_w$  is the density of water [kg/m<sup>3</sup>],  $c_w$  is the specific heat of water [J/kg·K],  $v$  is the average linear velocity of groundwater in the fracture [m/s], and  $e$  is the aperture of the fracture [m]. Heat exchange between the fracture and the matrix is handled through the  $g(x, y)$  term as follows [14]:

$$g(x, y) = \frac{K_r}{e/2} \frac{\partial T}{\partial y} \Big|_{y=e/2} \quad (3)$$

It has been shown under a range of conditions that the heat storage term may be omitted from (2) without significant error [13; 14]. This allows the governing equation for the fracture to be simplified to:

$$\frac{\partial T}{\partial x} = \frac{2K_r}{\rho_w c_w v e} \frac{\partial T}{\partial y} \Big|_{y=e/2} \quad (4)$$

and the system is reduced to a more tractable system of ordinary differential equations. Using this assumption, Lauwerier [15] developed a solution applicable to heat transfer between a body of rock and a single fracture; Yang et al. [16] published a similar solution that includes the effect of longitudinal conduction in the fracture. Gringarten [17] developed a Laplace-space solution for heat transfer between a body of rock and a set of parallel fractures. Lowell [18] simplified that solution by showing that, for the modeling of hot dry rock geothermal systems where fracture spacing is typically very large, little error is introduced by considering only a single fracture.

When the rock is heated directly, as is the case in TCH, a solution must consider multidimensional conduction and heat generation within the matrix. To the authors' knowledge, the solution of Cheng et al. [14] is the only semi-analytical solution to consider multidimensional heat conduction in the matrix. However, there does not appear to be a published solution to the case where heat is generated within the rock matrix.

Several features distinguish the present solution from previous analytical models. First is the explicit modeling of multiple parallel fractures with two-dimensional heat conduction in the rock matrix. Although previous analytical solutions have modeled parallel fractures or multidimensional heat conduction, no solution has included both. Second, the present solution provides for heat generation within the matrix, allowing the inclusion of an unlimited number of heater wells, located at arbitrary coordinates. Third, the solution is given in terms of elementary functions rather than special functions such as Bessel functions. This reduces computation time and provides improved accuracy when evaluating the temperature at points inside the rock matrix. The solution is not capable of modeling boiling within the fracture, or thermally-induced changes in rock properties.

A schematic of the two-dimensional model domain is presented in Figure B2. The domain comprises a two-dimensional strip of rock of infinite dimension in  $x$  and of finite width ( $H$ ) in  $y$ . At  $y = 0$ , water flows through a fracture of aperture  $e$  at an average linear velocity determined from a specified hydraulic gradient using the cubic law [e.g., 19]. The rock matrix is assumed to be impervious to the flow of groundwater.

Type I zero-temperature boundary conditions are assigned at  $x = \pm\infty$ , and homogeneous Type II (no-flux) boundaries are assigned at  $y = 0$  and  $y = H$  to represent lines of symmetry. Prior to heating, the temperature is equal to zero throughout the domain. It is important to note that the temperature rise will be computed; therefore, the computed temperature rise can be added to any desired uniform initial temperature. At  $t = 0$ , heater wells located at  $x = W_i$  begin generating heat at a constant rate of  $g$  watts per meter in the  $y$  direction. Although the rate of heat generation is assumed here to be constant, it will be seen that any function  $g(t)$  may be used, provided that its Laplace transform is known.

The solution to (1) is given in terms of Green's functions as [20]:

$$T(x, y, t) = \frac{\alpha_r}{K_r} \int_{\tau=0}^t \int_{y'=0}^H \int_{x'=-\infty}^{\infty} G(x-x', y-y', t-\tau) g(x', y', \tau) dx' dy' d\tau \quad (5)$$

where  $G(x-x', y-y', t-\tau)$  is a Green's function corresponding to the domain and boundary conditions described above and shown in Figure B2, and  $g(x', y', \tau)$  is the strength of an instantaneous point source. A more complete discussion of the Green's function used in this solution is found in the appendix. The Laplace transform of (5) can be taken using the convolution property, giving:

$$\bar{T}(x, y, s) = \frac{\alpha_r}{K_r} \int_{y'=0}^H \int_{x'=-\infty}^{\infty} \bar{G}(x-x', y-y', s) \bar{g}(x', y', s) dx' dy' \quad (6)$$

where  $s$  is the Laplace variable, and the overbar denotes a transformed quantity. Two vehicles of heat transfer to/from the rock matrix are present in this problem: heat generated by the thermal wells and heat exchange with groundwater in the fracture. The source function  $\bar{g}(x', y', s)$  can therefore be expanded as:

$$\bar{g}(x', y', s) = \bar{q}(x', s)\delta(y') + \frac{g_w}{s}\delta(W - x) \quad (7)$$

where  $\bar{q}(x', s)$  is an as yet unknown function of  $x'$  representing heat exchange between the rock matrix and groundwater in the fracture, and  $g_w$  is the constant strength of the thermal wells, expressed in W/m. Because the two heat source terms are linear and orthogonal, the two integrals of (7) may be separated, giving:

$$\bar{T}(x, y, s) = \frac{\alpha_r}{K_r} \int_{x'=-\infty}^{\infty} \bar{q}(x', s) \bar{G}(x - x', y - 0, s) dx' + \frac{g_w \alpha_r}{K_r s} \int_{y'=0}^H \bar{G}(W - x, y - y', s) dy' \quad (8)$$

By substituting the fracture heat balance (3) into the first integral of (8), integrating by parts, and evaluating at  $y = 0$ , the problem is converted into a Fredholm integral equation of the second kind:

$$\begin{aligned} \bar{T}(x, 0, s) = & \frac{ve\rho_w c_w}{2} \frac{\alpha_r}{K_r} \left\{ \int_{x'=-\infty}^{\infty} \bar{T}(x', 0, s) \frac{\partial \bar{G}}{\partial x'}(x - x', 0, s) dx' + \bar{T}(-\infty, 0, s) \bar{G}(x, 0, s) + \bar{T}(\infty, 0, s) \bar{G}(x, 0, s) \right\} \\ & + \frac{g_w \alpha_r}{K_r s} \int_{y'=0}^H \bar{G}(W - x, y', s) dy' \end{aligned} \quad (9)$$

The derivative of the Green's function,  $\partial \bar{G} / \partial x'$ , is singular as  $(x' - x) \rightarrow 0$ . In order to provide accurate results, (9) must be regularized. A subtraction method is used [e.g., 21]. The regularized form of (9) is given by:

$$\begin{aligned} \bar{T}(x, 0, s) = & \frac{ve\rho_w c_w}{2} \frac{\alpha_r}{K_r} \\ & \left\{ \int_{x'=-\infty}^{\infty} [\bar{T}(x', 0, s) - \bar{T}(x, 0, s)] \frac{\partial \bar{G}}{\partial x'}(x - x', 0, s) dx' \right. \\ & + \bar{T}(x, 0, s) \bar{G}(\infty, 0, s) - \bar{T}(x, 0, s) \bar{G}(-\infty, 0, s) \\ & \left. - \bar{T}(-\infty, 0, s) \bar{G}(-\infty, 0, s) + \bar{T}(\infty, 0, s) \bar{G}(\infty, 0, s) \right\} \\ & + \frac{g_w \alpha_r}{K_r s} \int_{y'=0}^H \bar{G}(W - x, y', s) dy' \end{aligned} \quad (10)$$

A wide array of techniques may be used to solve (10) numerically [e.g., 21]. Like Cheng et al. [14], our approach is to use a quadrature method to approximate the first integral. The result is an  $n \times n$  system of linear inhomogeneous equations. The  $i$ th equation is given by:

$$\begin{aligned} T_i = & \frac{ve\rho_w c_w}{2} \frac{\alpha_r}{K_r} \left\{ \sum_{j=1}^n w_j [T_j - T_i] \frac{\partial \bar{G}}{\partial x'}(x_i - x_j, 0, s) \right. \\ & \left. + T_1 \bar{G}(x_i, 0, s) - T_n \bar{G}(x_n - x_i, 0, s) + T_i \bar{G}(x_n - x_i, 0, s) \right\} \end{aligned}$$

$$+T_i(x_i,0,s)\} + \frac{g_w \alpha_r}{K_r s} \int_{y'=0}^H \bar{G}(W-x, y', s) dy' \quad (11)$$

$$i = 1 \dots n$$

where  $T_i$  is the Laplace-space temperature at  $x_i$ , and  $W_j$  are the values of the nodal weights. The values of  $x$  and  $w$  are dependent on the choice of quadrature; the formula is sufficiently general to allow the choice of any  $x, w$  pair. A quadrature method designed for infinite integration limits, such as Gauss-Hermite quadrature, may be used, but this requires that the temperature be scaled by a weighting function. An alternative is to evaluate only a finite portion of the integral, from  $x'=0$  to  $L$ . This approach is valid provided that  $T$  is equal to zero everywhere outside the evaluated portion. This condition will be satisfied if  $L$  is chosen to be sufficiently large, and the condition may be easily checked by examining the computed values of the temperature at the endpoints. Once the temperature on the boundary is known, the temperature at any point in the domain may be determined by:

$$\begin{aligned} \bar{T}(x, y, s) = & \frac{ve\rho_w c_w}{2} \frac{\alpha_r}{K_r} \left\{ \sum_{j=1}^n w_j [T_j - \bar{T}(x, 0, s)] \right. \\ & \frac{\partial \bar{G}}{\partial x'}(x-x_j, 0, s) + T_1(x, y, s) + T_n \bar{G}(L, y, s) \\ & \left. + \bar{T}(x, 0, s) \bar{G}(L-x, 0, s) + \bar{T}(x, 0, s) \bar{G}(x, 0, s) \right\} \\ & + \frac{g_w \alpha_r}{K_r s} \int_{y'=0}^H \bar{G}(W-x, y-y', s) dy' \quad (12) \\ & i = 1 \dots n \end{aligned}$$

A number of numerical Laplace inversion routines may be used to determine time-domain temperatures from the values calculated in (11) and (12). The authors have had success using the algorithms proposed by Weeks [22] and De Hoog et al. [23]. The special case of zero fracture aperture was verified against an analytical solution [24]. In addition, the numerical simulator TOUGH2 [25] was used to model the base case scenario (Table B1). The maximum difference in computed fracture temperatures between the semi-analytical solution and the numerical solution was 6%.

### B3. Outline of Simulations

The base case scenario (Table B1) consists of shale with 500  $\mu\text{m}$  horizontal fractures spaced at 1 m. Groundwater flows through the fractures subject to a hydraulic gradient ( $\nabla h$ ) of -0.005, resulting in an average linear velocity of 67 m/day (computed using  $\mu=1.31 \times 10^{-3}$  Pa·s). Heater wells, located at  $x = 30$  m and  $x = 33$  m, each provide a constant heat output ( $g_w$ ) of 100 W/m in the  $y$  direction. This output is equivalent to the spatially averaged heat flux generated by a row of heater wells perpendicular to the model plane, spaced at 3 m, each providing 300 W/m - well within the range attainable by the heater elements in current use [8]. Use of an analytical solution [24] shows that, in the absence of cooling from fractures, a target temperature of 100 °C would be reached throughout the interwell zone after 17 weeks of heating.

Parameter sensitivity was assessed through four sets of trials (Table B2). Three sets involved the variation of a hydrogeological parameter: hydraulic gradient, fracture aperture, or fracture spacing. In the fourth set, the host rock type was changed. Values for the thermal conductivity, density, and specific heat capacity of each rock type used (Table 3) were taken from the literature [26]. Although the thermal conductivity of sedimentary rocks tends to decline with temperature [e.g., 27], all rock properties were assumed to remain constant with temperature in order to preserve the linearity of the governing equations (1) and (4).

## B4. Results and Discussion

In order to facilitate direct comparison of the various trials, the temperature distribution in the system is summarized by two values: the minimum ( $T_{min}$ ) and maximum ( $T_{max}$ ) temperatures in the fracture between the two thermal wells after one year of heating. This time was chosen as a point for comparison because transient results (discussed later) show that the effect of changes in some parameters may not be apparent during the earlier part of the heating period.

Although groundwater influx generally skews the distribution of temperature contours near thermal wells, the contours remain primarily normal to the fracture plane (but with noticeable curvature at the fracture wall). Figure B3(a), for example, illustrates the two-dimensional distribution of temperatures after one year of heating in the vicinity of a single heater well for the case of  $e=1$  mm,  $2H=1$  m, and  $v=20$  m/day. Figure B3(b) illustrates the temperature distribution in the absence of groundwater flow. Because the temperature difference between the fracture and the center of the matrix is typically less than one degree,  $T_{min}$  and  $T_{max}$  provide good indicators of the overall temperature distribution in the treatment zone.

### B4.1 Sensitivity to Hydrogeological Parameters

Minimum and maximum interwell fracture temperatures ( $T_{min}$  and  $T_{max}$ ) after one year of heating are plotted in Figure B4(a) for the variation of hydraulic gradient between  $-10^{-4}$  and  $5 \times 10^{-2}$ . The semi-analytical solution is not capable modeling the boiling of water, so temperatures above 120 °C are not shown. Computed temperatures for the fracture aperture trials and fracture spacing trials are found in Figures B4(b) and B4(c), respectively. It can be observed that a high hydraulic gradient, or the presence of large-aperture or closely-spaced fractures can significantly inhibit heating in the treatment zone.

A variation in any of the hydrogeological parameters will have an impact on the bulk groundwater influx ( $q$ ). Since the matrix is considered to be impermeable,  $q$  can be calculated as:

$$q = \frac{\rho g e^3 (\nabla h)}{24 H \mu} \quad (13)$$

where  $\mu$  is the dynamic viscosity of water. For each of the hydrogeological parameter variation trials plotted in Figures B4(a-c), the bulk groundwater influx was calculated. Figure B4(d) presents  $T_{min}$  and  $T_{max}$  plotted against the calculated bulk groundwater influx values.

It is apparent from the temperatures plotted in Figure B4(d) that there is some degree of correlation between bulk influx and treatment zone temperatures. To test the robustness of this correlation, a series of tests was performed in which several combinations and/or values of hydrogeological parameters were employed to arrive at a single value of bulk groundwater influx. The semi-analytical solution was applied by assigning each combination of influx and spacing presented in Table B4 and adjusting the aperture accordingly, with a gradient fixed at -0.005. Results for the cases of  $q = 33.7 \text{ L/m}^2\cdot\text{day}$  and  $q=3.23 \text{ L/m}^2\cdot\text{day}$  are summarized in Figure B5, where transient temperature profiles are shown for the point in the fracture at the center ( $x=31.5 \text{ m}$ ) of the treatment zone (not necessarily the location of  $T_{min}$  or  $T_{max}$ ).

For the case of  $q = 33.7 \text{ L/m}^2\cdot\text{day}$ , the temperature profiles are in good agreement for fracture spacings of 2.5 m or less, but temperatures drop off when fracture spacing is increased beyond this threshold. Similarly, for the case of  $q = 323 \text{ L/m}^2\cdot\text{day}$  (not shown), deviation was observed for fracture spacings of 5 m and greater. When the bulk influx is decreased to  $3.23 \text{ L/m}^2\cdot\text{day}$  (Figure B5(b)), fracture spacing does not appear to play a large role in determining the temperature distribution. Results are not shown for the cases of lower influx, where there is no significant difference between the temperature profiles at any time during heating. Therefore, while the correlation between influx and  $T_{min}$  and  $T_{max}$  appears to be good in Figure B4(d), the temperature profiles in Figure B5(a) show that the correlation becomes weaker when more extreme combinations of parameters are used.

For a screening-level estimate of the extent of fracture cooling at sub-boiling temperatures for conditions of low to moderate influx, it may be necessary only to know the influx through the treatment area and not have knowledge of the particular combination of spacing and aperture. This forms a distinction between the problem of heat extraction from hot dry rock and subsurface heating using thermal wells. For example, Gringarten et al. [17] found that the number and size of fractures had a strong effect on heat extraction from a hot dry rock reservoir, even when the total flow rate was kept constant. This difference in behavior may be due to the different time scales of the two problems; it is after a reservoir has been in operation for several years that the predicted outlet temperature becomes dependent on the nature of the fractures carrying the flow.

## **B4.2 Sensitivity to Host Rock Type**

Using the four sets of rock properties (Table B3) and the base case properties (Table B1), the temperature in the fracture between the two thermal wells was computed. Figure B6 illustrates the fracture temperature profiles for each rock type after one month and one year of heating. Compared to the hydrogeological parameters, host rock material properties play a relatively minor role in determining temperature distributions throughout the treatment zone. This behavior is not surprising, as the range of material properties is far smaller than the range of hydrogeological parameters. Heating in rocks with low thermal diffusivity will progress more slowly than in rocks with high thermal diffusivity; yet, this variation does little to affect the shape of the steady-state temperature profile.

## **B4.3 Transient Behavior**

As an example of transient behavior during heating, the temperature in the fracture at the midpoint between the two heater wells is plotted in Figure B7 for eight different values of hydraulic gradient, using the base-case parameters of 500  $\mu\text{m}$  fractures spaced by 1 m. The transient temperature plot shows a correlation between the ground water influx (in this case determined by a varying hydraulic gradient) and the time needed to reach a steady-state temperature profile. Similar results are seen when the influx is varied by a change in aperture or fracture spacing.

For a given value of groundwater influx, a temperature threshold exists below which the fractures have little effect. When groundwater influx is very small (due to low-aperture or widely spaced fractures, shallow gradient, etc.) the cooling effect is negligible until temperatures approach 100 °C or higher. For a mid-level groundwater influx, such as the base case in this study, the cooling effect is negligible until a temperature of about 50 °C, where heating begins to lag before reaching a steady state. When the ground water influx is very high, the threshold temperature is so low that a steady state is reached almost immediately, before any significant heating occurs.

The semi-analytical solution was employed to model two methods of overcoming the groundwater influx cooling effect: the installation of a pre-heating well, and an increase in the thermal well heat production. Using the base case parameters (Table B1), the time to reach a target temperature of 100 °C was calculated for thermal well heat production rates between 70 W/m and 1000 W/m. The amount of energy required to achieve this target was calculated by the product of the heat generation rate [ $\text{W}/\text{m}^2$ ] and the time [days] to reach the target. Computed values for the time to reach the target and energy consumption are shown in Figure B8.

With these parameters, the target is not reached within three years at heat production rates below 140 W/m. However, the time required to reach the target decreases sharply above 140 W/m, reaching a minimum at approximately two weeks for heat fluxes above 900 W/m. Because the total power consumption is correlated to the heating time, it appears to be generally advantageous to generate heat at a high rate, although for the parameters used in this study, efficiency peaks at approximately 300 W/m.

Mitigation using a preheating well was also modeled (results not shown). Using the base case parameters, a third thermal well was placed 3 m upgradient of the first well ( $x = 27$  m), and the temperature in the original interwell zone was monitored through time. Although the preheating well caused a rise in the interwell temperatures, it was not sufficient to reach the target temperature throughout this entire zone.

## **B5. Conclusions**

Groundwater influx may prevent or delay the heating of fractured rock during application of thermal conductive heating (TCH). When bulk groundwater influx is high, temperatures in the fractures are influenced by the aperture and spacing of fractures. For medium and low values of influx, fracture properties do not appear to be important in determining the temperature in fractures. In these cases, it appears not to be important to characterize discrete fracture features

in the treatment zone; only a quantification of the total groundwater influx through the treatment zone is necessary.

Variations in material properties (rock density, rock thermal conductivity, and rock heat capacity) amongst rock types do have a small effect on the early-time temperature distribution in the rock, but on the whole are less significant than variations in hydrogeological parameters (hydraulic gradient, fracture aperture, and fracture spacing). It is noted that the range of variation in material properties is much smaller than the range of hydrogeological properties, which may vary by several orders of magnitude.

Transient analysis shows that influx cooling affects treatment zone temperatures only once a certain temperature threshold has been passed during heating. It is possible that, if target treatment temperatures are low, influx cooling may not pose a problem.

One solution to the problem of groundwater influx cooling is to simply increase the power delivered to the thermal wells. In the case where this may not be done due to equipment limitations or other concerns, preheating wells installed outside of the treatment zone may be used to partially mitigate the cooling effects.

## References

- [1] U.S. EPA, *Correcting the Henry's Law constant for soil temperature*, Technical report (June 2001).
- [2] B. E. Sleep, P. D. McClure, *The effect of temperature on adsorption of organic compounds to soils*, Canadian Geotechnical Journal 38 (2001) 46--52.
- [3] National Research Council, *Contaminants in the Subsurface: Source Zone Assessment and Remediation*, National Academy Press, Washington, 2004.
- [4] R. Baker, M. Kuhlman, *A description of the mechanics of in-situ thermal destruction (ISTD) reactions*, in: H. El-Akabi (Ed.), Proceedings of the 2nd International Conference on Oxidation and Reduction Technologies for Soil and Groundwater, ORTs-2, 2002.
- [5] R. Newmark, R. Aines, K. Knauss, R. Leif, M. Chiarappa, B. Hudson, C. Carrigan, A. Thompson, J. Richards, C. Eaker, R. Wiedner, T. Sciarotta, *In-situ destruction of contaminants via hydrous pyrolysis / oxidation: Visalia field test*, Report UCRL-ID-132671, Lawrence Livermore National Laboratory (1998).
- [6] E. Davis, N. Akladiss, R. Hoey, B. Brandon, M. Nalipinski, S. Carroll, G. Herom, K. Novakowski, K. Udell, *Steam enhanced remediation research for DNAPL in fractured rock*, Report EPA/540/R-05/010, Environmental Protection Agency (August 2005).
- [7] G. Beyke, D. Fleming, *In situ thermal remediation of DNAPL and LNAPL using electrical resistive heating*, Remediation Journal 15 (3) (2005) 5--22.
- [8] G. Stegemeier, H. Vinegar, *Thermal conduction heating for in-situ thermal desorption of soils*, in: C. H. Oh (Ed.), Hazardous & Radioactive Waste Treatment Technologies Handbook, CRC Press, Boca Raton, Florida, 2001, Ch. 4.6-1.
- [9] R. Baker, G. Heron, *In-situ delivery of heat by thermal conduction and steam injection for improved DNAPL remediation*, in: A. Gavaskar, A. Chen (Eds.), Proceedings of the Fourth International Conference on Remediation of Chlorinated and Recalcitrant Compounds, Battelle Press, Monterey, CA, 2004.
- [10] L. J. Elliott, G. A. Pope, R. T. Johns, *In-situ thermal remediation of contaminant below the water table*, No. SPE 81204, 2003.
- [11] L. J. Elliott, G. A. Pope, R. T. Johns, *Multidimensional numerical reservoir simulation of thermal remediation of contaminants below the water table*, in: A. Gavaskar, A. Chen (Eds.), Proceedings of the Fourth International Conference on Remediation of Chlorinated and Recalcitrant Compounds, Battelle Press, Monterey, CA, 2004.
- [12] M. N. Özişik, *Heat Conduction*, Wiley, New York, 1980.
- [13] D. P. Baston, *Analytical and numerical modeling of thermal conductive heating in fractured rock*, Master's thesis, Queen's University (April 2008).
- [14] A.-D. Cheng, A. Ghassemi, E. Detournay, *Integral equation solution of heat extraction from a fracture in hot dry rock*, International Journal for Numerical and Analytical Methods in Geomechanics 25 (2001) 1327--1338.
- [15] H. Lauwerier, *The transport of heat in an oil layer caused by the injection of hot fluid*, Applied Scientific Research A 5 (2--3) (1955) 145--150.
- [16] J. Yang, K. Latychev, R. Edwards, *Numerical computation of hydrothermal fluid circulation in fractured Earth structures*, Geophysics Journal International 135 (1998) 627--649.
- [17] A. Gringarten, P. Witherspoon, Y. Ohnishi, *Theory of heat extraction from fractured hot dry rock*, Journal of Geophysical Research 80 (8) (1975) 1120--1124.

- [18] R. Lowell, *Comments on 'Theory of heat extraction from fractured hot dry rock'* by A.C. Gringarten, P.A. Witherspoon, and Yuzo Ohnishi, *Journal of Geophysical Research* 81 (2) (1976) 359.
- [19] P. Witherspoon, J. Wang, K. Iwai, J. Gale, *Validity of cubic law for fluid flow in a deformable rock fracture*, *Water Resources Research* 16 (6) (1980) 1016--1024.
- [20] J. Beck, K. Cole, A. Haji-Sheikh, B. Litkouhi, *Heat Conduction Using Green's Functions*, Hemisphere, 1992.
- [21] L. Delves, J. Mohamed, *Computational methods for integral equations*, Cambridge University Press, 1985.
- [22] W. Weeks, *Numerical inversion of Laplace transforms using Laguerre functions*, *Journal of the Association for Computing Machinery* 13 (3) (1966) 419--426.
- [23] F. De Hoog, J. Knight, A. Stokes, *An improved method for the numerical inversion of Laplace transforms*, *SIAM Journal on Scientific and Statistical Computing* 3 (3) (1982) 357--366.
- [24] H. Carslaw, J. Jaeger, *Conduction of Heat in Solids*, 2nd Edition, Oxford University Press, New York, 1959.
- [25] K. Pruess, C. Oldenburg, G. Moridis, *TOUGH2 User's Guide, Version 2.0*, Report LBNL-43134, Lawrence Berkeley National Laboratory (November 1999).
- [26] V. Čermák, L. Rybach, *Thermal conductivity and specific heat of minerals and rocks*, in: G. Angenheister (Ed.), *Landolt-Börnstein: Numerical Data and Functional Relationships in Science and Tehcnology, Group V (Geophysics and Space Research), Volume 1a (Physical Properties of Rocks)*, Springer, Berlin-Heidelberg, 1982, pp. 305--343.
- [27] C. Clauser, E. Huenges, *Thermal conductivity of rocks and minerals*, in: *Rock Physics and Phase Relations -- A Handbook of Physical Constants*, American Geophysical Union, 1995, pp. 105--126.

## Tables

**Table B1: Base case parameters for sensitivity analysis**

Parameter	Unit	Value
Rock Type	-	Shale
Heater Well Locations	m	$x = 30, 33$
Heater Well Power ( $g_w$ )	W/m	100
Initial Temperature	°C	10
Fracture Aperture ( $e$ )	μm	500
Fracture Spacing ( $2H$ )	m	1
Hydraulic Gradient ( $\nabla h$ )	-	-0.005
Influent Temperature	°C	10

**Table B2: Summary of sensitivity testing trials**

Parameter	Range of Values	Bulk Influx Range (L/m <sup>2</sup> ·day)
$\nabla h$	0.0001 - 0.05	0.674 - 337
$e$	10 - 2000 μm	$2.69 \times 10^{-4}$ - 2160
$2H$	0.25 - 4 m	8.42 - 135
Rock Type	shale, limestone, dolomite, sandstone	

**Table B3: Rock material properties [26]**

Rock Type	$K_r$ (W/m·K)	$\rho$ (kg/m <sup>3</sup> )	$c$ (J/kg·K)
Shale	2.98	2757	1180
Sandstone	3.03	2391	960
Limestone	2.40	2520	890
Dolomite	2.87	2536	920

**Table B4: Parameters for runs used to assess correlation between bulk influx and treatment zone temperature**

Parameter	Unit	Values
Bulk Influx	(L/m <sup>2</sup> ·day)	33.7, 3.23, 0.323, 0.0323
Fracture spacing	m	0.25, 0.5, 1.0, 2.5, 5.0, 10.0

## Figures

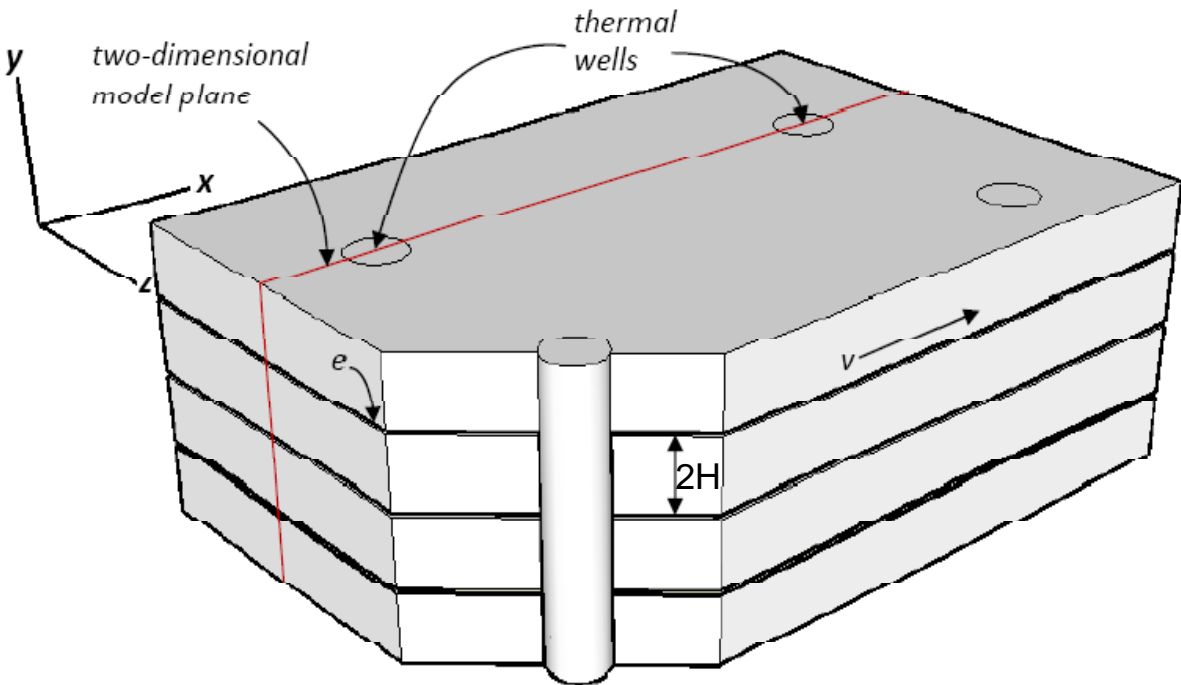


**Figure B9.1:** Conceptual model of fractured rock environment. Groundwater flows at velocity  $v$  within equally spaced ( $2H$ ) fractures of aperture  $e$ . The model plane ( $x$ - $y$ ) is oriented perpendicular to the fractures and in line with  $v$ .

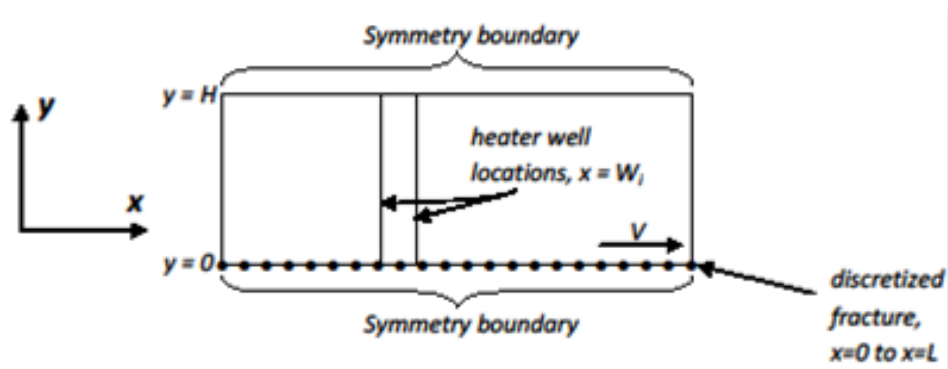


**Figure B9.2:** Schematic of model domain. Fractures are spaced at distance  $2H$ , groundwater flows through the fracture at velocity  $v$ , and heater wells are located at  $x=W_i$ .

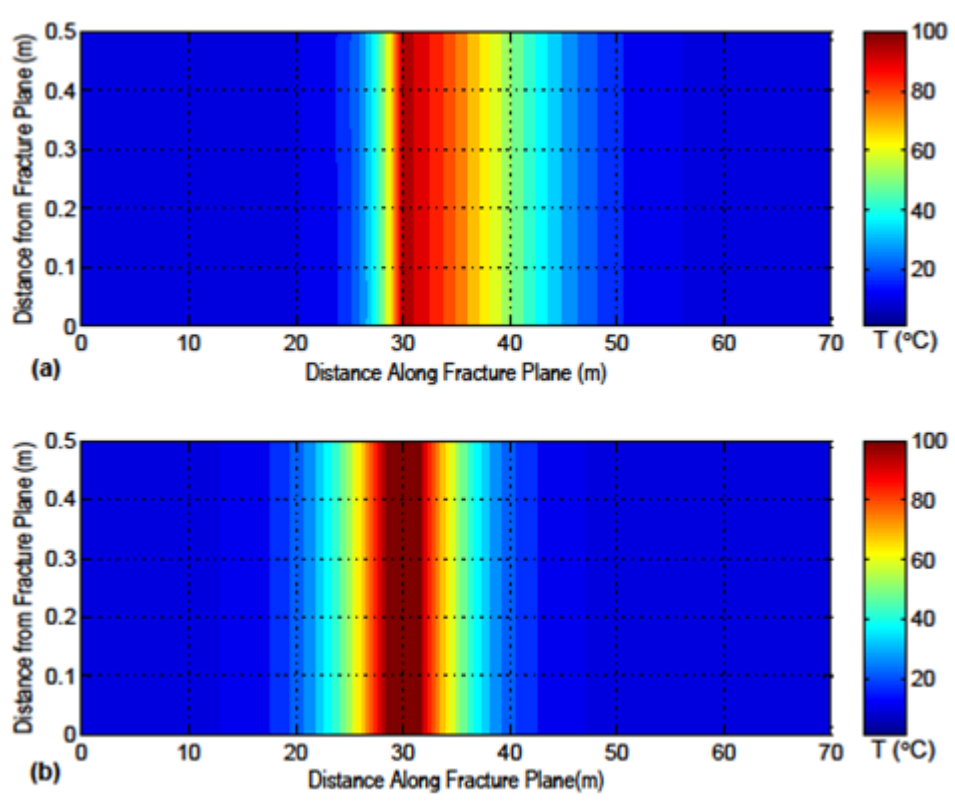


**Figure B9.3: Temperature distribution resulting from heating by a single thermal well, showing the general effect of groundwater influx. (a)  $v = 20$  m/day,  $2H = 1$  m,  $e = 1$  mm,  $g_w = 100$  W/m; (b) no flow,  $g_w = 100$  W/m. Note vertical exaggeration of 55.**

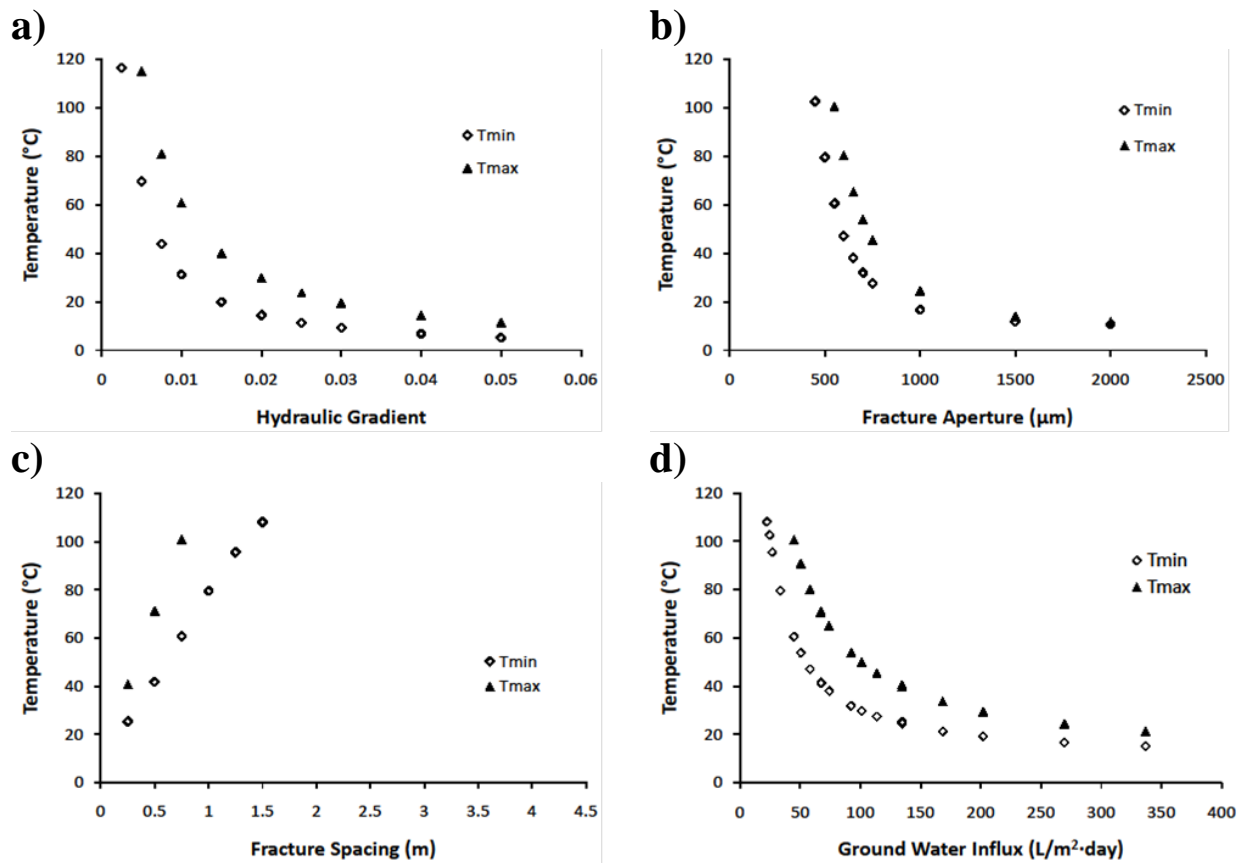


**Figure B9.4: Summary of computed one-year interwell fracture temperatures, showing effect of variation in hydraulic gradient (a), fracture aperture (b), fracture spacing (c), and bulk influx (d).**

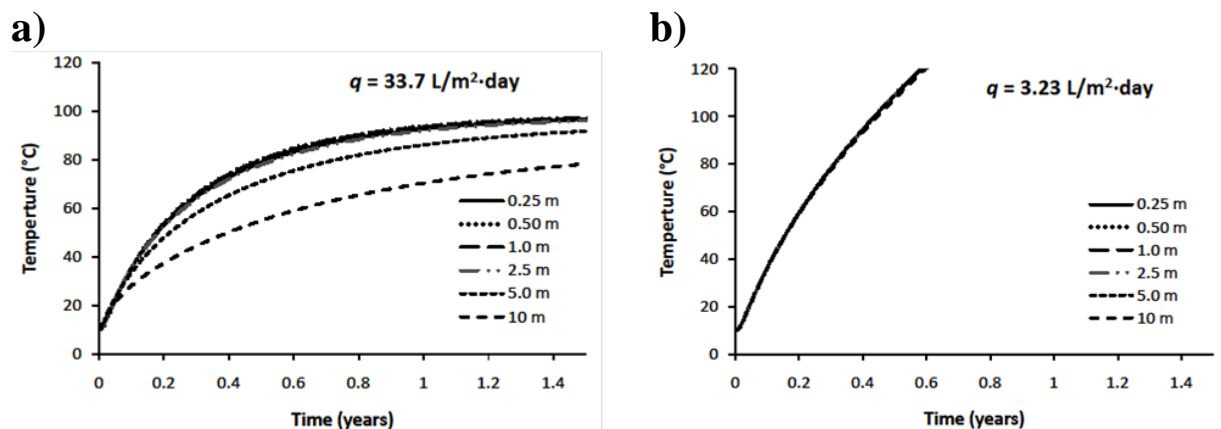
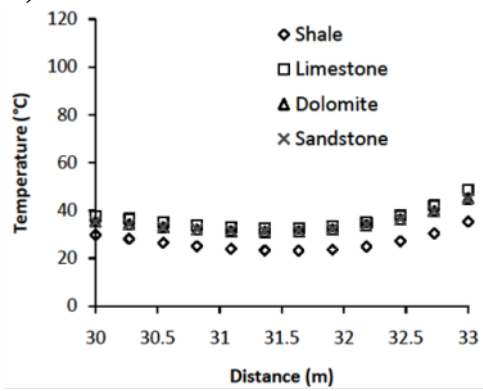


**Figure B9.5: Transient fracture temperature profiles at the center of the treatment zone for high (a) and mid-level (b) values of groundwater influx. Curves correspond to various fracture spacings.**

a)  $t = 1$  month



b)  $t = 1$  year

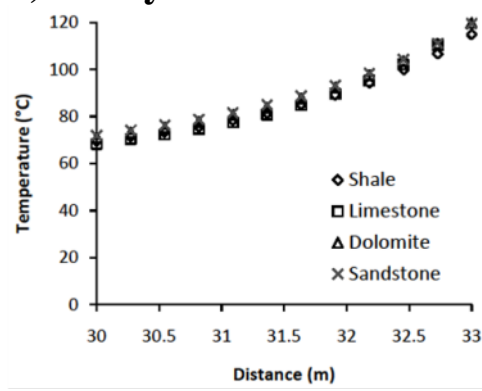
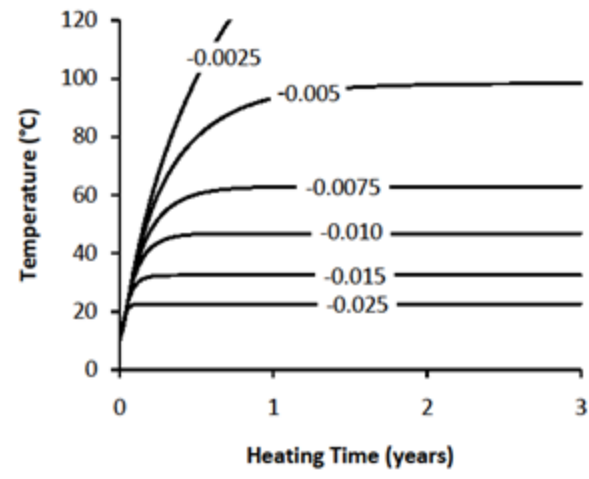
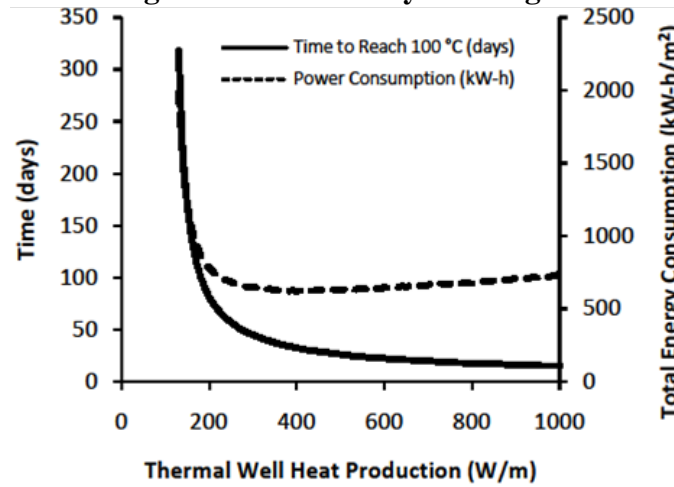


Figure B9.6: Early (a) and late-time (b) fracture temperature profiles for various rock types.



**Figure B9.7: Transient fracture temperature profiles at midpoint between heater wells, showing the influence of hydraulic gradient.**



**Figure B9.8: Effect of increased heat production on the time needed to reach a target temperature of 100 °C and total energy consumption.**

## Appendix: Green's Function

The Green's function used in the presented solution is determined by the product of two one-dimensional Green's functions:  $G_{x00}(x, t | x', \tau)$ , for an infinite domain in  $x$ , where the temperature vanishes as  $x \rightarrow \pm\infty$ ; and  $G_{y22}(y, t | y', \tau)$ , for finite domain in  $y$  of length  $H$ , with Type-II boundary conditions at  $y = 0$  and  $y = H$ . These functions are given by [20] as:

$$G_{x00}(x, t | x', \tau) = \left( \frac{1}{2\sqrt{\pi\alpha(t-\tau)}} \right) \exp\left( -\frac{(x-x')^2}{4\alpha(t-\tau)} \right) \quad (14)$$

$$G_{y22}(y, t | y', \tau) = \frac{1}{H} \left[ 1 + 2 \sum_{m=1}^{\infty} \exp\left( \frac{-m^2 \pi^2 \alpha (t-\tau)}{H^2} \right) \cos\left( \frac{m\pi y}{H} \right) \cos\left( \frac{m\pi y'}{H} \right) \right] \quad (15)$$

The effect of a point source function  $g(x', y', \tau)$  at  $(x, y, t)$  is given by:

$$T(x, y, t) = \frac{\alpha}{K} \int_{\tau=0}^t \int_{x'=a_1}^{a_2} \int_{y'=b_1}^{b_2} G_{x00}(x, t | x', \tau) G_{y22}(y, t | y', \tau) g(x', y', \tau) dy' dx' d\tau \quad (16)$$

where  $G$  is the product  $G_{x00}G_{y22}$ . From the convolution property of the Laplace transform, the Laplace transform of (16) is given by:

$$\bar{T}(x, y, s) = \frac{\alpha}{K} \int_{x'=a_1}^{a_2} \int_{y'=b_1}^{b_2} \mathbb{L}[G_{x00}(x, t | x', \tau) G_{y22}(y, t | y', \tau)] \mathbb{L}[g(x', y')] dy' dx' \quad (17)$$

where  $\bar{G}$ , the Laplace transform of  $G_{x00}G_{y22}$ , is given by:

$$\bar{G}(x, y | x', y') = \frac{1}{2H\sqrt{s\alpha}} \exp\left( -|x-x'| \sqrt{\frac{s}{\alpha}} \right) + \sum_{m=1}^{\infty} \frac{\exp\left( -|x-x'| \sqrt{\frac{s}{\alpha} + \frac{m^2 \pi^2}{H^2}} \right) \cos\left( \frac{m\pi y}{H} \right) \cos\left( \frac{m\pi y'}{H} \right)}{\sqrt{H^2 s + m^2 \pi^2 \alpha}} \quad (18)$$

## **Appendix C**

### **Numerical Modeling of TCH in Fractured Bedrock**

Baston, D.P., Falta, R.W. and Kueper, B.H., 2010. Numerical modeling of thermal conductive heating in bedrock. *Journal of Ground Water*, 48(6), pp. 836-843.

## **C1. Introduction**

Thermal methods of in-situ remediation attempt to take advantage of enhanced mass transfer processes occurring at elevated temperatures in order to remove organic contaminants from the subsurface, or destroy them in-situ. For many organic chemicals, elevated temperatures bring about enhanced dissolution, vaporization, volatilization, desorption and non-aqueous phase liquid (NAPL) mobility (e.g., NRC, 2004). A variety of methods have evolved for heating the subsurface; in this study, consideration is given to thermal conductive heating (TCH). TCH systems employ electrical heater wells to directly heat the subsurface to temperatures of up to 800 °C. The technology has been applied at several field sites in porous media, but has been used only recently in fractured rock environments.

The design of TCH systems may be significantly affected by the flow of cool groundwater into the treatment zone. This cooling effect has been examined in porous media modeling studies (Elliott et al., 2003, 2004) and a fractured media study (Baston and Kueper, 2009). For high values of bulk rock hydraulic conductivity or hydraulic gradient, target temperatures may not be attained unless the influx cooling is accommodated in the heating system design through the use of components such as preheating wells and impermeable barriers. Although the effect of influx on boiling has been studied in porous media (Elliot et al. 2003, 2004), no published study has examined how boiling during thermal treatment may be affected by the high degree of heterogeneity (i.e., large difference between matrix and fracture permeability) present in fractured rock environments. Using a two-dimensional semianalytical solution, Baston and Kueper (2009) found that for the prediction of treatment zone temperatures, the size and location of fractures is important when groundwater influx is high. However, the semianalytical solution used in that study was not able to model the boiling of water.

The present study examines the performance of a TCH system in a three-dimensional fractured shale where boiling of the water is considered. A numerical model is utilized to compute temperature distributions as well as liquid and vapor saturations in a hexagonal treatment zone heated by seven thermal wells. The importance of matrix permeability, matrix porosity, bulk permeability, and fracture spacing is examined.

## **C2. Numerical Model**

### **C2.1 Model Domain and Boundary Conditions**

Numerical modeling was conducted using the TOUGH2 simulator, which is capable of modeling nonisothermal multiphase flows (Pruess et al., 1999). The numerical simulations were designed to model a typical TCH configuration consisting of seven heater wells arranged in a hexagon, with a heater-extraction well at the center (Figure C1). This geometry permits the use of partial radial symmetry, whereby only a slice of the hexagon is modeled. The rock is a fractured shale, with assumed equal-aperture fractures occurring in the horizontal plane only and at regular spacing. The domain comprises one half of a fracture and adjacent matrix block in the vertical direction, making use of vertical symmetry (Figure C).

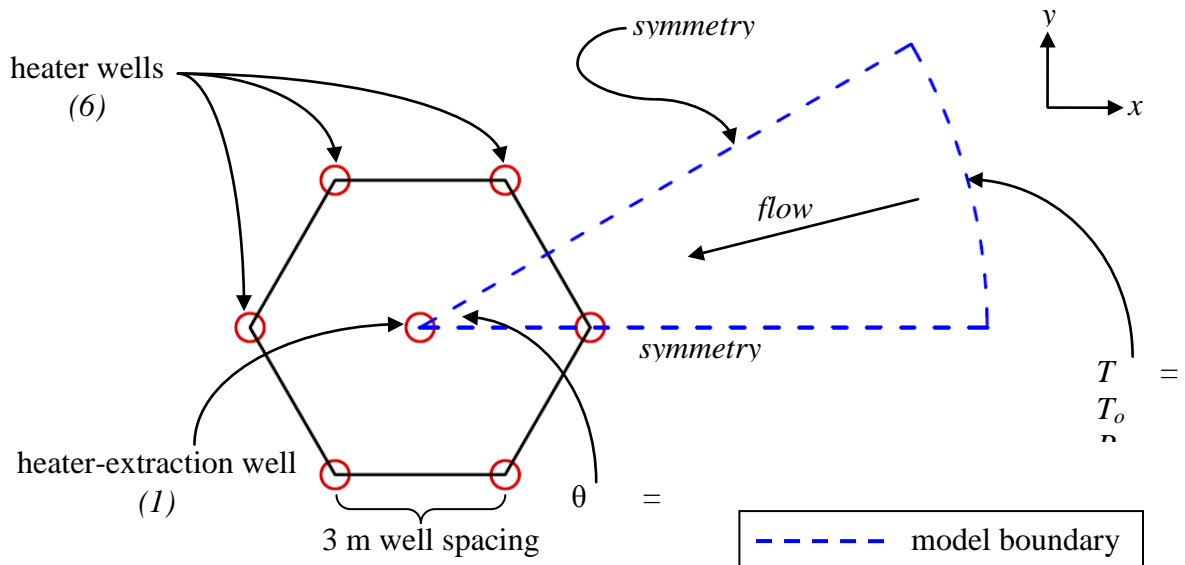


**Figure C9.9: Plan view of model domain**

The control volume formulation of TOUGH2 permits the use of irregularly shaped grids such as that employed in this study (Figure C2(b)). In order to represent the flow that would occur in fractures, a row of 1 mm thick fracture grid blocks with high permeability was created along the  $z = 0$  plane (Figure C). A grid sensitivity study and comparison with a semianalytical discrete fracture solution demonstrated that this approach results in temperature distributions that are nearly identical to those predicted by a discrete fracture model, while achieving much more rapid model convergence (Baston, 2008).

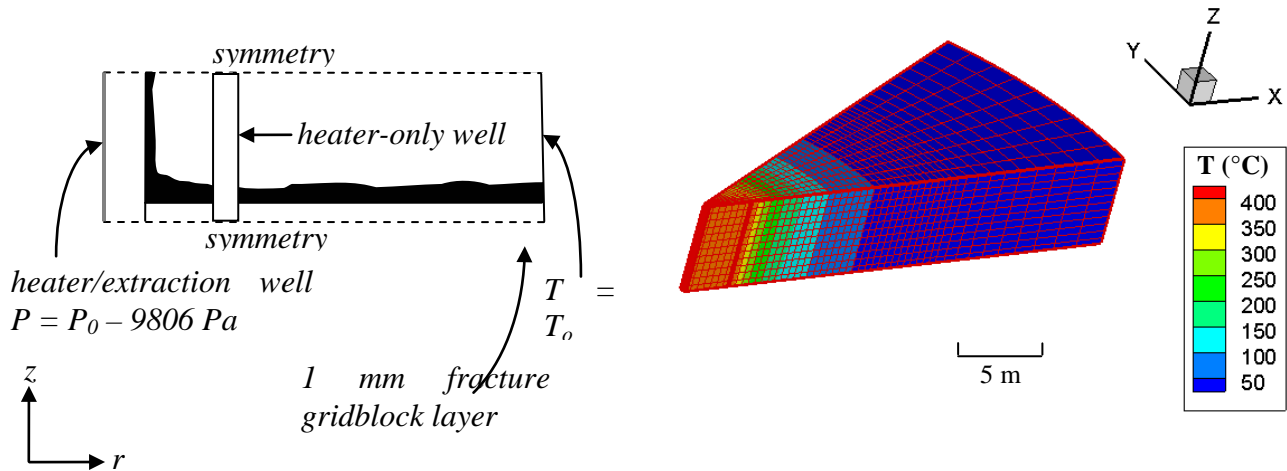


**Figure C9.10(a): Section of model domain in  $rz$  plane**      **Figure C2(b): Isometric view of model domain**

The initial temperature within the model domain is 10 °C and the initial pressure distribution is hydrostatic, with the pressure at  $z = 0$  corresponding to a depth of 15 m below the water table. Pressures in the extraction well for  $t > 0$  were held constant, corresponding to 1 m of water drawdown. Both temperature and hydrostatic pressure were held constant at the outer edge of the domain ( $r = 25$  m). A grid dependence analysis showed that increasing the size of the model domain in the radial direction did not significantly affect temperature or pressure distributions within the heated region (Baston, 2008). The two thermal wells located within the model domain, both assumed to generate heat at a steady rate of 800 W/m, were represented as line sources. The constitutive relationships of van Genuchten (1980) were used for capillary pressure and relative permeability functions. All properties of water and steam were computed using the EOS1 module of TOUGH2, which provides an implementation of the 1967 International Formulation Committee steam table equations (e.g., ASME, 1979). The model does not consider thermally-induced changes in rock properties or processes such as fracture creation or dilation that may occur under elevated pressures.

## C2.2 Rock Properties and Outline of Simulations

A series of simulations was conducted to examine the effect of matrix permeability ( $k_m$ ), matrix porosity ( $\phi$ ), bulk rock permeability ( $k_b$ ), and fracture spacing ( $2H$ ) on the temperature and time necessary to deplete all liquid water (superheated steam conditions) within the treatment zone, defined as the area within a 3 m radius of the center well (i.e., the circumscribed circle of the hexagon shown in Figure C1). A base case set of rock matrix and bulk medium properties is defined in Table C1. To evaluate the sensitivity to rock matrix properties,  $k_m$  and  $\phi$  were varied independently over the ranges in Table C2. The range of rock matrix permeabilities,  $10^{-18}$  m<sup>2</sup> to  $10^{-22}$  m<sup>2</sup>, is representative of literature values for the permeability of shale and other rock types such as granite, gneiss, and dolomite (e.g., Keith and Rimstidt, 1985; de Marsily, 1986; Hart et al., 2006). Rock thermal properties, variations in which have been shown to play a minor role in this context (Baston and Kueper, 2009) were held constant throughout the simulations.

Temperature dependent compressibility of water was incorporated into all simulations and it was assumed that the compressibility of the rock matrix was negligible compared to the compressibility of water.

To evaluate the sensitivity to bulk medium properties, a simulation was conducted for each combination of bulk permeability and fracture spacing in Table C2. For a given value of  $k_b$ , an increase in the fracture spacing corresponds to increased fracture permeability and therefore higher flow in the fracture gridblocks. The fracture gridblock permeability was calculated by considering the bulk permeability to be a depth weighted average of the matrix and fracture gridblock permeabilities as follows:

$$k_{fz} = \frac{k_b (\Delta z_m + \Delta z_{fz}) + k_m \Delta z_m}{\Delta z_{fz}} \quad (1)$$

where  $k_{fz}$  is the fracture gridblock permeability,  $\Delta z_m$  is the thickness of the matrix block, and  $\Delta z_{fz}$  is the thickness of the fracture gridblock (set to 1 mm in all simulations). Note that the fracture spacing,  $2H$ , is equal to  $\Delta z_m + \Delta z_{fz}$ . In addition to the five values of fracture spacing used, a simulation was run for each value of  $k_b$  using an equivalent porous medium (EPM) approximation. In the EPM approach, the rock mass is treated as a homogeneous porous medium that is assigned a permeability equal to  $k_b$ . This implies that there is no fracture zone within which preferential groundwater flow can occur.

**Table 9.1: Base case properties. Density, specific heat capacity, and thermal conductivity from Čermák and Rybach (1982)**

Property	Value
<i>Rock Matrix</i>	
Permeability (m <sup>2</sup> )	10 <sup>-18</sup>
Porosity (-)	0.03
Density (kg/m <sup>3</sup> )	2757
Specific heat capacity (J/kg·K)	1100
Thermal conductivity (W/m·K)	2.98
<i>Bulk Medium</i>	
Fracture Spacing (m)	2.5
Bulk permeability (m <sup>2</sup> )	10 <sup>-13</sup>

**Table 9.2: Parameters varied**

Parameter	Values Tested
<i>Rock Matrix</i>	
Permeability (m <sup>2</sup> )	10 <sup>-17</sup> , 10 <sup>-18</sup> , 10 <sup>-19</sup> , 10 <sup>-20</sup> , 10 <sup>-22</sup>
Porosity (-)	0.005, 0.01, 0.05, 0.10
<i>Bulk Medium</i>	
Bulk permeability (m <sup>2</sup> )	10 <sup>-11</sup> , 10 <sup>-12</sup> , 10 <sup>-13</sup> , 7.5*10 <sup>-14</sup> , 5*10 <sup>-14</sup> , 10 <sup>-14</sup> , 10 <sup>-15</sup> , 10 <sup>-16</sup>
Fracture spacing (m)	0 (EPM), 1, 2.5, 5, 7.5, 10

### C3. Results and Discussion

The fluid pressure response to the heating of a saturated rock mass depends on the relative influence of the thermal and hydraulic diffusivities of the rock (Palciauskas and Domenico, 1982). When the hydraulic diffusivity is much larger than the thermal diffusivity, the thermal expansion occurs at relatively constant pressure and the system responds as a drained medium

with water being easily expelled from the heated region. When the hydraulic diffusivity is less than the thermal diffusivity the system behaves as an undrained medium. In this case, the heated water is not able to escape and a significant pressure rise occurs (Palciauskas and Domenico, 1982). The thermal diffusivity of the rock matrix is less than or approximately equal to the hydraulic diffusivity for the rock considered in this study. In the fracture, however, the hydraulic diffusivity is far in excess of the thermal diffusivity. Consequently, the fractures act as drains for the fluid expansion in the rock matrix pores.

A steam front propagates radially outward away from the central well as boiling progresses in the treatment zone. When a gridblock on the steam front is heated, water within the pores expands. The mobility of this water is limited; it cannot flow radially inward toward the central well as a result of the expanding steam drive. Due to the low permeability of the rock matrix, the water can flow outward only slowly; consequently, the pressure in the gridblock rises. Because the pressure rise causes the boiling point of water to increase, the process is self-promoting: the boiling point elevation causes the water to expand more prior to boiling, with a concomitant increase in pressure. Finally, the water does boil and the pressure is relieved as the less viscous steam vapour flows toward the extraction well. Pressure relief is not immediate, requiring on the order of one to two times the time necessary for peak pressure to be reached.

The magnitude of this pressure spike, which effectively determines the time necessary to reach superheated steam conditions in the matrix, is determined in part by the fracture spacing, the matrix permeability, and the matrix porosity.

Typical pressure and temperature distributions during the early stage of boiling in the treatment zone are presented in Figures C3(a) and C3(b). Note that pressure build-up is strongest in the center of the rock matrix ( $z = 5$  m), directly between the two heater wells. Pressure is lower near the two heater wells, here boiling has already occurred and the pressure spike has passed.

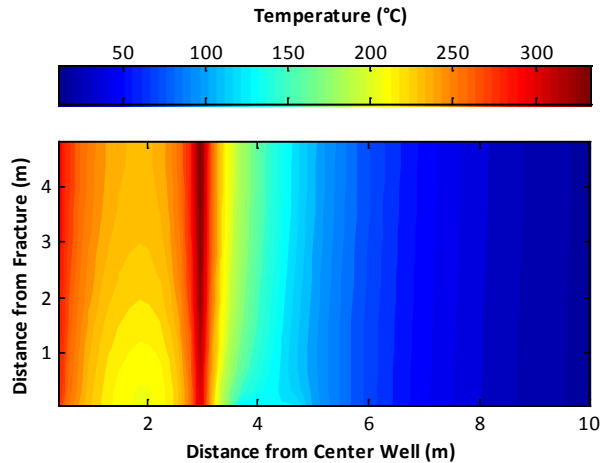


**Figure C9.11(a):** Example temperature distribution in  $r$ - $z$  plane after 168 days of heating, showing cooling effect adjacent to a fracture. Bulk permeability of  $10^{-13} \text{ m}^2$  and fracture spacing of 10 m used for this simulation.

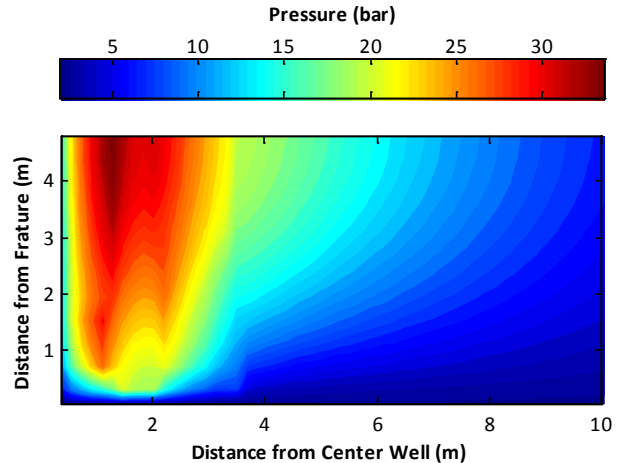


**Figure C3(b):** Example pressure distribution in  $r$ - $z$  plane after 168 days of heating, showing pressure buildup in rock matrix, away from fracture and center heater/extraction well. Bulk permeability of  $10^{-13} \text{ m}^2$  and fracture spacing of 10 m used for this simulation.

A typical pressure response is illustrated in Figure C for a location just outside the treatment zone ( $R = 3.88 \text{ m}$ ,  $\theta = 28.5^\circ$ ) using the base case parameters (Table 9.). The pressure distribution is very similar to that seen in a low-permeability medium subjected to an external loading. For example, a similar pore pressure distribution was calculated by Nogami and Li (2003) using an analytical solution for consolidation in a system of alternating horizontal sand and clay layers.

Because boiling in the rock matrix does not take place at constant pressure, the temperature may not remain constant throughout the boiling period. Consequently, a temperature plateau may not be observed in the rock matrix, as it typically is in the fracture. In Figure C, temperature is plotted against time for a reference block in the rock matrix ( $R = 2.96 \text{ m}$ ,  $\theta = 28.5^\circ$ ,  $z = 1.17 \text{ m}$ ) and in the fracture ( $R = 2.96 \text{ m}$ ,  $\theta = 28.5^\circ$ ,  $z = 0.5 \text{ mm}$ ) for the base case parameters (Table C1). Although a clear temperature plateau is observed during the boiling period in the fracture, the boiling period in the rock matrix cannot be discerned from temperature alone.

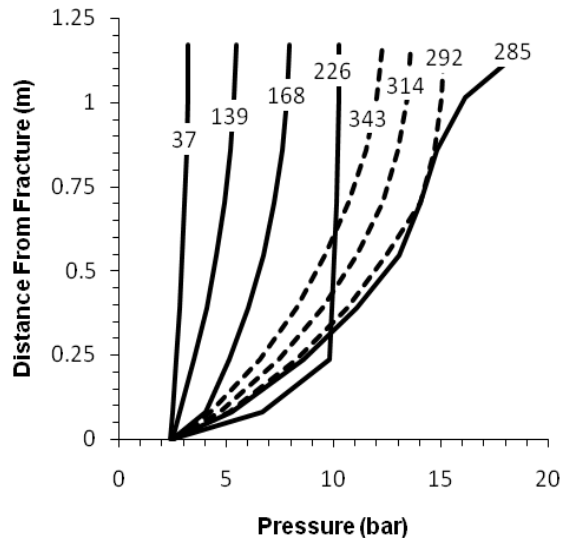


**Figure C9.12: Pressure versus distance from the fracture for an example location 3.05 m from the center well, just outside the treatment zone. Behavior at this location is characteristic of the last portion of the treatment zone to be depleted of liquid water. Heating time (days) is indicated for each line. Pressure profiles prior to reaching superheated steam conditions throughout the matrix are indicated with a solid line; profiles after reaching superheated steam conditions throughout the matrix are indicated with a dashed line.**

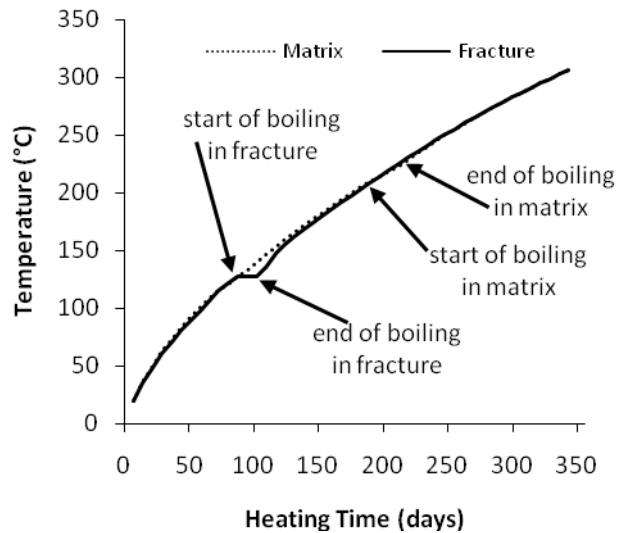


**Figure C9.13: Temperature versus time for a reference block in the rock matrix (dotted line) and fracture (solid line), at the outer boundary of the treatment zone. At the end of boiling in the fracture, the fracture is dry. At the end of boiling in the matrix, the matrix is dry.**

### **Influence of Matrix Permeability**

The lower the matrix permeability, the more slowly the heated water moves outwards and the larger the pressure rise, as illustrated in Figure C6a for a reference gridblock at the center of the rock matrix and edge of the treatment zone ( $R = 2.96$  m,  $\theta = 28.5^\circ$ ,  $z = 1.17$  m). The degree of boiling point elevation can be quite significant in a low permeability rock matrix. Even at treatment zone temperatures in excess of 200 °C, water in the matrix pores may still be in the liquid phase. It is conceivable, however, that stresses resulting from the high pore pressure in these cases could cause failure or micro fracturing of the rock, thus attenuating the pressure spike and reducing the boiling point elevation (Palciauskas and Domenico, 1982; Horseman and McEwen, 1996).

In cases where the boiling point elevation is large, the time necessary to bring about complete removal of liquid water throughout the treatment zone will increase significantly. In Figure C(b), the volume fraction of the treatment zone from which all liquid water has been removed is shown for several values of matrix permeability. The significance of the boiling point elevation may depend on the context of the thermal treatment. A boiling point of 300 °C may not affect

the treatment of high boiling point compounds such as PCBs, where the treatment temperature would need to exceed 300 °C even in the absence of boiling point elevation. However, boiling point elevation may significantly delay the treatment of volatile compounds, which would be treated at lower temperatures in a porous medium (LaChance et al., 2006).

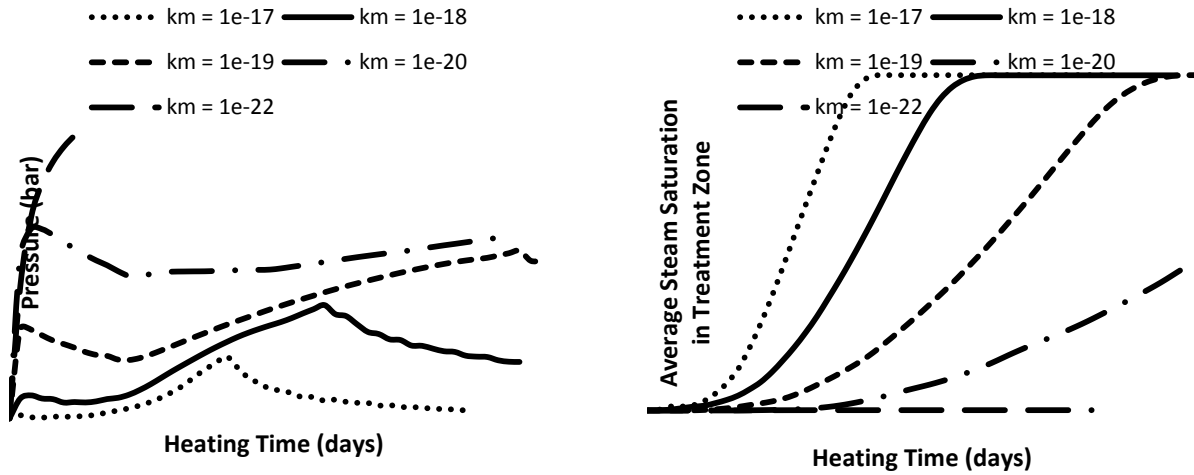


**Figure C9.14: Impact of matrix permeability ( $k_m$ ) on magnitude of pressure spike at center of rock matrix ( $z = H$ ), where pressure spike is most pronounced (a) and average vapor saturation within treatment zone (b).**

### Influence of Matrix Porosity

Figure C(a) presents the transient pressure response for a reference block near the center of the rock matrix, at the outer radius of the treatment zone. The time necessary to remove all liquid water increases with matrix porosity, which not only determines the quantity of water to be boiled, but also has an effect on the pressure distribution. For a given value of intrinsic permeability, an increase in the porosity causes a larger volume of water to undergo thermal expansion, without increasing the ability of the expanded water to flow outward. Consequently, the magnitude of the pressure spike will increase. For the range of porosities evaluated, the significance of matrix porosity is less than that of permeability in dictating the magnitude of the pressure spike.

The effect of porosity on vapor saturations in the treatment zone is shown in Figure C(b). In addition to boiling point elevation due to an increase in pore pressures, an increase in matrix porosity causes a larger amount of energy to be expended to overcome the latent heat of vaporization, thereby resulting in longer treatment times to boil away the liquid water.

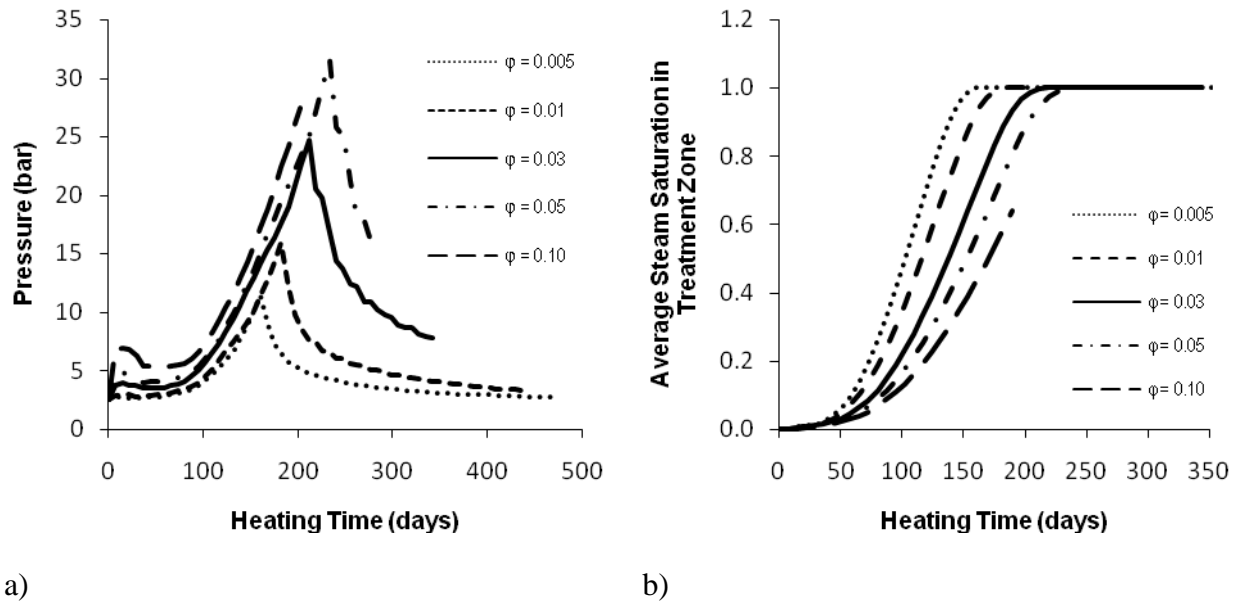


**Figure C9.15 Impact of porosity ( $\phi$ ) on magnitude of pressure spike at center of rock matrix (a) and average vapor saturation within the treatment zone (b).**

### Influence of bulk permeability and fracture properties

The importance of bulk permeability and fracture properties was assessed through an examination of treatment zone temperatures and the time necessary to reach complete superheated vapor conditions within the treatment zone. For each combination of bulk medium properties in Table C2, the minimum temperature and the average vapor saturation in the treatment zone were recorded at fixed time intervals.

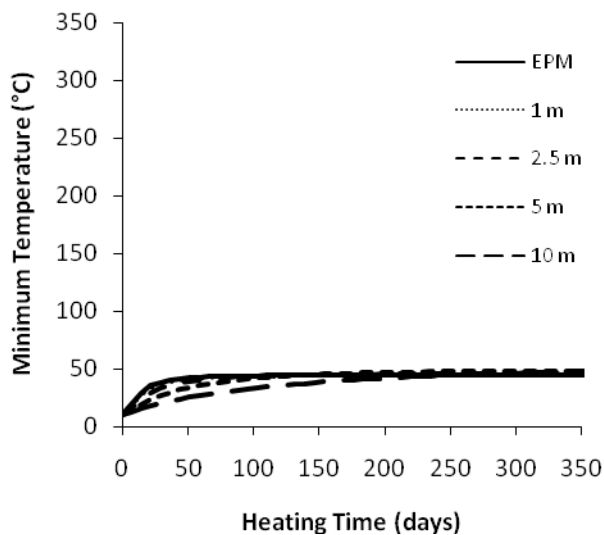
### Treatment Zone Temperatures

Figure C plots the minimum treatment zone temperature versus time for four values of bulk permeability. For each value of bulk permeability, the temperature is plotted as calculated using four different values of fracture spacing, as well as an equivalent porous medium. Because the location of the minimum treatment zone temperature may vary throughout time, the temperatures plotted do not necessarily correspond to one single location in space.

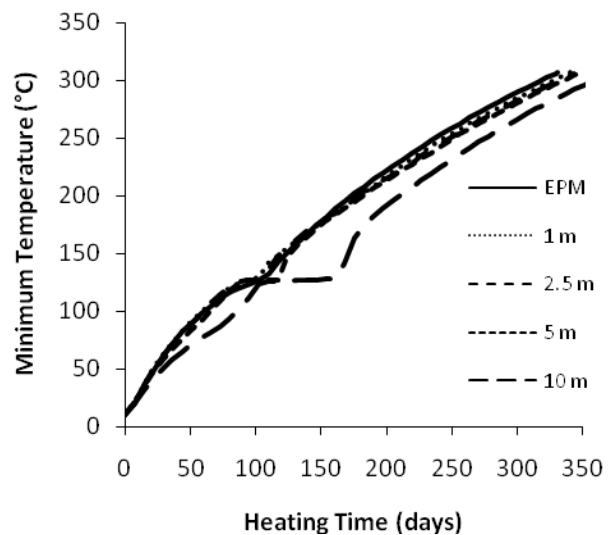
The temperature profiles are very dependent on the heterogeneity of the system at high values of bulk permeability. When  $k_b$  is equal to  $10^{-12} \text{ m}^2$ , the treatment zone does not reach boiling temperatures because of the excessive influx of groundwater and comes to a steady state with a minimum temperature of approximately  $50 \text{ }^\circ\text{C}$  (Figure C8a). The time needed to reach this steady state varies by a factor of approximately five, depending on the fracture spacing. For each case of fracture spacing, the final temperature is the same, illustrating that flow heterogeneity has an effect only at early and mid-time in this scenario.

When the bulk permeability is decreased to  $10^{-13} \text{ m}^2$ , cooling induced by flow in the fracture is insufficient to bring the system to a steady state at sub-boiling temperatures. For the parameters

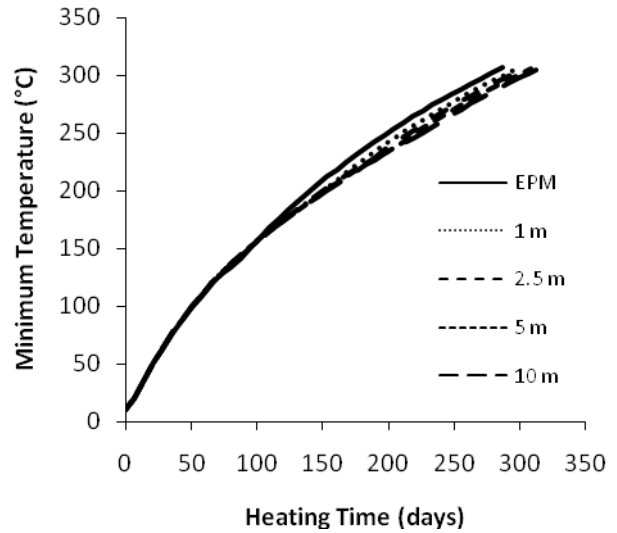
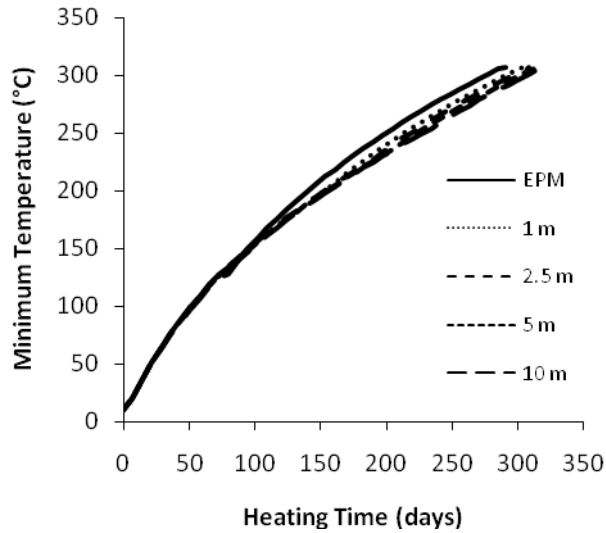
used in this study, the threshold permeability is between  $10^{-12}$  and  $10^{-13}$   $\text{m}^2$ , but this particular value is dependent on other values, such as the imposed hydraulic gradient and rate of energy delivery. For the case of a  $10^{-13}$   $\text{m}^2$  bulk permeability, the temperature profiles are closely spaced at early time and the profiles diverge as boiling is initiated in the fracture, but begin to converge some time after boiling has finished (Figure C8b). Once again, the differences between the trials are diminished at late-time. After 150 days of heating, only the temperature profile for the 10 m fracture spacing case is significantly different. For the cases of high fracture spacing in Figure C8(b), a temperature plateau lasting approximately 100 days can be observed. In these cases, the coldest point in the treatment zone is located in the fracture, where a plateau does develop during boiling. At smaller values of bulk permeability ( $k_b \leq 10^{-14}$   $\text{m}^2$ ), the differences between the trials become less significant. For both  $k_b = 10^{-14}$   $\text{m}^2$  and  $k_b = 10^{-15}$   $\text{m}^2$  (Figures C8c-C8d), the difference in predicted temperatures between the simulations rises gradually to a maximum of 7% at 226 days of heating, before declining.



a) Minimum temperature vs time for  $k_b = 10^{-12}$   $\text{m}^2$



b) Minimum temperature vs time for  $k_b = 10^{-13}$   $\text{m}^2$



c) Minimum temperature vs time for  $k_b = 10^{-14} \text{ m}^2$

d) Minimum temperature vs time for  $k_b = 10^{-15} \text{ m}^2$

**Figure C9.16: Minimum treatment zone temperature profiles for various values of fracture spacing, with (a)  $k_b = 10^{-12} \text{ m}^2$ , (b)  $k_b = 10^{-13} \text{ m}^2$ , (c)  $k_b = 10^{-14} \text{ m}^2$ , (d)  $k_b = 10^{-15} \text{ m}^2$ . Complete removal of liquid water is achieved in the entire treatment zone for all cases presented in figures (b) – (d).**

### Treatment Zone Boiling

Fracture properties can have a large impact on the time needed to reach complete steam saturation within the treatment zone, even in cases where temperatures seem to be little affected by flow heterogeneity. In the fracture, where there is no significant pressure spike, boiling will begin at a lower temperature than in the rock matrix. Consequently, for all parameters used in this study, boiling occurred in the fracture prior to in the matrix. An example of this behaviour is illustrated in Figure C, which shows the relationship between average steam saturation in a horizontal plane through the treatment zone and distance from the fracture plane for the base case simulation (Table C1). Although the entire fracture is void of liquid water after 117 days, the matrix is not depleted of liquid water until 263 days of heating.

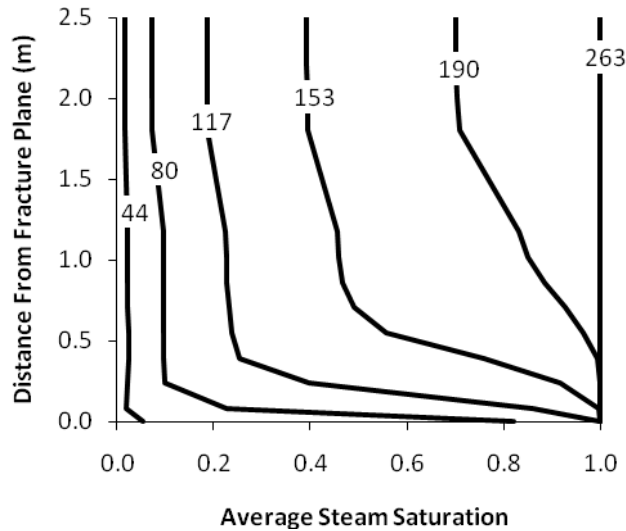


**Figure C9.17: Average steam saturation at a specified distance from the fracture plane, in the treatment zone for the base case simulation. The heating time (days) is indicated for each curve.**

Even in scenarios where changes in fracture spacing and bulk permeability do not have a significant effect on the amount of time needed to reach a target temperature, these factors can have a significant impact on the amount of time necessary to bring about complete removal of all liquid water in the treatment zone, as seen in Figure C. For example, there is no significant difference in computed temperatures between an EPM and 1 m-spaced fractures in any of the simulations presented in Figure C. However, the difference in time to reach complete steam saturation is significant: over 50% in some of the cases shown in Figure C.

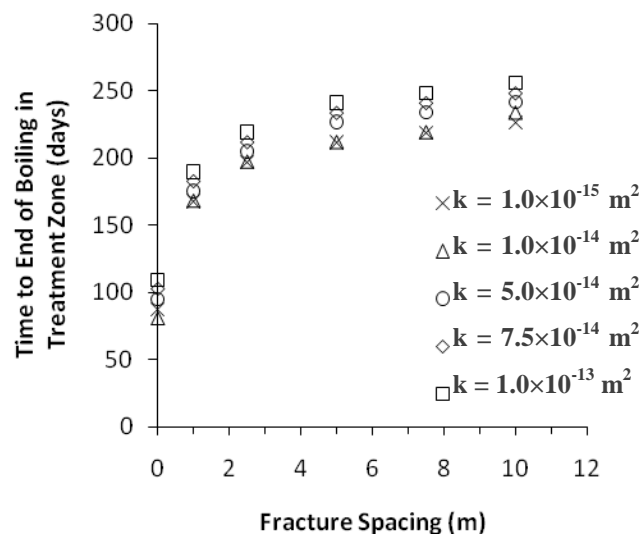


**Figure C9.18: Sensitivity of time to remove all liquid water in the treatment zone to bulk permeability. Fracture spacing of 0 corresponds to EPM simulation.**

When the fracture spacing is large, more time is necessary for water to drain into the fractures, due the larger distance between the center of the rock matrix and the closest fracture. Consequently, the pressure rise is larger and the boiling point more elevated. There appears to be a limit to this behavior, however; as seen in Figure C, incremental increases in fracture spacing have a progressively smaller impact on the time needed to remove all liquid water. The large variability in the time needed to reach complete steam saturation for a single value of bulk permeability suggests a potential challenge in predicting TCH treatment times in fractured bedrock if complete removal of all liquid water is the goal of treatment.

#### **C4. CONCLUSIONS**

The performance of thermal conductive heating in fractured rock environments is expected to be strongly dependent on the hydraulic properties of the rock matrix (permeability, porosity) and the aperture and spacing of fractures. If complete removal of all liquid water is the goal of thermal treatment, treatment time will be strongly governed by the magnitude of the pressure spike that occurs in the rock matrix during heating. When the rock matrix has a low permeability, high porosity, or sparse fracturing, this pressure rise may be enough to significantly raise the boiling point of water in the matrix, thus delaying treatment. Because a clear temperature plateau may not be observed in the matrix during boiling, it may be difficult to determine if boiling has occurred throughout a treatment area from temperature measurements alone.

Due to the importance of fracture spacing in determining the pressure rise in the matrix, a discrete fracture model is more appropriate than an equivalent porous medium model for simulating boiling in this context. However, treatment zone temperatures are only moderately affected by the location of fractures, for a given value of bulk permeability. An equivalent porous medium (EPM) model may provide an adequate estimation of treatment zone temperatures, especially when the bulk permeability is low or heating times are long.

## C5. REFERENCES

- American Society of Mechanical Engineers. 1977. "ASME Steam Tables." 3<sup>rd</sup> edition. ASME, New York.
- Baston, D.P. 2008. "Analytical and Numerical Modeling of Thermal Conductive Heating in Fractured Rock." M.Sc. Thesis, Queen's University.
- Baston, D.P. and Kueper, B.H., 2009. Thermal conductive heating in fractured bedrock: screening calculations to assess the effect of groundwater influx. *Advances in Water Resources*, 32, pp. 231-238.
- Čermák, V. and L. Rybach. 1982. Thermal conductivity and specific heat of minerals and rocks. In *Landolt-Börnstein: Numerical Data and Functional Relationships in Science and Technology, Group V (Geophysical and Space Research), Volume 1a (Physical Properties of Rocks)*, ed. G. Angenheister, 305—343. Springer: Berlin-Heidelberg.
- Elliott, L.J., G.A. Pope, and R.T. Johns. 2003. "In-Situ Thermal Remediation of Contaminant Below the Water Table." Paper SPE-81204. In: *Proceedings of the SPE/EPA/DOE Exploration and Production Environmental Conference*. San Antonio, TX.
- Elliott, L.J., G.A. Pope, and R.T. Johns. 2004. "Multi-Dimensional Numerical Reservoir Simulation of Thermal Remediation of Contaminants Below the Water Table." Paper 2B-08. In: A.R. Gavaskar and A.S.C. Chen (Eds.), *Proceedings of the Fourth International Conference on Remediation of Chlorinated and Recalcitrant Compounds*. Battelle Press, Columbus, OH (CD format).
- Hart, D.J., K.R. Bradbury, and D.T. Feinstein. 2006. "The Vertical Hydraulic Conductivity of an Aquitard at Two Spatial Scales." *Ground Water*. 44(2): 201—211.
- Horseman, S.T. and T.J. McEwen. 1996. "Thermal constraints on disposal of heat-emitting waste in argillaceous rocks." *Engineering Geology*. 41, 5—16.
- Keith, L.A. and J.D. Rimstidt. 1985. "A Numerical Compaction Model of Overpressuring in Shales." *Mathematical Geology*. 17(2). 115—135.
- de Marsily, G. 1986. *Quantitative Hydrogeology*. Academic Press, New York.
- Lachance, J., G. Heron, and R. Baker. 2006. "Verification of an Improved Approach for Implementing In-Situ Thermal Desorption for the Remediation of Chlorinated Solvents". In: B.M. Sass (Ed.), *Remediation of Chlorinated and Recalcitrant Compounds: Proceedings of the Fifth International Conference*. Battelle Press, Columbus, OH (CD format).
- National Research Council. 1996. *Rock Fractures and Fluid Flow: Contemporary Understanding and Applications*. National Academy Press, Washington.
- National Research Council. 2004. *Contaminants in the Subsurface: Source Zone Assessment and Remediation*. National Academy Press, Washington.
- Nogami, T., and M. Li. 2003. "Consolidation of Clay with a System of Vertical and Horizontal Drains." *Journal of Geotechnical and Geoenvironmental Engineering*. 129(9): 838—848.
- Palciauskas, V.V., and P.A. Domenico. 1982. "Characterization of Drained and Undrained Response of Thermally Loaded Repository Rocks." *Water Resources Research*. 18(2): 281—290.
- Pruess, K., C. Oldenburg, and G. Moridis. 1999. *TOUGH2 User's Guide, Version 2.0*. Report LBNL-43134. Lawrence Berkeley National Laboratory, Berkeley, CA.
- van Genuchten, M. Th. 1980. "A Closed-Form Equation for Predicting the Hydraulic Conductivity of Unsaturated Soils. *Soil Science Society of America Journal*. 44: 892—898.

## **Appendix D: Treatability Study Results (Queen's University)**

## Appendix D1 - Laboratory methodology and heating tests supplementary data

### Heating test methodology

The seven rock types selected for bench-scale assessment of TCH in fractured rock were tested in the following order: red mudstone, gray mudstone, black mudstone, siltstone, limestone, sandstone and dolostone. The experimental program was divided into two phases. Phase 1 started with the spiking of the three different mudstone types on May 5, 2008 and finished with the volatile organic compound (VOC) analyses of the mudstone samples after heating tests on April 1, 2009. Phase 2 started with the spiking of the siltstone, limestone, sandstone and dolostone samples on May 7, 2009 and finished with the VOC analysis of the corresponding heating tests on February 26, 2010.

Following is the methodology undertaken during the heating experiments in the laboratory to assess the relationships between temperature, heating duration and degree of contaminant mass removal.

1. After the end of the TCE spiking process, one de-aired water saturated disc was recovered from the water bath and drilled with a 1/8" x 3" type D rotary percussion bit from the periphery to the center of the disc. Drilling was performed at low RPM while water was used to cool down the disc and to avoid breakage.
2. The drilled disc was placed back into the de-aired water bath for 24h to restore and potential water loss caused by drilling.
3. After the 24h period, the drilled disc was taken from the de-aired water bath and a type T thermocouple was placed into the previously drilled hole. The thermocouple was sealed and secured in the rock disc using FluoroGrip SC-200 (Figure 1).



**Figure 1 – Photograph of the temperature monitoring disc for red mudstone with a thermocouple placed inside the drilled hole to monitor the temperature profile in the disc during the heating tests.**

4. The disc with the thermocouple was positioned in the center of the binder convection oven vented to a fume hood after the FluoroGrip was cured.
5. The thermocouple was connected to a data-logger (Data Translation Inc. DT9805) outside the oven to monitor the temperature of the rock disc during the heating test.
6. An additional thermocouple was connected to the data-logger and placed inside the oven, close to the temperature monitoring disc, to monitor the temperature of the surroundings inside the oven.
7. One of the two sets of six rock discs was selected and removed from TCE bath.



**Figure 2 – Photograph of the red mudstone, gray mudstone and black mudstone disc samples under TCE saturation at the left, and PCE saturation at the right.**

8. The six TCE saturated discs were placed on an absorbing mat in a fume hood for about a minute or until surface residual TCE was evaporated.
9. The TCE saturated discs were placed into the convection oven around the temperature monitoring disc to facilitate a uniform distribution of heat (Figure 3).



**Figure 3 – The distribution of the set of TCE saturated siltstone discs, the temperature monitoring disc and the extra thermocouple inside the convection oven.**

10. The discs were heated using the heating temperature profile to assess the effect of temperature on contaminant mass removal from the rock matrix.
11. The temperature of the convection oven was set to 200°C (105°C for the heating duration profile). The convection oven and data logger were simultaneously started to monitor the complete temperature profile.
12. One disc was recovered from the convection oven per each temperature point in the corresponding heating profile, and the disc was placed into a rock crusher specifically design for this purpose (Figure 4). The process of removing the disc sample was rapidly performed to avoid a drop in the temperature inside the convection oven.
13. To extract TCE from the disc sample, the sample was placed into the rock crusher and 40mL of methanol were added to cover the sample and avoid VOC loss.
14. The rock crusher was closed and the plunger was hit with a hammer to crush the disc.

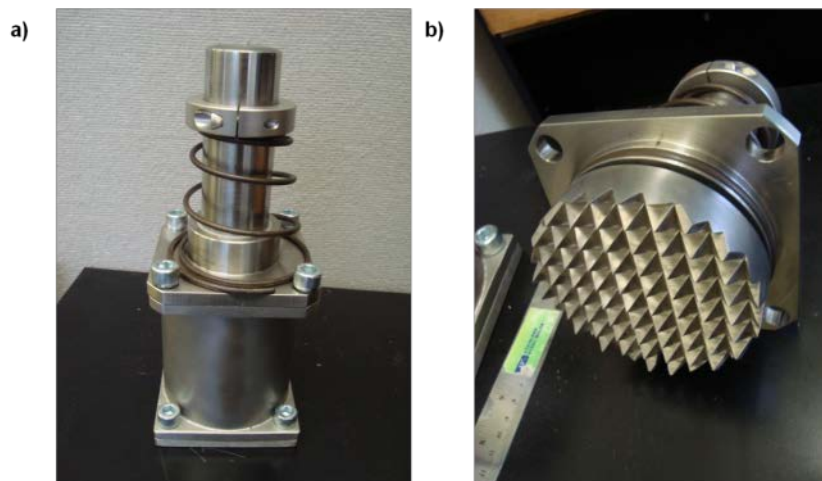


**Figure 4 – Photograph of the a) rock crusher and its b) upper teeth.**

15. The disc particles with the methanol extract were recovered after crushing and poured into a 125mL straight-sided glass jar with Teflon-lined cap (Figure 5).



**Figure 5 – Photograph of the 125mL jar containing the TCE extract from grey mudstone.**

16. The remaining particles inside the rock crusher were recovered by rinsing the bottom of the rock crusher with 40ml of methanol and adding the resulting extract into the 125mL jar.
17. The jar was closed to avoid extract losses by evaporation and placed on an orbital shaker for a period of 24h to attain the complete extraction of TCE and PCE (Figure 6).
18. The rock crusher was dissembled and the pieces were rinsed initially with distilled water and then with methanol to remove any residual TCE or disc particles remaining in any of the rock crusher elements.
19. After cleaning, the pieces of the rock crusher were placed in the fume hood for drying out the methanol and, consecutively re-assembled for subsequent rock disc crushing.



**Figure 6 – Photograph of the orbital shaker where the TCE and PCE extracts remained for 24 hours to attain complete extraction of VOCs.**

20. Steps 12 to 19 were repeated for the consecutive five rock discs, until the target temperature of 200°C in the heating temperature profile was reached (105°C @ 72 h for the heating duration profile).
21. After shaking for 24h, 10mL of the methanol were collected from each of the six extracts and placed into 15mL vials that were sent to the Analytical Services Unit (ASU) at Queen's University for VOC analysis.
22. Steps 1 to 22 were repeated for the second set of TCE saturated discs with the application of the heating duration profile.
23. The methodology was repeated for the two sets of six rock discs spiked with PCE and consecutively for the additional rock types.

## Analytical methodology

The TCE and PCE extracts were analyzed for TCE and PCE at the Analytical Service Unit (ASU). The analytical method followed United States Environmental Protection Agency methods 5035A (USEPA, 2002) and 8260B (USEPA, 1996), Closed-system Purge-and-Trap and Extraction for Volatile Organics in soil and waste samples and Volatile Organic Compounds by Gas Chromatography/Mass Spectrometry (GC/MS), respectively. The analyses were performed in a gas chromatograph/Mass selective detector model Hewlett Packard 5890 Series II Plus/ 5972 Series system with purge-and-trap concentrator (Teckmar LSC-2000). The method detection limits for TCE and PCE were both on the order of 2 ppb in methanol.

The calibration of the system was performed with a blank and five standard solutions at concentrations of 10 ppb, 40 ppb, 100 ppb, 200 ppb and 400 ppb for TCE. A blank and four standard solutions at concentrations of 10 ppb, 100 ppb, 200 ppb, and 500 ppb were utilized for PCE. The blank solution was composed solely of organic free deionized water. The standard solutions for TCE and PCE were prepared from a 20 ppm VOC mixture in methanol solution (1,1-Dichloroethylene, 1,1,1- Trichloroethane, 1,1,2-Trichloroethane, 1,2-Dichlorobenzene, 1,2-Dichloroethane, 1,2-Dichloropropane, 1,2,4-Trichlorobenzene, 1,4-Dichlorobenzene, Benzene, Bromodichloromethane, Bromoform, Carbon tetrachloride, Chlorobenzene, Chloroform, cis-1,2-Dichloroethylene, Dibromochloromethane, Dichloromethane, Ethylbenzene, m-Xylene, o-Xylene, p-Xylene, Styrene, Tetrachloroethylene, Toluene, trans-1,2-Dichloroethylene, Trichloroethylene, Vinyl chloride) purchased from AccuStandard, Inc. with a >99 % quality. The calibration curves for TCE and PCE are shown in Figure 7 and Figure 8, respectively. The maximum concentration in the standard solutions during the calibration experiments were selected to encompass the maximum concentration expected during TCE and PCE analyses. The system showed a linear response with a coefficient of determination ( $R^2$ ) of 0.9996 for TCE, and of 0.9998 for PCE.

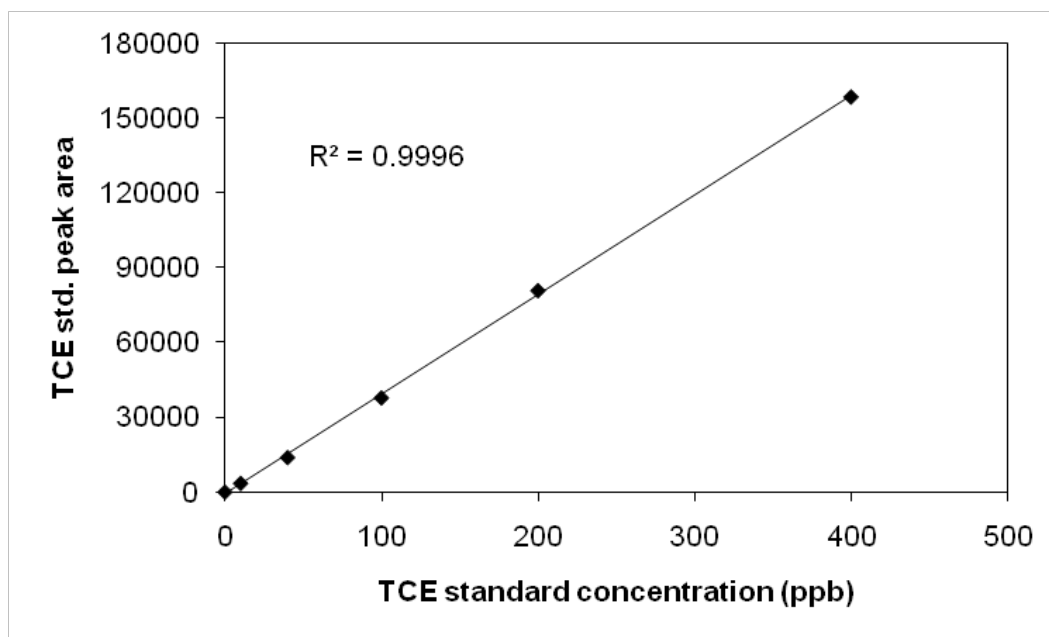
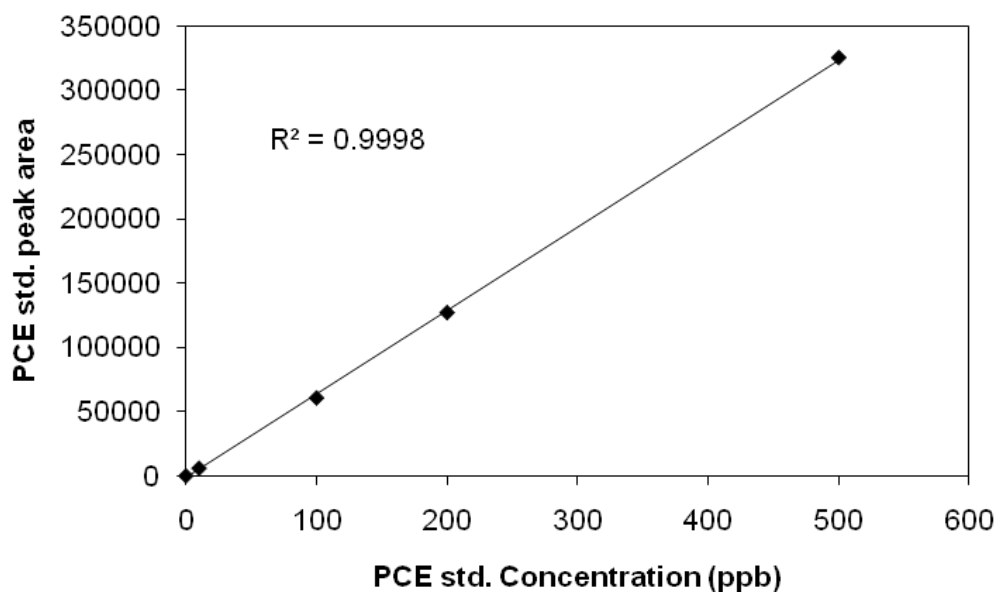
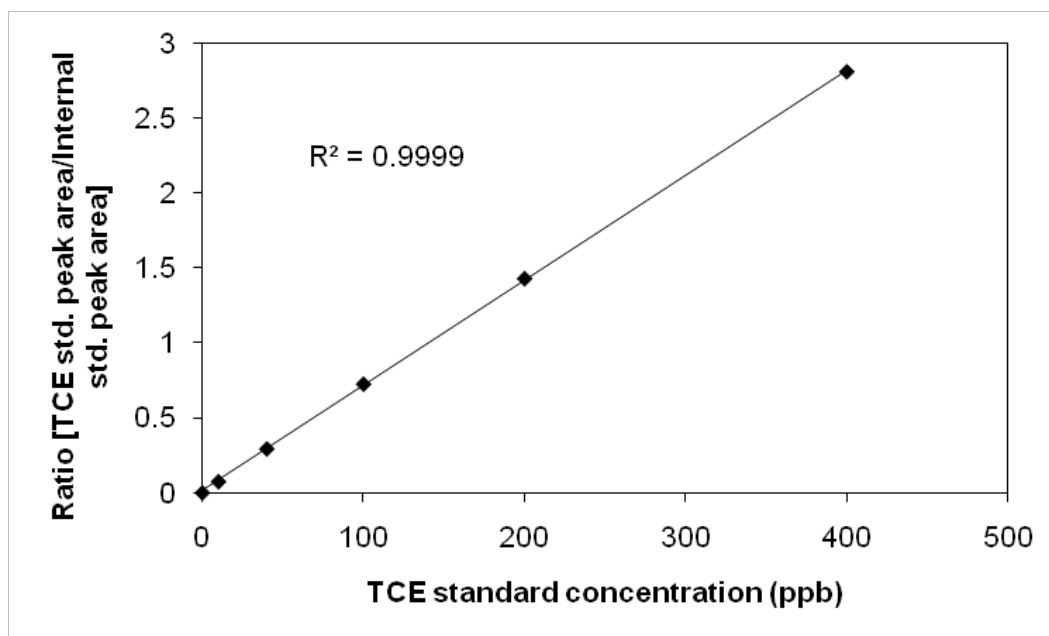


Figure 7 – TCE calibration experiment for purge-and-trap GC/MS analyses.



**Figure 8 – PCE calibration experiment for purge-and-trap GC/MS analyses.**

In addition to the TCE and PCE standards, an internal standard was used to improve the accuracy and precision of the analysis by eliminating the variability of the test. The internal standard at concentrations of 150 ppb for TCE and 1 ppm for PCE was prepared from a 20 ppm Fluorobenzene in methanol solution purchased from AccuStandard, Inc. with a >99 % quality. The internal standard improved the linearity of the experiment with a coefficient of determination ( $R^2$ ) of 0.9999 for TCE, and of 1 for PCE. The calibration curve for TCE with the adjusting factor of the internal standard is shown in Figure 9, while for PCE is shown in Figure 10.



**Figure 9 – TCE calibration experiment with internal standard for purge-and-trap GC/MS analyses.**

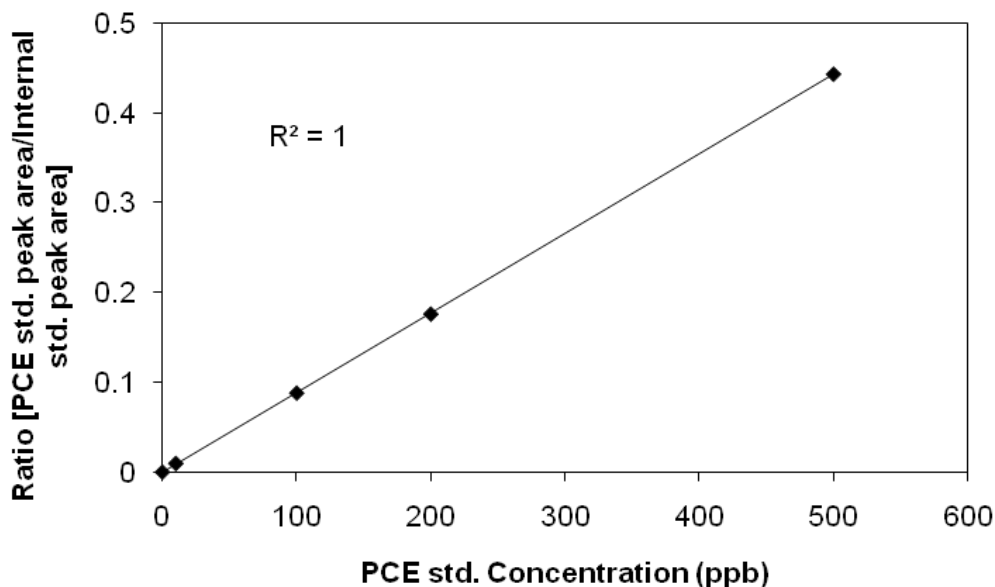


**Figure 10 – PCE calibration experiment with internal standard for purge-and-trap GC/MS analyses.**

Because of the linear behaviour of the system during the calibration experiments, a new calibration was not required for each set of six discs of either TCE or PCE extracts. However, during the VOC analyses, the system was verified for accuracy with a blank solution, consecutively with the VOC standard solution, and finally with the internal standard solution. The TCE and PCE standard solutions were injected with concentrations of 200 ppb, while the internal standard was injected with a concentration of 20 ppb during each extract analysis.

The basic calculation to compute the concentration of VOCs in the methanol extract ( ) is expressed as (Burghardt, 2007):

$$(1)$$

where is either the TCE or PCE standard concentration, is the peak area of the experimental sample, and is the peak area of either the TCE or PCE standard.

With the addition of the internal standard, Equation 1 becomes:

$$(2)$$

where is the peak area of the internal standard during calibration experiments, and is the peak area of the internal standard injected in the experimental sample.

## Results of the heating temperature profile and heating duration profile tests for TCE

A heating ‘temperature profile’ test involves evaluating VOC concentrations in the rock disks at temperatures of 20C, 60C, 95C, 105C, 150C and 200C. The evaluation at 20C (room temperature) involves analyzing a disk that is not placed into the heating oven. The remaining five evaluations are carried out with disks placed into the heating oven. The oven is set to 200C and as the internal rock temperature increases, one disk is removed from the oven at each target temperature (total of six disks to complete a temperature ‘profile’ test).

A heating ‘duration profile’ test involves evaluating VOC concentrations in the rock disks at temperatures of 20C, 60C, 95C and three disks at 105C. The first of the three disks at 105C will have been present in the oven for 24hr, the second for 48hr and the third for 72hr (total of 6 disks to complete a temperature ‘duration’ test).

Both temperature profile and duration profile heating tests were completed for all seven rock types, for both TCE and PCE, with one exception. The temperature profile test was conducted twice for the red mudstone spiked with TCE to evaluate reproducibility. A duration profile test was not completed for red mudstone spiked with TCE.

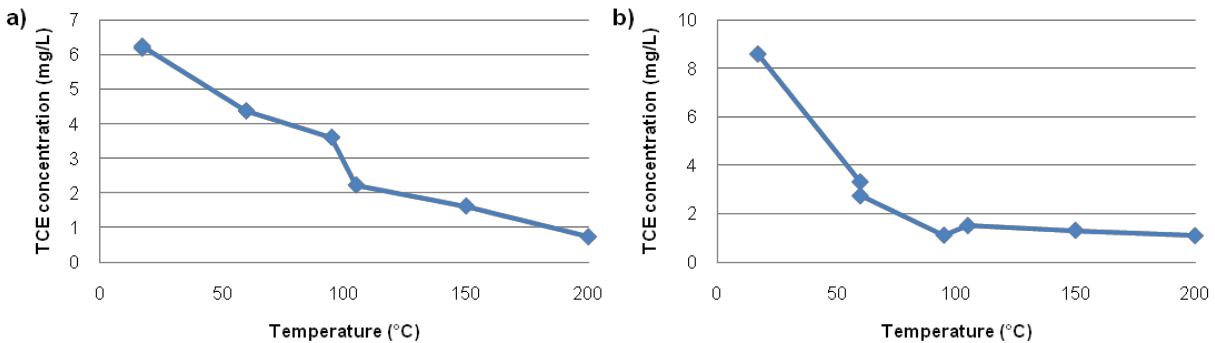


**Figure 11 – TCE concentration in red mudstone during heating experiments using a) the heating temperature profile and b) the duplicate of the experiment.**

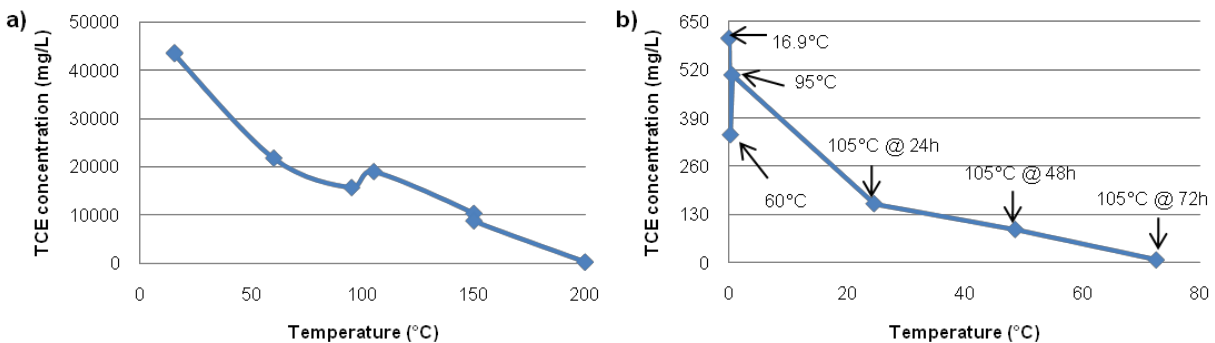


**Figure 12 – TCE concentration in gray mudstone during heating experiments using a) the heating temperature profile and b) the heating duration profile.**

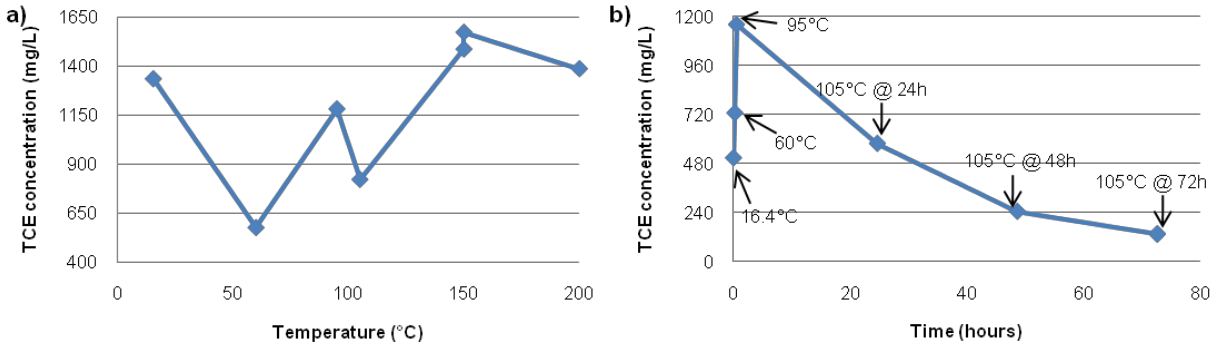


**Figure 13 – TCE concentration in black mudstone during heating experiments using a) the heating temperature profile and b) the heating duration profile.**

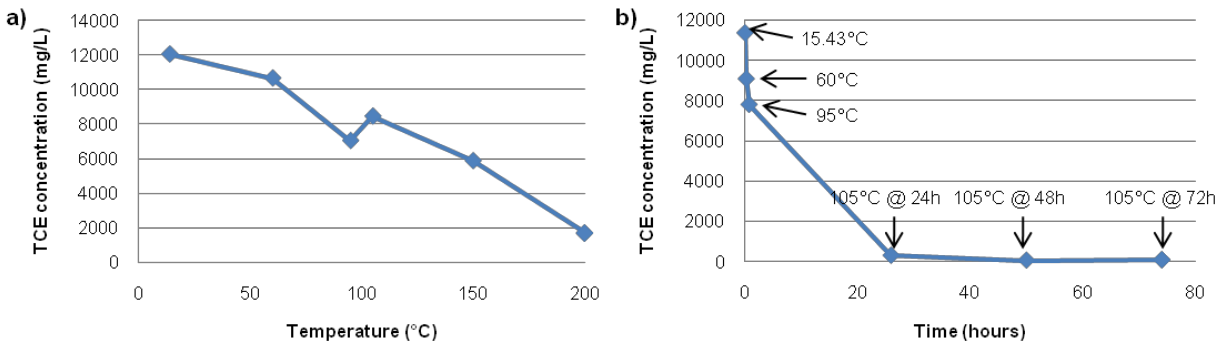


**Figure 14 – TCE concentration in siltstone during heating experiments using a) the heating temperature profile and b) the heating duration profile.**

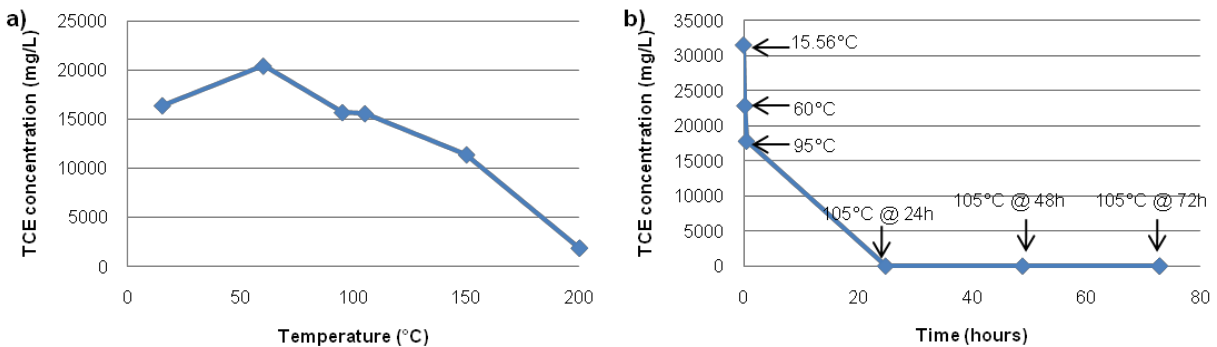


**Figure 15 – TCE concentration in limestone during heating experiments using a) the heating temperature profile and b) the heating duration profile.**

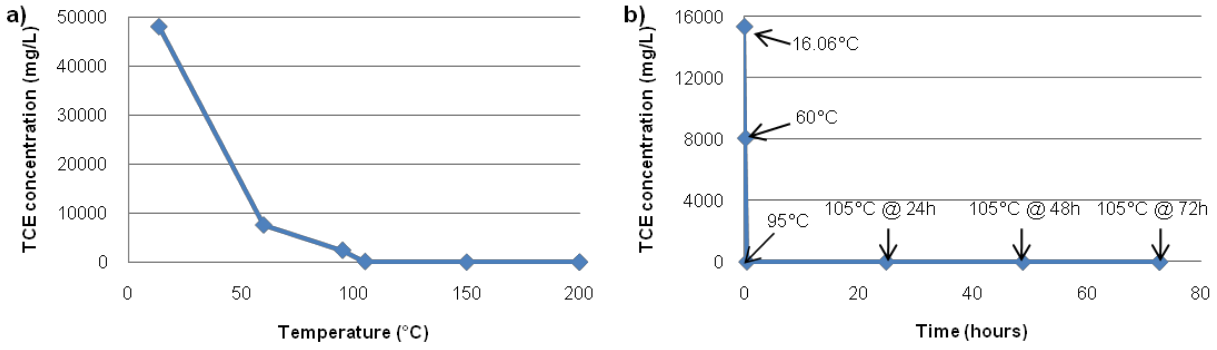


**Figure 16 – TCE concentration in sandstone during heating experiments using a) the heating temperature profile and b) the heating duration profile.**

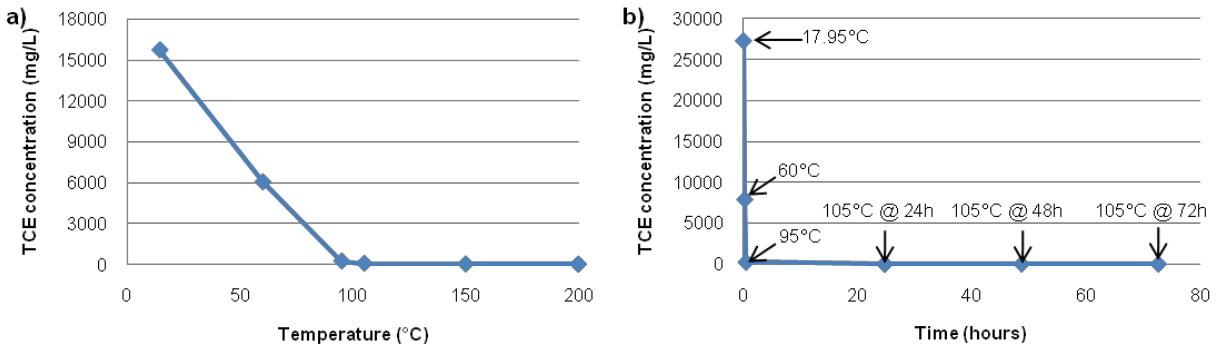


**Figure 17 – TCE concentration in dolostone during heating experiments using a) the heating temperature profile and b) the heating duration profile.**

**Results of the heating temperature profile and heating duration profile tests for PCE.**

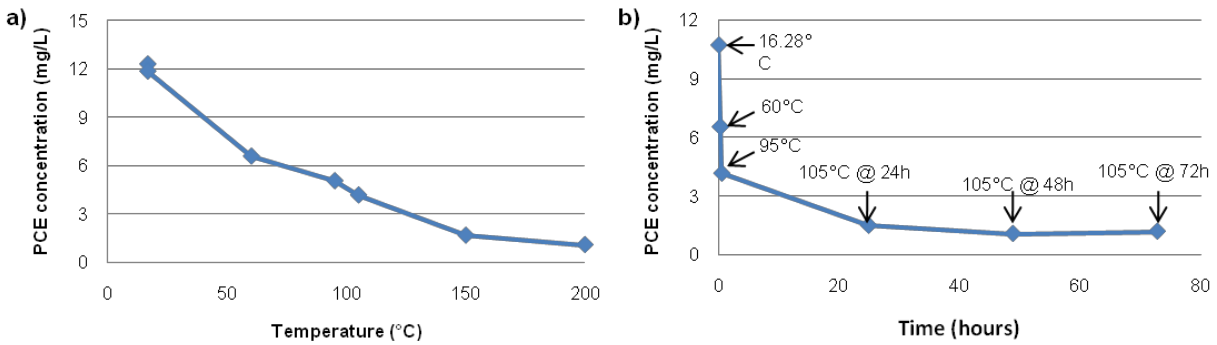


**Figure 18 – PCE concentration in red mudstone during heating experiments using a) the heating temperature profile and b) the heating duration profile.**

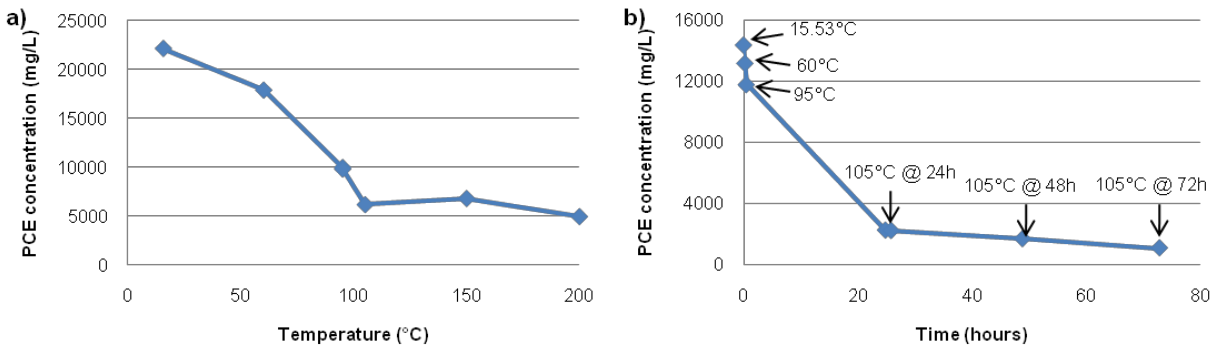


**Figure 19 – PCE concentration in gray mudstone during heating experiments using a) the heating temperature profile and b) the heating duration profile.**

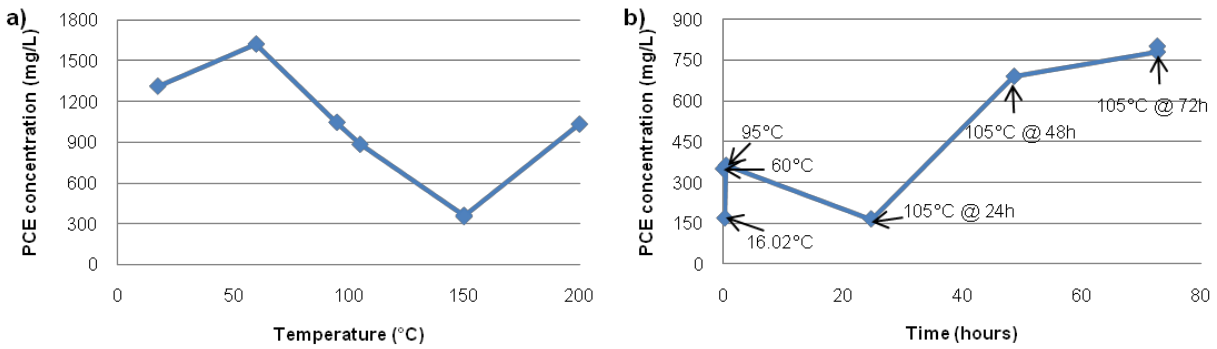


**Figure 20 – PCE concentration in black mudstone during heating experiments using a) the heating temperature profile and b) the heating duration profile.**

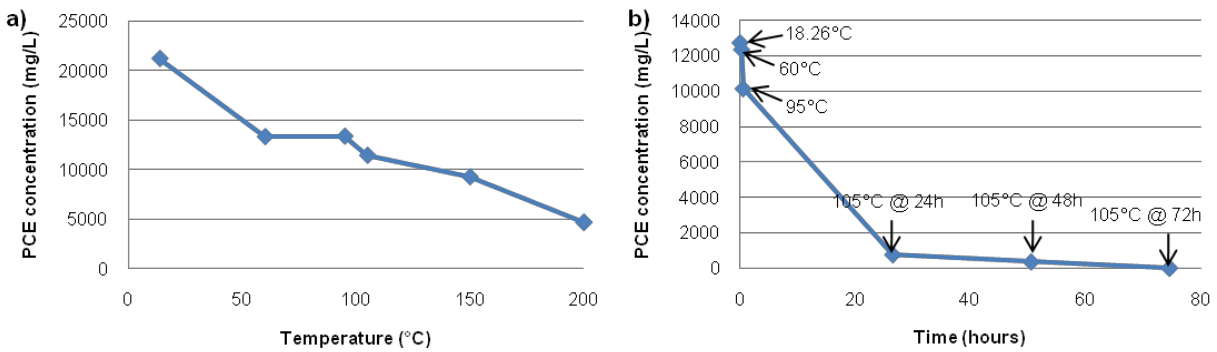


**Figure 21 – PCE concentration in siltstone during heating experiments using a) the heating temperature profile and b) the heating duration profile.**

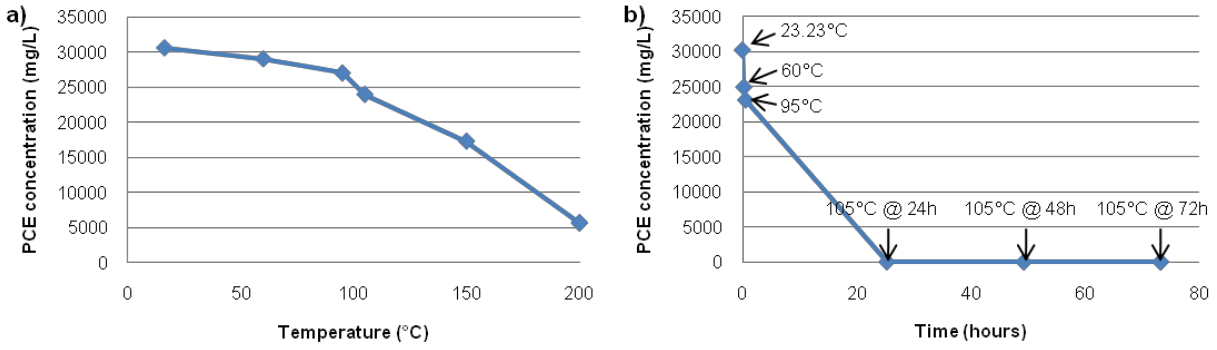


**Figure 22 – PCE concentration in limestone during heating experiments using a) the heating temperature profile and b) the heating duration profile.**

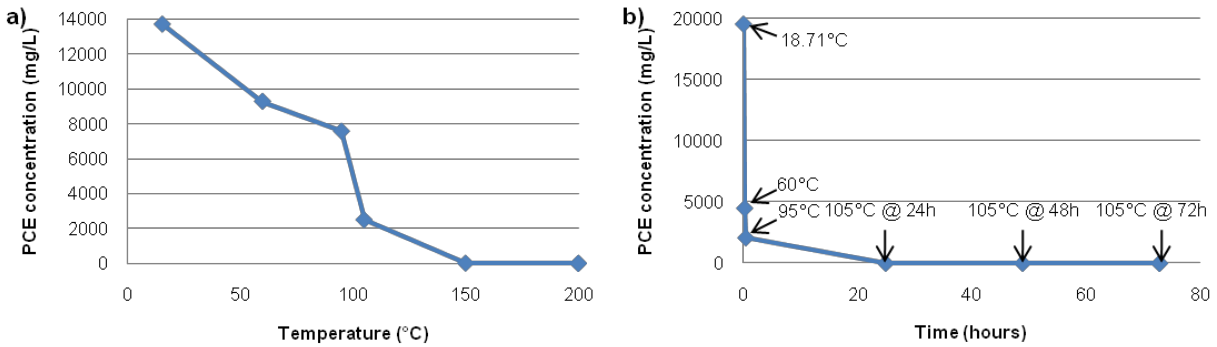


**Figure 23 – PCE concentration in sandstone during heating experiments using a) the heating temperature profile and b) the heating duration profile.**

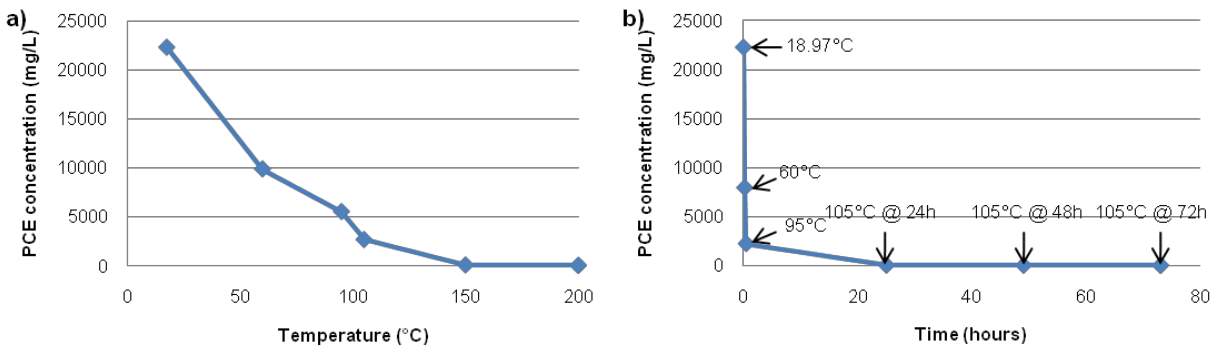


**Figure 24 – PCE concentration in dolostone during heating experiments using a) the heating temperature profile and b) the heating duration profile.**

**Temperature monitoring for the heating temperature profile and heating duration profile tests for TCE.**

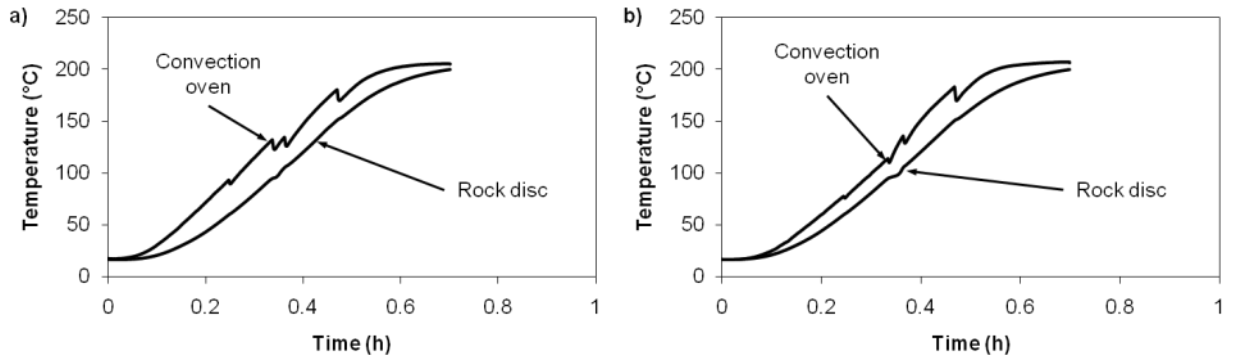


**Figure 25 – Convection oven and internal temperature of the red mudstone temperature monitoring disc, during a) the heating temperature profile and b) duplicate experiment for TCE.**

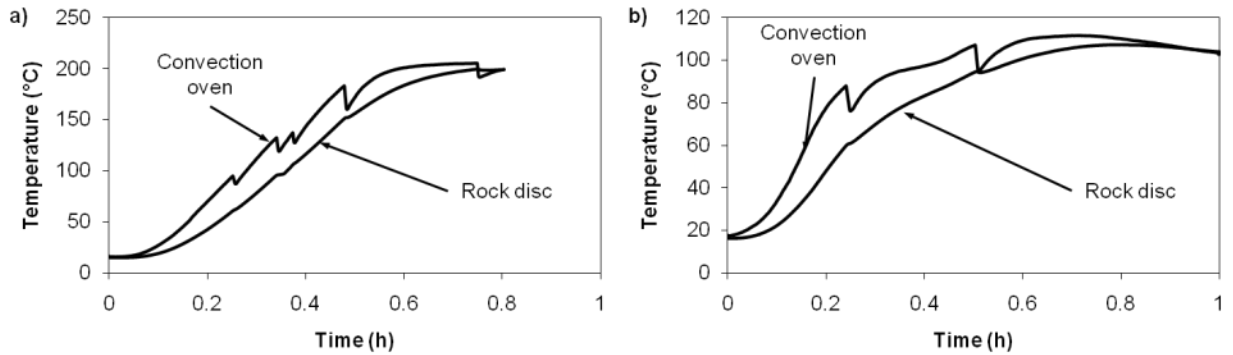


**Figure 26 – Convection oven and internal temperature of the gray mudstone temperature monitoring disc, during a) the heating temperature profile and b) the heating duration profiles tests for TCE.**

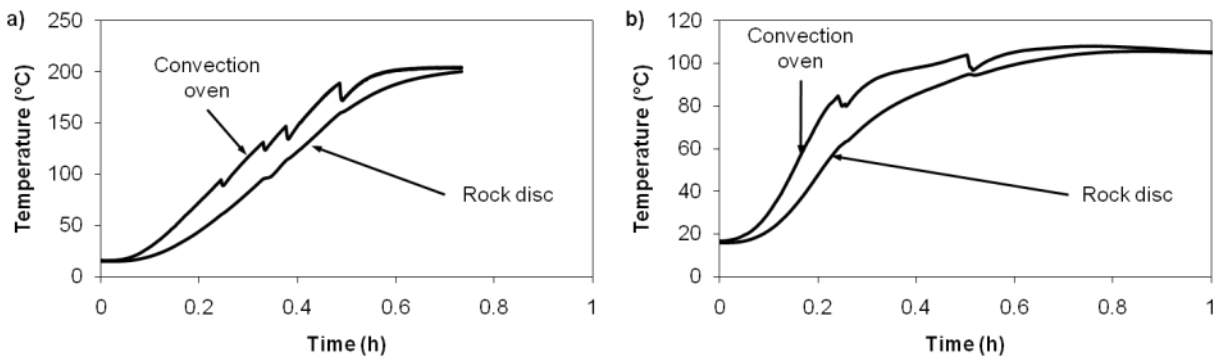


**Figure 27 – Convection oven and internal temperature of the black mudstone temperature monitoring disc, during a) the heating temperature profile and b) the heating duration profiles tests for TCE.**

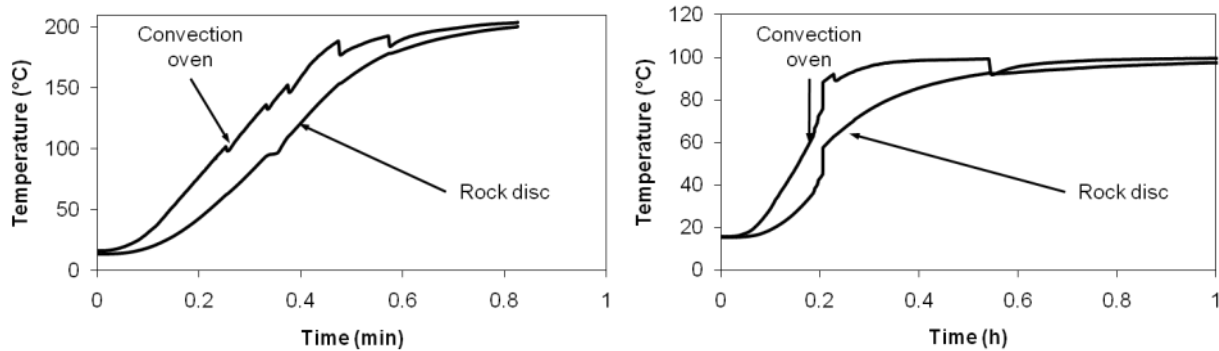


**Figure 28 – Convection oven and internal temperature of the siltstone temperature monitoring disc, during a) the heating temperature profile and b) the heating duration profiles tests for TCE.**

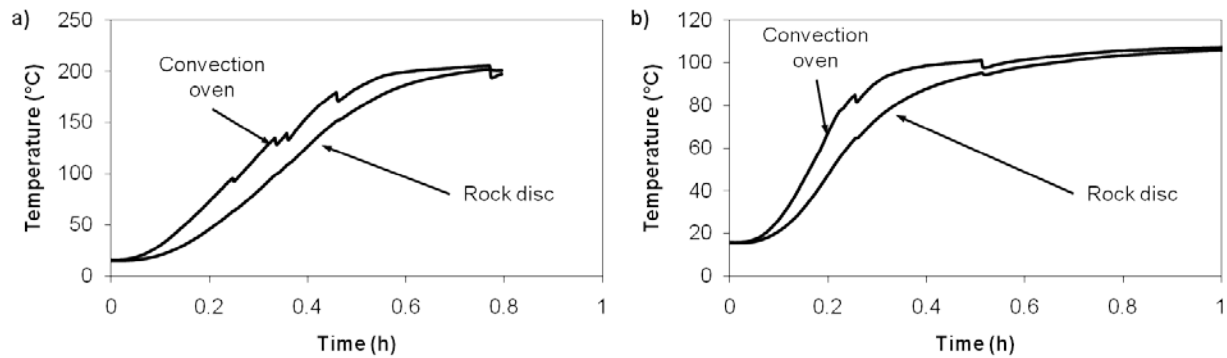


**Figure 29 – Convection oven and internal temperature of the limestone temperature monitoring disc, during a) the heating temperature profile and b) the heating duration profiles tests for TCE.**

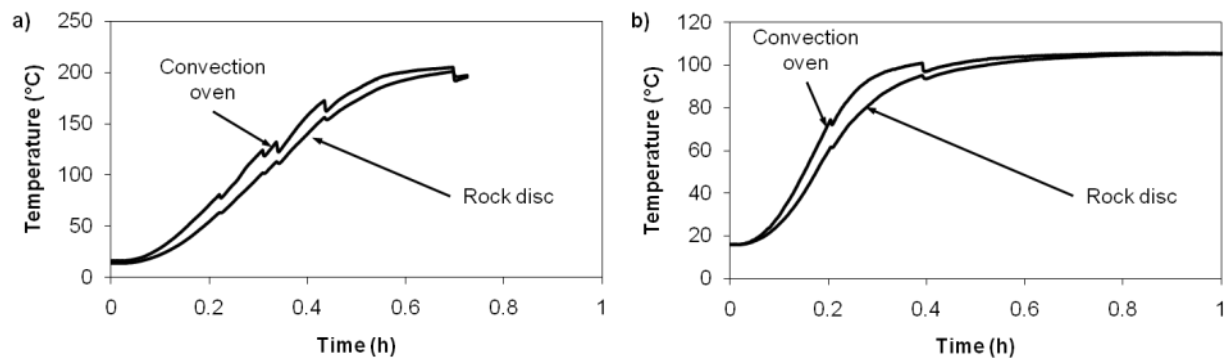


**Figure 30 – Convection oven and internal temperature of the sandstone temperature monitoring disc, during a) the heating temperature profile and b) the heating duration profiles tests for TCE.**

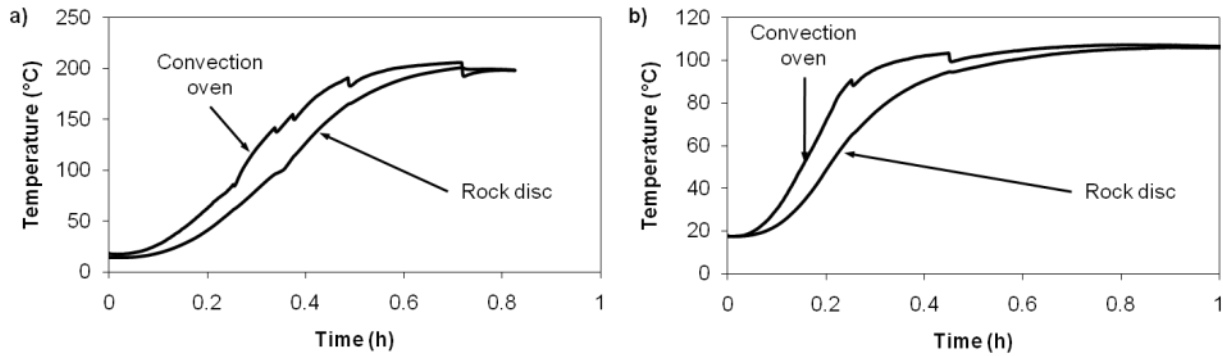


**Figure 31 – Convection oven and internal temperature of the dolostone temperature monitoring disc, during a) the heating temperature profile and b) the heating duration profiles tests for TCE.**

**Temperature monitoring for the heating temperature profile and heating duration profile tests for PCE.**

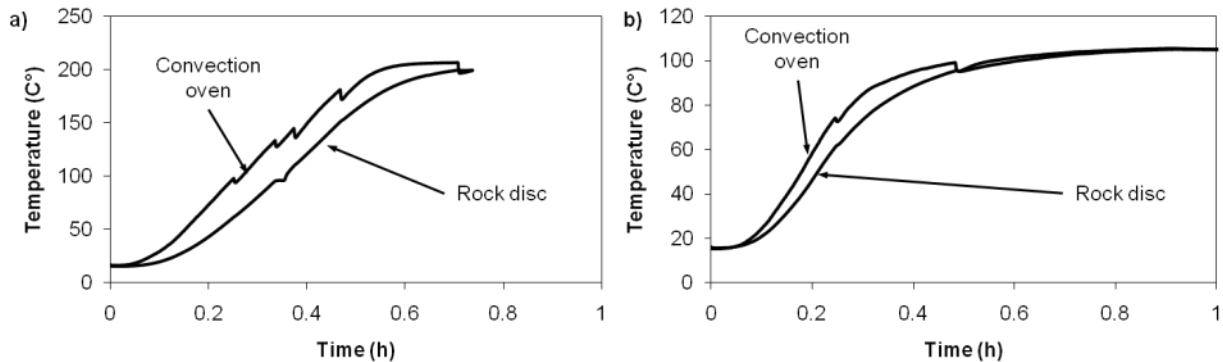


**Figure 32 – Convection oven and internal temperature of the red mudstone temperature monitoring disc, during a) the heating temperature profile and b) the heating duration profiles tests for PCE.**

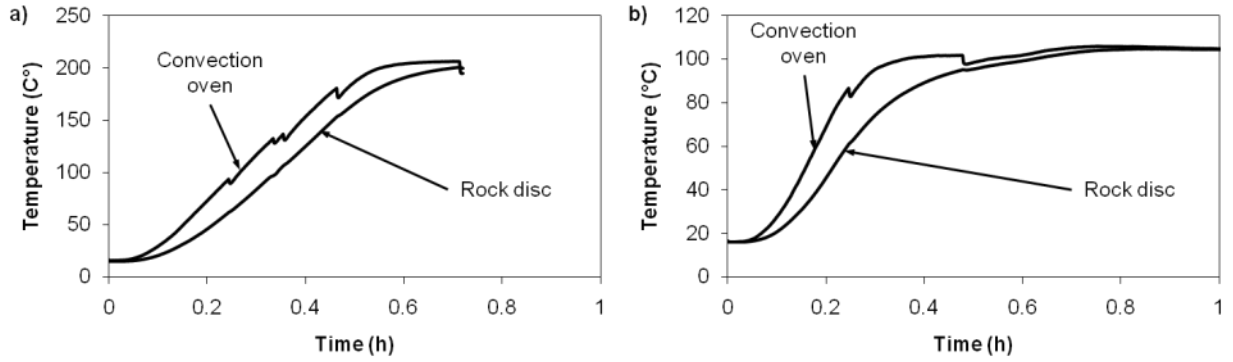


**Figure 33 – Convection oven and internal temperature of the gray mudstone temperature monitoring disc, during a) the heating temperature profile and b) the heating duration profiles tests for PCE.**

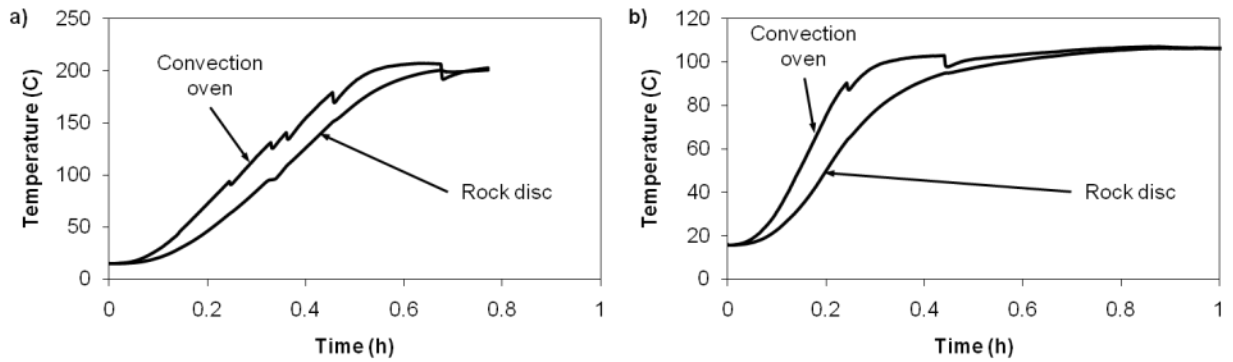


**Figure 34 – Convection oven and internal temperature of the black mudstone temperature monitoring disc, during a) the heating temperature profile and b) the heating duration profiles tests for PCE.**

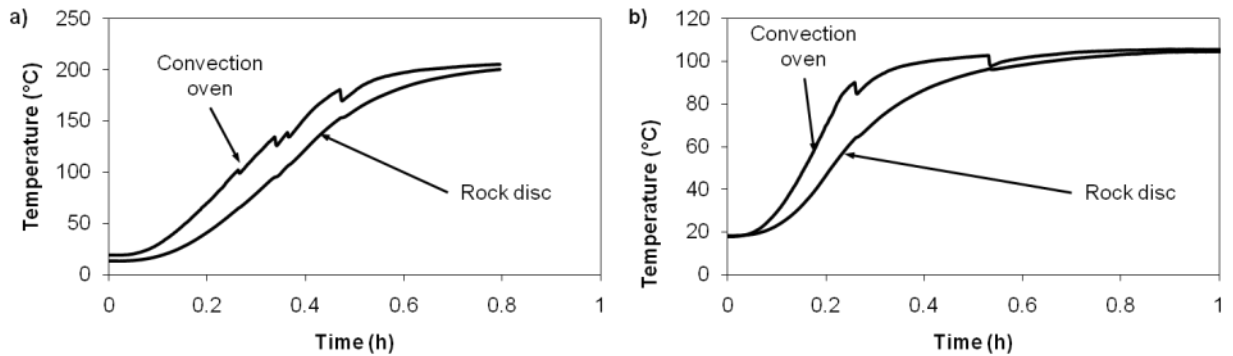


**Figure 35 – Convection oven and internal temperature of the siltstone temperature monitoring disc, during a) the heating temperature profile and b) the heating duration profiles tests for PCE.**

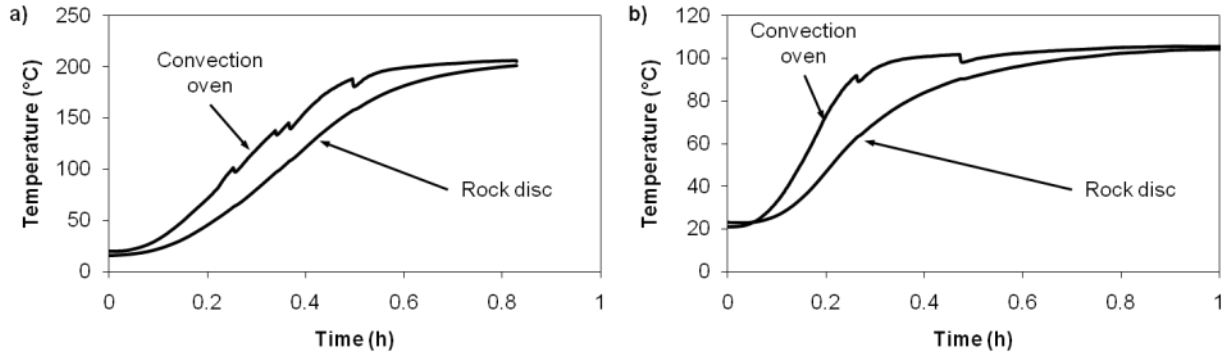


**Figure 36 – Convection oven and internal temperature of the limestone temperature monitoring disc, during a) the heating temperature profile and b) the heating duration profiles tests for PCE.**

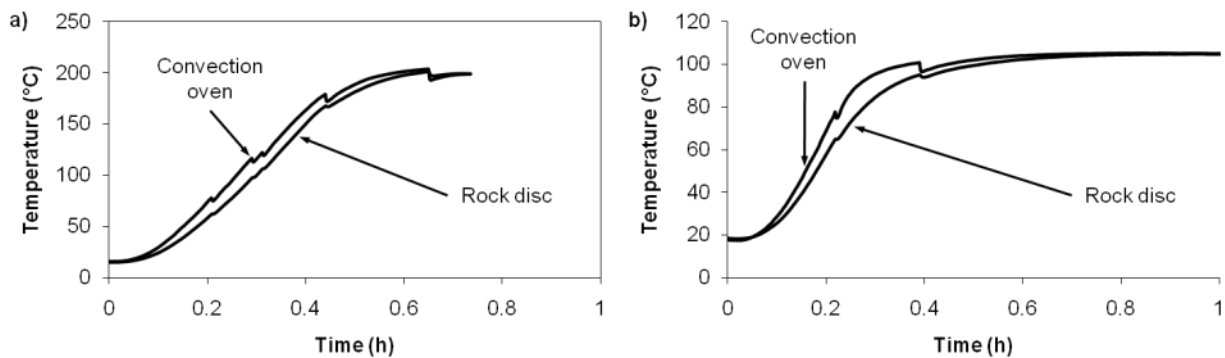


**Figure 37 – Convection oven and internal temperature of the sandstone temperature monitoring disc, during a) the heating temperature profile and b) the heating duration profiles tests for PCE.**

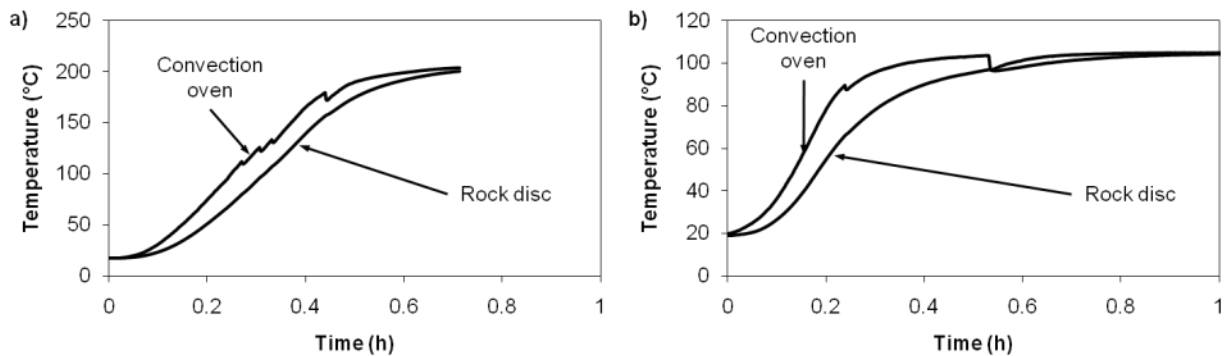


**Figure 38 – Convection oven and internal temperature of the dolostone temperature monitoring disc, during a) the heating temperature profile and b) the heating duration profiles tests for PCE.**

### Rock Analysis Results Summary (NAWC samples collected during pilot test)

Twelve 3.81 cm [1.5 inch] thick discs, of each type of rock (red mudstone, gray mudstone, black mudstone, siltstone, limestone, sandstone, dolostone) were sent for rock property analyses at PTS Laboratories in Santa Fe Springs, CA. These tests were conducted in triplicate and included measurements of dry bulk density using gravimetric method ASTM D2937-04 (ASTM, 2004a), fraction organic carbon using the Walkley-Black method EPA 9060 (USEPA, 1999), matrix porosity using mercury porosimetry method ASTM D4404-84 (ASTM, 2004b), and intrinsic permeability using method EPA 9100 (USEPA, 1986). The results of the analyses in triplicate for dry bulk density, fraction organic carbon, mercury porosimetry and intrinsic permeability are presented in Tables 1, 2, 3 and 4, respectively.

**Table 1 – Results of dry bulk density analysis**

PTS File No:	38225, 38521, 39380, 39609		PTS Laboratories
Client:	Queens University		
<b>PHYSICAL PROPERTIES DATA - DRY BULK DENSITY</b>			
PROJECT NAME:	DNAPL Removal		
PROJECT NO:	ER-0715		
		<b>METHODS:</b>	<b>API RP 40</b>
SAMPLE ID.	DEPTH, ft.	SAMPLE ORIENTATION (1)	DRY BULK DENSITY g/cm <sup>3</sup>
Red mudstone 1	287	N/A	2.59
Red mudstone 2	287	N/A	2.59
Red mudstone 3	287	N/A	2.59
Gray mudstone 1	260	N/A	2.75
Gray mudstone 2	260	N/A	2.67
Gray mudstone 3	260	N/A	2.65
Black mudstone 1	50	N/A	2.66
Black mudstone 2	50	N/A	3.10
Black mudstone 3	50	N/A	2.63
Siltstone 1	70	N/A	2.68
Siltstone 2	70	N/A	2.67
Siltstone 3	70	N/A	2.67
Limestone 1	70	N/A	2.70
Limestone 2	70	N/A	2.71
Limestone 3	70	N/A	2.71
Sandstone 1	38	V	2.58
Sandstone 2	38	V	2.51
Sandstone 3	38	V	2.44
Dolostone 1	45	V	2.68

Dolostone 2	45	V	2.65
Dolostone 3	45	V	2.59
(1) Sample Orientation: H = horizontal; V = vertical (2) Effective or Native = With as-received pore fluids in place			

**Table 2 – Results of total organic carbon analysis**

PTS File No:	38225, 38521, 39380, 39609			PTS Laboratories
Client:	Queen's University			
<b>ORGANIC CARBON DATA - TOC (foc)</b>				
PROJECT NAME:	NAWC			
PROJECT NO:	ER-0715			
		<b>METHOD:</b>	<b>WALKLEY-BLACK</b>	<b>WALKLEY-BLACK</b>
<b>SAMPLE ID.</b>	<b>DEPTH, ft.</b>	<b>SAMPLE MATRIX</b>	<b>FRACTION ORGANIC CARBON, g/g</b>	<b>TOTAL ORGANIC CARBON, mg/kg</b>
Red mudstone 1	287	SOIL	1.75E-03	1750
Red mudstone 2	287	SOIL	1.90E-03	1900
Red mudstone 3	287	SOIL	2.00E-03	2000
Gray mudstone 1	260	SOIL	4.00E-03	4000
Gray mudstone 2	260	SOIL	4.10E-03	4100
Gray mudstone 3	260	SOIL	4.15E-03	4150
Black mudstone 1	50	SOIL	7.55E-03	7550
Black mudstone 2	50	SOIL	8.65E-03	8650
Black mudstone 3	50	SOIL	9.65E-03	9650
Siltstone 1	70	SOIL	3.05E-03	3050
Siltstone 2	70	SOIL	2.40E-03	2400
Siltstone 3	70	SOIL	2.95E-03	2950
Limestone 1	70	SOIL	2.35E-03	2350
Limestone 2	70	SOIL	2.70E-03	2700
Limestone 3	70	SOIL	2.50E-03	2500
Sandstone 1	38	SOIL	9.30E-04	930
Sandstone 2	38	SOIL	2.40E-04	240
Sandstone 3	38	SOIL	6.00E-04	600
Dolostone 1	45	SOIL	1.35E-03	1350
Dolostone 2	45	SOIL	1.75E-03	1750

Dolostone 3	45	SOIL	2.30E-03	2300
-------------	----	------	----------	------

**Table 3 – Results of mercury porosimetry analysis**

PTS File No:	38225, 38521, 39380, 39609		PTS Laboratories
Client:	Queen's University		
<b>MERCURY INJECTION DATA SUMMARY</b>			
PROJECT NAME:	DNAPL Removal		
PROJECT NO:	ER-0715		
SAMPLE ID	DEPTH, feet feet	PERMEABILITY TO AIR,* md	MERCURY POROSITY, percent
Red mudstone 1	287	N/A	0.9
Red mudstone 2	287	N/A	0.8
Red mudstone 3	287	N/A	1.3
Gray mudstone 1	260	N/A	6.6
Gray mudstone 2	260	N/A	6.2
Gray mudstone 3	260	N/A	7.1
Black mudstone 1	50	N/A	0.2
Black mudstone 2	50	N/A	0.2
Black mudstone 3	50	N/A	0.1
Siltstone 1	70	N/A	0.6
Siltstone 2	70	N/A	0.6
Siltstone 3	70	N/A	0.3
Limestone 1	70	N/A	0.4
Limestone 2	70	N/A	3.2
Limestone 3	70	N/A	2.7
Sandstone 1	38	N/A	9.1
Sandstone 2	38	N/A	4.2
Sandstone 3	38	N/A	4.3
Dolostone 1	45	N/A	4.1
Dolostone 2	45	N/A	6.3
Dolostone 3	45	N/A	4.4
* After Swanson B.F., Journal of Petroleum Technology, December 1981			

**Table 4 – Results of intrinsic permeability analysis**

PTS File No:	38225, 38521, 39380, 39609		PTS Laboratories
Client:	Queen's University		
<b>PHYSICAL PROPERTIES DATA - PERMEABILITY</b>			
PROJECT NAME:	NAWC		
PROJECT NO:	ER-0715		

SAMPLE ID.	DEPTH, ft.	SAMPLE ORIENTATION (1)	500 PSI CONFINING STRESS INTRINSIC PERMEABILITY cm <sup>2</sup>
Red mudstone 1	287	V	<9.90E-15
Red mudstone 2	287	V	<9.90E-15
Red mudstone 3	260	V	<9.90E-15
Gray mudstone 1	260	V	2.66E-13
Gray mudstone 2	260	V	3.84E-13
Gray mudstone 3	260	V	4.56E-13
Black mudstone 1	50	V	5.56E-13
Black mudstone 2	50	V	6.63E-13
Black mudstone 3	50	V	8.10E-13
Siltstone 1	70	V	2.82E-12
Siltstone 2	70	V	2.47E-12
Siltstone 3	70	V	3.07E-12
Limestone 1	70	V	2.72E-14
Limestone 2	70	V	1.31E-12
Limestone 3	70	V	1.82E-12
Sandstone 1	38	V	5.40E-13
Sandstone 2	38	V	2.72E-13
Sandstone 3	38	V	2.36E-12
Dolostone 1	45	V	1.57E-10
Dolostone 2	45	V	2.56E-12
Dolostone 3	45	V	1.80E-13
(1) Sample Orientation: H = horizontal; V = vertical (2) Effective or Native = With as-received pore fluids in place			

## References

- ASTM, 2004a. Standard Test Method for Density of Soil in Place by the Drive-Cylinder Method. ASTM D2937-04. American Society for Testing and Materials (ASTM) International, West Conshohocken, Penn.
- ASTM, 2004b. Standard Test Method for Determination of Pore Volume and Pore Volume Distribution of Soil and Rock by Mercury Intrusion Porosimetry. ASTM D4404-84. American Society for Testing and Materials (ASTM) International, West Conshohocken, Penn.
- Burghardt, J.M., 2007. Laboratory study evaluating Thermo Remediation of Tetrachloroethylene impacted soil. M.Sc. Thesis, Department of Civil Engineering, Queen's University.
- USEPA, 1986. Method 9100: Saturated hydraulic conductivity, saturated leachate conductivity and intrinsic permeability. Test Methods for Evaluating Solid Waste, Physical/Chemical Methods. EPA/SW-846, Revision 0.
- USEPA, 1996. Method 8260B: Volatile Organic Compounds by Gas Chromatography/Mass Spectrometry (GC/MS). Test Methods for Evaluating Solid Waste, Physical/Chemical Methods. EPA/SW-846, Revision 2.

USEPA, 1999. Method 9060: Total Organic Carbon (TOC) in soil. Test Methods for Evaluating Solid Waste, Physical/Chemical Methods. EPA/SW-846, Revision 1.

USEPA, 2002. Method 5035A: Closed-system Purge-and-Trap and Extraction for Volatile Organics in soil and waste samples. Test Methods for Evaluating Solid Waste, Physical/Chemical Methods. EPA/SW-846, Revision 1.

**Appendix D2 – Rock Sample Physical Characterization Results (samples collected prior to pilot testing)**

**Table 1 – Results of the mercury porosimetry analysis on the red mudstone rock samples.**

PTS File No:	38225			<b>PTS</b> Laboratories
Client:	Queens University			
<b>MERCURY INJECTION SUMMARY</b>				
PROJECT NAME:	DNAPL Removal		SAMPLE ID:	Red mudstone 1
PROJECT NO:	ER-0715		DEPTH, ft.:	287
			POROSITY, %Vp:	0.9
*INJECTION PRESSURE, psia	PORE THROAT RADIUS, microns	NON-WETTING PHASE SATURATION:		WETTING PHASE SATURATION, percent
		INCREMENTAL, percent	CUMULATIVE, percent	
1.56	68.4	0.000	0.000	100.0
2.07	51.5	0.000	0.000	100.0
3.07	34.7	0.000	0.00	100.0
4.06	26.3	0.00	0.00	100.0
5.55	19.2	0.00	0.00	100.0
7.05	15.1	0.00	0.00	100.0
8.55	12.5	0.00	0.0	100.0
10.5	10.1	0.00	0.0	100.0
13.0	8.18	0.00	0.0	100.0
16.0	6.66	0.00	0.0	100.0
20.0	5.33	0.00	0.0	100.0
23.0	4.64	0.00	0.0	100.0
25.0	4.27	0.00	0.0	100.0
30.4	3.51	0.00	0.0	100.0
41.4	2.57	0.00	0.0	100.0
50.3	2.12	0.00	0.0	100.0
59.9	1.78	0.00	0.0	100.0
74.9	1.42	0.00	0.0	100.0
90.4	1.18	0.00	0.0	100.0
115	0.930	0.00	0.0	100.0
140	0.762	0.00	0.0	100.0
174	0.612	0.00	0.0	100.0
219	0.487	0.00	0.0	100.0
270	0.395	0.00	0.0	100.0

331	0.322	0.00	0.0	100.0
440	0.242	0.00	0.0	100.0
520	0.205	0.00	0.0	100.0
659	0.162	0.00	0.0	100.0
698	0.153	0.000	0.0	100.0
809	0.132	0.000	0.0	100.0
995	0.107	0.00	0.0	100.0
1240	0.086	0.000	0.0	100.0
1325	0.080	0.000	0.0	100.0
1424	0.075	0.000	0.0	100.0
1528	0.070	0.000	0.0	100.0
1626	0.066	0.000	0.0	100.0
1727	0.062	0.000	0.0	100.0
1916	0.056	0.000	0.0	100.0
2063	0.052	0.000	0.0	100.0
2214	0.048	0.000	0.0	100.0
2366	0.045	0.000	0.0	100.0
2510	0.042	0.000	0.0	100.0
2662	0.040	0.000	0.0	100.0
2711	0.039	0.000	0.0	100.0
2866	0.037	0.000	0.0	100.0
3015	0.035	0.000	0.0	100.0
3266	0.033	0.000	0.0	100.0
3498	0.030	0.000	0.0	100.0
3751	0.028	0.000	0.0	100.0
3993	0.027	0.000	0.0	100.0
4296	0.025	0.000	0.0	100.0
4523	0.024	0.000	0.0	100.0
4764	0.022	0.000	0.0	100.0
4986	0.021	0.000	0.0	100.0
5278	0.020	0.000	0.0	100.0
5488	0.019	0.000	0.0	100.0
5736	0.019	0.000	0.0	100.0
5978	0.018	0.000	0.0	100.0
6228	0.017	0.000	0.0	100.0
6478	0.016	0.000	0.0	100.0
6733	0.016	0.000	0.0	100.0
6974	0.015	0.000	0.0	100.0
7470	0.014	0.000	0.0	100.0
7968	0.013	0.000	0.0	100.0
8522	0.013	0.000	0.0	100.0
9031	0.012	0.000	0.0	100.0
9258	0.012	0.000	0.0	100.0
9602	0.011	0.000	0.0	100.0
10032	0.011	0.000	0.0	100.0
10504	0.010	0.000	0.0	100.0
11012	0.010	0.000	0.0	100.0
11482	0.009	0.000	0.0	100.0

11975	0.009	0.000	0.0	100.0
12589	0.008	0.000	0.0	100.0
13093	0.008	0.000	0.0	100.0
13616	0.008	0.000	0.0	100.0
13966	0.008	0.000	0.0	100.0
14321	0.007	0.000	0.0	100.0
14577	0.007	0.000	0.0	100.0
14991	0.007	0.000	0.0	100.0
15433	0.007	0.000	0.0	100.0
15771	0.007	0.000	0.0	100.0
16148	0.007	0.000	0.0	100.0
16670	0.006	0.000	0.0	100.0
17032	0.006	0.000	0.0	100.0
17353	0.006	0.000	0.0	100.0
17718	0.006	0.000	0.0	100.0
18094	0.006	0.000	0.0	100.0
18474	0.006	0.000	0.0	100.0
18807	0.006	0.000	0.0	100.0
19219	0.006	0.000	0.0	100.0
19790	0.005	0.000	0.0	100.0
20316	0.005	0.000	0.0	100.0
20814	0.005	0.000	0.0	100.0
21195	0.005	0.000	0.0	100.0
21662	0.005	0.000	0.0	100.0
22044	0.005	0.000	0.0	100.0
22612	0.005	0.000	0.0	100.0
23167	0.005	0.000	0.0	100.0
23727	0.004	0.000	0.0	100.0
24079	0.004	0.000	0.0	100.0
24638	0.004	0.000	0.0	100.0
24987	0.004	0.000	0.0	100.0
25417	0.004	0.000	0.0	100.0
25873	0.004	2.945	2.9	97.1
26415	0.004	5.882	8.8	91.2
26881	0.004	5.882	14.7	85.3
27344	0.004	5.882	20.6	79.4
27741	0.004	2.941	23.5	76.5
28216	0.004	2.941	26.5	73.5
28893	0.004	2.941	29.4	70.6
29435	0.004	2.941	32.4	67.6
29989	0.004	2.941	35.3	64.7
30495	0.003	0.000	35.3	64.7
30932	0.003	2.941	38.2	61.8
31325	0.003	2.941	41.2	58.8
31831	0.003	0.000	41.2	58.8
32372	0.003	2.941	44.1	55.9
32955	0.003	2.941	47.1	52.9
33486	0.003	2.941	50.0	50.0

34050	0.003	0.000	50.0	50.0
34662	0.003	2.941	52.9	47.1
35521	0.003	2.941	55.9	44.1
36224	0.003	2.941	58.8	41.2
36971	0.003	2.941	61.8	38.2
37667	0.003	2.941	64.7	35.3
38449	0.003	2.941	67.6	32.4
39199	0.003	0.000	67.6	32.4
40003	0.003	2.941	70.6	29.4
40652	0.003	0.000	70.6	29.4
41071	0.003	2.941	73.5	26.5
42524	0.003	2.941	76.5	23.5
43444	0.002	2.941	79.4	20.6
44139	0.002	0.000	79.4	20.6
45114	0.002	2.941	82.4	17.6
46517	0.002	2.941	85.3	14.7
48067	0.002	2.941	88.2	11.8
49476	0.002	2.941	91.2	8.8
50299	0.002	0.000	91.2	8.8
52872	0.002	2.941	94.1	5.9
54510	0.002	0.000	94.1	5.9
55992	0.002	2.941	97.1	2.9
57976	0.002	0.000	97.1	2.9
59954	0.002	2.941	100	0.0
* psia = pounds per square inch, absolute				



### PORE VOLUME FILLED vs PRESSURE

Mercury Pressure: 0 - 60000 psia  
(METHODOLOGY: ASTM D4404)

Project Name: NAWC  
Project No: ER-0715

Sample ID: Red mudstone 1  
Depth, ft.: 287  
Porosity, %Vp: 0.9

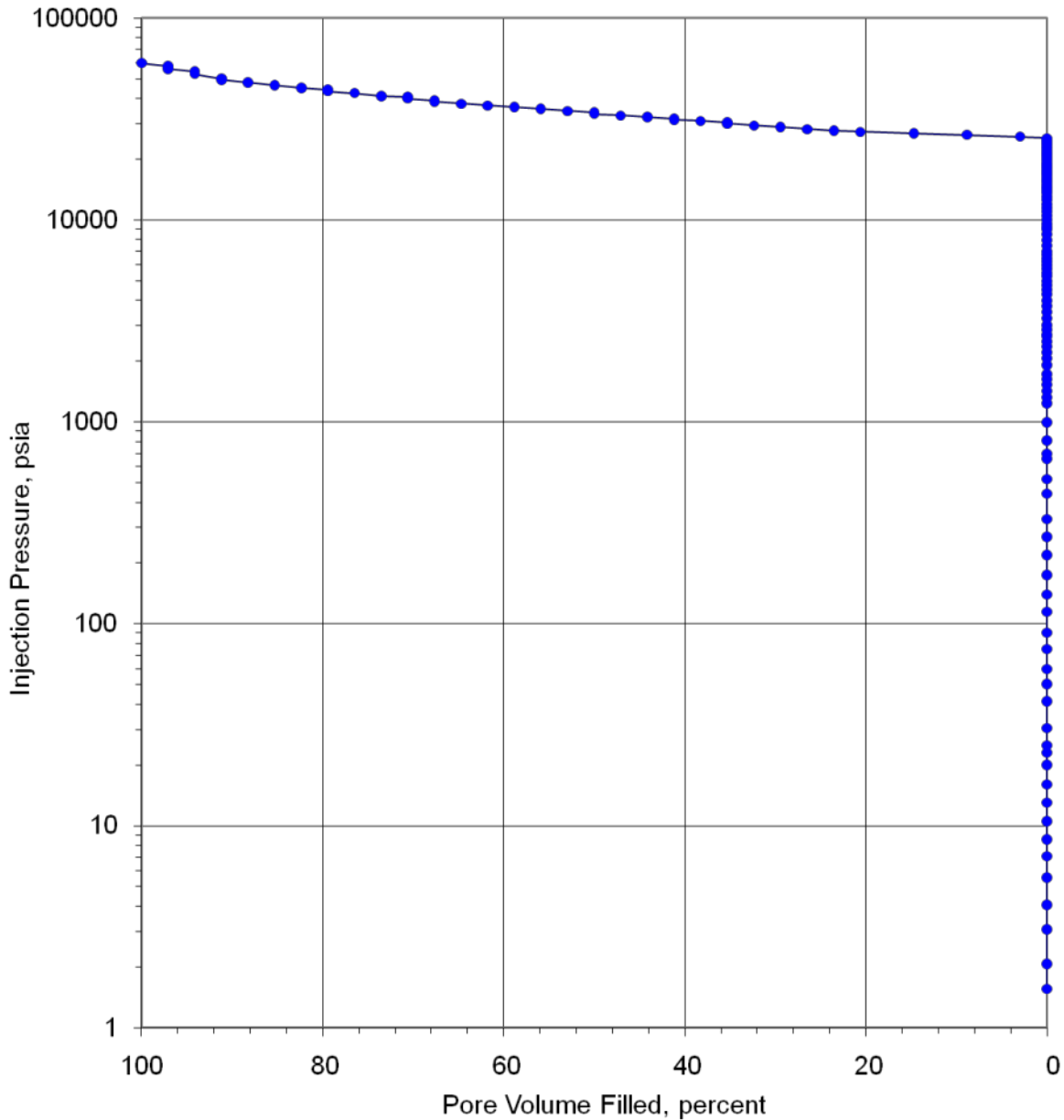


**Figure 1 – Results of the mercury porosimetry analysis on the red mudstone rock sample as pore volume filled per pressure unit.**



### CAPILLARY PRESSURE vs. WETTING PHASE SATURATION

Mercury Pressure: 0 - 60000  
(METHODOLOGY: ASTM D4404)

Project Name: NAWC  
Project No: ER-0715

Sample ID: Red mudstone 1  
Depth, ft.: 287  
Porosity, %Vp: 0.9

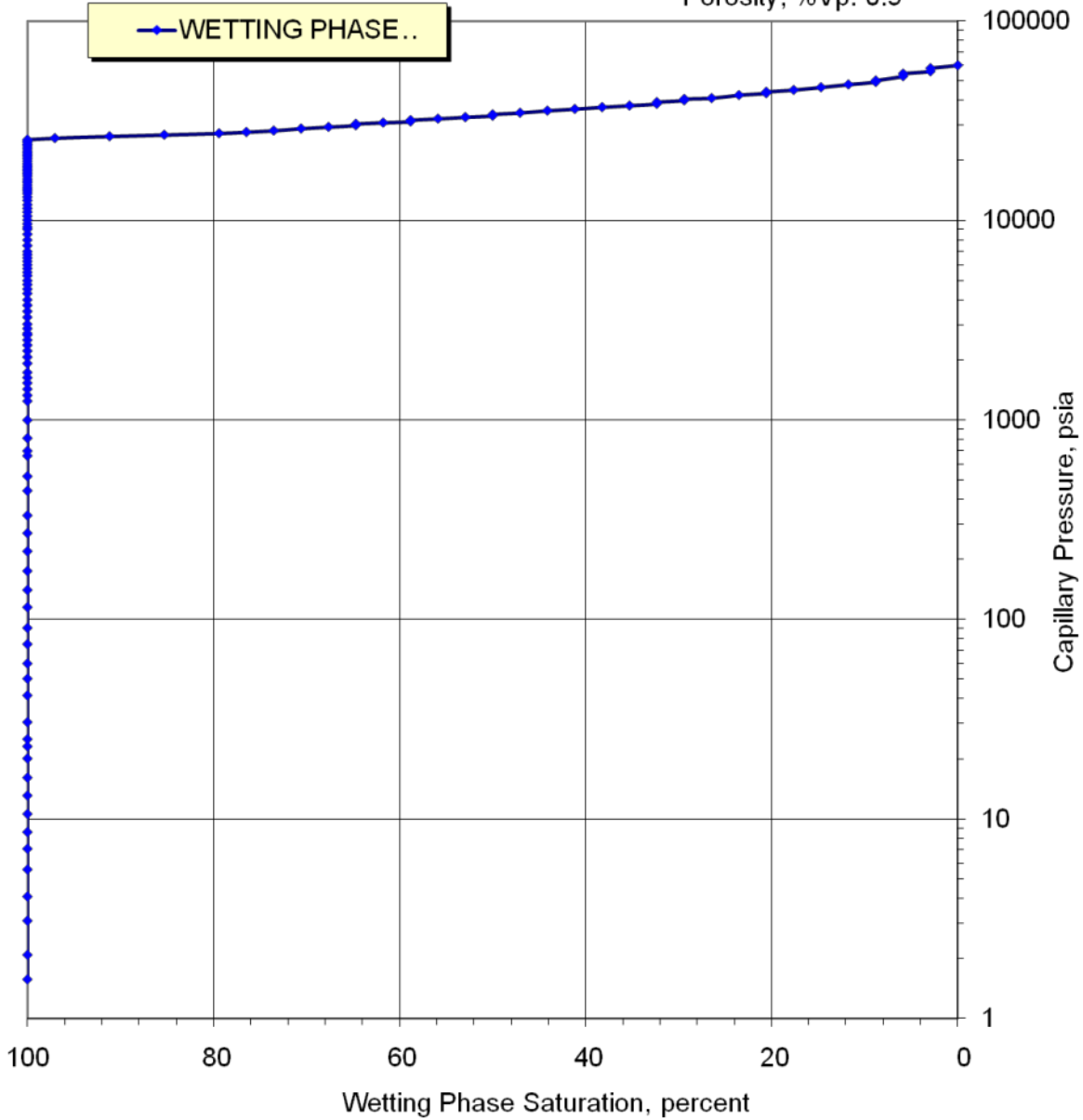


**Figure 2 – Results of the mercury porosimetry analysis on the red mudstone rock sample as wetting phase saturation per capillary pressure.**



### PORE THROAT RADIUS DISTRIBUTION

Mercury Pressure: 0 - 60000  
(METHODOLOGY: ASTM D4404)

Project Name: NAWC  
Project No:ER-0715

Sample ID: Red mudstone 1  
Depth, ft.: 287  
Porosity, %Vp: 0.9

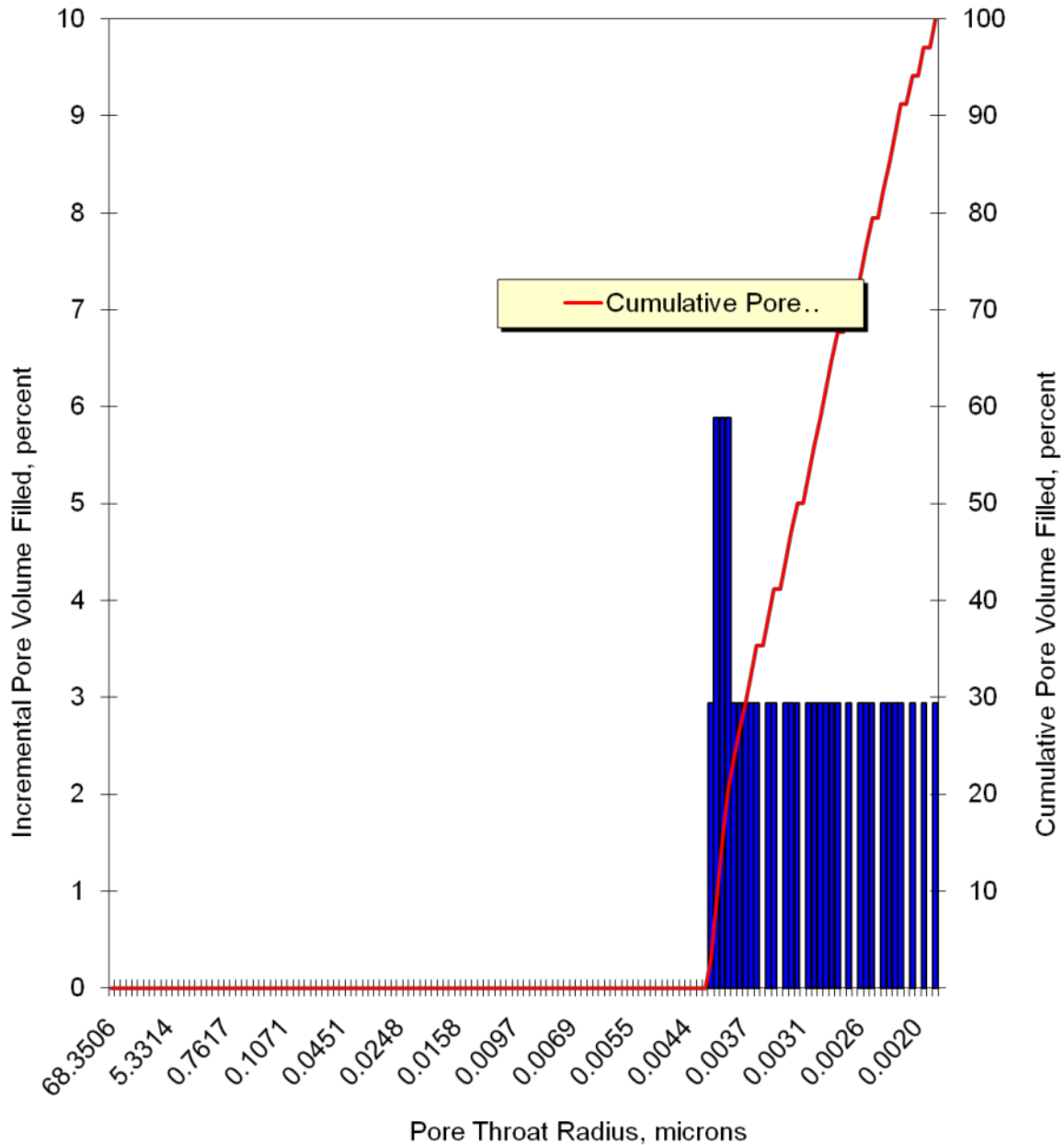


**Figure 3 – Pore throat radius distribution of the red mudstone sample during the mercury porosimetry analysis.**

**Table 2 – Results of the mercury porosimetry analysis on the duplicate red mudstone rock sample.**

PTS File No:	38225			PTS Laboratories
Client:	Queens University			
<b>MERCURY INJECTION SUMMARY</b>				
PROJECT NAME:	NAWC		SAMPLE ID:	Red mudstone 2
PROJECT NO:	ER-0715		DEPTH, ft.:	287
			POROSITY, %Vp:	0.8
*INJECTION PRESSURE, psia	PORE THROAT RADIUS, microns	NON-WETTING PHASE SATURATION:		WETTING PHASE SATURATION, percent
		INCREMENTAL, percent	CUMULATIVE, percent	
1.56	68.4	0.000	0.000	100.0
2.07	51.5	0.000	0.000	100.0
3.07	34.7	0.000	0.00	100.0
4.06	26.3	0.00	0.00	100.0
5.55	19.2	0.00	0.00	100.0
7.05	15.1	0.00	0.00	100.0
8.55	12.5	0.00	0.0	100.0
10.5	10.1	0.00	0.0	100.0
13.0	8.18	0.00	0.0	100.0
16.0	6.66	0.00	0.0	100.0
20.0	5.33	0.00	0.0	100.0
23.0	4.64	0.00	0.0	100.0
25.0	4.27	0.00	0.0	100.0
30.4	3.50	0.00	0.0	100.0
41.4	2.57	0.00	0.0	100.0
50.3	2.12	0.00	0.0	100.0
59.9	1.78	0.00	0.0	100.0
74.9	1.42	0.00	0.0	100.0
90.4	1.18	0.00	0.0	100.0
115	0.929	0.00	0.0	100.0
140	0.761	0.00	0.0	100.0
174	0.611	0.00	0.0	100.0
219	0.487	0.00	0.0	100.0
270	0.395	0.00	0.0	100.0
331	0.322	0.00	0.0	100.0
441	0.242	0.00	0.0	100.0
520	0.205	0.00	0.0	100.0
659	0.162	0.00	0.0	100.0
698	0.153	0.000	0.0	100.0
809	0.132	0.000	0.0	100.0
995	0.107	0.00	0.0	100.0
1240	0.086	0.000	0.0	100.0

1325	0.080	0.000	0.0	100.0
1424	0.075	0.000	0.0	100.0
1528	0.070	0.000	0.0	100.0
1626	0.066	0.000	0.0	100.0
1727	0.062	0.000	0.0	100.0
1916	0.056	0.000	0.0	100.0
2063	0.052	0.000	0.0	100.0
2214	0.048	0.000	0.0	100.0
2366	0.045	0.000	0.0	100.0
2510	0.042	0.000	0.0	100.0
2662	0.040	0.000	0.0	100.0
2711	0.039	0.000	0.0	100.0
2866	0.037	0.000	0.0	100.0
3015	0.035	0.000	0.0	100.0
3266	0.033	0.000	0.0	100.0
3498	0.030	0.000	0.0	100.0
3751	0.028	0.000	0.0	100.0
3993	0.027	1.663	1.7	98.3
4296	0.025	0.993	2.7	97.3
4523	0.024	0.993	3.6	96.4
4764	0.022	0.331	4.0	96.0
4986	0.021	0.993	5.0	95.0
5278	0.020	0.993	6.0	94.0
5488	0.019	0.993	7.0	93.0
5736	0.019	0.662	7.6	92.4
5978	0.018	0.662	8.3	91.7
6228	0.017	0.993	9.3	90.7
6478	0.016	0.993	10.3	89.7
6733	0.016	0.662	10.9	89.1
6974	0.015	0.662	11.6	88.4
7470	0.014	0.993	12.6	87.4
7968	0.013	0.993	13.6	86.4
8522	0.013	1.324	14.9	85.1
9031	0.012	1.324	16.2	83.8
9258	0.012	1.656	17.9	82.1
9602	0.011	2.649	20.5	79.5
10032	0.011	3.311	23.8	76.2
10504	0.010	0.000	23.8	76.2
11012	0.010	0.000	23.8	76.2
11482	0.009	3.311	27.2	72.8
11975	0.009	0.000	27.2	72.8
12588	0.008	3.311	30.5	69.5
13093	0.008	3.311	33.8	66.2
13616	0.008	0.000	33.8	66.2
13966	0.008	0.000	33.8	66.2
14321	0.007	3.311	37.1	62.9
14576	0.007	0.000	37.1	62.9
14991	0.007	3.311	40.4	59.6

15433	0.007	0.000	40.4	59.6
15771	0.007	0.000	40.4	59.6
16148	0.007	0.000	40.4	59.6
16669	0.006	3.311	43.7	56.3
17032	0.006	0.000	43.7	56.3
17353	0.006	0.000	43.7	56.3
17718	0.006	3.311	47.0	53.0
18094	0.006	0.000	47.0	53.0
18473	0.006	0.000	47.0	53.0
18805	0.006	3.311	50.3	49.7
19218	0.006	0.000	50.3	49.7
19789	0.005	0.000	50.3	49.7
20315	0.005	3.311	53.6	46.4
20812	0.005	0.000	53.6	46.4
21194	0.005	0.000	53.6	46.4
21660	0.005	3.311	57.0	43.0
22043	0.005	0.000	57.0	43.0
22611	0.005	0.000	57.0	43.0
23166	0.005	3.311	60.3	39.7
23726	0.004	0.000	60.3	39.7
24078	0.004	0.000	60.3	39.7
24636	0.004	3.311	63.6	36.4
24986	0.004	0.000	63.6	36.4
25416	0.004	3.311	66.9	33.1
25873	0.004	0.000	66.9	33.1
26415	0.004	0.000	66.9	33.1
26881	0.004	3.311	70.2	29.8
27344	0.004	0.000	70.2	29.8
27741	0.004	3.311	73.5	26.5
28216	0.004	0.000	73.5	26.5
28893	0.004	0.000	73.5	26.5
29435	0.004	3.311	76.8	23.2
29989	0.004	0.000	76.8	23.2
30495	0.003	0.000	76.8	23.2
30932	0.003	3.311	80.1	19.9
31325	0.003	0.000	80.1	19.9
31831	0.003	0.000	80.1	19.9
32372	0.003	3.311	83.4	16.6
32955	0.003	0.000	83.4	16.6
33486	0.003	0.000	83.4	16.6
34050	0.003	3.311	86.8	13.2
34662	0.003	0.000	86.8	13.2
35521	0.003	0.000	86.8	13.2
36224	0.003	3.311	90.1	9.9
36971	0.003	0.000	90.1	9.9
37667	0.003	0.000	90.1	9.9
38449	0.003	0.000	90.1	9.9
39199	0.003	3.311	93.4	6.6

40003	0.003	0.000	93.4	6.6
40652	0.003	0.000	93.4	6.6
41071	0.003	0.000	93.4	6.6
42524	0.003	3.311	96.7	3.3
43444	0.002	0.000	96.7	3.3
44139	0.002	0.000	96.7	3.3
45114	0.002	0.000	96.7	3.3
46517	0.002	3.311	100.0	0.0
48067	0.002	0.000	100.0	0.0
49476	0.002	0.000	100.0	0.0
50299	0.002	0.000	100.0	0.0
52872	0.002	0.000	100.0	0.0
54510	0.002	0.000	100.0	0.0
55992	0.002	0.000	100.0	0.0
57976	0.002	0.000	100.0	0.0
59954	0.002	0.000	100	0.0
* psia = pounds per square inch, absolute				



### PORE VOLUME FILLED vs PRESSURE

Mercury Pressure: 0 - 60000 psia  
(METHODOLOGY: ASTM D4404)

Project Name: NAWC  
Project No: ER-0715

Sample ID: Red mudstone 2  
Depth, ft.: 287  
Porosity, %Vp: 0.8

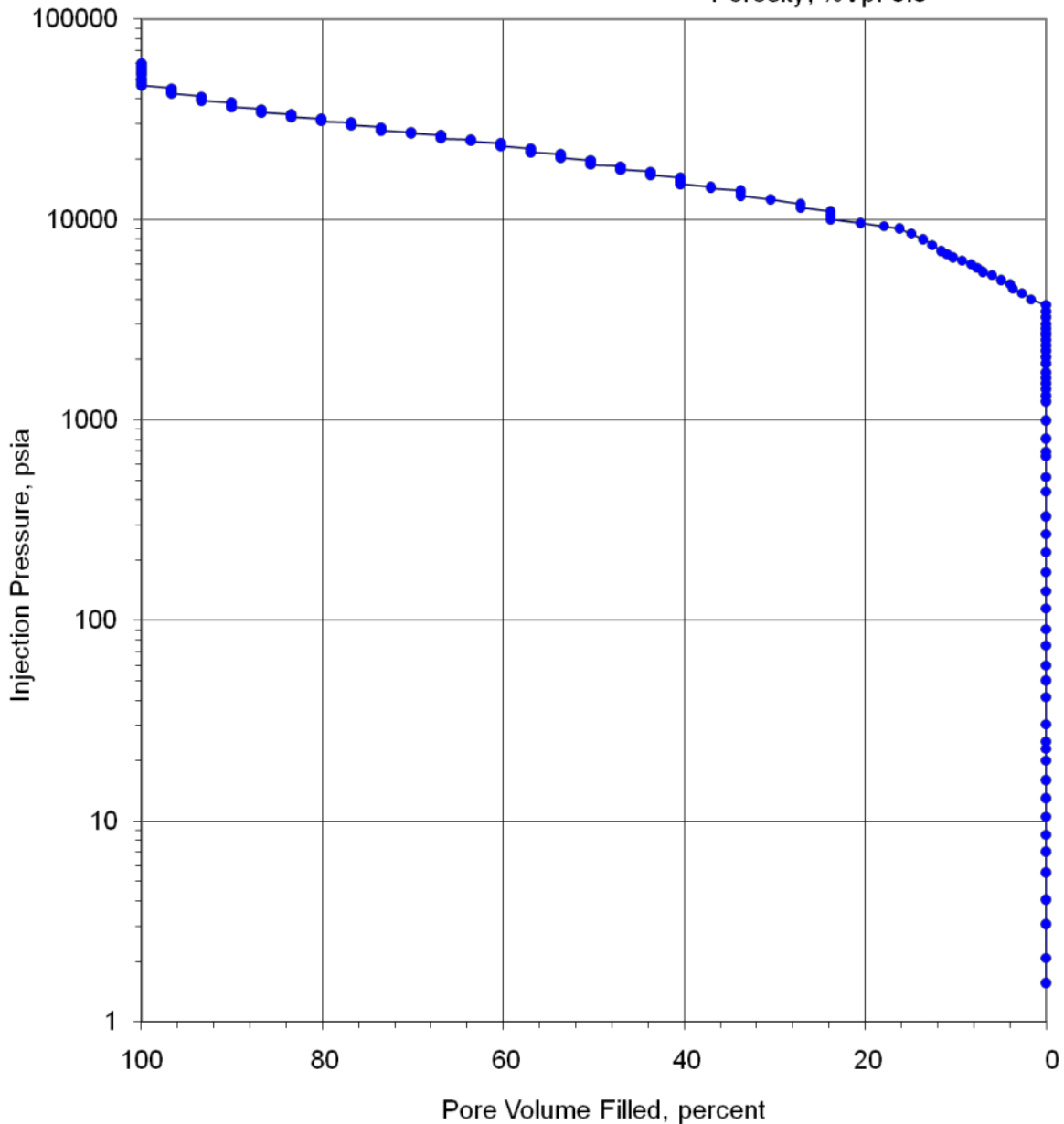


**Figure 4 – Results of the mercury porosimetry analysis on the duplicate red mudstone rock sample as pore volume filled per pressure unit.**



### CAPILLARY PRESSURE vs. WETTING PHASE SATURATION

Mercury Pressure: 0 - 60000  
(METHODOLOGY: ASTM D4404)

Project Name: NAWC  
Project No: ER-0715

Sample ID: Red mudstone 2  
Depth, ft.: 287  
Porosity, %Vp: 0.8

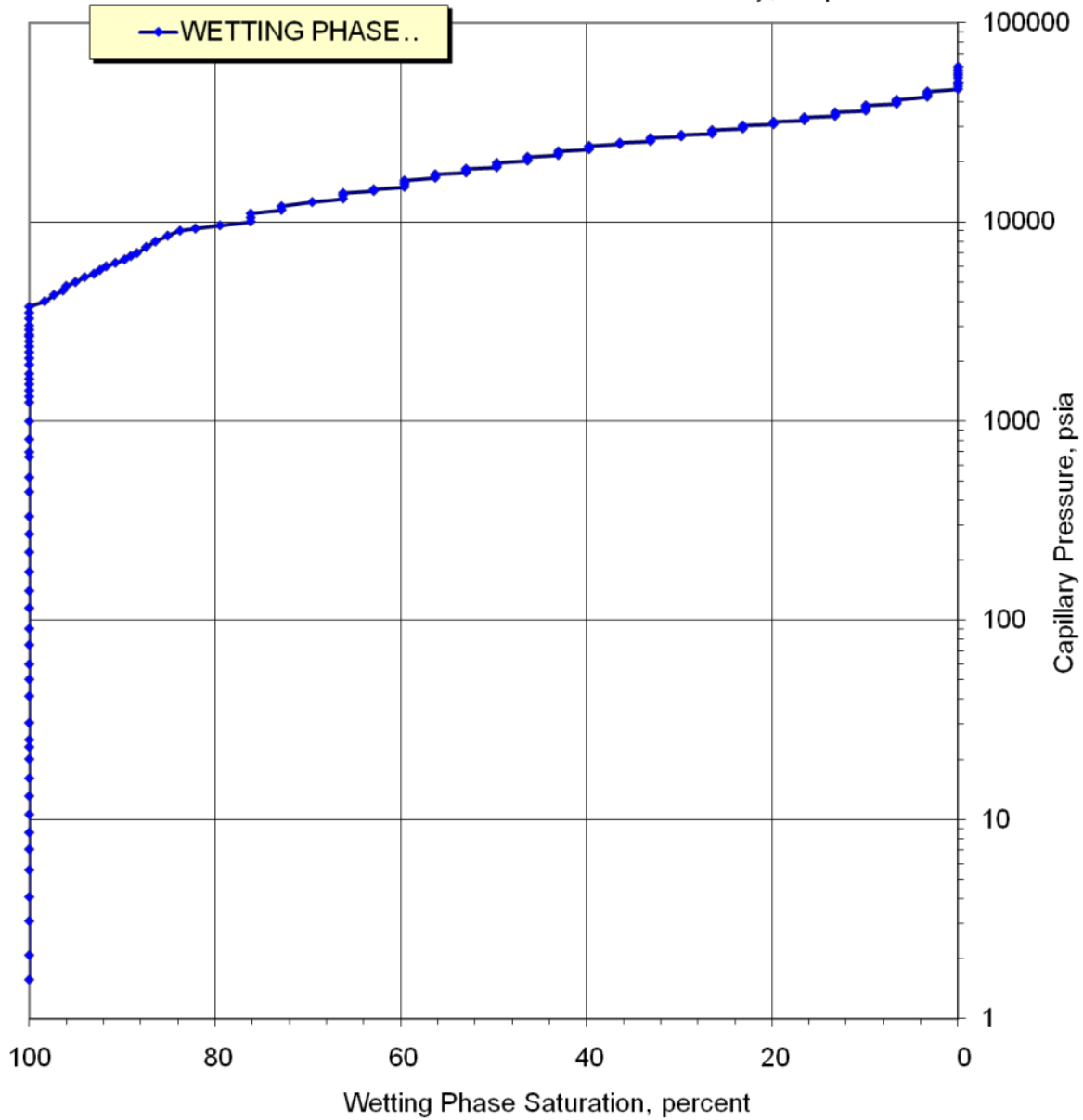


**Figure 5 – Results of the mercury porosimetry analysis on the duplicate red mudstone rock sample as wetting phase saturation per capillary pressure.**



### PORE THROAT RADIUS DISTRIBUTION

Mercury Pressure: 0 - 60000  
(METHODOLOGY: ASTM D4404)

Project Name: NAWC  
Project No: ER-0715

Sample ID: Red mudstone 2  
Depth, ft.: 287  
Porosity, %Vp: 0.8

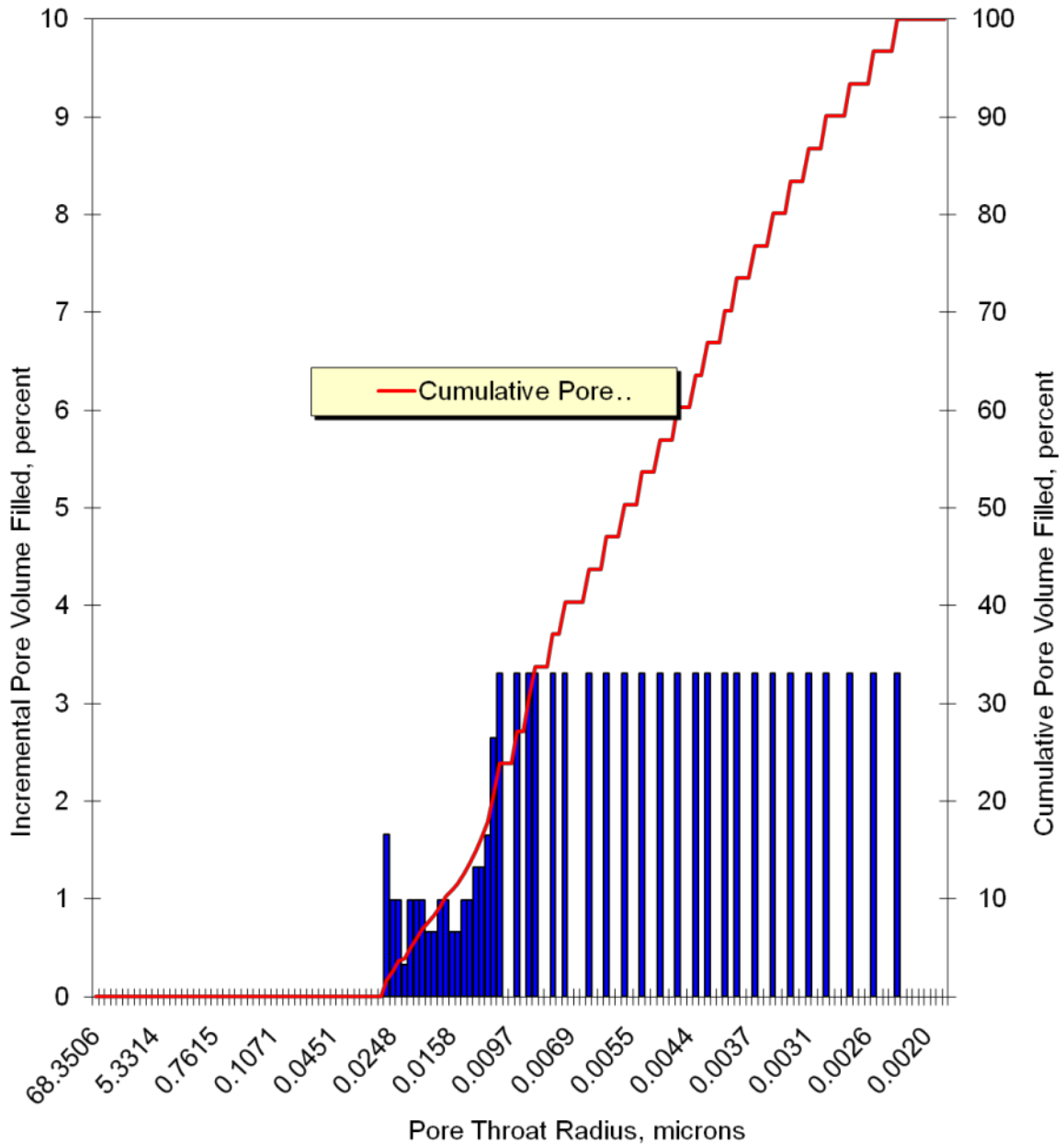


**Figure 6 – Pore throat radius distribution of the duplicate red mudstone sample during the mercury porosimetry analysis.**

**Table 3 – Results of the mercury porosimetry analysis on the triplicate red mudstone rock sample.**

PTS File No:	38225			PTS Laboratories
Client:	Queens University			
<b>MERCURY INJECTION SUMMARY</b>				
PROJECT NAME:	DNAPL Removal		SAMPLE ID:	Red mudstone 3
PROJECT NO:	ER-0715		DEPTH, ft.:	287
			POROSITY, %Vp:	1.3
*INJECTION PRESSURE, psia	PORE THROAT RADIUS, microns	NON-WETTING PHASE SATURATION:		WETTING PHASE SATURATION, percent
		INCREMENTAL, percent	CUMULATIVE, percent	
1.56	68.4	0.000	0.000	100.0
2.07	51.5	0.000	0.000	100.0
3.07	34.7	0.000	0.00	100.0
4.06	26.3	0.00	0.00	100.0
5.55	19.2	0.00	0.00	100.0
7.05	15.1	0.00	0.00	100.0
8.55	12.5	0.00	0.0	100.0
10.5	10.1	0.00	0.0	100.0
13.0	8.18	0.00	0.0	100.0
16.0	6.66	0.00	0.0	100.0
20.0	5.33	0.00	0.0	100.0
23.0	4.64	0.00	0.0	100.0
25.0	4.27	0.00	0.0	100.0
29.9	3.56	0.00	0.0	100.0
40.6	2.62	0.00	0.0	100.0
50.0	2.13	0.00	0.0	100.0
59.8	1.78	0.00	0.0	100.0
75.2	1.42	0.00	0.0	100.0
90.4	1.18	0.00	0.0	100.0
115	0.931	0.00	0.0	100.0
140	0.764	0.00	0.0	100.0
174	0.611	0.00	0.0	100.0
219	0.486	0.00	0.0	100.0
271	0.393	0.00	0.0	100.0
329	0.324	0.00	0.0	100.0
440	0.242	0.00	0.0	100.0
521	0.205	0.00	0.0	100.0
652	0.164	0.00	0.0	100.0
699	0.152	0.000	0.0	100.0
797	0.134	0.000	0.0	100.0
1030	0.103	0.00	0.0	100.0
1241	0.086	0.000	0.0	100.0
1328	0.080	0.000	0.0	100.0

1419	0.075	0.000	0.0	100.0
1526	0.070	0.000	0.0	100.0
1627	0.066	0.000	0.0	100.0
1718	0.062	0.000	0.0	100.0
1930	0.055	0.000	0.0	100.0
2084	0.051	0.000	0.0	100.0
2240	0.048	0.000	0.0	100.0
2382	0.045	0.000	0.0	100.0
2522	0.042	0.000	0.0	100.0
2671	0.040	0.000	0.0	100.0
2722	0.039	0.000	0.0	100.0
2868	0.037	0.000	0.0	100.0
3021	0.035	0.000	0.0	100.0
3271	0.033	0.000	0.0	100.0
3515	0.030	0.000	0.0	100.0
3750	0.028	0.000	0.0	100.0
4002	0.027	0.000	0.0	100.0
4304	0.025	0.000	0.0	100.0
4547	0.023	0.000	0.0	100.0
4762	0.022	0.000	0.0	100.0
4995	0.021	0.000	0.0	100.0
5302	0.020	1.610	1.6	98.4
5480	0.019	1.014	2.6	97.4
5741	0.019	1.014	3.6	96.4
5987	0.018	0.811	4.4	95.6
6235	0.017	0.406	4.9	95.1
6476	0.016	0.811	5.7	94.3
6723	0.016	0.811	6.5	93.5
6970	0.015	0.203	6.7	93.3
7471	0.014	1.014	7.7	92.3
7967	0.013	1.014	8.7	91.3
8515	0.013	1.014	9.7	90.3
8996	0.012	1.014	10.7	89.3
9307	0.011	1.014	11.8	88.2
9604	0.011	1.014	12.8	87.2
10054	0.011	1.014	13.8	86.2
10474	0.010	1.014	14.8	85.2
10990	0.010	1.014	15.8	84.2
11486	0.009	1.014	16.8	83.2
11985	0.009	1.014	17.8	82.2
12571	0.008	1.014	18.9	81.1
13086	0.008	2.029	20.9	79.1
13632	0.008	1.014	21.9	78.1
13968	0.008	1.014	22.9	77.1
14323	0.007	1.014	23.9	76.1
14564	0.007	1.014	24.9	75.1
14954	0.007	1.014	26.0	74.0
15417	0.007	1.014	27.0	73.0

15734	0.007	2.029	29.0	71.0
16141	0.007	1.014	30.0	70.0
16688	0.006	1.014	31.0	69.0
17035	0.006	2.029	33.1	66.9
17374	0.006	1.014	34.1	65.9
17727	0.006	1.014	35.1	64.9
18143	0.006	1.014	36.1	63.9
18467	0.006	1.014	37.1	62.9
18799	0.006	1.014	38.1	61.9
19195	0.006	1.014	39.1	60.9
19806	0.005	2.029	41.2	58.8
20287	0.005	1.014	42.2	57.8
20738	0.005	1.014	43.2	56.8
21192	0.005	2.029	45.2	54.8
21678	0.005	2.029	47.3	52.7
22016	0.005	1.014	48.3	51.7
22652	0.005	1.014	49.3	50.7
23176	0.005	2.029	51.3	48.7
23703	0.004	1.014	52.3	47.7
24097	0.004	1.014	53.3	46.7
24622	0.004	2.029	55.4	44.6
25011	0.004	2.029	57.4	42.6
25445	0.004	0.000	57.4	42.6
25867	0.004	2.029	59.4	40.6
26420	0.004	0.000	59.4	40.6
26904	0.004	2.029	61.5	38.5
27323	0.004	0.000	61.5	38.5
27732	0.004	2.029	63.5	36.5
28227	0.004	0.000	63.5	36.5
28934	0.004	2.029	65.5	34.5
29457	0.004	0.000	65.5	34.5
30008	0.004	2.029	67.5	32.5
30534	0.003	0.000	67.5	32.5
30942	0.003	0.000	67.5	32.5
31326	0.003	1.014	68.6	31.4
31863	0.003	1.014	69.6	30.4
32392	0.003	2.029	71.6	28.4
32919	0.003	0.811	72.4	27.6
33538	0.003	0.811	73.2	26.8
34082	0.003	0.406	73.6	26.4
34564	0.003	2.029	75.7	24.3
35536	0.003	2.029	77.7	22.3
36243	0.003	2.029	79.7	20.3
36983	0.003	2.029	81.7	18.3
37658	0.003	2.029	83.8	16.2
38452	0.003	0.000	83.8	16.2
39217	0.003	0.000	83.8	16.2
40112	0.003	2.029	85.8	14.2

40571	0.003	0.000	85.8	14.2
41117	0.003	2.029	87.8	12.2
42602	0.003	0.000	87.8	12.2
43439	0.002	2.029	89.9	10.1
44147	0.002	0.000	89.9	10.1
45113	0.002	2.029	91.9	8.1
46503	0.002	0.000	91.9	8.1
48006	0.002	2.029	93.9	6.1
49457	0.002	0.000	93.9	6.1
50202	0.002	0.000	93.9	6.1
53020	0.002	2.029	95.9	4.1
54530	0.002	2.029	98.0	2.0
56023	0.002	0.000	98.0	2.0
57930	0.002	0.000	98.0	2.0
60021	0.002	2.029	100	0.0

\* psia = pounds per square inch, absolute



Queens University  
PTS File No: 38225

### PORE VOLUME FILLED vs PRESSURE

Mercury Pressure: 0 - 60000 psia  
(METHODOLOGY: ASTM D4404)

Project Name: NAWC  
Project No: ER-0715

Sample ID: Red mudstone 3  
Depth, ft.: 287  
Porosity, %Vp: 1.3

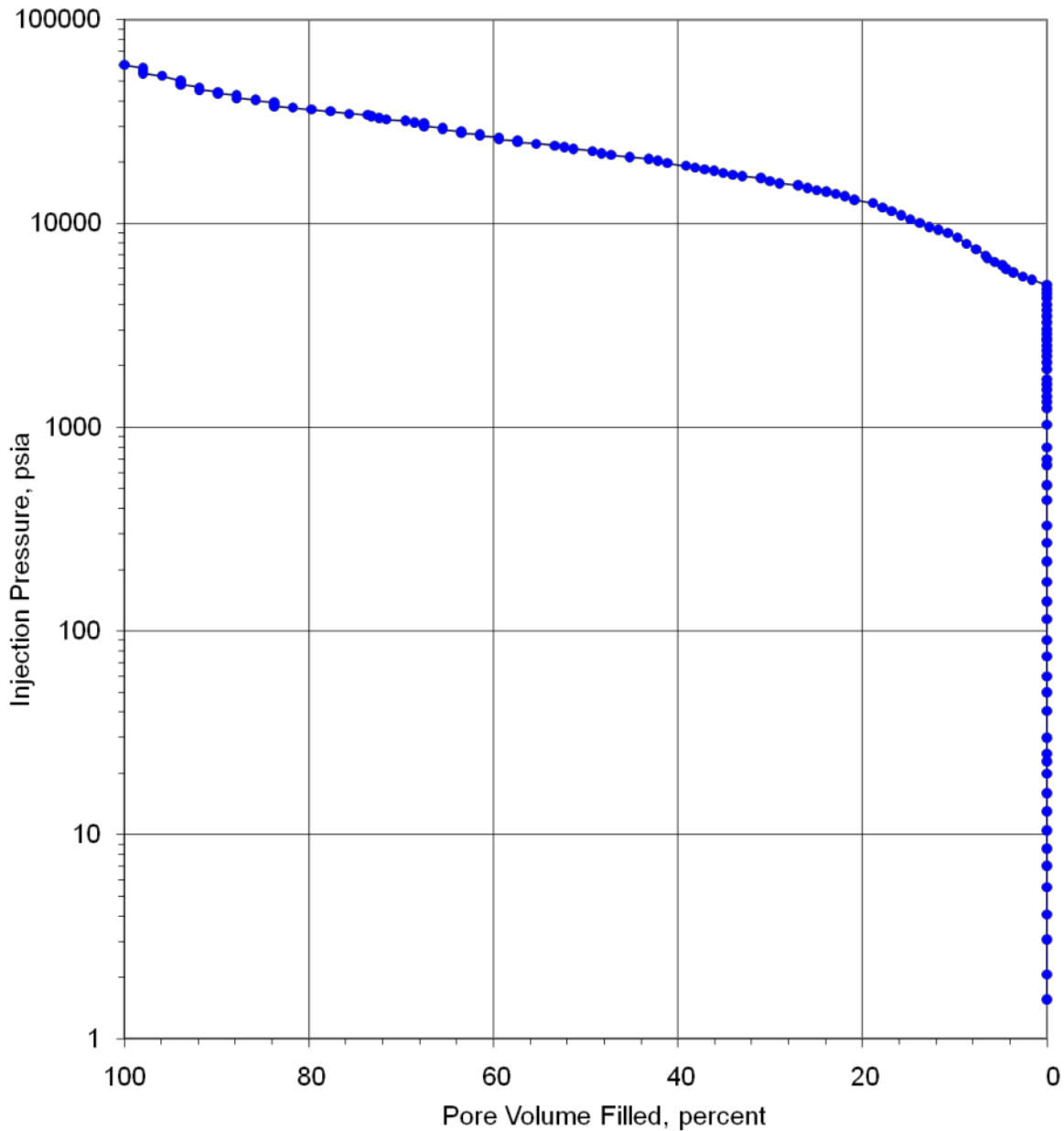


**Figure 7 – Results of the mercury porosimetry analysis on the triplicate red mudstone rock sample as pore volume filled per pressure unit.**



Queens University  
PTS File No: 38225

### CAPILLARY PRESSURE vs. WETTING PHASE SATURATION

Mercury Pressure: 0 - 60000  
(METHODOLOGY: ASTM D4404)

Project Name: NAWC  
Project No: ER-0715

Sample ID: Red mudstone 3  
Depth, ft.: 287  
Porosity, %Vp: 1.3

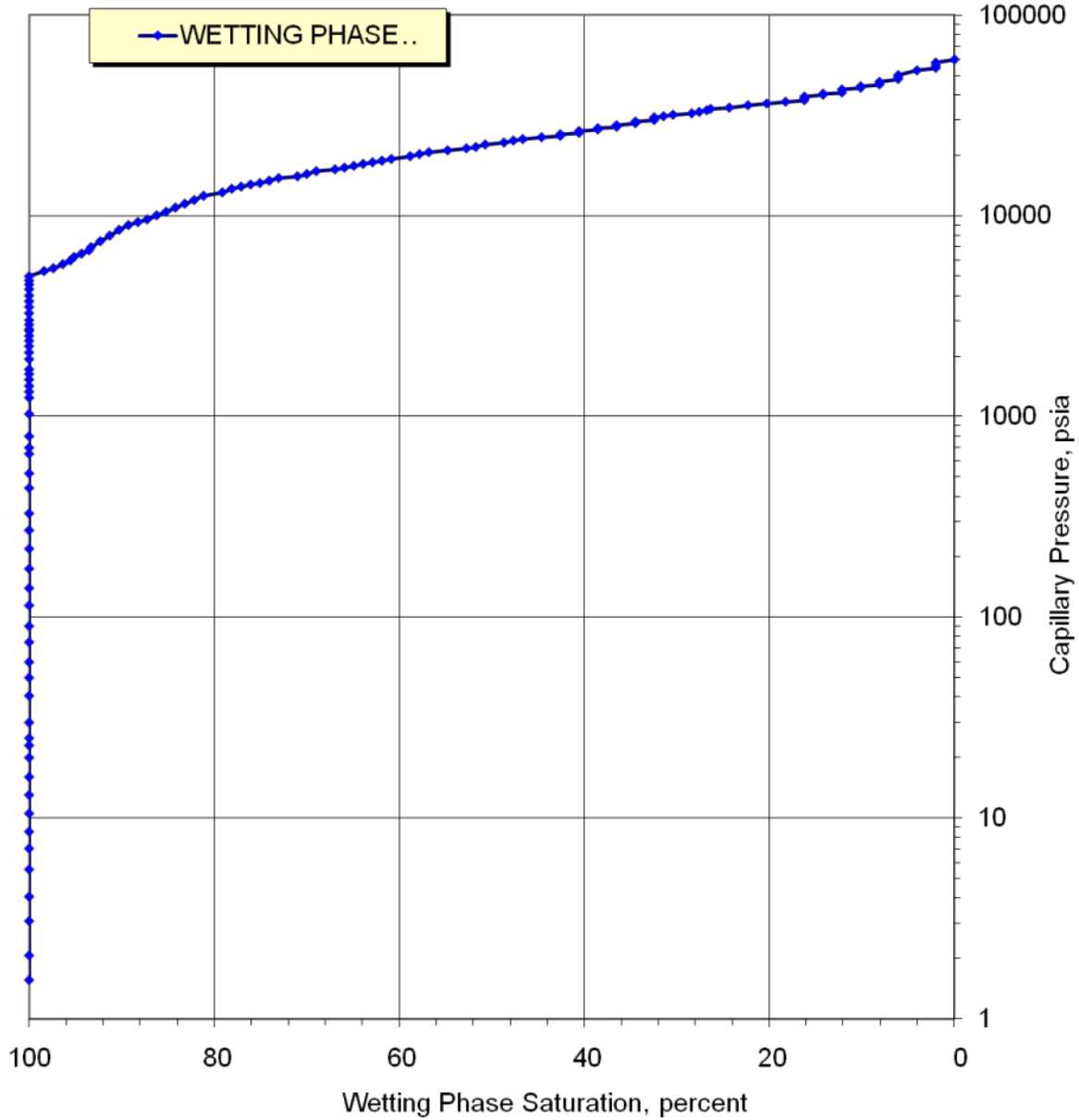


***Figure 8 – Results of the mercury injection during the mercury porosimetry analysis on the triplicate red mudstone rock sample as wetting phase saturation per capillary pressure.***



### PORE THROAT RADIUS DISTRIBUTION

Mercury Pressure: 0 - 60000  
(METHODOLOGY: ASTM D4404)

Project Name: NAWC  
Project No: ER-0715

Sample ID: Red mudstone 3  
Depth, ft.: 287  
Porosity, %Vp: 1.3

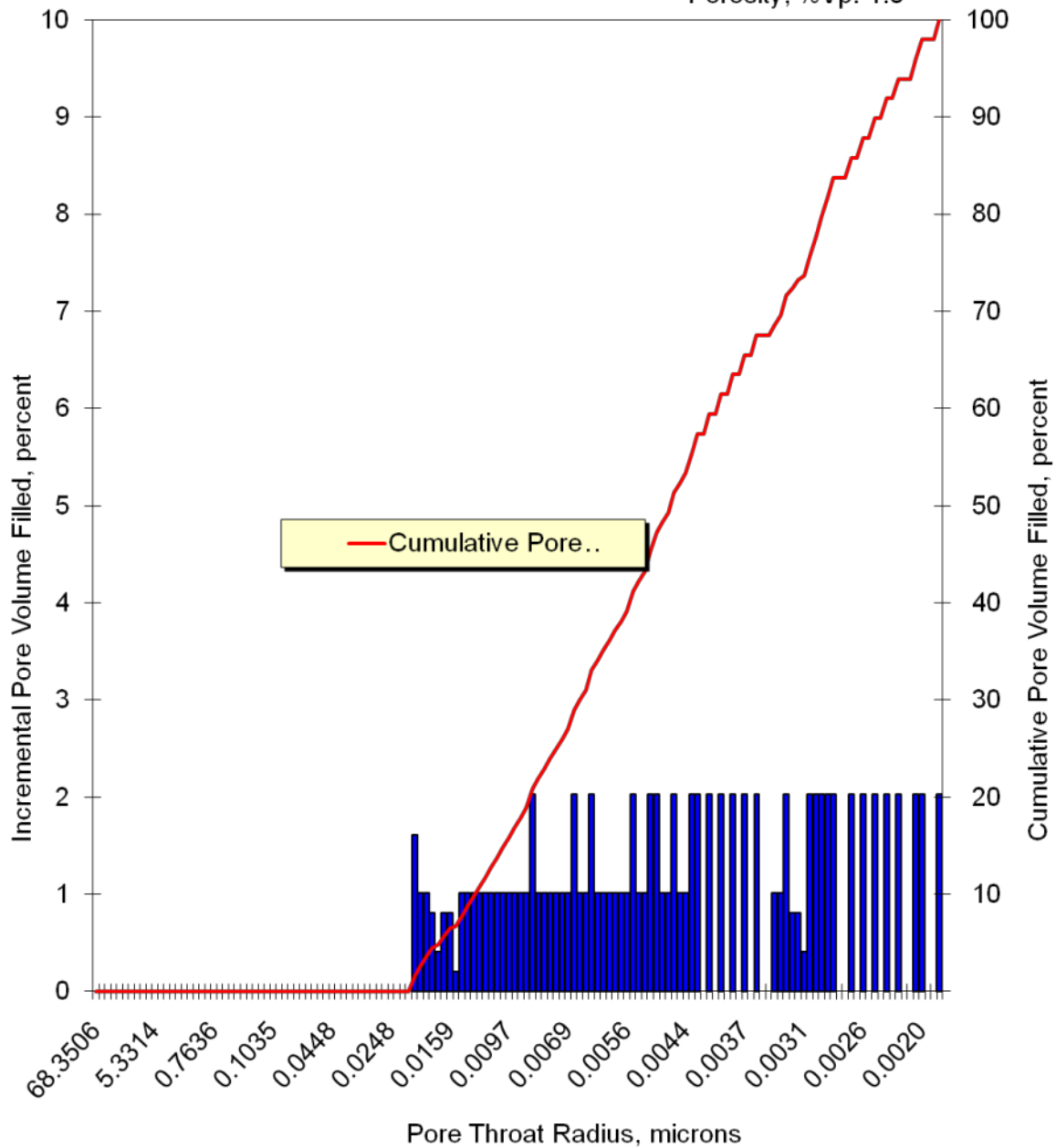


**Figure 9 – Pore throat radius distribution of the triplicate red mudstone sample during the mercury porosimetry analysis.**

**Table 4 – Results of the hg porosimetry analysis on the gray mudstone rock sample.**

PTS File No:	38521			<b>PTS</b>
Client:	Queen's University			Laboratories
<b>MERCURY INJECTION SUMMARY</b>				
PROJECT NAME:	NAWC		Sample ID:	Gray mudstone 1
PROJECT NO:	ER-0715		Depth, ft.:	260
			Porosity, %Vp:	6.6
*INJECTION PRESSURE, psia	PORE THROAT Radius, microns	NON-WETTING PHASE SATURATION		WETTING PHASE SATURATION, percent
		INCREMENTAL, percent	CUMULATIVE, percent	
1.50	71.1	0.000	0.000	100.0
1.99	53.6	0.000	0.000	100.0
2.99	35.7	0.000	0.000	100.0
3.99	26.7	0.000	0.000	100.0
5.49	19.4	0.000	0.000	100.0
6.99	15.3	0.000	0.000	100.0
8.49	12.6	0.000	0.000	100.0
10.5	10.2	0.000	0.000	100.0
13.0	8.21	0.000	0.000	100.0
16.0	6.67	0.000	0.000	100.0
20.0	5.33	0.000	0.000	100.0
23.0	4.64	0.000	0.000	100.0
25.0	4.27	0.000	0.000	100.0
27.1	3.94	0.000	0.000	100.0
35.8	2.98	0.000	0.000	100.0
47.3	2.26	0.000	0.000	100.0
56.7	1.88	0.000	0.000	100.0
72.1	1.48	0.000	0.000	100.0
86.9	1.23	0.000	0.000	100.0
112	0.955	0.000	0.000	100.0
137	0.781	0.000	0.000	100.0
172	0.621	0.000	0.000	100.0
217	0.492	0.000	0.000	100.0
266	0.401	0.000	0.000	100.0
327	0.326	0.000	0.000	100.0
417	0.256	0.000	0.000	100.0
517	0.206	0.000	0.000	100.0
637	0.167	0.000	0.000	100.0
697	0.153	0.000	0.000	100.0
799	0.134	0.000	0.000	100.0
988	0.108	0.000	0.000	100.0
1199	0.089	0.000	0.000	100.0
1298	0.082	0.000	0.000	100.0

1398	0.076	0.000	0.000	100.0
1496	0.071	0.000	0.000	100.0
1597	0.067	0.000	0.000	100.0
1697	0.063	0.000	0.000	100.0
1897	0.056	0.000	0.000	100.0
2045	0.052	0.000	0.000	100.0
2196	0.049	0.000	0.000	100.0
2345	0.045	0.000	0.000	100.0
2496	0.043	0.000	0.000	100.0
2645	0.040	0.000	0.000	100.0
2696	0.040	0.000	0.000	100.0
2845	0.037	0.000	0.000	100.0
2996	0.036	0.000	0.000	100.0
3245	0.033	0.000	0.000	100.0
3493	0.031	0.000	0.000	100.0
3742	0.028	0.000	0.000	100.0
3991	0.027	0.000	0.000	100.0
4246	0.025	0.000	0.000	100.0
4484	0.024	0.000	0.000	100.0
4730	0.023	0.675	0.675	99.3
4987	0.021	0.386	1.06	98.9
5294	0.020	0.773	1.83	98.2
5487	0.019	0.386	2.22	97.8
5746	0.019	0.773	2.99	97.0
5995	0.018	0.773	3.77	96.2
6247	0.017	1.16	4.93	95.1
6497	0.016	1.55	6.47	93.5
6745	0.016	0.773	7.24	92.8
6997	0.015	1.93	9.18	90.8
7497	0.014	3.48	12.7	87.3
7996	0.013	5.02	17.7	82.3
8496	0.013	4.25	21.9	78.1
8996	0.012	1.93	23.9	76.1
9278	0.011	0.773	24.6	75.4
9580	0.011	2.32	27.0	73.0
10026	0.011	3.48	30.4	69.6
10496	0.010	5.80	36.2	63.8
10996	0.010	3.86	40.1	59.9
11496	0.009	3.86	44.0	56.0
11994	0.009	3.86	47.8	52.2
12589	0.008	2.71	50.5	49.5
13089	0.008	3.48	54.0	46.0
13645	0.008	3.86	57.9	42.1
13996	0.008	3.86	61.7	38.3
14336	0.007	3.86	65.6	34.4
14595	0.007	2.32	67.9	32.1
14995	0.007	1.93	69.9	30.1
15446	0.007	2.71	72.6	27.4

15767	0.007	0.000	72.6	27.4
16196	0.007	2.71	75.3	24.7
16646	0.006	0.773	76.0	24.0
16996	0.006	2.32	78.4	21.6
17316	0.006	0.000	78.4	21.6
17695	0.006	1.16	79.5	20.5
18095	0.006	1.16	80.7	19.3
18442	0.006	0.773	81.4	18.6
18778	0.006	0.386	81.8	18.2
19196	0.006	1.16	83.0	17.0
19792	0.005	0.773	83.8	16.2
20294	0.005	1.16	84.9	15.1
20789	0.005	0.386	85.3	14.7
21180	0.005	0.386	85.7	14.3
21632	0.005	0.000	85.7	14.3
22045	0.005	1.16	86.9	13.1
22643	0.005	0.773	87.6	12.4
23191	0.005	0.386	88.0	12.0
23743	0.004	0.773	88.8	11.2
24088	0.004	0.000	88.8	11.2
24644	0.004	0.773	89.6	10.4
25042	0.004	0.386	90.0	10.0
25443	0.004	0.000	90.0	10.0
25890	0.004	0.386	90.3	9.7
26441	0.004	0.000	90.3	9.7
26946	0.004	0.773	91.1	8.9
27393	0.004	0.386	91.5	8.5
27793	0.004	0.386	91.9	8.1
28242	0.004	0.000	91.9	8.1
28989	0.004	0.386	92.3	7.7
29494	0.004	0.386	92.7	7.3
29993	0.004	0.000	92.7	7.3
30443	0.004	0.386	93.0	7.0
30894	0.003	0.386	93.4	6.6
31294	0.003	0.000	93.4	6.6
31791	0.003	0.386	93.8	6.2
32342	0.003	0.000	93.8	6.2
32893	0.003	0.386	94.2	5.8
33493	0.003	0.386	94.6	5.4
33992	0.003	0.000	94.6	5.4
34639	0.003	0.386	95.0	5.0
35491	0.003	0.386	95.4	4.6
36185	0.003	0.000	95.4	4.6
36984	0.003	0.386	95.7	4.3
37630	0.003	0.000	95.7	4.3
38430	0.003	0.000	95.7	4.3
39179	0.003	0.000	95.7	4.3
39985	0.003	0.773	96.5	3.5

40482	0.003	0.000	96.5	3.5
40981	0.003	0.386	96.9	3.1
42482	0.003	0.386	97.3	2.7
43331	0.002	0.000	97.3	2.7
43981	0.002	0.386	97.7	2.3
44984	0.002	0.000	97.7	2.3
46479	0.002	0.386	98.1	1.9
47970	0.002	0.386	98.5	1.5
49472	0.002	0.386	98.8	1.2
50173	0.002	0.000	98.8	1.2
52960	0.002	0.000	98.8	1.2
54469	0.002	0.386	99.2	0.8
55963	0.002	0.386	99.6	0.4
57955	0.002	0.386	100	0.0
59957	0.002	0.000	100	0.0



**PORE VOLUME FILLED vs PRESSURE**  
Mercury Pressure: 0 - 60000 psia  
(METHODOLOGY: ASTM D4404, API RP40)

Project Name: NAWC  
Project No.: ER-0715

Sample ID: Gray mudstone 1  
Depth, ft.: 260  
Porosity, %Vp: 6.6

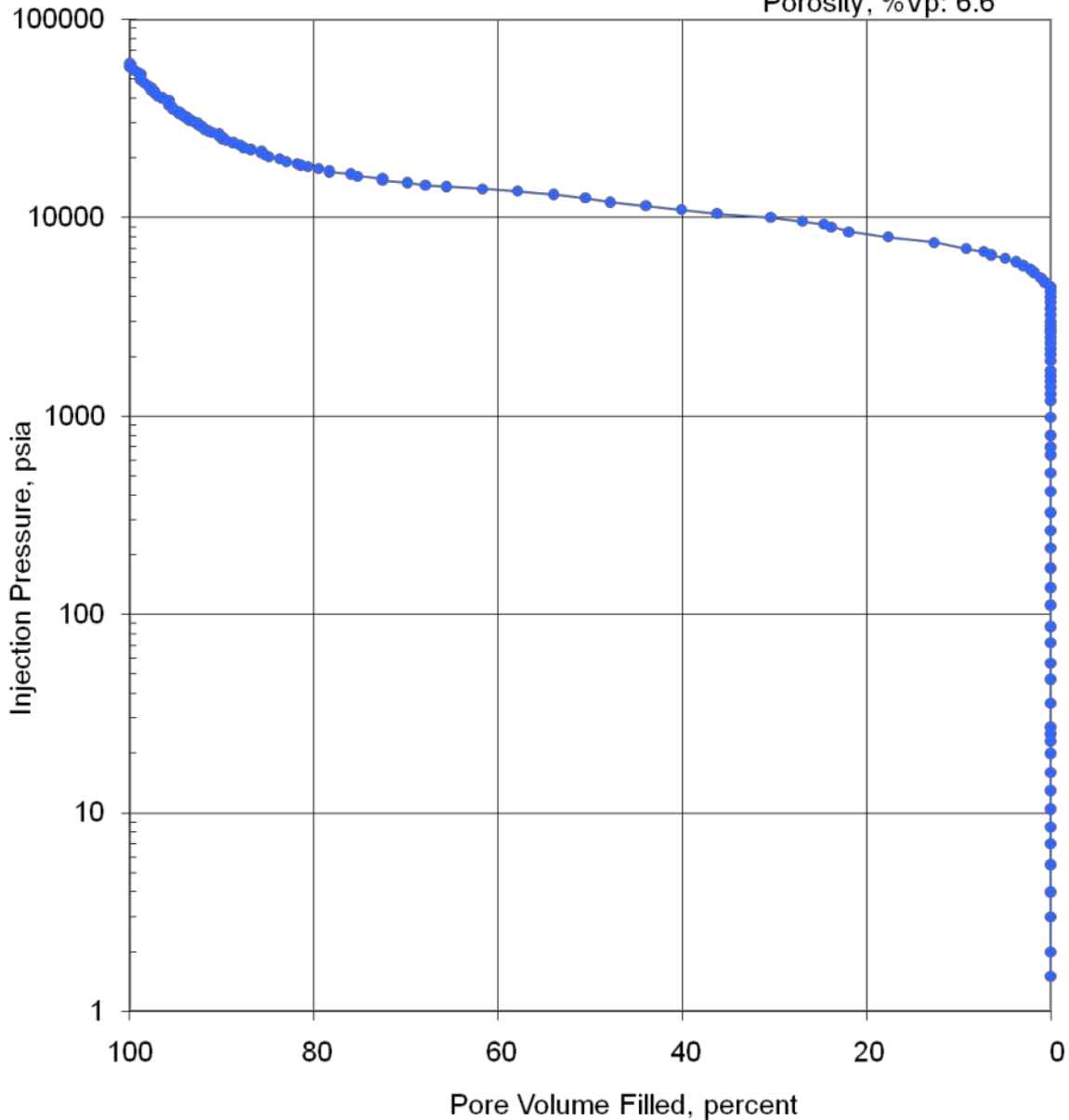


**Figure 10 – Results of the mercury porosimetry analysis on the gray mudstone rock sample as pore volume filled per pressure unit.**



### CAPILLARY PRESSURE vs. WETTING PHASE SATURATION

Mercury Pressure: 0 - 60000  
(METHODOLOGY: ASTM D4404, API RP40)

Project Name: NAWC  
Project No.: ER-0715

Sample ID: Gray mudstone 1  
Depth, ft.: 260  
Porosity, %Vp: 6.6

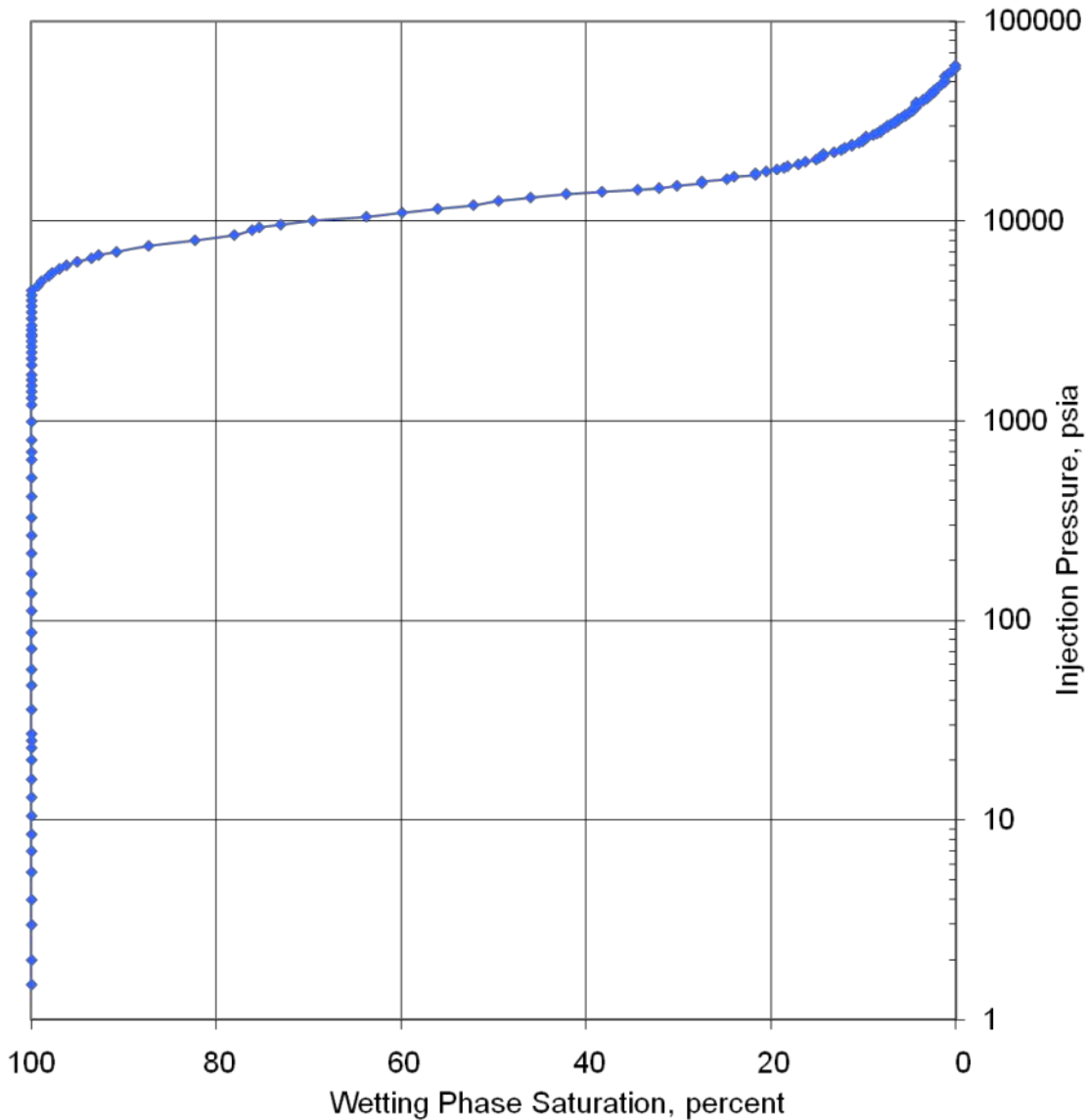


**Figure 11 – Results of the mercury porosimetry analysis on the gray mudstone rock sample as wetting phase saturation per capillary pressure.**



**PORE THROAT RADIUS DISTRIBUTION**  
Mercury Pressure: 0 - 60000  
(METHODOLOGY: ASTM D4404, API RP40)

Project Name: NAWC  
Project No.: ER-0715

Sample ID: Gray mudstone 1  
Depth, ft.: 260  
Porosity, %Vp: 6.6

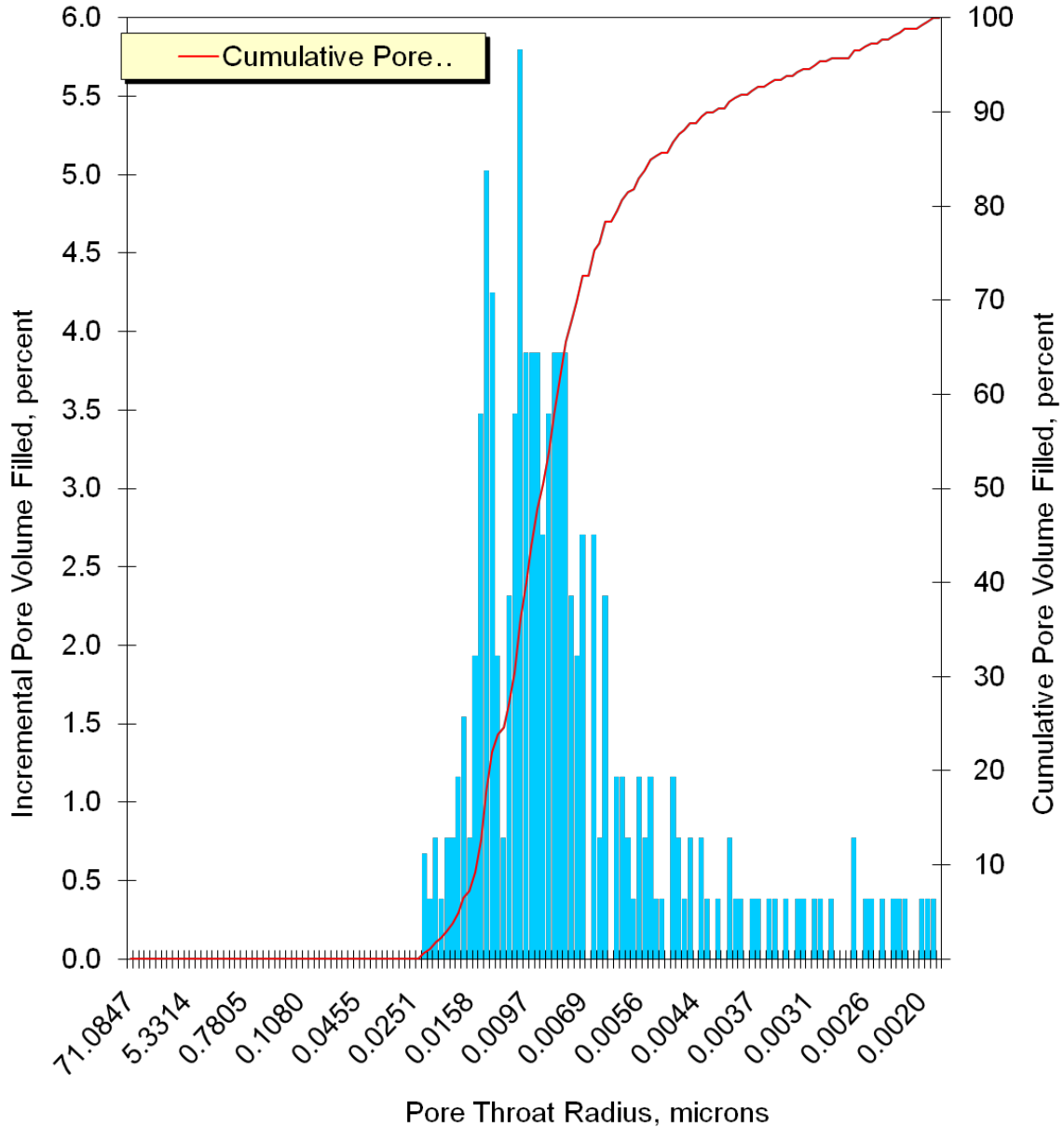


**Figure 12 – Pore throat radius distribution of the gray mudstone sample during the mercury porosimetry analysis.**

**Table 5 – Results of the mercury porosimetry analysis on duplicate the gray mudstone rock sample.**

PTS File No:	38521			PTS Laboratories
Client:	Queen's University			
<b>MERCURY INJECTION SUMMARY</b>				
PROJECT NAME:	NAWC		Sample ID:	Gray mudstone 2
PROJECT NO:	ER-0715		Depth, ft.:	260
			Porosity, %Vp:	6.2
*INJECTION PRESSURE, psia	PORE THROAT Radius, microns	NON-WETTING PHASE SATURATION		WETTING PHASE SATURATION, percent
		INCREMENTAL, percent	CUMULATIVE, percent	
1.50	71.1	0.000	0.000	100.0
1.99	53.6	0.000	0.000	100.0
2.99	35.7	0.000	0.000	100.0
3.99	26.7	0.000	0.000	100.0
5.49	19.4	0.000	0.000	100.0
6.99	15.3	0.000	0.000	100.0
8.49	12.6	0.000	0.000	100.0
10.5	10.2	0.000	0.000	100.0
13.0	8.21	0.000	0.000	100.0
16.0	6.67	0.000	0.000	100.0
20.0	5.33	0.000	0.000	100.0
23.0	4.64	0.000	0.000	100.0
25.0	4.27	0.000	0.000	100.0
26.7	3.99	0.000	0.000	100.0
35.4	3.01	0.000	0.000	100.0
46.9	2.27	0.000	0.000	100.0
56.4	1.89	0.000	0.000	100.0
71.6	1.49	0.000	0.000	100.0
86.5	1.23	0.000	0.000	100.0
111	0.958	0.000	0.000	100.0
136	0.782	0.000	0.000	100.0
171	0.622	0.000	0.000	100.0
216	0.493	0.000	0.000	100.0
266	0.401	0.000	0.000	100.0
326	0.327	0.000	0.000	100.0
416	0.256	0.000	0.000	100.0
517	0.206	0.000	0.000	100.0
637	0.167	0.000	0.000	100.0
697	0.153	0.000	0.000	100.0
798	0.134	0.000	0.000	100.0
987	0.108	0.000	0.000	100.0
1198	0.089	0.000	0.000	100.0

1298	0.082	0.000	0.000	100.0
1397	0.076	0.000	0.000	100.0
1496	0.071	0.000	0.000	100.0
1597	0.067	0.000	0.000	100.0
1697	0.063	0.000	0.000	100.0
1897	0.056	0.000	0.000	100.0
2045	0.052	0.000	0.000	100.0
2196	0.049	0.000	0.000	100.0
2345	0.045	0.000	0.000	100.0
2496	0.043	0.000	0.000	100.0
2644	0.040	0.000	0.000	100.0
2695	0.040	0.000	0.000	100.0
2844	0.037	0.000	0.000	100.0
2995	0.036	0.000	0.000	100.0
3245	0.033	0.000	0.000	100.0
3493	0.031	0.000	0.000	100.0
3742	0.028	0.000	0.000	100.0
3991	0.027	0.000	0.000	100.0
4246	0.025	0.000	0.000	100.0
4483	0.024	0.000	0.000	100.0
4730	0.023	0.317	0.317	99.7
4987	0.021	0.410	0.727	99.3
5293	0.020	0.410	1.14	98.9
5487	0.019	0.410	1.55	98.5
5746	0.019	0.820	2.37	97.6
5995	0.018	0.410	2.78	97.2
6247	0.017	0.820	3.60	96.4
6496	0.016	0.820	4.42	95.6
6745	0.016	0.410	4.83	95.2
6996	0.015	1.23	6.06	93.9
7496	0.014	2.46	8.52	91.5
7996	0.013	3.28	11.8	88.2
8496	0.013	3.28	15.1	84.9
8996	0.012	2.46	17.5	82.5
9277	0.011	2.05	19.6	80.4
9580	0.011	3.69	23.3	76.7
10026	0.011	3.69	27.0	73.0
10496	0.010	3.69	30.7	69.3
10996	0.010	3.28	34.0	66.0
11496	0.009	2.87	36.8	63.2
11994	0.009	2.05	38.9	61.1
12589	0.008	2.87	41.7	58.3
13089	0.008	3.28	45.0	55.0
13645	0.008	3.28	48.3	51.7
13996	0.008	3.69	52.0	48.0
14336	0.007	4.10	56.1	43.9
14595	0.007	2.05	58.2	41.8
14995	0.007	2.05	60.2	39.8

15446	0.007	2.46	62.7	37.3
15767	0.007	0.000	62.7	37.3
16196	0.007	2.87	65.5	34.5
16646	0.006	1.64	67.2	32.8
16996	0.006	2.05	69.2	30.8
17316	0.006	0.410	69.6	30.4
17695	0.006	1.23	70.9	29.1
18095	0.006	1.23	72.1	27.9
18442	0.006	1.23	73.3	26.7
18778	0.006	0.410	73.7	26.3
19196	0.006	1.64	75.4	24.6
19792	0.005	1.23	76.6	23.4
20294	0.005	1.23	77.8	22.2
20789	0.005	0.820	78.7	21.3
21180	0.005	0.410	79.1	20.9
21632	0.005	0.410	79.5	20.5
22045	0.005	1.23	80.7	19.3
22643	0.005	1.23	82.0	18.0
23191	0.005	0.820	82.8	17.2
23743	0.004	0.410	83.2	16.8
24088	0.004	0.410	83.6	16.4
24644	0.004	1.23	84.8	15.2
25042	0.004	0.410	85.2	14.8
25443	0.004	0.410	85.6	14.4
25890	0.004	0.820	86.5	13.5
26441	0.004	0.000	86.5	13.5
26946	0.004	0.820	87.3	12.7
27393	0.004	0.820	88.1	11.9
27793	0.004	0.410	88.5	11.5
28242	0.004	0.410	88.9	11.1
28989	0.004	0.410	89.3	10.7
29494	0.004	0.410	89.7	10.3
29993	0.004	0.410	90.2	9.8
30443	0.004	0.410	90.6	9.4
30894	0.003	0.410	91.0	9.0
31294	0.003	0.410	91.4	8.6
31791	0.003	0.410	91.8	8.2
32342	0.003	0.000	91.8	8.2
32893	0.003	0.410	92.2	7.8
33493	0.003	0.410	92.6	7.4
33992	0.003	0.410	93.0	7.0
34639	0.003	0.000	93.0	7.0
35491	0.003	0.820	93.8	6.2
36185	0.003	0.000	93.8	6.2
36984	0.003	0.410	94.3	5.7
37630	0.003	0.410	94.7	5.3
38429	0.003	0.000	94.7	5.3
39179	0.003	0.410	95.1	4.9

39985	0.003	0.410	95.5	4.5
40482	0.003	0.410	95.9	4.1
40981	0.003	0.000	95.9	4.1
42482	0.003	0.820	96.7	3.3
43331	0.002	0.000	96.7	3.3
43981	0.002	0.410	97.1	2.9
44984	0.002	0.410	97.5	2.5
46479	0.002	0.000	97.5	2.5
47970	0.002	0.410	97.9	2.1
49472	0.002	0.410	98.4	1.6
50173	0.002	0.410	98.8	1.2
52960	0.002	0.000	98.8	1.2
54469	0.002	0.410	99.2	0.8
55963	0.002	0.410	99.6	0.4
57955	0.002	0.000	100	0.4
59957	0.002	0.410	100	0.0



PORE VOLUME FILLED vs PRESSURE  
Mercury Pressure: 0 - 60000 psia  
(METHODOLOGY: ASTM D4404, API RP40)

Project Name: NAWC  
Project No.: ER-0715

Sample ID: Gray mudstone 2  
Depth, ft.: 260  
Porosity, %Vp: 6.2

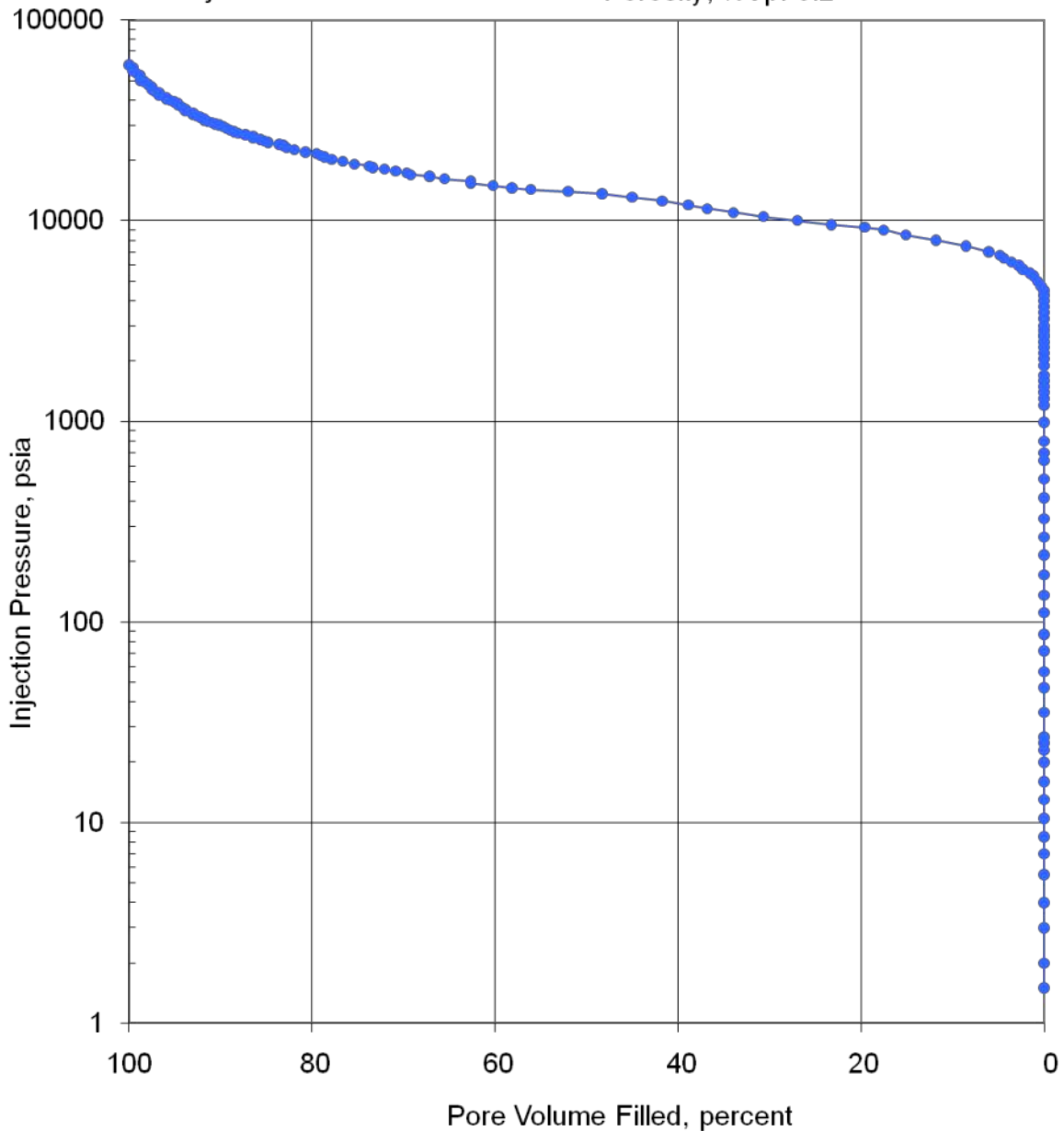


**Figure 13 – Results of the mercury porosimetry analysis on the duplicate gray mudstone rock sample as pore volume filled per pressure unit.**



Queen's University  
PTS File No.: 38521

### CAPILLARY PRESSURE vs. WETTING PHASE SATURATION

Mercury Pressure: 0 - 60000  
(METHODOLOGY: ASTM D4404, API RP40)

Project Name: NAWC  
Project No.: ER-0715

Sample ID: Gray mudstone 2  
Depth, ft.: 260  
Porosity, %Vp: 6.2

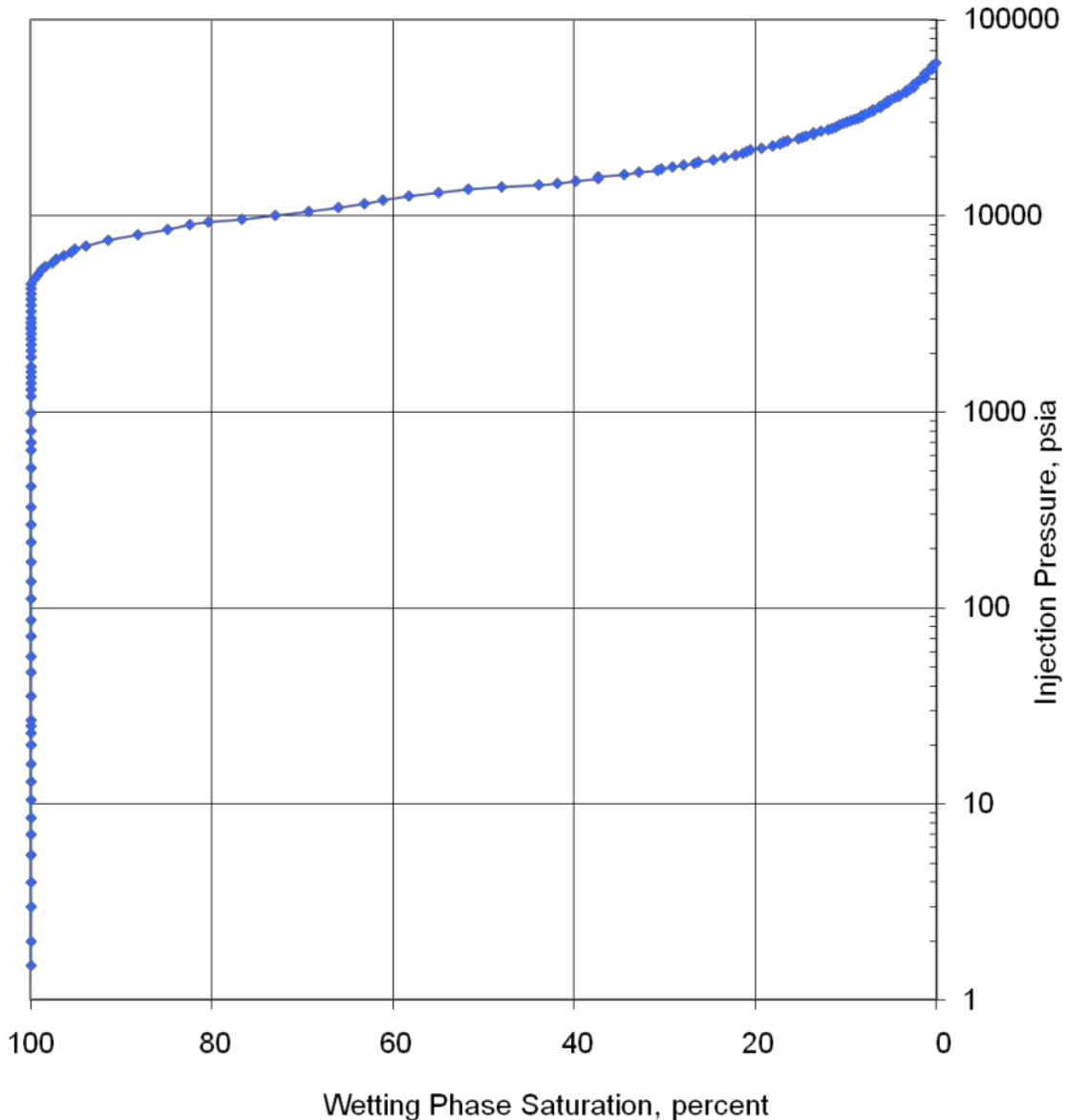


**Figure 14 – Results of the mercury porosimetry analysis on the duplicate gray mudstone rock sample as wetting phase saturation per capillary pressure.**



**PORE THROAT RADIUS DISTRIBUTION**  
Mercury Pressure: 0 - 60000  
(METHODOLOGY: ASTM D4404, API RP40)

Project Name: NAWC  
Project No.: ER-0715

Sample ID: Gray mudstone 2  
Depth, ft.: 260  
Porosity, %Vp: 6.2

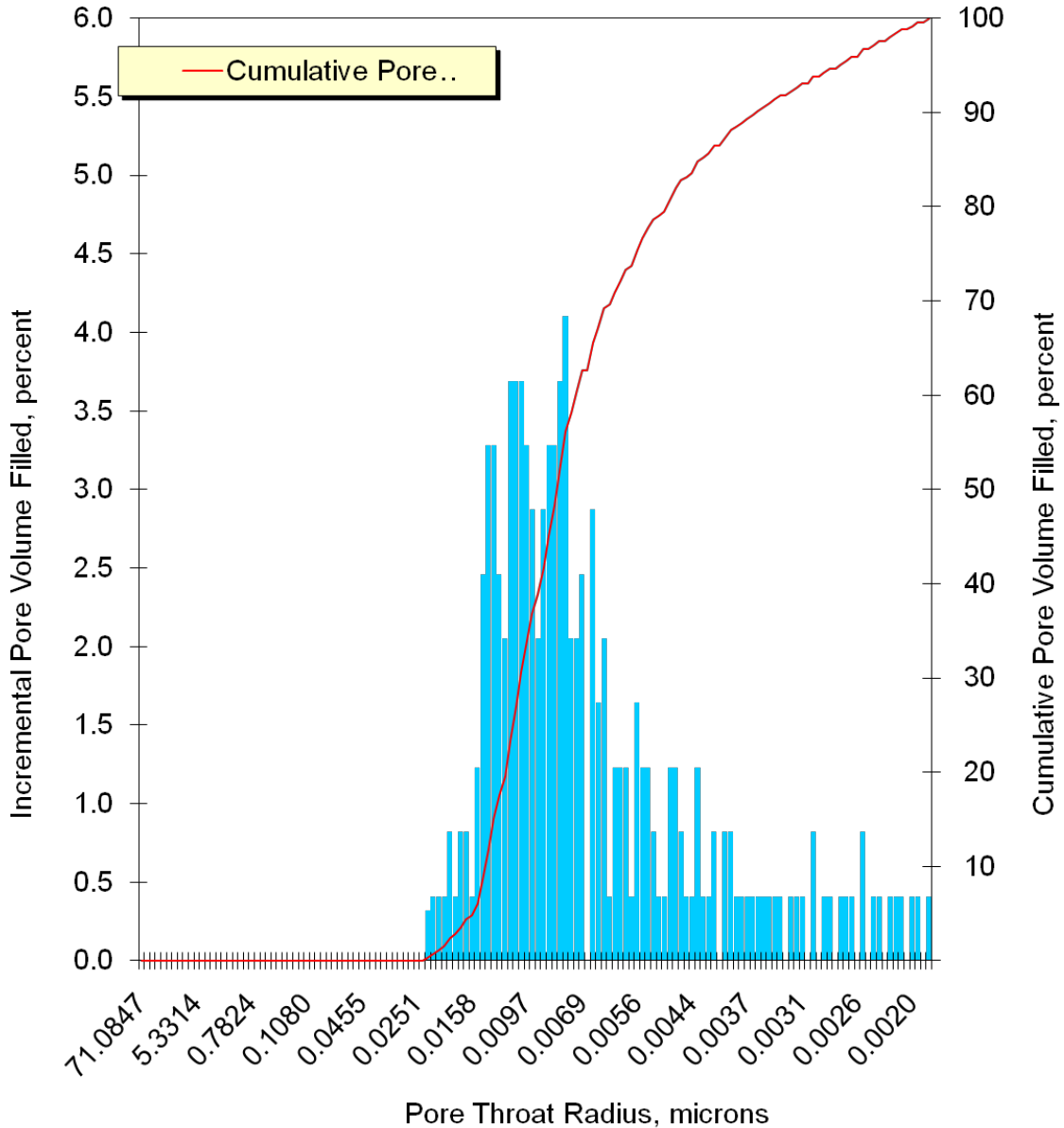


**Figure 15 – Pore throat radius distribution of the duplicate gray mudstone sample during the hg porosimetry analysis.**

**Table 6 – Results of the mercury porosimetry analysis on the triplicate gray  
mudstone rock sample.**

PTS File No:	38521			<b>PTS Laboratories</b>
Client:	Queen's University			
<b>MERCURY INJECTION SUMMARY</b>				
PROJECT NAME:	NAWC		Sample ID:	Gray mudstone 3
PROJECT NO:	ER-0715		Depth, ft.:	260
			Porosity, %Vp:	7.1
*INJECTION PRESSURE, psia	PORE THROAT Radius, microns	NON-WETTING PHASE SATURATION INCREMENTAL, percent	CUMULATIVE, percent	WETTING PHASE SATURATION, percent
1.50	71.1	0.000	0.000	100.0
1.99	53.6	0.000	0.000	100.0
2.99	35.7	0.000	0.000	100.0
3.99	26.7	0.000	0.000	100.0
5.49	19.4	0.000	0.000	100.0
6.99	15.3	0.000	0.000	100.0
8.49	12.6	0.000	0.000	100.0
10.5	10.2	0.000	0.000	100.0
13.0	8.21	0.000	0.000	100.0
16.0	6.67	0.000	0.000	100.0
20.0	5.33	0.000	0.000	100.0
23.0	4.64	0.000	0.000	100.0
25.0	4.27	0.000	0.000	100.0
26.1	4.08	0.000	0.000	100.0
37.3	2.86	0.000	0.000	100.0
46.5	2.30	0.000	0.000	100.0
56.2	1.90	0.000	0.000	100.0
72.1	1.48	0.000	0.000	100.0
87.4	1.22	0.000	0.000	100.0
112	0.949	0.000	0.000	100.0
138	0.772	0.000	0.000	100.0
172	0.620	0.000	0.000	100.0
219	0.486	0.000	0.000	100.0
266	0.400	0.000	0.000	100.0
327	0.326	0.000	0.000	100.0
417	0.256	0.000	0.000	100.0
518	0.206	0.000	0.000	100.0
637	0.167	0.000	0.000	100.0
697	0.153	0.000	0.000	100.0
797	0.134	0.000	0.000	100.0
988	0.108	0.000	0.000	100.0
1197	0.089	0.000	0.000	100.0
1298	0.082	0.000	0.000	100.0

1399	0.076	0.000	0.000	100.0
1498	0.071	0.000	0.000	100.0
1599	0.067	0.000	0.000	100.0
1696	0.063	0.000	0.000	100.0
1896	0.056	0.000	0.000	100.0
2046	0.052	0.000	0.000	100.0
2196	0.049	0.000	0.000	100.0
2345	0.045	0.000	0.000	100.0
2496	0.043	0.000	0.000	100.0
2645	0.040	0.000	0.000	100.0
2695	0.040	0.000	0.000	100.0
2845	0.037	0.000	0.000	100.0
2994	0.036	0.000	0.000	100.0
3244	0.033	0.000	0.000	100.0
3497	0.030	0.000	0.000	100.0
3743	0.028	0.378	0.378	99.6
3992	0.027	0.424	0.802	99.2
4240	0.025	0.000	0.802	99.2
4486	0.024	0.424	1.23	98.8
4733	0.023	0.848	2.07	97.9
4990	0.021	0.424	2.50	97.5
5292	0.020	0.848	3.35	96.7
5488	0.019	0.424	3.77	96.2
5731	0.019	0.424	4.19	95.8
5986	0.018	0.000	4.19	95.8
6246	0.017	1.27	5.47	94.5
6495	0.016	1.27	6.74	93.3
6736	0.016	0.424	7.16	92.8
6996	0.015	1.27	8.43	91.6
7494	0.014	1.27	9.70	90.3
7996	0.013	4.24	13.9	86.1
8496	0.013	2.12	16.1	83.9
8997	0.012	4.24	20.3	79.7
9296	0.011	2.54	22.8	77.2
9597	0.011	2.12	25.0	75.0
10046	0.011	2.97	27.9	72.1
10496	0.010	2.12	30.1	69.9
10996	0.010	2.54	32.6	67.4
11496	0.009	5.09	37.7	62.3
11996	0.009	5.09	42.8	57.2
12577	0.008	2.12	44.9	55.1
13090	0.008	2.54	47.4	52.6
13627	0.008	2.54	50.0	50.0
13972	0.008	2.12	52.1	47.9
14310	0.007	1.70	53.8	46.2
14571	0.007	1.27	55.1	44.9
14973	0.007	1.27	56.3	43.7
15424	0.007	1.70	58.0	42.0

15769	0.007	1.70	59.7	40.3
16178	0.007	0.848	60.6	39.4
16634	0.006	1.27	61.8	38.2
16995	0.006	1.70	63.5	36.5
17332	0.006	1.70	65.2	34.8
17696	0.006	1.70	66.9	33.1
18096	0.006	1.27	68.2	31.8
18441	0.006	2.12	70.3	29.7
18793	0.006	1.70	72.0	28.0
19193	0.006	1.70	73.7	26.3
19793	0.005	1.70	75.4	24.6
20292	0.005	1.27	76.7	23.3
20793	0.005	2.54	79.2	20.8
21190	0.005	2.12	81.3	18.7
21639	0.005	2.54	83.9	16.1
22038	0.005	2.12	86.0	14.0
22640	0.005	0.848	86.9	13.1
23193	0.005	0.424	87.3	12.7
23742	0.004	0.424	87.7	12.3
24095	0.004	0.848	88.6	11.4
24642	0.004	0.424	89.0	11.0
25039	0.004	0.000	89.0	11.0
25440	0.004	0.424	89.4	10.6
25893	0.004	0.424	89.8	10.2
26446	0.004	0.424	90.2	9.8
26937	0.004	0.424	90.7	9.3
27392	0.004	0.000	90.7	9.3
27793	0.004	0.424	91.1	8.9
28243	0.004	0.424	91.5	8.5
28993	0.004	0.848	92.4	7.6
29488	0.004	0.000	92.4	7.6
29990	0.004	0.000	92.4	7.6
30441	0.004	0.424	92.8	7.2
30891	0.003	0.000	92.8	7.2
31292	0.003	0.424	93.2	6.8
31794	0.003	0.848	94.1	5.9
32342	0.003	0.000	94.1	5.9
32891	0.003	0.000	94.1	5.9
33491	0.003	0.000	94.1	5.9
33992	0.003	0.424	94.5	5.5
34642	0.003	0.848	95.3	4.7
35490	0.003	0.424	95.8	4.2
36184	0.003	0.000	95.8	4.2
36981	0.003	0.000	95.8	4.2
37628	0.003	0.000	95.8	4.2
38428	0.003	0.000	95.8	4.2
39187	0.003	0.848	96.6	3.4
39983	0.003	0.000	96.6	3.4

40480	0.003	0.424	97.0	3.0
40979	0.003	0.424	97.5	2.5
42485	0.003	0.424	97.9	2.1
43327	0.002	0.000	97.9	2.1
43977	0.002	0.000	97.9	2.1
44979	0.002	0.000	97.9	2.1
46489	0.002	0.848	98.7	1.3
47976	0.002	0.000	98.7	1.3
49477	0.002	0.424	99.2	0.8
50171	0.002	0.424	99.6	0.4
52965	0.002	0.424	100	0.0
54463	0.002	0.000	100	0.0
55961	0.002	0.000	100	0.0
57960	0.002	0.000	100	0.0
59960	0.002	0.000	100	0.0



PORE VOLUME FILLED vs PRESSURE  
Mercury Pressure: 0 - 60000 psia  
(METHODOLOGY: ASTM D4404, API RP40)

Project Name: NAWC  
Project No.: ER-0715

Sample ID: Gray mudstone 3  
Depth, ft.: 260  
Porosity, %Vp: 7.1

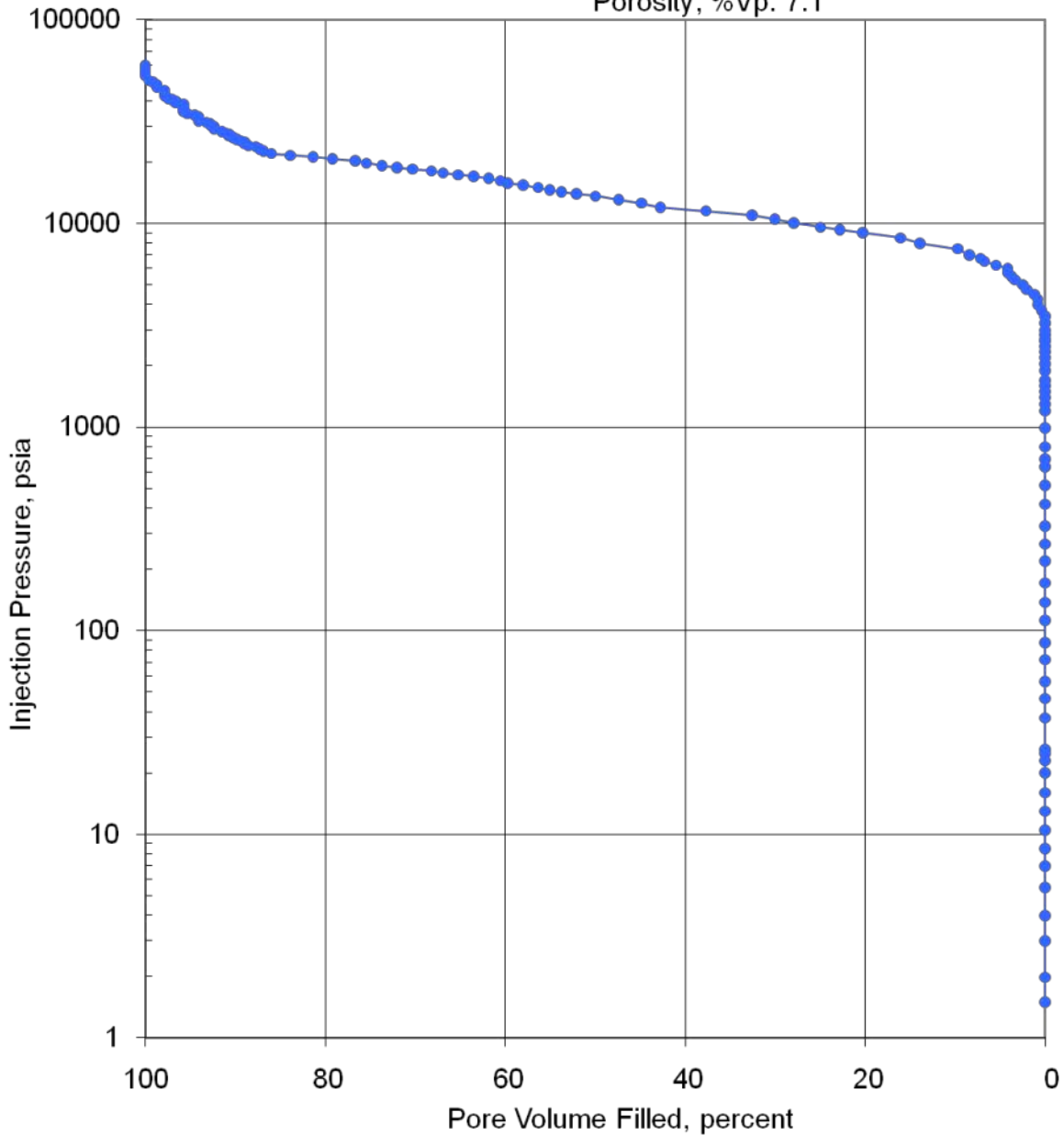


**Figure 16 – Results of the mercury porosimetry analysis on the triplicate gray mudstone rock sample as pore volume filled per pressure unit.**



Queen's University  
PTS File No.: 38521

### CAPILLARY PRESSURE vs. WETTING PHASE SATURATION

Mercury Pressure: 0 - 60000  
(METHODOLOGY: ASTM D4404, API RP40)

Project Name: NAWC  
Project No.: ER-0715

Sample ID: Gray mudstone 3  
Depth, ft.: 260  
Porosity, %Vp: 7.1

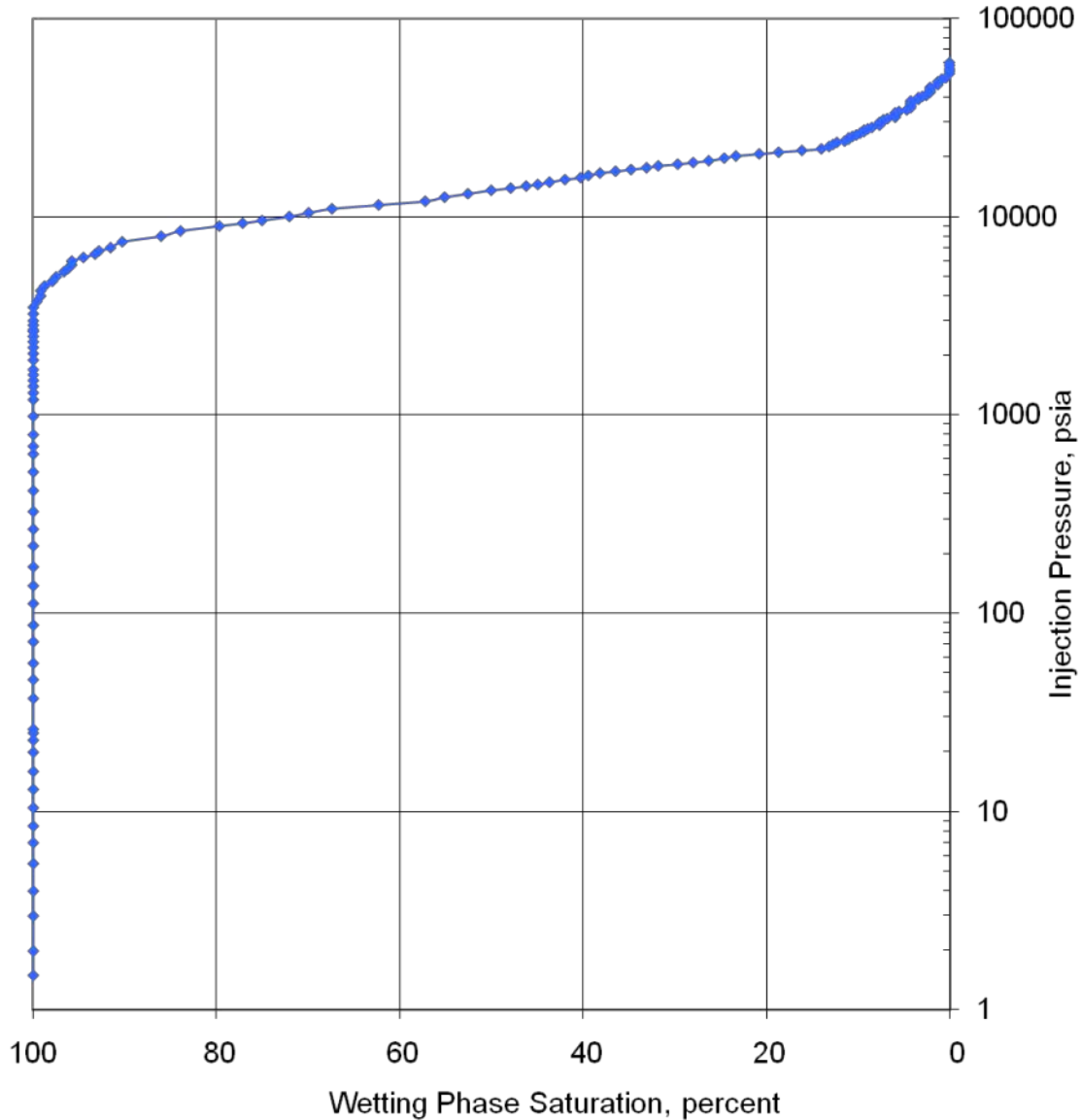


**Figure 17 – Results of the mercury porosimetry analysis on the triplicate gray mudstone rock sample as wetting phase saturation per capillary pressure.**

PORE THROAT RADIUS DISTRIBUTION  
Mercury Pressure: 0 - 60000  
(METHODOLOGY: ASTM D4404, API RP40)

Project Name: NAWC  
Project No.: ER-0715

Sample ID: Gray mudstone 3  
Depth, ft.: 260  
Porosity, %Vp: 7.1

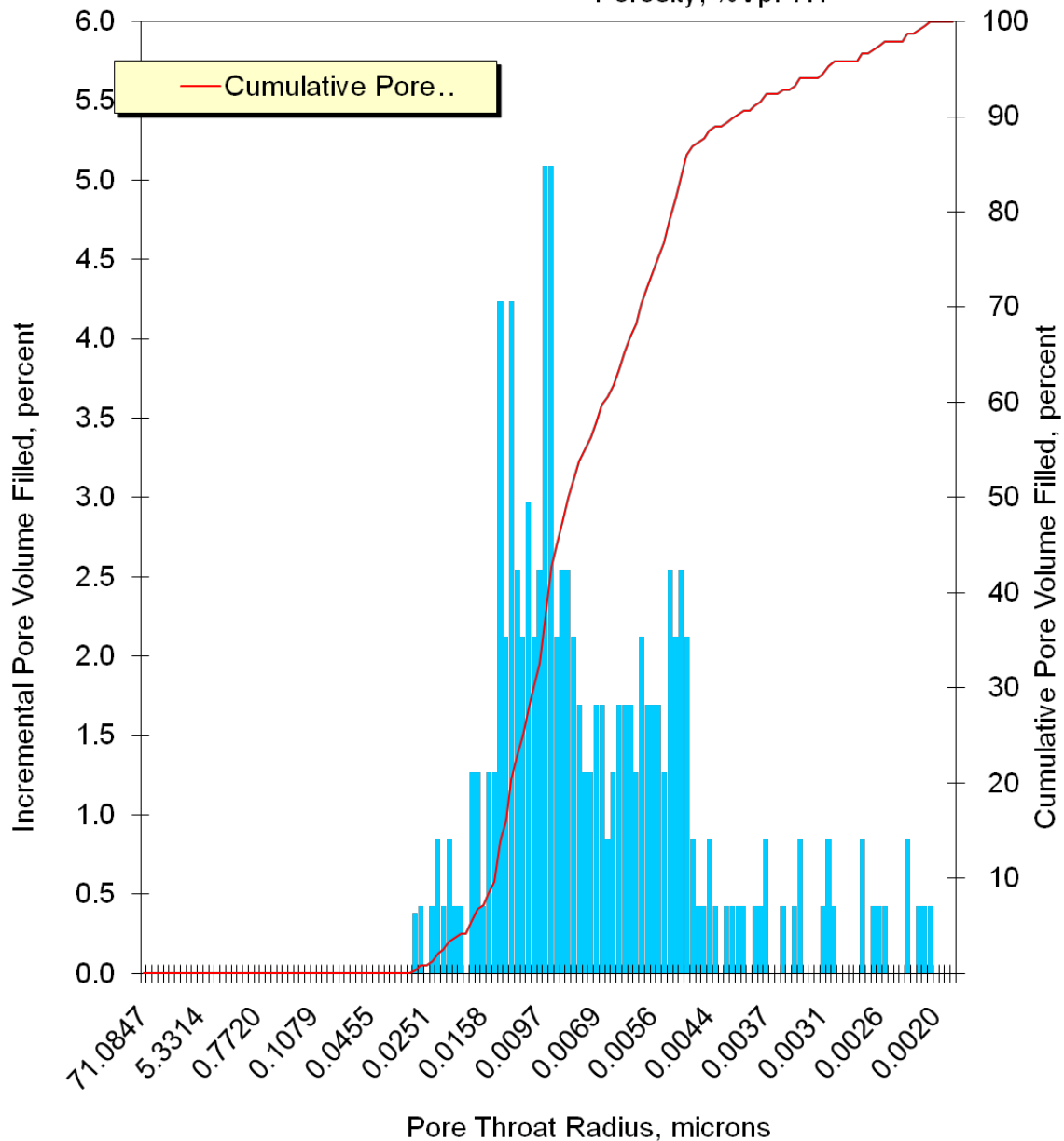


**Figure 18 – Pore throat radius distribution of the triplicate gray mudstone sample during the mercury porosimetry analysis.**

**Table 7 – Results of the mercury porosimetry analysis on the black mudstone  
rock sample.**

PTS File No:	38521			<b>PTS Laboratories</b>
Client:	Queen's University			
<b>MERCURY INJECTION SUMMARY</b>				
PROJECT NAME:	NAWC		Sample ID:	Black mudstone 1
PROJECT NO:	ER-0715		Depth, ft.:	50
			Porosity, %Vp:	0.2
*INJECTION PRESSURE, psia	PORE THROAT Radius, microns	NON-WETTING PHASE SATURATION		WETTING PHASE SATURATION, percent
		INCREMENTAL, percent	CUMULATIVE, percent	
1.57	67.9	0.000	0.000	100.0
2.07	51.5	11.1	11.1	88.9
3.06	34.8	22.2	33.3	66.7
4.07	26.2	11.1	44.4	55.6
5.57	19.1	11.1	55.6	44.4
7.06	15.1	0.000	55.6	44.4
8.55	12.5	11.1	66.7	33.3
10.5	10.1	0.000	66.7	33.3
13.0	8.18	22.2	88.9	11.1
16.0	6.66	0.000	88.9	11.1
20.0	5.33	0.000	88.9	11.1
23.0	4.64	0.000	88.9	11.1
25.0	4.27	11.1	100	0.000
30.2	3.53	0.000	100	0.000
40.5	2.63	0.000	100	0.000
50.2	2.12	0.000	100	0.000
60.1	1.78	0.000	100	0.000
75.1	1.42	0.000	100	0.000
89.7	1.19	0.000	100	0.000
115	0.928	0.000	100	0.000
140	0.764	0.000	100	0.000
174	0.612	0.000	100	0.000
220	0.484	0.000	100	0.000
270	0.395	0.000	100	0.000
329	0.325	0.000	100	0.000
418	0.255	0.000	100	0.000
529	0.201	0.000	100	0.000
639	0.167	0.000	100	0.000
701	0.152	0.000	100	0.000
805	0.132	0.000	100	0.000
1025	0.104	0.000	100	0.000
1242	0.086	0.000	100	0.000
1324	0.081	0.000	100	0.000

1426	0.075	0.000	100	0.000
1519	0.070	0.000	100	0.000
1617	0.066	0.000	100	0.000
1712	0.062	0.000	100	0.000
1915	0.056	0.000	100	0.000
2069	0.052	0.000	100	0.000
2213	0.048	0.000	100	0.000
2369	0.045	0.000	100	0.000
2515	0.042	0.000	100	0.000
2661	0.040	0.000	100	0.000
2714	0.039	0.000	100	0.000
2861	0.037	0.000	100	0.000
3009	0.035	0.000	100	0.000
3266	0.033	0.000	100	0.000
3512	0.030	0.000	100	0.000
3743	0.028	0.000	100	0.000
3997	0.027	0.000	100	0.000
4290	0.025	0.000	100	0.000
4511	0.024	0.000	100	0.000
4757	0.022	0.000	100	0.000
4985	0.021	0.000	100	0.000
5287	0.020	0.000	100	0.000
5495	0.019	0.000	100	0.000
5739	0.019	0.000	100	0.000
5992	0.018	0.000	100	0.000
6231	0.017	0.000	100	0.000
6480	0.016	0.000	100	0.000
6730	0.016	0.000	100	0.000
6978	0.015	0.000	100	0.000
7467	0.014	0.000	100	0.000
7981	0.013	0.000	100	0.000
8494	0.013	0.000	100	0.000
9010	0.012	0.000	100	0.000
9303	0.011	0.000	100	0.000
9615	0.011	0.000	100	0.000
10043	0.011	0.000	100	0.000
10509	0.010	0.000	100	0.000
10979	0.010	0.000	100	0.000
11508	0.009	0.000	100	0.000
11962	0.009	0.000	100	0.000
12576	0.008	0.000	100	0.000
13060	0.008	0.000	100	0.000
13615	0.008	0.000	100	0.000
13961	0.008	0.000	100	0.000
14312	0.007	0.000	100	0.000
14563	0.007	0.000	100	0.000
14961	0.007	0.000	100	0.000
15422	0.007	0.000	100	0.000

15756	0.007	0.000	100	0.000
16155	0.007	0.000	100	0.000
16658	0.006	0.000	100	0.000
17027	0.006	0.000	100	0.000
17386	0.006	0.000	100	0.000
17687	0.006	0.000	100	0.000
18076	0.006	0.000	100	0.000
18435	0.006	0.000	100	0.000
18838	0.006	0.000	100	0.000
19221	0.006	0.000	100	0.000
19777	0.005	0.000	100	0.000
20333	0.005	0.000	100	0.000
20828	0.005	0.000	100	0.000
21183	0.005	0.000	100	0.000
21636	0.005	0.000	100	0.000
22036	0.005	0.000	100	0.000
22622	0.005	0.000	100	0.000
23146	0.005	0.000	100	0.000
23725	0.004	0.000	100	0.000
24086	0.004	0.000	100	0.000
24599	0.004	0.000	100	0.000
25026	0.004	0.000	100	0.000
25405	0.004	0.000	100	0.000
25865	0.004	0.000	100	0.000
26394	0.004	0.000	100	0.000
26890	0.004	0.000	100	0.000
27360	0.004	0.000	100	0.000
27762	0.004	0.000	100	0.000
28170	0.004	0.000	100	0.000
28927	0.004	0.000	100	0.000
29429	0.004	0.000	100	0.000
29997	0.004	0.000	100	0.000
30457	0.004	0.000	100	0.000
30938	0.003	0.000	100	0.000
31325	0.003	0.000	100	0.000
31889	0.003	0.000	100	0.000
32415	0.003	0.000	100	0.000
32929	0.003	0.000	100	0.000
33503	0.003	0.000	100	0.000
34008	0.003	0.000	100	0.000
34658	0.003	0.000	100	0.000
35510	0.003	0.000	100	0.000
36225	0.003	0.000	100	0.000
37004	0.003	0.000	100	0.000
37672	0.003	0.000	100	0.000
38446	0.003	0.000	100	0.000
39169	0.003	0.000	100	0.000
40140	0.003	0.000	100	0.000

40647	0.003	0.000	100	0.000
41050	0.003	0.000	100	0.000
42593	0.003	0.000	100	0.000
43388	0.002	0.000	100	0.000
44072	0.002	0.000	100	0.000
45107	0.002	0.000	100	0.000
46460	0.002	0.000	100	0.000
48072	0.002	0.000	100	0.000
49573	0.002	0.000	100	0.000
50214	0.002	0.000	100	0.000
52962	0.002	0.000	100	0.000
54524	0.002	0.000	100	0.000
55959	0.002	0.000	100	0.000
57919	0.002	0.000	100	0.000
59894	0.002	0.000	100	0.000





### CAPILLARY PRESSURE vs. WETTING PHASE SATURATION

Mercury Pressure: 0 - 60000  
(METHODOLOGY: ASTM D4404, API RP40)

Project Name: NAWC  
Project No.: ER-0715

Sample ID: Black mudstone 1  
Depth, ft.: 50  
Porosity, %Vp: 0.2

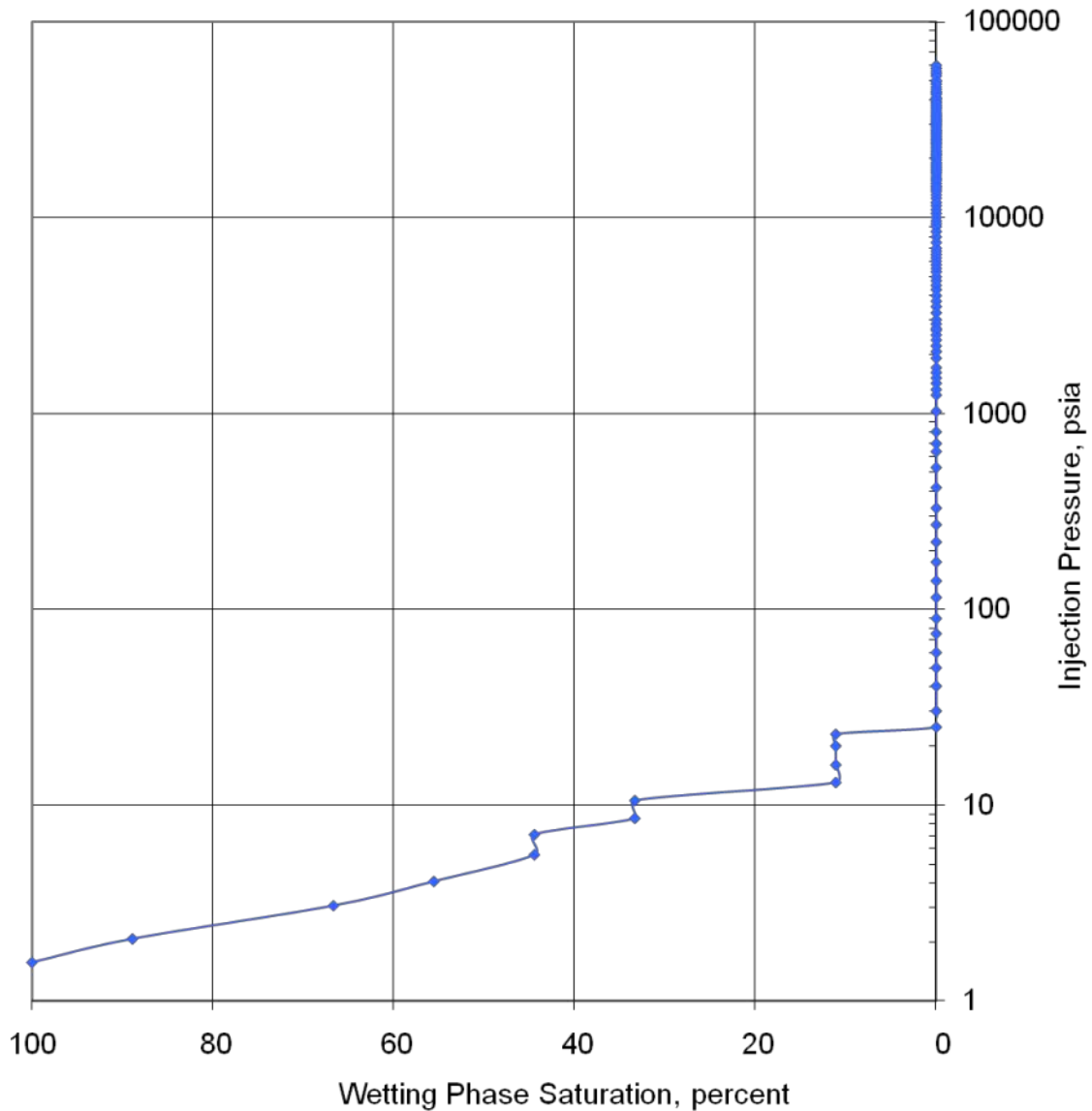


**Figure 20 – Results of the mercury porosimetry analysis on the black mudstone rock sample as wetting phase saturation per capillary pressure.**



PORE THROAT RADIUS DISTRIBUTION  
Mercury Pressure: 0 - 60000  
(METHODOLOGY: ASTM D4404, API RP40)

Project Name: NAWC  
Project No.: ER-0715

Sample ID: Black mudstone 1  
Depth, ft.: 50  
Porosity, %Vp: 0.2

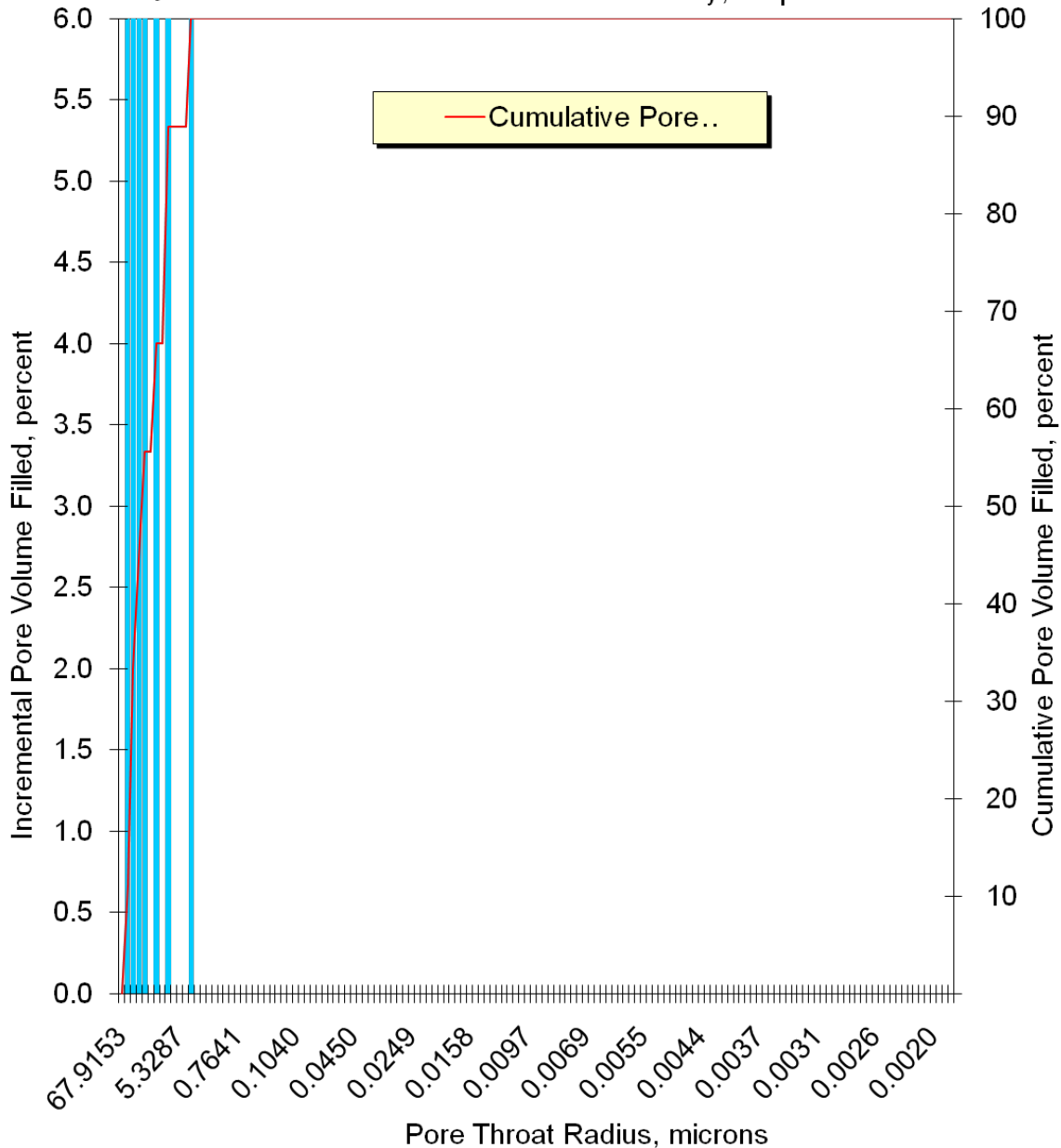


**Figure 21 – Pore throat radius distribution of the black mudstone sample during the mercury porosimetry analysis.**

**Table 8 – Results of the mercury porosimetry analysis on the duplicate black mudstone rock sample.**

PTS File No:	38521			<b>PTS</b>
Client:	Queen's University			Laboratories
<b>MERCURY INJECTION SUMMARY</b>				
PROJECT NAME:	NAWC		Sample ID:	Black mudstone 2
PROJECT NO:	ER-0715		Depth, ft.:	50
			Porosity, %Vp:	0.2
*INJECTION PRESSURE, psia	PORE THROAT Radius, microns	NON-WETTING PHASE SATURATION		WETTING PHASE SATURATION, percent
		INCREMENTAL, percent	CUMULATIVE, percent	
1.57	67.9	0.000	0.000	100.0
2.07	51.5	16.7	16.7	83.3
3.06	34.8	0.0	16.7	83.3
4.07	26.2	16.7	33.3	66.7
5.57	19.1	16.7	50.0	50.0
7.06	15.1	16.7	66.7	33.3
8.55	12.5	0.000	66.7	33.3
10.5	10.1	16.7	83.3	16.7
13.0	8.18	0.000	83.3	16.7
16.0	6.66	0.000	83.3	16.7
20.0	5.33	0.000	83.3	16.7
23.0	4.64	16.7	100	0.000
25.0	4.27	0.000	100	0.000
30.3	3.52	0.000	100	0.000
40.6	2.62	0.000	100	0.000
50.3	2.12	0.000	100	0.000
60.2	1.77	0.000	100	0.000
75.2	1.42	0.000	100	0.000
89.8	1.19	0.000	100	0.000
115	0.928	0.000	100	0.000
140	0.763	0.000	100	0.000
174	0.611	0.000	100	0.000
220	0.484	0.000	100	0.000
270	0.395	0.000	100	0.000
329	0.324	0.000	100	0.000
418	0.255	0.000	100	0.000
529	0.201	0.000	100	0.000
639	0.167	0.000	100	0.000
701	0.152	0.000	100	0.000
805	0.132	0.000	100	0.000
1025	0.104	0.000	100	0.000
1242	0.086	0.000	100	0.000
1324	0.081	0.000	100	0.000

1426	0.075	0.000	100	0.000
1519	0.070	0.000	100	0.000
1617	0.066	0.000	100	0.000
1712	0.062	0.000	100	0.000
1916	0.056	0.000	100	0.000
2069	0.052	0.000	100	0.000
2213	0.048	0.000	100	0.000
2369	0.045	0.000	100	0.000
2515	0.042	0.000	100	0.000
2661	0.040	0.000	100	0.000
2714	0.039	0.000	100	0.000
2861	0.037	0.000	100	0.000
3009	0.035	0.000	100	0.000
3266	0.033	0.000	100	0.000
3512	0.030	0.000	100	0.000
3743	0.028	0.000	100	0.000
3997	0.027	0.000	100	0.000
4290	0.025	0.000	100	0.000
4511	0.024	0.000	100	0.000
4758	0.022	0.000	100	0.000
4985	0.021	0.000	100	0.000
5287	0.020	0.000	100	0.000
5495	0.019	0.000	100	0.000
5739	0.019	0.000	100	0.000
5992	0.018	0.000	100	0.000
6231	0.017	0.000	100	0.000
6480	0.016	0.000	100	0.000
6731	0.016	0.000	100	0.000
6978	0.015	0.000	100	0.000
7467	0.014	0.000	100	0.000
7981	0.013	0.000	100	0.000
8494	0.013	0.000	100	0.000
9010	0.012	0.000	100	0.000
9303	0.011	0.000	100	0.000
9616	0.011	0.000	100	0.000
10043	0.011	0.000	100	0.000
10509	0.010	0.000	100	0.000
10979	0.010	0.000	100	0.000
11508	0.009	0.000	100	0.000
11963	0.009	0.000	100	0.000
12576	0.008	0.000	100	0.000
13060	0.008	0.000	100	0.000
13615	0.008	0.000	100	0.000
13961	0.008	0.000	100	0.000
14312	0.007	0.000	100	0.000
14563	0.007	0.000	100	0.000
14961	0.007	0.000	100	0.000
15423	0.007	0.000	100	0.000

15756	0.007	0.000	100	0.000
16155	0.007	0.000	100	0.000
16658	0.006	0.000	100	0.000
17027	0.006	0.000	100	0.000
17386	0.006	0.000	100	0.000
17687	0.006	0.000	100	0.000
18076	0.006	0.000	100	0.000
18435	0.006	0.000	100	0.000
18838	0.006	0.000	100	0.000
19221	0.006	0.000	100	0.000
19777	0.005	0.000	100	0.000
20333	0.005	0.000	100	0.000
20828	0.005	0.000	100	0.000
21183	0.005	0.000	100	0.000
21636	0.005	0.000	100	0.000
22036	0.005	0.000	100	0.000
22622	0.005	0.000	100	0.000
23146	0.005	0.000	100	0.000
23725	0.004	0.000	100	0.000
24087	0.004	0.000	100	0.000
24599	0.004	0.000	100	0.000
25026	0.004	0.000	100	0.000
25405	0.004	0.000	100	0.000
25865	0.004	0.000	100	0.000
26394	0.004	0.000	100	0.000
26890	0.004	0.000	100	0.000
27361	0.004	0.000	100	0.000
27763	0.004	0.000	100	0.000
28170	0.004	0.000	100	0.000
28927	0.004	0.000	100	0.000
29430	0.004	0.000	100	0.000
29998	0.004	0.000	100	0.000
30457	0.004	0.000	100	0.000
30939	0.003	0.000	100	0.000
31325	0.003	0.000	100	0.000
31890	0.003	0.000	100	0.000
32415	0.003	0.000	100	0.000
32929	0.003	0.000	100	0.000
33503	0.003	0.000	100	0.000
34009	0.003	0.000	100	0.000
34659	0.003	0.000	100	0.000
35510	0.003	0.000	100	0.000
36226	0.003	0.000	100	0.000
37005	0.003	0.000	100	0.000
37672	0.003	0.000	100	0.000
38446	0.003	0.000	100	0.000
39169	0.003	0.000	100	0.000
40140	0.003	0.000	100	0.000

40647	0.003	0.000	100	0.000
41050	0.003	0.000	100	0.000
42593	0.003	0.000	100	0.000
43388	0.002	0.000	100	0.000
44072	0.002	0.000	100	0.000
45107	0.002	0.000	100	0.000
46460	0.002	0.000	100	0.000
48073	0.002	0.000	100	0.000
49574	0.002	0.000	100	0.000
50214	0.002	0.000	100	0.000
52962	0.002	0.000	100	0.000
54525	0.002	0.000	100	0.000
55959	0.002	0.000	100	0.000
57919	0.002	0.000	100	0.000
59894	0.002	0.000	100	0.000



PORE VOLUME FILLED vs PRESSURE  
Mercury Pressure: 0 - 60000 psia  
(METHODOLOGY: ASTM D4404, API RP40)

Project Name: NAWC  
Project No.: ER-0715

Sample ID: Black mudstone 2  
Depth, ft.: 50  
Porosity, %Vp: 0.2

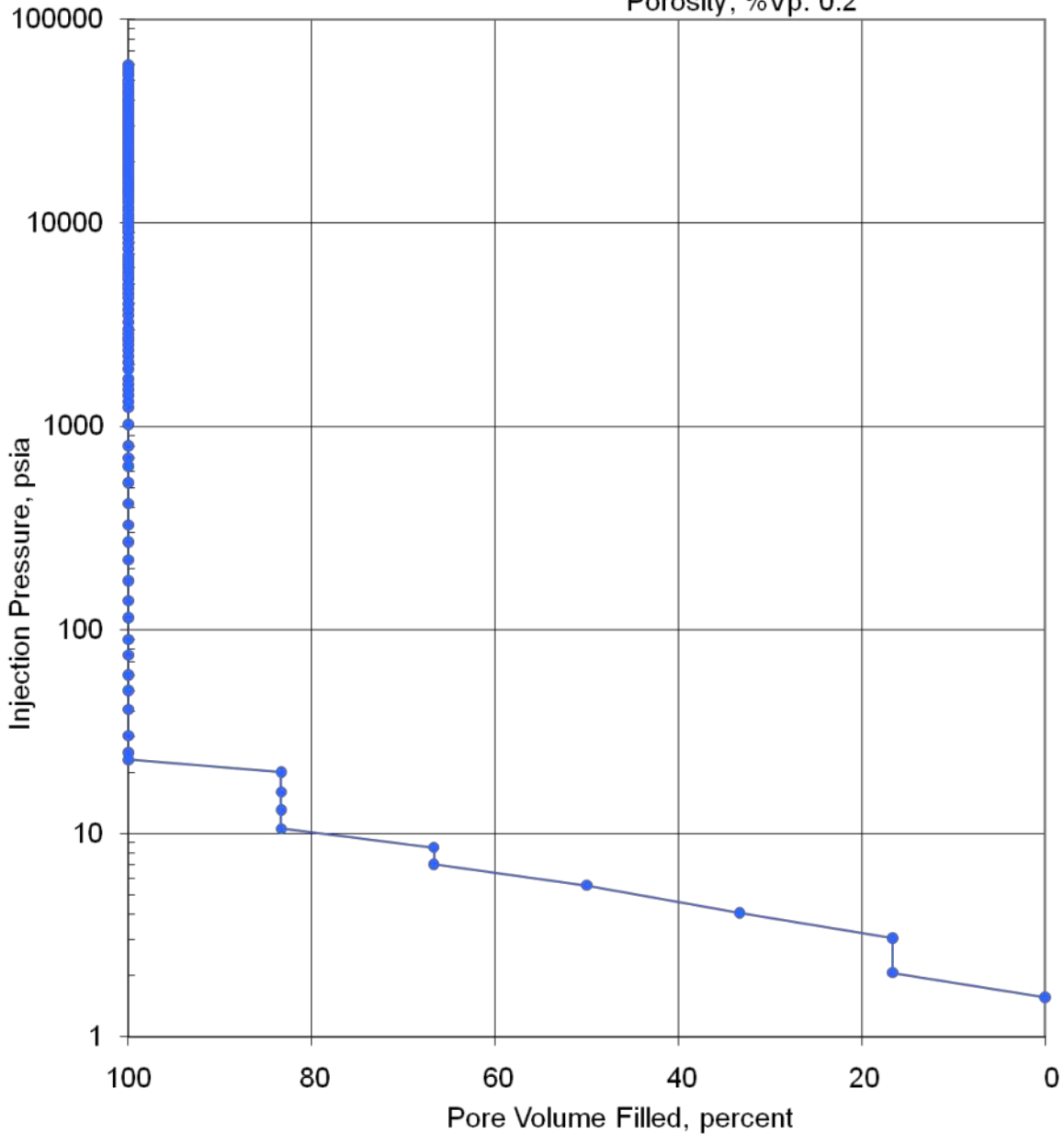


**Figure 22 – Results of the mercury porosimetry analysis on the duplicate black mudstone rock sample as pore volume filled per pressure unit.**



### CAPILLARY PRESSURE vs. WETTING PHASE SATURATION

Mercury Pressure: 0 - 60000

(METHODOLOGY: ASTM D4404, API RP40)

Project Name: NAWC  
Project No.: ER-0715

Sample ID: Black mudstone 2  
Depth, ft.: 50  
Porosity, %Vp: 0.2

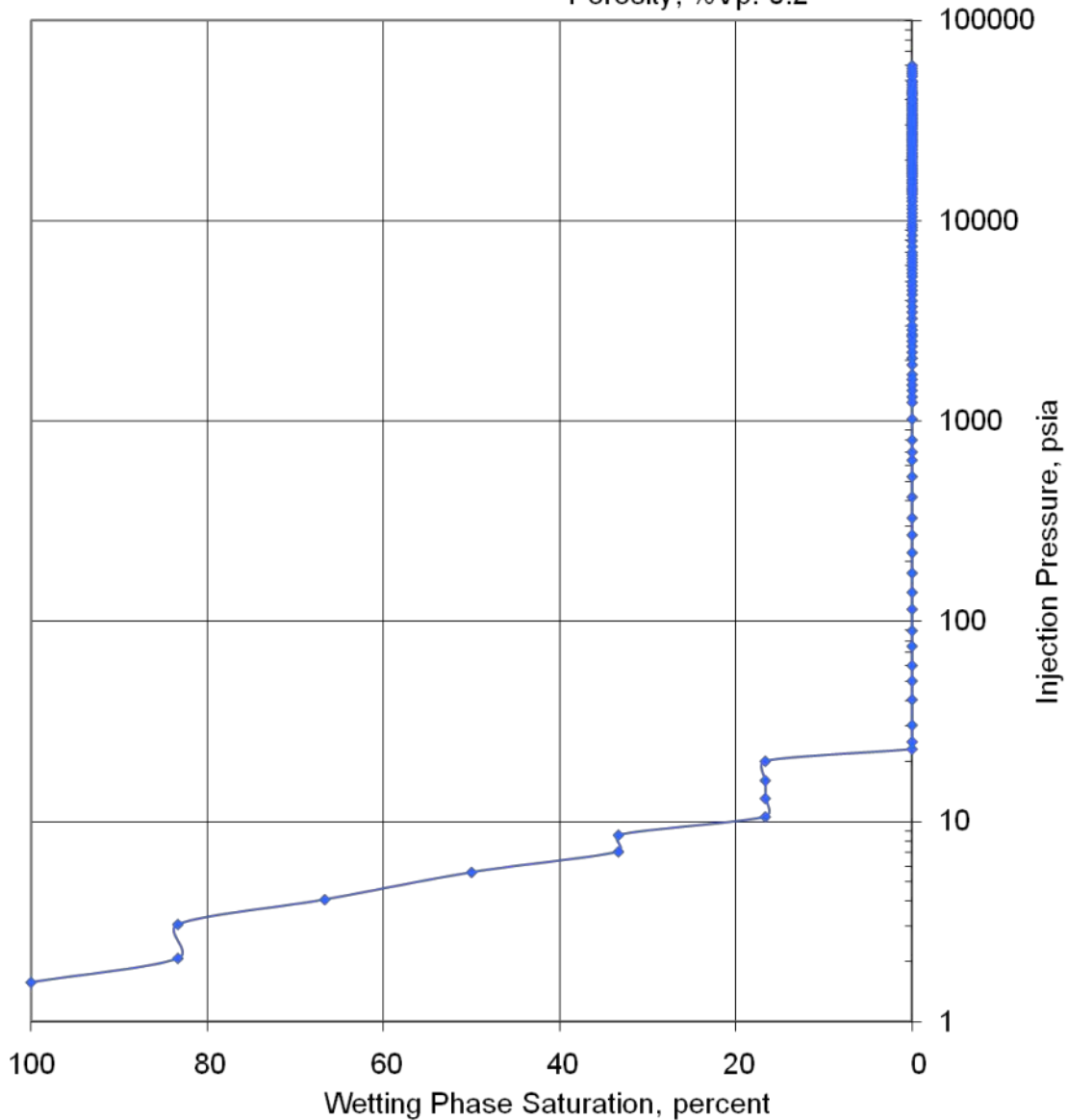


**Figure 23 – Results of the mercury porosimetry analysis on the duplicate black mudstone rock sample as wetting phase saturation per capillary pressure.**



PORE THROAT RADIUS DISTRIBUTION  
Mercury Pressure: 0 - 60000  
(METHODOLOGY: ASTM D4404, API RP40)

Project Name: NAWC  
Project No.: ER-0715

Sample ID: Black mudstone 2  
Depth, ft.: 50  
Porosity, %Vp: 0.2

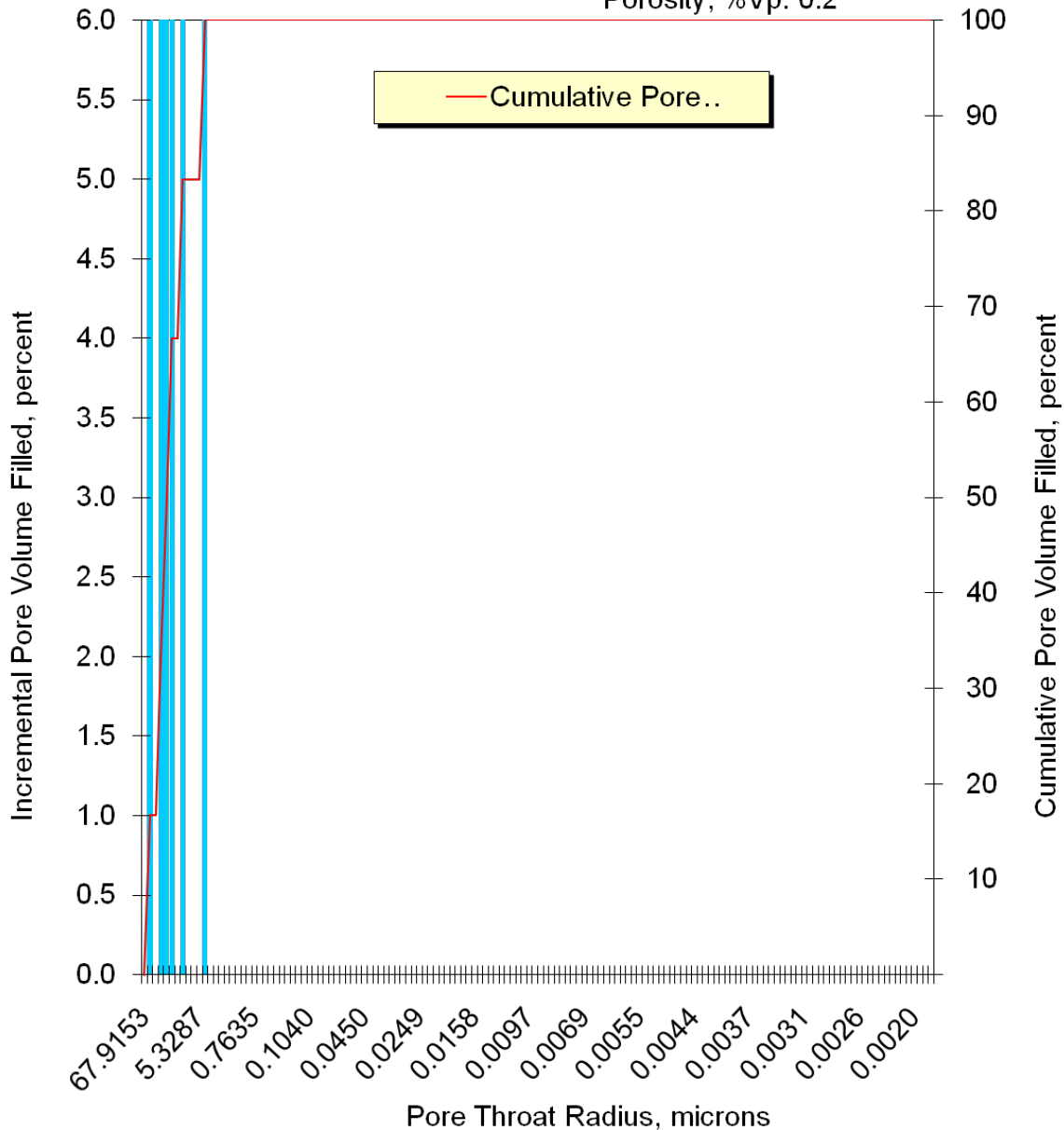


**Figure 24 – Pore throat radius distribution of the duplicate black mudstone sample during the mercury porosimetry analysis.**

**Table 9 – Results of the mercury porosimetry analysis on the triplicate black mudstone rock sample.**

PTS File No:	38521			PTS Laboratories
Client:	Queen's University			
<b>MERCURY INJECTION SUMMARY</b>				
PROJECT NAME:	NAWC		Sample ID:	Black mudstone 3
PROJECT NO:	ER-0715		Depth, ft.:	50
			Porosity, %Vp:	0.1
*INJECTION PRESSURE, psia	PORE THROAT Radius, microns	NON-WETTING PHASE SATURATION		WETTING PHASE SATURATION, percent
		INCREMENTAL, percent	CUMULATIVE, percent	
1.57	67.9	0.000	0.000	100.0
2.07	51.5	20.0	20.0	80.0
3.06	34.8	20.0	40.0	60.0
4.07	26.2	20.0	60.0	40.0
5.57	19.1	0.0	60.0	40.0
7.06	15.1	0.0	60.0	40.0
8.55	12.5	20.000	80.0	20.0
10.5	10.1	0.0	80.0	20.0
13.0	8.18	0.000	80.0	20.0
16.0	6.66	0.000	80.0	20.0
20.0	5.33	0.000	80.0	20.0
23.0	4.64	0.0	80.0	20.0
25.0	4.27	20.000	100	0.000
30.1	3.54	0.000	100	0.000
40.4	2.64	0.000	100	0.000
50.1	2.13	0.000	100	0.000
59.9	1.78	0.000	100	0.000
74.7	1.43	0.000	100	0.000
89.9	1.19	0.000	100	0.000
115	0.931	0.000	100	0.000
140	0.760	0.000	100	0.000
176	0.607	0.000	100	0.000
219	0.486	0.000	100	0.000
275	0.388	0.000	100	0.000
330	0.323	0.000	100	0.000
433	0.246	0.000	100	0.000
533	0.200	0.000	100	0.000
638	0.167	0.000	100	0.000
698	0.153	0.000	100	0.000
800	0.133	0.000	100	0.000
1019	0.105	0.000	100	0.000
1244	0.086	0.000	100	0.000
1316	0.081	0.000	100	0.000

1420	0.075	0.000	100	0.000
1524	0.070	0.000	100	0.000
1618	0.066	0.000	100	0.000
1730	0.062	0.000	100	0.000
1916	0.056	0.000	100	0.000
2076	0.051	0.000	100	0.000
2216	0.048	0.000	100	0.000
2369	0.045	0.000	100	0.000
2518	0.042	0.000	100	0.000
2668	0.040	0.000	100	0.000
2714	0.039	0.000	100	0.000
2866	0.037	0.000	100	0.000
3019	0.035	0.000	100	0.000
3271	0.033	0.000	100	0.000
3518	0.030	0.000	100	0.000
3750	0.028	0.000	100	0.000
4001	0.027	0.000	100	0.000
4301	0.025	0.000	100	0.000
4539	0.023	0.000	100	0.000
4767	0.022	0.000	100	0.000
4985	0.021	0.000	100	0.000
5288	0.020	0.000	100	0.000
5486	0.019	0.000	100	0.000
5745	0.019	0.000	100	0.000
5990	0.018	0.000	100	0.000
6229	0.017	0.000	100	0.000
6476	0.016	0.000	100	0.000
6727	0.016	0.000	100	0.000
6971	0.015	0.000	100	0.000
7463	0.014	0.000	100	0.000
7968	0.013	0.000	100	0.000
8514	0.013	0.000	100	0.000
8992	0.012	0.000	100	0.000
9303	0.011	0.000	100	0.000
9589	0.011	0.000	100	0.000
10024	0.011	0.000	100	0.000
10469	0.010	0.000	100	0.000
10996	0.010	0.000	100	0.000
11476	0.009	0.000	100	0.000
11988	0.009	0.000	100	0.000
12589	0.008	0.000	100	0.000
13065	0.008	0.000	100	0.000
13622	0.008	0.000	100	0.000
13954	0.008	0.000	100	0.000
14300	0.007	0.000	100	0.000
14573	0.007	0.000	100	0.000
14949	0.007	0.000	100	0.000
15399	0.007	0.000	100	0.000

15758	0.007	0.000	100	0.000
16151	0.007	0.000	100	0.000
16658	0.006	0.000	100	0.000
16999	0.006	0.000	100	0.000
17337	0.006	0.000	100	0.000
17682	0.006	0.000	100	0.000
18097	0.006	0.000	100	0.000
18475	0.006	0.000	100	0.000
18771	0.006	0.000	100	0.000
19179	0.006	0.000	100	0.000
19792	0.005	0.000	100	0.000
20281	0.005	0.000	100	0.000
20783	0.005	0.000	100	0.000
21152	0.005	0.000	100	0.000
21620	0.005	0.000	100	0.000
22035	0.005	0.000	100	0.000
22613	0.005	0.000	100	0.000
23167	0.005	0.000	100	0.000
23716	0.004	0.000	100	0.000
24050	0.004	0.000	100	0.000
24590	0.004	0.000	100	0.000
25012	0.004	0.000	100	0.000
25397	0.004	0.000	100	0.000
25850	0.004	0.000	100	0.000
26408	0.004	0.000	100	0.000
26864	0.004	0.000	100	0.000
27334	0.004	0.000	100	0.000
27728	0.004	0.000	100	0.000
28167	0.004	0.000	100	0.000
28935	0.004	0.000	100	0.000
29413	0.004	0.000	100	0.000
29937	0.004	0.000	100	0.000
30529	0.003	0.000	100	0.000
30949	0.003	0.000	100	0.000
31330	0.003	0.000	100	0.000
31855	0.003	0.000	100	0.000
32405	0.003	0.000	100	0.000
32908	0.003	0.000	100	0.000
33478	0.003	0.000	100	0.000
34057	0.003	0.000	100	0.000
34676	0.003	0.000	100	0.000
35475	0.003	0.000	100	0.000
36193	0.003	0.000	100	0.000
37034	0.003	0.000	100	0.000
37652	0.003	0.000	100	0.000
38457	0.003	0.000	100	0.000
39191	0.003	0.000	100	0.000
40080	0.003	0.000	100	0.000

40596	0.003	0.000	100	0.000
41070	0.003	0.000	100	0.000
42615	0.003	0.000	100	0.000
43433	0.002	0.000	100	0.000
44041	0.002	0.000	100	0.000
45060	0.002	0.000	100	0.000
46508	0.002	0.000	100	0.000
47978	0.002	0.000	100	0.000
49455	0.002	0.000	100	0.000
50171	0.002	0.000	100	0.000
52965	0.002	0.000	100	0.000
54416	0.002	0.000	100	0.000
55903	0.002	0.000	100	0.000
57913	0.002	0.000	100	0.000
59876	0.002	0.000	100	0.000



**PORE VOLUME FILLED vs PRESSURE**  
Mercury Pressure: 0 - 60000 psia  
(METHODOLOGY: ASTM D4404, API RP40)

Project Name: NAWC  
Project No.: ER-0715

Sample ID: Black mudstone 3  
Depth, ft.: 50  
Porosity, %Vp: 0.1

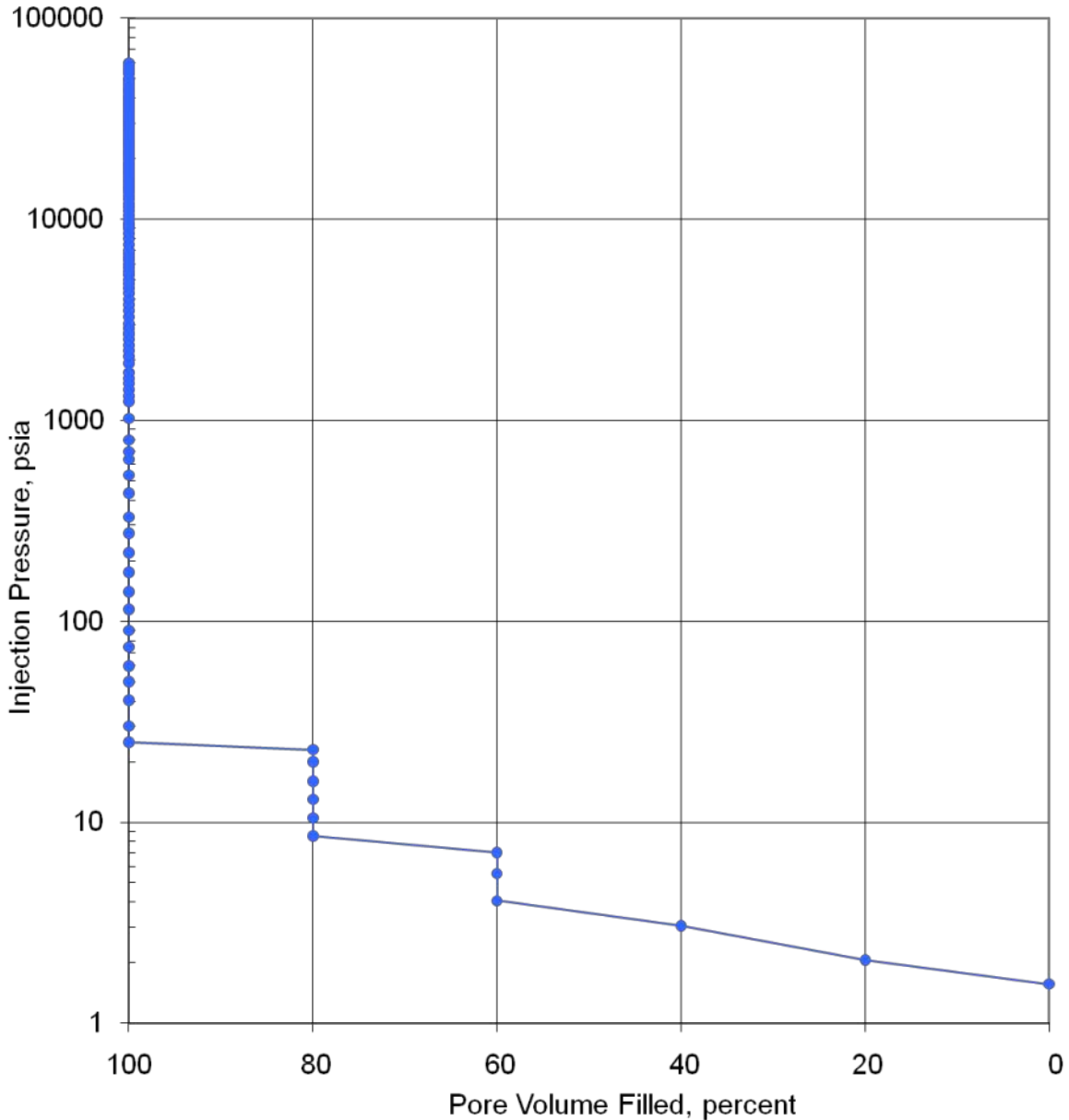


**Figure 25 – Results of the mercury porosimetry analysis on the triplicate black mudstone rock sample as pore volume filled per pressure unit.**



### CAPILLARY PRESSURE vs. WETTING PHASE SATURATION

Mercury Pressure: 0 - 60000  
(METHODOLOGY: ASTM D4404, API RP40)

Project Name: NAWC  
Project No.: ER-0715

Sample ID: Black mudstone 3  
Depth, ft.: 50  
Porosity, %Vp: 0.1

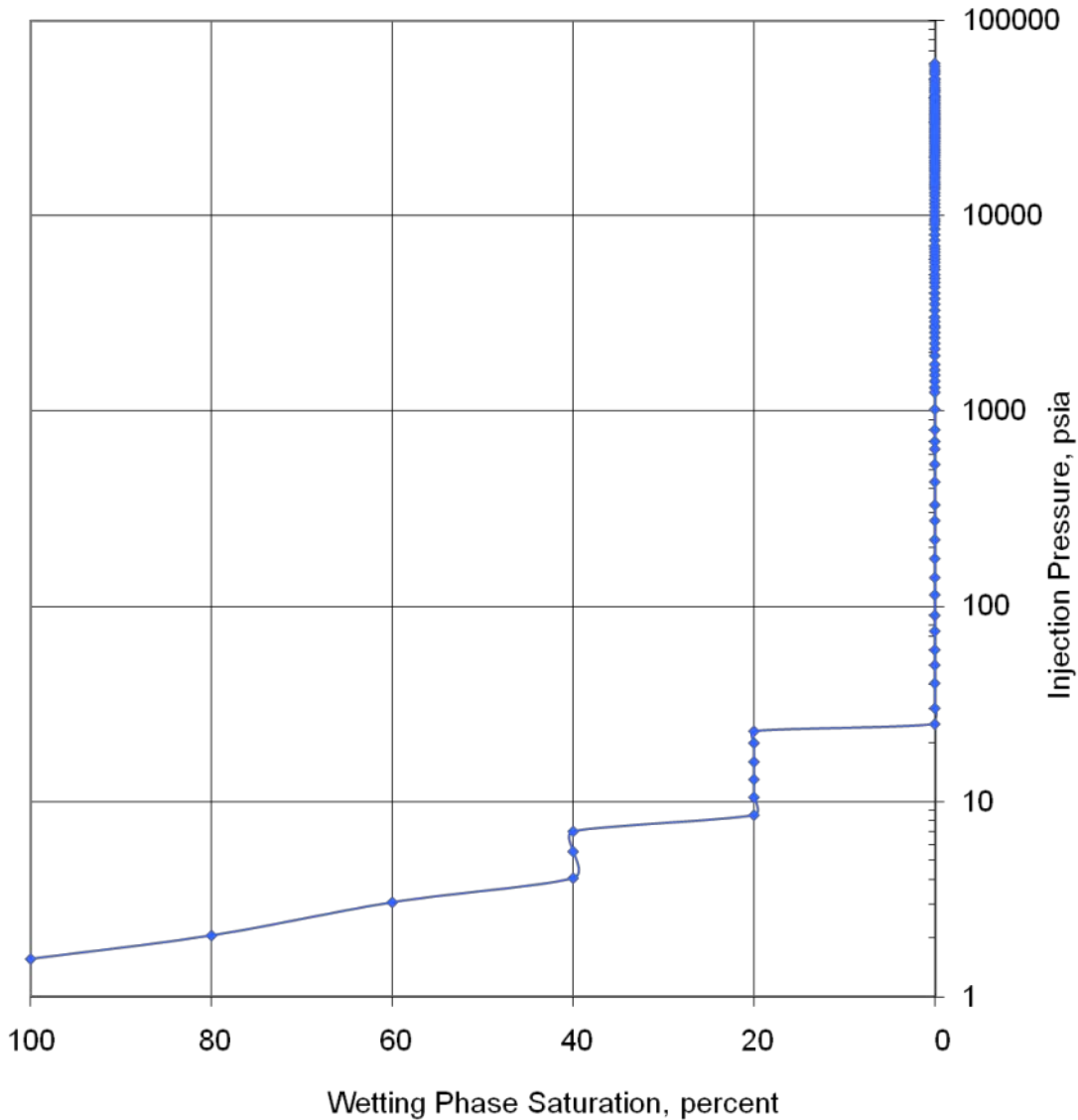


**Figure 26 – Results of the mercury porosimetry analysis on the triplicate black mudstone rock sample as wetting phase saturation per capillary pressure.**



PORE THROAT RADIUS DISTRIBUTION  
Mercury Pressure: 0 - 60000  
(METHODOLOGY: ASTM D4404, API RP40)

Project Name: NAWC  
Project No.: ER-0715

Sample ID: Black mudstone 3  
Depth, ft.: 50  
Porosity, %Vp: 0.1

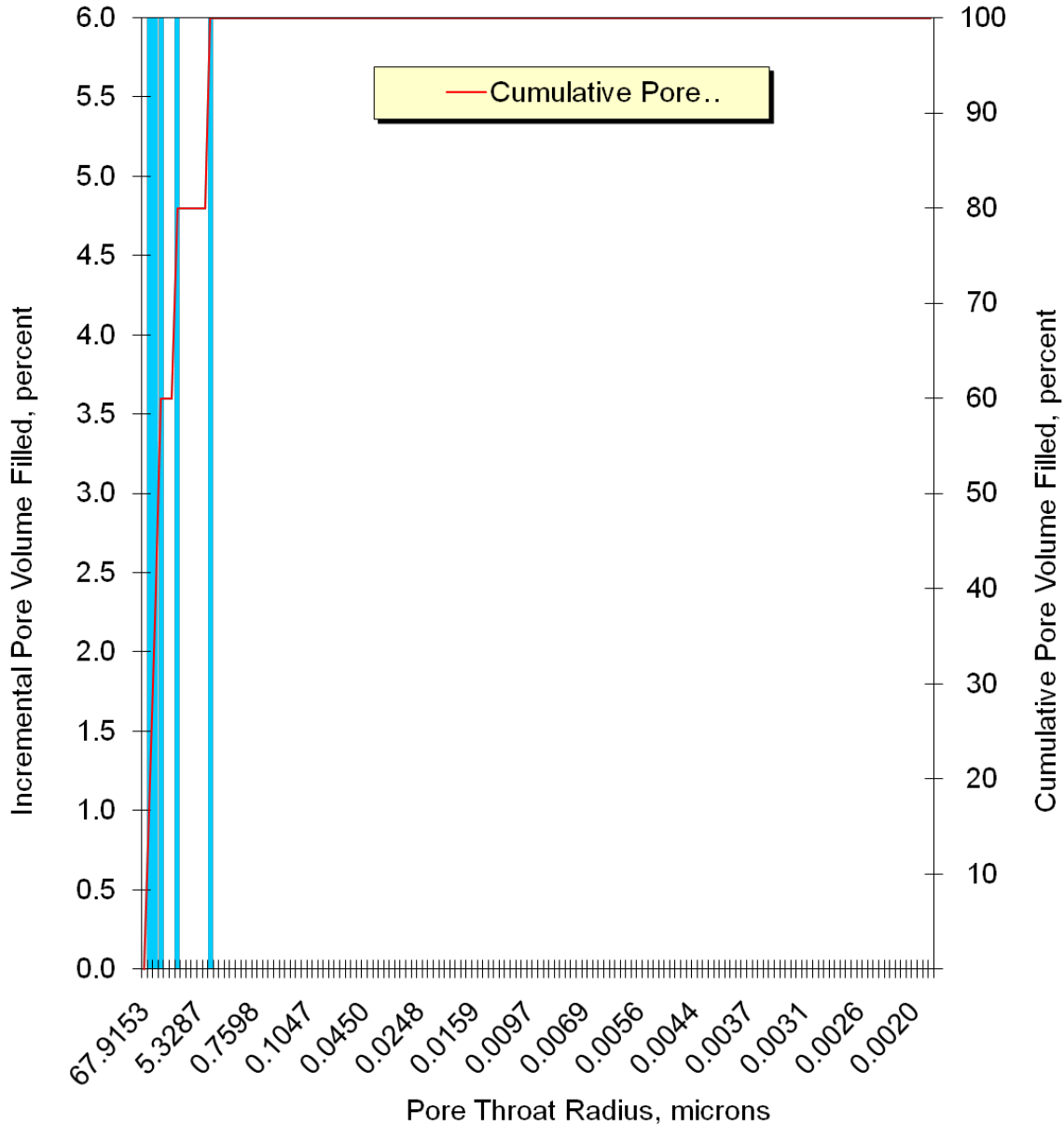


**Figure 27 – Pore throat radius distribution of the triplicate black mudstone sample during the mercury porosimetry analysis.**

**Table 10 – Results of the mercury porosimetry analysis on the siltstone rock sample.**

PTS File No:	39380			<b>PTS</b> Laboratories
Client:	Queen's University			
<b>MERCURY INJECTION SUMMARY</b>				
PROJECT NAME:	NAWC		Sample ID:	Siltstone 1
PROJECT NO:	ER-0715		Depth, ft.:	70
			Porosity, %Vp:	0.6
*INJECTION PRESSURE, psia	PORE THROAT Radius, microns	NON-WETTING PHASE SATURATION		WETTING PHASE SATURATION, percent
		INCREMENTAL, percent	CUMULATIVE, percent	
0.510	209	0.000	0.000	100.0
0.560	190	0.000	0.000	100.0
0.600	178	0.000	0.000	100.0
0.640	167	0.000	0.000	100.0
0.690	155	0.000	0.000	100.0
0.730	146	0.000	0.000	100.0
0.790	135	0.000	0.000	100.0
0.860	124	0.000	0.000	100.0
0.920	116	0.000	0.000	100.0
0.990	108	0.000	0.000	100.0
1.05	102	0.000	0.000	100.0
1.13	94.4	0.000	0.000	100.0
1.22	87.4	0.000	0.000	100.0
1.31	81.4	0.000	0.000	100.0
1.41	75.6	0.000	0.000	100.0
1.51	70.6	0.000	0.000	100.0
1.62	65.8	0.000	0.000	100.0
1.74	61.3	0.000	0.000	100.0
1.87	57.0	0.000	0.000	100.0
2.01	53.0	0.000	0.000	100.0
2.16	49.4	0.000	0.000	100.0
2.32	46.0	0.000	0.000	100.0
2.51	42.5	0.000	0.000	100.0
2.69	39.6	0.000	0.000	100.0
2.91	36.6	0.000	0.000	100.0
3.12	34.2	0.000	0.000	100.0
3.36	31.7	0.000	0.000	100.0
3.61	29.5	0.000	0.000	100.0
3.89	27.4	0.000	0.000	100.0
4.19	25.4	0.000	0.000	100.0
4.50	23.7	0.000	0.000	100.0
4.85	22.0	0.000	0.000	100.0
5.22	20.4	0.000	0.000	100.0

5.62	19.0	0.000	0.000	100.0
6.04	17.7	0.000	0.000	100.0
6.50	16.4	0.000	0.000	100.0
7.00	15.2	0.000	0.000	100.0
7.53	14.2	0.000	0.000	100.0
8.11	13.1	0.000	0.000	100.0
8.73	12.2	0.000	0.000	100.0
9.39	11.4	0.000	0.000	100.0
10.1	10.6	0.000	0.000	100.0
10.9	9.79	0.000	0.000	100.0
11.7	9.12	0.000	0.000	100.0
12.6	8.47	0.000	0.000	100.0
13.6	7.85	0.000	0.000	100.0
14.6	7.31	0.000	0.000	100.0
15.7	6.80	0.000	0.000	100.0
16.9	6.31	0.000	0.000	100.0
18.2	5.86	0.000	0.000	100.0
19.6	5.44	0.000	0.000	100.0
21.1	5.06	0.000	0.000	100.0
22.7	4.70	0.000	0.000	100.0
23.4	4.56	0.000	0.000	100.0
25.9	4.11	0.000	0.000	100.0
26.9	3.97	0.000	0.000	100.0
30.3	3.52	0.000	0.000	100.0
32.6	3.28	0.000	0.000	100.0
35.3	3.02	0.000	0.000	100.0
39.0	2.74	0.000	0.000	100.0
41.2	2.59	0.000	0.000	100.0
45.1	2.36	0.000	0.000	100.0
48.9	2.18	0.000	0.000	100.0
52.4	2.03	0.000	0.000	100.0
56.4	1.89	0.000	0.000	100.0
62.5	1.71	0.000	0.000	100.0
65.3	1.63	0.000	0.000	100.0
71.2	1.50	0.000	0.000	100.0
75.1	1.42	0.000	0.000	100.0
81.9	1.30	0.000	0.000	100.0
89.9	1.19	0.000	0.000	100.0
96.7	1.10	0.000	0.000	100.0
103	1.04	0.000	0.000	100.0
112	0.950	0.000	0.000	100.0
119	0.894	0.000	0.000	100.0
129	0.826	0.000	0.000	100.0
139	0.765	0.000	0.000	100.0
151	0.704	0.000	0.000	100.0
162	0.658	0.000	0.000	100.0
174	0.613	0.000	0.000	100.0
188	0.568	0.000	0.000	100.0

202	0.528	0.000	0.000	100.0
216	0.494	0.000	0.000	100.0
234	0.455	0.000	0.000	100.0
252	0.423	0.000	0.000	100.0
272	0.391	0.000	0.000	100.0
293	0.364	0.000	0.000	100.0
315	0.339	0.000	0.000	100.0
339	0.315	0.000	0.000	100.0
364	0.293	0.000	0.000	100.0
394	0.271	0.000	0.000	100.0
424	0.252	0.000	0.000	100.0
457	0.234	0.000	0.000	100.0
491	0.217	0.000	0.000	100.0
529	0.201	0.000	0.000	100.0
570	0.187	0.000	0.000	100.0
612	0.174	0.000	0.000	100.0
661	0.161	0.000	0.000	100.0
709	0.150	0.000	0.000	100.0
764	0.139	0.000	0.000	100.0
823	0.129	0.000	0.000	100.0
886	0.120	0.000	0.000	100.0
954	0.112	0.000	0.000	100.0
1027	0.104	0.000	0.000	100.0
1105	0.097	0.000	0.000	100.0
1188	0.090	0.000	0.000	100.0
1280	0.083	0.000	0.000	100.0
1374	0.078	0.000	0.000	100.0
1482	0.072	0.000	0.000	100.0
1595	0.067	0.000	0.000	100.0
1714	0.062	0.000	0.000	100.0
1846	0.058	0.000	0.000	100.0
1987	0.054	0.000	0.000	100.0
2138	0.050	0.000	0.000	100.0
2300	0.046	0.000	0.000	100.0
2474	0.043	0.000	0.000	100.0
2663	0.040	0.000	0.000	100.0
2866	0.037	0.000	0.000	100.0
3082	0.035	0.000	0.000	100.0
3318	0.032	0.000	0.000	100.0
3571	0.030	0.000	0.000	100.0
3840	0.028	0.000	0.000	100.0
4129	0.026	0.000	0.000	100.0
4441	0.024	0.000	0.000	100.0
4778	0.022	0.000	0.000	100.0
5144	0.021	0.000	0.000	100.0
5534	0.019	0.000	0.000	100.0
5958	0.018	0.000	0.000	100.0
6407	0.017	0.000	0.000	100.0

6899	0.015	0.000	0.000	100.0
7424	0.014	0.000	0.000	100.0
7997	0.013	0.000	0.000	100.0
8599	0.012	0.000	0.000	100.0
9261	0.012	0.000	0.000	100.0
9965	0.011	0.000	0.000	100.0
10725	0.010	0.000	0.000	100.0
11542	0.009	0.000	0.000	100.0
12422	0.009	2.35	2.35	97.7
13369	0.008	1.37	3.72	96.3
14388	0.007	0.456	4.17	95.8
15482	0.007	2.28	6.45	93.5
16660	0.006	2.28	8.74	91.3
17929	0.006	1.37	10.1	89.9
19295	0.006	0.456	10.6	89.4
20771	0.005	0.91	11.5	88.5
22361	0.005	2.74	14.2	85.8
24067	0.004	3.65	17.9	82.1
25900	0.004	4.56	22.4	77.6
27874	0.004	4.56	27.0	73.0
29996	0.004	4.56	31.6	68.4
32279	0.003	4.56	36.1	63.9
34736	0.003	4.56	40.7	59.3
37376	0.003	4.56	45.2	54.8
40217	0.003	8.21	53.5	46.5
43282	0.002	10.0	63.5	36.5
46582	0.002	9.13	72.6	27.4
50126	0.002	9.13	81.7	18.3
53924	0.002	9.13	90.9	9.13
58038	0.002	9.13	100	0.000



**PORE VOLUME FILLED vs PRESSURE**  
Mercury Pressure: 0 - 60000 psia  
(METHODOLOGY: ASTM D4404, API RP40)

Project Name: NAWC  
Project No.: ER-0715

Sample ID: Siltstone 1  
Depth, ft.: 70  
Porosity, %Vp: 0.6

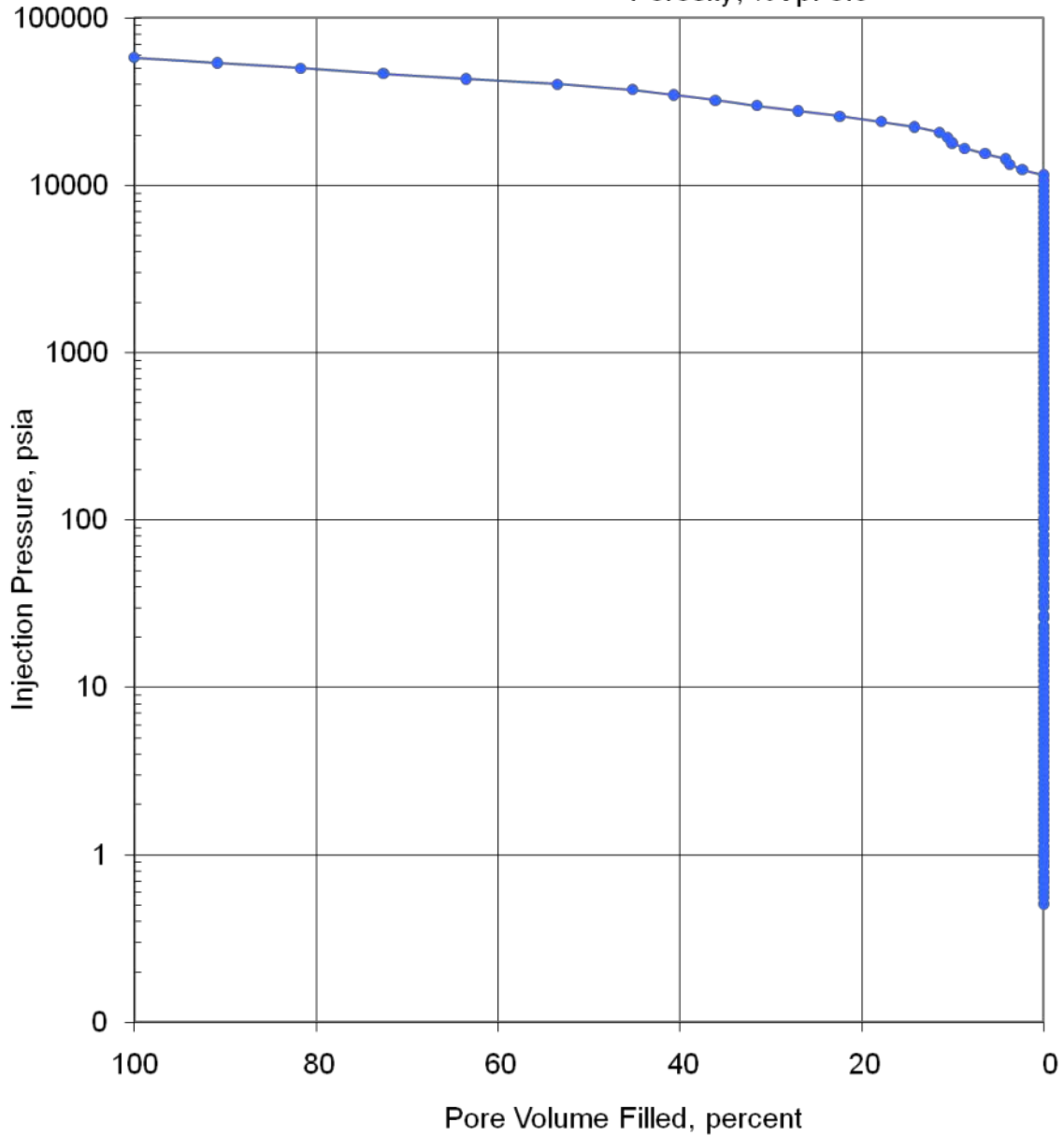


**Figure 28 – Results of the mercury porosimetry analysis on the siltstone rock sample as pore volume filled per pressure unit.**



### CAPILLARY PRESSURE vs. WETTING PHASE SATURATION

Mercury Pressure: 0 - 60000  
(METHODOLOGY: ASTM D4404, API RP40)

Project Name: NAWC  
Project No.: ER-0715

Sample ID: Siltstone 1  
Depth, ft.: 70  
Porosity, %Vp: 0.6

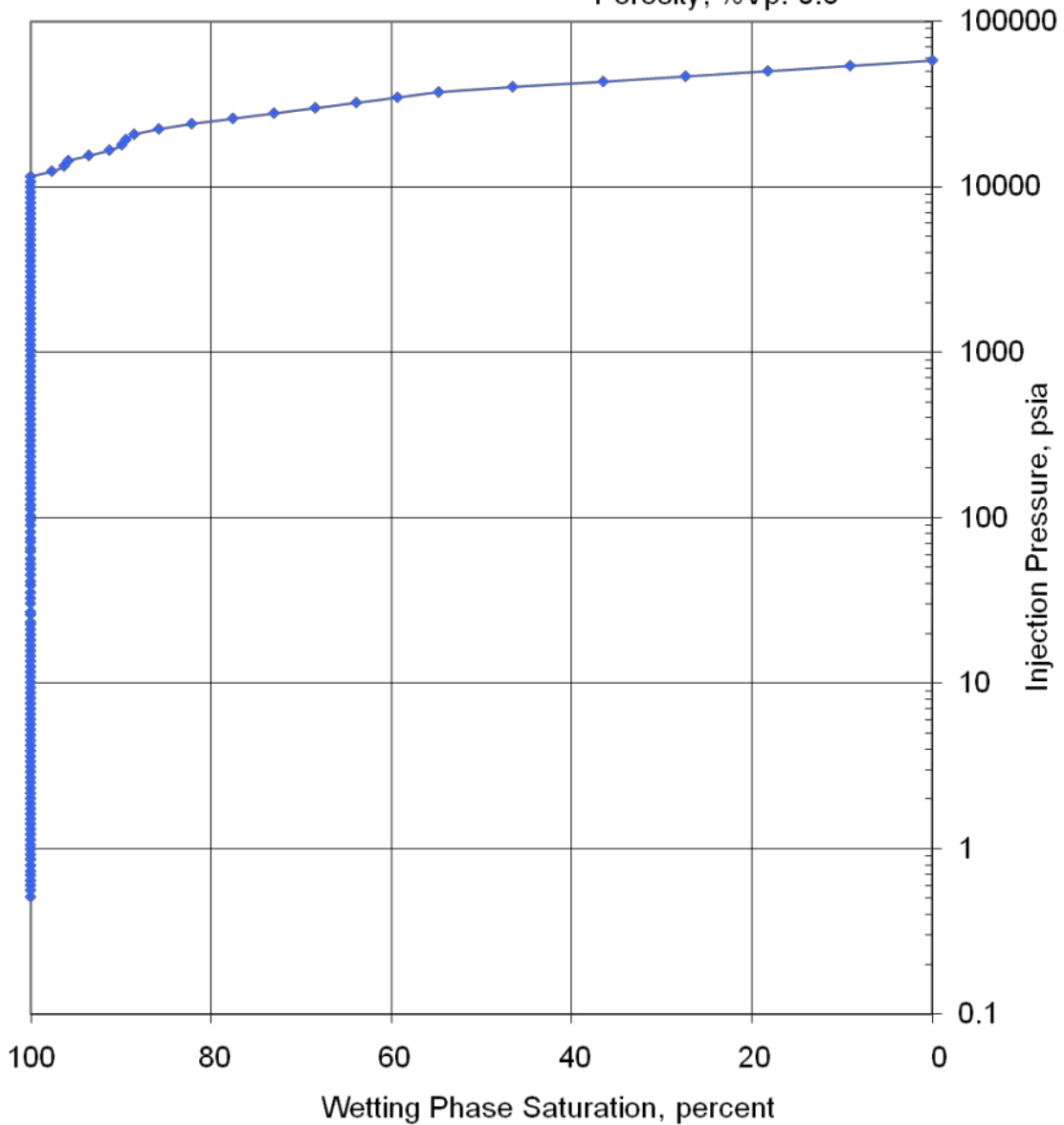


**Figure 29 – Results of the mercury porosimetry analysis on the siltstone rock sample as wetting phase saturation per capillary pressure.**



**PORE THROAT RADIUS DISTRIBUTION**  
Mercury Pressure: 0 - 60000  
(METHODOLOGY: ASTM D4404, API RP40)

Project Name: NAWC  
Project No.: ER-0715

Sample ID: Siltstone 1  
Depth, ft.: 70  
Porosity, %Vp: 0.6

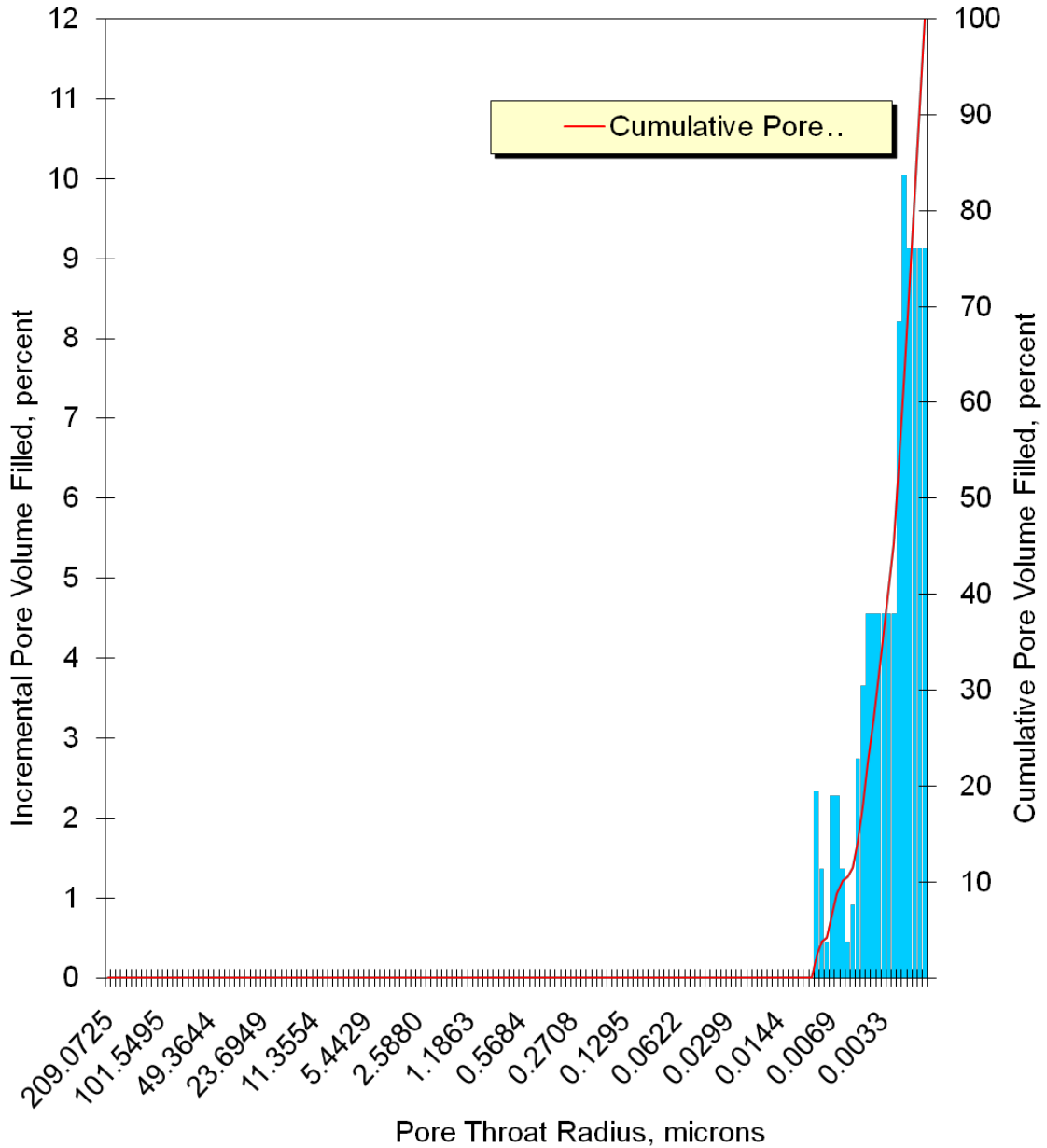


**Figure 30 – Pore throat radius distribution of the siltstone sample during the mercury porosimetry analysis.**

**Table 11 – Results of the mercury porosimetry analysis on the duplicate siltstone rock sample.**

PTS File No:	39380			<b>PTS</b> Laboratories
Client:	Queen's University			
<b>MERCURY INJECTION SUMMARY</b>				
PROJECT NAME:	NAWC		Sample ID:	Siltstone 2
PROJECT NO:	ER-0715		Depth, ft.:	70
			Porosity, %Vp:	0.6
*INJECTION PRESSURE, psia	PORE THROAT Radius, microns	NON-WETTING PHASE SATURATION		WETTING PHASE SATURATION, percent
		INCREMENTAL, percent	CUMULATIVE, percent	
0.510	209	0.000	0.000	100.0
0.560	190	0.000	0.000	100.0
0.600	178	0.000	0.000	100.0
0.640	167	0.000	0.000	100.0
0.690	155	0.000	0.000	100.0
0.730	146	0.000	0.000	100.0
0.790	135	0.000	0.000	100.0
0.860	124	0.000	0.000	100.0
0.920	116	0.000	0.000	100.0
0.990	108	0.000	0.000	100.0
1.05	102	0.000	0.000	100.0
1.13	94.4	0.000	0.000	100.0
1.22	87.4	0.000	0.000	100.0
1.31	81.4	0.000	0.000	100.0
1.41	75.6	0.000	0.000	100.0
1.51	70.6	0.000	0.000	100.0
1.62	65.8	0.000	0.000	100.0
1.74	61.3	0.000	0.000	100.0
1.87	57.0	0.000	0.000	100.0
2.01	53.0	0.000	0.000	100.0
2.16	49.4	0.000	0.000	100.0
2.32	46.0	0.000	0.000	100.0
2.51	42.5	0.000	0.000	100.0
2.69	39.6	0.000	0.000	100.0
2.91	36.6	0.000	0.000	100.0
3.12	34.2	0.000	0.000	100.0
3.36	31.7	0.000	0.000	100.0
3.61	29.5	0.000	0.000	100.0
3.89	27.4	0.000	0.000	100.0
4.19	25.4	0.000	0.000	100.0
4.50	23.7	0.000	0.000	100.0
4.85	22.0	0.000	0.000	100.0
5.22	20.4	0.000	0.000	100.0

5.62	19.0	0.000	0.000	100.0
6.04	17.7	0.000	0.000	100.0
6.50	16.4	0.000	0.000	100.0
7.00	15.2	0.000	0.000	100.0
7.53	14.2	0.000	0.000	100.0
8.11	13.1	0.000	0.000	100.0
8.73	12.2	0.000	0.000	100.0
9.39	11.4	0.000	0.000	100.0
10.1	10.6	0.000	0.000	100.0
10.9	9.79	0.000	0.000	100.0
11.7	9.12	0.000	0.000	100.0
12.6	8.47	0.000	0.000	100.0
13.6	7.85	0.000	0.000	100.0
14.6	7.31	0.000	0.000	100.0
15.7	6.80	0.000	0.000	100.0
16.9	6.31	0.000	0.000	100.0
18.2	5.86	0.000	0.000	100.0
19.6	5.44	0.000	0.000	100.0
21.1	5.06	0.000	0.000	100.0
22.7	4.70	0.000	0.000	100.0
24.4	4.37	0.000	0.000	100.0
26.5	4.02	0.000	0.000	100.0
29.9	3.57	0.000	0.000	100.0
32.6	3.27	0.000	0.000	100.0
34.9	3.06	0.000	0.000	100.0
37.3	2.86	0.000	0.000	100.0
39.8	2.68	0.000	0.000	100.0
43.5	2.45	0.000	0.000	100.0
47.3	2.26	0.000	0.000	100.0
50.5	2.11	0.000	0.000	100.0
55.1	1.94	0.000	0.000	100.0
59.2	1.80	0.000	0.000	100.0
63.9	1.67	0.000	0.000	100.0
70.3	1.52	0.000	0.000	100.0
75.3	1.42	0.000	0.000	100.0
81.2	1.31	0.000	0.000	100.0
88.4	1.21	0.000	0.000	100.0
95.6	1.12	0.000	0.000	100.0
103.4	1.03	0.000	0.000	100.0
112	0.96	0.000	0.000	100.0
118	0.900	0.000	0.000	100.0
129	0.829	0.000	0.000	100.0
139	0.768	0.000	0.000	100.0
150	0.709	0.000	0.000	100.0
161	0.664	0.000	0.000	100.0
174	0.612	0.000	0.000	100.0
186	0.574	0.000	0.000	100.0
203	0.526	0.000	0.000	100.0

218	0.488	0.000	0.000	100.0
234	0.456	0.000	0.000	100.0
252	0.423	0.000	0.000	100.0
270	0.394	0.000	0.000	100.0
293	0.364	0.000	0.000	100.0
315	0.338	0.000	0.000	100.0
337	0.316	0.000	0.000	100.0
366	0.291	0.000	0.000	100.0
393	0.271	0.000	0.000	100.0
422	0.253	0.000	0.000	100.0
455	0.234	0.000	0.000	100.0
492	0.217	0.000	0.000	100.0
530	0.201	0.000	0.000	100.0
570	0.187	0.000	0.000	100.0
612	0.174	0.000	0.000	100.0
659	0.162	0.000	0.000	100.0
710	0.150	0.000	0.000	100.0
764	0.140	0.000	0.000	100.0
823	0.130	0.000	0.000	100.0
884	0.121	0.000	0.000	100.0
952	0.112	0.000	0.000	100.0
1025	0.104	0.000	0.000	100.0
1103	0.097	0.000	0.000	100.0
1187	0.090	0.000	0.000	100.0
1278	0.083	0.000	0.000	100.0
1374	0.078	0.000	0.000	100.0
1480	0.072	0.000	0.000	100.0
1592	0.067	0.000	0.000	100.0
1714	0.062	0.000	0.000	100.0
1845	0.058	0.000	0.000	100.0
1986	0.054	0.000	0.000	100.0
2136	0.050	0.000	0.000	100.0
2299	0.046	0.000	0.000	100.0
2475	0.043	0.000	0.000	100.0
2661	0.040	0.000	0.000	100.0
2865	0.037	0.000	0.000	100.0
3082	0.035	0.000	0.000	100.0
3318	0.032	0.000	0.000	100.0
3567	0.030	0.000	0.000	100.0
3839	0.028	0.000	0.000	100.0
4128	0.026	0.000	0.000	100.0
4440	0.024	0.000	0.000	100.0
4776	0.022	0.000	0.000	100.0
5140	0.021	0.000	0.000	100.0
5534	0.019	0.000	0.000	100.0
5956	0.018	0.000	0.000	100.0
6413	0.017	0.000	0.000	100.0
6898	0.015	0.000	0.000	100.0

7425	0.014	0.000	0.000	100.0
7994	0.013	0.000	0.000	100.0
8602	0.012	0.000	0.000	100.0
9261	0.012	0.000	0.000	100.0
9967	0.011	0.000	0.000	100.0
10722	0.010	0.000	0.000	100.0
11540	0.009	1.48	1.48	98.5
12419	0.009	1.43	2.91	97.1
13365	0.008	0.952	3.86	96.1
14385	0.007	1.90	5.76	94.2
15486	0.007	2.38	8.14	91.9
16677	0.006	3.33	11.5	88.5
17950	0.006	2.86	14.3	85.7
19312	0.006	4.76	19.1	80.9
20787	0.005	4.76	23.8	76.2
22370	0.005	9.52	33.4	66.6
24072	0.004	8.09	41.5	58.5
25907	0.004	6.19	47.6	52.4
27873	0.004	9.52	57.2	42.8
29987	0.004	8.09	65.3	34.7
32283	0.003	6.19	71.4	28.6
34739	0.003	4.76	76.2	23.8
37372	0.003	4.76	81.0	19.0
40213	0.003	4.76	85.7	14.3
43278	0.002	4.76	90.5	9.52
46573	0.002	2.38	92.9	7.14
50115	0.002	2.38	95.2	4.76
53935	0.002	2.38	97.6	2.38
58020	0.002	2.38	100	0.000



PORE VOLUME FILLED vs PRESSURE  
Mercury Pressure: 0 - 60000 psia  
(METHODOLOGY: ASTM D4404, API RP40)

Project Name: NAWC  
Project No.: ER-0715

Sample ID: Siltstone 2  
Depth, ft.: 70  
Porosity, %Vp: 0.6

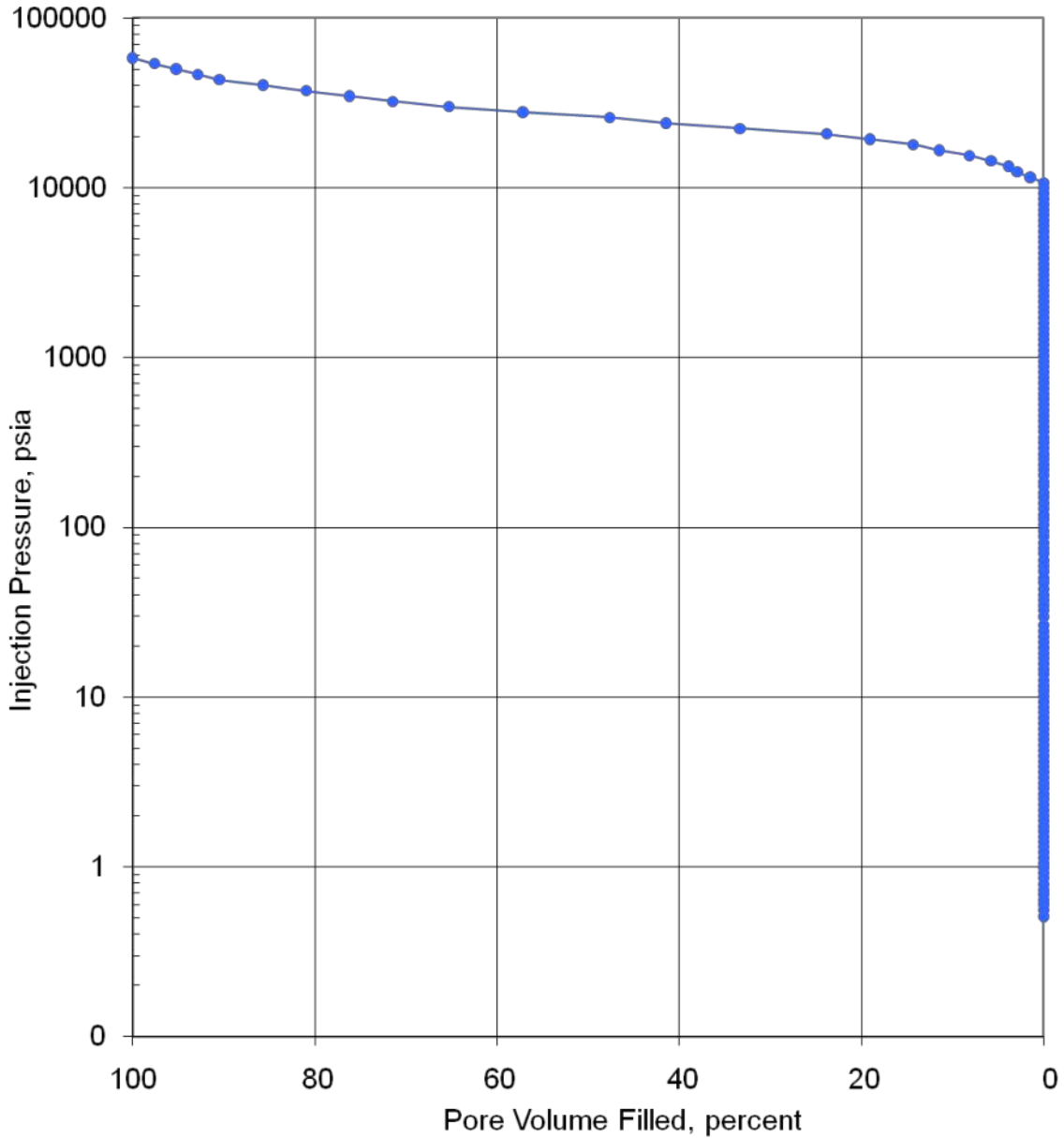


**Figure 31 – Results of the mercury porosimetry analysis on the duplicate siltstone rock sample as pore volume filled per pressure unit.**



### CAPILLARY PRESSURE vs. WETTING PHASE SATURATION

Mercury Pressure: 0 - 60000  
(METHODOLOGY: ASTM D4404, API RP40)

Project Name: NAWC  
Project No.: ER-0715

Sample ID: Siltstone 2  
Depth, ft.: 70  
Porosity, %Vp: 0.6

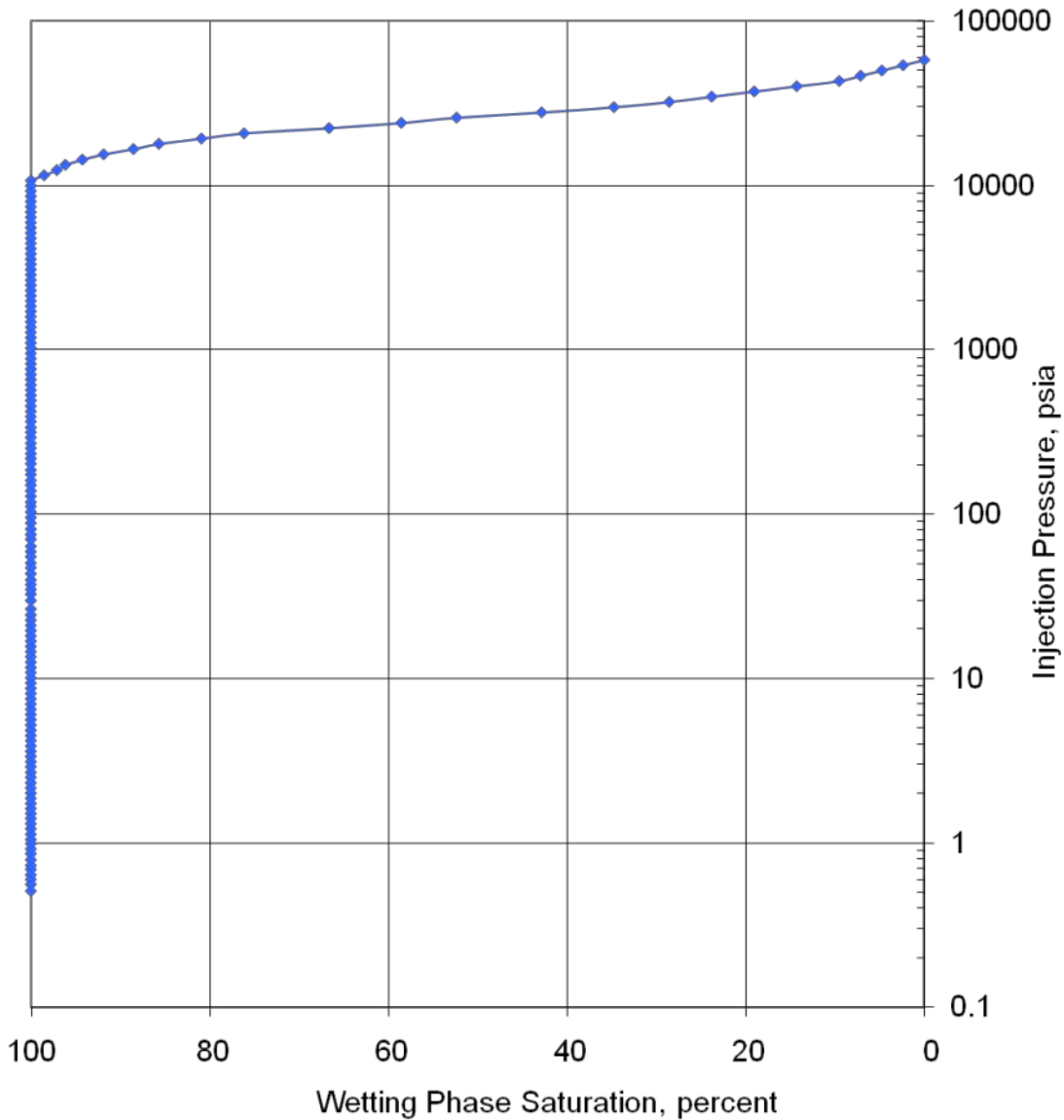


**Figure 32 – Results of the mercury porosimetry analysis on the duplicate siltstone rock sample as wetting phase saturation per capillary pressure.**



### PORE THROAT RADIUS DISTRIBUTION

Mercury Pressure: 0 - 60000

(METHODOLOGY: ASTM D4404, API RP40)

Project Name: NAWC  
Project No.: ER-0715

Sample ID: Siltstone 2  
Depth, ft.: 70  
Porosity, %Vp: 0.6

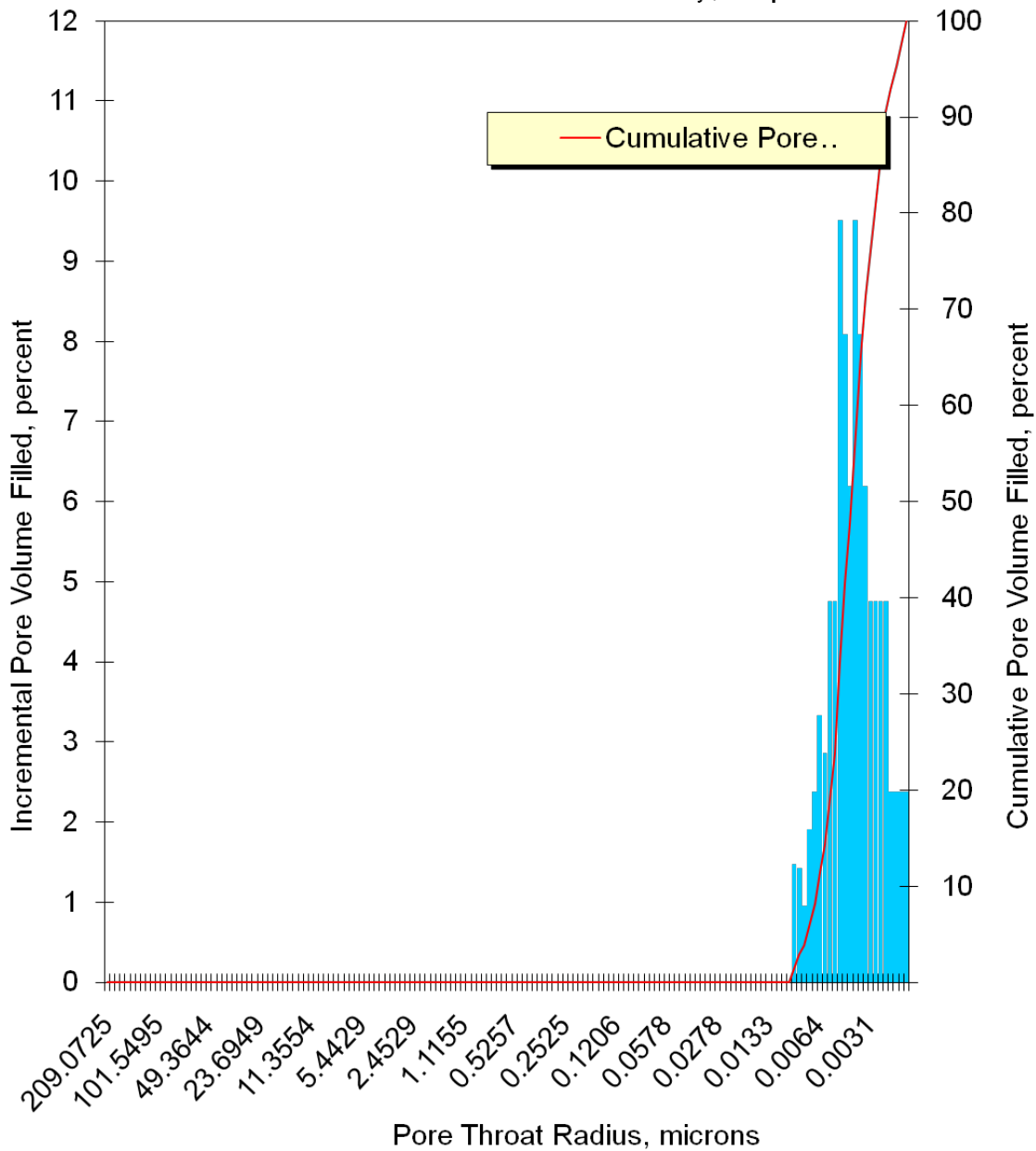


**Figure 33 – Pore throat radius distribution of the duplicate siltstone sample during the mercury porosimetry analysis.**

**Table 12 – Results of the mercury porosimetry analysis on the triplicate siltstone rock sample.**

PTS File No:	39380			<b>PTS</b> Laboratories
Client:	Queen's University			
<b>MERCURY INJECTION SUMMARY</b>				
PROJECT NAME:	NAWC		Sample ID:	Siltstone 3
PROJECT NO:	ER-0715		Depth, ft.:	70
			Porosity, %Vp:	0.3
*INJECTION PRESSURE, psia	PORE THROAT	NON-WETTING PHASE SATURATION		WETTING PHASE SATURATION, percent
	Radius, microns	INCREMENTAL, percent	CUMULATIVE, percent	
0.510	209	0.000	0.000	100.0
0.560	190	0.000	0.000	100.0
0.600	178	0.000	0.000	100.0
0.630	169	0.000	0.000	100.0
0.670	159	0.000	0.000	100.0
0.740	144	0.000	0.000	100.0
0.790	135	0.000	0.000	100.0
0.860	124	0.000	0.000	100.0
0.920	116	0.000	0.000	100.0
0.990	108	0.000	0.000	100.0
1.05	102	0.000	0.000	100.0
1.13	94.4	0.000	0.000	100.0
1.23	86.7	0.000	0.000	100.0
1.31	81.4	0.000	0.000	100.0
1.41	75.6	0.000	0.000	100.0
1.51	70.6	0.000	0.000	100.0
1.62	65.8	0.000	0.000	100.0
1.74	61.3	0.000	0.000	100.0
1.87	57.0	0.000	0.000	100.0
2.01	53.0	0.000	0.000	100.0
2.16	49.4	0.000	0.000	100.0
2.33	45.8	0.000	0.000	100.0
2.51	42.5	0.000	0.000	100.0
2.69	39.6	0.000	0.000	100.0
2.91	36.6	0.000	0.000	100.0
3.12	34.2	0.000	0.000	100.0
3.37	31.6	0.000	0.000	100.0
3.61	29.5	0.000	0.000	100.0
3.89	27.4	0.000	0.000	100.0
4.19	25.4	0.000	0.000	100.0
4.50	23.7	0.000	0.000	100.0
4.85	22.0	0.000	0.000	100.0
5.22	20.4	0.000	0.000	100.0

5.62	19.0	0.000	0.000	100.0
6.04	17.7	0.000	0.000	100.0
6.50	16.4	0.000	0.000	100.0
7.00	15.2	0.000	0.000	100.0
7.53	14.2	0.000	0.000	100.0
8.11	13.1	0.000	0.000	100.0
8.73	12.2	0.000	0.000	100.0
9.39	11.4	0.000	0.000	100.0
10.1	10.6	0.000	0.000	100.0
10.9	9.79	0.000	0.000	100.0
11.7	9.11	0.000	0.000	100.0
12.6	8.47	0.000	0.000	100.0
13.6	7.85	0.000	0.000	100.0
14.6	7.31	0.000	0.000	100.0
15.7	6.80	0.000	0.000	100.0
16.9	6.31	0.000	0.000	100.0
18.2	5.86	0.000	0.000	100.0
19.6	5.44	0.000	0.000	100.0
21.1	5.06	0.000	0.000	100.0
22.7	4.70	0.000	0.000	100.0
24.4	4.37	0.000	0.000	100.0
24.6	4.33	0.000	0.000	100.0
26.7	4.00	0.000	0.000	100.0
29.8	3.57	0.000	0.000	100.0
31.7	3.36	0.000	0.000	100.0
35.1	3.04	0.000	0.000	100.0
37.5	2.84	0.000	0.000	100.0
40.5	2.63	0.000	0.000	100.0
44.1	2.42	0.000	0.000	100.0
47.6	2.24	0.000	0.000	100.0
51.4	2.08	0.000	0.000	100.0
55.4	1.92	0.000	0.000	100.0
59.1	1.81	0.000	0.000	100.0
64.6	1.65	0.000	0.000	100.0
69.8	1.53	0.000	0.000	100.0
74.6	1.43	0.000	0.000	100.0
82.4	1.29	0.000	0.000	100.0
88.4	1.21	0.000	0.000	100.0
94.7	1.13	0.000	0.000	100.0
104	1.03	0.000	0.000	100.0
110	0.969	0.000	0.000	100.0
118	0.903	0.000	0.000	100.0
128	0.834	0.000	0.000	100.0
139	0.765	0.000	0.000	100.0
149	0.715	0.000	0.000	100.0
161	0.664	0.000	0.000	100.0
174	0.611	0.000	0.000	100.0
187	0.572	0.000	0.000	100.0

203	0.525	0.000	0.000	100.0
216	0.494	0.000	0.000	100.0
234	0.456	0.000	0.000	100.0
251	0.425	0.000	0.000	100.0
270	0.395	0.000	0.000	100.0
291	0.366	0.000	0.000	100.0
315	0.338	0.000	0.000	100.0
338	0.315	0.000	0.000	100.0
365	0.292	0.000	0.000	100.0
394	0.270	0.000	0.000	100.0
422	0.252	0.000	0.000	100.0
459	0.232	0.000	0.000	100.0
491	0.217	0.000	0.000	100.0
528	0.202	0.000	0.000	100.0
569	0.187	0.000	0.000	100.0
611	0.174	0.000	0.000	100.0
660	0.162	0.000	0.000	100.0
709	0.150	0.000	0.000	100.0
763	0.140	0.000	0.000	100.0
823	0.130	0.000	0.000	100.0
885	0.120	0.000	0.000	100.0
953	0.112	0.000	0.000	100.0
1026	0.104	0.000	0.000	100.0
1103	0.097	0.000	0.000	100.0
1188	0.090	0.000	0.000	100.0
1278	0.083	0.000	0.000	100.0
1375	0.078	0.000	0.000	100.0
1481	0.072	0.000	0.000	100.0
1593	0.067	0.000	0.000	100.0
1714	0.062	0.000	0.000	100.0
1845	0.058	0.000	0.000	100.0
1984	0.054	0.000	0.000	100.0
2136	0.050	0.000	0.000	100.0
2299	0.046	0.000	0.000	100.0
2473	0.043	0.000	0.000	100.0
2662	0.040	0.000	0.000	100.0
2865	0.037	0.000	0.000	100.0
3084	0.035	0.000	0.000	100.0
3317	0.032	0.000	0.000	100.0
3569	0.030	0.000	0.000	100.0
3836	0.028	0.000	0.000	100.0
4129	0.026	0.000	0.000	100.0
4439	0.024	0.000	0.000	100.0
4777	0.022	0.000	0.000	100.0
5142	0.021	0.000	0.000	100.0
5536	0.019	0.000	0.000	100.0
5955	0.018	0.000	0.000	100.0
6411	0.017	0.000	0.000	100.0

6901	0.015	0.000	0.000	100.0
7428	0.014	0.000	0.000	100.0
7993	0.013	0.000	0.000	100.0
8602	0.012	0.000	0.000	100.0
9259	0.012	0.000	0.000	100.0
9967	0.011	0.000	0.000	100.0
10737	0.010	0.000	0.000	100.0
11558	0.009	0.000	0.00	100.0
12438	0.009	0.000	0.00	100.0
13385	0.008	5.68	5.68	94.3
14404	0.007	7.18	12.9	87.1
15482	0.007	5.13	18.0	82.0
16659	0.006	5.13	23.1	76.9
17949	0.006	6.15	29.3	70.7
19316	0.006	9.23	38.5	61.5
20788	0.005	10.3	48.7	51.3
22371	0.005	7.18	55.9	44.1
24070	0.004	8.20	64.1	35.9
25905	0.004	5.13	69.2	30.8
27879	0.004	8.20	77.4	22.6
30001	0.004	7.18	84.6	15.4
32282	0.003	5.13	89.7	10.3
34734	0.003	4.10	93.8	6.15
37377	0.003	2.05	95.9	4.10
40224	0.003	2.05	97.9	2.05
43288	0.002	2.05	100	0.000
46574	0.002	0.000	100	0.000
50120	0.002	0.000	100	0.000
53932	0.002	0.000	100	0.000
58031	0.002	0.000	100	0.000



**PORE VOLUME FILLED vs PRESSURE**  
Mercury Pressure: 0 - 60000 psia  
(METHODOLOGY: ASTM D4404, API RP40)

Project Name: ANWC  
Project No.: ER-0715

Sample ID: Siltstone 3  
Depth, ft.: 70  
Porosity, %Vp: 0.3

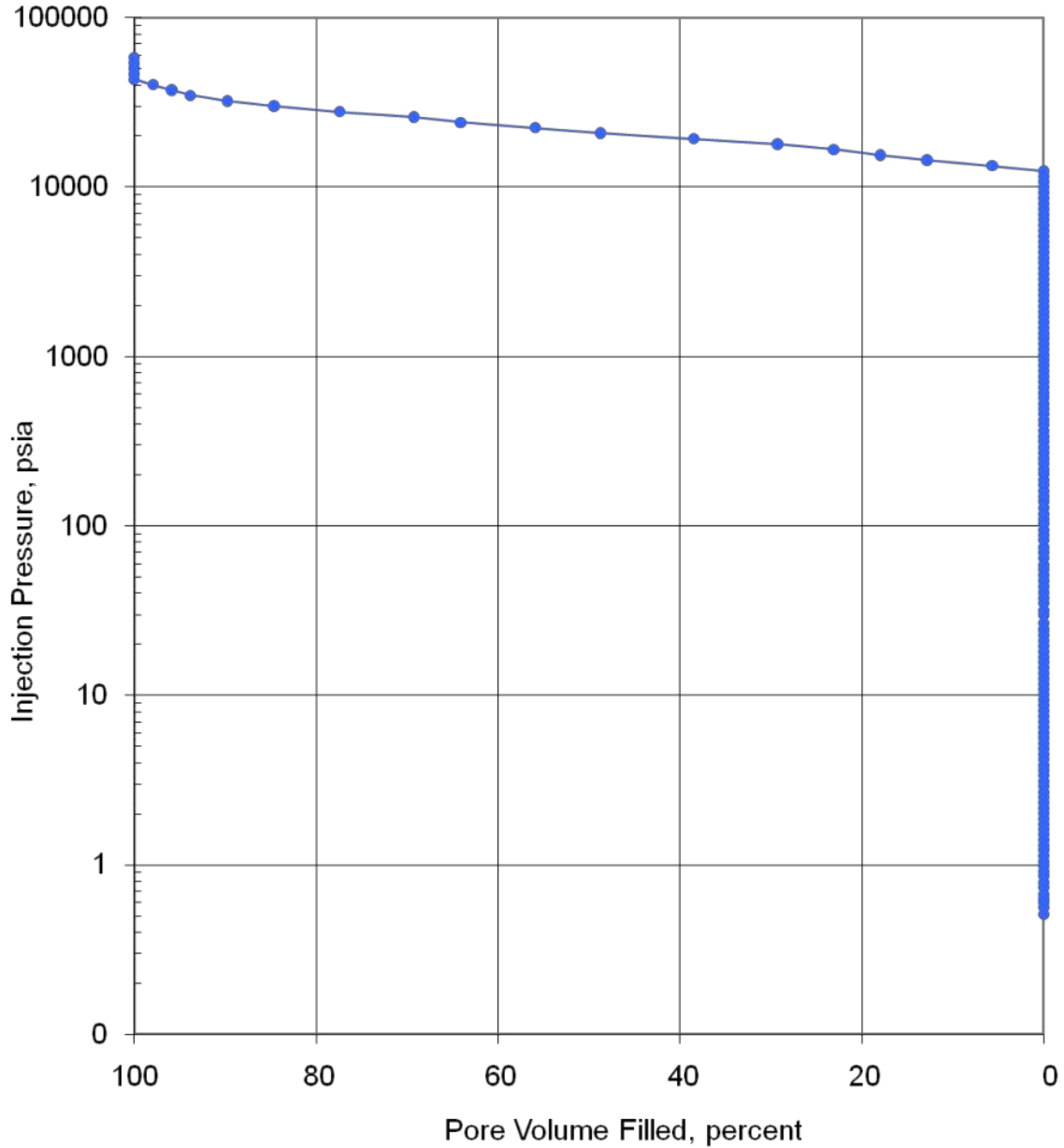


**Figure 34 – Results of the mercury porosimetry analysis on the triplicate siltstone rock sample as pore volume filled per pressure unit.**



### CAPILLARY PRESSURE vs. WETTING PHASE SATURATION

Mercury Pressure: 0 - 60000

(METHODOLOGY: ASTM D4404, API RP40)

Project Name: NAWC  
Project No.: ER-0715

Sample ID: Siltstone 3  
Depth, ft.: 70  
Porosity, %Vp: 0.3

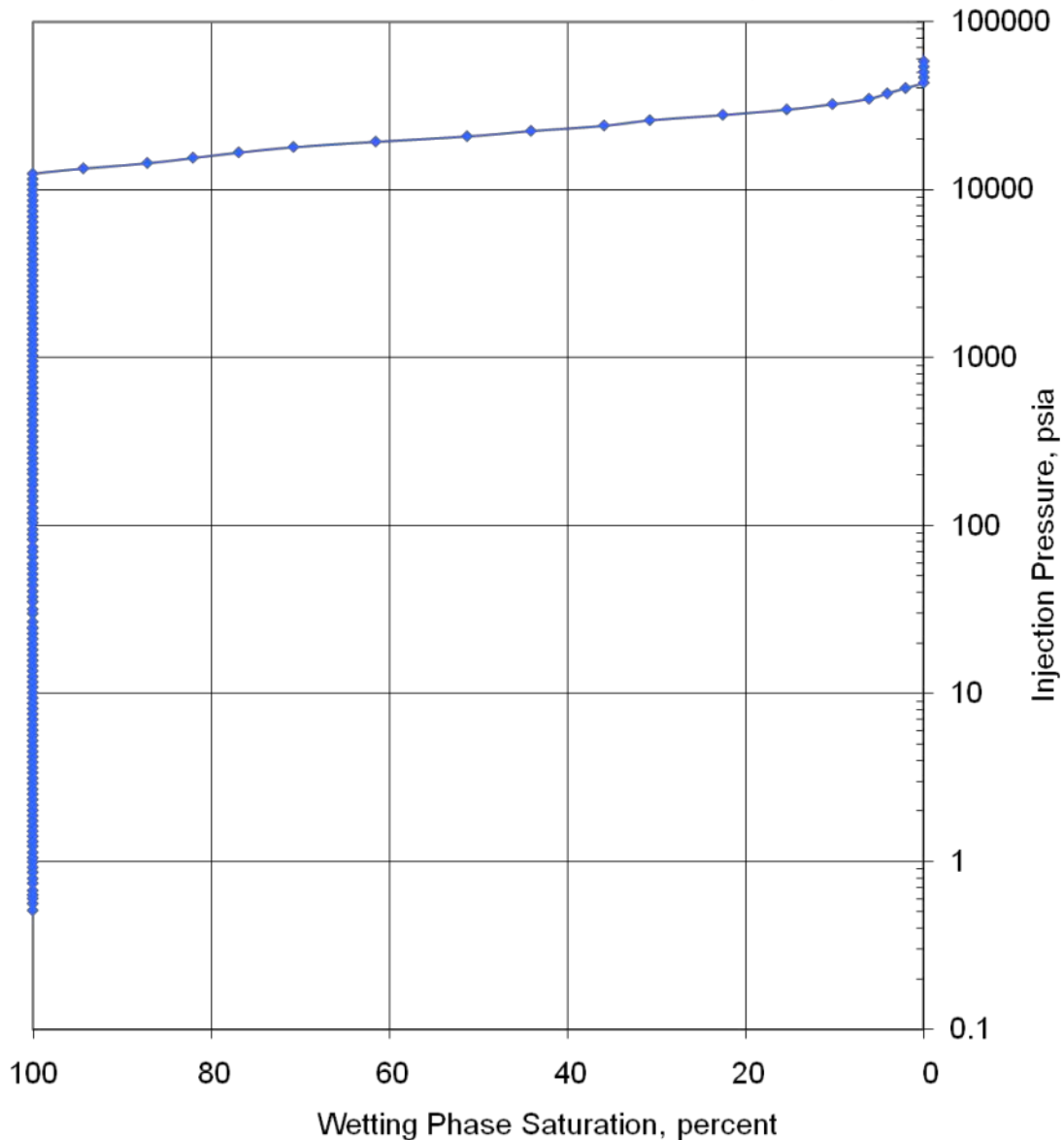


**Figure 35 – Results of the mercury porosimetry analysis on the triplicate siltstone rock sample as wetting phase saturation per capillary pressure.**



**PORE THROAT RADIUS DISTRIBUTION**  
Mercury Pressure: 0 - 60000  
(METHODOLOGY: ASTM D4404, API RP40)

Project Name: NAWC  
Project No.: ER-0715

Sample ID: Siltstone 3  
Depth, ft.: 70  
Porosity, %Vp: 0.3

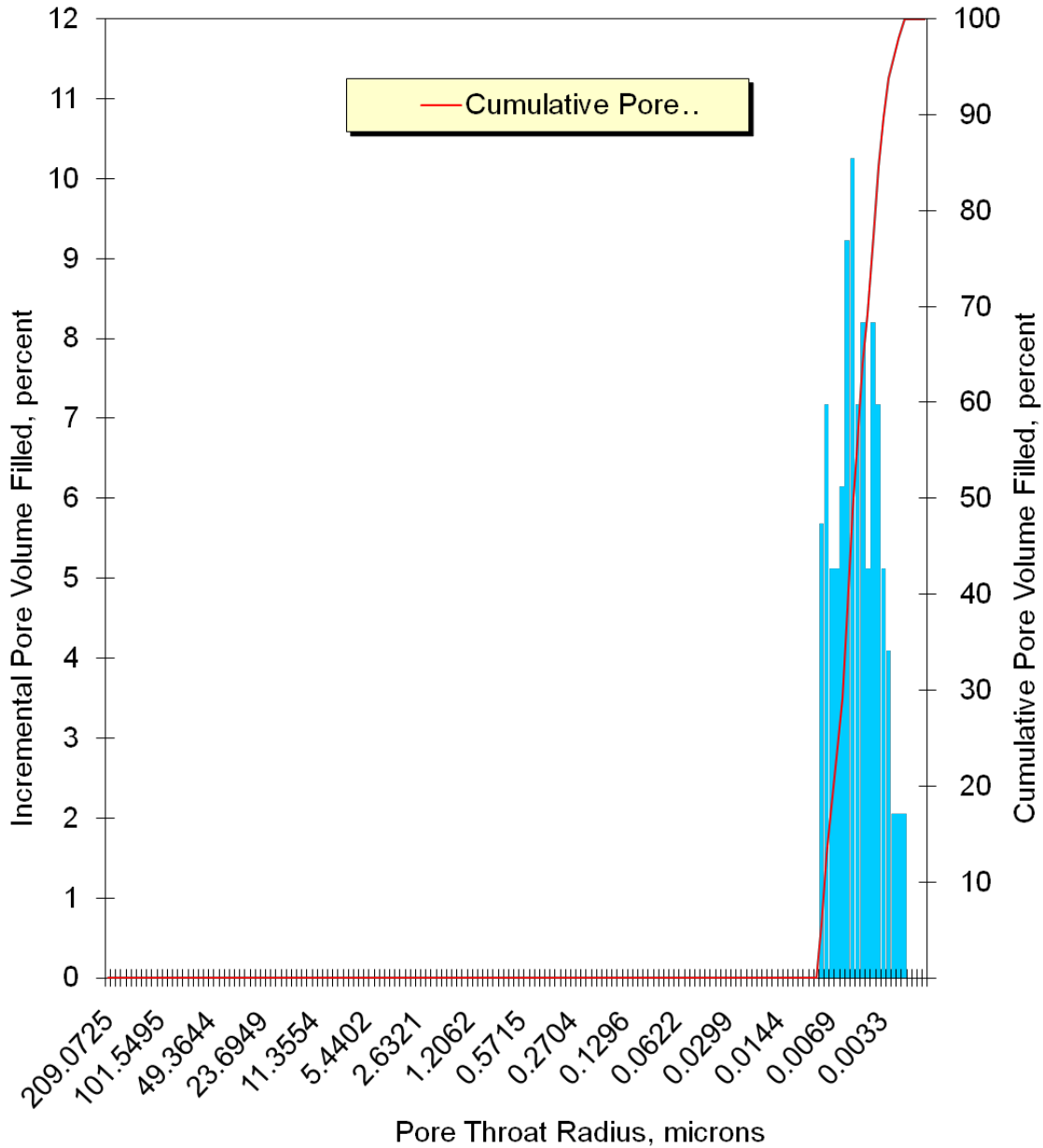


**Figure 36 – Pore throat radius distribution of the triplicate siltstone sample during the mercury porosimetry analysis.**

**Table 13 – Results of the mercury porosimetry analysis on the limestone rock sample.**

PTS File No:	39380			<b>PTS</b> Laboratories
Client:	Queen's University			
<b>MERCURY INJECTION SUMMARY</b>				
PROJECT NAME:	NAWC		Sample ID:	Limestone 1
PROJECT NO:	ER-0715		Depth, ft.:	70
			Porosity, %Vp:	0.4
*INJECTION PRESSURE, psia	PORE THROAT Radius, microns	NON-WETTING PHASE SATURATION		WETTING PHASE SATURATION, percent
		INCREMENTAL, percent	CUMULATIVE, percent	
0.510	209	0.000	0.000	100.0
0.560	190	0.000	0.000	100.0
0.600	178	0.000	0.000	100.0
0.640	167	0.000	0.000	100.0
0.690	155	0.000	0.000	100.0
0.730	146	0.000	0.000	100.0
0.790	135	0.000	0.000	100.0
0.860	124	0.000	0.000	100.0
0.920	116	0.000	0.000	100.0
0.990	108	0.000	0.000	100.0
1.05	102	0.000	0.000	100.0
1.13	94.4	0.000	0.000	100.0
1.22	87.4	0.000	0.000	100.0
1.31	81.4	0.000	0.000	100.0
1.41	75.6	0.000	0.000	100.0
1.51	70.6	0.000	0.000	100.0
1.62	65.8	0.000	0.000	100.0
1.74	61.3	0.000	0.000	100.0
1.87	57.0	0.000	0.000	100.0
2.01	53.0	0.000	0.000	100.0
2.16	49.4	0.000	0.000	100.0
2.32	46.0	0.000	0.000	100.0
2.51	42.5	0.000	0.000	100.0
2.69	39.6	0.000	0.000	100.0
2.91	36.6	0.000	0.000	100.0
3.12	34.2	0.000	0.000	100.0
3.36	31.7	0.000	0.000	100.0
3.61	29.5	0.000	0.000	100.0
3.89	27.4	0.000	0.000	100.0
4.19	25.4	0.000	0.000	100.0
4.50	23.7	0.000	0.000	100.0
4.85	22.0	0.000	0.000	100.0
5.22	20.4	0.000	0.000	100.0

5.62	19.0	0.000	0.000	100.0
6.04	17.7	0.000	0.000	100.0
6.50	16.4	0.000	0.000	100.0
7.00	15.2	0.000	0.000	100.0
7.53	14.2	0.000	0.000	100.0
8.11	13.1	0.000	0.000	100.0
8.73	12.2	0.000	0.000	100.0
9.39	11.4	0.000	0.000	100.0
10.1	10.6	0.000	0.000	100.0
10.9	9.79	0.000	0.000	100.0
11.7	9.12	0.000	0.000	100.0
12.6	8.47	0.000	0.000	100.0
13.6	7.85	0.000	0.000	100.0
14.6	7.31	0.000	0.000	100.0
15.7	6.80	0.000	0.000	100.0
16.9	6.31	0.000	0.000	100.0
18.2	5.86	0.000	0.000	100.0
19.6	5.44	0.000	0.000	100.0
21.1	5.06	0.000	0.000	100.0
22.7	4.70	0.000	0.000	100.0
24.4	4.37	0.000	0.000	100.0
25.3	4.22	0.000	0.000	100.0
26.2	4.07	0.000	0.000	100.0
29.6	3.60	0.000	0.000	100.0
31.9	3.34	0.000	0.000	100.0
34.7	3.08	0.000	0.000	100.0
38.3	2.78	0.000	0.000	100.0
40.6	2.63	0.000	0.000	100.0
44.5	2.40	0.000	0.000	100.0
48.3	2.21	0.000	0.000	100.0
51.8	2.06	0.000	0.000	100.0
55.7	1.91	0.000	0.000	100.0
61.6	1.73	0.000	0.000	100.0
64.7	1.65	0.000	0.000	100.0
70.6	1.51	0.000	0.000	100.0
74.5	1.43	0.000	0.000	100.0
81.3	1.31	0.000	0.000	100.0
89.2	1.19	0.000	0.000	100.0
96.1	1.11	0.000	0.000	100.0
102	1.05	0.000	0.000	100.0
112	0.955	0.000	0.000	100.0
119	0.899	0.000	0.000	100.0
128	0.830	0.000	0.000	100.0
139	0.768	0.000	0.000	100.0
150	0.710	0.000	0.000	100.0
161	0.661	0.000	0.000	100.0
173	0.615	0.000	0.000	100.0
187	0.570	0.000	0.000	100.0

201	0.530	0.000	0.000	100.0
215	0.496	0.000	0.000	100.0
234	0.456	0.000	0.000	100.0
251	0.424	0.000	0.000	100.0
272	0.392	0.000	0.000	100.0
292	0.365	0.000	0.000	100.0
314	0.339	0.000	0.000	100.0
338	0.315	0.000	0.000	100.0
364	0.293	0.000	0.000	100.0
393	0.271	0.000	0.000	100.0
423	0.252	0.000	0.000	100.0
456	0.234	0.000	0.000	100.0
491	0.217	0.000	0.000	100.0
529	0.202	0.000	0.000	100.0
569	0.187	0.000	0.000	100.0
611	0.174	0.000	0.000	100.0
661	0.161	0.000	0.000	100.0
709	0.150	0.000	0.000	100.0
764	0.140	0.000	0.000	100.0
823	0.130	0.000	0.000	100.0
885	0.120	0.000	0.000	100.0
953	0.112	0.000	0.000	100.0
1026	0.104	0.000	0.000	100.0
1104	0.097	0.000	0.000	100.0
1188	0.090	0.000	0.000	100.0
1279	0.083	0.000	0.000	100.0
1373	0.078	0.000	0.000	100.0
1481	0.072	0.000	0.000	100.0
1594	0.067	0.000	0.000	100.0
1714	0.062	0.000	0.000	100.0
1845	0.058	0.000	0.000	100.0
1986	0.054	0.000	0.000	100.0
2137	0.050	0.000	0.000	100.0
2299	0.046	0.000	0.000	100.0
2474	0.043	0.000	0.000	100.0
2662	0.040	0.000	0.000	100.0
2865	0.037	0.000	0.000	100.0
3081	0.035	0.000	0.000	100.0
3317	0.032	0.000	0.000	100.0
3570	0.030	0.000	0.000	100.0
3839	0.028	0.000	0.000	100.0
4129	0.026	0.000	0.000	100.0
4440	0.024	0.000	0.000	100.0
4778	0.022	0.000	0.000	100.0
5144	0.021	0.000	0.000	100.0
5533	0.019	0.000	0.000	100.0
5957	0.018	0.000	0.000	100.0
6407	0.017	2.16	2.16	97.8

6899	0.015	1.19	3.35	96.6
7424	0.014	1.19	4.55	95.5
7996	0.013	1.79	6.34	93.7
8598	0.012	1.79	8.13	91.9
9261	0.012	1.79	9.92	90.1
9965	0.011	0.597	10.5	89.5
10724	0.010	1.79	12.3	87.7
11541	0.009	1.79	14.1	85.9
12422	0.009	1.79	15.9	84.1
13368	0.008	2.39	18.3	81.7
14387	0.007	1.79	20.1	79.9
15481	0.007	1.79	21.8	78.2
16659	0.006	2.39	24.2	75.8
17929	0.006	1.79	26.0	74.0
19294	0.006	1.79	27.8	72.2
20771	0.005	2.39	30.2	69.8
22361	0.005	1.79	32.0	68.0
24067	0.004	1.79	33.8	66.2
25900	0.004	2.39	36.2	63.8
27874	0.004	1.79	38.0	62.0
29996	0.004	1.79	39.7	60.3
32278	0.003	1.79	41.5	58.5
34735	0.003	2.39	43.9	56.1
37375	0.003	5.37	49.3	50.7
40217	0.003	7.16	56.4	43.6
43281	0.002	7.16	63.6	36.4
46581	0.002	10.1	73.8	26.2
50125	0.002	8.35	82.1	17.9
53923	0.002	8.35	90.5	9.55
58037	0.002	9.55	100	0.000



**PORE VOLUME FILLED vs PRESSURE**  
Mercury Pressure: 0 - 60000 psia  
(METHODOLOGY: ASTM D4404, API RP40)

Project Name: NAWC  
Project No.: ER-0715

Sample ID: Limestone 1  
Depth, ft.: 70  
Porosity, %Vp: 0.4

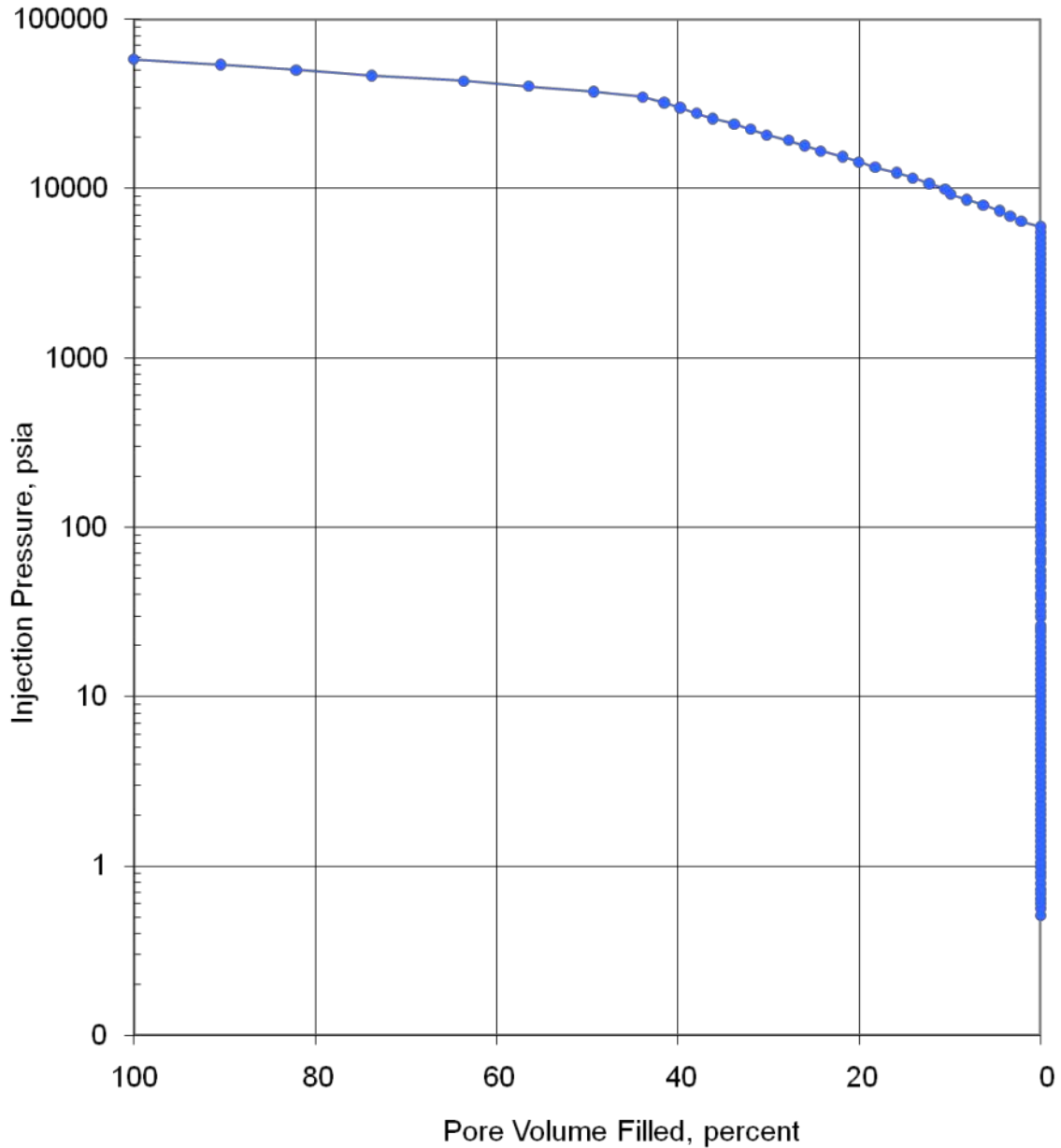


**Figure 37 – Results of the mercury porosimetry analysis on the limestone rock sample as pore volume filled per pressure unit.**



### CAPILLARY PRESSURE vs. WETTING PHASE SATURATION

Mercury Pressure: 0 - 60000  
(METHODOLOGY: ASTM D4404, API RP40)

Project Name: NAWC  
Project No.: ER-0715

Sample ID: Limestone 1  
Depth, ft.: 70  
Porosity, %Vp: 0.4

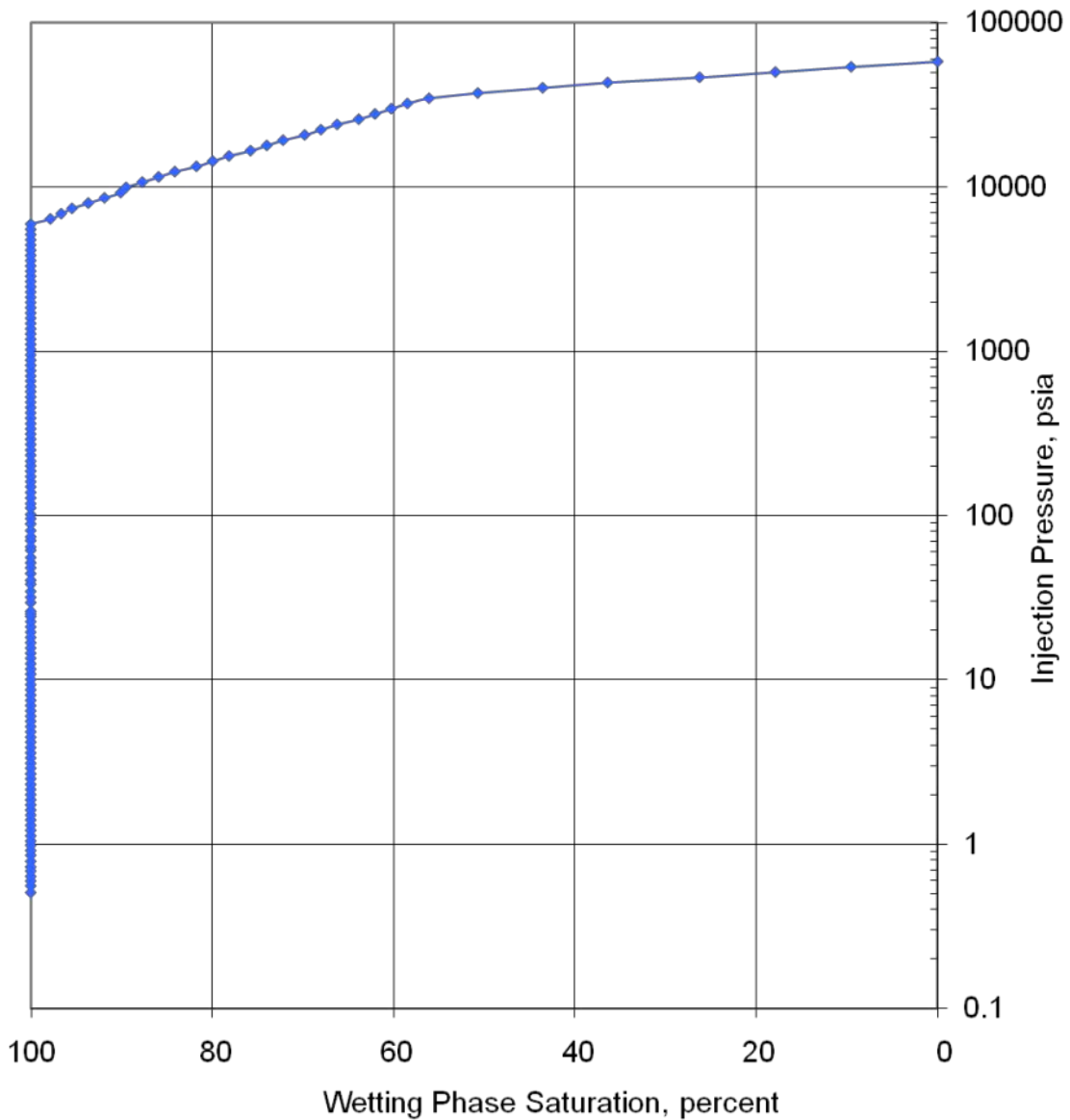


**Figure 38 – Results of the mercury porosimetry analysis on the limestone rock sample as wetting phase saturation per capillary pressure.**



**PORE THROAT RADIUS DISTRIBUTION**  
Mercury Pressure: 0 - 60000  
(METHODOLOGY: ASTM D4404, API RP40)

Project Name: NAWC  
Project No.: ER-0715

Sample ID: Limestone 1  
Depth, ft.: 70  
Porosity, %Vp: 0.4

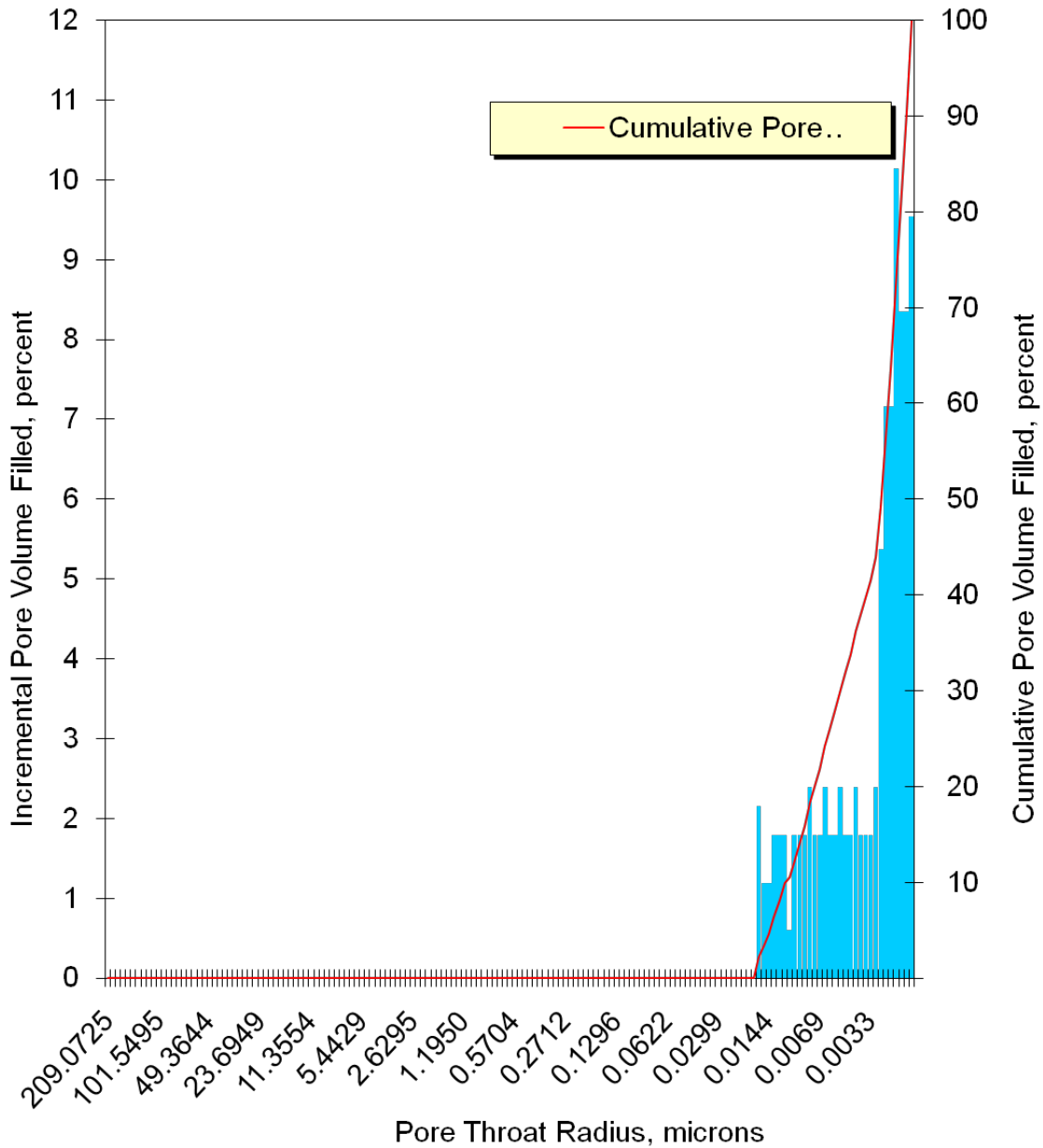


**Figure 39 – Pore throat radius distribution of the limestone sample during the mercury porosimetry analysis.**

**Table 14 – Results of the mercury porosimetry analysis on the duplicate limestone rock sample.**

PTS File No:	39380			<b>PTS</b>
Client:	Queen's University			Laboratories
<b>MERCURY INJECTION SUMMARY</b>				
PROJECT NAME:	NAWC		Sample ID:	Limestone 2
PROJECT NO:	ER-0715		Depth, ft.:	70
			Porosity, %Vp:	3.2
*INJECTION PRESSURE, psia	PORE THROAT Radius, microns	NON-WETTING PHASE SATURATION		WETTING PHASE SATURATION, percent
		INCREMENTAL, percent	CUMULATIVE, percent	
0.510	209	0.000	0.000	100.0
0.560	190	0.000	0.000	100.0
0.600	178	0.000	0.000	100.0
0.640	167	0.000	0.000	100.0
0.690	155	0.000	0.000	100.0
0.730	146	0.000	0.000	100.0
0.790	135	0.000	0.000	100.0
0.860	124	0.000	0.000	100.0
0.920	116	0.000	0.000	100.0
0.990	108	0.000	0.000	100.0
1.05	102	0.000	0.000	100.0
1.13	94.4	0.000	0.000	100.0
1.22	87.4	0.000	0.000	100.0
1.31	81.4	0.000	0.000	100.0
1.41	75.6	0.000	0.000	100.0
1.51	70.6	0.000	0.000	100.0
1.62	65.8	0.000	0.000	100.0
1.74	61.3	0.000	0.000	100.0
1.87	57.0	0.000	0.000	100.0
2.01	53.0	0.000	0.000	100.0
2.16	49.4	0.000	0.000	100.0
2.32	46.0	0.000	0.000	100.0
2.51	42.5	0.000	0.000	100.0
2.69	39.6	0.000	0.000	100.0
2.91	36.6	0.000	0.000	100.0
3.12	34.2	0.000	0.000	100.0
3.36	31.7	0.000	0.000	100.0
3.61	29.5	0.000	0.000	100.0
3.89	27.4	0.000	0.000	100.0
4.19	25.4	0.000	0.000	100.0
4.50	23.7	0.000	0.000	100.0
4.85	22.0	0.000	0.000	100.0
5.22	20.4	0.000	0.000	100.0

5.62	19.0	0.000	0.000	100.0
6.04	17.7	0.000	0.000	100.0
6.50	16.4	0.000	0.000	100.0
7.00	15.2	0.000	0.000	100.0
7.53	14.2	0.000	0.000	100.0
8.11	13.1	0.000	0.000	100.0
8.73	12.2	0.000	0.000	100.0
9.39	11.4	0.000	0.000	100.0
10.1	10.6	0.000	0.000	100.0
10.9	9.79	0.000	0.000	100.0
11.7	9.12	0.000	0.000	100.0
12.6	8.47	0.000	0.000	100.0
13.6	7.85	0.000	0.000	100.0
14.6	7.31	0.000	0.000	100.0
15.7	6.80	0.000	0.000	100.0
16.9	6.31	0.000	0.000	100.0
18.2	5.86	0.000	0.000	100.0
19.6	5.44	0.000	0.000	100.0
21.1	5.06	0.000	0.000	100.0
22.7	4.70	0.000	0.000	100.0
24.4	4.37	0.000	0.000	100.0
26.6	4.01	0.000	0.000	100.0
29.9	3.57	0.000	0.000	100.0
32.7	3.26	0.000	0.000	100.0
34.9	3.06	0.000	0.000	100.0
37.4	2.85	0.000	0.000	100.0
39.9	2.68	0.000	0.000	100.0
43.5	2.45	0.000	0.000	100.0
47.3	2.25	0.000	0.000	100.0
50.5	2.11	0.000	0.000	100.0
55.1	1.93	0.000	0.000	100.0
59.3	1.80	0.000	0.000	100.0
63.9	1.67	0.000	0.000	100.0
70.4	1.52	0.000	0.000	100.0
75.3	1.42	0.000	0.000	100.0
81.2	1.31	0.000	0.000	100.0
88.5	1.21	0.000	0.000	100.0
95.6	1.12	0.000	0.000	100.0
103.1	1.03	0.000	0.000	100.0
112	0.96	0.000	0.000	100.0
118	0.900	0.000	0.000	100.0
129	0.829	0.000	0.000	100.0
139	0.768	0.000	0.000	100.0
150	0.710	0.000	0.000	100.0
161	0.664	0.000	0.000	100.0
174	0.612	0.000	0.000	100.0
186	0.574	0.000	0.000	100.0
203	0.526	0.000	0.000	100.0

218	0.488	0.000	0.000	100.0
234	0.456	0.000	0.000	100.0
252	0.423	0.000	0.000	100.0
270	0.394	0.000	0.000	100.0
293	0.364	0.000	0.000	100.0
315	0.338	0.000	0.000	100.0
338	0.316	0.000	0.000	100.0
366	0.291	0.000	0.000	100.0
393	0.271	0.000	0.000	100.0
422	0.253	0.000	0.000	100.0
455	0.234	0.000	0.000	100.0
492	0.217	0.000	0.000	100.0
530	0.201	0.000	0.000	100.0
570	0.187	0.000	0.000	100.0
612	0.174	0.000	0.000	100.0
659	0.162	0.000	0.000	100.0
710	0.150	0.000	0.000	100.0
764	0.140	0.000	0.000	100.0
823	0.130	0.000	0.000	100.0
884	0.121	0.000	0.000	100.0
952	0.112	0.000	0.000	100.0
1025	0.104	0.000	0.000	100.0
1103	0.097	0.000	0.000	100.0
1187	0.090	0.000	0.000	100.0
1279	0.083	0.000	0.000	100.0
1374	0.078	0.000	0.000	100.0
1480	0.072	0.000	0.000	100.0
1592	0.067	0.000	0.000	100.0
1714	0.062	0.000	0.000	100.0
1845	0.058	0.000	0.000	100.0
1986	0.054	0.000	0.000	100.0
2136	0.050	0.000	0.000	100.0
2299	0.046	0.000	0.000	100.0
2475	0.043	0.000	0.000	100.0
2661	0.040	0.000	0.000	100.0
2865	0.037	0.000	0.000	100.0
3082	0.035	0.000	0.000	100.0
3318	0.032	0.000	0.000	100.0
3567	0.030	0.000	0.000	100.0
3839	0.028	0.000	0.000	100.0
4128	0.026	0.000	0.000	100.0
4440	0.024	0.000	0.000	100.0
4776	0.022	0.000	0.000	100.0
5140	0.021	0.000	0.000	100.0
5534	0.019	0.000	0.000	100.0
5956	0.018	0.000	0.000	100.0
6413	0.017	0.000	0.000	100.0
6898	0.015	0.000	0.000	100.0

7425	0.014	0.000	0.000	100.0
7994	0.013	0.000	0.000	100.0
8602	0.012	0.000	0.000	100.0
9261	0.012	0.000	0.000	100.0
9967	0.011	0.000	0.000	100.0
10722	0.010	0.000	0.000	100.0
11540	0.009	0.000	0.000	100.0
12419	0.009	0.000	0.000	100.0
13365	0.008	0.000	0.000	100.0
14385	0.007	0.517	0.517	99.5
15486	0.007	0.809	1.33	98.7
16677	0.006	0.809	2.13	97.9
17950	0.006	1.62	3.75	96.2
19312	0.006	1.62	5.37	94.6
20786	0.005	1.62	6.99	93.0
22370	0.005	4.04	11.0	89.0
24072	0.004	4.04	15.1	84.9
25907	0.004	8.09	23.2	76.8
27873	0.004	8.09	31.3	68.7
29987	0.004	8.90	40.1	59.9
32283	0.003	7.28	47.4	52.6
34739	0.003	8.09	55.5	44.5
37372	0.003	8.09	63.6	36.4
40213	0.003	8.09	71.7	28.3
43277	0.002	4.04	75.7	24.3
46573	0.002	5.66	81.4	18.6
50114	0.002	3.07	84.5	15.5
53934	0.002	7.44	91.9	8.09
58019	0.002	8.09	100	0.00



PORE VOLUME FILLED vs PRESSURE  
Mercury Pressure: 0 - 60000 psia  
(METHODOLOGY: ASTM D4404, API RP40)

Project Name: NAWC  
Project No.: ER-0715

Sample ID: Limestone 2  
Depth, ft.: 70  
Porosity, %Vp: 3.2

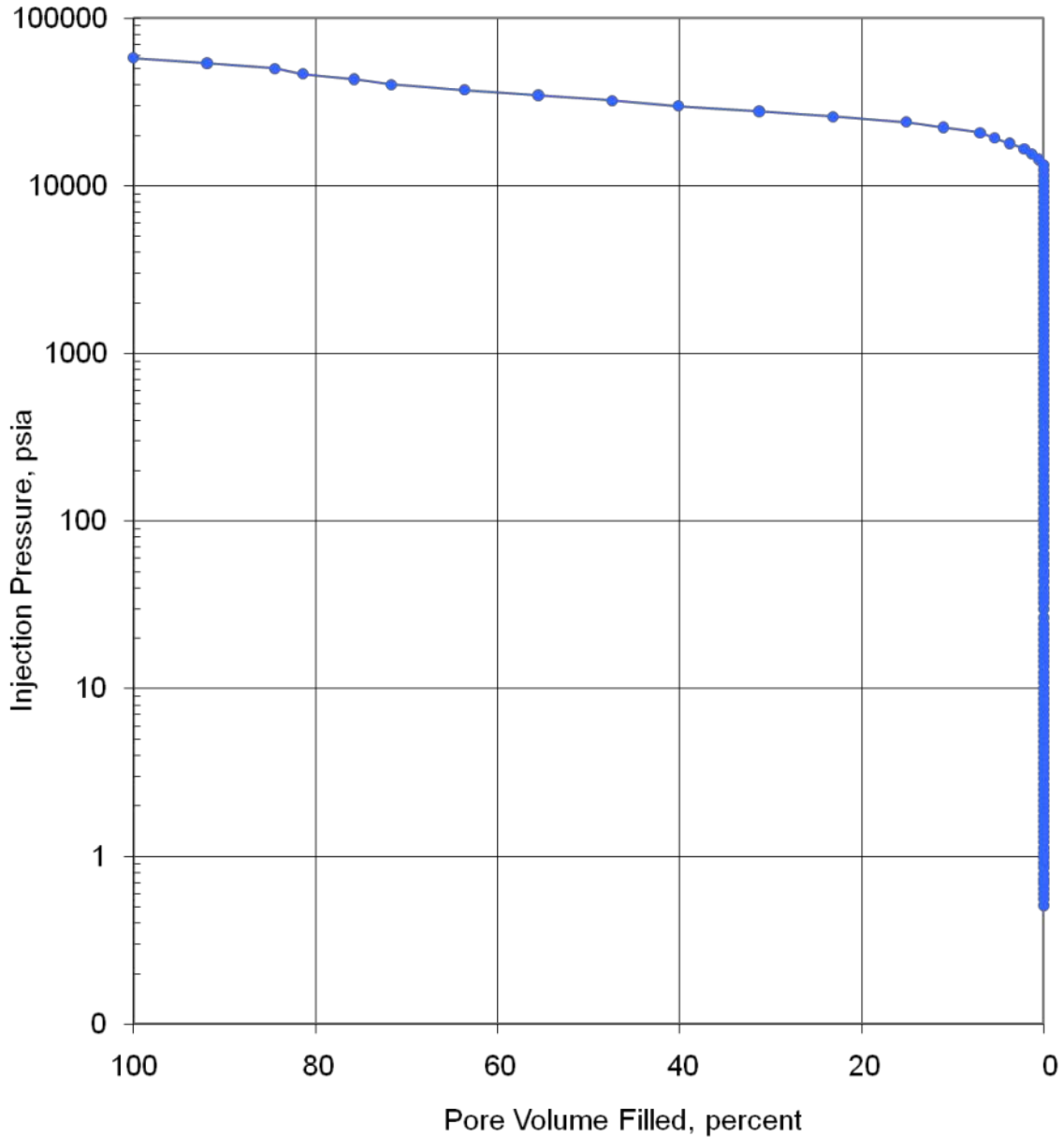


**Figure 40 – Results of the mercury porosimetry analysis on the duplicate limestone rock sample as pore volume filled per pressure unit.**



### CAPILLARY PRESSURE vs. WETTING PHASE SATURATION

Mercury Pressure: 0 - 60000

(METHODOLOGY: ASTM D4404, API RP40)

Project Name: NAWC  
Project No.: ER-0715

Sample ID: Limestone 2  
Depth, ft.: 70  
Porosity, %Vp: 3.2

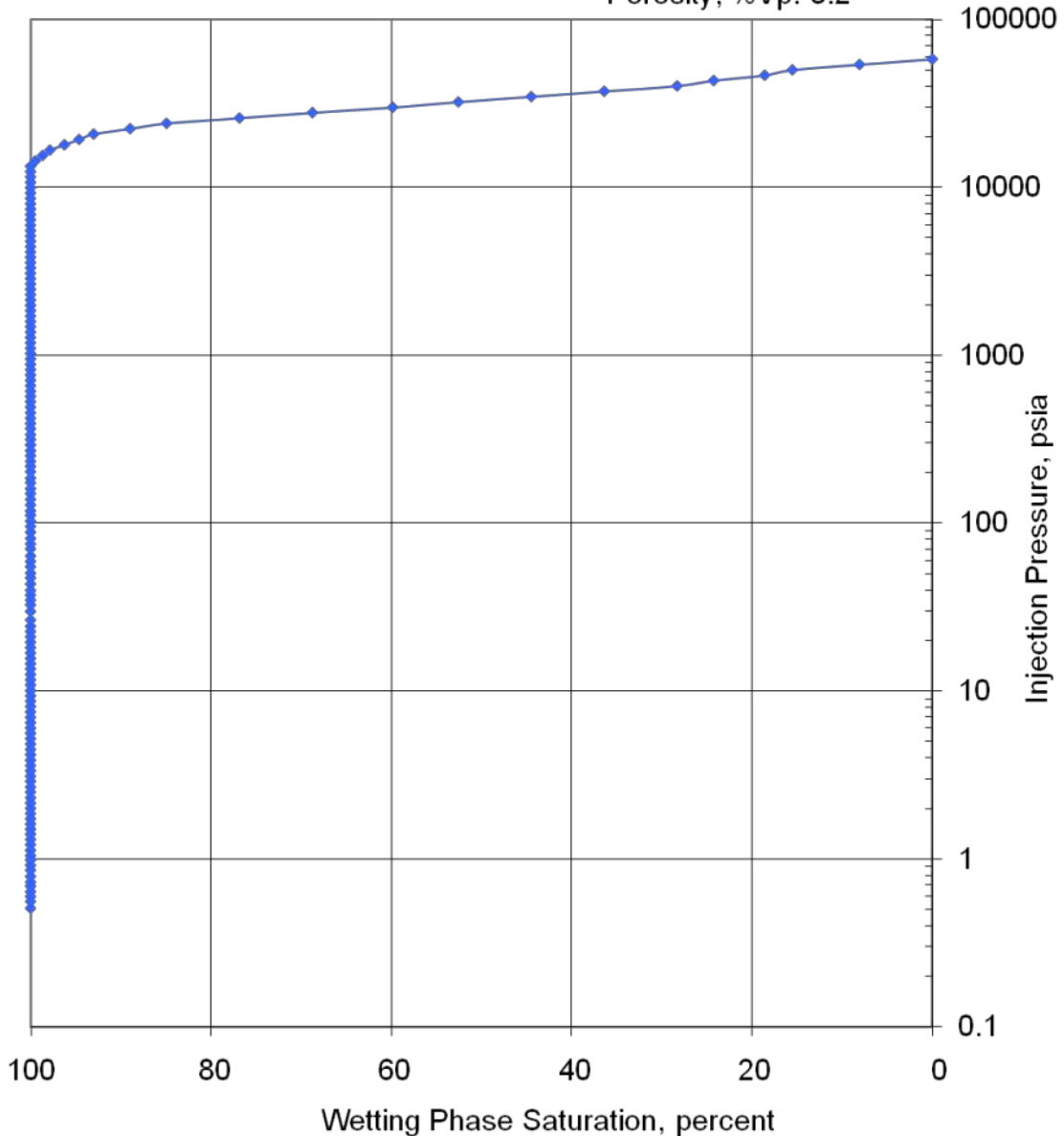


**Figure 41 – Results of the mercury porosimetry analysis on the duplicate limestone rock sample as wetting phase saturation per capillary pressure.**



**PORE THROAT RADIUS DISTRIBUTION**  
Mercury Pressure: 0 - 60000  
(METHODOLOGY: ASTM D4404, API RP40)

Project Name: NAWC  
Project No.: ER-0715

Sample ID: Limestone 2  
Depth, ft.: 70  
Porosity, %Vp: 3.2

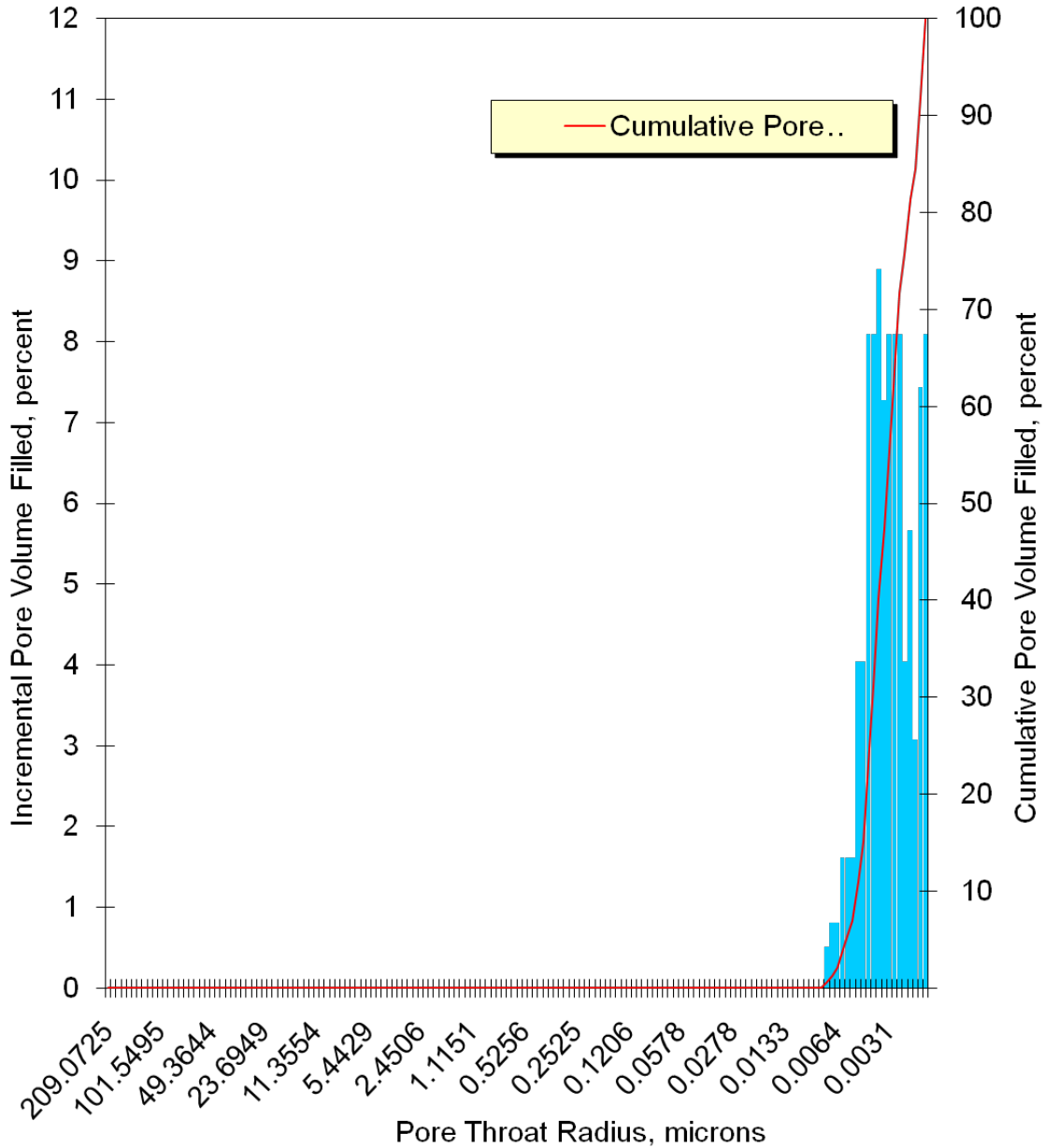


**Figure 42 – Pore throat radius distribution of the duplicate limestone sample during the mercury porosimetry analysis.**

**Table 15 – Results of the mercury porosimetry analysis on the triplicate limestone rock sample.**

PTS File No:	39380			<b>PTS</b> Laboratories
Client:	Queen's University			
<b>MERCURY INJECTION SUMMARY</b>				
PROJECT NAME:	NAWC		Sample ID:	Limestone 3
PROJECT NO:	ER-0715		Depth, ft.:	70
			Porosity, %Vp:	2.7
*INJECTION PRESSURE, psia	PORE THROAT Radius, microns	NON-WETTING PHASE SATURATION		WETTING PHASE SATURATION, percent
		INCREMENTAL, percent	CUMULATIVE, percent	
0.510	209	0.000	0.000	100.0
0.560	190	0.000	0.000	100.0
0.600	178	0.000	0.000	100.0
0.630	169	0.000	0.000	100.0
0.680	157	0.000	0.000	100.0
0.740	144	0.000	0.000	100.0
0.790	135	0.000	0.000	100.0
0.860	124	0.000	0.000	100.0
0.920	116	0.000	0.000	100.0
0.990	108	0.000	0.000	100.0
1.05	102	0.000	0.000	100.0
1.13	94.4	0.000	0.000	100.0
1.23	86.7	0.000	0.000	100.0
1.31	81.4	0.000	0.000	100.0
1.41	75.6	0.000	0.000	100.0
1.51	70.6	0.000	0.000	100.0
1.62	65.8	0.000	0.000	100.0
1.74	61.3	0.000	0.000	100.0
1.87	57.0	0.000	0.000	100.0
2.01	53.0	0.000	0.000	100.0
2.16	49.4	0.000	0.000	100.0
2.33	45.8	0.000	0.000	100.0
2.51	42.5	0.000	0.000	100.0
2.69	39.6	0.000	0.000	100.0
2.91	36.6	0.000	0.000	100.0
3.12	34.2	0.000	0.000	100.0
3.37	31.6	0.000	0.000	100.0
3.61	29.5	0.000	0.000	100.0
3.89	27.4	0.000	0.000	100.0
4.19	25.4	0.000	0.000	100.0
4.50	23.7	0.000	0.000	100.0
4.85	22.0	0.000	0.000	100.0
5.22	20.4	0.000	0.000	100.0

5.62	19.0	0.000	0.000	100.0
6.04	17.7	0.000	0.000	100.0
6.50	16.4	0.000	0.000	100.0
7.00	15.2	0.000	0.000	100.0
7.53	14.2	0.000	0.000	100.0
8.11	13.1	0.000	0.000	100.0
8.73	12.2	0.000	0.000	100.0
9.39	11.4	0.000	0.000	100.0
10.1	10.6	0.000	0.000	100.0
10.9	9.79	0.000	0.000	100.0
11.7	9.11	0.000	0.000	100.0
12.6	8.47	0.000	0.000	100.0
13.6	7.85	0.000	0.000	100.0
14.6	7.31	0.000	0.000	100.0
15.7	6.80	0.000	0.000	100.0
16.9	6.31	0.000	0.000	100.0
18.2	5.86	0.000	0.000	100.0
19.6	5.44	0.000	0.000	100.0
21.1	5.06	0.000	0.000	100.0
22.7	4.70	0.000	0.000	100.0
24.4	4.37	0.000	0.000	100.0
24.7	4.33	0.000	0.000	100.0
26.7	4.00	0.000	0.000	100.0
29.9	3.57	0.000	0.000	100.0
31.7	3.36	0.000	0.000	100.0
35.1	3.04	0.000	0.000	100.0
37.5	2.84	0.000	0.000	100.0
40.5	2.63	0.000	0.000	100.0
44.1	2.42	0.000	0.000	100.0
47.6	2.24	0.000	0.000	100.0
51.4	2.08	0.000	0.000	100.0
55.4	1.92	0.000	0.000	100.0
59.1	1.81	0.000	0.000	100.0
64.6	1.65	0.000	0.000	100.0
69.8	1.53	0.000	0.000	100.0
74.7	1.43	0.000	0.000	100.0
82.4	1.29	0.000	0.000	100.0
88.4	1.21	0.000	0.000	100.0
94.7	1.13	0.000	0.000	100.0
104	1.03	0.000	0.000	100.0
110	0.969	0.000	0.000	100.0
118	0.903	0.000	0.000	100.0
128	0.834	0.000	0.000	100.0
139	0.765	0.000	0.000	100.0
149	0.715	0.000	0.000	100.0
161	0.664	0.000	0.000	100.0
174	0.611	0.000	0.000	100.0
187	0.571	0.000	0.000	100.0

203	0.525	0.000	0.000	100.0
216	0.494	0.000	0.000	100.0
234	0.456	0.000	0.000	100.0
251	0.425	0.000	0.000	100.0
270	0.395	0.000	0.000	100.0
291	0.366	0.000	0.000	100.0
315	0.338	0.000	0.000	100.0
338	0.315	0.000	0.000	100.0
365	0.292	0.000	0.000	100.0
394	0.270	0.000	0.000	100.0
422	0.252	0.000	0.000	100.0
459	0.232	0.000	0.000	100.0
491	0.217	0.000	0.000	100.0
528	0.202	0.000	0.000	100.0
569	0.187	0.000	0.000	100.0
611	0.174	0.000	0.000	100.0
660	0.162	0.000	0.000	100.0
709	0.150	0.000	0.000	100.0
763	0.140	0.000	0.000	100.0
823	0.130	0.000	0.000	100.0
885	0.120	0.000	0.000	100.0
953	0.112	0.000	0.000	100.0
1026	0.104	0.000	0.000	100.0
1103	0.097	0.000	0.000	100.0
1188	0.090	0.000	0.000	100.0
1278	0.083	0.000	0.000	100.0
1375	0.078	0.000	0.000	100.0
1481	0.072	0.000	0.000	100.0
1593	0.067	0.000	0.000	100.0
1714	0.062	0.000	0.000	100.0
1845	0.058	0.000	0.000	100.0
1984	0.054	0.000	0.000	100.0
2136	0.050	0.000	0.000	100.0
2299	0.046	0.000	0.000	100.0
2473	0.043	0.000	0.000	100.0
2662	0.040	0.000	0.000	100.0
2865	0.037	0.000	0.000	100.0
3084	0.035	0.000	0.000	100.0
3317	0.032	0.000	0.000	100.0
3569	0.030	0.000	0.000	100.0
3836	0.028	0.000	0.000	100.0
4129	0.026	0.000	0.000	100.0
4439	0.024	0.000	0.000	100.0
4777	0.022	0.000	0.000	100.0
5142	0.021	0.000	0.000	100.0
5536	0.019	0.000	0.000	100.0
5955	0.018	0.000	0.000	100.0
6411	0.017	0.000	0.000	100.0

6901	0.015	0.000	0.000	100.0
7427	0.014	0.000	0.000	100.0
7993	0.013	0.000	0.000	100.0
8602	0.012	0.000	0.000	100.0
9259	0.012	0.000	0.000	100.0
9967	0.011	0.000	0.000	100.0
10737	0.010	0.231	0.231	99.8
11558	0.009	1.59	1.82	98.2
12438	0.009	2.38	4.21	95.8
13385	0.008	3.58	7.78	92.2
14404	0.007	3.58	11.4	88.6
15481	0.007	3.97	15.3	84.7
16658	0.006	5.96	21.3	78.7
17948	0.006	9.94	31.2	68.8
19315	0.006	10.3	41.6	58.4
20787	0.005	11.5	53.1	46.9
22370	0.005	7.15	60.3	39.7
24069	0.004	4.77	65.0	35.0
25904	0.004	5.56	70.6	29.4
27877	0.004	4.37	75.0	25.0
30000	0.004	5.56	80.5	19.5
32281	0.003	4.37	84.9	15.1
34733	0.003	3.58	88.5	11.5
37376	0.003	2.78	91.3	8.7
40222	0.003	2.78	94.0	5.96
43286	0.002	1.99	96.0	3.97
46572	0.002	1.19	97.2	2.78
50118	0.002	1.19	98.4	1.59
53931	0.002	1.19	100	0.397
58030	0.002	0.397	100	0.000



**PORE VOLUME FILLED vs PRESSURE**  
Mercury Pressure: 0 - 60000 psia  
(METHODOLOGY: ASTM D4404, API RP40)

Project Name: NAWC  
Project No.: ER-0715

Sample ID: Limestone 3  
Depth, ft.: 70  
Porosity, %Vp: 2.7

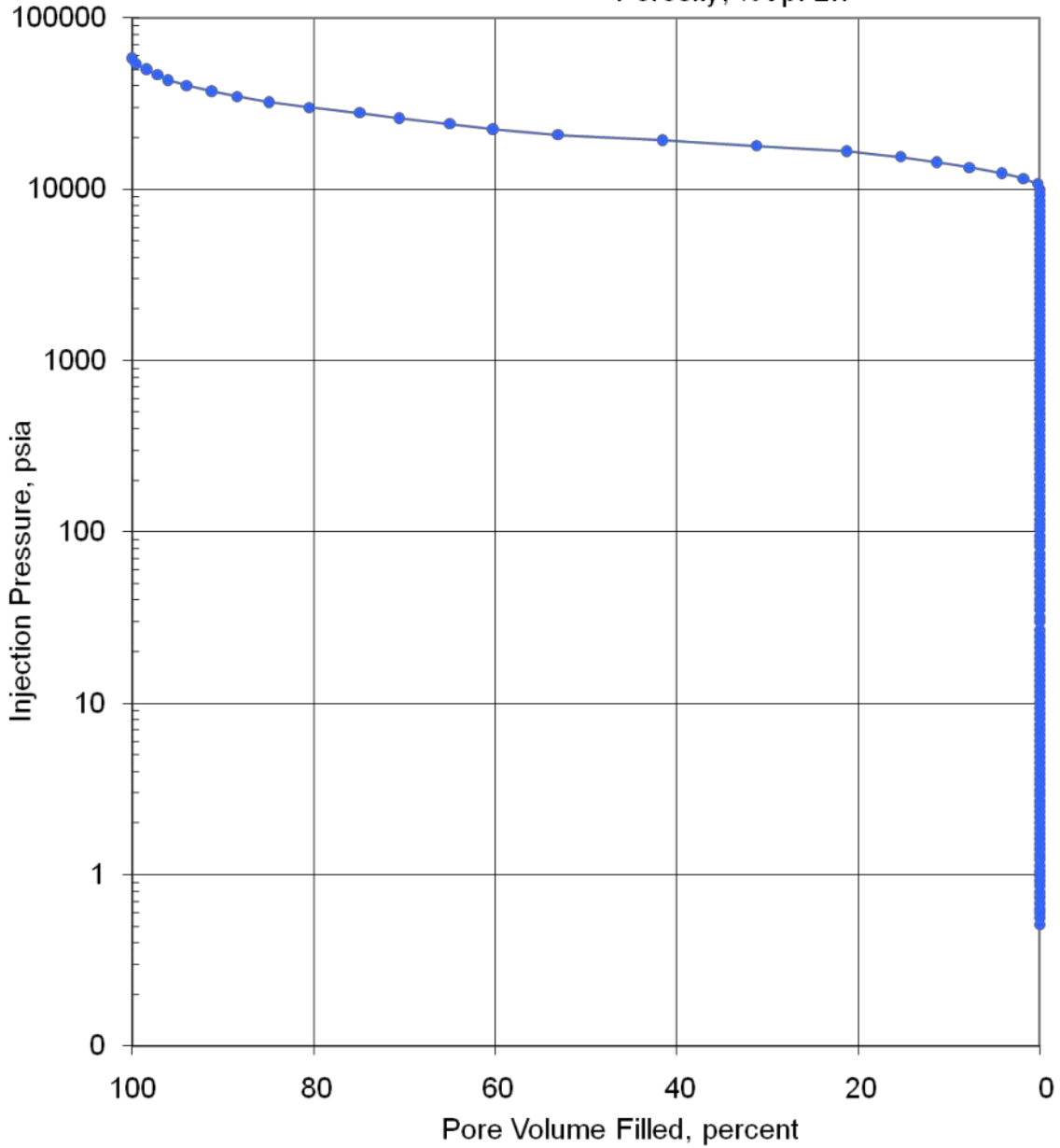


**Figure 43 – Results of the mercury porosimetry analysis on the triplicate limestone rock sample as pore volume filled per pressure unit.**



### CAPILLARY PRESSURE vs. WETTING PHASE SATURATION

Mercury Pressure: 0 - 60000  
(METHODOLOGY: ASTM D4404, API RP40)

Project Name: NAWC  
Project No.: ER-0715

Sample ID: Limestone 3  
Depth, ft.: 70  
Porosity, %Vp: 2.7

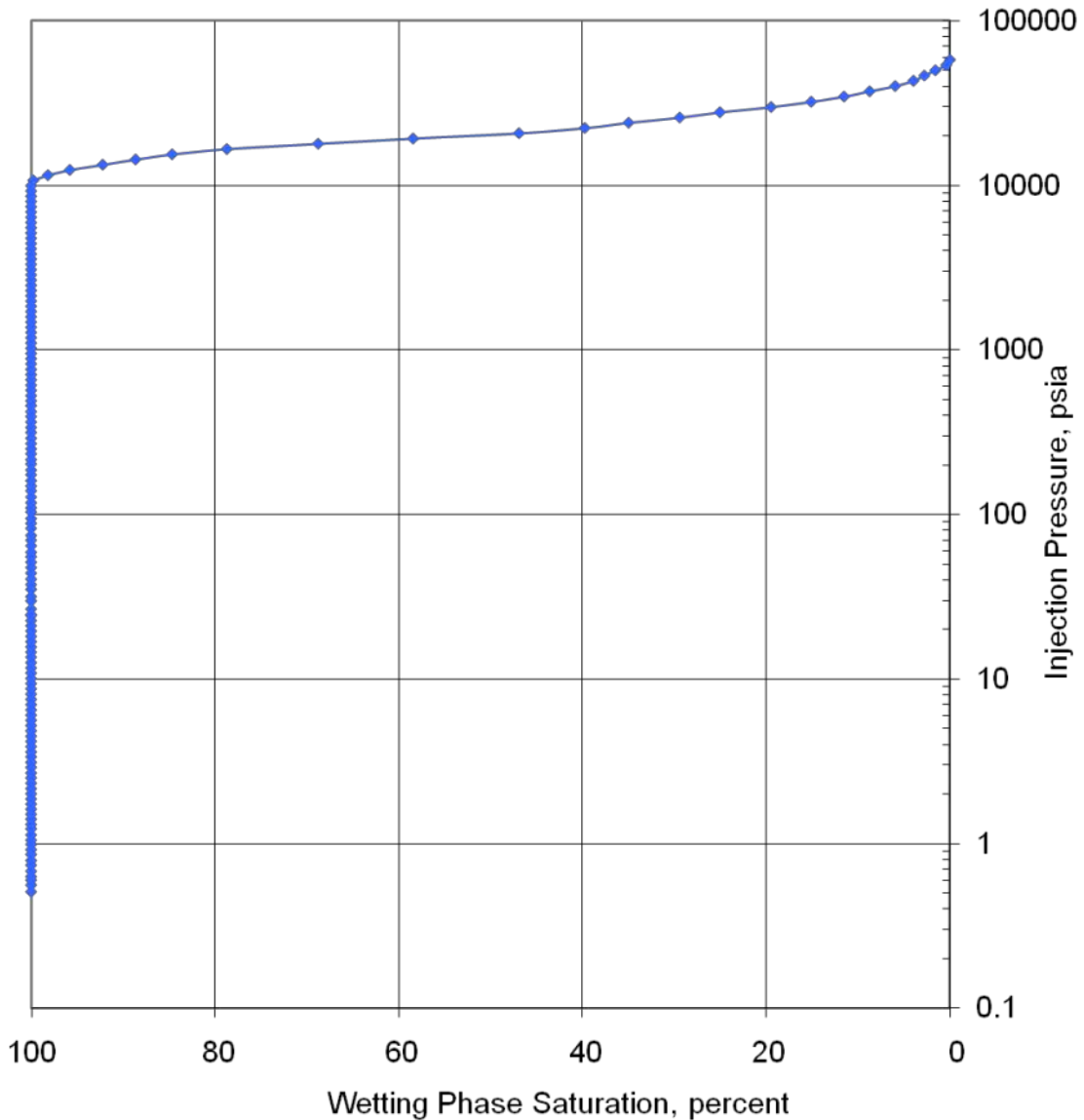


**Figure 44 – Results of the mercury porosimetry analysis on the triplicate limestone rock sample as wetting phase saturation per capillary pressure.**



**PORE THROAT RADIUS DISTRIBUTION**  
Mercury Pressure: 0 - 60000  
(METHODOLOGY: ASTM D4404, API RP40)

Project Name: NAWC  
Project No.: ER-0715

Sample ID: Limestone 3  
Depth, ft.: 70  
Porosity, %Vp: 2.7

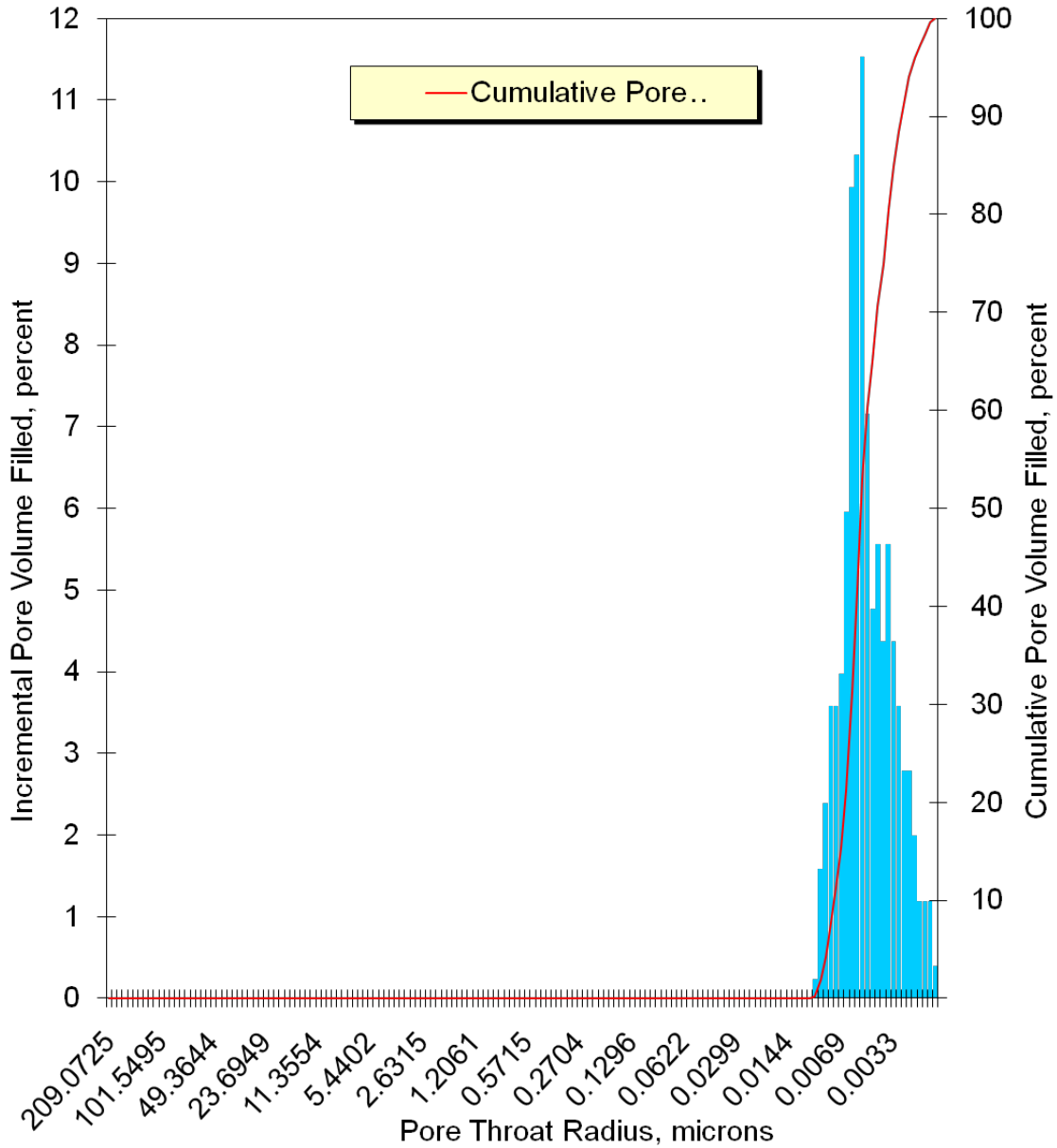


**Figure 45 – Pore throat radius distribution of the triplicate limestone sample during the mercury porosimetry analysis.**

**Table 16 – Results of the mercury porosimetry analysis on the sandstone rock sample.**

PTS File No:	39609			PTS Laboratories
Client:	Queen's University			
<b>MERCURY INJECTION SUMMARY</b>				
PROJECT NAME:	NAWC		Sample ID:	Sandstone 1
PROJECT NO:	ER-0715		Depth, ft.:	38
			Porosity, %Vp:	9.1
*INJECTION PRESSURE, psia	PORE THROAT Radius, microns	NON-WETTING PHASE SATURATION		WETTING PHASE SATURATION, percent
		INCREMENTAL, percent	CUMULATIVE, percent	
0.510	209	0.000	0.000	100.0
0.550	194	0.000	0.000	100.0
0.600	178	0.000	0.000	100.0
0.630	169	0.000	0.000	100.0
0.680	157	0.000	0.000	100.0
0.730	146	0.000	0.000	100.0
0.790	135	0.000	0.000	100.0
0.850	125	0.000	0.000	100.0
0.920	116	0.000	0.000	100.0
0.990	108	0.000	0.000	100.0
1.05	102	0.000	0.000	100.0
1.12	95.2	0.000	0.000	100.0
1.22	87.4	0.000	0.000	100.0
1.31	81.4	0.000	0.000	100.0
1.41	75.6	0.000	0.000	100.0
1.51	70.6	0.000	0.000	100.0
1.62	65.8	0.000	0.000	100.0
1.73	61.6	0.000	0.000	100.0
1.87	57.0	0.000	0.000	100.0
2.01	53.0	0.000	0.000	100.0
2.16	49.4	0.000	0.000	100.0
2.32	46.0	0.000	0.000	100.0
2.50	42.7	0.000	0.000	100.0
2.69	39.6	0.000	0.000	100.0
2.90	36.8	0.000	0.000	100.0
3.12	34.2	0.000	0.000	100.0
3.36	31.7	0.000	0.000	100.0
3.61	29.5	0.000	0.000	100.0
3.89	27.4	0.000	0.000	100.0
4.19	25.4	0.000	0.000	100.0
4.50	23.7	0.000	0.000	100.0
4.85	22.0	0.000	0.000	100.0
5.23	20.4	0.000	0.000	100.0
5.63	18.9	0.000	0.000	100.0

6.04	17.7	0.000	0.000	100.0
6.50	16.4	0.000	0.000	100.0
7.00	15.2	0.000	0.000	100.0
7.53	14.2	0.000	0.000	100.0
8.11	13.1	0.000	0.000	100.0
8.73	12.2	0.000	0.000	100.0
9.39	11.4	0.000	0.000	100.0
10.1	10.6	0.000	0.000	100.0
10.9	9.79	0.000	0.000	100.0
11.7	9.12	0.624	0.624	99.4
12.6	8.47	1.139	1.763	98.2
13.6	7.85	1.139	2.902	97.1
14.6	7.31	1.139	4.041	96.0
15.7	6.80	1.424	5.465	94.5
16.9	6.31	1.708	7.173	92.8
18.2	5.86	1.708	8.882	91.1
19.6	5.44	1.708	10.590	89.4
21.1	5.06	1.993	12.584	87.4
22.7	4.70	1.993	14.577	85.4
24.4	4.37	1.993	16.570	83.4
25.1	4.25	0.000	16.570	83.4
29.4	3.62	1.708	18.278	81.7
29.8	3.57	2.563	20.841	79.2
35.7	2.99	1.993	22.834	77.2
38.2	2.79	1.708	24.543	75.5
38.4	2.78	0.854	25.397	74.6
43.2	2.47	3.132	28.529	71.5
46.1	2.31	1.139	29.668	70.3
49.8	2.14	3.132	32.800	67.2
53.1	2.01	1.993	34.794	65.2
57.2	1.86	1.993	36.787	63.2
62.1	1.72	2.847	39.634	60.4
68.2	1.56	2.563	42.197	57.8
70.6	1.51	0.854	43.051	56.9
78.1	1.37	3.132	46.183	53.8
83.5	1.28	1.424	47.607	52.4
90.7	1.18	2.278	49.885	50.1
97.3	1.10	1.708	51.594	48.4
104	1.02	1.424	53.017	47.0
112	0.954	1.993	55.010	45.0
119	0.894	1.139	56.149	43.9
129	0.825	1.993	58.143	41.9
142	0.752	1.993	60.136	39.9
152	0.700	1.708	61.844	38.2
163	0.655	1.424	63.268	36.7
177	0.603	1.993	65.261	34.7
188	0.568	1.424	66.685	33.3
205	0.521	1.993	68.678	31.3

219	0.488	1.708	70.387	29.6
237	0.451	1.708	72.095	27.9
254	0.420	1.424	73.519	26.5
272	0.392	1.708	75.227	24.8
293	0.364	1.424	76.651	23.3
317	0.336	1.993	78.644	21.4
340	0.314	1.139	79.783	20.2
367	0.291	1.708	81.492	18.5
396	0.269	1.139	82.631	17.4
424	0.251	1.424	84.054	15.9
458	0.233	1.139	85.193	14.8
493	0.216	0.854	86.048	14.0
530	0.201	1.139	87.187	12.8
572	0.186	0.854	88.041	12.0
614	0.174	0.854	88.895	11.1
661	0.161	0.569	89.464	10.5
711	0.150	0.854	90.319	9.7
765	0.139	0.569	90.888	9.1
824	0.129	0.569	91.458	8.5
885	0.121	0.569	92.027	8.0
954	0.112	0.569	92.597	7.4
1026	0.104	0.569	93.166	6.8
1104	0.097	0.569	93.736	6.3
1189	0.090	0.285	94.020	6.0
1281	0.083	0.569	94.590	5.4
1376	0.077	0.285	94.875	5.1
1483	0.072	0.569	95.444	4.6
1594	0.067	0.285	95.729	4.3
1716	0.062	0.285	96.014	4.0
1846	0.058	0.569	96.583	3.4
1988	0.054	0.285	96.868	3.1
2141	0.050	0.285	97.153	2.8
2301	0.046	0.285	97.437	2.6
2475	0.043	0.285	97.722	2.3
2664	0.040	0.285	98.007	2.0
2866	0.037	0.000	98.007	2.0
3083	0.035	0.285	98.292	1.7
3317	0.032	0.285	98.576	1.4
3569	0.030	0.285	98.861	1.1
3838	0.028	0.000	98.861	1.1
4130	0.026	0.285	99.146	0.9
4444	0.024	0.000	99.146	0.9
4775	0.022	0.285	99.431	0.6
5139	0.021	0.000	99.431	0.6
5535	0.019	0.000	99.431	0.6
5957	0.018	0.285	99.715	0.3
6412	0.017	0.000	99.715	0.3
6900	0.015	0.000	99.715	0.3

7426	0.014	0.000	99.715	0.3
7992	0.013	0.285	100.000	0.0
8603	0.012	0.000	100.000	0.0
9262	0.012	0.000	100.000	0.0
9966	0.011	0.000	100.000	0.0
10725	0.010	0.000	100.000	0.0
11543	0.009	0.000	100.00	0.0
12421	0.009	0.000	100.00	0.0
13367	0.008	0.00	100.00	0.0
14382	0.007	0.00	100.0	0.0
15481	0.007	0.00	100.0	0.0
16659	0.006	0.00	100.0	0.0
17927	0.006	0.00	100.0	0.0
19294	0.006	0.00	100.0	0.0
20771	0.005	0.0	100.0	0.0
22360	0.005	0.00	100.0	0.0
24067	0.004	0.00	100.0	0.0
25902	0.004	0.00	100.0	0.0
27873	0.004	0.00	100.0	0.0
29996	0.004	0.00	100.0	0.0
32279	0.003	0.00	100.0	0.0
34735	0.003	0.00	100.0	0.00
37375	0.003	0.00	100.0	0.00
40216	0.003	0.00	100.0	0.00
43278	0.002	0.00	100	0.000
46564	0.002	0.000	100	0.000
50114	0.002	0.000	100	0.000
53920	0.002	0.000	100	0.000
58022	0.002	0.000	100	0.000



**PORE VOLUME FILLED vs PRESSURE**  
Mercury Pressure: 0 - 60000 psia  
(METHODOLOGY: ASTM D4404, API RP40)

Project Name: NAWC  
Project No.: ER-0715

Sample ID: Sandstone 1  
Depth, ft.: 38  
Porosity, %Vp: 9.1

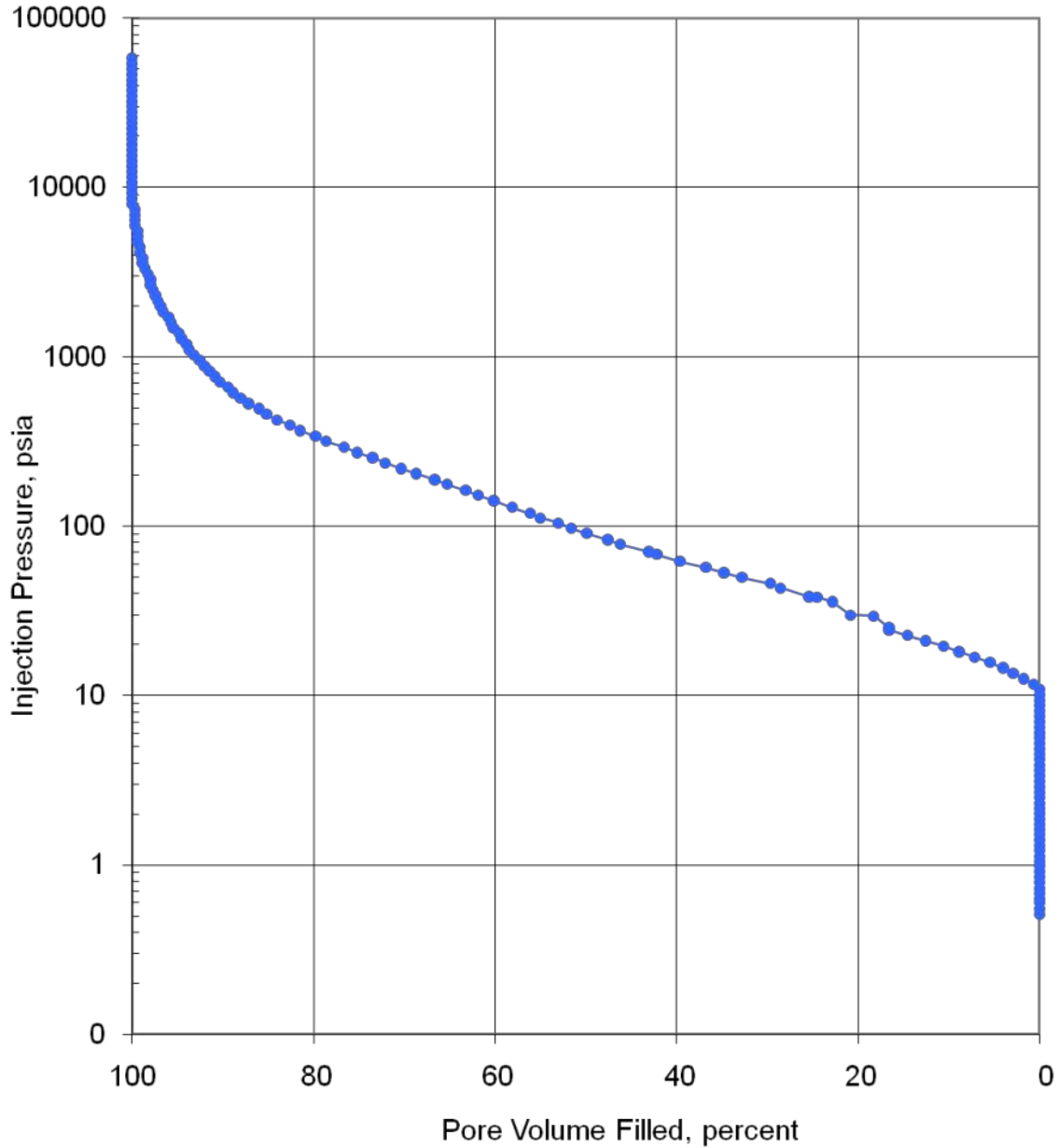


**Figure 46 – Results of the mercury porosimetry analysis on the sandstone rock sample as pore volume filled per pressure unit.**



### CAPILLARY PRESSURE vs. WETTING PHASE SATURATION

Mercury Pressure: 0 - 60000  
(METHODOLOGY: ASTM D4404, API RP40)

Project Name: NAWC  
Project No.: ER-0715

Sample ID: Sandstone 1  
Depth, ft.: 38  
Porosity, %Vp: 9.1

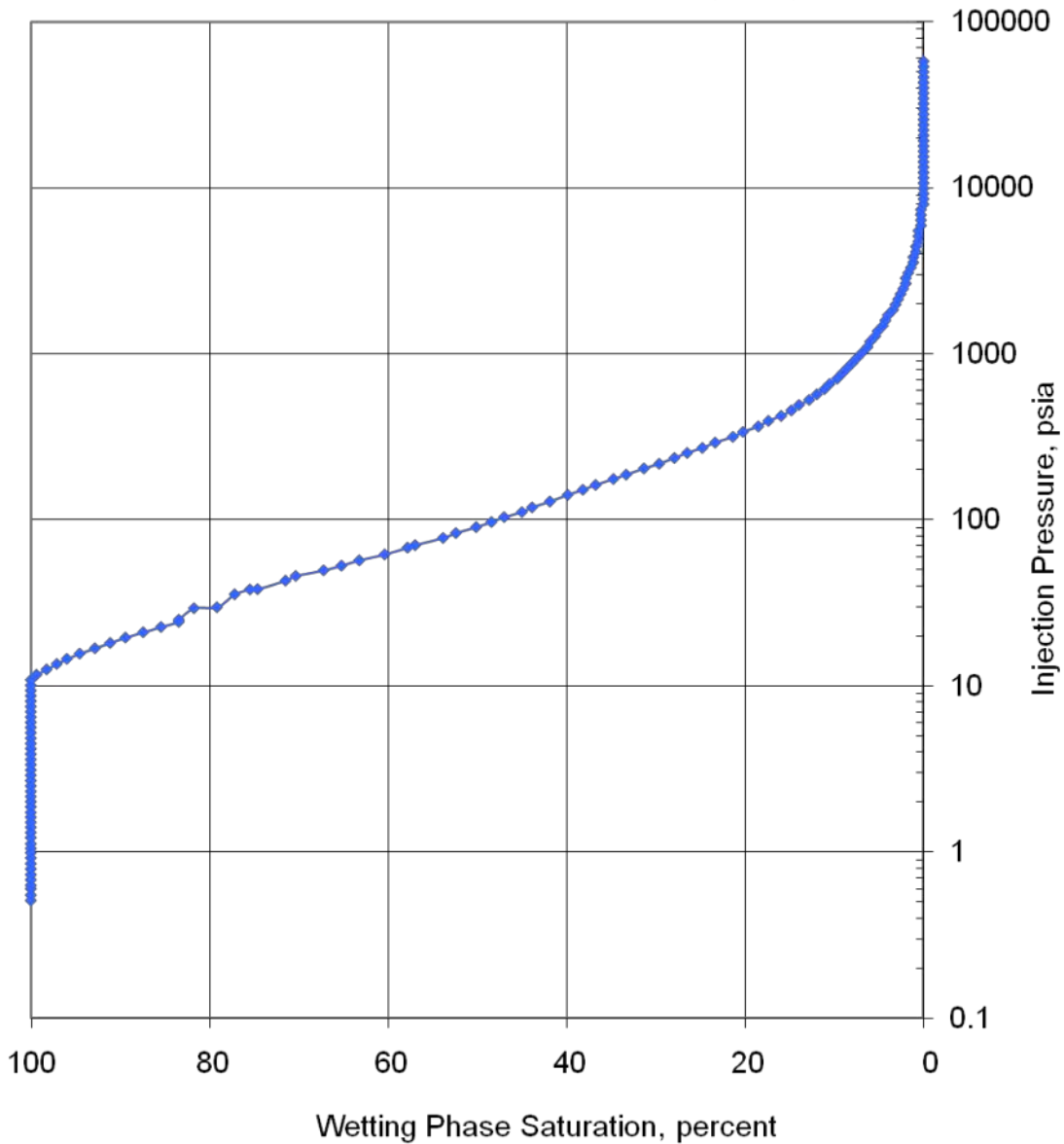


**Figure 47 – Results of the mercury porosimetry analysis on the sandstone rock sample as wetting phase saturation per capillary pressure.**



**PORE THROAT RADIUS DISTRIBUTION**  
Mercury Pressure: 0 - 60000  
(METHODOLOGY: ASTM D4404, API RP40)

Project Name: NAWC  
Project No.: ER-0715

Sample ID: Sandstone 1  
Depth, ft.: 38  
Porosity, %Vp: 9.1

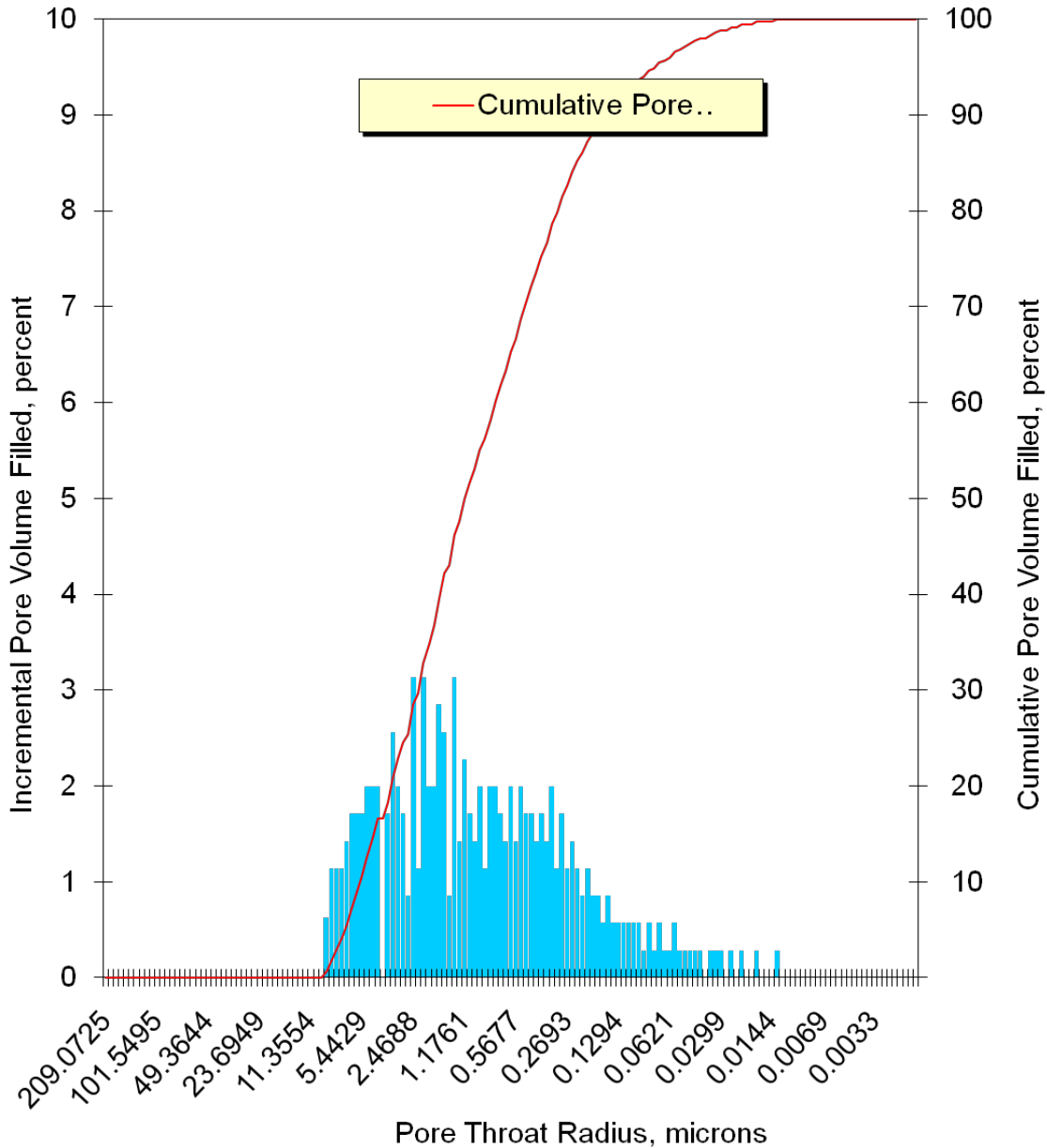


**Figure 48 – Pore throat radius distribution of the sandstone sample during the mercury porosimetry analysis.**

**Table D.17 – Results of the mercury porosimetry analysis on the duplicate sandstone rock sample.**

PTS File No:	39609			PTS Laboratories
Client:	Queen's University			
<b>MERCURY INJECTION SUMMARY</b>				
PROJECT NAME:	NAWC		Sample ID:	Sandstone 2
PROJECT NO:	ER-0715		Depth, ft.:	38
			Porosity, %Vp:	4.2
*INJECTION PRESSURE, psia	PORE THROAT Radius, microns	NON-WETTING PHASE SATURATION		WETTING PHASE SATURATION, percent
		INCREMENTAL, percent	CUMULATIVE, percent	
0.510	209	0.000	0.000	100.0
0.550	194	0.000	0.000	100.0
0.600	178	0.000	0.000	100.0
0.630	169	0.000	0.000	100.0
0.680	157	0.000	0.000	100.0
0.730	146	0.000	0.000	100.0
0.790	135	0.000	0.000	100.0
0.850	125	0.000	0.000	100.0
0.920	116	0.000	0.000	100.0
0.990	108	0.000	0.000	100.0
1.05	102	0.000	0.000	100.0
1.12	95.2	0.000	0.000	100.0
1.22	87.4	0.000	0.000	100.0
1.31	81.4	0.000	0.000	100.0
1.41	75.6	0.000	0.000	100.0
1.51	70.6	0.000	0.000	100.0
1.62	65.8	0.000	0.000	100.0
1.73	61.6	0.000	0.000	100.0
1.87	57.0	0.000	0.000	100.0
2.01	53.0	0.000	0.000	100.0
2.16	49.4	0.000	0.000	100.0
2.32	46.0	0.000	0.000	100.0
2.50	42.7	0.000	0.000	100.0
2.69	39.6	0.000	0.000	100.0
2.90	36.8	0.000	0.000	100.0
3.12	34.2	0.000	0.000	100.0
3.36	31.7	0.000	0.000	100.0
3.61	29.5	0.000	0.000	100.0
3.89	27.4	0.000	0.000	100.0
4.19	25.4	0.000	0.000	100.0
4.50	23.7	0.000	0.000	100.0
4.85	22.0	0.000	0.000	100.0
5.23	20.4	0.000	0.000	100.0

5.63	18.9	0.000	0.000	100.0
6.04	17.7	0.000	0.000	100.0
6.50	16.4	0.000	0.000	100.0
7.00	15.2	0.000	0.000	100.0
7.53	14.2	0.000	0.000	100.0
8.11	13.1	0.000	0.000	100.0
8.73	12.2	0.000	0.000	100.0
9.39	11.4	0.000	0.000	100.0
10.1	10.6	0.000	0.000	100.0
10.9	9.79	0.000	0.000	100.0
11.7	9.12	0.000	0.000	100.0
12.6	8.47	0.000	0.000	100.0
13.6	7.85	0.000	0.000	100.0
14.6	7.31	0.000	0.000	100.0
15.7	6.80	0.000	0.000	100.0
16.9	6.31	0.000	0.000	100.0
18.2	5.86	0.000	0.000	100.0
19.6	5.44	0.000	0.000	100.0
21.1	5.06	0.000	0.000	100.0
22.7	4.70	0.000	0.000	100.0
24.4	4.37	0.000	0.000	100.0
30.3	3.52	0.000	0.000	100.0
30.4	3.50	0.000	0.000	100.0
35.0	3.05	0.000	0.000	100.0
35.4	3.01	0.000	0.000	100.0
39.7	2.69	0.000	0.000	100.0
40.8	2.61	0.000	0.000	100.0
44.4	2.40	0.000	0.000	100.0
47.4	2.25	0.000	0.000	100.0
55.0	1.94	0.000	0.000	100.0
56.1	1.90	0.000	0.000	100.0
61.2	1.74	0.000	0.000	100.0
66.3	1.61	0.000	0.000	100.0
69.2	1.54	0.000	0.000	100.0
75.7	1.41	0.000	0.000	100.0
83.2	1.28	0.000	0.000	100.0
89.5	1.19	0.853	0.853	99.1
96.1	1.11	1.29	2.14	97.9
104.5	1.02	1.29	3.43	96.6
112	0.95	0.644	4.07	95.9
120	0.885	1.29	5.36	94.6
130	0.819	1.29	6.65	93.4
139	0.770	1.29	7.94	92.1
152	0.701	1.93	9.87	90.1
162	0.658	1.29	11.2	88.8
175	0.610	1.29	12.4	87.6
188	0.567	2.58	15.0	85.0
204	0.524	1.93	16.9	83.1

218	0.489	1.93	18.9	81.1
236	0.453	1.93	20.8	79.2
254	0.420	1.93	22.7	77.3
272	0.391	2.58	25.3	74.7
293	0.364	1.93	27.2	72.8
317	0.337	2.58	29.8	70.2
341	0.313	3.22	33.0	67.0
366	0.292	2.58	35.6	64.4
394	0.270	2.58	38.2	61.8
424	0.252	2.58	40.8	59.2
457	0.233	2.58	43.3	56.7
493	0.216	2.58	45.9	54.1
529	0.202	2.58	48.5	51.5
571	0.187	2.58	51.1	48.9
613	0.174	1.93	53.0	47.0
660	0.162	2.58	55.6	44.4
710	0.150	2.58	58.2	41.8
765	0.139	3.22	61.4	38.6
823	0.130	2.58	63.9	36.1
887	0.120	2.58	66.5	33.5
954	0.112	3.22	69.7	30.3
1027	0.104	2.58	72.3	27.7
1105	0.097	3.22	75.5	24.5
1187	0.090	2.58	78.1	21.9
1279	0.083	2.58	80.7	19.3
1376	0.077	1.93	82.6	17.4
1481	0.072	1.93	84.5	15.5
1594	0.067	1.93	86.5	13.5
1715	0.062	1.93	88.4	11.6
1845	0.058	1.29	89.7	10.3
1986	0.054	0.644	90.3	9.66
2135	0.050	1.29	91.6	8.37
2300	0.046	0.644	92.3	7.73
2474	0.043	0.644	92.9	7.08
2662	0.040	0.644	93.6	6.44
2865	0.037	0.644	94.2	5.79
3081	0.035	0.644	94.8	5.15
3316	0.032	0.644	95.5	4.51
3566	0.030	0.000	95.5	4.51
3835	0.028	0.644	96.1	3.86
4128	0.026	0.644	96.8	3.22
4440	0.024	0.000	96.8	3.22
4776	0.022	0.644	97.4	2.58
5142	0.021	0.000	97.4	2.58
5534	0.019	0.000	97.4	2.58
5957	0.018	0.644	98.1	1.93
6411	0.017	0.000	98.1	1.93
6897	0.015	0.000	98.1	1.93

7427	0.014	0.644	98.7	1.29
7993	0.013	0.000	98.7	1.29
8603	0.012	0.000	98.7	1.29
9260	0.012	0.000	98.7	1.29
9964	0.011	0.644	99.4	0.644
10722	0.010	0.000	99.4	0.644
11542	0.009	0.000	99.4	0.644
12421	0.009	0.000	99.4	0.644
13365	0.008	0.000	99.4	0.644
14385	0.007	0.000	99.4	0.644
15481	0.007	0.644	100.0	0.000
16657	0.006	0.000	100.0	0.000
17927	0.006	0.000	100.0	0.000
19293	0.006	0.000	100.0	0.000
20768	0.005	0.000	100.0	0.000
22359	0.005	0.000	100.0	0.000
24066	0.004	0.000	100.0	0.000
25900	0.004	0.000	100.0	0.000
27873	0.004	0.000	100.0	0.000
29993	0.004	0.000	100.0	0.000
32269	0.003	0.000	100.0	0.000
34734	0.003	0.000	100.0	0.000
37374	0.003	0.000	100.0	0.000
40214	0.003	0.000	100.0	0.000
43277	0.002	0.000	100.0	0.000
46574	0.002	0.000	100.0	0.000
50110	0.002	0.000	100.0	0.000
53919	0.002	0.000	100.0	0.000
58022	0.002	0.000	100.0	0.000
58022	0.002	0.000	100.0	0.000



**PORE VOLUME FILLED vs PRESSURE**  
Mercury Pressure: 0 - 60000 psia  
(METHODOLOGY: ASTM D4404, API RP40)

Project Name: NAWC  
Project No.: ER-0715

Sample ID: Sandstone 2  
Depth, ft.: 38  
Porosity, %Vp: 4.2

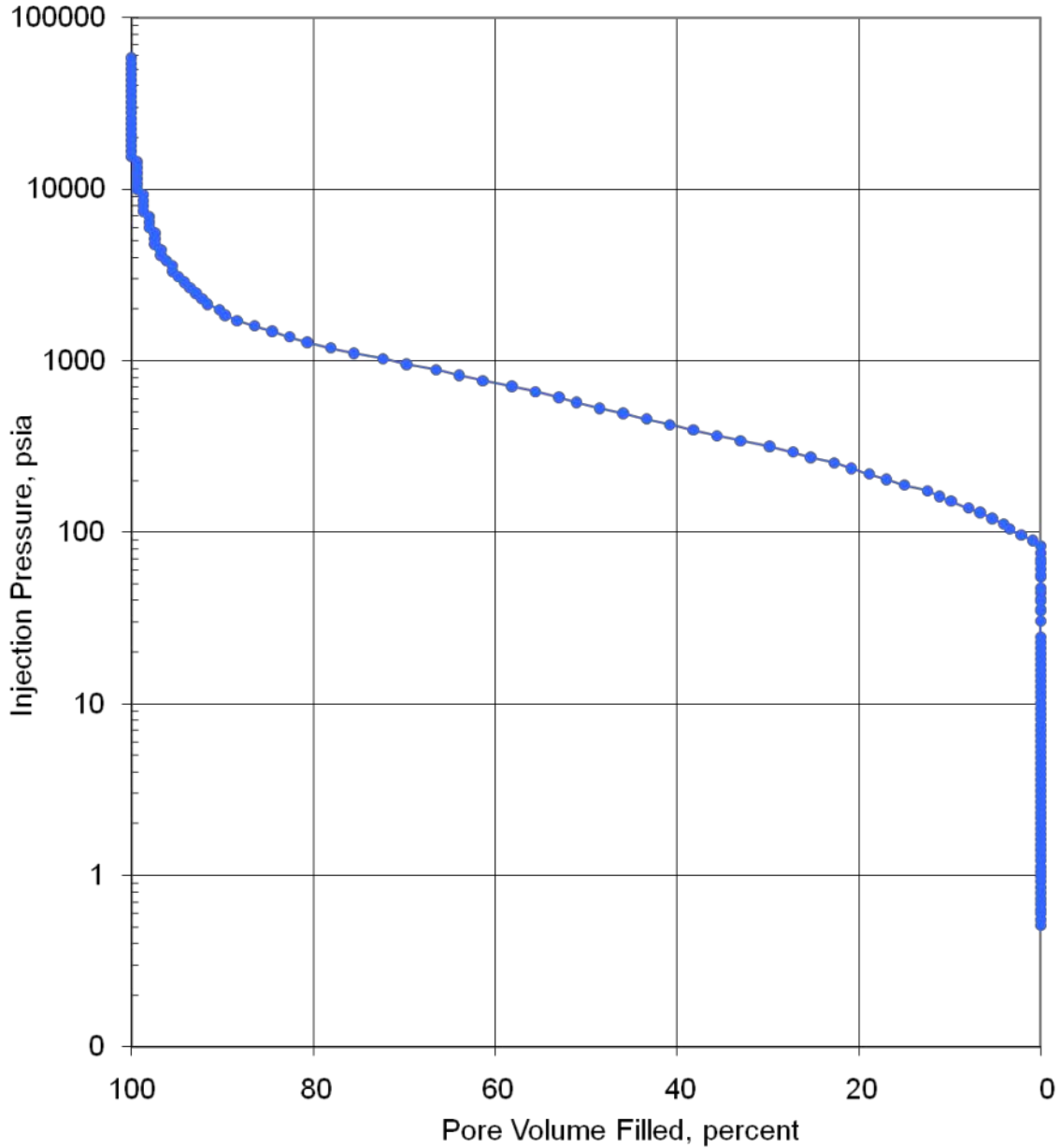


**Figure 49 – Results of the mercury porosimetry analysis on the duplicate sandstone rock sample as pore volume filled per pressure unit.**



### CAPILLARY PRESSURE vs. WETTING PHASE SATURATION

Mercury Pressure: 0 - 60000  
(METHODOLOGY: ASTM D4404, API RP40)

Project Name: NAWC  
Project No.: ER-0715

Sample ID: Sandstone 2  
Depth, ft.: 38  
Porosity, %Vp: 4.2

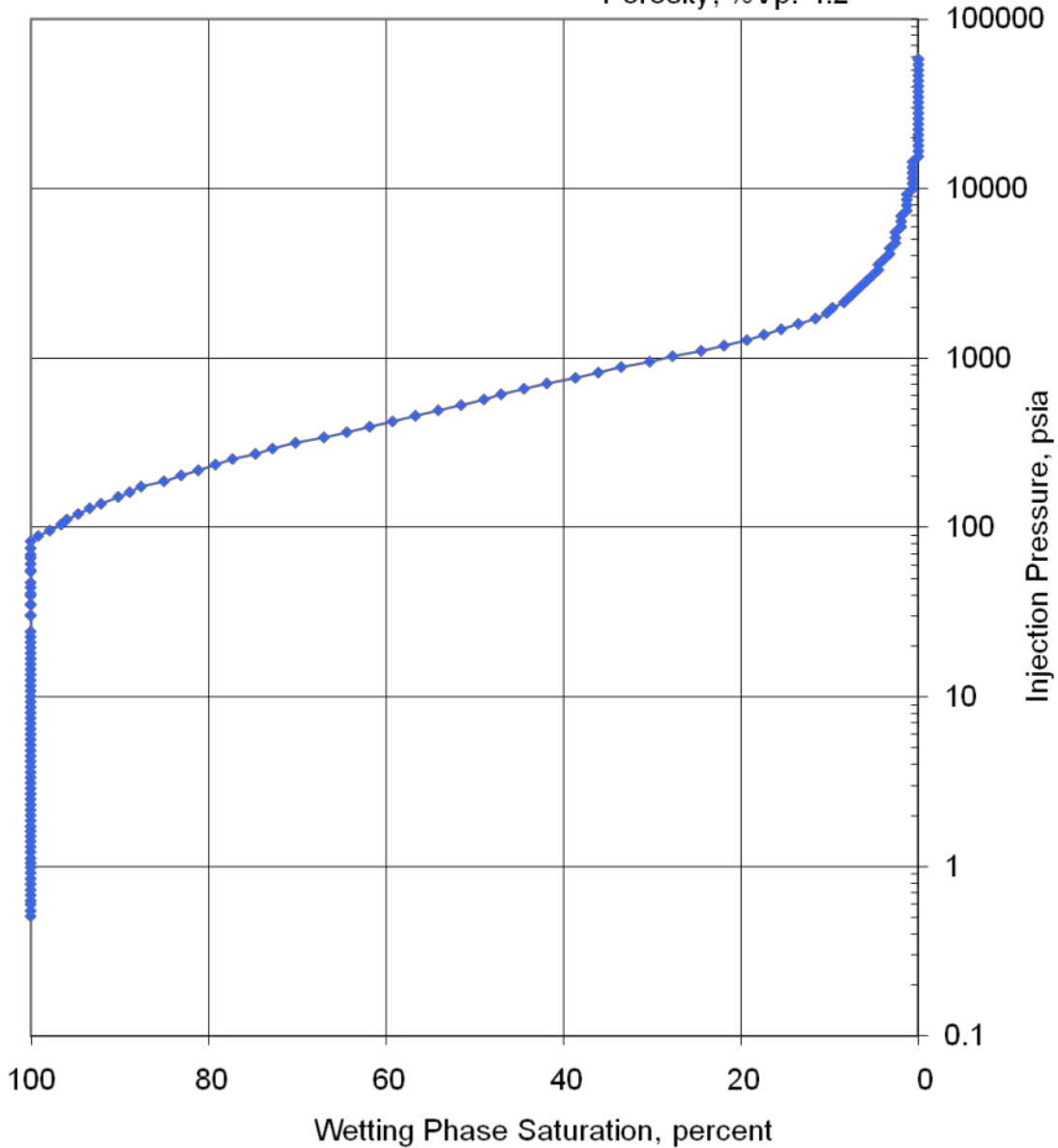


**Figure 50 – Results of the mercury porosimetry analysis on the duplicate sandstone rock sample as wetting phase saturation per capillary pressure.**



**PORE THROAT RADIUS DISTRIBUTION**  
Mercury Pressure: 0 - 60000  
(METHODOLOGY: ASTM D4404, API RP40)

Project Name: NAWC  
Project No.: ER-0715

Sample ID: Sandstone 2  
Depth, ft.: 38  
Porosity, %Vp: 4.2

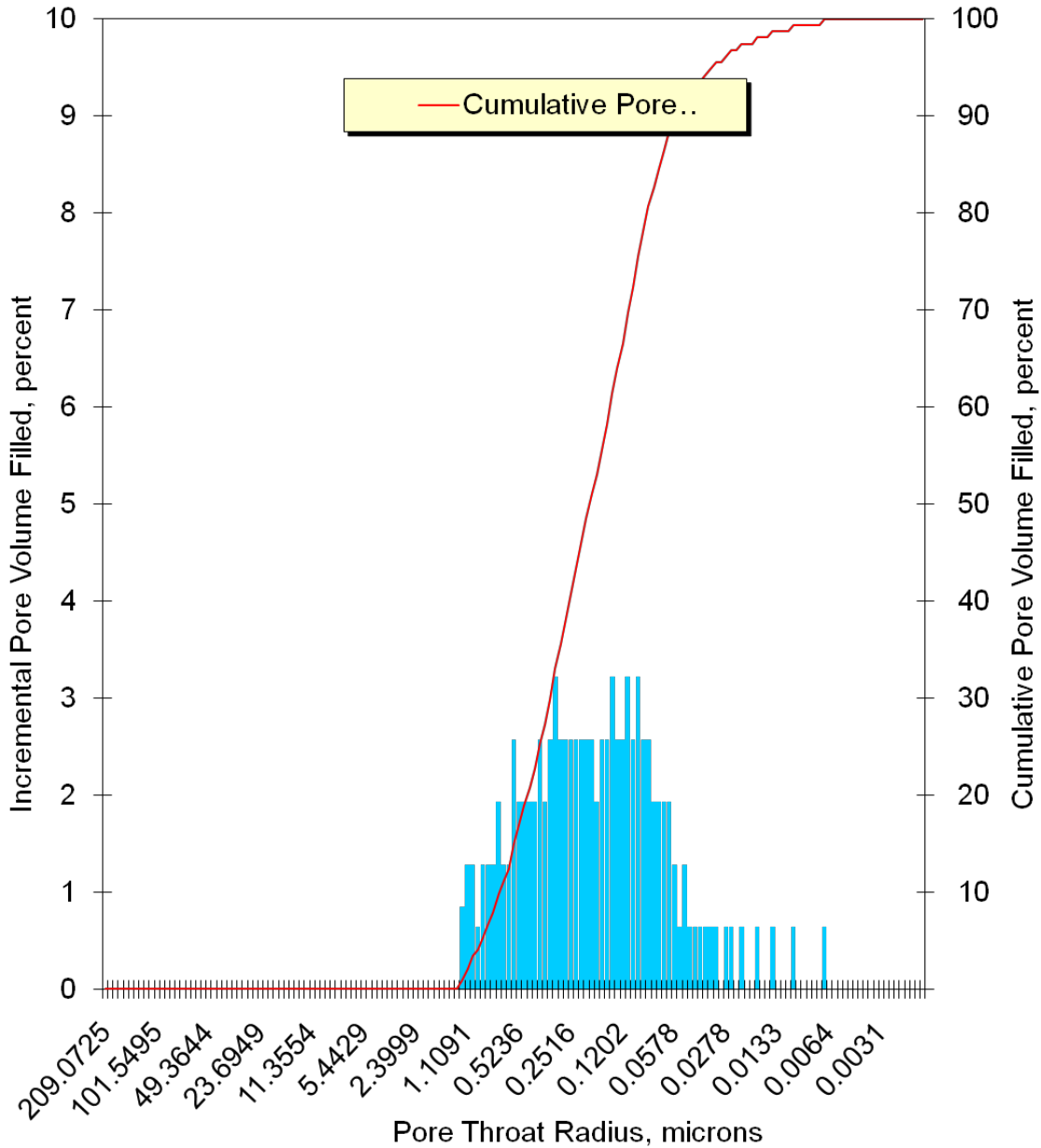


**Figure 51 – Pore throat radius distribution of the duplicate sandstone sample during the mercury porosimetry analysis.**

**Table 18 – Results of the hg porosimetry analysis on the triplicate sandstone rock sample.**

PTS File No:	39609			<b>PTS</b> Laboratories
Client:	Queen's University			
<b>MERCURY INJECTION SUMMARY</b>				
PROJECT NAME:	NAWC		Sample ID:	Sandstone 3
PROJECT NO:	ER-0715		Depth, ft.:	38
			Porosity, %Vp:	4.3
*INJECTION PRESSURE, psia	PORE THROAT Radius, microns	NON-WETTING PHASE SATURATION		WETTING PHASE SATURATION, percent
		INCREMENTAL, percent	CUMULATIVE, percent	
0.510	209	0.000	0.000	100.0
0.550	194	0.000	0.000	100.0
0.600	178	0.000	0.000	100.0
0.630	169	0.000	0.000	100.0
0.680	157	0.000	0.000	100.0
0.730	146	0.000	0.000	100.0
0.790	135	0.000	0.000	100.0
0.850	125	0.000	0.000	100.0
0.920	116	0.000	0.000	100.0
0.990	108	0.000	0.000	100.0
1.05	102	0.000	0.000	100.0
1.12	95.2	0.000	0.000	100.0
1.22	87.4	0.000	0.000	100.0
1.31	81.4	0.000	0.000	100.0
1.41	75.6	0.000	0.000	100.0
1.51	70.6	0.000	0.000	100.0
1.62	65.8	0.000	0.000	100.0
1.73	61.6	0.000	0.000	100.0
1.87	57.0	0.000	0.000	100.0
2.01	53.0	0.000	0.000	100.0
2.16	49.4	0.000	0.000	100.0
2.32	46.0	0.000	0.000	100.0
2.50	42.7	0.000	0.000	100.0
2.69	39.6	0.000	0.000	100.0
2.90	36.8	0.000	0.000	100.0
3.12	34.2	0.000	0.000	100.0
3.36	31.7	0.000	0.000	100.0
3.61	29.5	0.000	0.000	100.0
3.89	27.4	0.000	0.000	100.0
4.19	25.4	0.000	0.000	100.0
4.50	23.7	0.000	0.000	100.0
4.85	22.0	0.000	0.000	100.0

5.23	20.4	0.000	0.000	100.0
5.63	18.9	0.000	0.000	100.0
6.04	17.7	0.000	0.000	100.0
6.50	16.4	0.000	0.000	100.0
7.00	15.2	0.000	0.000	100.0
7.53	14.2	0.000	0.000	100.0
8.11	13.1	0.000	0.000	100.0
8.73	12.2	0.000	0.000	100.0
9.39	11.4	0.000	0.000	100.0
10.1	10.6	0.000	0.000	100.0
10.9	9.79	0.000	0.000	100.0
11.7	9.12	0.000	0.000	100.0
12.6	8.47	0.000	0.000	100.0
13.6	7.85	0.000	0.000	100.0
14.6	7.31	0.000	0.000	100.0
15.7	6.80	0.000	0.000	100.0
16.9	6.31	0.000	0.000	100.0
18.2	5.86	0.000	0.000	100.0
19.6	5.44	0.000	0.000	100.0
21.1	5.06	0.000	0.000	100.0
22.7	4.70	0.000	0.000	100.0
24.4	4.37	0.000	0.000	100.0
30.7	3.47	0.000	0.000	100.0
30.8	3.46	0.000	0.000	100.0
35.4	3.01	0.000	0.000	100.0
35.8	2.98	0.000	0.000	100.0
40.2	2.66	0.000	0.000	100.0
41.3	2.58	0.000	0.000	100.0
44.9	2.37	0.000	0.000	100.0
47.9	2.22	0.000	0.000	100.0
55.6	1.92	0.000	0.000	100.0
56.7	1.88	0.000	0.000	100.0
61.7	1.73	0.000	0.000	100.0
66.9	1.59	0.000	0.000	100.0
69.8	1.53	0.000	0.000	100.0
76.3	1.40	0.000	0.000	100.0
83.8	1.27	0.000	0.000	100.0
90.1	1.18	0.000	0.000	100.0
96.8	1.10	0.000	0.000	100.0
105.2	1.01	0.000	0.000	100.0
112	0.95	0.000	0.000	100.0
121	0.880	0.000	0.000	100.0
131	0.814	0.000	0.000	100.0
139	0.766	0.000	0.000	100.0
153	0.698	0.000	0.000	100.0
163	0.655	0.000	0.000	100.0
176	0.607	0.000	0.000	100.0
189	0.564	0.000	0.000	100.0

205	0.521	0.000	0.000	100.0
219	0.487	0.000	0.000	100.0
237	0.451	0.000	0.000	100.0
255	0.418	0.000	0.000	100.0
273	0.390	0.000	0.000	100.0
294	0.363	0.532	0.532	99.5
318	0.335	0.607	1.14	98.9
342	0.312	1.21	2.35	97.6
367	0.291	1.82	4.17	95.8
396	0.270	1.82	5.99	94.0
425	0.251	3.03	9.02	91.0
459	0.232	3.03	12.1	87.9
494	0.216	4.25	16.3	83.7
530	0.201	4.25	20.5	79.5
572	0.186	4.85	25.4	74.6
614	0.174	4.85	30.3	69.7
662	0.161	4.85	35.1	64.9
711	0.150	4.25	39.3	60.7
767	0.139	3.64	43.0	57.0
824	0.129	2.43	45.4	54.6
888	0.120	2.43	47.8	52.2
955	0.112	1.82	49.7	50.3
1028	0.104	1.82	51.5	48.5
1106	0.096	1.21	52.7	47.3
1189	0.090	1.82	54.5	45.5
1281	0.083	1.21	55.7	44.3
1378	0.077	1.82	57.5	42.5
1483	0.072	1.21	58.8	41.2
1596	0.067	1.21	60.0	40.0
1716	0.062	1.21	61.2	38.8
1847	0.058	1.21	62.4	37.6
1987	0.054	0.607	63.0	37.0
2137	0.050	1.21	64.2	35.8
2301	0.046	1.21	65.4	34.6
2475	0.043	1.21	66.6	33.4
2664	0.040	0.607	67.2	32.8
2867	0.037	1.21	68.5	31.5
3082	0.035	0.607	69.1	30.9
3318	0.032	1.21	70.3	29.7
3568	0.030	0.607	70.9	29.1
3837	0.028	1.21	72.1	27.9
4130	0.026	0.607	72.7	27.3
4442	0.024	1.21	73.9	26.1
4778	0.022	0.607	74.5	25.5
5144	0.021	1.21	75.7	24.3
5536	0.019	1.21	77.0	23.0
5959	0.018	0.607	77.6	22.4
6413	0.017	1.21	78.8	21.2

6899	0.015	0.607	79.4	20.6
7428	0.014	1.21	80.6	19.4
7995	0.013	1.21	81.8	18.2
8605	0.012	0.607	82.4	17.6
9262	0.012	1.21	83.6	16.4
9966	0.011	1.21	84.8	15.2
10724	0.010	1.21	86.1	13.9
11544	0.009	0.607	86.7	13.3
12423	0.009	1.21	87.9	12.1
13367	0.008	0.607	88.5	11.5
14387	0.007	0.607	89.1	10.9
15483	0.007	0.607	89.7	10.3
16659	0.006	1.21	90.9	9.10
17929	0.006	0.000	90.9	9.10
19295	0.006	0.607	91.5	8.49
20770	0.005	0.607	92.1	7.88
22361	0.005	0.607	92.7	7.28
24068	0.004	0.000	92.7	7.28
25902	0.004	0.607	93.3	6.67
27875	0.004	0.000	93.3	6.67
29995	0.004	0.607	93.9	6.07
32271	0.003	0.000	93.9	6.07
34735	0.003	0.607	94.5	5.46
37376	0.003	0.000	94.5	5.46
40216	0.003	0.000	94.5	5.46
43279	0.002	0.607	95.1	4.85
46575	0.002	0.607	95.8	4.25
50112	0.002	0.000	95.8	4.25
53920	0.002	1.82	97.6	2.43
58024	0.002	2.43	100.0	0.000
58022	0.002	0.000	100.0	0.000



**PORE VOLUME FILLED vs PRESSURE**  
Mercury Pressure: 0 - 60000 psia  
(METHODOLOGY: ASTM D4404, API RP40)

Project Name: NAWC  
Project No.: ER-0715

Sample ID: Sandstone 3  
Depth, ft.: 38  
Porosity, %Vp: 4.3

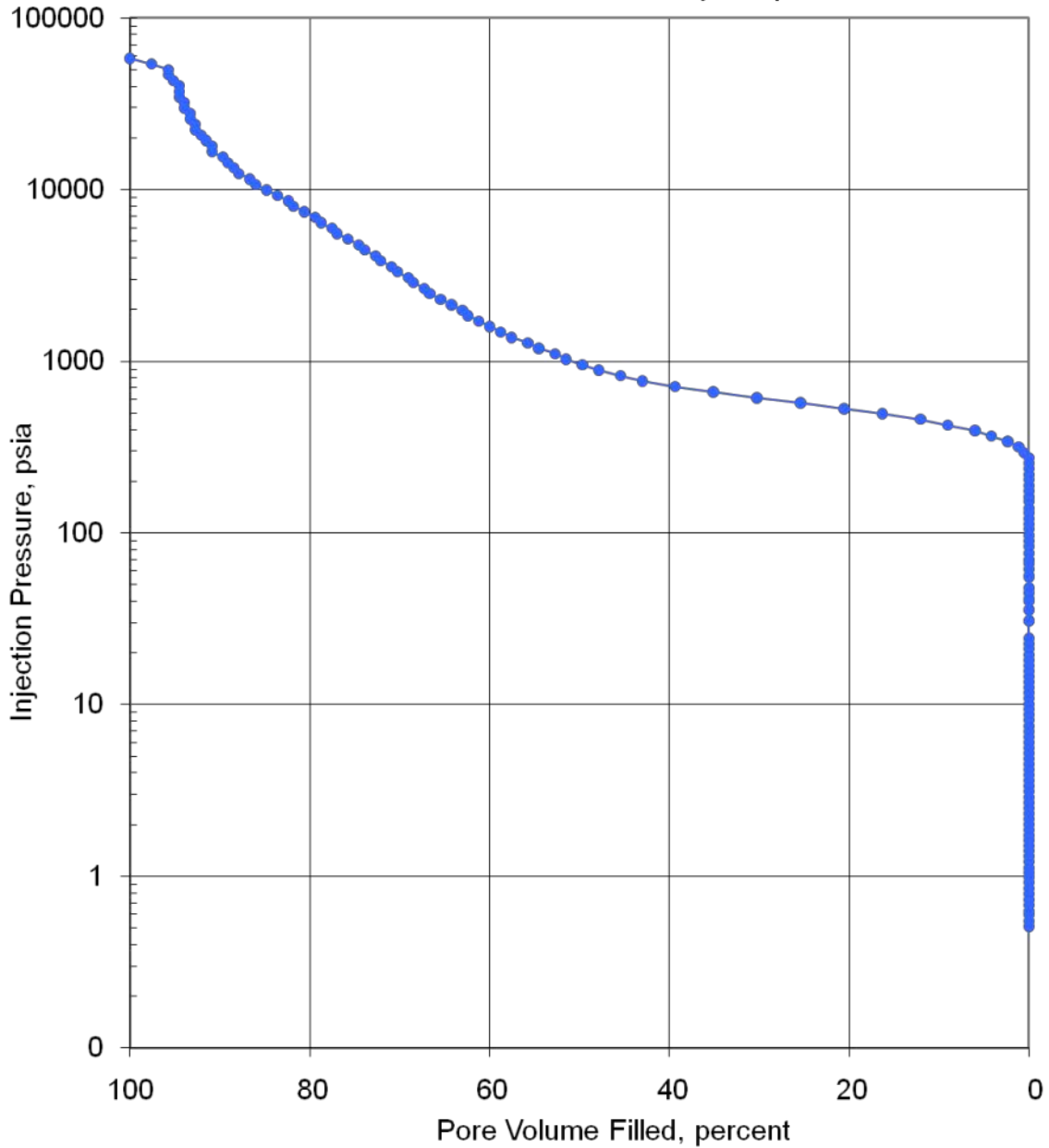


**Figure 52 – Results of the mercury porosimetry analysis on the triplicate sandstone rock sample as pore volume filled per pressure unit.**



### CAPILLARY PRESSURE vs. WETTING PHASE SATURATION

Mercury Pressure: 0 - 60000  
(METHODOLOGY: ASTM D4404, API RP40)

Project Name: NAWC  
Project No.: ER-0715

Sample ID: Sandstone 3  
Depth, ft.: 38  
Porosity, %Vp: 4.3

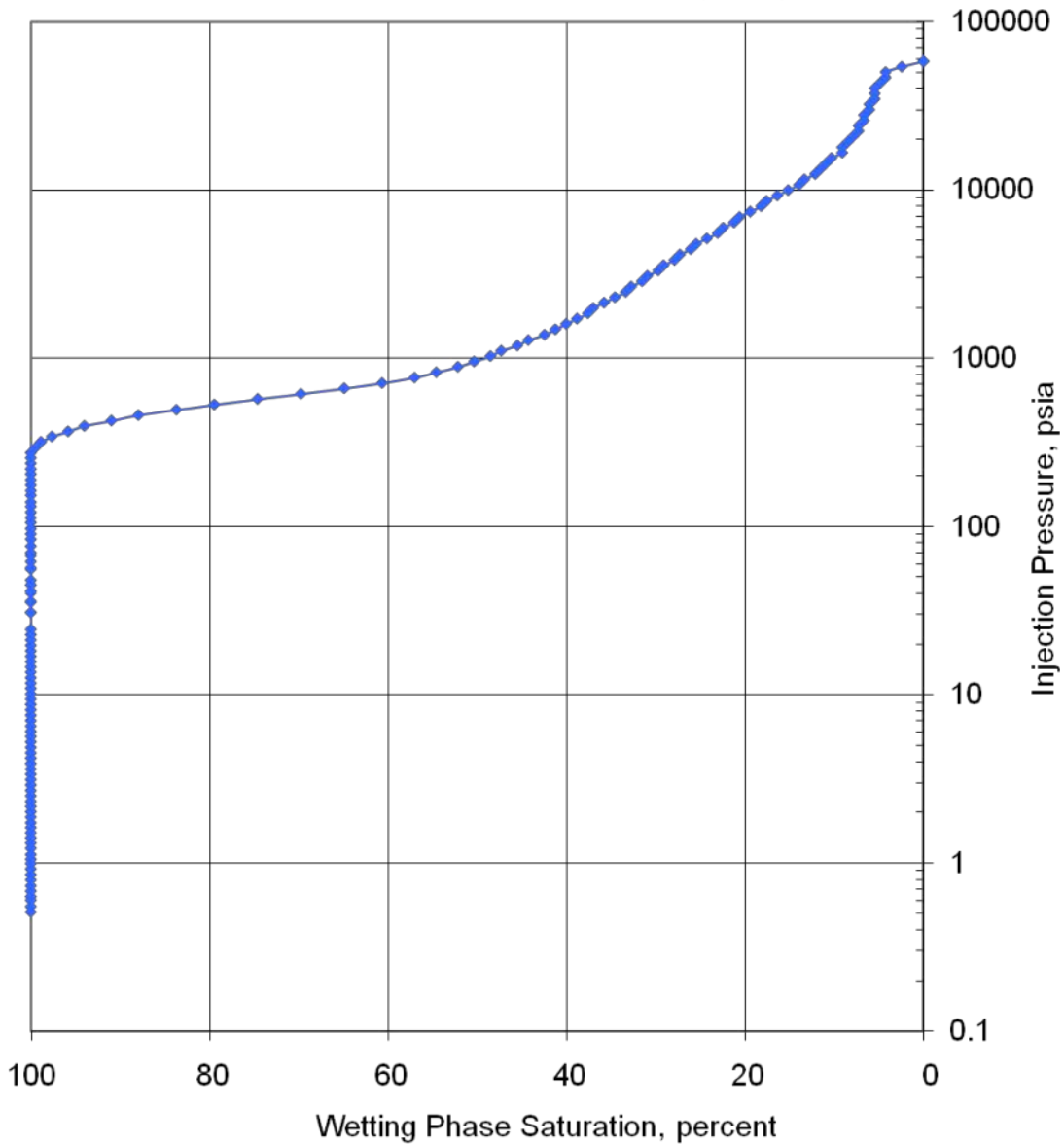


**Figure 53 – Results of the mercury porosimetry analysis on the triplicate sandstone rock sample as wetting phase saturation per capillary pressure.**



**PORE THROAT RADIUS DISTRIBUTION**  
Mercury Pressure: 0 - 60000  
(METHODOLOGY: ASTM D4404, API RP40)

Project Name: NAWC  
Project No.: ER-0715

Sample ID: Sandstone 3  
Depth, ft.: 38  
Porosity, %Vp: 4.3

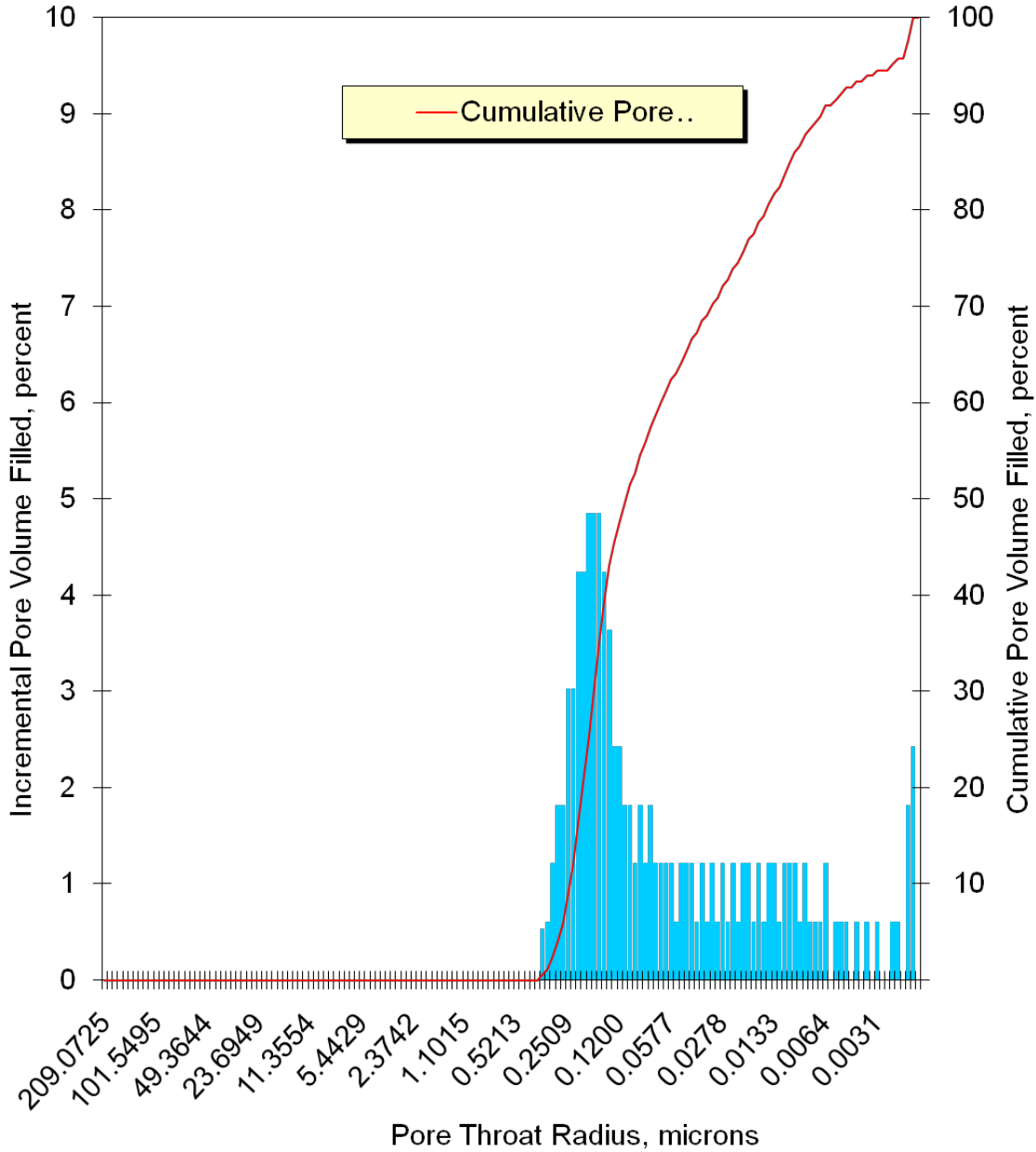


**Figure 54 – Pore throat radius distribution of the triplicate sandstone sample during the mercury porosimetry analysis.**

**Table D.19 – Results of the mercury porosimetry analysis on the dolostone rock sample.**

PTS File No:	39609			<b>PTS</b> Laboratories
Client:	Queen's University			
<b>MERCURY INJECTION SUMMARY</b>				
PROJECT NAME:	NAWC		Sample ID:	Dolostone 1
PROJECT NO:	ER-0715		Depth, ft.:	45
			Porosity, %Vp:	4.1
*INJECTION PRESSURE, psia	PORE THROAT Radius, microns	NON-WETTING PHASE SATURATION		WETTING PHASE SATURATION, percent
		INCREMENTAL, percent	CUMULATIVE, percent	
0.510	209	0.000	0.000	100.0
0.550	194	0.000	0.000	100.0
0.600	178	0.000	0.000	100.0
0.630	169	0.000	0.000	100.0
0.680	157	0.000	0.000	100.0
0.730	146	0.000	0.000	100.0
0.790	135	0.000	0.000	100.0
0.850	125	0.000	0.000	100.0
0.910	117	0.000	0.000	100.0
0.980	109	0.000	0.000	100.0
1.05	102	0.000	0.000	100.0
1.13	94.4	0.000	0.000	100.0
1.22	87.4	0.000	0.000	100.0
1.31	81.4	0.000	0.000	100.0
1.40	76.2	0.000	0.000	100.0
1.51	70.6	0.000	0.000	100.0
1.61	66.2	0.000	0.000	100.0
1.74	61.3	0.000	0.000	100.0
1.87	57.0	0.000	0.000	100.0
2.01	53.0	0.000	0.000	100.0
2.16	49.4	0.000	0.000	100.0
2.32	46.0	0.000	0.000	100.0
2.50	42.7	0.000	0.000	100.0
2.69	39.6	0.000	0.000	100.0
2.90	36.8	0.000	0.000	100.0
3.12	34.2	0.000	0.000	100.0
3.36	31.7	0.000	0.000	100.0
3.61	29.5	0.000	0.000	100.0
3.89	27.4	0.000	0.000	100.0
4.19	25.4	0.000	0.000	100.0
4.50	23.7	0.000	0.000	100.0
4.85	22.0	0.000	0.000	100.0
5.22	20.4	0.000	0.000	100.0

5.62	19.0	0.000	0.000	100.0
6.04	17.7	0.000	0.000	100.0
6.50	16.4	0.000	0.000	100.0
7.00	15.2	0.000	0.000	100.0
7.53	14.2	0.000	0.000	100.0
8.11	13.1	0.000	0.000	100.0
8.73	12.2	0.000	0.000	100.0
9.39	11.4	0.000	0.000	100.0
10.1	10.6	0.000	0.000	100.0
10.9	9.79	0.000	0.000	100.0
11.7	9.12	0.000	0.000	100.0
12.6	8.47	0.000	0.000	100.0
13.6	7.85	0.000	0.000	100.0
14.6	7.31	0.000	0.000	100.0
15.7	6.80	0.000	0.000	100.0
16.9	6.31	0.000	0.000	100.0
18.2	5.86	0.000	0.000	100.0
19.6	5.44	0.000	0.000	100.0
21.1	5.06	0.000	0.000	100.0
22.7	4.70	0.000	0.000	100.0
24.4	4.37	0.000	0.000	100.0
25.4	4.20	0.000	0.000	100.0
27.3	3.91	0.000	0.000	100.0
28.6	3.73	0.000	0.000	100.0
31.5	3.39	0.000	0.000	100.0
35.1	3.04	0.000	0.000	100.0
37.0	2.88	0.000	0.000	100.0
40.5	2.63	0.000	0.000	100.0
43.7	2.44	0.000	0.000	100.0
47.1	2.26	0.000	0.000	100.0
50.8	2.10	0.000	0.000	100.0
56.0	1.90	0.000	0.000	100.0
60.2	1.77	0.000	0.000	100.0
64.5	1.65	0.000	0.000	100.0
70.0	1.52	0.000	0.000	100.0
74.4	1.43	0.000	0.000	100.0
83.9	1.27	0.000	0.000	100.0
88.7	1.20	0.000	0.000	100.0
96.1	1.11	0.000	0.000	100.0
103	1.03	0.000	0.000	100.0
111	0.961	0.000	0.000	100.0
119	0.900	0.000	0.000	100.0
128	0.831	0.000	0.000	100.0
140	0.760	0.759	0.759	99.2
150	0.710	0.628	1.39	98.6
162	0.660	0.628	2.02	98.0
176	0.607	1.88	3.90	96.1
189	0.565	1.88	5.78	94.2

203	0.525	3.14	8.92	91.1
218	0.490	3.77	12.7	87.3
237	0.451	5.65	18.3	81.7
254	0.420	5.65	24.0	76.0
274	0.390	6.28	30.3	69.7
293	0.364	5.65	35.9	64.1
317	0.337	5.65	41.6	58.4
341	0.313	5.02	46.6	53.4
367	0.291	4.40	51.0	49.0
394	0.270	4.40	55.4	44.6
425	0.251	3.77	59.2	40.8
457	0.233	3.77	62.9	37.1
492	0.217	3.14	66.1	33.9
530	0.201	3.14	69.2	30.8
571	0.187	2.51	71.7	28.3
613	0.174	2.51	74.2	25.8
660	0.162	1.88	76.1	23.9
710	0.150	1.88	78.0	22.0
763	0.140	1.26	79.3	20.7
822	0.130	1.88	81.2	18.8
885	0.121	1.26	82.4	17.6
953	0.112	0.628	83.0	17.0
1027	0.104	1.26	84.3	15.7
1103	0.097	0.628	84.9	15.1
1187	0.090	1.26	86.2	13.8
1278	0.083	0.628	86.8	13.2
1376	0.077	0.628	87.4	12.6
1481	0.072	0.628	88.1	11.9
1592	0.067	0.628	88.7	11.3
1713	0.062	0.628	89.3	10.7
1845	0.058	0.628	90.0	10.0
1985	0.054	0.000	90.0	10.0
2135	0.050	0.628	90.6	9.42
2299	0.046	0.628	91.2	8.79
2473	0.043	0.000	91.2	8.79
2662	0.040	0.628	91.8	8.17
2864	0.037	0.000	91.8	8.17
3082	0.035	0.628	92.5	7.54
3317	0.032	0.628	93.1	6.91
3568	0.030	0.000	93.1	6.91
3838	0.028	0.628	93.7	6.28
4130	0.026	0.000	93.7	6.28
4440	0.024	0.628	94.3	5.65
4778	0.022	0.000	94.3	5.65
5141	0.021	0.628	95.0	5.02
5533	0.019	0.000	95.0	5.02
5956	0.018	0.628	95.6	4.40
6411	0.017	0.000	95.6	4.40

6898	0.015	0.628	96.2	3.77
7427	0.014	0.000	96.2	3.77
7995	0.013	0.628	96.9	3.14
8603	0.012	0.628	97.5	2.51
9258	0.012	0.000	97.5	2.51
9964	0.011	0.628	98.1	1.88
10727	0.010	0.000	98.1	1.88
11541	0.009	0.628	98.7	1.26
12421	0.009	0.000	98.7	1.26
13368	0.008	0.628	99.4	0.628
14385	0.007	0.000	99.4	0.628
15477	0.007	0.628	100.0	0.000
16660	0.006	0.000	100.0	0.000
17927	0.006	0.000	100.0	0.000
19294	0.006	0.000	100.0	0.000
20772	0.005	0.000	100.0	0.000
22361	0.005	0.000	100.0	0.000
24066	0.004	0.000	100.0	0.000
25901	0.004	0.000	100.0	0.000
27873	0.004	0.000	100.0	0.000
29995	0.004	0.000	100.0	0.000
32279	0.003	0.000	100.0	0.000
34735	0.003	0.000	100.0	0.000
37375	0.003	0.000	100.0	0.000
40215	0.003	0.000	100.0	0.000
43277	0.002	0.000	100.0	0.000
46564	0.002	0.000	100.0	0.000
50114	0.002	0.000	100.0	0.000
53920	0.002	0.000	100.0	0.000
58023	0.002	0.000	100.0	0.000



**PORE VOLUME FILLED vs PRESSURE**  
Mercury Pressure: 0 - 60000 psia  
(METHODOLOGY: ASTM D4404, API RP40)

Project Name: NAWC  
Project No.: ER-0715

Sample ID: Dolostone 1  
Depth, ft.: 45  
Porosity, %Vp: 4.1

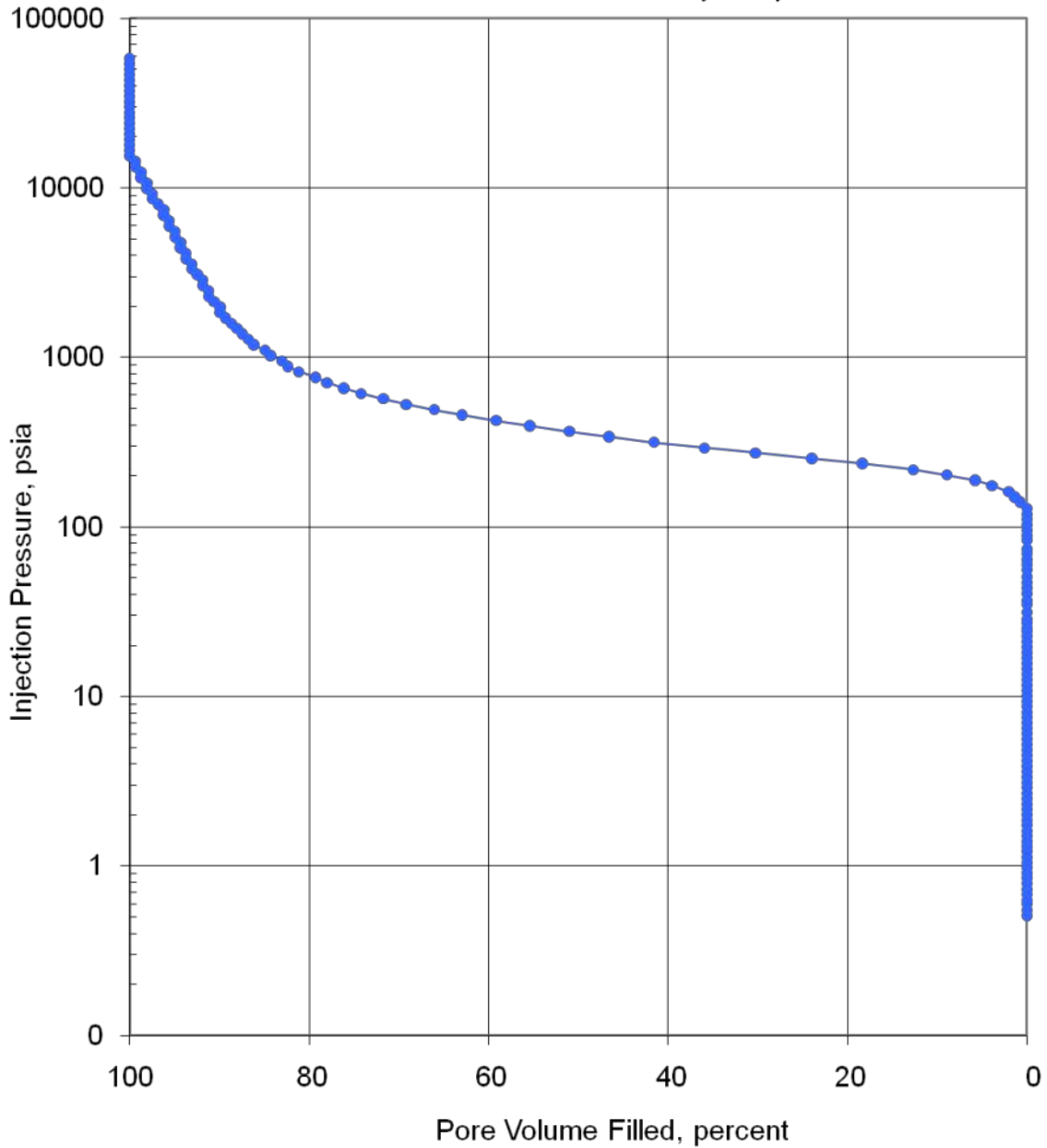


**Figure 55 – Results of the mercury porosimetry analysis on the dolostone rock sample as pore volume filled per pressure unit.**



### CAPILLARY PRESSURE vs. WETTING PHASE SATURATION

Mercury Pressure: 0 - 60000  
(METHODOLOGY: ASTM D4404, API RP40)

Project Name: NAWC  
Project No.: ER-0715

Sample ID: Dolostone 1  
Depth, ft.: 45  
Porosity, %Vp: 4.1

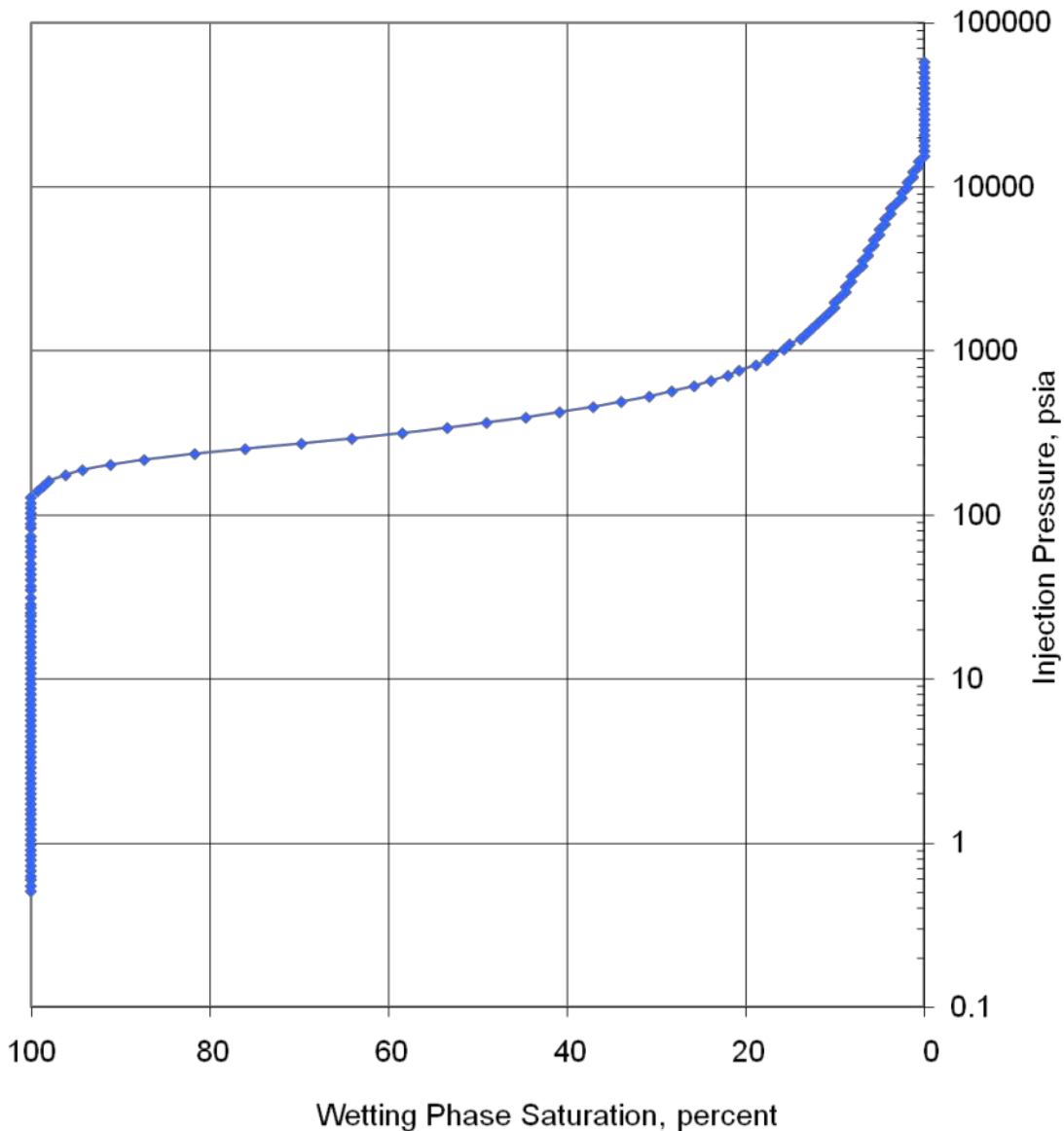


**Figure 56 – Results of the mercury porosimetry analysis on the dolostone rock sample as wetting phase saturation per capillary pressure.**



**PORE THROAT RADIUS DISTRIBUTION**  
Mercury Pressure: 0 - 60000  
(METHODOLOGY: ASTM D4404, API RP40)

Project Name: NAWC  
Project No.: ER-0715

Sample ID: Dolostone 1  
Depth, ft.: 45  
Porosity, %Vp: 4.1

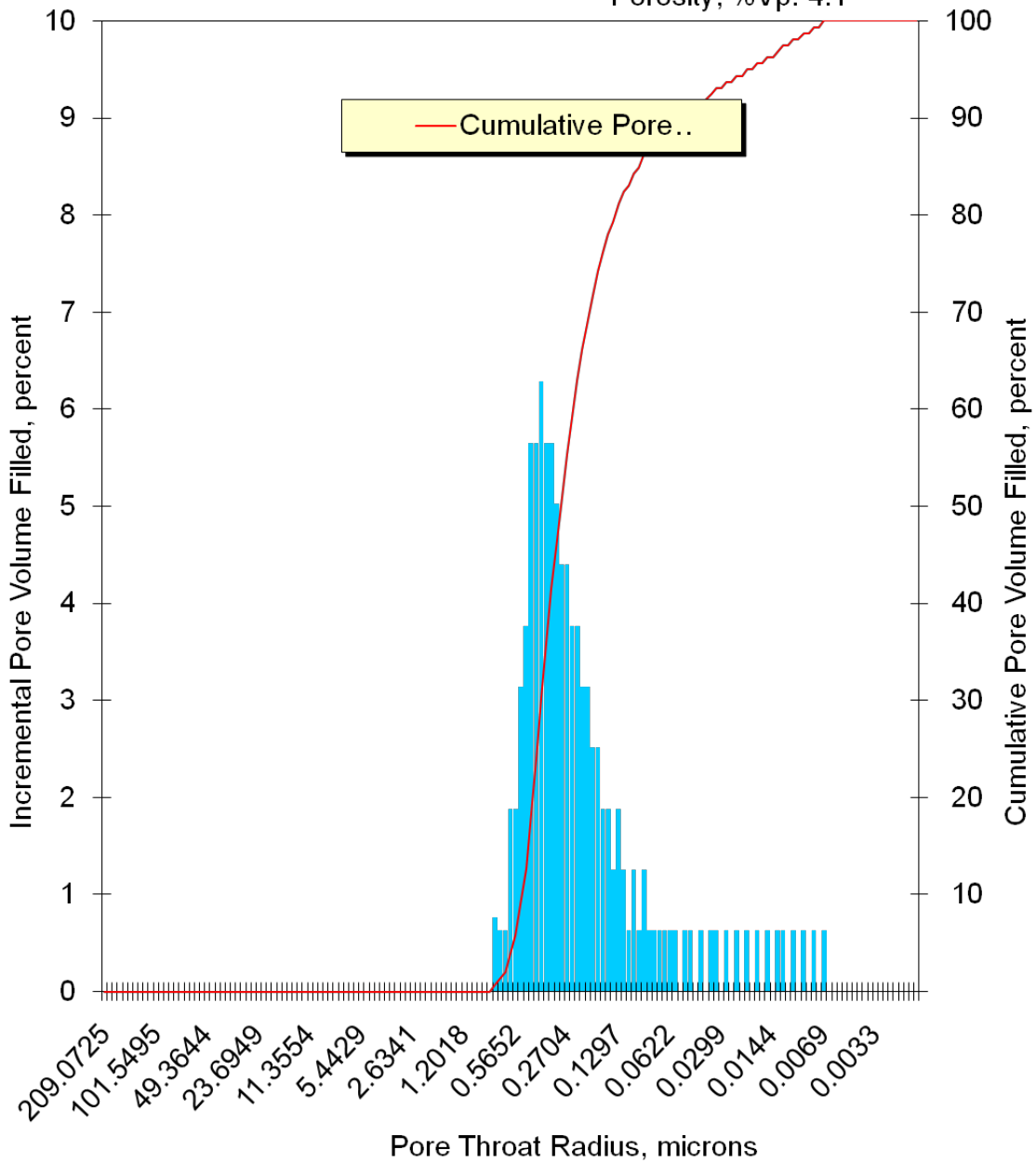


**Figure 57 – Pore throat radius distribution of the dolostone sample during the mercury porosimetry analysis.**

**Table 20 – Results of the mercury porosimetry analysis on the duplicate dolostone rock sample.**

PTS File No:	39609			PTS Laboratories
Client:	Queen's University			
<b>MERCURY INJECTION SUMMARY</b>				
PROJECT NAME:	NAWC		Sample ID:	Dolostone 2
PROJECT NO:	ER-0715		Depth, ft.:	45
			Porosity, %Vp:	6.3
*INJECTION PRESSURE, psia	PORE THROAT Radius, microns	NON-WETTING PHASE SATURATION		WETTING PHASE SATURATION, percent
		INCREMENTAL, percent	CUMULATIVE, percent	
0.510	209	0.000	0.000	100.0
0.550	194	0.000	0.000	100.0
0.600	178	0.000	0.000	100.0
0.630	169	0.000	0.000	100.0
0.680	157	0.000	0.000	100.0
0.730	146	0.000	0.000	100.0
0.790	135	0.000	0.000	100.0
0.850	125	0.000	0.000	100.0
0.910	117	0.000	0.000	100.0
0.980	109	0.000	0.000	100.0
1.05	102	0.000	0.000	100.0
1.13	94.4	0.000	0.000	100.0
1.22	87.4	0.000	0.000	100.0
1.31	81.4	0.000	0.000	100.0
1.40	76.2	0.000	0.000	100.0
1.51	70.6	0.000	0.000	100.0
1.61	66.2	0.000	0.000	100.0
1.74	61.3	0.000	0.000	100.0
1.87	57.0	0.000	0.000	100.0
2.01	53.0	0.000	0.000	100.0
2.16	49.4	0.000	0.000	100.0
2.32	46.0	0.000	0.000	100.0
2.50	42.7	0.000	0.000	100.0
2.69	39.6	0.000	0.000	100.0
2.90	36.8	0.000	0.000	100.0
3.12	34.2	0.000	0.000	100.0
3.36	31.7	0.000	0.000	100.0
3.61	29.5	0.000	0.000	100.0
3.89	27.4	0.000	0.000	100.0
4.19	25.4	0.000	0.000	100.0
4.50	23.7	0.000	0.000	100.0
4.85	22.0	0.000	0.000	100.0

5.22	20.4	0.000	0.000	100.0
5.62	19.0	0.000	0.000	100.0
6.04	17.7	0.000	0.000	100.0
6.50	16.4	0.000	0.000	100.0
7.00	15.2	0.000	0.000	100.0
7.53	14.2	0.000	0.000	100.0
8.11	13.1	0.000	0.000	100.0
8.73	12.2	0.000	0.000	100.0
9.39	11.4	0.000	0.000	100.0
10.1	10.6	0.000	0.000	100.0
10.9	9.79	0.000	0.000	100.0
11.7	9.12	0.000	0.000	100.0
12.6	8.47	0.000	0.000	100.0
13.6	7.85	0.000	0.000	100.0
14.6	7.31	0.000	0.000	100.0
15.7	6.80	0.000	0.000	100.0
16.9	6.31	0.000	0.000	100.0
18.2	5.86	0.000	0.000	100.0
19.6	5.44	0.000	0.000	100.0
21.1	5.06	0.000	0.000	100.0
22.7	4.70	0.000	0.000	100.0
24.4	4.37	0.000	0.000	100.0
25.8	4.13	0.000	0.000	100.0
27.7	3.85	0.000	0.000	100.0
29.0	3.67	0.000	0.000	100.0
31.9	3.34	0.000	0.000	100.0
35.5	3.01	0.000	0.000	100.0
37.4	2.85	0.000	0.000	100.0
40.9	2.61	0.000	0.000	100.0
44.1	2.42	0.000	0.000	100.0
47.5	2.24	0.000	0.000	100.0
51.2	2.08	0.000	0.000	100.0
56.5	1.89	0.000	0.000	100.0
60.6	1.76	0.000	0.000	100.0
65.0	1.64	0.000	0.000	100.0
70.4	1.51	0.000	0.000	100.0
74.9	1.42	0.000	0.000	100.0
84.4	1.26	0.000	0.000	100.0
89.2	1.20	0.000	0.000	100.0
96.6	1.10	0.000	0.000	100.0
104	1.03	0.000	0.000	100.0
111	0.957	0.000	0.000	100.0
119	0.896	0.000	0.000	100.0
129	0.828	0.000	0.000	100.0
141	0.757	0.000	0.000	100.0
151	0.708	0.477	0.477	99.5
162	0.657	0.395	0.872	99.1
176	0.605	1.58	2.45	97.5

189	0.563	3.16	5.61	94.4
204	0.524	5.92	11.5	88.5
218	0.488	6.32	17.9	82.1
237	0.450	6.71	24.6	75.4
254	0.419	6.32	30.9	69.1
274	0.388	5.13	36.0	64.0
294	0.362	4.34	40.4	59.6
318	0.336	3.95	44.3	55.7
342	0.312	3.55	47.9	52.1
368	0.290	3.55	51.4	48.6
396	0.270	2.76	54.2	45.8
426	0.250	2.76	57.0	43.0
459	0.233	2.76	59.7	40.3
494	0.216	2.37	62.1	37.9
531	0.201	1.97	64.1	35.9
572	0.186	1.97	66.0	34.0
615	0.173	1.97	68.0	32.0
661	0.161	1.58	69.6	30.4
712	0.150	1.58	71.2	28.8
765	0.139	1.18	72.4	27.6
824	0.129	1.58	73.9	26.1
886	0.120	1.18	75.1	24.9
955	0.112	1.18	76.3	23.7
1028	0.104	1.18	77.5	22.5
1105	0.096	0.790	78.3	21.7
1189	0.090	1.18	79.5	20.5
1280	0.083	0.790	80.3	19.7
1378	0.077	0.790	81.0	19.0
1483	0.072	1.18	82.2	17.8
1594	0.067	0.790	83.0	17.0
1715	0.062	0.395	83.4	16.6
1847	0.058	0.790	84.2	15.8
1987	0.054	0.790	85.0	15.0
2137	0.050	0.790	85.8	14.2
2301	0.046	0.790	86.6	13.4
2475	0.043	0.395	87.0	13.0
2664	0.040	0.790	87.8	12.2
2866	0.037	0.395	88.2	11.8
3084	0.035	0.395	88.5	11.5
3318	0.032	0.790	89.3	10.7
3569	0.030	0.395	89.7	10.3
3840	0.028	0.395	90.1	9.87
4132	0.026	0.395	90.5	9.48
4442	0.024	0.790	91.3	8.69
4780	0.022	0.395	91.7	8.29
5143	0.021	0.395	92.1	7.90
5535	0.019	0.395	92.5	7.50
5958	0.018	0.395	92.9	7.11

6413	0.017	0.790	93.7	6.32
6900	0.015	0.395	94.1	5.92
7429	0.014	0.395	94.5	5.53
7997	0.013	0.790	95.3	4.74
8605	0.012	0.395	95.7	4.34
9260	0.012	0.790	96.4	3.55
9966	0.011	0.395	96.8	3.16
10729	0.010	0.395	97.2	2.76
11543	0.009	0.790	98.0	1.97
12423	0.009	0.395	98.4	1.58
13370	0.008	0.395	98.8	1.18
14387	0.007	0.395	99.2	0.790
15479	0.007	0.000	99.2	0.790
16662	0.006	0.395	99.6	0.395
17929	0.006	0.000	99.6	0.395
19296	0.006	0.000	99.6	0.395
20774	0.005	0.395	100.0	0.000
22363	0.005	0.000	100.0	0.000
24068	0.004	0.000	100.0	0.000
25903	0.004	0.000	100.0	0.000
27875	0.004	0.000	100.0	0.000
29997	0.004	0.000	100.0	0.000
32281	0.003	0.000	100.0	0.000
34737	0.003	0.000	100.0	0.000
37377	0.003	0.000	100.0	0.000
40217	0.003	0.000	100.0	0.000
43279	0.002	0.000	100.0	0.000
46566	0.002	0.000	100.0	0.000
50116	0.002	0.000	100.0	0.000
53922	0.002	0.000	100.0	0.000
58025	0.002	0.000	100.0	0.000



**PORE VOLUME FILLED vs PRESSURE**  
Mercury Pressure: 0 - 60000 psia  
(METHODOLOGY: ASTM D4404, API RP40)

Project Name: NAWC  
Project No.: ER-0715

Sample ID: Dolostone 2  
Depth, ft.: 45  
Porosity, %Vp: 6.3

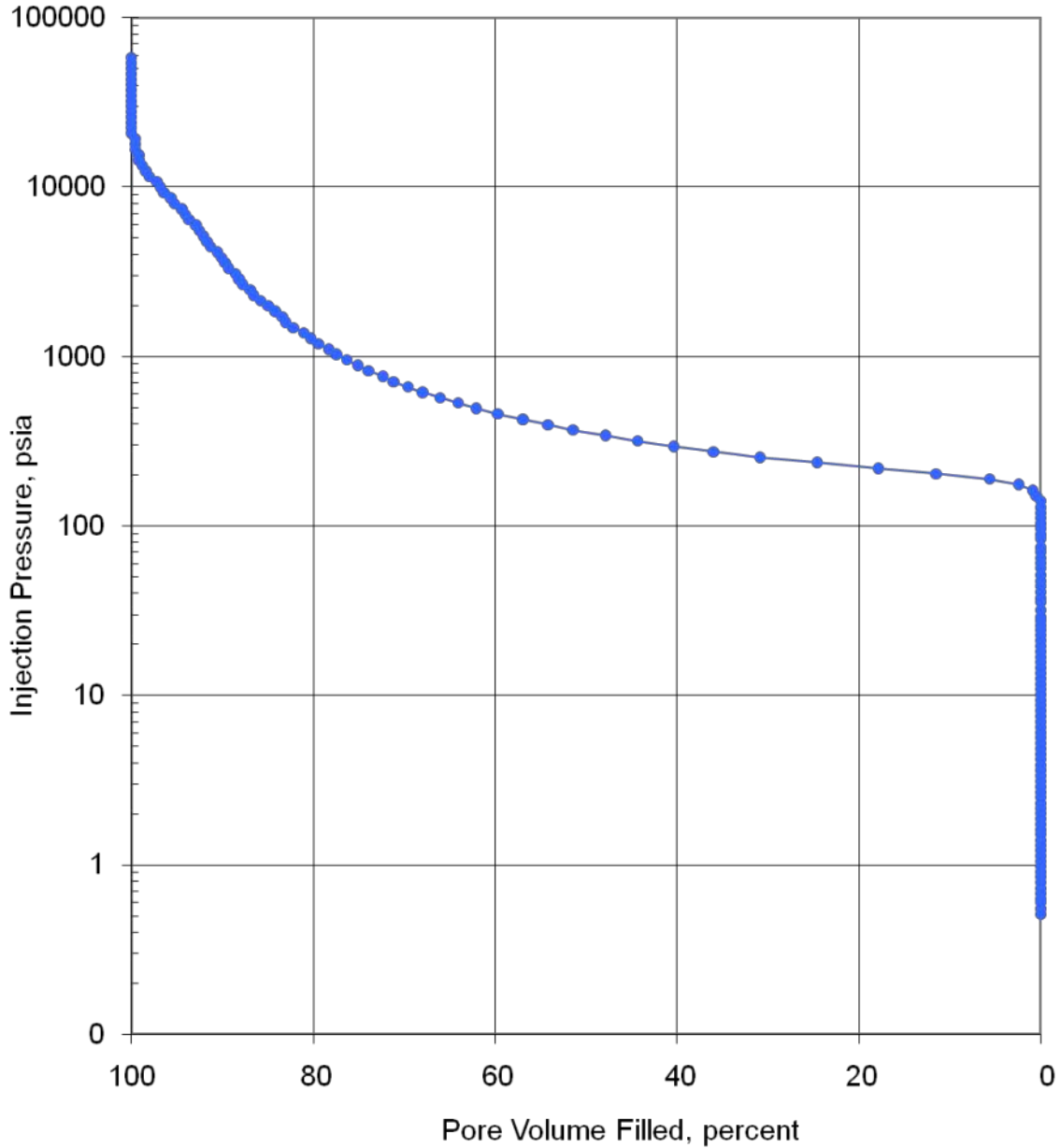


**Figure 58 – Results of the mercury porosimetry analysis on the duplicate dolostone rock sample as pore volume filled per pressure unit.**



### CAPILLARY PRESSURE vs. WETTING PHASE SATURATION

Mercury Pressure: 0 - 60000  
(METHODOLOGY: ASTM D4404, API RP40)

Project Name: NAWC  
Project No.: ER-0715

Sample ID: Dolostone 2  
Depth, ft.: 45  
Porosity, %Vp: 6.3

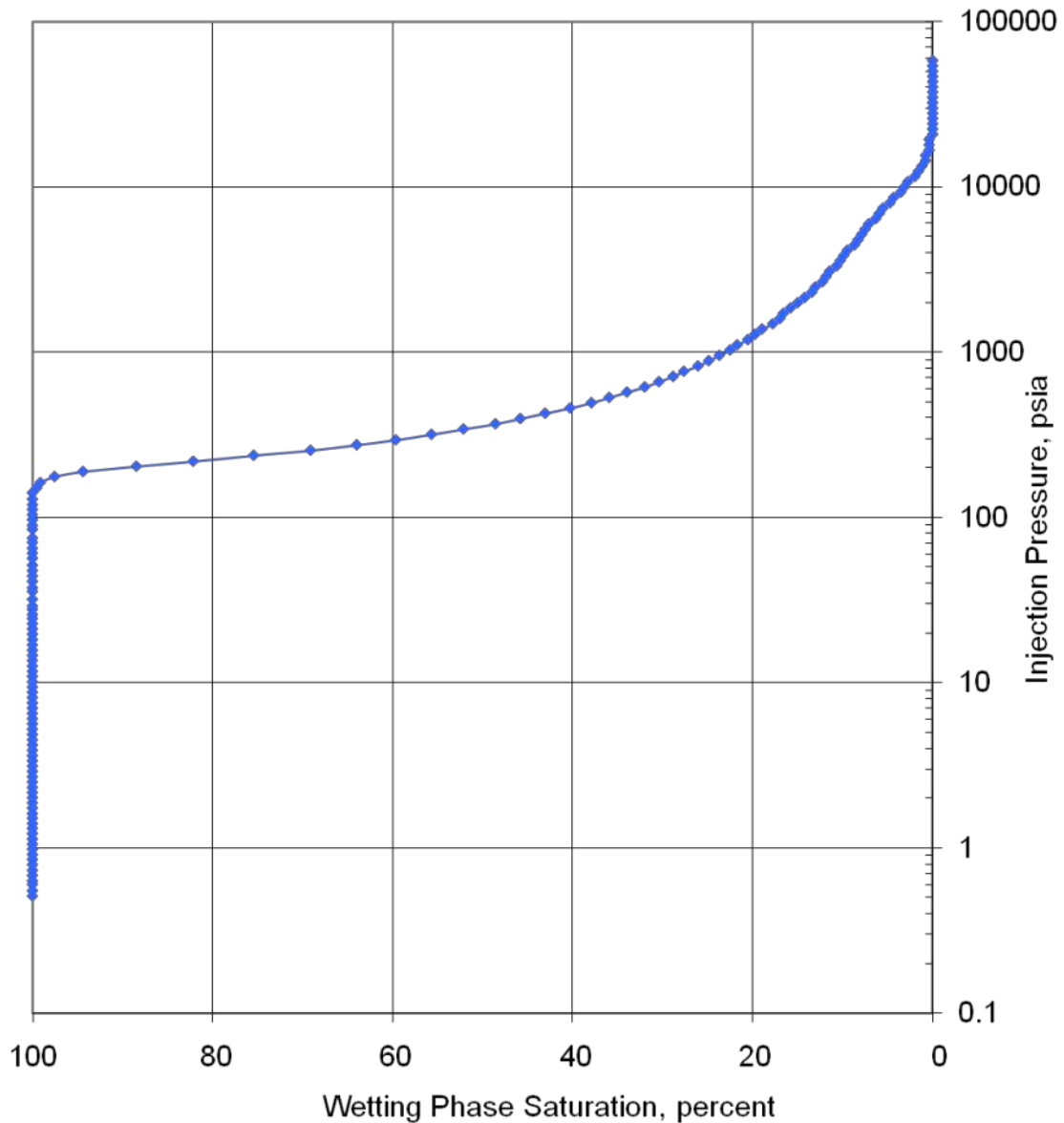


**Figure 59 – Results of the mercury porosimetry analysis on the duplicate dolostone rock sample as wetting phase saturation per capillary pressure.**



**PORE THROAT RADIUS DISTRIBUTION**  
Mercury Pressure: 0 - 60000  
(METHODOLOGY: ASTM D4404, API RP40)

Project Name: NAWC  
Project No.: ER-0715

Sample ID: Dolostone 2  
Depth, ft.: 45  
Porosity, %Vp: 6.3

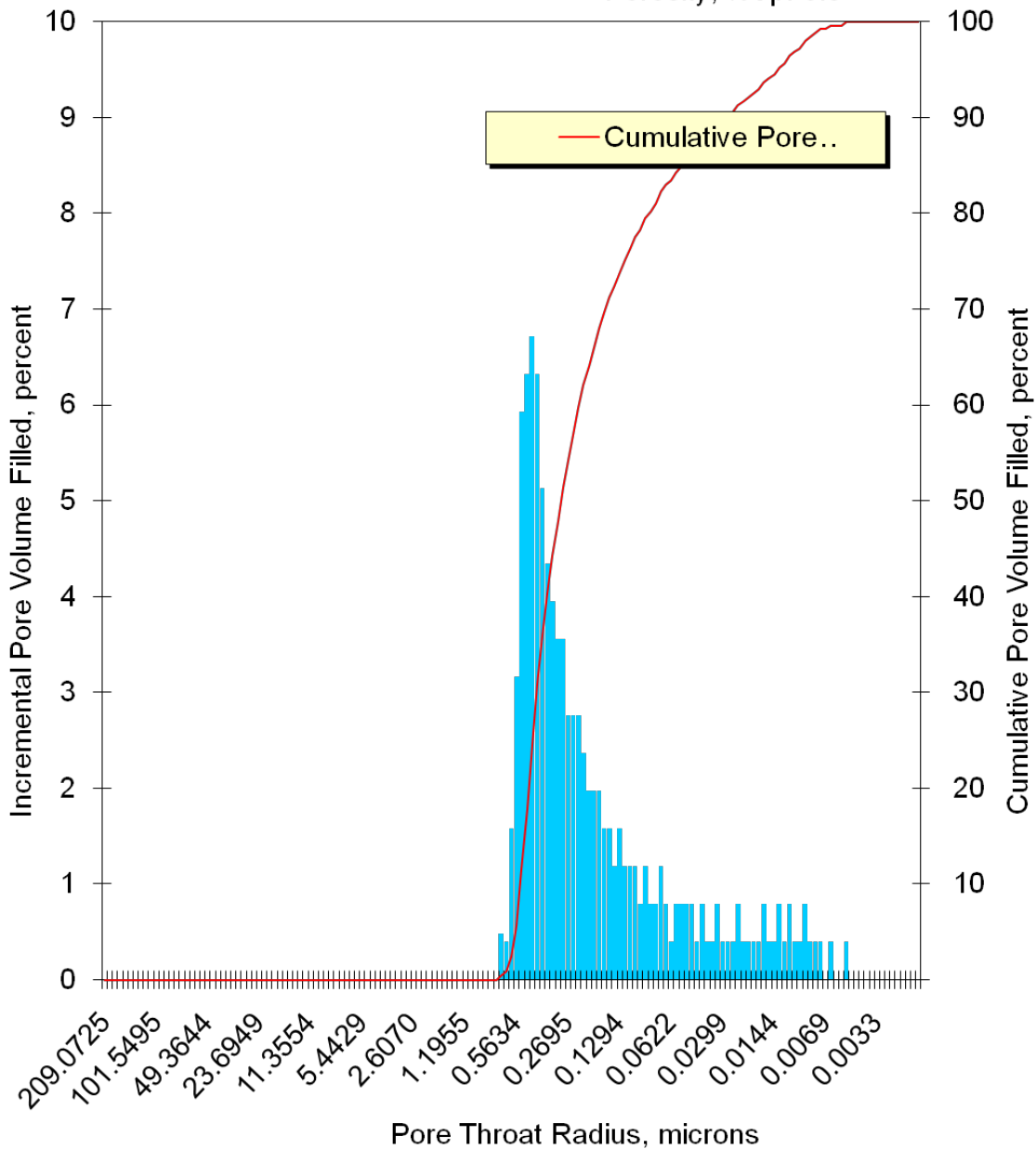


**Figure 60 – Pore throat radius distribution of the duplicate dolostone sample during the mercury porosimetry analysis.**

**Table 21 – Results of the mercury porosimetry analysis on the triplicate dolostone rock sample.**

PTS File No:	39609			<b>PTS Laboratories</b>
Client:	Queen's University			
<b>MERCURY INJECTION SUMMARY</b>				
PROJECT NAME:	NAWC		Sample ID:	Dolostone 3
PROJECT NO:	ER-0715		Depth, ft.:	45
			Porosity, %Vp:	4.4
*INJECTION PRESSURE, psia	PORE THROAT Radius, microns	NON-WETTING PHASE SATURATION		WETTING PHASE SATURATION, percent
		INCREMENTAL, percent	CUMULATIVE, percent	
0.510	209	0.000	0.000	100.0
0.550	194	0.000	0.000	100.0
0.600	178	0.000	0.000	100.0
0.630	169	0.000	0.000	100.0
0.680	157	0.000	0.000	100.0
0.730	146	0.000	0.000	100.0
0.790	135	0.000	0.000	100.0
0.850	125	0.000	0.000	100.0
0.920	116	0.000	0.000	100.0
0.990	108	0.000	0.000	100.0
1.05	102	0.000	0.000	100.0
1.12	95.2	0.000	0.000	100.0
1.22	87.4	0.000	0.000	100.0
1.31	81.4	0.000	0.000	100.0
1.41	75.6	0.000	0.000	100.0
1.51	70.6	0.000	0.000	100.0
1.62	65.8	0.000	0.000	100.0
1.73	61.6	0.000	0.000	100.0
1.87	57.0	0.000	0.000	100.0
2.01	53.0	0.000	0.000	100.0
2.16	49.4	0.000	0.000	100.0
2.32	46.0	0.000	0.000	100.0
2.50	42.7	0.000	0.000	100.0
2.69	39.6	0.000	0.000	100.0
2.90	36.8	0.000	0.000	100.0
3.12	34.2	0.000	0.000	100.0
3.36	31.7	0.000	0.000	100.0
3.61	29.5	0.000	0.000	100.0
3.89	27.4	0.000	0.000	100.0
4.19	25.4	0.000	0.000	100.0

4.50	23.7	0.000	0.000	100.0
4.85	22.0	0.000	0.000	100.0
5.23	20.4	0.000	0.000	100.0
5.63	18.9	0.000	0.000	100.0
6.04	17.7	0.000	0.000	100.0
6.50	16.4	0.000	0.000	100.0
7.00	15.2	0.000	0.000	100.0
7.53	14.2	0.000	0.000	100.0
8.11	13.1	0.000	0.000	100.0
8.73	12.2	0.000	0.000	100.0
9.39	11.4	0.000	0.000	100.0
10.1	10.6	0.000	0.000	100.0
10.9	9.79	0.000	0.000	100.0
11.7	9.12	0.000	0.000	100.0
12.6	8.47	0.000	0.000	100.0
13.6	7.85	0.000	0.000	100.0
14.6	7.31	0.000	0.000	100.0
15.7	6.80	0.000	0.000	100.0
16.9	6.31	0.000	0.000	100.0
18.2	5.86	0.000	0.000	100.0
19.6	5.44	0.000	0.000	100.0
21.1	5.06	0.000	0.000	100.0
22.7	4.70	0.000	0.000	100.0
24.4	4.37	0.000	0.000	100.0
24.5	4.35	0.000	0.000	100.0
28.9	3.69	0.000	0.000	100.0
29.3	3.64	0.000	0.000	100.0
35.2	3.03	0.000	0.000	100.0
37.7	2.83	0.000	0.000	100.0
37.8	2.82	0.000	0.000	100.0
42.6	2.50	2.43	2.43	97.6
45.5	2.34	0.577	3.01	97.0
49.3	2.17	2.31	5.32	94.7
52.6	2.03	1.73	7.05	92.9
56.7	1.88	0.577	7.63	92.4
61.6	1.73	2.31	9.94	90.1
67.7	1.58	1.73	11.7	88.3
70.1	1.52	2.89	14.6	85.4
77.6	1.37	4.04	18.6	81.4
83.0	1.29	1.73	20.3	79.7
90.2	1.18	1.73	22.1	77.9
96.9	1.10	2.31	24.4	75.6
104	1.03	1.15	25.5	74.5
111	0.958	1.15	26.7	73.3
119	0.897	0.577	27.3	72.7
129	0.827	1.73	29.0	71.0
141	0.754	2.31	31.3	68.7
152	0.702	1.15	32.5	67.5

162	0.656	1.73	34.2	65.8
176	0.605	1.73	35.9	64.1
187	0.569	1.15	37.1	62.9
204	0.522	1.73	38.8	61.2
218	0.489	1.73	40.5	59.5
236	0.451	1.15	41.7	58.3
253	0.421	1.73	43.4	56.6
272	0.392	1.15	44.6	55.4
292	0.365	1.15	45.7	54.3
317	0.336	1.15	46.9	53.1
339	0.314	1.15	48.0	52.0
367	0.291	1.15	49.2	50.8
396	0.270	1.15	50.4	49.6
424	0.251	1.73	52.1	47.9
457	0.233	1.15	53.2	46.8
493	0.216	1.15	54.4	45.6
529	0.201	1.15	55.5	44.5
572	0.186	1.73	57.3	42.7
614	0.174	1.73	59.0	41.0
660	0.161	1.73	60.7	39.3
710	0.150	1.73	62.5	37.5
765	0.139	2.31	64.8	35.2
823	0.129	1.73	66.5	33.5
884	0.121	2.31	68.8	31.2
954	0.112	1.73	70.6	29.4
1026	0.104	2.31	72.9	27.1
1104	0.097	2.31	75.2	24.8
1189	0.090	1.73	76.9	23.1
1280	0.083	1.73	78.6	21.4
1376	0.077	1.73	80.4	19.6
1482	0.072	1.73	82.1	17.9
1594	0.067	1.73	83.8	16.2
1716	0.062	1.73	85.6	14.4
1845	0.058	1.73	87.3	12.7
1987	0.054	1.73	89.0	11.0
2140	0.050	1.15	90.2	9.81
2301	0.046	1.15	91.3	8.66
2474	0.043	1.15	92.5	7.51
2663	0.040	1.15	93.6	6.35
2865	0.037	0.577	94.2	5.77
3083	0.035	1.15	95.4	4.62
3317	0.032	0.577	96.0	4.04
3568	0.030	0.577	96.5	3.46
3837	0.028	0.000	96.5	3.46
4129	0.026	0.577	97.1	2.89
4443	0.024	0.577	97.7	2.31
4775	0.022	0.000	97.7	2.31
5138	0.021	0.577	98.3	1.73

5534	0.019	0.000	98.3	1.73
5956	0.018	0.577	98.8	1.15
6411	0.017	0.000	98.8	1.15
6899	0.015	0.577	99.4	0.577
7426	0.014	0.000	99.4	0.577
7992	0.013	0.000	99.4	0.577
8603	0.012	0.000	99.4	0.577
9261	0.012	0.577	100.0	0.000
9965	0.011	0.000	100.0	0.000
10725	0.010	0.000	100.0	0.000
11543	0.009	0.000	100.0	0.000
12420	0.009	0.000	100.0	0.000
13366	0.008	0.000	100.0	0.000
14381	0.007	0.000	100.0	0.000
15481	0.007	0.000	100.0	0.000
16658	0.006	0.000	100.0	0.000
17927	0.006	0.000	100.0	0.000
19293	0.006	0.000	100.0	0.000
20770	0.005	0.000	100.0	0.000
22360	0.005	0.000	100.0	0.000
24066	0.004	0.000	100.0	0.000
25901	0.004	0.000	100.0	0.000
27873	0.004	0.000	100.0	0.000
29996	0.004	0.000	100.0	0.000
32278	0.003	0.000	100.0	0.000
34735	0.003	0.000	100.0	0.000
37375	0.003	0.000	100.0	0.000
40215	0.003	0.000	100.0	0.000
43278	0.002	0.000	100.0	0.000
46564	0.002	0.000	100.0	0.000
50113	0.002	0.000	100.0	0.000
53919	0.002	0.000	100.0	0.000
58022	0.002	0.000	100.0	0.000



### PORE VOLUME FILLED vs PRESSURE

Mercury Pressure: 0 - 60000 psia

(METHODOLOGY: ASTM D4404, API RP40)

Project Name: NAWC  
Project No.: ER-0715

Sample ID: Dolostone 3  
Depth, ft.: 45  
Porosity, %Vp: 4.4

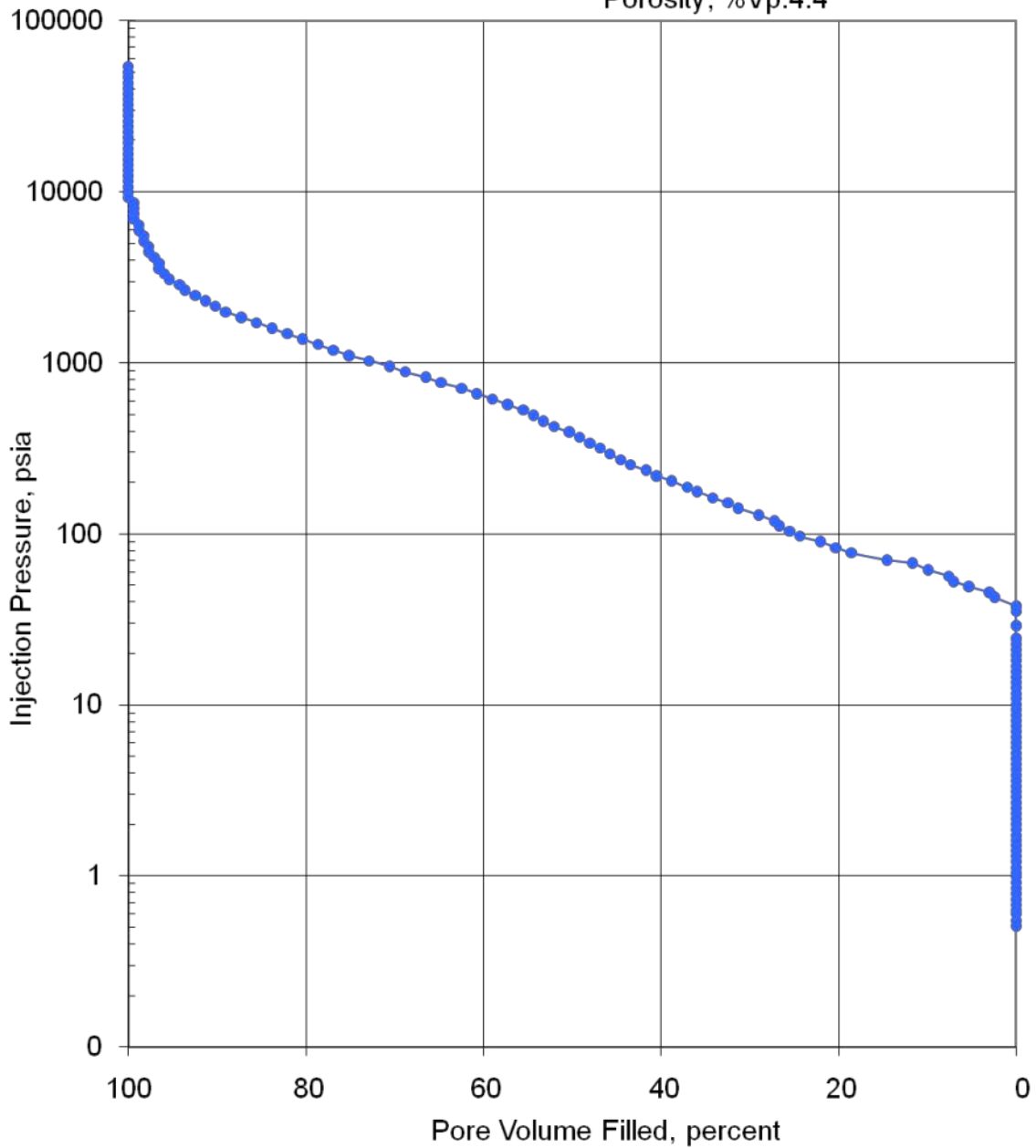


**Figure 61 – Results of the mercury porosimetry analysis on the triplicate dolostone rock sample as pore volume filled per pressure unit.**



### CAPILLARY PRESSURE vs. WETTING PHASE SATURATION

Mercury Pressure: 0 - 60000  
(METHODOLOGY: ASTM D4404, API RP40)

Project Name: NAWC  
Project No.: ER-075

Sample ID: Dolostone 3  
Depth, ft.: 45  
Porosity, %Vp: 4.4

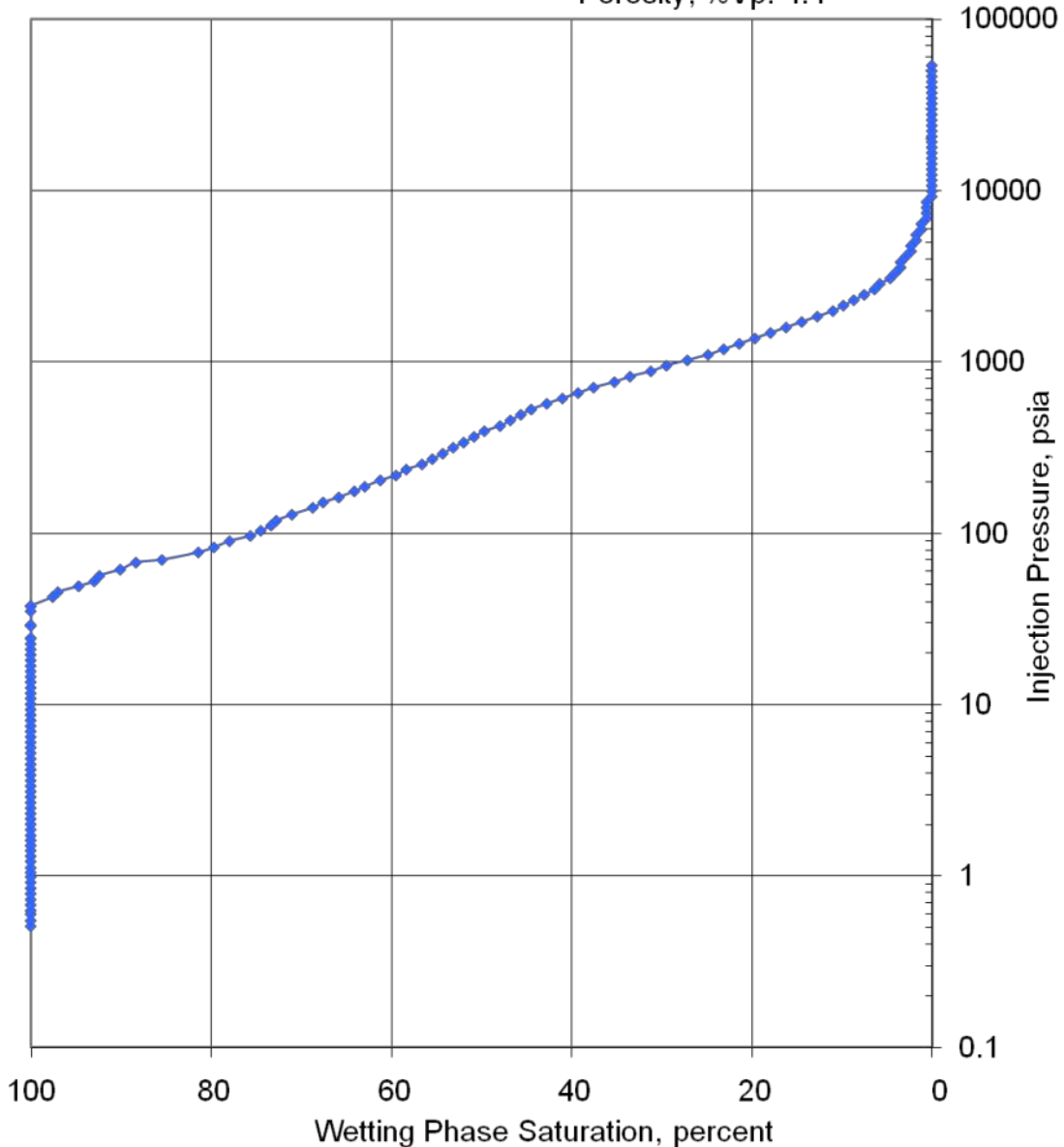


**Figure 62 – Results of the mercury porosimetry analysis on the triplicate dolostone rock sample as wetting phase saturation per capillary pressure.**



**PORE THROAT RADIUS DISTRIBUTION**  
Mercury Pressure: 0 - 60000  
(METHODOLOGY: ASTM D4404, API RP40)

Project Name: NAWC  
Project No. ER-0715:

Sample ID: Dolostone 3  
Depth, ft.: 45  
Porosity, %Vp: 4.4

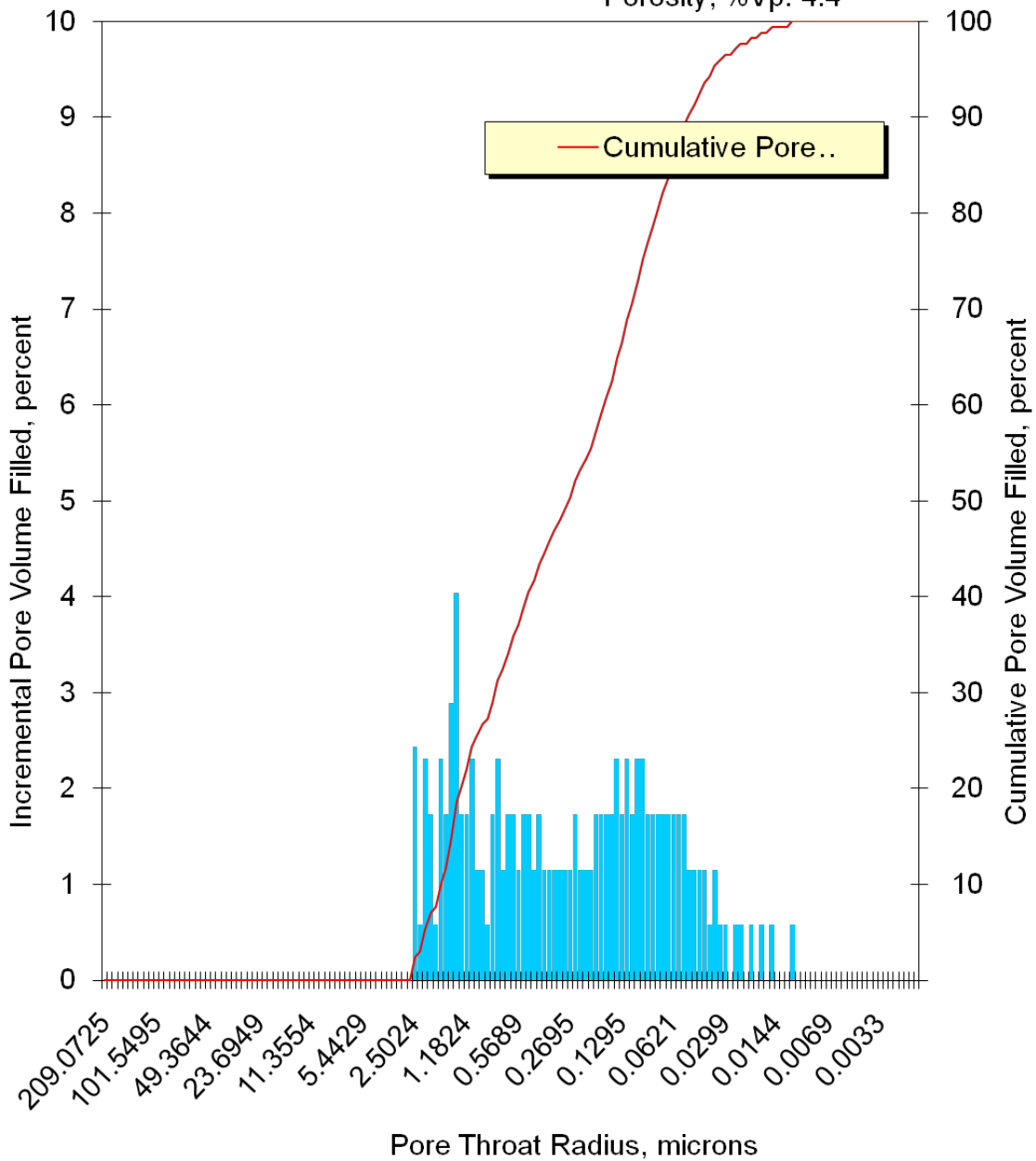


**Figure 63 – Pore throat radius distribution of the triplicate dolostone sample during the mercury porosimetry analysis.**

## Appendix D3 - Field VOC extraction methodology and related data from NAWC Site.

Rock cores were extracted from the NAWC site to assess the performance of TCH in removing TCE from fractured bedrock. The following is the methodology undertaken during the core recovery to determine the VOC concentration in the rock matrix before and after the application of the TCH pilot system (Figure 1). The VOC analysis had the objective of determining the degree of contaminant mass removal resulting from thermal treatment.



**Figure 1 – Photograph of the TCH pilot-system installed for the source zone remediation of TCE at the NAWC site, including a diagram indicating the location of the heating wells, temperature measurement points and bore holes for core sample collection.**

24. Immediately after drilling, the collected core sample from BR1 was characterized giving a brief description and report of its geological features and properties.
25. 1 cm thick discs were cut out of the rock core at 1 foot intervals using a diamond saw. Cutting the disc out of the core was performed immediately after collecting the core to avoid TCE losses by volatilization (Figure 2).



**Figure 2 – Photograph of the cutting of the 1 cm thick discs from the recollected rock core at the NAWC site.**

26. The disc was placed into the rock crusher adding 50 ml of methanol to cover the sample and avoid VOC losses.
27. The rock crusher was sealed and the plunger was punched with a hammer to crush the rock disc.
28. The disc particles with the methanol extract were recovered after crushing and poured into a 250 mL straight-sided glass jar with Teflon-lined cap (figure 3a).
29. The remaining particles of methanol inside the rock crusher were recovered by rinsing the bottom of the rock crusher with 100ml of methanol and adding the resulting extract into the 250 mL jar.
30. The jar was closed to avoid extract losses by evaporation and, placed on an orbital shaker for a period of 24 hours (Figure 3b).

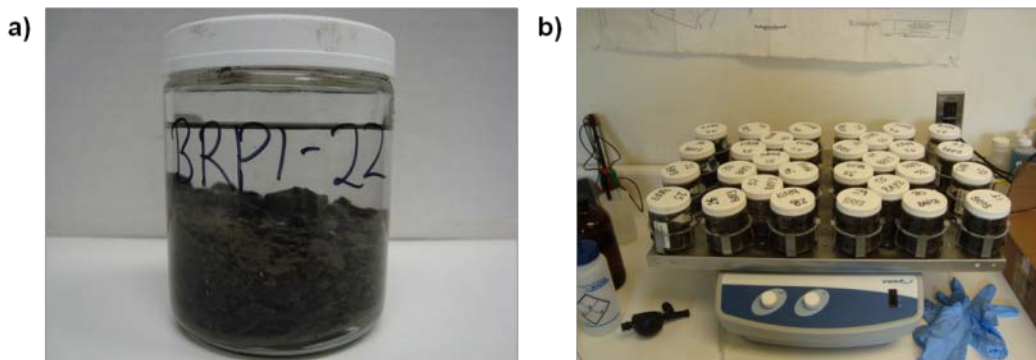


**Figure 3 – Photograph of the a) 250mL straight-sided glass jar with Teflon-lined cap containing the TCE extract and, b) the orbital shaker.**

31. The rock crusher was disassembled and the pieces were rinsed with distilled water and methanol to clean up any residual TCE or disc particles remaining in any of the rock crusher elements.
32. After the pieces dried out, the rock crusher was re-assembled for subsequent rock disc crushing.
33. Steps 3 to 9 were repeated for the consecutive rock discs, until the last disc, corresponding to 16.8 m [55 ft] deep, was crushed.
34. After 24 hours of shaking 20 mL of the extract were collected from each of the 50 jars and placed into 20 ml vials that were sent to Test America Laboratories for Volatile Organics in soil and waste samples and Volatile Organic Compounds by Gas Chromatography/Mass Spectrometry (GC/MS).
35. Steps 1 to 11 were repeated for rock core samples from boreholes BR2 and BR3.
36. Steps 1 to 12 were repeated for post remedy core samples from boreholes BRP-1, BRP-2 and BRP-3.

### Rock analysis results

Eight 3.81 cm [1.5 inch] thick discs, of core samples collected in the treatment zone at the Naval Air Warfare Center were sent for rock property analyses at PTS Laboratories in Santa Fe Springs, CA. These tests were conducted in duplicate and included measurements of dry bulk density using gravimetric method ASTM D2937-04 (ASTM, 2004a), fraction organic carbon using the Walkley-Black method EPA 9060 (USEPA, 1999), matrix porosity using mercury porosimetry method ASTM D4404-84 (ASTM, 2004b), and intrinsic permeability using method EPA 9100 (USEPA, 1986). The results of the analyses in triplicate for dry bulk density, fraction organic carbon, mercury porosimetry and intrinsic permeability are presented in Tables 1, 2, 3 and 4, respectively.

**Table 1 – Results of dry bulk density**

PTS File No:	38225, 38521, 39380, 39609		<b>PTS</b> Laboratories
Client:	Queens University		
<b>PHYSICAL PROPERTIES DATA - DRY BULK DENSITY</b>			
PROJECT NAME:	DNAPL Removal		
PROJECT NO:	ER-0715		
		<b>METHODS:</b>	<b>API RP 40</b>
SAMPLE ID.	DEPTH, ft.	SAMPLE ORIENTATION (1)	DRY BULK DENSITY g/cm <sup>3</sup>
NAWC mudstone 1	30	V	2.52
NAWC mudstone 2	30	V	2.51
(1) Sample Orientation: H = horizontal; V = vertical (2) Effective or Native = With as-received pore fluids in place			

**Table 2 – Results of total organic carbon analysis**

PTS File No:	38225, 38521, 39380, 39609			PTS Laboratories
Client:	Queen's University			
<b>ORGANIC CARBON DATA - TOC (foc)</b>				
PROJECT NAME:	NAWC			
PROJECT NO:	ER-0715			
		<b>METHOD:</b>	<b>WALKLEY-BLACK</b>	<b>WALKLEY-BLACK</b>
<b>SAMPLE ID.</b>	<b>DEPTH, ft.</b>	<b>SAMPLE MATRIX</b>	<b>FRACTION ORGANIC CARBON, g/g</b>	<b>TOTAL ORGANIC CARBON, mg/kg</b>
NAWC mudstone 1	30	SOIL	3.60E-03	3600
NAWC mudstone 2	30	SOIL	1.21E-02	12100

**Table 3 – Results of mercury porosimetry**

PTS File No:	38225, 38521, 39380, 39609			PTS Laboratories
Client:	Queen's University			
<b>MERCURY INJECTION DATA SUMMARY</b>				
PROJECT NAME:	DNAPL Removal			
PROJECT NO:	ER-0715			
<b>SAMPLE ID</b>	<b>DEPTH, feet</b> feet	<b>PERMEABILITY TO AIR,*</b> md	<b>MERCURY POROSITY,</b> percent	
NAWC mudstone 1	30	N/A	3.5	
NAWC mudstone 2	30	N/A	3.1	
* After Swanson B.F., Journal of Petroleum Technology, December 1981				

**Table 4 – Results of intrinsic permeability**

PTS File No:	38225, 38521, 39380, 39609			PTS Laboratories
Client:	Queen's University			
<b>PHYSICAL PROPERTIES DATA - PERMEABILITY</b>				
PROJECT NAME:	NAWC			
PROJECT NO:	ER-0715			

SAMPLE ID.	DEPTH, ft.	SAMPLE ORIENTATION (1)	500 PSI CONFINING STRESS INTRINSIC PERMEABILITY cm <sup>2</sup>
NAWC mudstone 1	30	V	2.47E-14
NAWC mudstone 2	30	V	1.71E-13
(1) Sample Orientation: H = horizontal; V = vertical (2) Effective or Native = With as-received pore fluids in place			

**Table 5 – Results of the mercury porosimetry analysis on a rock sample from the treatment zone at the NAWC site.**

PTS File No:	39609			PTS Laboratories
Client:	Queen's University			
MERCURY INJECTION SUMMARY				
PROJECT NAME:	NAWC		Sample ID:	Mudstone 1
PROJECT NO:	ER-0715		Depth, ft.:	30
			Porosity, %Vp:	3.5
*INJECTION PRESSURE, psia	PORE THROAT Radius, microns	NON-WETTING PHASE SATURATION		WETTING PHASE SATURATION, percent
		INCREMENTAL, percent	CUMULATIVE, percent	
0.510	209	0.000	0.000	100.0
0.550	194	0.000	0.000	100.0
0.600	178	0.000	0.000	100.0
0.630	169	0.000	0.000	100.0
0.680	157	0.000	0.000	100.0
0.730	146	0.000	0.000	100.0
0.790	135	0.000	0.000	100.0
0.850	125	0.000	0.000	100.0
0.910	117	0.000	0.000	100.0
0.980	109	0.000	0.000	100.0
1.05	102	0.000	0.000	100.0
1.13	94.4	0.000	0.000	100.0
1.22	87.4	0.000	0.000	100.0
1.31	81.4	0.000	0.000	100.0
1.40	76.2	0.000	0.000	100.0
1.51	70.6	0.000	0.000	100.0
1.61	66.2	0.000	0.000	100.0
1.74	61.3	0.000	0.000	100.0
1.87	57.0	0.000	0.000	100.0
2.01	53.0	0.000	0.000	100.0
2.16	49.4	0.000	0.000	100.0
2.32	46.0	0.000	0.000	100.0
2.50	42.7	0.000	0.000	100.0
2.69	39.6	0.000	0.000	100.0

2.90	36.8	0.000	0.000	100.0
3.12	34.2	0.000	0.000	100.0
3.36	31.7	0.000	0.000	100.0
3.61	29.5	0.000	0.000	100.0
3.89	27.4	0.000	0.000	100.0
4.19	25.4	0.000	0.000	100.0
4.50	23.7	0.000	0.000	100.0
4.85	22.0	0.000	0.000	100.0
5.22	20.4	0.000	0.000	100.0
5.62	19.0	0.000	0.000	100.0
6.04	17.7	0.000	0.000	100.0
6.50	16.4	0.000	0.000	100.0
7.00	15.2	0.000	0.000	100.0
7.53	14.2	0.000	0.000	100.0
8.11	13.1	0.000	0.000	100.0
8.73	12.2	0.000	0.000	100.0
9.39	11.4	0.000	0.000	100.0
10.1	10.6	0.000	0.000	100.0
10.9	9.79	0.000	0.000	100.0
11.7	9.12	0.000	0.000	100.0
12.6	8.47	0.000	0.000	100.0
13.6	7.85	0.000	0.000	100.0
14.6	7.31	0.000	0.000	100.0
15.7	6.80	0.000	0.000	100.0
16.9	6.31	0.000	0.000	100.0
18.2	5.86	0.000	0.000	100.0
19.6	5.44	0.000	0.000	100.0
21.1	5.06	0.000	0.000	100.0
22.7	4.70	0.000	0.000	100.0
24.4	4.37	0.000	0.000	100.0
25.6	4.17	0.000	0.000	100.0
28.2	3.78	0.000	0.000	100.0
29.7	3.59	0.000	0.000	100.0
32.9	3.24	0.000	0.000	100.0
36.4	2.93	0.000	0.000	100.0
38.7	2.76	0.000	0.000	100.0
41.3	2.58	0.000	0.000	100.0
44.4	2.40	0.000	0.000	100.0
48.3	2.21	0.000	0.000	100.0
52.4	2.04	0.000	0.000	100.0
56.0	1.91	0.000	0.000	100.0
61.4	1.74	0.000	0.000	100.0
64.9	1.64	0.000	0.000	100.0
71.3	1.50	0.000	0.000	100.0
76.4	1.40	0.000	0.000	100.0
82.5	1.29	0.000	0.000	100.0
89.2	1.20	0.000	0.000	100.0
98.2	1.09	0.000	0.000	100.0

103	1.04	0.000	0.000	100.0
111	0.957	0.000	0.000	100.0
120	0.889	0.000	0.000	100.0
130	0.819	0.000	0.000	100.0
140	0.761	0.000	0.000	100.0
151	0.705	0.000	0.000	100.0
162	0.660	0.000	0.000	100.0
175	0.610	0.000	0.000	100.0
189	0.563	0.000	0.000	100.0
202	0.528	0.000	0.000	100.0
219	0.488	0.000	0.000	100.0
236	0.451	0.000	0.000	100.0
252	0.423	0.000	0.000	100.0
272	0.392	0.000	0.000	100.0
293	0.364	0.000	0.000	100.0
315	0.338	0.000	0.000	100.0
340	0.314	0.000	0.000	100.0
366	0.292	0.000	0.000	100.0
394	0.270	0.000	0.000	100.0
424	0.251	0.000	0.000	100.0
458	0.233	0.000	0.000	100.0
492	0.217	0.000	0.000	100.0
529	0.201	0.000	0.000	100.0
570	0.187	0.000	0.000	100.0
614	0.174	0.000	0.000	100.0
661	0.161	0.000	0.000	100.0
710	0.150	0.000	0.000	100.0
766	0.139	0.000	0.000	100.0
824	0.129	0.000	0.000	100.0
886	0.120	0.000	0.000	100.0
955	0.112	0.000	0.000	100.0
1027	0.104	0.000	0.000	100.0
1105	0.097	0.000	0.000	100.0
1189	0.090	0.000	0.000	100.0
1280	0.083	0.000	0.000	100.0
1375	0.078	0.000	0.000	100.0
1481	0.072	0.000	0.000	100.0
1595	0.067	0.000	0.000	100.0
1716	0.062	0.000	0.000	100.0
1845	0.058	0.000	0.000	100.0
1986	0.054	0.000	0.000	100.0
2137	0.050	0.000	0.000	100.0
2300	0.046	0.000	0.000	100.0
2476	0.043	0.000	0.000	100.0
2662	0.040	0.000	0.000	100.0
2865	0.037	0.000	0.000	100.0
3084	0.035	0.000	0.000	100.0
3317	0.032	0.000	0.000	100.0

3567	0.030	0.000	0.000	100.0
3840	0.028	0.000	0.000	100.0
4130	0.026	0.000	0.000	100.0
4441	0.024	0.000	0.000	100.0
4778	0.022	0.000	0.000	100.0
5144	0.021	0.000	0.000	100.0
5534	0.019	0.000	0.000	100.0
5962	0.018	0.000	0.000	100.0
6415	0.017	0.000	0.000	100.0
6901	0.015	0.000	0.000	100.0
7430	0.014	0.507	0.507	99.5
7991	0.013	0.737	1.24	98.8
8611	0.012	1.474	2.72	97.3
9269	0.012	1.474	4.19	95.8
9976	0.011	0.737	4.93	95.1
10736	0.010	1.474	6.40	93.6
11559	0.009	2.211	8.61	91.4
12439	0.009	3.685	12.3	87.7
13368	0.008	2.211	14.5	85.5
14405	0.007	2.211	16.7	83.3
15495	0.007	2.948	19.7	80.3
16681	0.006	5.159	24.8	75.2
17947	0.006	2.948	27.8	72.2
19312	0.006	3.685	31.5	68.5
20789	0.005	5.896	37.4	62.6
22362	0.005	6.633	44.0	56.0
24072	0.004	5.159	49.1	50.9
25902	0.004	4.422	53.6	46.4
27876	0.004	2.948	56.5	43.5
29998	0.004	5.896	62.4	37.6
32286	0.003	6.633	69.0	31.0
34736	0.003	5.896	74.9	25.1
37381	0.003	3.685	78.6	21.4
40226	0.003	5.159	83.8	16.2
43285	0.002	2.948	86.7	13.3
46574	0.002	2.211	88.9	11.1
50127	0.002	2.948	91.9	8.11
53919	0.002	4.422	96.3	3.68
58022	0.002	3.685	100.0	0.000



### PORE VOLUME FILLED vs PRESSURE

Mercury Pressure: 0 - 60000 psia

(METHODOLOGY: ASTM D4404, API RP40)

Project Name: NAWC  
Project No.: ER-0715

Sample ID: Mudstone 1  
Depth, ft.: 30  
Porosity, %Vp: 3.5

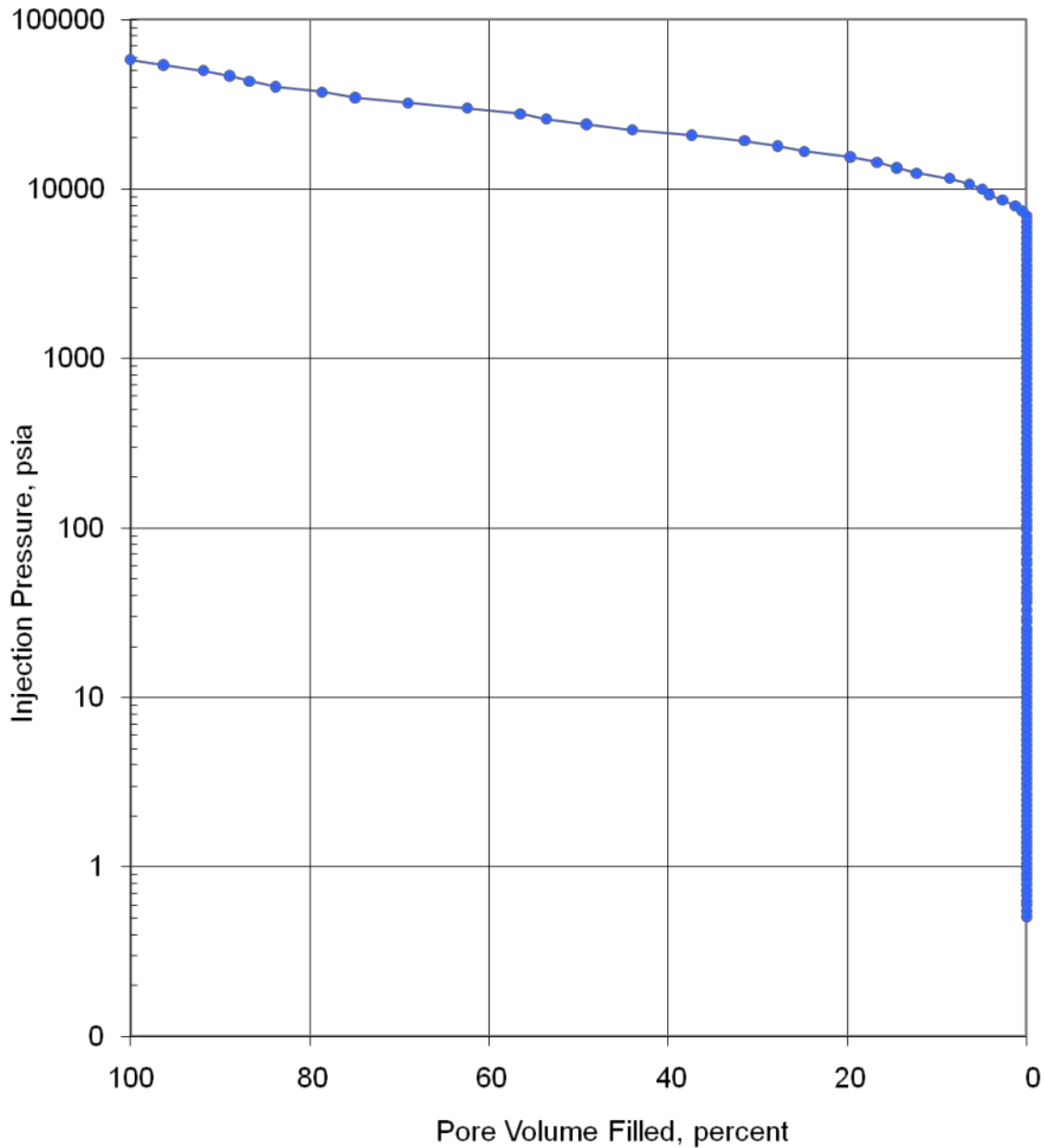


Figure 4 – Results of the mercury injection during the hg porosimetry analysis on the treatment zone rock sample from the NAWC site as pore volume filled per pressure unit.



### CAPILLARY PRESSURE vs. WETTING PHASE SATURATION

Mercury Pressure: 0 - 60000  
(METHODOLOGY: ASTM D4404, API RP40)

Project Name: NAWC  
Project No.: ER-0715

Sample ID: Mudstone 1  
Depth, ft.: 30  
Porosity, %Vp: 3.5

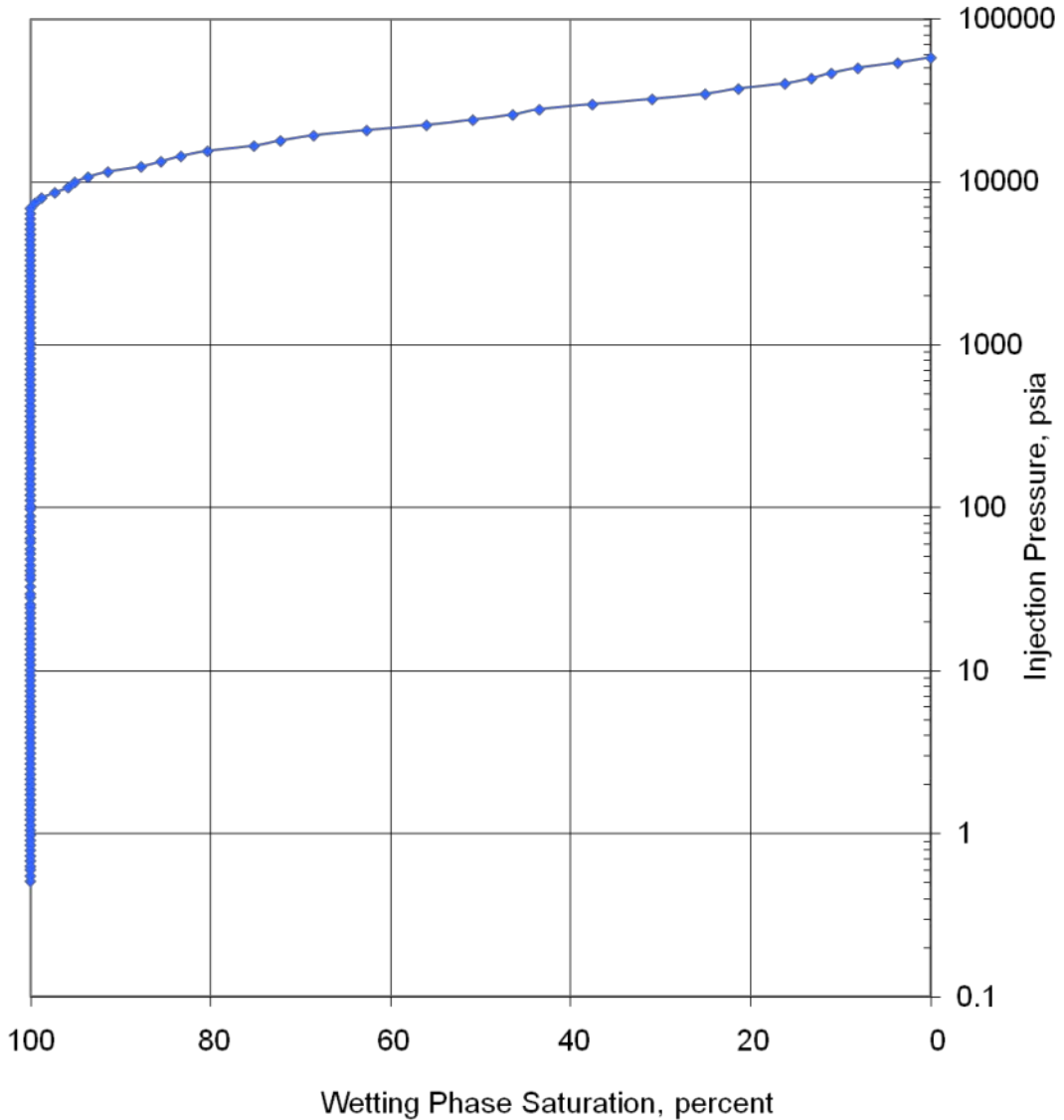


**Figure 5 – Results of the mercury injection during the hg porosimetry analysis on the treatment zone rock sample from the NAWC site as wetting phase saturation per capillary pressure.**



**PORE THROAT RADIUS DISTRIBUTION**  
Mercury Pressure: 0 - 60000  
(METHODOLOGY: ASTM D4404, API RP40)

Project Name: NAWC  
Project No.: ER-0715

Sample ID: Mudstone 1  
Depth, ft.: 30  
Porosity, %Vp: 3.5

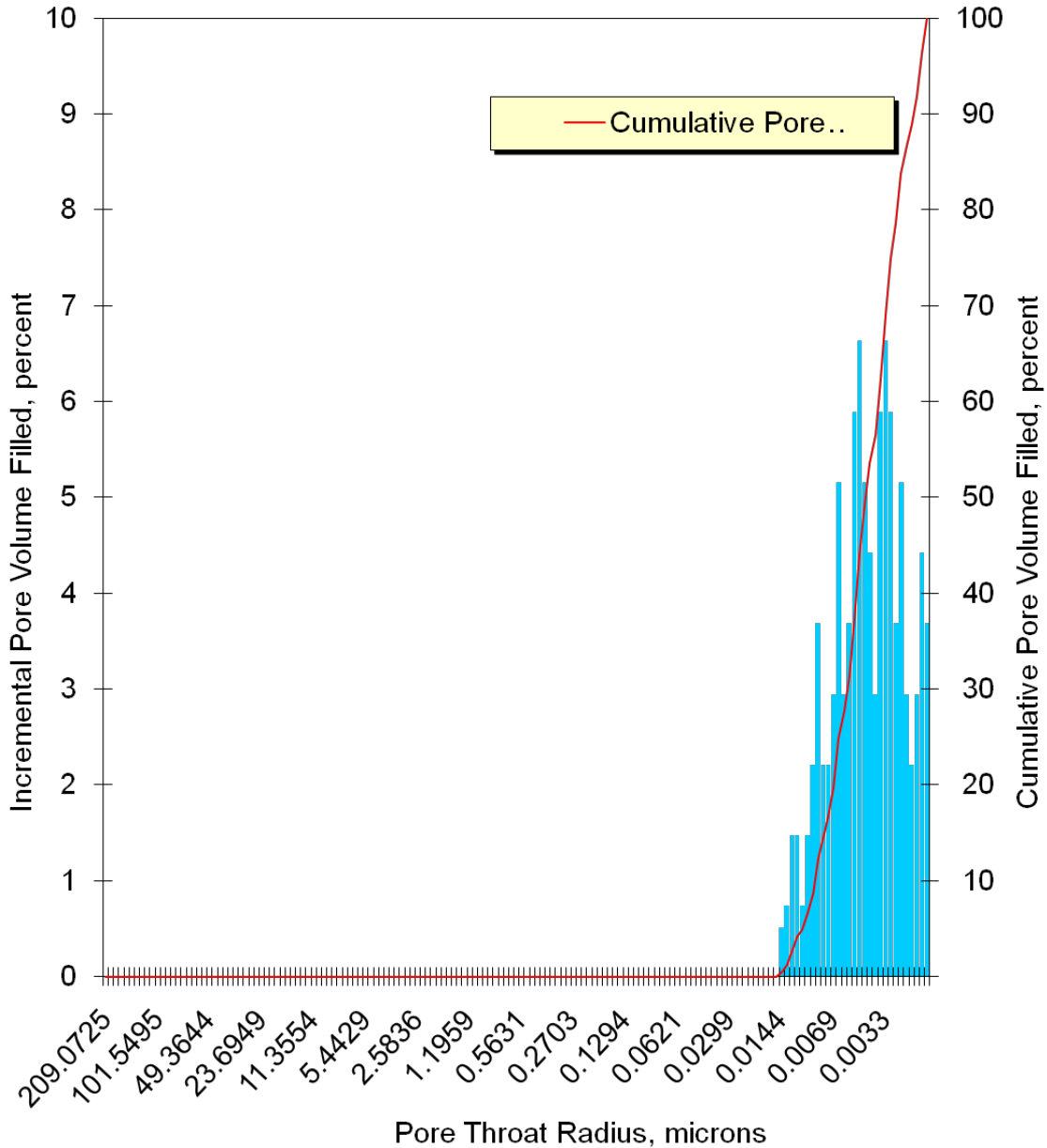


**Figure 6 – Pore throat radius distribution of the treatment zone rock sample from the NAWC site during the hg porosimetry analysis.**

**Table 6 – Results of the mercury porosimetry analysis on a duplicate rock sample from the treatment zone at the NAWC site.**

PTS File No:	39609			<b>PTS Laboratories</b>
Client:	Queen's University			
<b>MERCURY INJECTION SUMMARY</b>				
PROJECT NAME:	NAWC		Sample ID:	Mudstone 2
PROJECT NO:	ER-0715		Depth, ft.:	30
			Porosity, %Vp:	3.1
*INJECTION PRESSURE, psia	PORE THROAT Radius, microns	NON-WETTING PHASE SATURATION		WETTING PHASE SATURATION, percent
		INCREMENTAL, percent	CUMULATIVE, percent	
0.510	209	0.000	0.000	100.0
0.550	194	0.000	0.000	100.0
0.600	178	0.000	0.000	100.0
0.630	169	0.000	0.000	100.0
0.680	157	0.000	0.000	100.0
0.730	146	0.000	0.000	100.0
0.790	135	0.000	0.000	100.0
0.850	125	0.000	0.000	100.0
0.910	117	0.000	0.000	100.0
0.980	109	0.000	0.000	100.0
1.05	102	0.000	0.000	100.0
1.13	94.4	0.000	0.000	100.0
1.22	87.4	0.000	0.000	100.0
1.31	81.4	0.000	0.000	100.0
1.40	76.2	0.000	0.000	100.0
1.51	70.6	0.000	0.000	100.0
1.61	66.2	0.000	0.000	100.0
1.74	61.3	0.000	0.000	100.0
1.87	57.0	0.000	0.000	100.0
2.01	53.0	0.000	0.000	100.0
2.16	49.4	0.000	0.000	100.0
2.32	46.0	0.000	0.000	100.0
2.50	42.7	0.000	0.000	100.0
2.69	39.6	0.000	0.000	100.0
2.90	36.8	0.000	0.000	100.0
3.12	34.2	0.000	0.000	100.0
3.36	31.7	0.000	0.000	100.0
3.61	29.5	0.000	0.000	100.0
3.89	27.4	0.000	0.000	100.0
4.19	25.4	0.000	0.000	100.0
4.50	23.7	0.000	0.000	100.0
4.85	22.0	0.000	0.000	100.0
5.22	20.4	0.000	0.000	100.0
5.62	19.0	0.000	0.000	100.0

6.04	17.7	0.000	0.000	100.0
6.50	16.4	0.000	0.000	100.0
7.00	15.2	0.000	0.000	100.0
7.53	14.2	0.000	0.000	100.0
8.11	13.1	0.000	0.000	100.0
8.73	12.2	0.000	0.000	100.0
9.39	11.4	0.000	0.000	100.0
10.1	10.6	0.000	0.000	100.0
10.9	9.79	0.000	0.000	100.0
11.7	9.12	0.000	0.000	100.0
12.6	8.47	0.000	0.000	100.0
13.6	7.85	0.000	0.000	100.0
14.6	7.31	0.000	0.000	100.0
15.7	6.80	0.000	0.000	100.0
16.9	6.31	0.000	0.000	100.0
18.2	5.86	0.000	0.000	100.0
19.6	5.44	0.000	0.000	100.0
21.1	5.06	0.000	0.000	100.0
22.7	4.70	0.000	0.000	100.0
24.4	4.37	0.000	0.000	100.0
24.5	4.35	0.000	0.000	100.0
27.1	3.94	0.000	0.000	100.0
28.6	3.73	0.000	0.000	100.0
31.8	3.36	0.000	0.000	100.0
35.3	3.02	0.000	0.000	100.0
37.6	2.84	0.000	0.000	100.0
40.2	2.66	0.000	0.000	100.0
43.3	2.46	0.000	0.000	100.0
47.2	2.26	0.000	0.000	100.0
51.3	2.08	0.000	0.000	100.0
54.9	1.94	0.000	0.000	100.0
60.3	1.77	0.000	0.000	100.0
63.8	1.67	0.000	0.000	100.0
70.1	1.52	0.000	0.000	100.0
75.3	1.42	0.000	0.000	100.0
81.4	1.31	0.000	0.000	100.0
88.1	1.21	0.000	0.000	100.0
97.1	1.10	0.000	0.000	100.0
102	1.05	0.000	0.000	100.0
110	0.967	0.000	0.000	100.0
119	0.897	0.000	0.000	100.0
129	0.826	0.000	0.000	100.0
139	0.767	0.000	0.000	100.0
150	0.710	0.000	0.000	100.0
161	0.664	0.000	0.000	100.0
174	0.614	0.000	0.000	100.0
188	0.566	0.000	0.000	100.0
201	0.531	0.000	0.000	100.0

217	0.490	0.000	0.000	100.0
235	0.454	0.000	0.000	100.0
251	0.425	0.000	0.000	100.0
271	0.393	0.000	0.000	100.0
291	0.366	0.000	0.000	100.0
314	0.340	0.000	0.000	100.0
338	0.315	0.000	0.000	100.0
365	0.292	0.000	0.000	100.0
393	0.271	0.000	0.000	100.0
423	0.252	0.000	0.000	100.0
457	0.233	0.000	0.000	100.0
491	0.217	0.000	0.000	100.0
528	0.202	0.000	0.000	100.0
569	0.187	0.000	0.000	100.0
613	0.174	0.000	0.000	100.0
660	0.162	0.000	0.000	100.0
709	0.150	0.000	0.000	100.0
765	0.139	0.000	0.000	100.0
823	0.130	0.000	0.000	100.0
884	0.121	0.000	0.000	100.0
954	0.112	0.000	0.000	100.0
1026	0.104	0.000	0.000	100.0
1104	0.097	0.000	0.000	100.0
1188	0.090	0.000	0.000	100.0
1279	0.083	0.000	0.000	100.0
1374	0.078	0.000	0.000	100.0
1479	0.072	0.000	0.000	100.0
1594	0.067	0.000	0.000	100.0
1715	0.062	0.000	0.000	100.0
1844	0.058	0.000	0.000	100.0
1985	0.054	0.000	0.000	100.0
2136	0.050	0.000	0.000	100.0
2298	0.046	0.000	0.000	100.0
2474	0.043	0.000	0.000	100.0
2661	0.040	0.000	0.000	100.0
2864	0.037	0.000	0.000	100.0
3083	0.035	0.000	0.000	100.0
3316	0.032	0.000	0.000	100.0
3566	0.030	0.000	0.000	100.0
3839	0.028	0.000	0.000	100.0
4129	0.026	0.000	0.000	100.0
4440	0.024	0.000	0.000	100.0
4777	0.022	0.000	0.000	100.0
5143	0.021	0.000	0.000	100.0
5533	0.019	0.000	0.000	100.0
5961	0.018	0.000	0.000	100.0
6413	0.017	0.000	0.000	100.0
6899	0.015	0.000	0.000	100.0

7429	0.014	0.000	0.000	100.0
7990	0.013	0.000	0.000	100.0
8610	0.012	1.55	1.55	98.5
9268	0.012	0.827	2.38	97.6
9975	0.011	0.827	3.20	96.8
10735	0.010	1.65	4.86	95.1
11558	0.009	1.65	6.51	93.5
12438	0.009	1.65	8.17	91.8
13366	0.008	1.65	9.82	90.2
14404	0.007	3.31	13.1	86.9
15494	0.007	2.48	15.6	84.4
16680	0.006	4.14	19.7	80.3
17945	0.006	2.48	22.2	77.8
19311	0.006	3.31	25.5	74.5
20788	0.005	7.45	33.0	67.0
22360	0.005	4.14	37.1	62.9
24070	0.004	5.79	42.9	57.1
25901	0.004	4.14	47.1	52.9
27875	0.004	3.31	50.4	49.6
29996	0.004	4.96	55.3	44.7
32284	0.003	8.27	63.6	36.4
34734	0.003	6.62	70.2	29.8
37379	0.003	4.14	74.4	25.6
40224	0.003	6.62	81.0	19.0
43284	0.002	3.31	84.3	15.7
46572	0.002	2.48	86.8	13.2
50125	0.002	4.14	90.9	9.10
53917	0.002	5.79	96.7	3.31
58020	0.002	3.31	100.0	0.000



**PORE VOLUME FILLED vs PRESSURE**  
Mercury Pressure: 0 - 60000 psia  
(METHODOLOGY: ASTM D4404, API RP40)

Project Name: NAWC  
Project No.: ER-0715

Sample ID: Mudstone 2  
Depth, ft.: 30  
Porosity, %Vp: 3.1

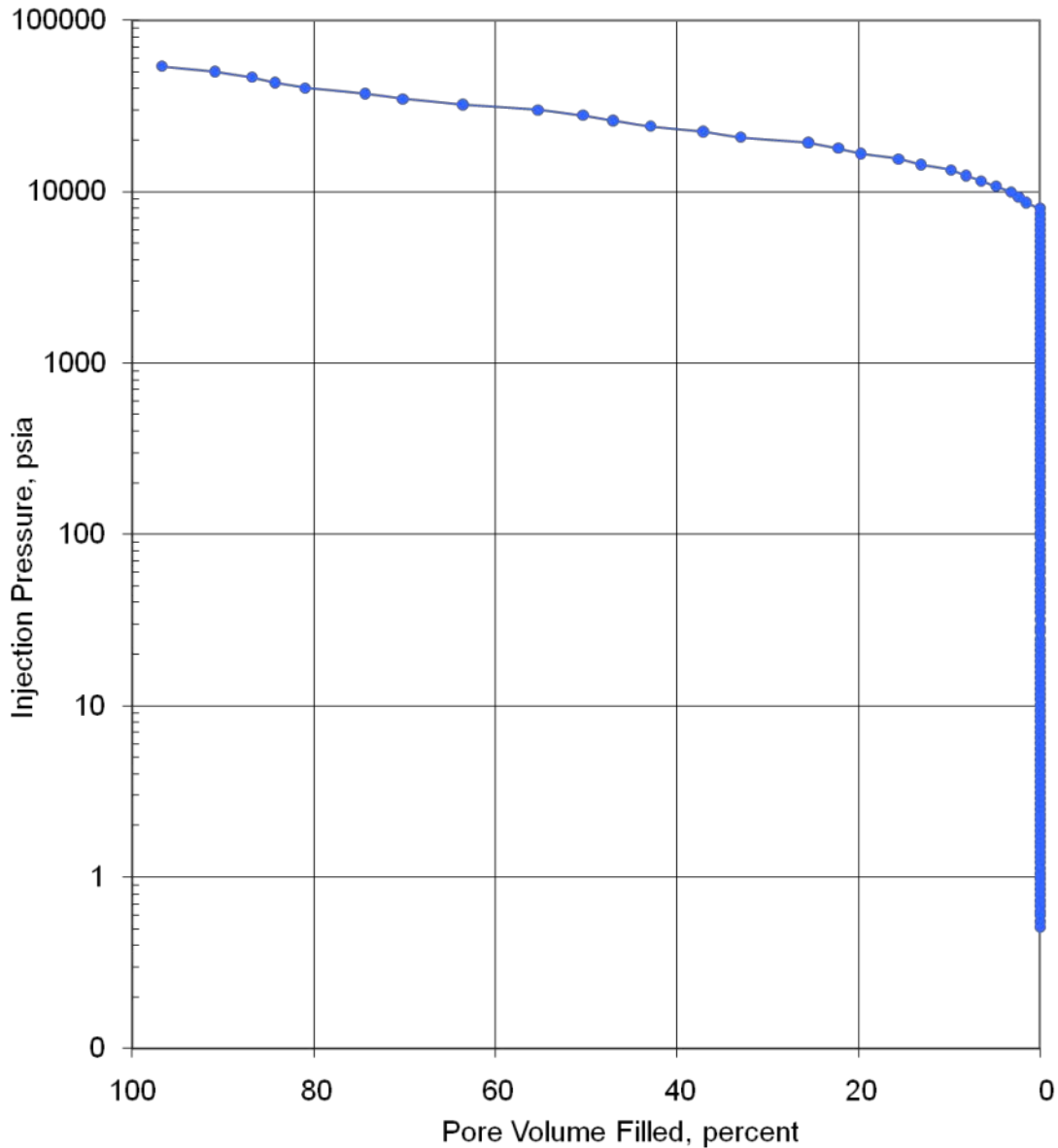


**Figure 7 – Results of the mercury injection during the hg porosimetry analysis on the duplicate treatment zone rock sample from the NAWC site as pore volume filled per pressure unit.**



### CAPILLARY PRESSURE vs. WETTING PHASE SATURATION

Mercury Pressure: 0 - 60000

(METHODOLOGY: ASTM D4404, API RP40)

Project Name: NAWC  
Project No.: ER-0715

Sample ID: Mudstone 2  
Depth, ft.: 30  
Porosity, %Vp: 3.1

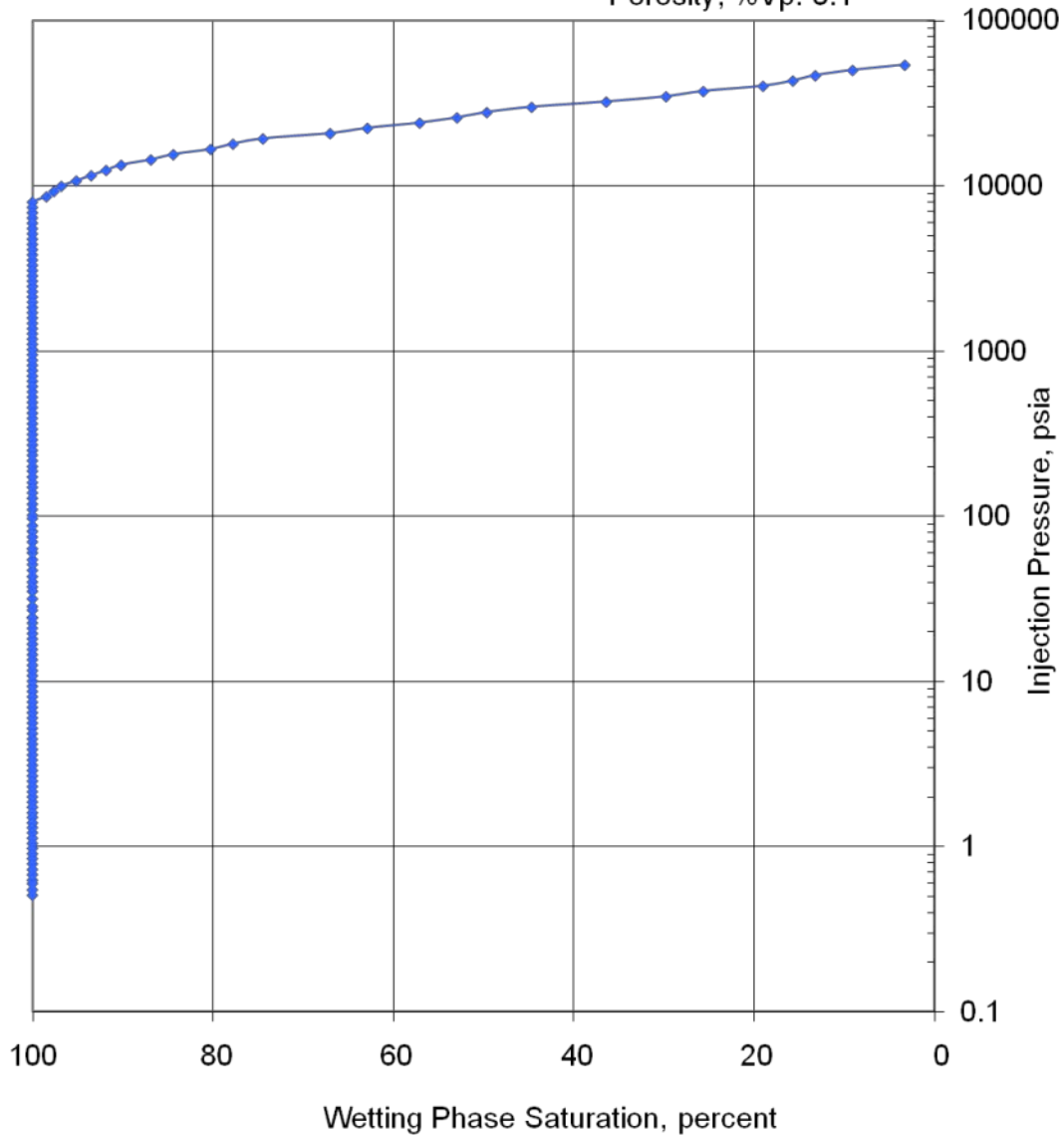


**Figure 8 – Results of the mercury injection during the mercury porosimetry analysis on the duplicate treatment zone rock sample from the NAWC site as wetting phase saturation per capillary pressure.**



**PORE THROAT RADIUS DISTRIBUTION**  
Mercury Pressure: 0 - 60000  
(METHODOLOGY: ASTM D4404, API RP40)

Project Name: NAWC  
Project No.: ER-0715

Sample ID: Mudstone 2  
Depth, ft.: 30  
Porosity, %Vp: 3.1

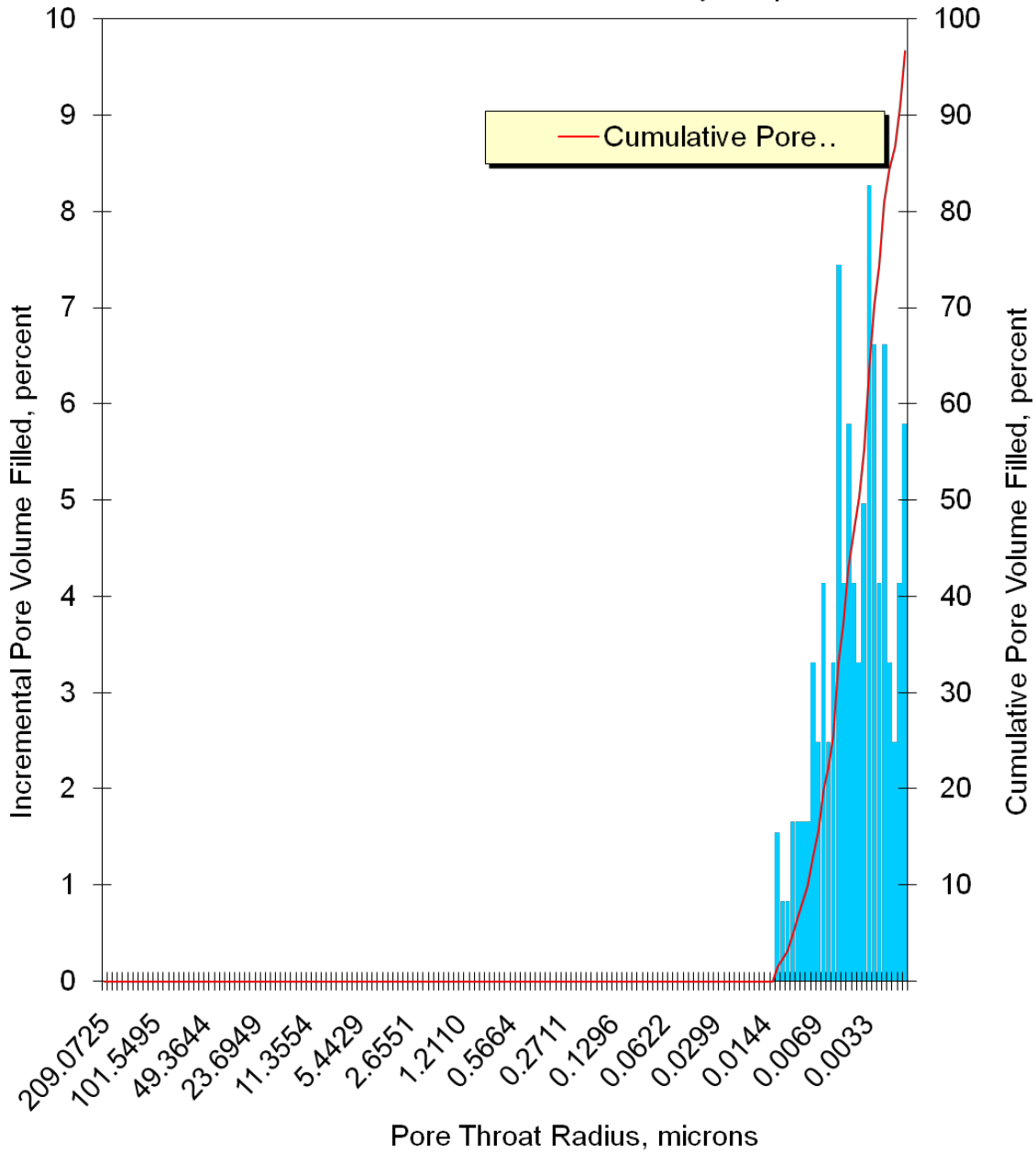


**Figure 9 – Pore throat radius distribution of the duplicate treatment zone rock sample from the NAWC site during the mercury porosimetry analysis.**

## References

- ASTM, 2004a. Standard Test Method for Density of Soil in Place by the Drive-Cylinder Method. ASTM D2937-04. American Society for Testing and Materials (ASTM) International, West Conshohocken, Penn.
- ASTM, 2004b. Standard Test Method for Determination of Pore Volume and Pore Volume Distribution of Soil and Rock by Mercury Intrusion Porosimetry. ASTM D4404-84. American Society for Testing and Materials (ASTM) International, West Conshohocken, Penn.
- USEPA, 1986. Method 9100: Saturated hydraulic conductivity, saturated leachate conductivity and intrinsic permeability. Test Methods for Evaluating Solid Waste, Physical/Chemical Methods. EPA/SW-846, Revision 0.
- USEPA, 1999. Method 9060: Total Organic Carbon (TOC) in soil. Test Methods for Evaluating Solid Waste, Physical/Chemical Methods. EPA/SW-846, Revision 1.

## Appendix E – Numerical Modeling of TCE Pilot Test

### Introduction

The remediation of dense, non-aqueous phase liquids (DNAPLs) such as creosote, coal tar and chlorinated solvents in bedrock is a challenging task given the discrete nature of flow through fractures and the potential for back diffusion of contaminants in many rock types. Technologies that rely upon fluid injection, such as steam injection, in-situ chemical oxidation, enhanced in-situ bioremediation, and co-solvent flushing are typically limited by sweep efficiency and a general inability to address contaminants sequestered in the low permeability porous rock matrix in a timely manner. Thermal conductive heating (TCH), which relies largely upon heat conduction rather than the delivery of injected fluids, has potential applicability in fractured rock because it can deliver heat to not only open fractures, but to the rock matrix as well. The general physical layout of a TCH application, including depiction of a power supply, produced fluids treatment components, temperature monitoring points, and pressure monitoring points is illustrated in Figure 1.

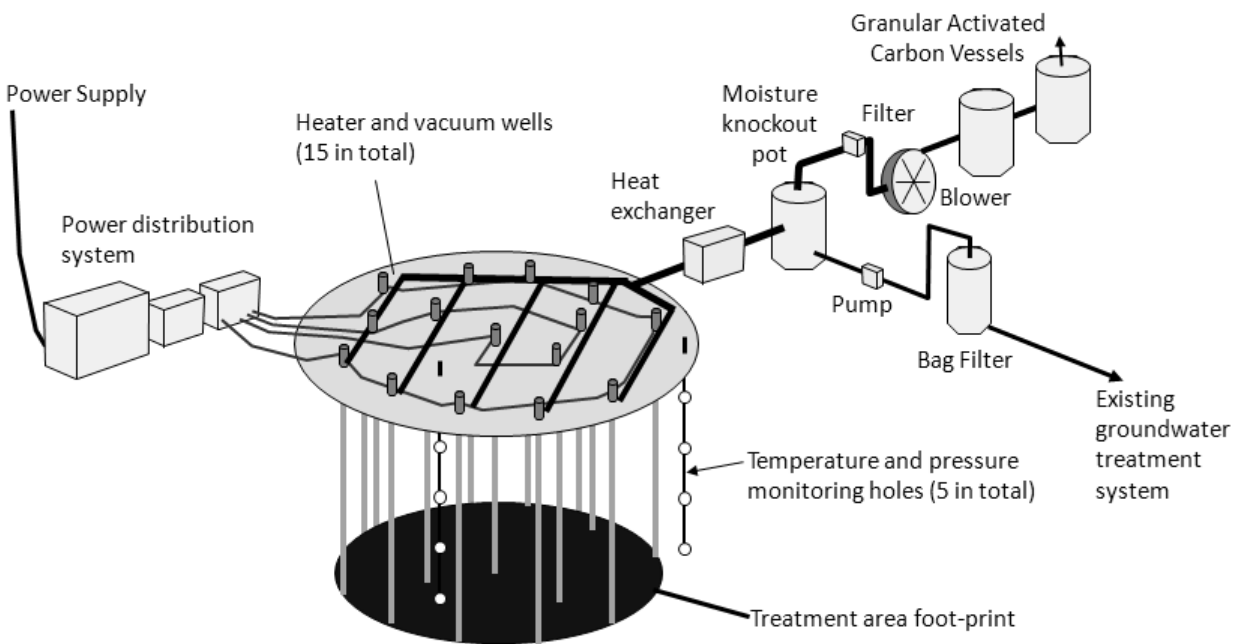


**Figure 1 – Typical configuration for thermal conductive heating (Johnson et al., 2009, Appendix A: Heron and Baker).**

Using data collected at the site during the pilot test and associated site characterization activities, a two-dimensional (2D) radial finite difference model was developed using TMVOC (Pruess and Battistelli, 2002). TMVOC is capable of simulating multiphase flow, heat transfer, and transport of volatile organic compounds (VOCs) in three-dimensional heterogeneous porous media or fractured rock. The developed model was employed to evaluate the reduction of TCE concentrations in the rock matrix upon application of TCH. A sensitivity analysis was performed to evaluate how TCE removal from the rock matrix is influenced by specific heat capacity,

matrix porosity, energy input into the subsurface and the duration of heating. The results from this study will generate recommendations for future TCH remediation applications in fractured bedrock aquifers.

### TCH Pilot Test

A TCH pilot test was performed by TerraTherm Inc. at the NAWC facility between April 10 and July 24, 2009. A network of 15 heater/extraction wells (vapor and liquid extraction) was installed over an area of 45.6 m<sup>2</sup>. The wells were installed to a depth of 16.8 m below ground surface (bgs) and screened their entire length to allow for maximum extraction of fluids. The top of bedrock at the NAWC Facility varies from 1 to 8 m depths and consists of highly fractured weathered mudstones that are part of the Lockatong Formation (Tiedeman et al., 2010; Lacombe and Burton, 2010). The water table across the NAWC Facility varies from 1 to 5 m below ground (Tiedeman et al., 2010). The top of bedrock was encountered at a depth of approximately 1.8 m in the area of the TCH test pilot and the water table is located at 1.52 m below ground surface. Further details pertaining to the pilot test are described in Rodriguez et al. (2012) and Lebron et al. (2012).

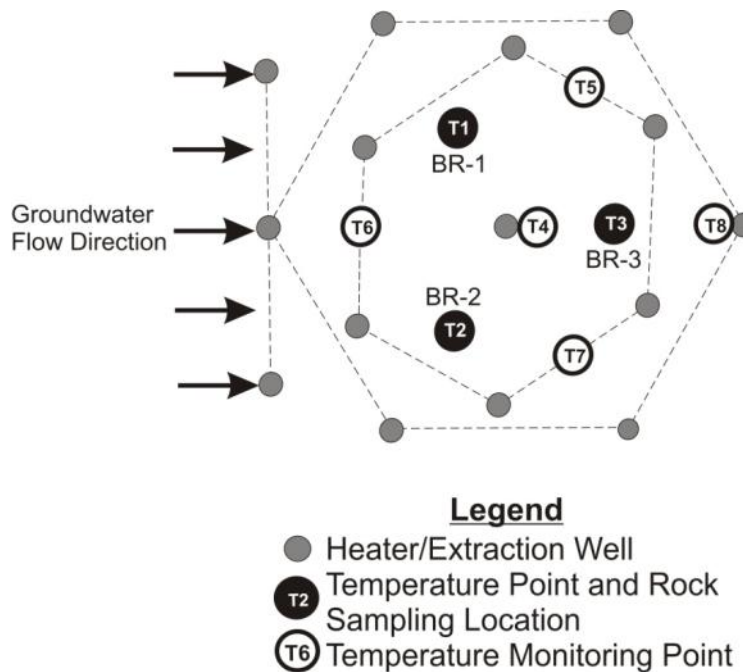


**Figure 2 – Configuration of heater/extraction wells and temperature monitoring points**

Figure 2 illustrates the configuration of heater/extraction wells and temperature monitoring points associated with the field pilot test. Three wells were installed on the upgradient side of the heating network to aid in reducing heat losses due to incoming groundwater flow. A total of eight temperature monitoring borings (T1 to T8) were completed with 10 temperature measurement points in each spaced at 1.52 m intervals beginning at 1.52 m below ground surface. A concrete cap was placed on top of the treatment zone to reduce heat losses at ground surface. The pilot test included combined heating and fluid extraction for 98 days, followed by

fluid extraction alone for 4 days post-heating. Steady-state temperatures achieved in the treatment zone varied from approximately 60 °C to approximately 110 °C with an average of 98 °C (Figure 3). Temperatures in the bottom 4.6 m of the test interval did not reach 100 °C, likely because of the cooling influence of inflowing groundwater at those depths.

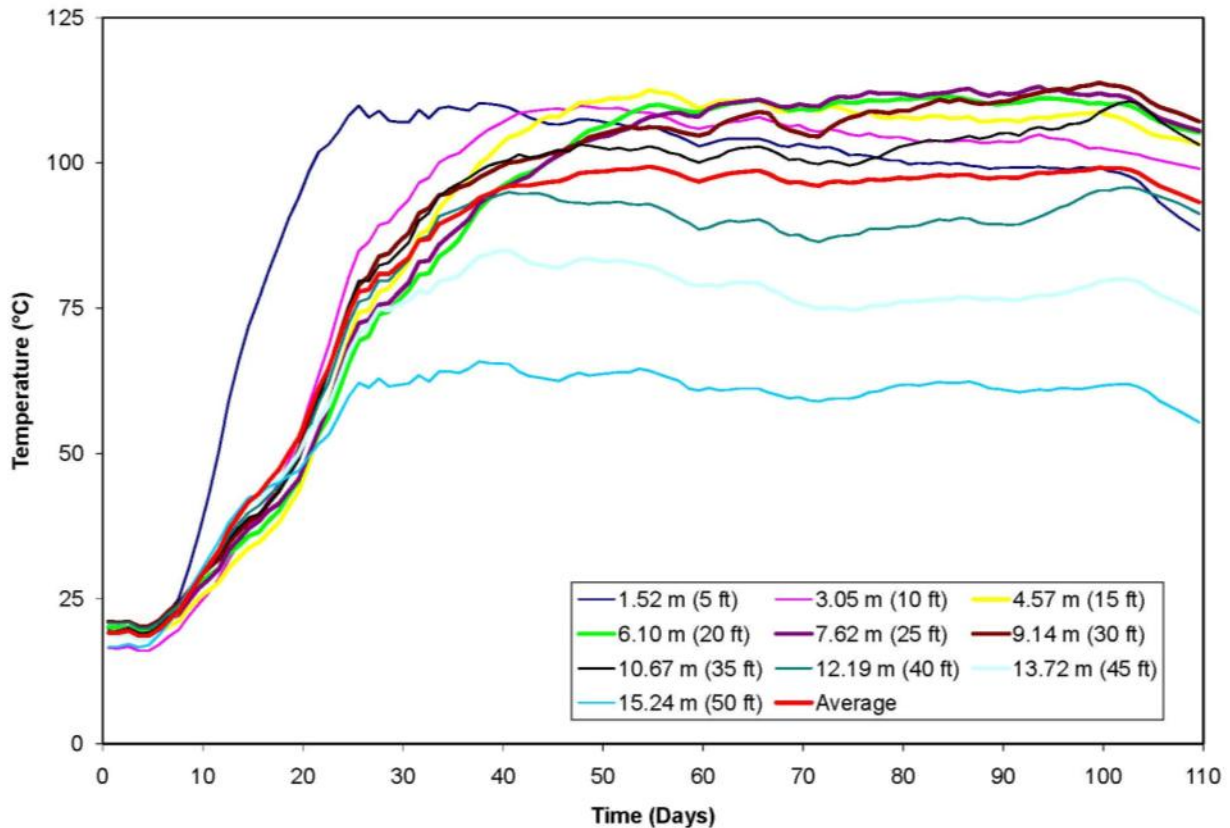


**Figure 3 – Average temperature for eight temperature monitor borings (T1-T8) that had 1.52 m interval temperature points from 1.52 m to 15.24 m below ground surface during the NAWC pilot test.**

To evaluate the removal of TCE from the rock matrix, three boreholes (BR-1, BR-2, and BR-3) were drilled in the centre of the treatment area in which samples were collected both pre- and post-treatment in adjacent boreholes (Figure 2). The samples were placed in a rock crushing device, preserved in methanol and shaken for 24 hours to allow the TCE to partition into the methanol (Rodriguez et al., 2012). The methanol solution was then extracted from each rock sample and analyzed for TCE concentration by an external laboratory. Figure 4 presents the rock matrix sampling results as a function of depth from the BR-1 pair of coring locations pre- and post-treatment. This location exhibited higher initial concentrations of TCE in the rock matrix than BR-2 and BR-3 and contained a greater number of discrete sample results. Considering results from all three paired locations, approximately 63.5% of the TCE was removed from the rock matrix as a result of TCH application.

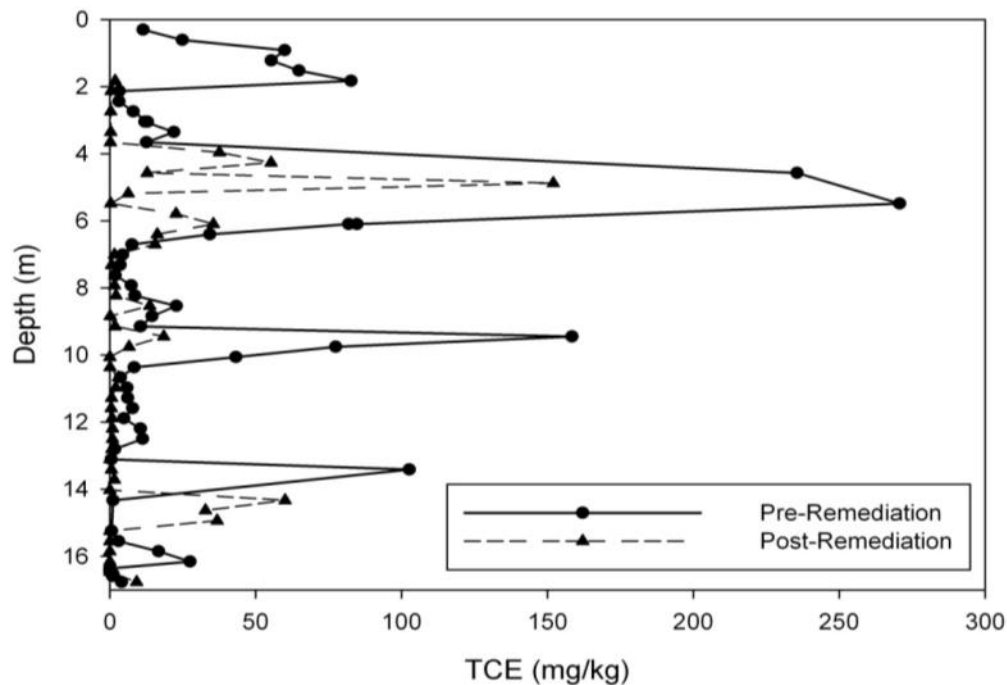


**Figure 4 – TCE concentration in the rock matrix from location BR-1 pre- and post-treatment.**

## Model Development

### Site Characterization Input

The local geology at the pilot test site consists of fill and weathered saprolite to approximately 1.8 m below ground surface (bgs). The saprolite is composed primarily of silt and clay and has a bulk average permeability of  $6.5 \times 10^{-13} \text{ m}^2$  (Tiedman et al., 2010). This layer is underlain by a highly fractured, weathered grey mudstone. Laboratory testing shows that the weathered mudstone has a bulk density of  $2520 \text{ kg/m}^3$ , a matrix permeability of  $1 \times 10^{-17} \text{ m}^2$ , a matrix porosity of 3.3% and a matrix fraction organic carbon of 0.0079 (average properties from Rodriguez et al., 2012). The weathered mudstone varies in depth up to 30 m bgs (Tiedman et al., 2010) and was the primary geologic unit encountered during rock coring in the area of the TCH pilot test. The hydraulic gradient at the site in the pilot test area was approximately 0.008 (Tiedman et al., 2010).

### Model Domain and Boundary Conditions

TMVOC was employed to create a two-dimensional (2D) radial finite difference model to simulate TCE removal from the rock matrix using data collected from the pilot test. Figures 5 and 6 display the conceptual 2D model upon which the numerical model is based. The numerical simulations were designed to simulate the heater/extraction well that is located in the center of the well network (Figure 5). The inside radius of the numerical domain represents a fixed boundary at the center heater/extraction well. The outside radius was set as a symmetry boundary

to account for the first ring of heater/extraction wells. The observation location is the outermost column of cells, which is located 1.25 m away from the center well and is located approximately half way between the inner well and first ring of wells in the field pilot test.

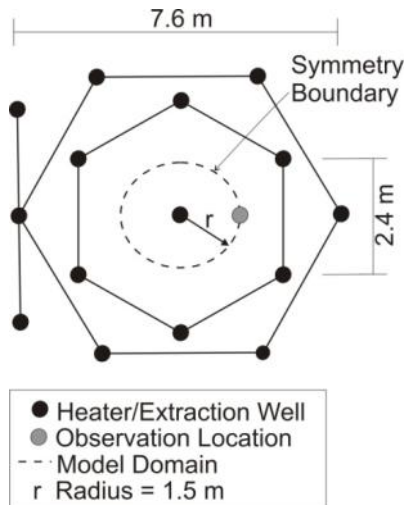


**Figure 5 – Plan view of the conceptual model.**

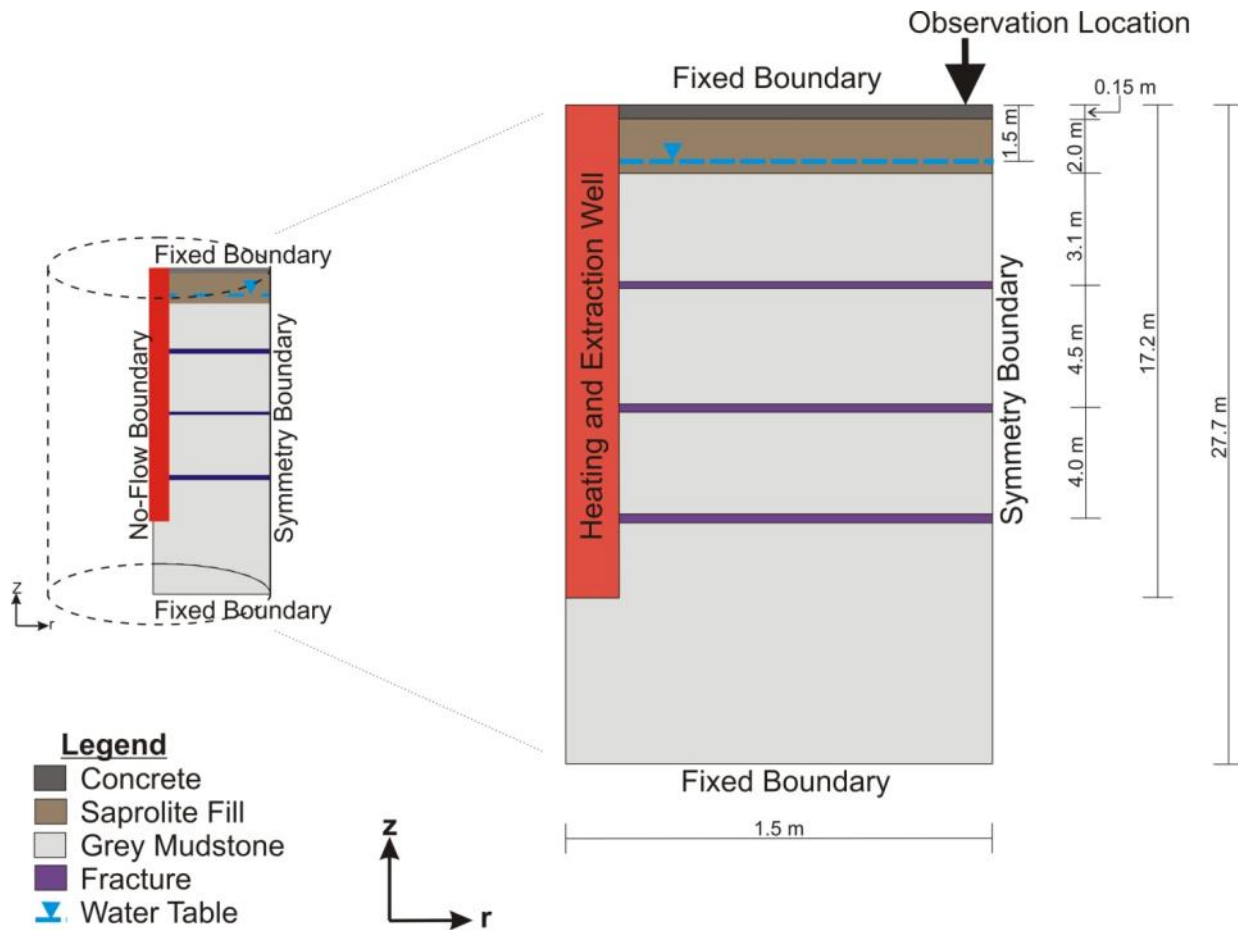


**Figure 6 – Cross-sectional view of the conceptual 2D radial symmetric model.**

The top and bottom boundaries were set to no-flow boundaries for all fluid phases with a constant temperature of 10 °C. A constant pressure on the top boundary of 101,325 Pa (representing atmospheric conditions) and 356,231 Pa at the bottom boundary was used to create a water table approximately 1.5 m below the top of the model. The bottom boundary was extended below the treatment zone in order to reduce the influence of the bottom boundary condition on the model results.

Three fractures were incorporated into the model domain as illustrated in Figure 6. The fracture locations were selected based on the sharp spikes in TCE concentration found in the rock matrix pre-remediation samples as shown in Figure 4. The TCE concentration profile found in the rock matrix in BR-1 pre-remediation was used in the numerical simulations as the baseline condition. The fracture zone cells had a 1 cm thickness and were assigned a permeability calculated according to the following depth-weighted arithmetic mean:

$$(1)$$

where  $k_{fz}$  is the permeability assigned to the fracture zone cells,  $k_f$  is the fracture permeability calculated as  $e^2/12$ ,  $e$  is the fracture hydraulic aperture assumed to be equal to the mechanical aperture,  $k_m$  is the matrix permeability, and  $z_{fz}$  is the thickness of the fracture zone cell (1 cm).

The fracture hydraulic aperture was calculated on the basis of hydraulic testing completed at the site by TerraTherm, Inc. in borings BR-1 through BR-3. A total of 32 hydraulic aperture values were calculated ranging from 54 microns to 234 microns with an arithmetic mean value of 138 microns. The average aperture was used in Equation 1 to calculate the permeability of the fracture zone cells and assigned to each of the three fractures in the model domain. A matrix permeability of  $1.0 \times 10^{-17} \text{ m}^2$  was assigned to the mudstone, which represents the arithmetic mean of 2 measurements performed on rock disks cut from pre-remediation rock core obtained from within the treatment zone. The resulting fracture zone permeability is calculated to be  $1.0 \times 10^{-11} \text{ m}^2$ .

A summary of the model input parameters is provided in Table 1. Thermal conductivity, specific heat capacity, pore compressibility and the Klinkenberg parameter were assumed to be equal for the saprolite and bedrock. Scaled power functions were used by TMVOC to calculate the gas and liquid water phase relative permeabilities following Stone (1970). The capillary pressure functions were adapted from Falta et al. (1992), which were calculated using modified versions of the van Genuchten (1980) constitutive model given by Parker et al. (1987).

**Table 1 – Baseline model input parameters.**

Parameter	Units	Saprolite	Mudstone Bedrock	Fracture Cells	Zone
Density	kg/m <sup>3</sup>	2520	2520	2520	
Permeability	m <sup>2</sup>	$6.5 \times 10^{-13}$	$1.0 \times 10^{-17}$	$1.0 \times 10^{-11}$	
Porosity <sup>1</sup>	%	30	3.3	3.3	
C <sub>wet</sub> <sup>2</sup>	W/m°C	2.84	2.84	2.84	
C <sub>dry</sub> <sup>2</sup>	W/m°C	2.19	2.19	2.19	
Specific heat capacity <sup>3</sup>	J/kg°C	1000	1000	1000	
Pore compressibility <sup>4</sup>	Pa <sup>-1</sup>	$3.0 \times 10^{-9}$	$3.0 \times 10^{-9}$	$3.0 \times 10^{-9}$	
Klinkenberg parameter <sup>5</sup>	Pa <sup>-1</sup>	$2.4 \times 10^{-6}$	$2.4 \times 10^{-6}$	$2.4 \times 10^{-6}$	
Fraction organic carbon	-	0.0079	0.0079	0.00	

1. The saprolite layers were assumed to have a porosity of 30% which is a common porosity for silts and clays as specified by Hough (1957).
2. C<sub>wet</sub> is the thermal conductivity under saturated conditions and C<sub>dry</sub> is the thermal conductivity under de-saturated conditions. This parameter was calculated using the equations in Woodside and Messmer (1961) with a thermal conductivity of the matrix of 3.0 W/m°C.
3. Schärli and Rybach (2001); Čermák and Rybach (1982).
4. Zimmerman (1991).
5. Webb and Pruess (2003).

## **Baseline Model Establishment**

The measured daily average amount of energy applied to the subsurface during the pilot test was specified in the numerical simulations. Use of the measured energy values resulted in model-predicted temperatures that exceeded temperatures measured during the pilot test (Figure 7 – Modeled Temperature 1). This would suggest that the field pilot test was prone to greater heat losses than represented in the numerical model. This is likely due, in part, to the fact that the model domain incorporated three fractures without vertical connections, while the bedrock within the test zone likely contained several interconnected micro-fractures creating additional pathways for heat losses due to groundwater flow. In addition, the numerical model does not incorporate a hydraulic gradient since it is radial symmetric. Groundwater flowing through the test zone may have represented a heat sink despite the fact that three heater/extraction wells were placed hydraulically up gradient of the target heating zone. Due to the numerical model's ideal conditions, the average temperature recorded at measurement points T1 through T8 during the pilot test were matched by adjusting the daily energy input into the model. This is justified given that the objective of the numerical simulations was to compare rock matrix mass removal achieved during the pilot test to that predicted by the model when subjected to similar heating conditions (i.e., temperature history). The resulting calibrated model match to the field measured temperature data is depicted in Figure 7 as Modeled Temperature 2.

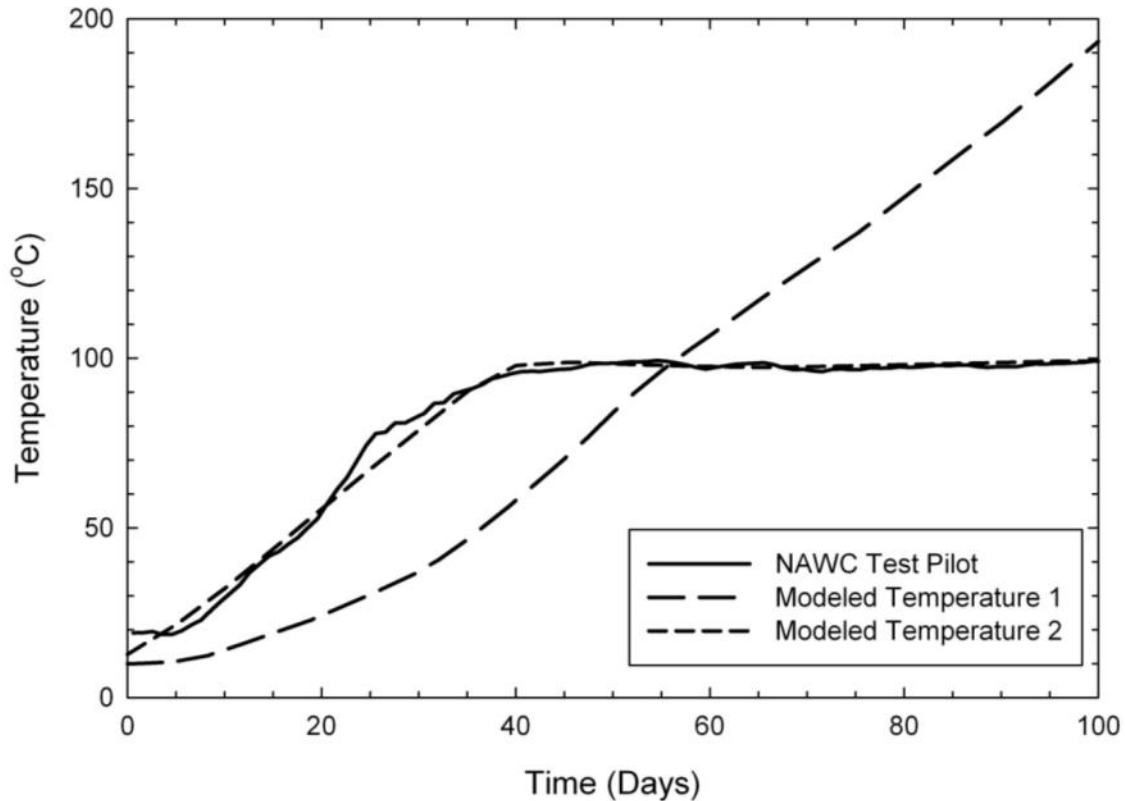


**Figure 7 – Temperature versus time for the recorded temperatures in the rock matrix at locations T1 through T8 compared to model predicted temperatures. Modeled Temperature 1 is based on a simulation incorporating the measured energy during the pilot test; Modeled Temperature 2 adopted a reduced energy input and represents the calibrated baseline model.**

The total mass of TCE removed from the rock matrix during the pilot test was estimated to be 63.5% of the initial amount (Rodriguez et al., 2012). The Modeled Temperature 1 simulation predicted 75% TCE mass removal while the calibrated baseline model (Modeled Temperature 2) predicted 31% TCE mass removal. The calibrated model predicted half the amount of mass removal as compared to the TCE removed during the pilot test. This is because the calibrated model represents an idealized scenario. The test pilot at the NAWC site was conducted in a highly fractured, weathered grey mudstone which would allow for liquid and vapour extraction through the various fracture networks. The calibrated model represents three primary fractures and assumes a competent bedrock matrix in between therefore the primary path for extraction to occur is through those three discrete fractures.

Figure 8 displays the model-predicted TCE profile in the rock matrix at the observation location over time. This figure shows that as the maximum temperature in the rock matrix is reached (average of 99°C), and steam begins to collect in the fractures, the TCE concentration in the fractures increases (concentration spikes at 35 days). At 45 days, extraction TCE fluid mass is occurring primarily in the fracture zone cells in the upper two fractures, and at 55 days extraction is taking place in all three fractures as well as slightly above and below in the rock matrix. Due to over idealized conditions in the calibrated model (i.e., 3 primary fractures with competent

bedrock in between), there is little to no extraction in the rock matrix between the three fractures as shown in Figure 8 at 100 days. The grey line represents the initial TCE profile in the rock matrix as compared to 100 days of remediation. At 100 days, the TCE removed continues to be primarily in the fracture zone cells which have a higher permeability than the rock matrix. This is further shown in Appendix D, which displays the water saturation profiles over time illustrating that extraction primarily occurs in the areas where steam is created (in the fracture zone cells with higher permeability).

### Sensitivity Analysis Outline

The baseline calibrated model was employed to perform a sensitivity analysis to examine what parameters are most influential in dictating the amount of TCE mass removal from the rock matrix. Table 2 summarizes the parameters varied in the sensitivity analysis, which comprise specific heat capacity, matrix porosity, energy rate, and length of energy application.

**Table 2 – Sensitivity analysis parameters.**

<b>Parameter</b>	<b>Unit</b>	<b>Baseline Model</b>	<b>Values Considered</b>
<i>Field Parameters</i>			
Specific Heat Capacity	J/kg°C	1000	800, 900, 1100, 1200
Matrix Porosity	%	3.3	1, 5, 10
<i>Thermal Conductive Heating Parameters</i>			
Energy Rate	J/s	field match	temperature -10%, +10%, +20%, +30%
<i>Matrix Clean-up</i>			
Length of energy application	Days	100	125, 150, 175, 200

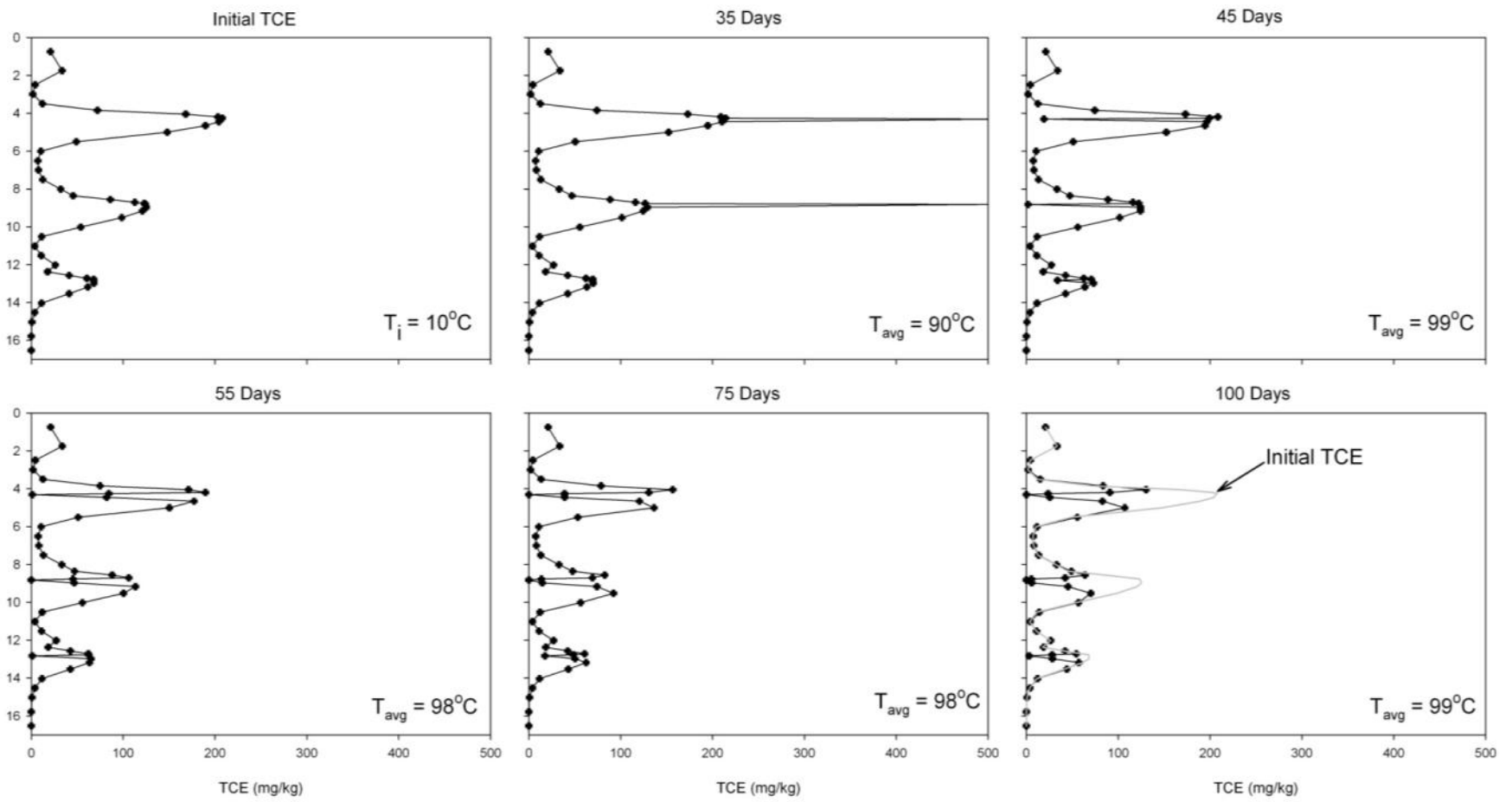


**Figure 8 – Model-predicted TCE profile in the rock matrix at the observation location over time.**

## Sensitivity Results and Discussion

### Specific Heat Capacity

The specific heat capacity of an object is the amount of energy that is required to increase the temperature of a material by one degree Celsius. The specific heat capacity varies with temperature and pressure. The specific heat capacity for mudstone can vary from 800 to 1200 J/kg°C with an average of 1000 J/kg°C used in the baseline model (Schärli and Rybach, 2001; Čermák and Rybach, 1982). Figure 9 displays the temperature-time curves at the observation point for various values of specific heat capacity.

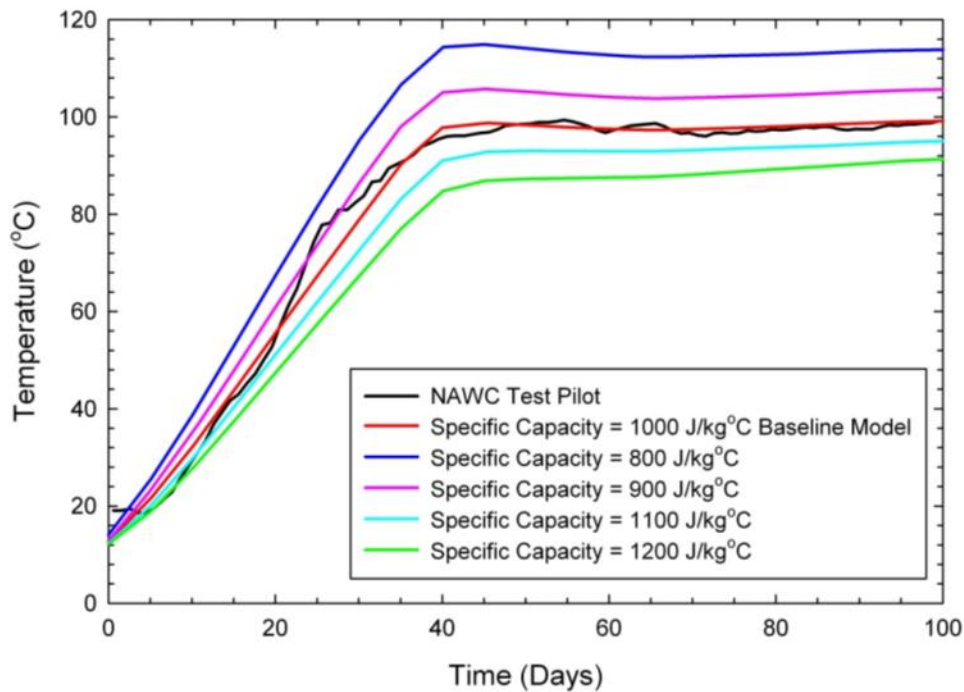


**Figure 9 – Temperature versus time curves displaying the influence of the specific heat capacity of the rock matrix.**

As the specific heat capacity is decreased, the ultimate temperature reached in the rock matrix increases. With a lower specific heat capacity, less energy is required to increase the temperature of the rock. The average maximum temperature sustained for the baseline model was 98 °C. When the specific heat capacity is decreased to 800 J/kg°C, the maximum temperature achieved becomes 118 °C, while when the specific heat capacity is increased to 1200 J/kg°C, the maximum temperature decreases to 86 °C, which is approximately the boiling point of TCE, but below the boiling point of water. Examining the percentage of TCE removed from the rock matrix at 100 days shows that when a higher temperature is reached, the TCE removed also increases as shown in Figure 10.

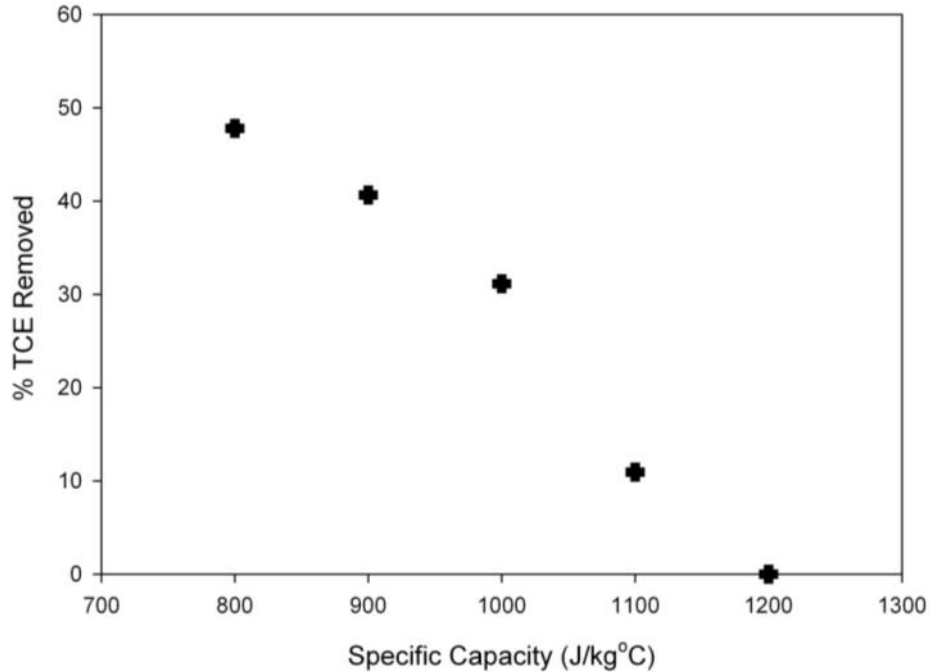


**Figure 10 – Percentage of TCE removed from the rock matrix at 100 days for values of specific heat capacity from 800 to 1200 J/kg°C.**

### **Matrix Porosity**

Primary porosity is created when the rock is formed and is referred to here as the matrix porosity; secondary porosity is created due to geological processes such as weathering and fracturing (Singhal and Gupta, 1999). The 2D simulations only considered primary porosity with the baseline model having a matrix porosity of 3.3%, determined through laboratory testing on core samples obtained from within the target heating zone.

Figure 11 displays the model-predicted temperature-time curves when the matrix porosity is altered between 1 and 10%. Figure 12 displays the percentage of TCE removed as a function of matrix porosity. Figures 11 and 12 illustrate that the matrix porosity does not significantly affect the temperature of the rock matrix when the same amount of energy is applied in the numerical model. However, the matrix porosity does influence the percentage of TCE removed from the rock matrix. As the porosity increases, the TCE removed at 100 days also increases.

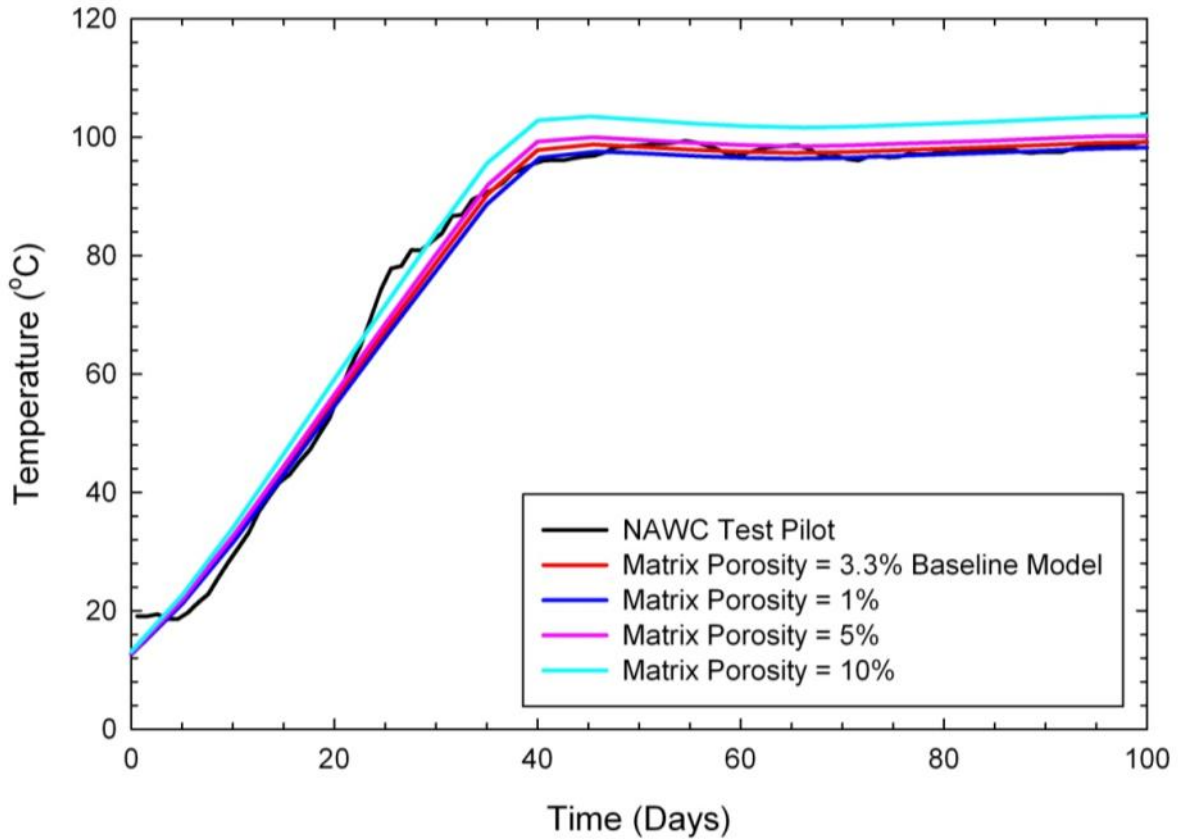


**Figure 11 - Temperature versus time curve displaying the influence of matrix porosity.**

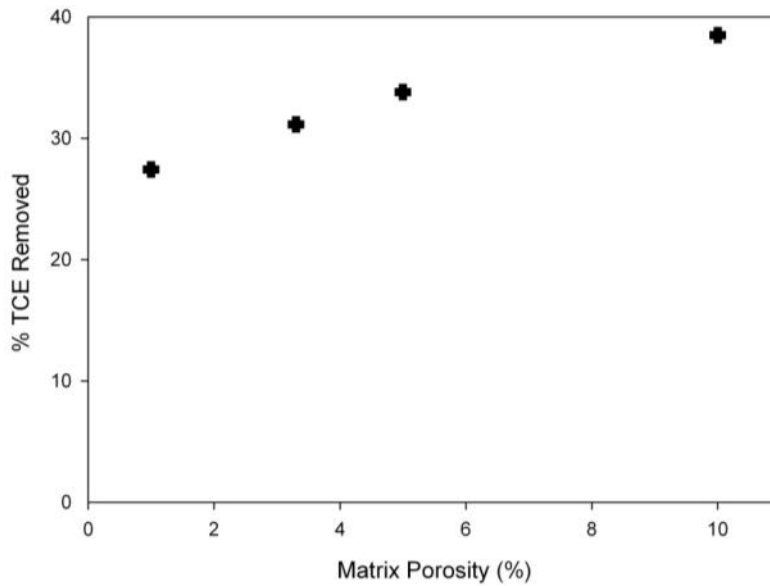


**Figure 12 - Percentage of TCE removed from the rock matrix at 100 days when the matrix porosity is varied from 1 to 10%.**

## Energy Rate

A variable energy rate (J/s) was applied to the column of matrix blocks where the heater/extraction well was located on the inner radius of the model domain. A higher energy was applied until the maximum average temperature was reached in which the energy was then reduced to sustain that temperature. The baseline model had an energy input that created a temperature-time profile similar to what was recorded during the NAWC pilot test. This energy was then increased or decreased to examine what effects the energy input into the rock matrix has on TCE removal.

The baseline model energy input was varied from a 10% decrease in energy to a 30% increase in energy, as shown in Figure 13. More energy into the rock matrix resulted in higher maximum temperatures reached in the model. With a 30% increase in energy input, the maximum temperature achieved in the rock matrix was 120 °C. Similar to varying the specific heat capacity, when the temperature in the rock matrix is increased by increasing the energy input, the percentage of TCE removed is also increased (Figure 13). A decrease in energy rate by 10% reduces the temperature to near the boiling temperature of TCE and this resulted in 5% of TCE being removed from the rock matrix.

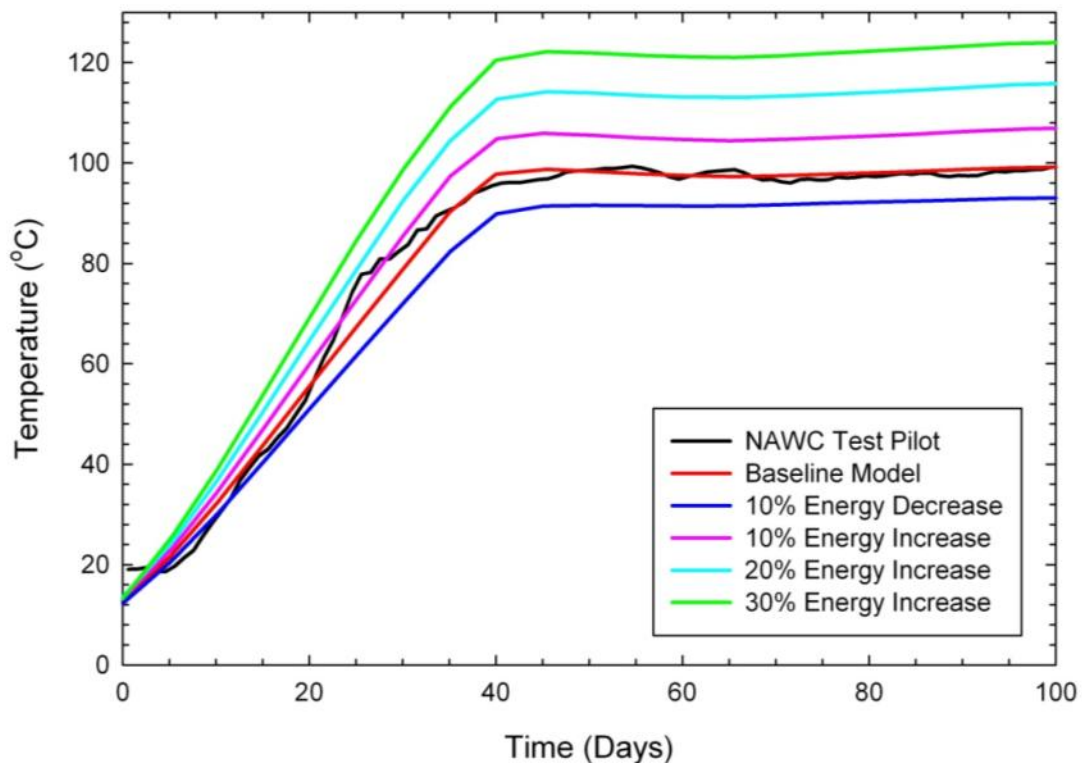


**Figure 13 - Temperature versus time curve displaying the influence of a change in energy input to the rock matrix.**

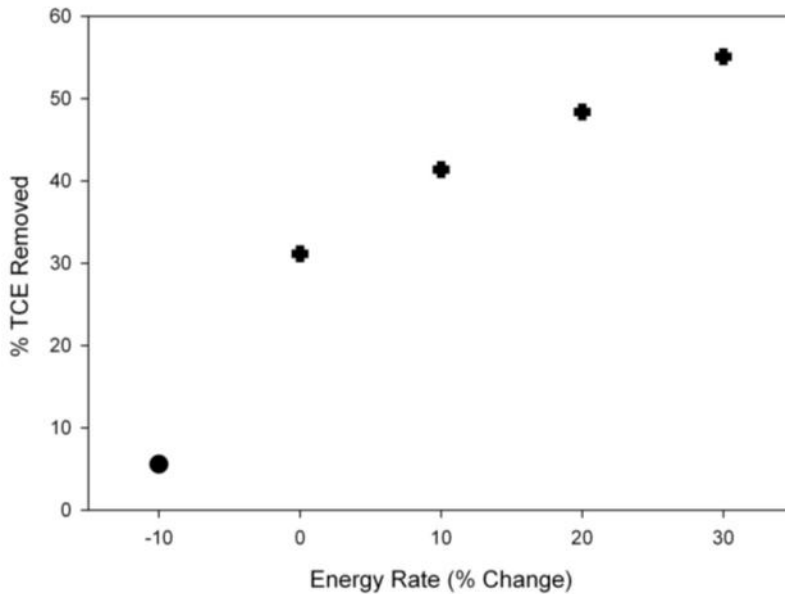


**Figure 14 - Percentage of TCE removed from the rock matrix at 100 days when the energy input into the 2D simulations is varied.**

### Duration of Remediation

Lastly, the duration of remediation in the rock matrix was examined. The energy input into the rock matrix was held constant for the baseline model at 98 °C for up to 200 days. The percentage of TCE removed from the rock matrix increased as the bedrock was heated for a longer amount of time as shown in Figure 15.

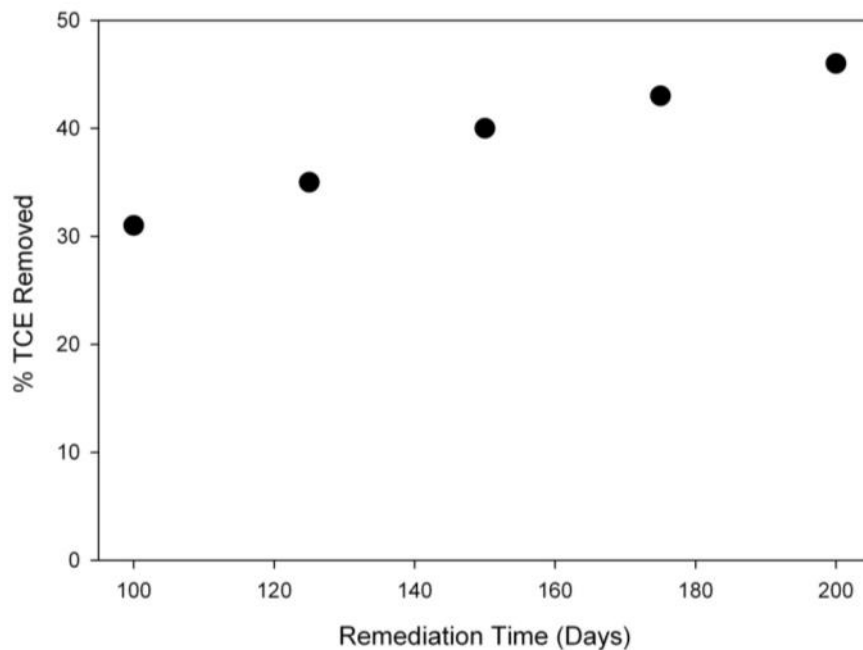


## **Figure 15 – Percentage of TCE removed from the rock matrix when remediation time is increased.**

### **Conclusions**

A thermal conductive heating field pilot test was conducted in 2009 at the Naval Air Warfare Center in West Trenton, New Jersey in which historical TCE contamination is found in fractured mudstone bedrock. The pilot test consisted of a network of 15 heater/extraction wells that were operated for 102 days to examine the TCE removal in the rock matrix. Using the data collected at the site, a 2D model was created using TMVOC in which the primary objective was to examine the TCE mass removal in the rock matrix from the numerical simulations compared to the pilot test.

The pilot test was found to have a TCE removal in the rock matrix of 63.5% as compared to the baseline model simulation which had a removal of 31%. The numerical model presented ideal conditions, such as only 3 fractures separated by competent bedrock and no hydraulic gradient, therefore reducing the percentage of TCE being removed. The fracture zone cells were identified to be the primary area where TCE removal occurred due to the higher permeability in these cells compared to the lower permeability in the rock matrix.

A sensitivity analysis concluded that the greater the maximum temperature sustained in the model, the greater the percentage of TCE removed from the rock matrix. The numerical simulations showed that the greater the duration of remediation at the maximum objective temperature, the greater amount contaminant removed. The field specific parameter of specific heat capacity showed that a lower heat capacity resulted in higher rock matrix temperatures. This parameter is site specific and should be measured prior to designing TCH projects as this may alter the energy input required to heat the subsurface to the desired temperatures.

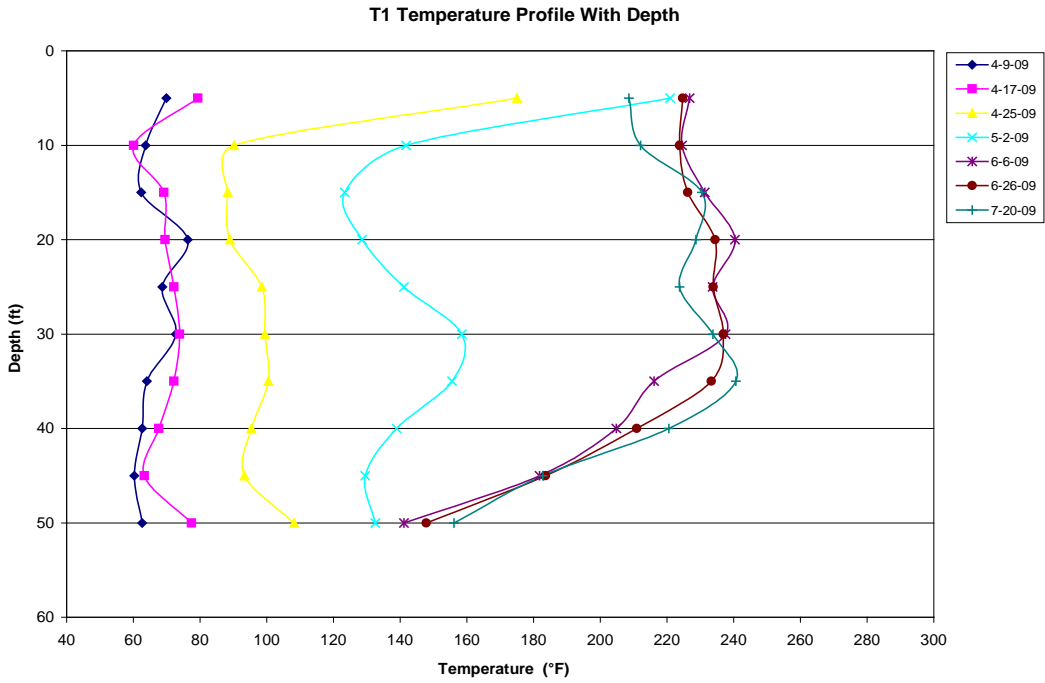
### **References**

- Baker, R.S. & Kuhlman, K. (2002). A Description of the Mechanisms of In-Situ Thermal Destruction (ISTD) Reactions. In: H. Al-Ekabi (Ed.), *Current Practices in Oxidation and Reduction Technologies for Soil and Groundwater*, Presented at the 2<sup>nd</sup> International Conference on Oxidation and Remediation Technologies for Soil and Groundwater, ORTs-2, Toronto, Ontario, Canada, Nov. 17-21, 2002.
- Baston, D.P. & Kueper, B.H. (2009) Thermal conductive heating in fractured bedrock: Screening calculations to assess the effect of groundwater influx. *Advances in Water Resources* 32, 231-238.
- Čermák, V., and Rybach, L. (1982). Thermal conductivity and specific heat of minerals and rocks. In G. Angenheister (Ed.) *Landolt-Börnstein: Numerical Data and Functional Relationships in Science and Tehcnology, Group V (Geophysics and Space Research), Volume 1a (Physical Properties of Rocks)*, (pp. 305{343). Springer, Berlin-Heidelberg.
- Falta, R.W., Pruess, K., Javandel, I., and Witherspoon, P.A. 1992. Numerical Model of Steam Injection for the Removal of Nonaqueous Phase Liquids From the Subsurface: 2. Code Validation and Application. *Water Resources Research* 28: 451-465.

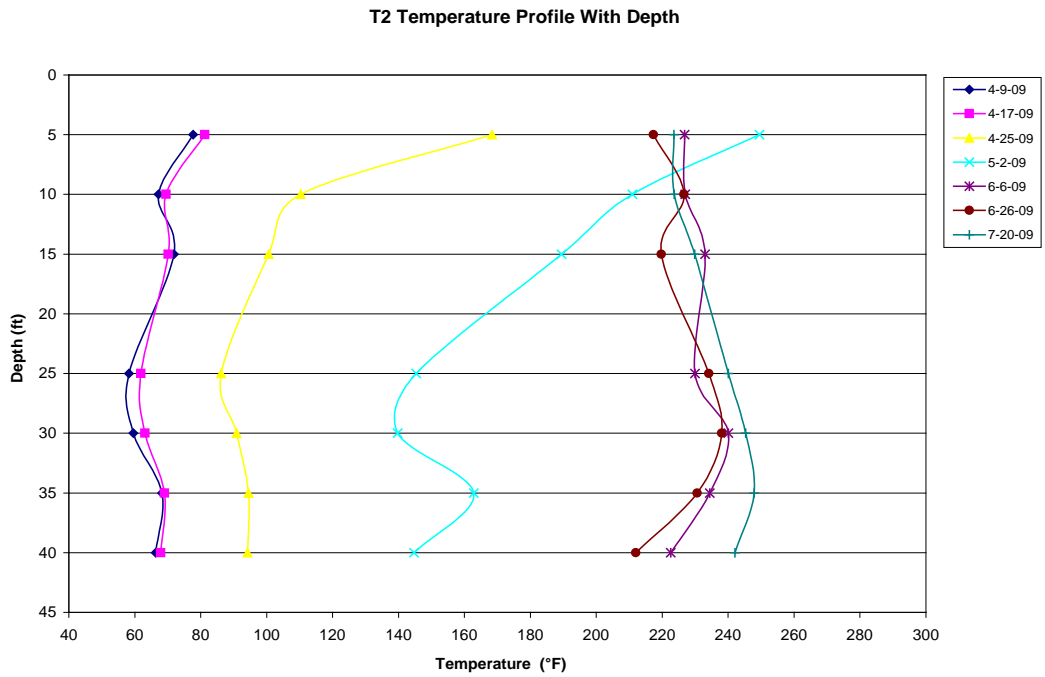
- Heron, G., Parker, K., Galligan, J., and Holmes, T.C. 2009. Thermal Treatment of Eight CVOC Source Zones to Near Nondetect Concentrations. *Ground Water Monitoring and Remediation* 29: 56-65.
- Hough, B.K. (19657). Basic Soils Engineering. Ronald Press Co., New York.
- Johnson, P., Dahlen, P., Triplett, J., Foote, E., and Williams, S. 2009. State-of-the-Practice Overview: Critical Evaluation of State-of-the-Art In Situ Thermal Treatment Technologies for DNAPL Source Zone Treatment. ESTCP Project ER-0314.
- Parker, J.C., Lenhard, R.J., and Kuppusamy, T. 1987. A parametric model for constitutive properties governing multiphase flow in porous media. *Water Resources Research* 23: 618-624.
- Pruess, K., & Battistelli, A. (2002). TMVOC, A Numerical Simulator for Three-Phase Non-isothermal Flows of Multicomponent Hydrocarbon Mixtures in Saturated-Unsaturated Heterogeneous Media. Lawrence Berkeley National Laboratory, Berkeley, CA.
- Rodriguez, D.J., and Kueper, B.H. (2012). Assessment of Thermal Conductive Heating for the Remediation of DNAPL Contaminated Fractured Bedrock. (In Progress).
- Schärli, U., and Rybach, L. 2001. Determination of specific heat capacity on rock fragments. *Geothermics* 30: 93-110.
- Singhal, B.B.S., & Gupta, R.P. (1999) Applied Hydrogeology of Fractured Rocks. Kluwer Academic Press, Netherlands.
- Stone, H.L. 1970. Probability Model for Estimating Three-Phase Relative Permeability. *Journal of Petroleum Technology* February: 214-218.
- Tiedeman, C.R., Lacombe, P.J., and Goode, D.J. 2010. Multiple Well-Shutdown Test and Site-Scale Flow Simulation in Fractured Rocks. *Ground Water*, 45(3):May-June 401-415.
- van Genuchten, M.T. 1980. A closed-form equation for predicting the hydraulic conductivity of unsaturated soils. *Soil Science Society of America Journal* 44: 892-898.
- Woodside, W., and Messmer, J. 1961. Thermal conductivity of porous media. *Journal of Applied Physics*, 32: 1688-1706.
- Webb, S.W., and Pruess, K. 2003. The Use of Fick's Law for Modeling Trace Gas Diffusion in Porous Media. *Transport in Porous Media* 51: 327-341.
- Zimmerman, R.W. 1991. Compressibility of sandstones, *Developments in Petroleum Science* 29, Elsevier, New York, NY, USA.

# Appendix D: Temperature Profiles

## Temperature Profiles during Operation

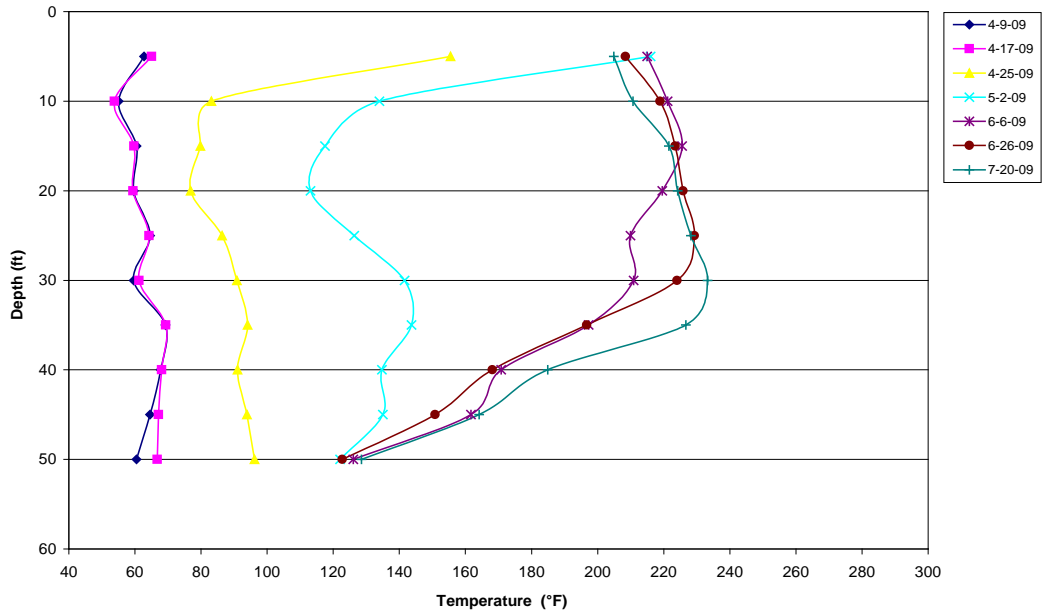


## Temperature at T1 during Heating Operations



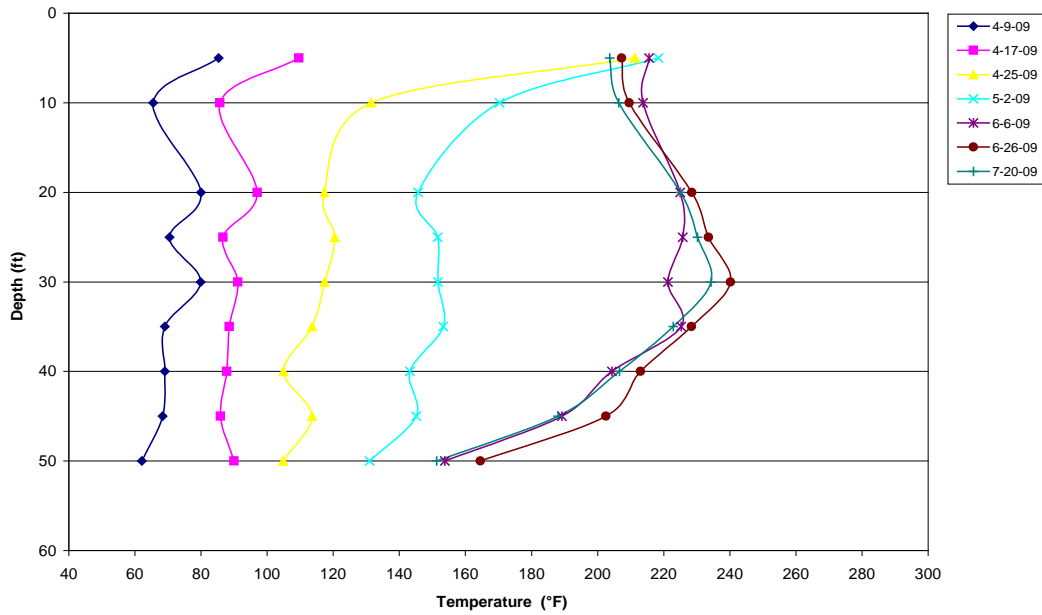
## Temperature at T2 during Heating Operations

**T3 Temperature Profile With Depth**



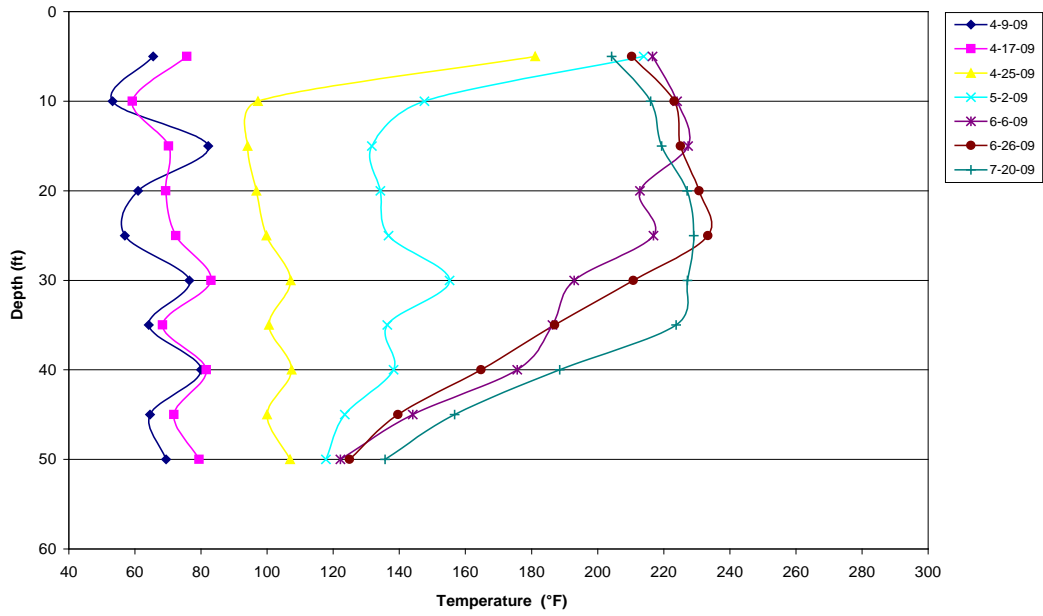
**Temperature at T3 during Heating Operations**

**T4 Temperature Profile With Depth**



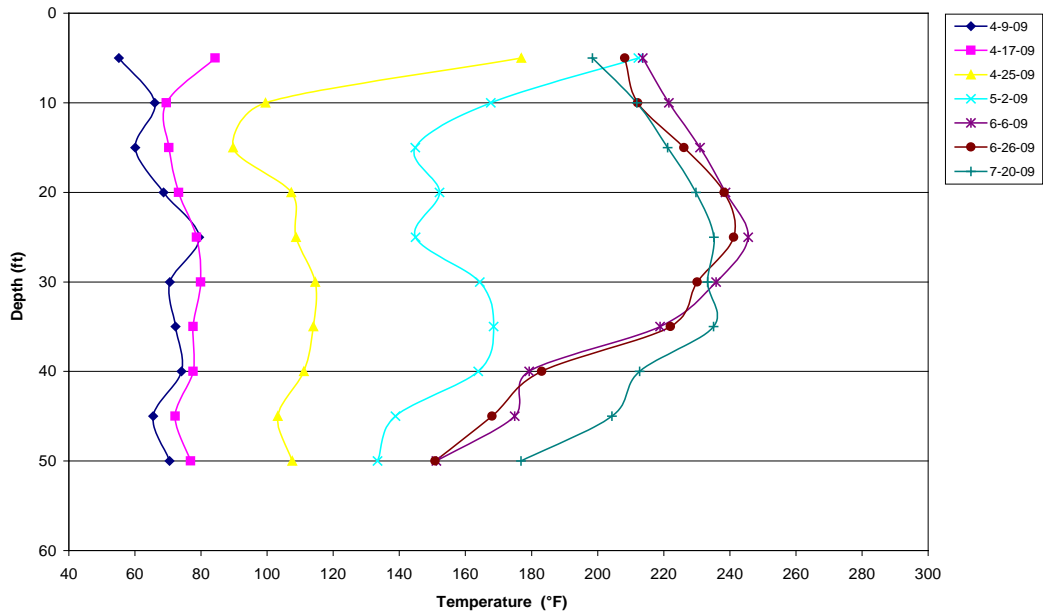
**Temperature at T4 during Heating Operations**

T5 Temperature Profile With Depth



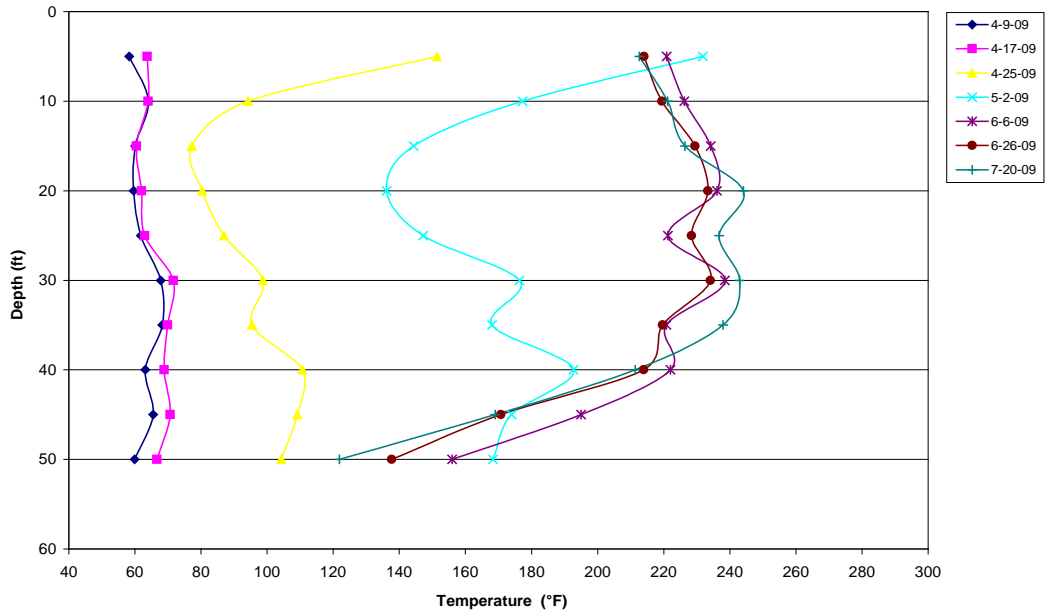
Temperature at T5 during Heating Operations

T6 Temperature Profile With Depth



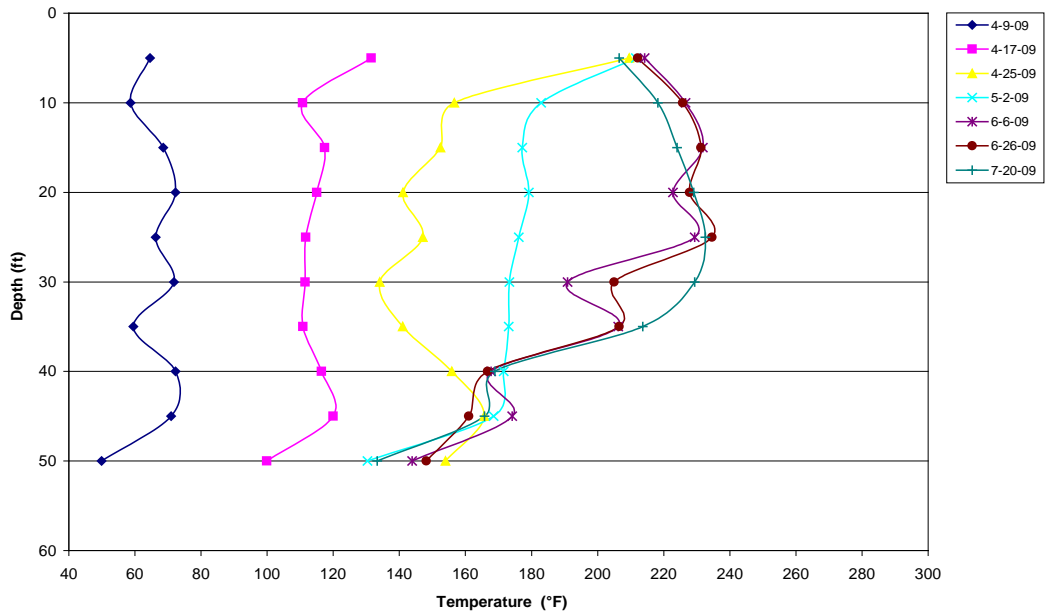
Temperature at T6 during Heating Operations

**T7 Temperature Profile With Depth**



**Temperature at T7 during Heating Operations**

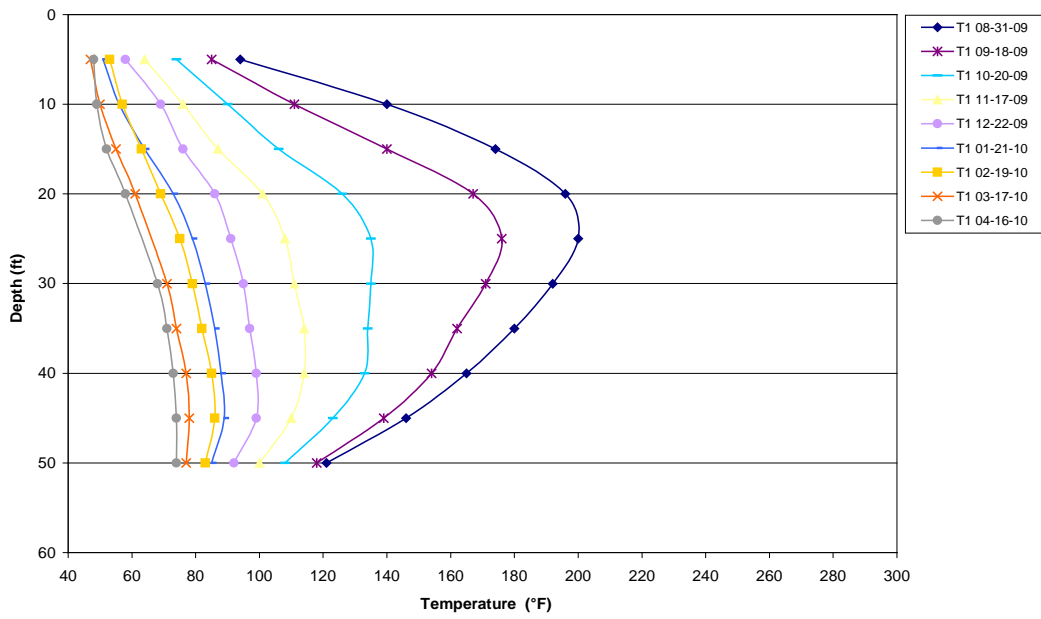
**T8 Temperature Profile With Depth**



**Temperature at T8 during Heating Operations**

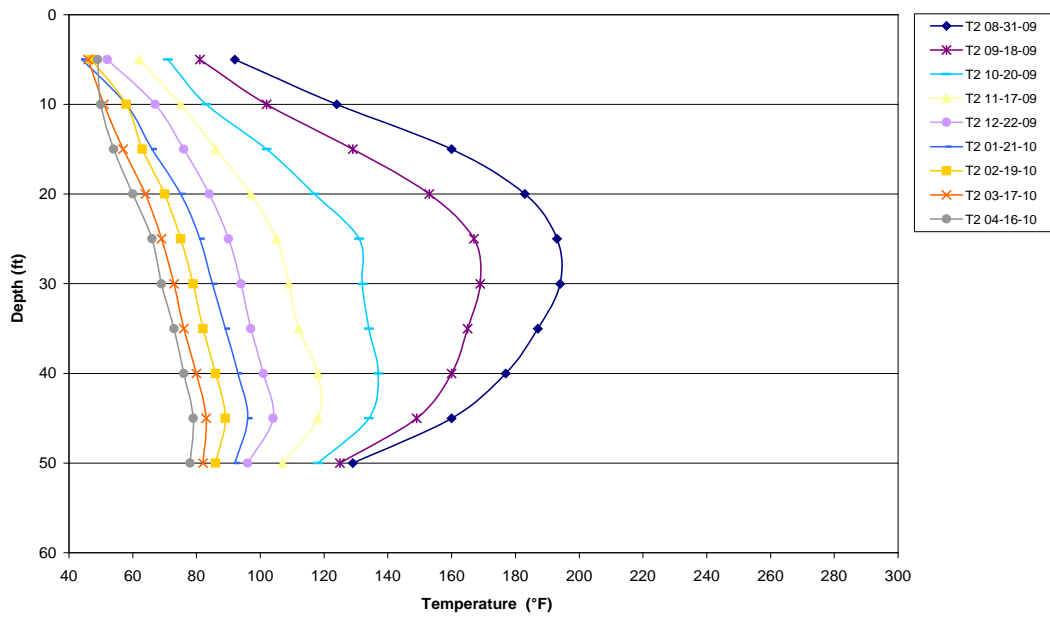
**Temperature Profiles during Cool-down**

T1 Temperature Profile With Depth



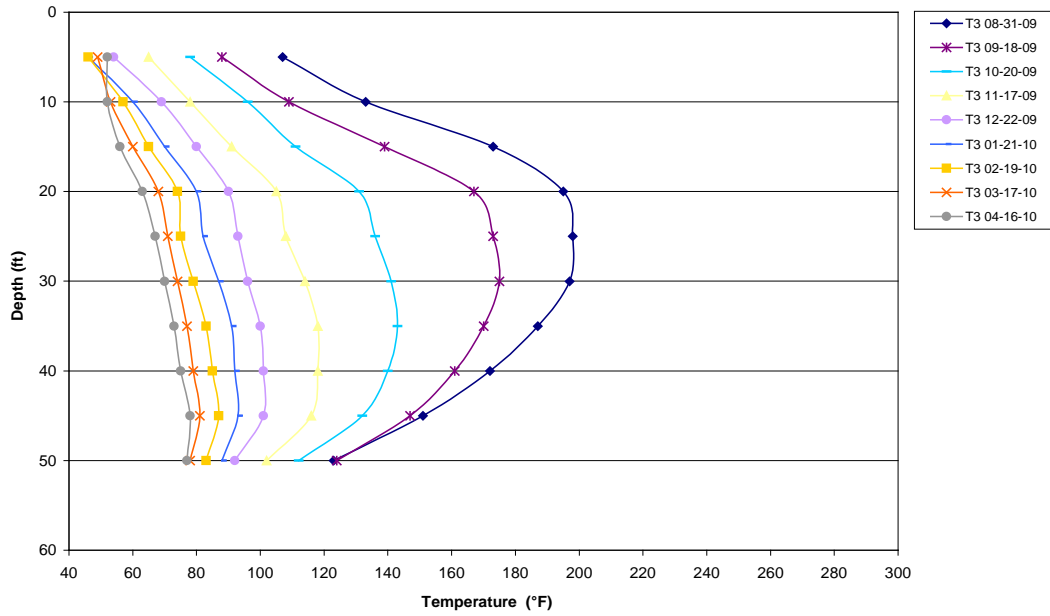
Temperature at T1 during Cool-down

T2 Temperature Profile With Depth



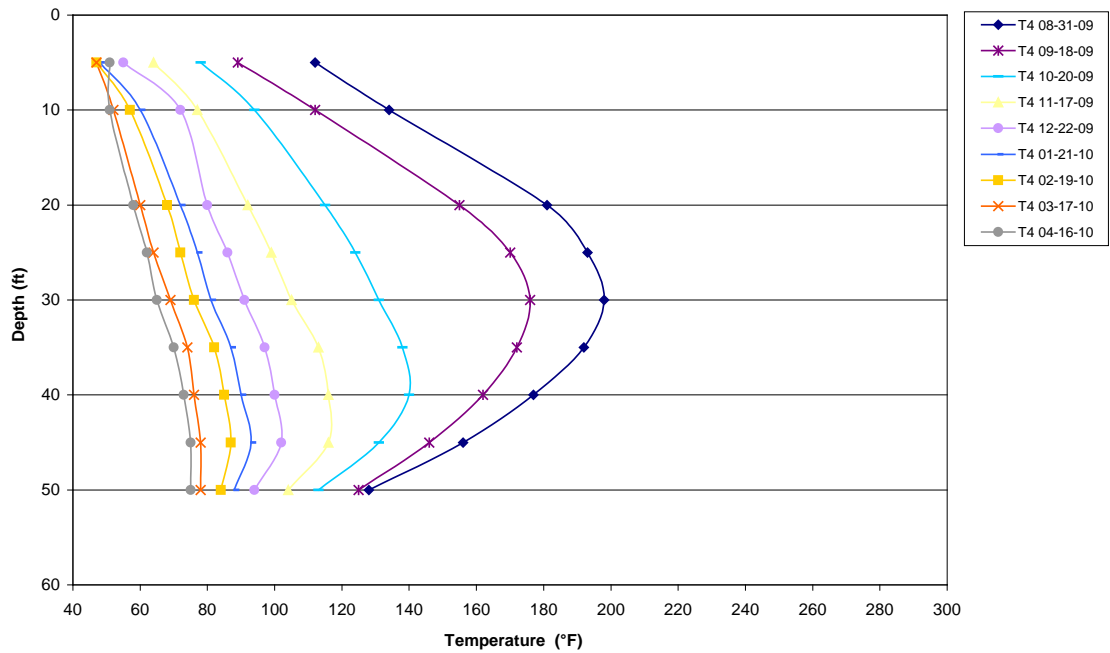
Temperature at T2 during Cool-down

**T3 Temperature Profile With Depth**



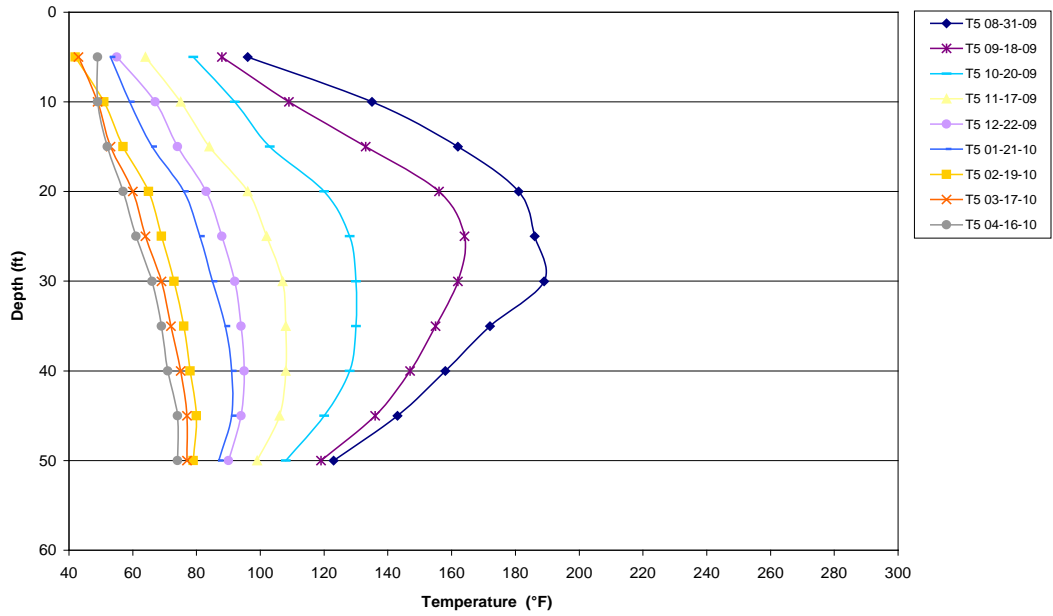
**Temperature at T3 during Cool-down**

**T4 Temperature Profile With Depth**



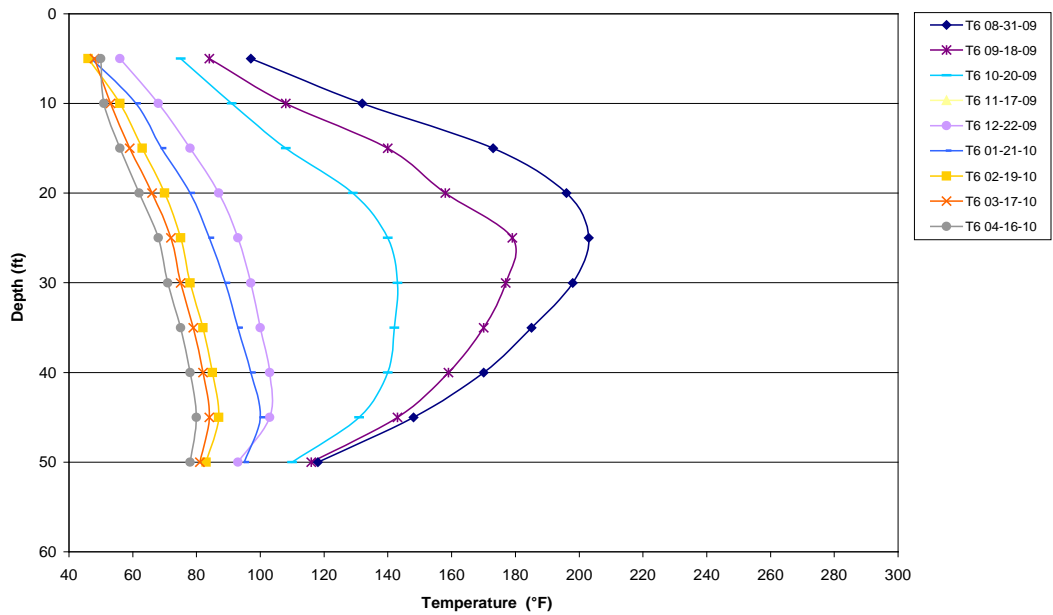
**Temperature at T4 during Cool-down**

T5 Temperature Profile With Depth



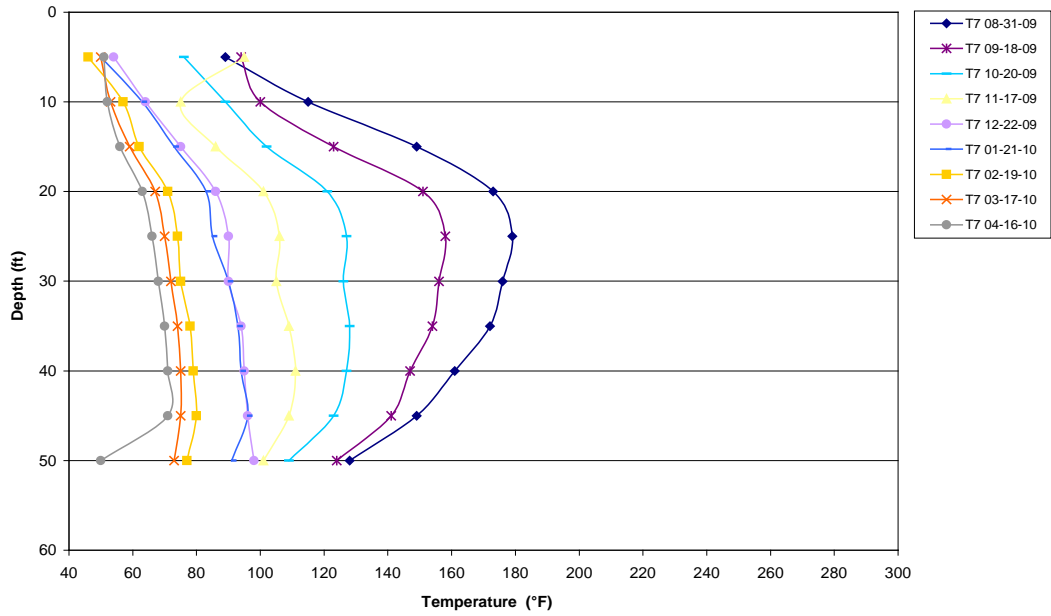
Temperature at T5 during Cool-down

T6 Temperature Profile With Depth



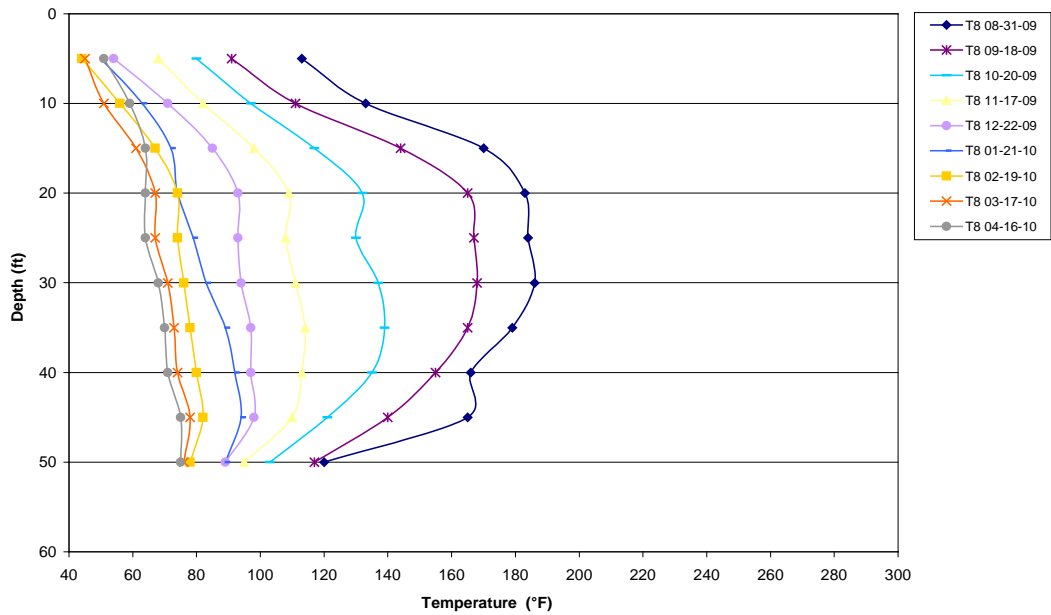
Temperature at T6 during Cool-down

T7 Temperature Profile With Depth



Temperature at T7 during Cool-down

T8 Temperature Profile With Depth



Temperature at T8 during Cool-down

## **Appendix E: Decontamination and Calibration**

Proper personal and equipment decontamination during construction, operation, and demobilization of the thermal remedy assured that residual COCs were contained to the TCH field demonstration area and were not transported via personnel or equipment out of the demonstration area and to the surrounding environment. Personal and equipment decontamination procedures are detailed below.

### **Personal Decontamination**

Proper decontamination was required of all personnel before leaving the site. Decontamination occurred within the contamination reduction zone (CRZ) setup at the site. Disposable personal protective equipment (PPE) was removed in the decontamination zone.

If worn, respirators were cleaned after each use with respirator wipe pads and stored in plastic bags after cleaning.

Water and liquid soap were available, so employees could wash their hands and face before leaving the site. Toilet facilities were also available on site.

### **Equipment Decontamination**

Drill rigs and forklifts used during the field demonstration were decontaminated via dry brushing and pressure washing. The equipment could not leave the site until the Site Safety Officer (SSO) released it.

All samples were collected by using new sample equipment or by equipment decontaminated off site by the analytical laboratory (e.g., Summa canisters). The only exception to this was the rock sample crusher used during the pre- and post-treatment rock sampling events.

Tedlar bags were used to collect PID vapor samples at the GAC vessels and from vapor extraction points in the wellfield. Tedlar bags were dedicated to a specific sample port and only reused at the same sample port after flushing with clean air.

### **Calibration of Analytical Equipment**

The MiniRae 2000 PID meter and the YSI 556 water quality meter were the only devices used during the project that required calibration. Manufacturer manuals for both detailing calibration procedures are attached.